BULLETIN OF THE EARTHQUAKE RESEARCH INSTITUTE,
UNIVERSITY OF TOKYO. Vol. 36, Part 1. March, 1958.

東京大學
地震研究所彙報

第 36 號　第 1 册

昭和 33 年 3 月

目　次

論文及報告

頁
1. 日本に於ける地磁気短周期変化の異常と地下構造（第 7 報）（英文）... 力武常次・横山泉・上田誠也・行武毅・中川英子 1
2. 震源の性状に関する地震学的及び測地学的研究（二）（英文）........... 笠原慶一 21
3. 電磁地震計の特性を周波数分析によつて求める方法（英文）............ 松本利松 55
4. 宮城県白石市附近の地震（1956 年 9 月 30 日）と水準測量の結果（邦文）
.... 岡田惇 65

(The titles in occidental languages are given on the back cover.)

地震研究所彙報は，年4回定期に（ただし，第1号より第6号までは不定期に，第7号は3冊として刊行された），彙報別冊は不定期に刊行される．

この彙報に載せられた論文及び報告についての責任は，すべてその著者のみにある．

この彙報についての照会通信は，すべて東京大学地震研究所長にあてられたい．

The Bulletin is published quarterly. (Vols. 1-6 were published at irregular intervals and Vol. 7 consisted of three parts.)
Supplementary Volume is published at irregular interval.

The authors of the papers alone are responsible for the statements and opinions contained in their respective papers.

All communications relating to this Bulletin should be addressed to the Director of the Earthquake Research Institute, University of Tokyo, Japan.

Earthquake Research Institute, University of Tokyo
Address:
No. 1, Motofuji-cho, Bunkyo-ku,
Tokyo Metropolis, Japan.
Telephone: 92-3188.
Cable address: ZISINKEN, TOKYO.

東京大学地震研究所
所在地
東京都文京区本富士町一番地
電話 小石川 92—3188
電略 ブンケウ トウダイ チシン

**Bulletin of the Earthquake
Research Institute**
Vol. 36 (1958), pp. 1-20

1. *The Anomalous Behaviour of Geomagnetic Variations fo Short Period in Japan and Its Relation to the Subterranean Structure. The 7th report.*

By Tsuneji RIKITAKE, Izumi YOKOYAMA, Seiya UYEDA,
Takesi YUKUTAKE and Eiko NAKAGAWA,

Earthquake Research Institute.

(Read Nov. 26, 1957.—Received Dec. 28, 1957.)

Summary

The writers carried out simultaneous observations of three geomagnetic components at four stations situated in the central part of Japan. With the aid of magnetograms sent from five other magnetic observatories distributed all over Japan, analyses of various phases of a magnetic storm that occurred on March 10, 1957 are made. It is found that all the components change regularly throughout all the stations in the case of the main phase in spite of anomalous behaviour of vertical component at central Japan in the cases of *SC* and bay, so that it is presumed that the particular distribution of electrical conductivity which seems to play an important role for short-period variations is nearly transparent for slower variations such as *Dst*.

1. Introduction

The writers have been investigating the anomalous behaviour of short-period geomagnetic variations in Japan and their findings have been published in a series of papers in this bulletin[1),2)] and elsewhere[3),4)]. Although it had been clarified that the anomalously large amplitudes of the vertical component of geomagnetic variations are observed only at stations situated in the central part of Japan and that this anomaly

---

1) T. RIKITAKE, I. YOKOYAMA and Y. HISHIYAMA, *Bull. Earthq. Res. Inst.*, **30** (1952), 207; **31** (1953), 19, 89, 101 and 119.

2) T. RIKITAKE and I. YOKOYAMA, *Bull. Earthq. Res. Inst.*, **33** (1955), 297.

3) T. RIKITAKE and I. YOKOYAMA, *Journ. Geomagn. Geoeletr.*, **5** (1953), 59.

4) T. RIKITAKE and I. YOKOYAMA, *Naturwissenschaften*, **41** (1954), 420.

originates from inside the earth, more detailed observations have been required in order to see the real cause of this rather extraordinary phenomenon.

In February and March, 1957, the writers had an opportunity to test the magnetic variometers which were constructed for observations in the Antarctica by the Japanese Antarctic Research Expedition. At the same time, magnetograms from three magnetic stations belonging to the Earthquake Research Institute were also available. Furthermore, copies of magnetograms were kindly supplied at the writers' request from five more observatories distributed all over Japan.

With these magnetograms, the writers were able to conduct fairly detailed analyses with respect to various phases of a magnetic storm that occurred on March 10, 1957. It is intended to bring out differences between the distribution for respective phases such as *SC*, polar storm and *Dst*, because there is a possibility of inferring the depth of the peculiar distribution of induced electric currents by analysing variations of different duration.

2. Magnetic stations, instruments and data

Since last year, variometers of three geomanetic components have been working at the Komoro Branch Station of the Earthquake Research Institute near Mt. Asama, while those at Aburatsubo and Maze are also at work as usual. The magnetometer room at Komoro is shown in Fig. 1.

One of the writers (T. R.), who has been appointed chief of the section of geomgnetism, Special Committee for Antarctic Observation, Science Council of Japan, designed a magnetograph (*RMM* magnetograph), specially constructed so as to make observations easy even at very low temperatures. Although the *D*(declination), *H*(horizontal intensity) and *Z*(vertical intensity) magnetometers are of the usual type, all adjustable screws are made bigger than those of usual magnetometers. The clamping devices of the magnets are also specially designed so as to be able to be handled with gloved fingers. The suspending wire of the *MK* magnets of the *D* and *H* magnetometers are quartz fibres of respectively 10 and 50 *microns* in diameter for ordinary use. A sensibility of a few *gammas* per *mm* is easily attained in the case of *H* magnetometer with a 2*m* optical lever. The *MK* magnet of the *Z* magnetometer is horizontally suspended with a fine quartz fibre as usual. With a 1*m* optical lever, a sensibility of a few *gammas* per *mm* is normally adopted. The sensibilities of the three magnetometers can be checked by the Helmholtz coils attached. These magnetometers are set on a frame work together with the recorder and lamp houses as can be seen in Fig. 2. The general arrangement is also shown in Fig. 3.

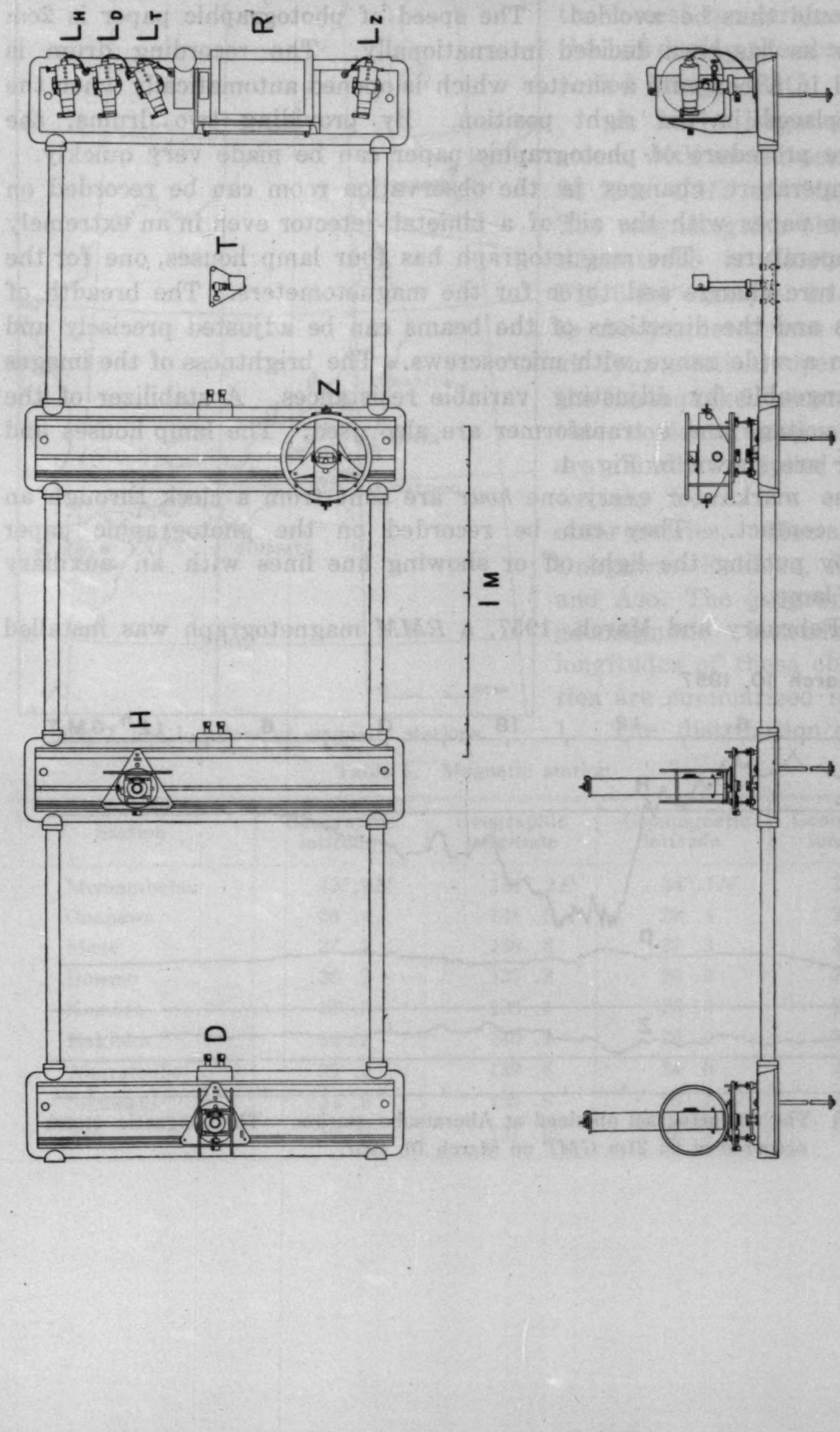

Fig. 3 The plan and elevation of RMM magnetograph. D: declination-, H: horizontal intensity- and Z: vertical intensity variometers. T: temperature change detector, R: recorder, L_H, L_D, L_T and L_Z: lamp houses.

The beams reflected from the mirrors attached to the magnets and fix-mirrors are focussed on photographic paper wound on a rotating drum which is driven by clock work. No spring is used in the clock work, its driving force being provided by a falling weight hung on a nylon string. Possible influences of very low temperatures on the clock work would thus be avoided. The speed of photographic paper is 2*cm* per *hour* as has been decided internationally. The recording drum is mounted in a box with a shutter which is opened automatically when the box is placed in the right position. By providing two drums, the exchange procedure of photographic paper can be made very quickly.

Temperature changes in the observation room can be recorded on the same paper with the aid of a bimetal detector even in an extremely low temperature. The magnetograph has four lamp houses, one for the temperature change and three for the magnetometers. The breadth of the slits and the directions of the beams can be adjusted precisely and easily in a wide range with microscrews. The brightness of the images are changeable by adjusting variable resistances. A stabilizer of the electric voltage and a transformer are also used. The lamp houses and recorder are shown in Fig. 4.

Time marks for every one *hour* are sent from a clock through an electric contact. They can be recorded on the photographic paper either by putting the light off or showing fine lines with an auxiliary electric lamp.

In February and March, 1957, a *RMM* magnetograph was installed

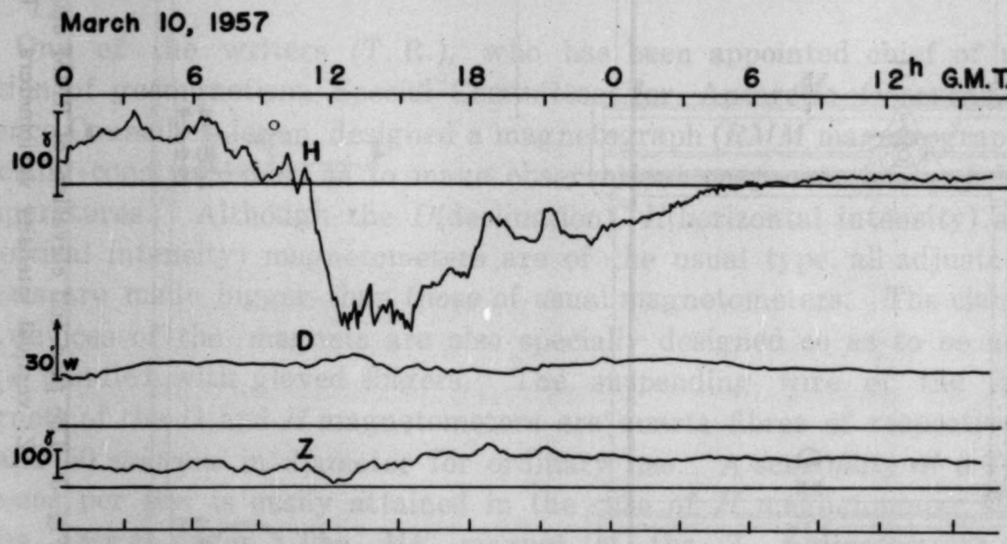

Fig. 6 The magnetogram obtained at Aburatsubo station. The magnetic storm occurred at 0*h* 21*m* *GMT* on March 10, 1957.

in a small hut at Hosono on the foot of Mt. Shirouma, Nagano Prefecture, where we usually have a lot of snow during the winter. The observation hut is shown in Fig. 5. It was proved that the magnetograph works satisfactorily in low temperatures, the lowest temperature inside the hut during the observation period being $-8°C$.

A fairly large magnetic storm with an *SC* occurred at 0*h* 21*m* *GMT* on March 10. The magnetogram obtained at Aburatsubo is illustrated in Fig. 6 for example. In addition to the magnetograms obtained at four stations operated by the Earthquake Research Institute, copies of magnetograms are kindly supplied to the writers from five magnetic observatories, Memambetsu, Onagawa, Kakioka, Simosato and Aso. The geographic and geomagnetic latitudes and longitudes of these observatories are summarized in Table 1. The distribution of these

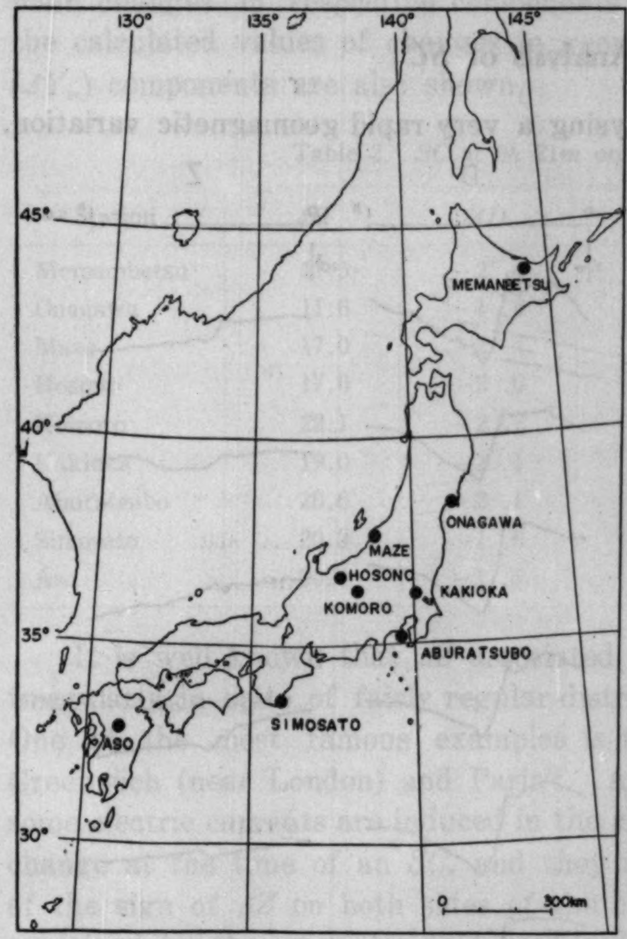

Fig. 7 The locations of magnetic stations.

Table 1. Magnetic station

Station	Geographic latitude	Geographic longitude	Geomagnetic latitude	Geomagnetic longitude
Memambetsu	43°.9*N*	144°.2*E*	34°.1*N*	208°.3*E*
Onagawa	38 .4	141 .5	28 .4	206 .7
Maze	37 .7	138 .8	27 .3	204 .5
Hosono	36 .7	137 .8	26 .2	203 .8
Komoro	36 .3	138 .4	26 .0	204 .4
Kakioka	36 .2	140 .2	26 .0	206 .0
Aburatsubo	35 .2	139 .6	24 .0	205 .6
Simosato	33 .6	135 .9	23 .1	202 .3
Aso	32 .9	131 .0	22 .1	198 .1

stations can be seen in Fig. 7. It may be said that we had fairly many stations in the central part of Japan, though it is regrettable that we could not have any observation on islands in the south sea.

3. Analysis of *SC*

With the intention of analysing a very rapid geomagnetic variation,

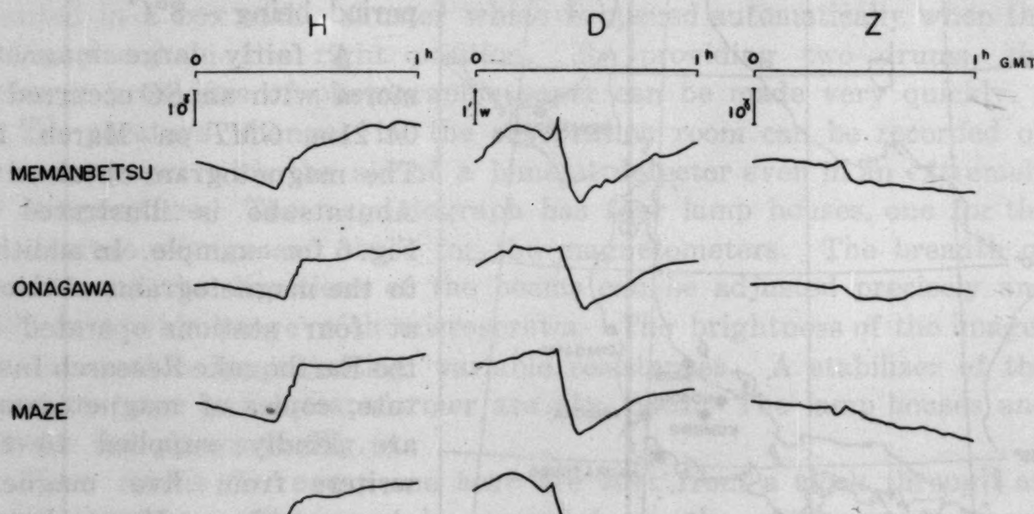

Fig. 8 The changes in the three geomagnetic components at the time of the *SC* on March 10, 1957.

the *SC* with which the magnetic storm begins is studied. The changes in the three geomagnetic components ΔH, ΔD, and ΔZ from $0h$ to $1h$ *GMT* are reproduced in Fig. 8 for respective stations. The amounts of main changes in respective components are given in Table 2 in which the calculated values of changes in geomagnetic north (ΔX_m) and east (ΔY_m) components are also shown.

Table 2. *SC* at $0h$ $21m$ on March 10, 1957.

Station	ΔH	ΔD	ΔZ	ΔX_m	ΔY_m
Memambetsu	11.5γ	$-2'.4$	1.5γ	15.9γ	-15.2γ
Onagawa	11.6	$-1\ .8$	1.0	14.9	-12.0
Maze	17.0	$-2\ .4$	-2.0	21.3	-16.3
Hosono	17.0	$-2\ .0$	-5.2	20.4	-13.4
Komoro	22.1	$-2\ .2$	-1.5	25.8	-13.9
Kakioka	19.0	$-2\ .1$	8.0	22.5	-13.9
Aburatsubo	20.6	$-2\ .1$	10.5	24.3	-13.9
Simosato	20.3	$-1\ .6$	15.0	22.7	-10.5
Aso	20.4	$-1\ .5$	7.0	23.5	-10.0

It is well known that ΔZ associated with an *SC* is distributed very irregularly in spite of fairly regular distribution of horizontal component. One of the most famous examples is the opposition of sign of ΔZ at Greenwich (near London) and Paris[5]. As measured by N. F. Barber[6], some electric currents are induced in the English Channel by geomagnetic change at the time of an *SC*, and they are so intense that the reversal of the sign of ΔZ on both sides of the channel may be approximately explained by the magnetic field produced by these currents. Hence, it is apparent that the distribution of *SC* is affected by irregular distribution of land and sea. However, we sometimes observe that the signs of ΔZ of *SC* differ from one another at relatively near observatories on land areas. H. Wiese[7] has demonstrated some examples in Europe. He has shown a few examples in which it can be seen that ΔZ is negative at Niemegk, Istanbul-Kandilli, Surlai and Helwan, positive at Rude Skov, Abinger, Ebro and very small at Chambon-la-Forêt, Witteveen, Fürstenfeldbruck and Wingst. It is likely that the distribution is closely related to the underground high conducting zone which is

---

5) S. CHAPMAN and J. BARTELS, *Geomagnetism*. Oxford (1940), 297.

6) N. F. BARBER, *M.N.R.A.S. Geophys. Suppl.*, **5** (1948), 258.

7) H. WIESE, *Meteorol. Hydrol. Diens'. DDR Abh. Geomag. Inst. Obs. Potsdam-Niemegk* **No. 18** (1956).

supposed to exist beneath North Germany as has been thoroughly studied by geomagnetic bays7),8),9), though the mode of distribution seems a little different for *SC's* and bays.

The behaviour of *SC* in Japan has been examined in one of the previous papers1). It has been pointed out by the writers that ΔZ at Kakioka is usually positive and large, while that at Wakkanai, the northern extremity of Japan, is always negative. Since, however, we had not as many stations as at this time, no detailed distribution over Japan could be obtained.

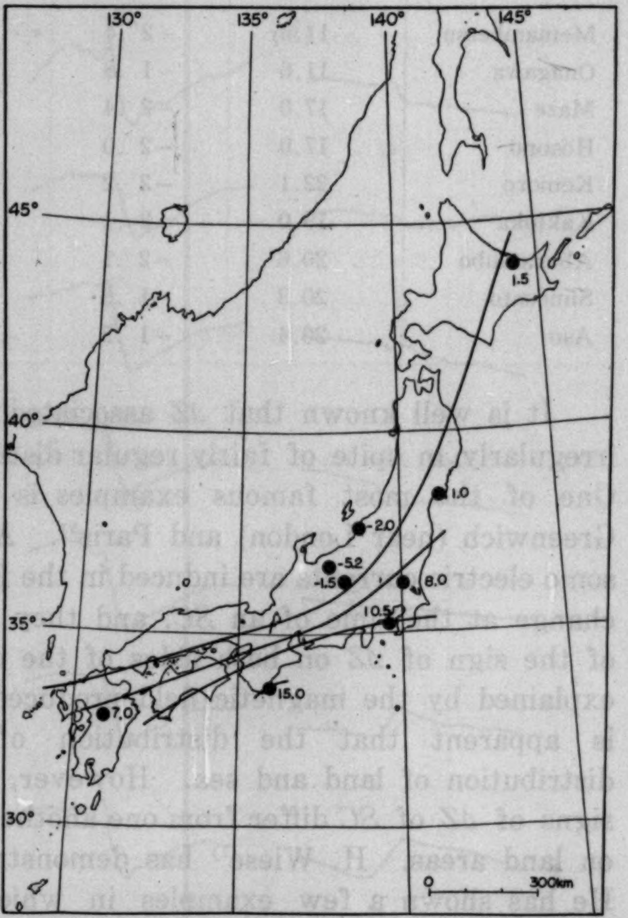

Fig. 9 The distribution of ΔZ of the main pulse of the *SC*. (Unit: *gammas*)

ΔZ, that has been given in Table 2, is shown on a map as can be seen in Fig. 9. It is interesting that we observe large positive ΔZ at Kakioka, Aburatsubo, Simosato and Aso, while the signs are reversed at Maze, Hosono and Komoro.

Taking into consideration the fact that the distance between Komoro and Aburatsubo or Kakioka amounts to only 170 *km*, it is striking that ΔZ shows such a great gradient. It is also interesting that the area in which we observe large positive ΔZ is slightly narrower than that for bays. But detailed comparisons between the distributions for different variations will be made later.

Since it has been approximately proved by the writers in their previous paper that the part of *SC* which originates from outside the earth has nothing particular, this sort of anomalous distribution is certainly caused by the electric currents induced in the earth beneath Japan where we naturally expect

---

8) U. FLEISCHER, *Naturwissenschaften*, **41** (1954), 114.
9) H. WIESE, *Zeits. f. Meteorol.*, **8** (1954), 77.

a complicated distribution of the electrical conductivity. Even in a uniformly conducting earth, the theory of electromagnetic induction shows that some changes of internal origin should come out in connection with changes in the external magnetic fields. In order to detect the changes purely due to the anomalous distribution of electrical conductivity under Japan, the general part of ΔZ which is caused by the electric currents induced in the earth of which the conductivity is determined as an average for the whole earth should be eliminated. But no accurate analysis of *SC* has been made yet because of local irregularities. The writers' previous analysis of the *SC* on June 18, 1936 suggests that mean ΔZ is nearly zero. This would be due to the fact that, as far as the conductivity takes non-zero value, no matter how small it is, the induced currents at the very beginning will flow on the earth's surface so as to cancel the normal component of the inducing field applied suddenly from outside, while the rate of decay of the induced currents necessarily depends on the conductivity. At any rate, the proportion of the general field which originates from inside the earth would be very small for a rapid variation such as *SC*, so that the anomalous distribution of ΔZ obtained above can be approximately regarded as the one produced by the electric currents induced in the earth having some particular conditions. As has been emphasized in one of the previous papers²⁾, the influence of the Pacific Ocean would not be of the type which accounts for the occurrence of such a distribution.

4. Analysis of polar magnetic storm

At about 18*h* and 21*h* on March 10, two marked changes were observed. Being superposed on the recovery phase of the storm, they are likely to be polar magnetic storms, the origin of such changes being overhead electric current systems similar to that of a bay. As has been studied in the 4 th report, the anomaly of ΔZ in Japan can be seen most clearly in the cases of polar magnetic storms and bays so that it would add something to the previous knowledge of the anomalous behaviour of geomagnetic variations to study the changes in detail with so many stations as this time.

In order to pick up only the polar magnetic storm, the influence of *Dst* should be eliminated. For that purpose, the writers made running averages by averaging 13 readings of every 10 *minutes* for all the components. After subtracting the averages from the original values,

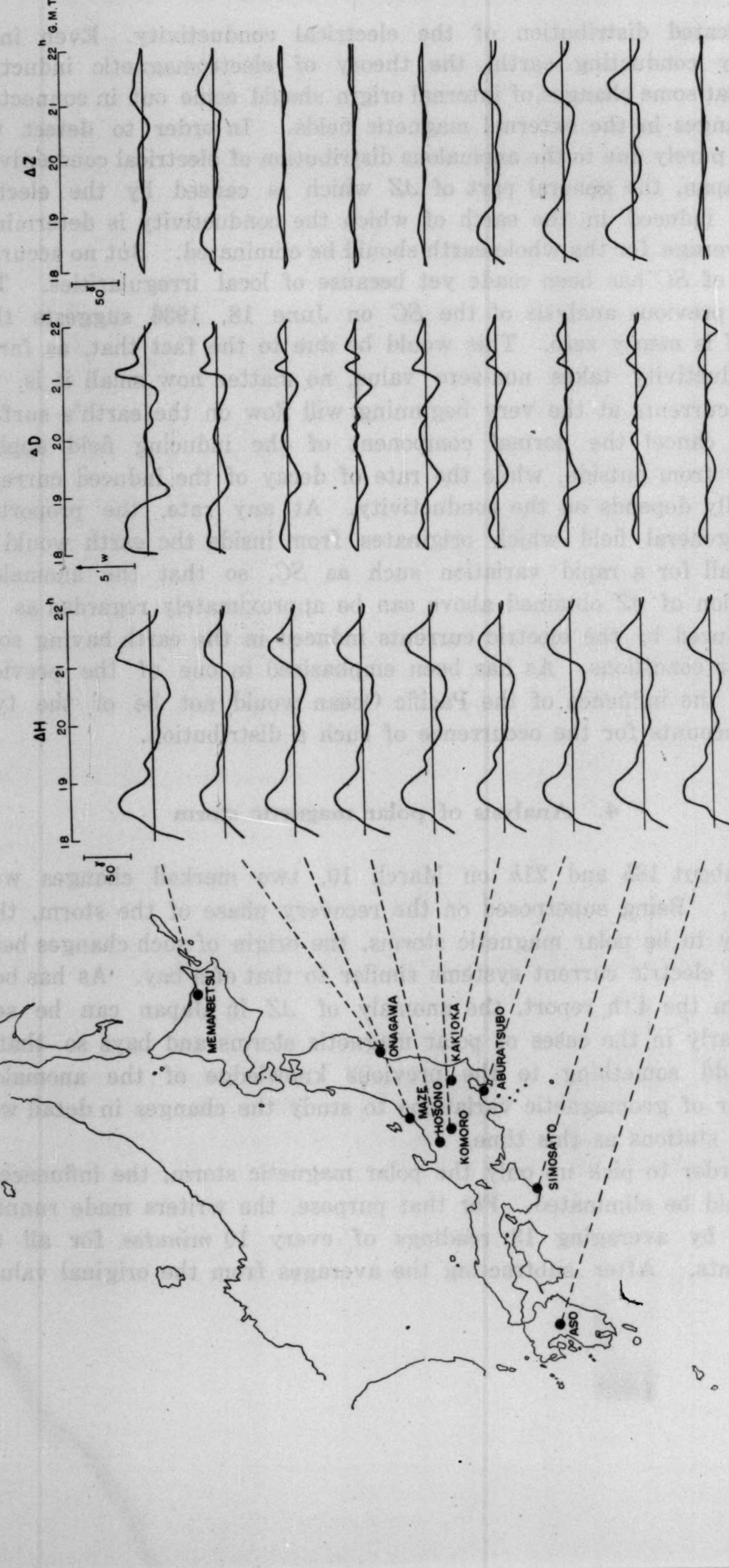

Fig. 10 The changes in the three geomagnetic components at the time of the successive polar magnetic storms on March 10, the locations of the magnetic stations being also shown.

we obtain ΔH, ΔD and ΔZ which are approximately free from the influence of long period variations. In Fig. 10, ΔH, ΔD and ΔZ during the period from $18h$ to $22h$ are graphically shown for the various stations. Looking at these curves, it is noticeable that ΔH and ΔD run quite regularly. We observe, however, a marked tendency for ΔZ to be extraordinarily large in the central part of Japan, the anomalous area seeming likely to extend along the main island with a roughly elliptical shape. At stations in the area, the shape of ΔZ-curve is nearly the same as that of ΔH-curve. It is again striking that ΔZ-curves at Komoro and Aburatsubo, the distance between these two stations amounting only 170 *km*, differ so much from one another.

The values of ΔZ at the stations situated in the central part of Japan are plotted against the latitude for epochs of every 10 *minutes* as can be seen in Fig. 11. It is noticeable that the line passing the points corresponding to Aburatsubo, Komoro and Hosono is always parallel to that connecting Kakioka with Maze. As we can see in Fig. 7, the direction of the Aburatsubo-Komoro-Hosono line is nearly parallel to that of the Kakioka-Maze line, so that we see that the fact shown in Fig. 11 suggests that the gradient of ΔZ is approximately directed to the direction of the two lines. The direction is roughly $N\,45°\,W$ and perpendicular to the general trend of Japan Islands.

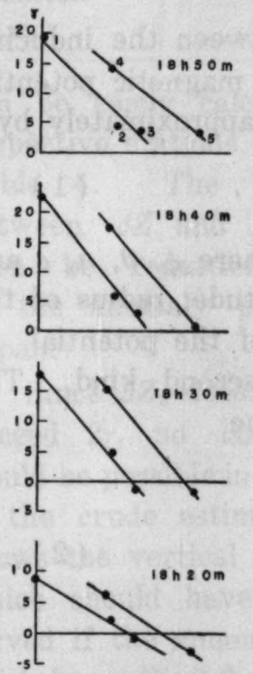

Fig. 11 The distribution of ΔZ at epochs of every 10 *minutes* for the magnetic stations situated in the central part of Japan. 1: Aburatsubo, 2: Komoro, 3: Hosono, 4: Kakioka, 5: Maze.

In order to see the geographic distribution of the anomaly, the values at $18h$ $40m$, when the polar magnetic storm reached its maximum, are selected and given in Table 3 in which ΔX_m and ΔY_m are also obtained from ΔH and ΔD.

The internal part of ΔZ thus deduced will consist of two parts, one caused by the anomalous conditions underneath Japan and the other produced by the induced currents flowing in the high conducting part of the earth below a depth a few hundred *kilometers*.

We call the latter the normal internal part, the nature of which has been examined by a number of authors.[10),11),12),13)] Strictly speaking, these two parts should electro-

---

10) A. SCHUSTER, *Phil. Trans. Roy. Soc. London A*, **208** (1908), 163.

Table 3. Polar magnetic storm at 18*h* 40*m* on March 10, 1957.

Station	ΔH	ΔD	ΔZ	ΔX_m	ΔY_m
Memambetsu	35.5γ	−1′.5	4.1γ	37.3γ	−2.5γ
Onagawa	22.9	−0 .9	14.4	23.0	−2.3
Maze	29.5	−0 .4	0.8	29.4	3.7
Hosono	31.1	−0 .2	2.9	30.7	5.6
Komoro	32.8	−0 .5	4.8	32.9	3.2
Kakioka	26.1	−0 .5	17.5	26.4	1.6
Aburatsubo	30.1	−0 .1	22.4	29.4	6.1
Simosato	30.4	−0 .3	25.3	30.3	3.3
Aso	29.5	−0 .1	5.8	29.2	4.5

magnetically couple with one another, but the coupling may be neglected for the first appoximation.

As to the normal internal part, the relation between the inducing and induced fields has been well known. Meanwhile, magnetic potential of polar magnetic storms or bays may be expressed approximately by

$$\Delta W=a\left\{\left(\frac{r}{a}\right)e+\left(\frac{r}{a}\right)^{-2}i\right\}\sin\phi\, Q_1^1(\cos\theta)\,, \tag{1}$$

as far as low and middle latitudes are concerned, where ϕ, θ, a, e and i denote respectively geomagnetic longitude, co-latitude, radius of the earth, external and internal parts of the coefficient of the potential. Q_1^1 denotes the associated Legendre function of the second kind. The components of the magnetic field at $r=a$ then become

$$\left.\begin{aligned}\Delta X_m&=(e+i)\ \sin\phi\,\frac{dQ_1^1}{d\theta}\,,\\ \Delta Y_m&=-(e+i)\ \cos\phi\,\frac{Q_1^1}{\sin\theta}\,,\\ \Delta Z&=(e-2i)\ \sin\phi\, Q_1^1\,.\end{aligned}\right\} \tag{2}$$

If the electrical conductivity that has been hitherto obtained[14] is adopted, the relation between e and i is given by

$$i=0.415\,e\,. \tag{3}$$

Although it is not possible to obtain e and i from data obtained

---

11) S. CHAPMAN, *Phil. Trans. Roy. Soc. London A*, **218** (1919), 1.

12) S. CHAPMAN and A. T. PRICE, *Phil. Trans. Roy. Soc. London A*, **229** (1930), 427.

13) B. N. LAHIRI and A. T. PRICE, *Phil. Trans. Roy. Soc. London A*, **237** (1939), 509.

14) T. RIKITAKE, *Bull. Earthq. Res. Inst.*, **28** (1950), 45, 219 and 263; **29** (1951), 61 and 539.

Table 4.

Station	ΔZ_n	$\delta Z = \Delta Z - \Delta Z_n$
Memambetsu	-2.1γ	6.2γ
Onagawa	-1.8	16.2
Maze	-1.7	2.5
Hosono	-1.6	4.5
Komoro	-1.6	6.4
Kakioka	-1.6	19.1
Aburatsubo	-1.5	23.9
Simosato	-1.4	26.7
Aso	-1.4	7.1

only in a restricted area of the earth's surface, we may estimate $e+i$ from ΔX_m in Table 3 by assuming that ΔX_m is of the type given by (2) and that the influence of the anomaly is not so large for horizontal components. Actually, no marked differences such as found in ΔZ are observed in the case of ΔH. If the assumption is taken for granted, $e+i$ can be obtained by least square method, hence, by taking into account (3), e and i of the normal part can be calculated. With these, $e-2i$ and consequently ΔZ_n (subscript n means normal part) can be easily calculated for respective stations as given in Table 4. The differences between ΔZ and ΔZ_n would then be regarded as due to the anomaly peculiar to Japan.

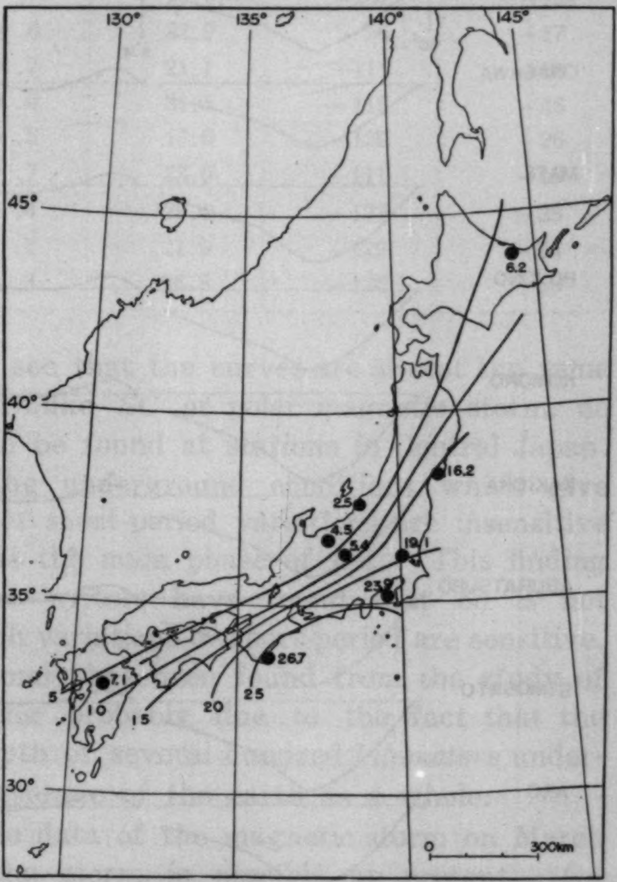

Fig. 12 The distribution of δZ for the polar magnetic storm. (Unit: *gammas*)

Since ΔZ_n does not much exceed 2γ, no large errors would be possible in δZ in spite of the crude estimate. ΔZ_n shows the vertical component which should have been observed if the anomaly did not exist, hence the influence of the anomalous field is so large that we actually observe variations of reversed sign all over Japan as well as extraordinarily large amplitude in the central part. The distribution of δZ is shown on a map in Fig. 12 which should be compared with Fig. 2

of the 6 th report. We see that the anomalous area extends roughly elliptically covering Kii, Izu and Boso peninsulas, its southern boundary being still unknown. We may also compare Fig. 12 to Fig. 9, similar chart for the *SC*, whence it is observed that the area is slightly larger in this case and its centre is likely to be shifted a little to *NE*.

5. Analysis of main phase of *Dst*

It is of much interest to see whether or not geomagnetic variations of a different period show the same tendency as those which have been described in the previous two sections. Since we know daily variation on quiet days (*Sq*) behaves quite differently as has been discussed by

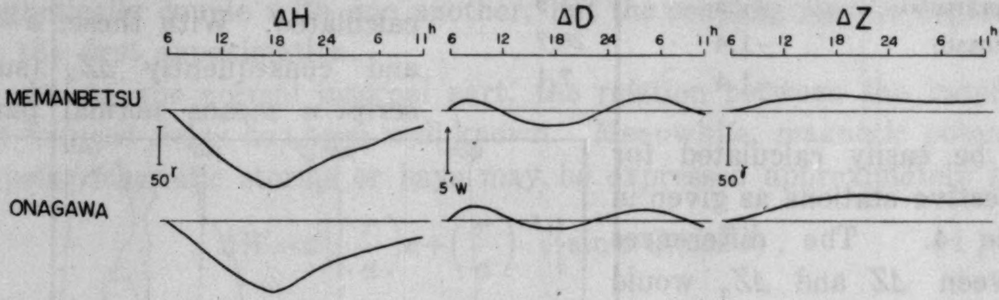

Fig. 13 The running average of the main phase of *Dst* for respective stations.

the writers[15)], it is highly desirable to conduct an analysis of much slower variations with respect to geomagnetic data from well-distributed observatories in Japan. In order to carry out such a study, the writers would here like to analyse the main phase of *Dst* of the magnetic storm.

Short-period variations are eliminated by taking running averages every one *hour*. The averages of 13 readings are made and shown in Fig. 13 for each station.

The values at 18*h* are tentatively assumed as those of the initial state, so that these curves in Fig. 13 express the departures from the initial values. All the elements at the maximum stage of the main phase are given in Table 5.

Table 5. *Dst* at 18*h* on March 10, 1957.

Station	ΔH	ΔD	ΔZ	ΔX_m	ΔY_m
Memambetsu	−107γ	1′.7	21.6γ	−107γ	−15γ
Onagawa	−97	0 .8	32.9	−96	−17
Maze	−112	0 .7	21.1	−111	−20
Hosono	−118	0 .0	31.3	−115	−26
Komoro	−131	0 .3	17.0	−129	−26
Kakioka	−112	0 .7	23.0	−111	−19
Aburatsubo	−129	0 .4	26.4	−127	−25
Simosato	−131	0 .1	21.5	−129	−24
Aso	−128	0 .3	26.8	−126	−19

At a glance of Fig. 13, we see that the curves are almost the same throughout all the stations. Unlike *SC* or polar magnetic storm, no anomalous distribution of ΔZ can be found at stations in Central Japan. The fact would suggest that the underground conditions which give rise to the anomalous behaviour of short-period variations are insensitive to much slower variation such as the main phase of *Dst*. This finding is of great interest because the writers have found that *Sq* is not affected by the conditions to which variations of short period are sensitive. However, another sort of anomaly has been found from the study of *Sq* in Japan, the anomaly being probably due to the fact that the electrical conductivity at the depth of several hundred *kilometers* underneath Japan is lower than the average of the earth as a whole.

Since we have no world-wide data of the magnetic storm on March 10, no complete analysis of the storm is possible at present. On

---

15) T. RIKITAKE, I. YOKOYAMA and S. SATO, *Bull. Earthq. Res. Inst.*, **34** (1956), 198.

assuming some nature of *Dst*, however, separation of the internal part of the magnetic potential from the external one will be effected in the following. It has been well known that the magnetic potential of *Dst* can be expressed fairly well by

$$\Delta W = a\{(r/a)e + (r/a)^{-2}i\} P_1(\cos\theta)\,, \tag{4}$$

where all the notations have the same meaning as those related to (1). It follows that

$$\left.\begin{aligned} \Delta X_m &= -(e+i)\sin\theta\,, \\ \Delta Z &= (e-2i)\cos\theta\,. \end{aligned}\right\} \tag{5}$$

Under the assumption that ΔX_m and ΔZ which are given in Table 5 can be used for the determination of e and i, we make use of least square methods from which we obtain

$$e+i=131\gamma,\ e-2i=55\gamma\,,$$

and then

$$e=105\gamma\,,\ i=25\gamma,\ e/i=4.2\,.$$

Meanwhile, the ratio e/i of *Dst* at the maximum stage of the main phase has been obtained to be 3 or thereabout from analyses of world-wide data[12),16)]. It is of interest that the internal part is considerably small when the coefficients are determined from observations in Japan only. The fact would suggest that the electrical state at a depth of several hundred *kilometers* underneath Japan is likely to differ from what we have obtained for the mean state of the earth. Under Japan, it may be presumed that either the conductivity below a depth of a few hundred *kilometers* is smaller than the mean value of the earth as a whole or the depth of the non-conducting layer is larger than that for the mean earth. Although it is difficult to determine which conclusion is more likely, the results seem to agree very well with that deduced from the study[15)] on *Sq* in Japan.

6. Discussion

From the analyses of *SC*, polar magnetic storm and main phase of *Dst* of the magnetic storm that occurred on March 10, 1957, we have seen that the anomalies of ΔZ for rapid variations differ greatly from those for much slower variations. Since it has been well known that, in the case of an earth having a conductivity-distribution of spherical

---

16) T. RIKITAKE and S. SATO, *Bull. Earthq. Res. Inst.*, **35** (1957), 7.

symmetry, the longer the period of a geomagnetic variation is, the deeper the induced currents penetrate into the earth, the different behaviours between these variations, rapid and slow, would give some clue to the investigation of the cause of the anomaly concerned.

In one of the previous papers[1)], it has been pointed out that there will be two kinds of local characteristics for geomagnetic variations of short period, one sensitive to *SC's* but not to bays or polar magnetic storms as can be found at British observatories, and the other sensitive to both variations. Although the anomaly in Japan is found to be of the latter type, it has been made clear that the detailed features of both the variations do not agree with one another. On comparing Fig. 9 with Fig. 12, we see that the area in which ΔZ of *SC* is anomalously large becomes wider and its centre is shifted to the *NE* direction in the case of polar storm. It has been also reported that the mode of distribution of ΔZ which is found in North Germany shows some differences for *SC's* and bays, the difference being likely to be of a similar character to that of Japan. If the anomaly is supposed to be caused by some particular distribution of electrical conductivity, we see that the response of this distribution is different when the inducing fields have different periods though some more observations would be necessary for clarifying the characteristics of the response.

As to the details of the underground distribution of electrical conductivity, nothing definite can be said yet. A roughly circular or elliptical circuit which has been imagined in the previous papers still seems to be the best model by which we can understand the peculiar behaviour of short-period geomagnetic variations in Japan. Let us imagine a circular circuit of a circular wire. The self-inductance of the circuit is given by

$$L=4\pi A\left(\log_e \frac{A}{\rho}+0.33\right),$$

where A and ρ are the radius of the circuit and the wire respectively. If a voltage E is applied to the circuit, the electric current I is described by

$$L\frac{dI}{dt}+RI=E,$$

where R denotes the resistance of the circuit. In the case of an alternating voltage of which the angular frequency is ω, therefore, the phase difference ψ between E and I is given as

$$\psi=\tan^{-1}(\omega L/R)\ .$$

Suppose that the underground circuit consists of the passage of electric currents, the radius of the section of which is assumed as 10*km*, L for $A=100$ and 1000*km* become respectively 5.5×10^{9} and 5.5×10^{11} *cm*. If we take the electrical conductivity of the material, of which the passage is composed to be 10^{-12}*e.m.u.* (that is the conductivity below the depth of 400 *km* for the normal part of the earth), R is obtained as 2.0×10^{9} and 2.0×10^{11}*e.m.u.* respectively. Furthermore, the period of the alternating current is taken as 1 *hour*. In that case, $\omega L/R$ is estimated at 0.0041 and 0.041 respectively for $A=100$ and 1000 *km*, so that there is practically no phase difference between the applied voltage and electric current in the circuit. The fact that we observe no phase difference between ΔH and ΔZ in the anomalous area may thus be understandable provided we suppose the existence of such a circuit whose radius has been thought to amount roughly to several hundred *kilometers*.

In the case of the main phase of *Dst*, it is of much interest that we do not observe any anomaly which seems to be related to the circuit supposed here. This is just the case for *Sq* as has been examined by the writers in the previous paper[15]. It is then presumed that the supposed circuit has nothing or very little to do with such slower variations as *Dst* and *Sq*. We may naturally speculate that the electric currents induced by these geomagnetic variations flow in deeper parts of the earth, so that no appreciable amount of electric currents is induced in the circuit which is supposed to exist at a depth of less than a few hundred *kilometers*. However, another sort of anomaly should be considered in relation to *Sq* and *Dst*. Although it is difficult to carry out an exact analysis, it is likely that, underneath Japan, the electrical conductivity below a depth of a few hundred *kilometers* is considerably lower than the usual value, which has been obtained for the mean state of the earth. It is not possible to determine the accurate boundaries of this region. However, one of the writers (T. R.)[17] has speculated that this sort of condition would have an important bearing on the formation of an orogenetic zone.

7. Concluding remarks

The analyses of various phases of the magnetic storm that occurred on March 10, 1957, are described in this report. On the basis of data from four magnetic stations belonging to the Earthquake Research Institute together with those from five other magnetic observatories in Japan, analyses that are more detailed than those hitherto conducted are made with respect to the *SC* and polar magnetic storm. Although the present analyses serve only to confirm the local characteristics of short-period geomagnetic variations which have been so far known, the northern boundary of the area in which we observe anomalously large ΔZ is well located by magnetograms from Komoro and Hosono which are newly added. As for the origin or cause of the anomaly, the previous idea that presumes circular or elliptical electrical circuit would still be the best explanation.

---

[17] T. RIKITAKE, *Bull. Earthq. Res. Inst.*, **34** (1956), 291.

The analysis of the main phase of *Dst* results in a notable finding that no anomaly such as found in the cases of short-period variations is associated, the result being agreed with the analysis of the *Sq* in Japan. We therefore presume that the hypothetical underground circuit of induced electric currents has no or very little effect on slower variations such as *Sq* and *Dst*. Meanwhile, anomaly of another kind is likely to exist in the earth's mantle as deep as several hundred *kilometers* beneath Japan. The relation between the external and internal parts of *Dst* as well as of *Sq* suggests that either the conductivity is low or the non-conducting outer layer is penetrating the mantle.

On summarizing all the results of the analyses of geomagnetic variations, it may be said that the electrical condition underneath Japan differs very much from the mean state of the earth which has been studied from the standpoint of the theory of electromagnetic induction. A crude picture, though very incomplete, of the conductivity distribution is speculated on as follows. Beneath Japan, the conductivity at a depth of several hundred *kilometers* seems likely to be very low, probably something of the order of 10^{-15}*e.m.u.* in contrast to 10^{-12}*e.m.u.* for the averaged value for the whole earth. The boundaries of the low conducting region are not known. Above the low conducting part, there would be a high conducting passage of electric currents. It is supposed that both the ends of the circuit are connected with the high conducting region extending outside the said low conducting part of the mantle in order to account for strong electric currents flowing in the circuit. Although no accurate estimate of the dimension of the circuit is possible, there seems no objection to assuming that the width of the roughly elliptical circuit amounts to more than a few hundred *kilometers*.

The bearing of the extraordinary distribution of the electrical conductivity on geophysical or geological problems is not known. However, as has been once speculated by one of the writers (T. R.), it would be possible to suppose that seismicity or volcanism might be correlated to the special condition beneath Japan.

In conclusion, the writers express cordial thanks to all the members of the Branch Stations of the Earthquake Research Institute who carried out magnetic observations. Their hearty thanks are also due to the members of Memambetsu, Onagawa, Kakioka, Simosato and Aso Magnetic Observatories. A part of this study has been made with the financial aid of a Research Grant from the Ministry of Education, for which the writers would like to extend their thanks to the Ministry.

---

1. 日本に於ける地磁気短周期変化の異常と地下構造（第7報）

地震研究所
力武常次
横山泉
上田誠也
行武毅
中川英子

南極地域観測用 *RMM* 磁力計の冬季テストをかねて，長野県細野，小諸，新潟県間瀬および神奈川県油壺に於て，地磁気3成分同時観測を行つた．この結果に女満別，女川，柿岡，下里および阿蘇観測所の観測結果を加えて，1957 年3月 10～11 日の磁気嵐の各相について解析を行つた．磁気嵐の急始，極磁気嵐等については従来とほぼ同様な結果を得たが，主相については，短周期変化を起す地下構造の影響を受けないことをたしかめ，また内部磁場が地球の平均状態の場合にくらべて小さいことを見出した．

これらの結果および *Sq* の解析結果にもとづいて，日本地下の電気的状態を推測した．

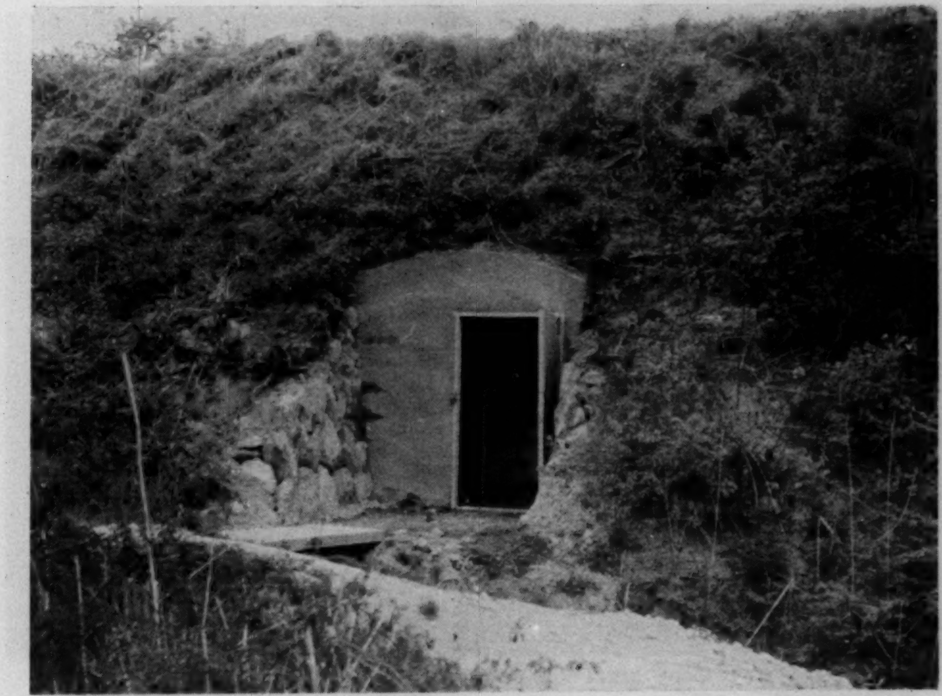

Fig. 1. The entrance of the magnetometer-room at Komoro Station.

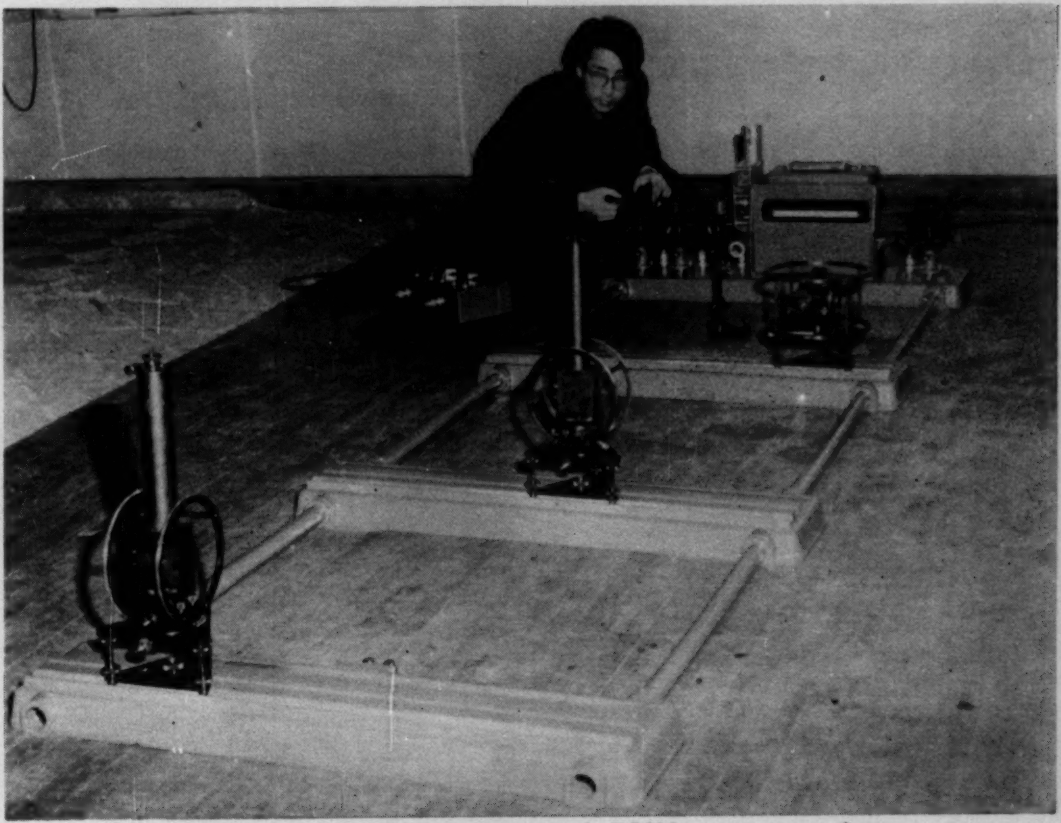

Fig. 2. General arrangement of *RMM* magnetograph.

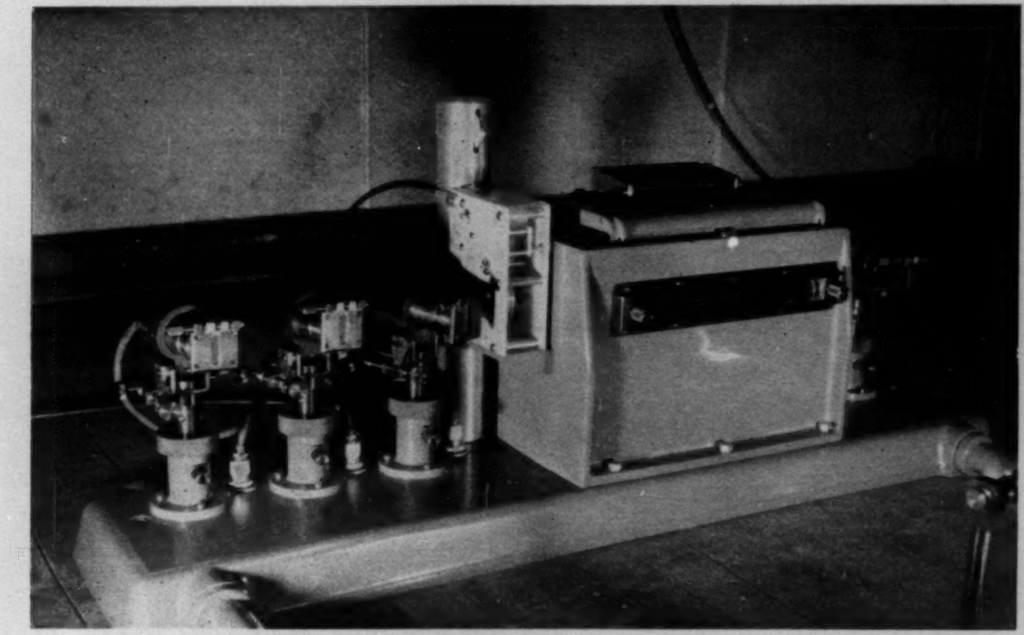

Fig. 4. The recorder and lamp houses.

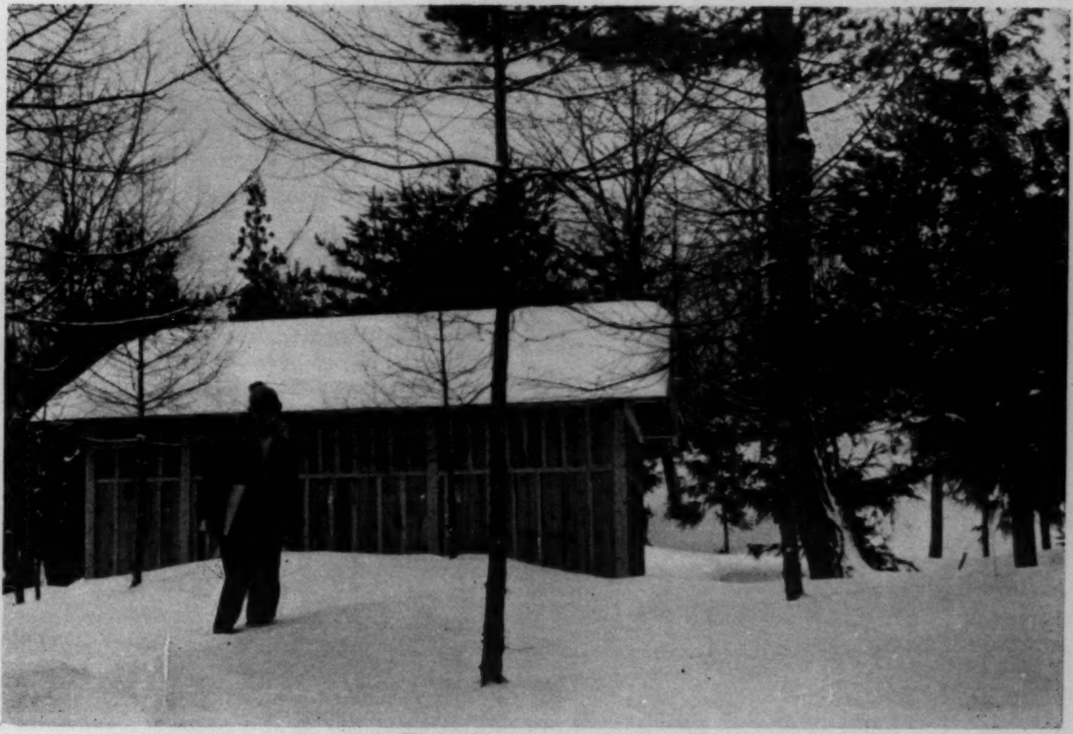

Fig. 5. The observation hut at Hosono.

**Bulletin of the Earthquake
Research Institute**
Vol. 36 (1958), pp. 21-53

2. *The Nature of Seismic Origins as Inferred from Seismological and Geodetic Observations* (2).*

By Keichi KASAHARA,

Earthquake Research Institute.

(Read November 26, 1957.—Received December 28, 1957.)

CONTENTS.

Page
Chapter V. Wave Generation from a Fault Plane 22
1. Introduction 22
2. Production of a fault plane and elastic waves caused by it 23
3. Spectrum and azimuthal effect of the model 30

Chapter VI. Fault Movement as a Possible Model of Earthquake Origins.... 34
1. Introduction 34
2. Proposed model of the Tango earthquake 35
3. Rapidity of fault production in the crust 40
4. Remarks on further application of the model to the other cases 43

Chapter VII. Strain Accumulation in the Crust 44
1. Introduction 44
2. Mechanism of strain accumulation in the crust 45
3. Strain accumulation in the visco-elastic crust 46
4. Continuous observations of crustal deformation associated with strain accumulation in the crust 47

Concluding Summary 48
Acknowledgements 52

---

*) Continued from p. 532 of the Bulletin of the Earthquake Research Institute, vol. 35 (1957).

Chapter V.

Wave Generation from a Fault Plane.

1. Introduction.

Most papers on wave generation have dealt with seismic origins which are assumed to be a spherical surface. It can not be denied that they achieved remarkable successes in interpreting some aspects of natural earthquakes, such as the azimuthal distribution of P- and S-waves, the relation between the magnitude and the period of seismic waves, and so on. Judging from the good agreement between the theory and the observational results, we may suppose that the model of spherical origins is plausible so far as we are concerned with the seismometrical aspects of earthquake phenomena.

We can not but feel, however, some hesitation in accepting that the actual shape of a seismic origin is always spherical. This feeling comes into effect particularly when we deal with the cases of destructive earthquakes which are accompanied by crustal deformations. As S. Homma pointed out, the most predominant characteristics of crustal deformations observed after the North-Izu earthquake could hardly be interpreted from the above-mentioned standpoint(82), and furthermore, it seems unnatural to accept the existence of fracture taking place on a spherical surface in the crust.

It was so many years ago when seismologists entertained the opinion that rapid occurrence of faulting might be the immediate cause of great earthquakes. A remarkable development has been made, since then, to find out clear proof of this supposition and we are now confident, to a certain extent, in concluding that many earthquakes take place in consequence of fault-like events in the earth. It should be mentiond, however, that such a conclusion is mainly on the basis of the "fault-plane solution" derived from push-pull distribution of the initial waves,(83) whereas no enough check has been made yet with respect to the other aspects of earthquakes.

Discussion in the previous chapter(84) has enabled us to estimate the most probable conditions of the Gômura fault and others, by which we can explain the geodetic aspects of the earthquakes concerned. Sup-

---

82) S. HOMMA, *loc. cit.*, 64).

83) *f.i.* P. BYERLY, *Geol. Soc. Amer., Special Paper* 62 (1955), 762.
J. H. HODGSON, *Bull. Geol. Soc. Amer.*, **68** (1957), 611.

84) see Chapter IV.

pose we could explain, at the same time, the seismological aspects by taking the conditions as inferred previously, we would be more confident in accepting the proposed model as reasonable. In the present chapter, therefore, we shall study what mode of characteristics is to be derived from the model of fault movement.

2. Production of a fault plane and elastic waves caused by it.

The mechanism of fracture production is of so complicated a nature that we can not get a complete solution for it even in the simplest case. The actual process of fault production in the earth would be quite a difficult problem to deal with theoretically. So that we have to take a simple model of it to develop the following discussion. We suppose that a homogeneous medium is initially subject to uniform shear stress which results in a single fracture plane of finite length, at a certain moment. The fracture plane being free from the initial stress, approximately, we may replace it by the apparent negative stress working along all the extent of the plane so as to cancel the initial stress. According to the analyses made in the last chapter, the depth of the Gômura fault, for instance, is estimated as about one half of its length, but the complete treatment of such a condition would be so difficult to solve that we are obliged to assume that the fault is infinitely deep. For the sake of simplicity, we also ignore the influence of the free surface, so that the problem is reduced to two-dimensional one.

It is convenient for us to study the problem with respect to the elliptic coordinates (ξ,η), taking the eccentric distance $2c$ equal to the length of the fault (Fig. 45). Wave equations in the present system are written as follows.

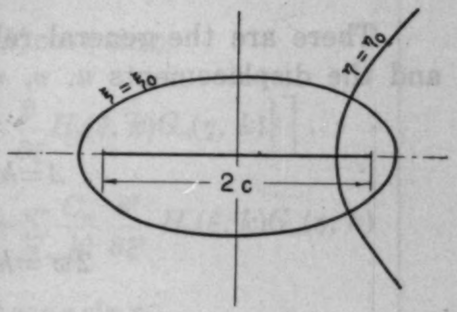

Fig. 45. Elliptic coordinates.

$$\left.\begin{aligned}\rho\frac{\partial^2\varDelta}{\partial t^2}&=\frac{\lambda+2\mu}{c^2(\cosh^2\xi-\cos^2\eta)}\left(\frac{\partial^2\varDelta}{\partial\xi^2}+\frac{\partial^2\varDelta}{\partial\eta^2}\right),\\ \rho\frac{\partial^2\varpi}{\partial t^2}&=\frac{\mu}{c^2(\cosh^2\xi-\cos^2\eta)}\left(\frac{\partial^2\varpi}{\partial\xi^2}+\frac{\partial^2\varpi}{\partial\eta^2}\right),\end{aligned}\right\}\quad(76)$$

where, λ, μ and ρ denote Lamé's constants and the density of the medium, respectively, while $\varDelta$ and ϖ are the dilatational and the distortional components of strain.

According to K. Sezawa,[85] the general expression of solutions for (76) is,

$$\left.\begin{aligned} \Delta &= \sum_n B_n H_n(\xi, h) G_n(\eta, h) e^{ipt} , \\ 2\varpi &= \sum_n C_n H_n(\xi, k) G_n(\eta, k) e^{ipt} , \end{aligned}\right\} \tag{77}$$

where,

$$h^2 = \frac{\rho}{\lambda + 2\mu} p^2 , \quad k^2 = \frac{\rho}{\mu} p^2 , \tag{78}$$

and, $H_n(\xi, h)$, $G_n(\eta, h)$, $H_n(\xi, k)$ and $G_n(\eta, k)$ are the functions as derived from the following relations.

$$\left.\begin{aligned} &\frac{\partial^2}{\partial \xi^2} H_n(\xi, h) + \left(\frac{h^2 c^2}{2} \cosh 2\xi - a_n\right) H_n(\xi, h) = 0 , \\ &\frac{\partial^2}{\partial \xi^2} H_n(\xi, k) + \left(\frac{k^2 c^2}{2} \cosh 2\xi - a_n'\right) H_n(\xi, k) = 0 , \\ &\frac{\partial^2}{\partial \eta^2} G_n(\eta, h) - \left(\frac{h^2 c^2}{2} \cos 2\eta - a_n\right) G_n(\eta, h) = 0 , \\ &\frac{\partial^2}{\partial \eta^2} G_n(\eta, k) - \left(\frac{k^2 c^2}{2} \cos 2\eta - a_n'\right) G_n(\eta, k) = 0 . \end{aligned}\right\} \tag{79}$$

There are the general relations between the strain components Δ, ϖ and the displacements u, v, *viz.*,

$$\left.\begin{aligned} \Delta &= h_1^2 \left\{ \frac{\partial}{\partial \xi}\left(\frac{u}{h_1}\right) + \frac{\partial}{\partial \eta}\left(\frac{v}{h_1}\right) \right\} , \\ 2\varpi &= h_1^2 \left\{ \frac{\partial}{\partial \xi}\left(\frac{v}{h_1}\right) - \frac{\partial}{\partial \eta}\left(\frac{u}{h_1}\right) \right\} , \end{aligned}\right\} \tag{80}$$

where, u, and v denote the displacements in the ξ- and η-directions, respectively, and

$$1/h_1^2 = c^2(\cosh^2 \xi - \cos^2 \eta) . \tag{81}$$

With the aid of (77) and (80), we get,

---

[85] K. SEZAWA, *Bull. Earthq. Res. Inst.*, **5** (1928), 59.

$$\left.\begin{aligned}
u_1&=-\sum_n\frac{h_1B_n}{h^2}\frac{\partial}{\partial\xi}H_n(\xi,h)G_n(\eta,h)e^{ipt}\\
v_1&=-\sum_n\frac{h_1B_n}{h^2}\,H_n(\xi,h)\frac{\partial}{\partial\eta}G_n(\eta,h)e^{ipt}\,,\\
u_2&=\sum_n\frac{h_1C_n}{k^2}\,H_n(\xi,k)\frac{\partial}{\partial\eta}G_n(\eta,k)e^{ipt}\,,\\
v_2&=-\sum_n\frac{h_1C_n}{k^2}\frac{\partial}{\partial\xi}H_n(\xi,k)G_n(\eta,k)e^{ipt}\,,
\end{aligned}\right\}\tag{82}$$

in which, u and v with the suffix 1 contribute to the dilatational wave, whereas those with the suffix 2, to the distortional one.

The stress-strain relations in the elliptic coordinates are given as,

$$\left.\begin{aligned}
\widehat{\xi\xi}&=\lambda\Delta+2\mu\left[h_1\frac{\partial}{\partial\xi}(u_1+u_2)+h_1^2(v_1+v_2)\frac{\partial}{\partial\eta}\left(\frac{1}{h_1}\right)\right],\\
\widehat{\xi\eta}&=\mu\left[\frac{\partial}{\partial\xi}h_1(v_1+v_2)+\frac{\partial}{\partial\eta}h_1(u_1+u_2)\right].
\end{aligned}\right\}\tag{83}$$

Hence we get the following relations.

$$\left.\begin{aligned}
\widehat{\xi\xi}=&\lambda\sum_n B_nH_n(\xi,h)G_n(\eta,h)+2\mu\Bigg[h_1\frac{\partial}{\partial\xi}h_1\Bigg\{-\sum_n\frac{B_n}{h^2}\frac{\partial}{\partial\xi}H_n(\xi,h)G_n(\eta,h)\\
&+\sum_n\frac{C_n}{k^2}H_n(\xi,k)\frac{\partial}{\partial\eta}G_n(\eta,k)\Bigg\}+h_1^2\Bigg\{-\sum_n\frac{B_n}{h^2}\frac{\partial^2}{\partial\xi^2}H_n(\xi,h)G_n(\eta,h)\\
&+\sum_n\frac{C_n}{k^2}\frac{\partial}{\partial\xi}H_n(\xi,k)\frac{\partial}{\partial\eta}G_n(\eta,k)\Bigg\}-2c^2h_1^4\cos\eta\sin\eta\\
&\times\Bigg\{\sum_n\frac{B_n}{h^2}H_n(\xi,h)\frac{\partial}{\partial\eta}G_n(\eta,h)+\sum_n\frac{C_n}{k^2}\frac{\partial}{\partial\xi}H_n(\xi,k)G_n(\eta,k)\Bigg\}\Bigg],\\
\widehat{\xi\eta}=&\mu\Bigg[-h_1^2\Bigg\{\sum_n\frac{2B_n}{h^2}\frac{\partial}{\partial\xi}H_n(\xi,h)\frac{\partial}{\partial\eta}G_n(\eta,h)+\sum_n\frac{C_n}{k^2}\frac{\partial^2}{\partial\xi^2}H_n(\xi,k)G_n(\eta,k)\\
&-\sum_n\frac{C_n}{k^2}H_n(\xi,k)\frac{\partial^2}{\partial\eta^2}G_n(\eta,k)\Bigg\}-2c^2h_1^4\cos\eta\sin\eta\\
&\times\Bigg\{\sum_n\frac{B_n}{h^2}\frac{\partial}{\partial\xi}H_n(\xi,h)G_n(\eta,h)-\sum_n\frac{C_n}{k^2}H_n(\xi,k)\frac{\partial}{\partial\eta}G_n(\eta,k)\Bigg\}\Bigg].
\end{aligned}\right\}\tag{84}$$

These equations give the boundary conditions along an elliptic-cylindrical surface ($\xi=\xi_0$).

It is convenient for the following study to deal with the boundary conditions on the plane lying between the foci of the (ξ, η) coordinates, so that we have to reduce (84) to the case of $\xi_0=0$. When ξ_0 approaches 0 asymptotic relations are known such as,

$$\left.\begin{aligned} &H_n(\xi, h)\to 1,\ \frac{\partial}{\partial\xi}H_n(\xi, h)\to -i\sqrt{2q-a_n}\ ,\\ &H_n(\xi, k)\to 1,\ \frac{\partial}{\partial\xi}H_n(\xi, k)\to -i\sqrt{2q'-a'_n}\ . \end{aligned}\right\} \tag{85}$$

Assuming that $\lambda=\mu$, we get the following relations[86].

$$\left.\begin{aligned} (\widehat{\xi\xi})_{\xi_0=0}=\mu\Big[&\sum_n B_nG_n+\frac{2}{\sin^2\eta}\Big\{-\sum_n\gamma\alpha_n^2B_nG_n+\sum_n\gamma'\alpha'_nC_n\frac{\partial}{\partial\eta}G'_n\Big\}\\ &-\frac{2\cos\eta}{\sin^3\eta}\Big\{\sum_n\gamma B_n\frac{\partial}{\partial\eta}G_n+\sum_n\gamma'\alpha'_nC_nG'_n\Big\}\Big]\ ,\\ (\widehat{\xi\eta})_{\xi_0=0}=\mu\Big[&\frac{1}{\sin^2\eta}\Big\{-\sum_n 2\gamma\alpha_nB_n\frac{\partial}{\partial\eta}G_n-\sum_n\gamma'\alpha_n'^2C_nC'_n+\sum_n\gamma'C_n\ \frac{\partial^2}{\partial\eta^2}G'_n\Big\}\\ &+\frac{2\cos\eta}{\sin^3\eta}\Big\{\sum_n\gamma\alpha_nB_nG_n-\sum_n\gamma'C_n\ \frac{\partial}{\partial\eta}G'_n\Big\}\Big]\ , \end{aligned}\right\} \tag{86}$$

where,

$$\left.\begin{aligned} &\alpha_n=-i\sqrt{2q-a_n}\ ,\quad \alpha'_n=-i\sqrt{2q'-a'_n}\\ &\gamma=\frac{1}{4q}\ ,\quad \gamma'=\frac{1}{4q'}\ ,\\ &q=\frac{h^2p^2}{4}\ ,\quad q'=\frac{k^2p^2}{4}\ , \end{aligned}\right\}$$

G_n and G'_n in (86) are used in place of $G_n(\eta,h)$ and $G_n(\eta, k)$, respectively, and the term e^{ipt} is neglected from the expressions for the sake of simplicity.

We now consider that the system is subject to the initial stress in the following way (*cf.* Fig. 46).

$$-\widehat{xy}=\widehat{yx}=S,\quad \widehat{xx}=\widehat{yy}=0\ . \tag{87}$$

There is a relation between the (x, y) coordinates and the (ξ, η) ones, *viz.*,

$$\left.\begin{aligned} x&=c\cosh\xi\cos\eta\\ y&=c\sinh\xi\sin\eta \end{aligned}\right\} \tag{88}$$

With the aid of it, the stress condition of (87) can be transformed into the following equation.

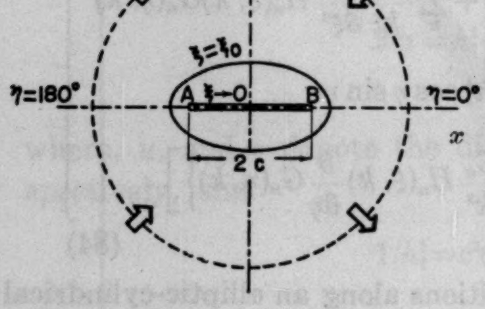

Fig. 46. Type of the initial stress.

$$\left.\begin{aligned}\widehat{\xi\xi}&=\frac{S}{2}\,\frac{\sinh^2\xi\sin 2\eta}{\cosh^2\xi-\cos^2\eta}\,,\\ \widehat{\xi\eta}&=S\,\frac{\cosh^2\xi\cos 2\eta-\cos^2\eta}{\cosh^2\xi-\cos^2\eta}\,.\end{aligned}\right\}\tag{89}$$

When ξ approaches infinity, we get,

$$\widehat{\xi\xi}\to S\sin 2\eta \text{ and } \widehat{\xi\eta}\to S\cos 2\eta\,. \tag{90}$$

This expression is identical with the condition (87) transformed into the polar coordinates. On the contrary, when $\xi=0$,

$$\begin{aligned}\widehat{\xi\xi}&=0\,,\\ \widehat{\xi\eta}&=S\,.\end{aligned}\tag{91}$$

We know, therefore, that the condition of the plane surface AB being suddenly free from the initial stress can be replaced by the additional stress working there in the negative sense, *viz.*,

$$(\widehat{\xi\xi})_{\xi=0}=0,\ \ (\widehat{\xi\eta})_{\xi=0}=-S\cdot f(t)\,, \tag{92}$$

where, $f(t)$ is a time-function of stress change which is to be written, in the case of the step-like change, as follows,

$$f(t)=\int_{-\infty}^{\infty}\frac{1}{\omega}e^{i\omega t}d\omega\,. \tag{93}$$

This means that, once we get the solution for the case of the periodic stress change, we can easily obtain the solution for the case of (93). So that the following calculation of this section will be made for the periodic case.

Meanwhile, (79) shows that $G_n(\eta, h)$ and $G_n(\eta, k)$ are reduced to Mathieu functions, $\mathrm{ce}_n(\eta, q)$ and $\mathrm{se}_n(\eta, q')$, the characteristic numbers of which are a_n and a_n', respectively. The characteristic numbers are expanded into power series of q, or q' in the following way.[87)]

$$\left.\begin{aligned}a_n&=n^2+x_1q+x_2q^2+x_3q^3+x_4q^4+\cdots\,,\\ a_n'&=n^2+y_1q'+y_2q'^2+y_3q'^3+y_4q'^4+\cdots\,,\end{aligned}\right\}\tag{94}$$

where, x_n and y_n are the constants which depends on n. When q and q' are very small, or in the case of the wave-length being far longer than the fracture, we might put $a_n=n^2$, $a_n'=n^2$, as Inouye assumed[88)]; however, the following discussion being concerned with the case of

---

86) W. INOUYE, *Bull. Earthq. Res. Inst.*, **15** (1937), 674.

87) N. W. MCLACHLAN, *Theory and Application of Mathieu Functions*, (1947) p. 10.

88) W. INOUYE, *loc. cit.*, 86).

shorter wave-length, we can not always make this simplification. From the physical consideration we know that the dilatational component is odd with respect to η, whereas the distortional is even. We may also infer that Mathieu functions of odd degree have nothing to do with the boundary conditions, so that we can replace $G_n(\eta, h)$ with $se_2(\eta, q)$, $se_4(\eta, q)$, $se_6(\eta, q)$, $\cdots$, and $G_n(\eta, k)$, with $ce_0(\eta, q'), ce_2(\eta, q')$, $ce_4(\eta, q')$, $ce_6(\eta, q')$, $\cdots$.

The next step of the study is to determine the constants B_2, B_4, B_6, $\cdots$, C_0, C_2, C_4, C_6, $\cdots$ so as to let them satisfy the boundary conditions given by (92). Eq. (86) being composed of infinite series $ce_n(\eta, q')$ and $se_n(\eta, q)$, it would be impossible to get complete solution numerically, so that we neglect the effect coming from those terms of higher than 4th degree. (92) is reduced, then, into the following expression, that is,

$$\left.\begin{aligned}&\text{normal stress } (\widehat{\xi\xi})_{\xi_0-0}=l_1B_2+l_2B_4+l_3B_0+l_4C_2+l_5C_4\,,\\&\text{tangential stress } (\widehat{\xi\eta})_{\xi_0-0}=m_1B_2+m_2B_4+m_3C_0+m_4C_2+m_5C_4\,,\end{aligned}\right\}\quad(95)$$

where,

$$\left.\begin{aligned}
l_1&=\left\{\left(\frac{1}{\gamma'}\sin^3\eta-6\alpha_2^2\sin\eta\right)se_2(\eta, q)-6\cos\eta\frac{\partial}{\partial\eta}se_2(\eta, q)\right\}F\,,\\
l_2&=\left\{\left(\frac{1}{\gamma'}\sin^3\eta-6\alpha_4^2\sin\eta\right)se_4(\eta, q)-6\cos\eta\frac{\partial}{\partial\eta}se_4(\eta, q)\right\}F\,,\\
l_3&=2\alpha_0'\left\{\sin\eta\frac{\partial}{\partial\eta}ce_0(\eta, q')-\cos\eta\; ce_0(\eta, q')\right\}F\,,\\
l_4&=2\alpha_2'\left\{\sin\eta\frac{\partial}{\partial\eta}ce_2(\eta, q')-\cos\eta\; ce_2(\eta, q')\right\}F\,,\\
l_5&=2\alpha_4'\left\{\sin\eta\frac{\partial}{\partial\eta}ce_4(\eta, q')-\cos\eta\; ce_4(\eta, q')\right\}F\,,\\
m_1&=6\alpha_2\left\{\cos\eta\, se_2(\eta, q)-\sin\eta\frac{\partial}{\partial\eta}se_2(\eta, q)\right\}F\,,\\
m_2&=6\alpha_4\left\{\cos\eta\, se_4(\eta, q)-\sin\eta\frac{\partial}{\partial\eta}se_4(\eta, q)\right\}F\,,\\
m_3&=-\left\{\sin\eta\,\alpha_0'^2ce_0(\eta, q')-\sin\eta\frac{\partial^2}{\partial\eta^2}ce_0(\eta, q')+2\cos\eta\frac{\partial}{\partial\eta}ce_0(\eta, q')\right\}F\,,\\
m_4&=-\left\{\sin\eta\,\alpha_2'^2ce_2(\eta, q')-\sin\eta\frac{\partial^2}{\partial\eta^2}ce_2(\eta, q')+2\cos\eta\frac{\partial}{\partial\eta}ce_2(\eta, q')\right\}F\,,\\
m_5&=-\left\{\sin\eta\,\alpha_4'^2ce_4(\eta, q')-\sin\eta\frac{\partial^2}{\partial\eta_2}ce_4(\eta, q')+2\cos\eta\frac{\partial}{\partial\eta}ce_4(\eta, q')\right\}F\,,
\end{aligned}\right\}$$

$$\text{and} \qquad F=\frac{\gamma'}{\sin^3\eta}\,. \qquad \Bigg\} \tag{96}$$

Suppose we find out a set of the constants (B_2, B_4, C_0, C_2, C_4) which fits most suitably the stress conditions (92) at many points along the fault, it would be accepted as the solution for the problem. In practice, we apply (92) to the points of $\eta=15, 30, 45, 60, 75, 90°, \cdots (\xi=0)$ and determine the most probable values of the constants by means of the least square method. The conditions at the points of $\eta=0°$ and $180°$ are not used, because the factor F in (96) becomes infinitely large at those points. This tendency corresponds to the physical condition that the stress at the extremities of a fracture is infinitely large.

Since the constants would be complex numbers, in general, we have to deal with a set of simultaneous equations in order to determine the real and the imaginary parts of these five constants. The normal equation is given, therefore, in the following way,

$$\left.\begin{array}{l}
d_{00}b_2+d_{01}b_4+d_{02}c_0+d_{03}c_2+d_{04}c_4+d_{05}b'_2+d_{06}b'_4+d_{07}c'_0+d_{08}c'_2+d_{09}c'_4=S_0\ , \\
d_{10}b_2+d_{11}b_4+d_{12}c^0+d_{13}c_2+d_{14}c_4+d_{15}b'_2+d_{16}b'_4+d_{17}c'_0+d_{18}c'_2+d_{19}c'_4=S_1\ , \\
d_{20}b_2+d_{21}b_4+d_{22}c_0+\cdot\cdot\cdot\cdot\cdot\cdot\cdot\cdot\cdot\cdot\cdot\cdot\cdot\cdot\cdot\cdot\cdot \\
\cdot\cdot\cdot\cdot\cdot\cdot\cdot\cdot\cdot\cdot\cdot\cdot\cdot\cdot\cdot\cdot\cdot\cdot\cdot\cdot\cdot\cdot\cdot\cdot\cdot \\
d_{90}b_2+d_{91}b_4+d_{92}c_2+d_{93}c_2+d_{94}c_4+d_{95}b'_2+d_{96}b'_4+d_{97}c'_0+d_{98}c'_2+d_{99}c'_4=S_9\ ,
\end{array}\right\} \tag{97}$$

where $B_n=b_n+ib'_n$ and $C_n=c_n+ic'_n$.

We apply the relaxation method to (97) in order to obtain the approximate solution. In the case of $q'=2.000$, for instance, the constants are determined as follows (unit : $S/4\mu$),

$$\left.\begin{array}{rl}
B_2= & 0.092+0.049i \\
B_4= & 0.005+0.001i \\
C_0= & 0.268-0.051i \\
C_2= & -0.244-0.087i \\
C_4= & -0.033+0.003i\ .
\end{array}\right\}$$

These values have been derived, of course, from an approximated treatment of (95), so that some check would be necessary in order to see their accuracies. We substitute them into the right-hand side of (92) again and calculate $(\xi\xi)_{\xi=0}$ and $(\widehat{\xi\eta})_{\xi=0}$. If the result of numericial calculation is enough accurate, $(\widehat{\xi\xi})_{\xi=0}$ and the imaginary part of $(\widehat{\xi\eta})_{\xi=0}$ would be infinitely small along the fault, while the real part of $(\widehat{\xi\eta})_{\xi=0}$

would be as large as $-S$. The curves in Fig. 47 looks likely to satisfy the said condition with errors less than ten percents.

In a similar way, we get the solution for the various values of q' as shown in Table X, wherein $\lambda_s/2c$ means the ratio of the wave-length (S-wave) to the length of the fault.

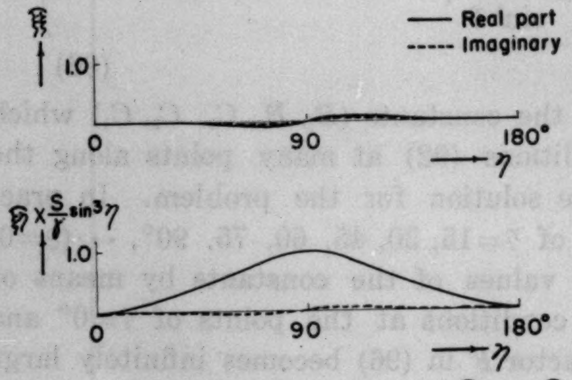

Fig. 47. Real and imaginary parts of $\widehat{\xi\xi}$ and $\widehat{\xi\eta}$.

Table X. Values of B_2, B_4, C_0, C_2 and C_4 given for the various values of $q'\left(\text{unit: } \frac{S}{4\mu}\right)$

q'	$\lambda_s/2c$	B_2	B_4	C_0	C_2	C_4
0.00	∞	0.000	0.000	0.000	0.000	0.000
0.20	3.14	0.025+0.004i	0.000+0.000i	0.037−0.069i	−0.056−0.005i	0.000+0.000i
0.60	2.01	0.054+0.009i	0.000+0.000i	0.088−0.133i	−0.109−0.011i	0.000+0.002i
1.00	1.57	0.083+0.041i	0.000+0.000i	0.216−0.259i	−0.190−0.067i	0.000+0.006i
2.00	1.12	0.092+0.049i	0.005+0.001i	0.268−0.051i	−0.244−0.087i	−0.033+0.003i
3.00	0.94	0.068+0.024i	0.007+0.004i	0.141−0.039i	−0.064−0.144i	−0.049−0.016i

3. Spectrum and azimuthal effect of the model

Substituting those constants determined above into (82), we obtain the displacements at a distant point ($\xi\to\infty$). When ξ is large, there is the asymptotic expression for Mathieu function such as,

$$H_n(\xi, h)\to\frac{e^{-ihc\sinh\xi}}{\sqrt{hc\sinh\xi}}\,,\qquad H_n'(\xi, k)\to\frac{e^{-ikc\sinh\xi}}{\sqrt{kc\sinh\xi}}\,. \tag{98}$$

Putting (96) in (82), we obtain u_1 and v_2 for a distant point, *viz.*,

$$\left.\begin{aligned} u_1&=\sum_n\frac{iB_n}{h_1^{(3/2)}R^{(1/2)}}se_n(\eta, q)e^{i(pt-hR)}\,,\\ v_2&=\sum_n\frac{iC_n}{h_1^{(3/2)}R^{(1/2)}}ce_n(\eta, q')e^{i(1t-kR)}\,,\end{aligned}\right\} \tag{99}$$

where R denotes the distance from the origin. Taking the case for $q'=2.000$ as an example, we show the patterns of azimuthal distribution of u_1 as well as v_2 in Fig. 48, in which we see that the pattern for u_1 (P-wave) is of the quadrant type characterized by two nodal lines, one being parallel to the fracture whereas another, perpendicular to it. As for the pattern for v_2 (S-wave), on the other hand, the maximum amplitude is observed at $\eta=90°$ and $270°$, while the amplitude at $\eta=0°$ and $180°$ are not so large. We therefore see that the pattern differs slightly from that of the quadrant type. Similar pictures for the other cases would be illustrated quite easily by taking account of the results shown in Table X. The phase angles of the disturbances, however, are scattered so widely for different values of q' that it would not be simple to illustrate the characteristics in a general way. Since the main object of this section is to compare the theory with the observed characteristics of seismic waves, we are able to obtain necessary information about them without drawing patterns for all the cases.

Referring to Table X, we know that u_1 at distant points depends mainly on $B_2 se_2(\eta, q)$, which means that P-wave shows a quadrant pattern for all the frequencies except for the cases of very large q'. Since it is not B_4 but B_2 that affects most seriously the amplitude of P-wave at a fixed point, we can approximately infer the spectrum of P-wave (impulsive excitation of the origin) from B_2 plotted as the function of q' (see the broken line in Fig. 49). In the picture we see that

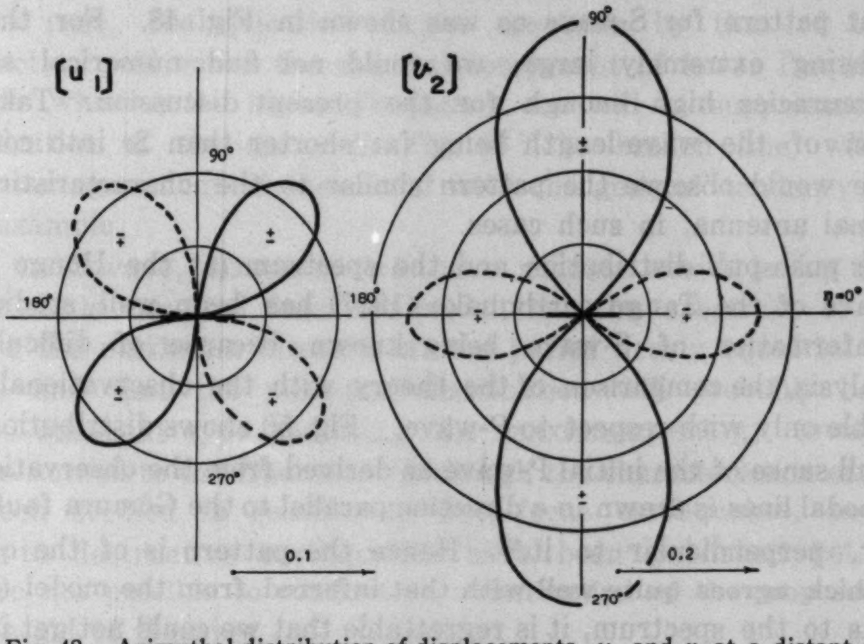

Fig. 48. Azimuthal distribution of displacements, u_1 and v_2 at a distant point caused by periodic excitation of the origin ($q'=2.000$, real part).

B_2 increases from 0 as q' increases and takes the maximum value (the first peak of the spectrum) when q' is about 1∼2. This fact suggests that the spectral intensity of P-wave will take the maximum value for the component whose wave-length is 1.2∼1.5 times as long as the fracture.

On the other hand, the pattern and the spectral structure of S-wave will be more complicated. We would not observe the quadrant type of distribution for all the frequencies, because v_2 is contributed not only by $C_2 ce_2(\eta, q')$ but also by $C_0 ce_0(\eta, q')$, and this condition makes the distribution pattern roughly circular rather than quadrant. Such cases will come into effect when q' is very small, wherein C_0 is larger than C_2 (*cf.* Table *X*) and $ce_0(\eta, q')$ and $ce_2(\eta, q')$ can be regarded approximately as 1 and cos 2η, respectively. The larger q' becomes, the larger value C_2 takes and the cos 2η-component in $ce_0(\eta, q')$ becomes predominant; and so we shall obtain the distorted quadrant pattern for S-wave as was shown in Fig. 48. For the cases of q' being extremely large, we could not find numerical solutions with accuracies high enough for the present discussion. Taking the condition of the wave-length being far shorter than $2c$ into consideration, we would observe the pattern similar to the characteristics of a directional antenna, in such cases.

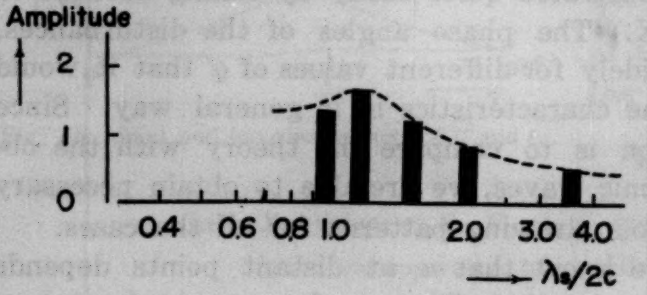

Fig. 49. Amplitude of B_2 plotted against $\lambda/2c$.

The push-pull distribution and the spectrum (at the Hongo station) of P-wave of the Tango earthquake (1927) has been well studied. No such information of S-wave being known because of difficulties on the analysis, the comparison of the theory with the observational results is possible only with respect to P-wave. Fig. 50 shows distribution of the push-pull sense of the initial P-wave as derived from the observation. One of the nodal lines is drawn in a direction parallel to the Gômura fault, while another, perpendicular to it.[89] Hence the pattern is of the quadrant type which agrees quite well with that inferred from the model (*cf.* Fig. 48). As to the spectrum, it is regrettable that we could not get information from many stations because there were few seismographs suitable for recording long-period waves. The only data available for the comparision was that recorded at the Hongo station with the Omori's type pendulum as shown in Fig. 19 (see Part I), in which we see that the maximum intensity occurs at the period of 23 sec. The model concerning the present chapter will result in the characteristic period of 11 sec, provided we take the length of the fault as 30 km and the velocity of S-wave, 3.2 km/sec. This result is based on the assumption that the origin is subject to an impulsive excitation. But a longer period, 20 sec or more say, is to be derived if we assume a step-like excitation. For, the unit step-function is composed of the spectrum as shown in Fig. 22, so that the model will result in a longer characteristic period than that of the impulsive case. Multiplication of the spectrum by that of the unit step-function will make the spectral component of lower frequency remarkable whereas the higher frequency one will be suppressed. Such a modification of the curve in Fig. 48 (the broken line) will result in a better agreement of the model with the general tendency of the actual example.

---

[89] S. KUNITOMI, *Geophys. Mag.*, **2** (1930), 65.

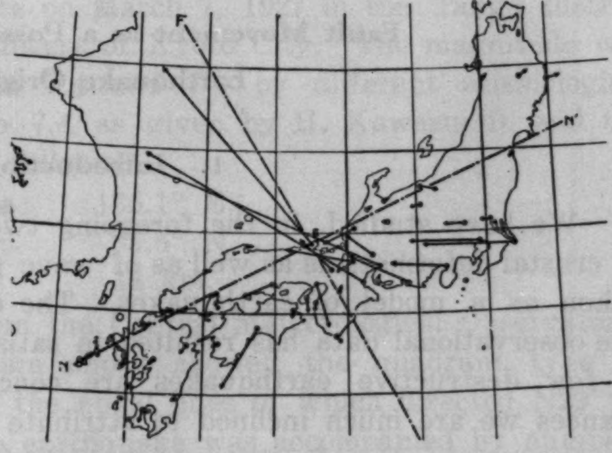

Fig. 50. Azimuthal effect of the push-pull distribution (initial P-wave) as observed in the case of the Tango earthquake (after S. Kunitomi).

As to S-wave, however, we have no data available for the comparison. It is expected from the model that the spectrum of S-wave will give the maximum intensity at the period nearly equal to that of P-wave, and that the push-pull distribution will probably be of the distorted quadrant type radiating the maximum energy towards the direction normal to the fracture. Although the characteristics of S-wave have been studied in relation to deep-focus earthquakes, no papers relating to destructive earthquakes have been published yet. It is therefore not possible to conduct an examination of the proposed model with the aid of S-waves.

Chapter VI.

Fault Movement as a Possible Model of Earthquake Origins.

1. Introduction.

We have studied, in the foregoing two chapters, the characteristics of crustal deformations as well as of wave generation from a fault plane taken as a model of earthquakes. The comparison of the model with the observational data has resulted in satisfactory agreement so long as a few destructive earthquakes are concerned. Under these circumstances we are much inclined to attribute the mechanism of earthquake occurrence to the fault movement taking place in such a way as assumed previously.

The mechanism of earthquake occurrence has been discussed since the beginning of seismology. All through the studies accumulated by now, the idea that earthquakes are likely to be caused by fracture production tends to be widely supported by seismologists. This kind of thinking is based, more or less, on the elastic rebound theory due to Reid ; numbers of papers that have been written along this line served to increase our knowledge concerning mechanism of earthquakes. The writer is much interested in the development of this field of seismology, though he considers, at the same time, that such an important proposal of models should be accepted only after all the necessary examinations are made. That is to say, the fault models that have so far been proposed are on the basis of qualitative discussion of the fact that the push-pull distribution of waves and the direction of the surface movements (if it were observed) seem likely to suggest the fault plane existing as the earthquake origin. In addittion to the points mentioned above, however, there are many kinds of phenomena which can be observed by seismometrical and the geodetic methods, so that we have to examine whether or not the proposed model is consistent with all of them.

Although it is not always possible to have a complete set of such information in all the cases, we still know a few examples which are provided with rich information as have been dealt with in the previous chapters. Since the Tango earthquake is thought to be the best example, we shall discuss it in the following.

2. Proposed model of the Tango earthquake.

The earthquake took place on March 7, 1927 in the Tango district which is located 90 km northwest of Kyoto City. The magnitude was estimated at a value between 7.4 and $7^3/_4$ by different seismologists (the present paper refers to 7.4 as given by H. Kawasumi), and the location of the origin was as follows[90],

longitude :	135.1° E,
latitude :	35.6° N,
depth :	14 km.

According to the report from the Central Meteorological Observatory, the initial P-wave of the main shock showed the quadrant type of push-pull distribution, one of the nodal lines of which directed N29°W, and another, N61°E[91]. The earthquake was accompanied by numbers of aftershocks taking place around the hypocentre of the main shock[92], and it was also accompanied by remarkable crustal deformations along two seismic faults, known as the Gômura and the Yamada fault, respectively. The Gômura fault, which was more remarkable than the latter, started from Kuchi-ôno town and extended to N30°W, crossing the neck of the Tango Peninsula. N. Yamasaki and F. Tada, who worked out a topographical study of the Tango district, stated that the earthquake was nothing but the effect of the blocking movement, which had been repeated in the old dislocated block of the Oku-Tango Peninsula on the west coast of the Bay of Wakasa[93].

It was not possible to trace the Gômura fault to the end, because it extended into the Japan Sea ; judging from the distribution of crustal deformations as well as of aftershocks, however, the said fault is presumed to be some 30 km long, as discussed in Chapter III. Another notable fact was the good coincidence of the fault with one of the nodal lines bounding the push- and pull-sense area of the initial P-wave. This coincidence could not be disregarded as an accidental event but seemed to have essential bearing upon the mechanism of the earthquake[94].

The spectral analysis made in Chapter III indicated that the radius of the origin would be as large as 16 km, apparently. This value being derived from the application of the spherical model, we might imagine such a spherical surface for stress change as shown in Fig. 51 (broken line). We know, of course, that the sphere is a tentative one drawn only to explain the characteristic period and the push-pull distribution of seismic waves, so that it is no longer acceptable when we undertake to account for the other kind of aspects. The stress change taking place on such a spherical surface can hardly be accepted from our common experiences of fracture production in a brittle material, and, furthermore, the model of a spherical origin is less suitable for understanding the most outstanding fact of crustal deformations that indicates remarkable shearing along a nodal line of push-pull distribution[95]. Recalling the results of Chapter III as shown in Figs. 21 and 26, the above-mentioned radius of the origin must bring an essential information about the "dimension" of the earthquake origin, even though we can not accept the model as real one.

---

[90] *Seis. Bull., C.M.O., For 1950*, (1952), 99; S. Kunitomi, *loc. cit.*, 89).

[91] S. Kunitomi, *ditto.*
J. H. Hodgson, *Bull. Seis. Soc. Amer.*, **45** (1955), 37.

[92] N. Nasu, *Bull. Earthq. Res. Inst.*, **13** (1935), 335.

[93] N. Yamasaki and F. Tada, *Bull. Earthq. Res. Inst.*, **4** (1928), 159.

[94] H. Honda, *loc. cit.*, 8).

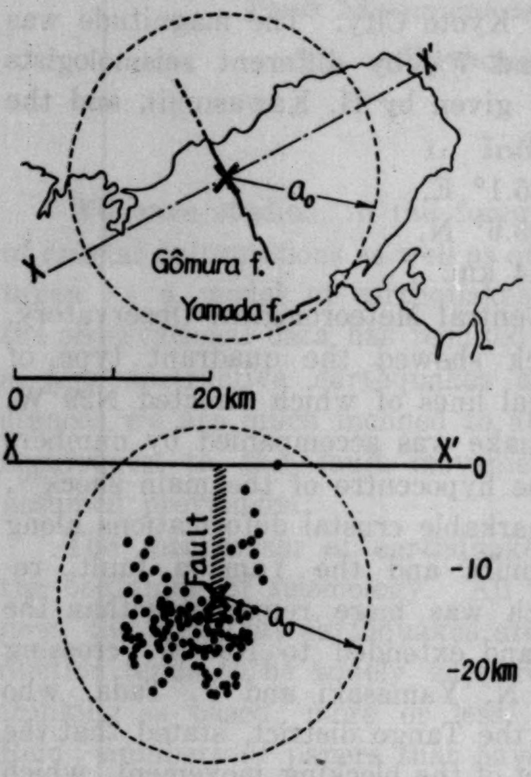

Fig. 51. Schematic view of the origin of the Tango earthquake. —— and ------: seismic faults, ×: hypocentre of the main shock, ●: aftershocks. The sphere (broken lines) refers to the model of spherical origin (*cf.* Chapter III).

The improvement of the model should be made, therefore, in a way not to spoil the advantageous points of the primary model. Under these considerations we shall propose another one to be examined as follows.

The improved model for the Tango earthquake assumes that a considerably large space of the crust has been subject to uniform strain accumulating over a long period. The principal axes lie horizontally with the directions of NW and NE, respectively. When the strain exceeds the ultimate strain of the crust (say 10^{-4}), single fracture takes place abruptly resulting into a fault plane, which is 30 km long, 15 km deep, and of the strike and the dip being N29°W, 90°, respectively[96]. At the moment of fracture production, the initial stress on the said plane (tangential stress only) decreases as large as 3×10^7 c.g.s. giving rise to the seismic waves as well as the crustal deformations around it.

---

[95] S. HOMMA, *loc. cit.*, 64).

Such conditions are shown in the central part of Fig. 52, in which the symbols H, L, θ, φ, and $(X_y)_{x=z=0}$ denote respectively such quantities as given previously. It was hardly possible to get complete solution for the seismological and the geodetic characteristics of the proposed model (we denote it as Model A). So that we have taken more simplified models under the consideration not to disturb the cardinal points of discussion. One of the simplification was realized in Chapter IV by assuming that the fault is infinitely long (Model B). This assumption is considered to bring no serious troubles in treating the

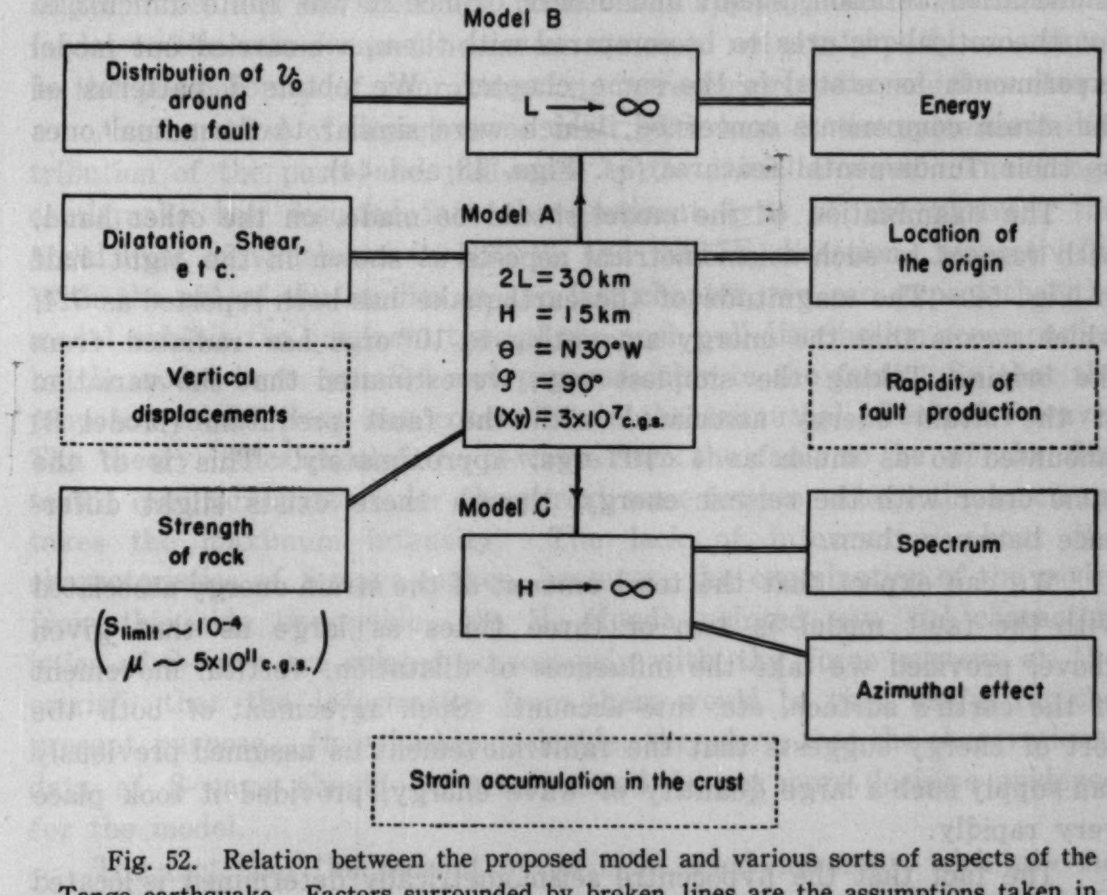
Model B
Distribution of v_0 around the fault
$L \longrightarrow \infty$
Energy
Model A
Dilatation, Shear, etc.
Location of the origin
$2L = 30$ km
$H = 15$ km
$\theta = $ N30°W
$\varphi = 90°$
$(X_y) = 3\times10^7$ c.g.s.
Vertical displacements
Rapidity of fault production
Model C
Strength of rock
Spectrum
$H \longrightarrow \infty$
$\left(\begin{matrix} S_{limit} \sim 10^{-4} \\ \mu \sim 5\times10^{11} \text{ c.g.s.}\end{matrix}\right)$
Azimuthal effect
Strain accumulation in the crust

Fig. 52. Relation between the proposed model and various sorts of aspects of the Tango earthquake. Factors surrounded by broken lines are the assumptions taken in the discussion.

---

96) *cf.* Chapter IV. The dip of the Gômura fault has been estimated as 70° by A. Imamura, while as 60°-80° by N. Yamasaki and F. Tada. We assume it, however, as 90°, for the sake of simplicity.

crustal deformation observed in the central part of the area. Another simplification was introduced to Model C, in which the depth of the fault plane was taken as infinitely large (*cf.* Chapter V). This condition means that the model is a two-dimensional system, which can be approximately accepted as far as the wave generation from a fault plane is concerned.

We see, in the figure, various sorts of aspects of the earthquake, among which the geodetic ones are arranged on the left side of the proposed model, while the seismometrical ones, on the right. Referring to the discussion made in Chapter IV, the diminution effect of horizontal displacements around the Gômura fault can be interpreted satisfactorily with Model B (*cf.* Fig. 35). Another sort of geodetic aspect which is observed around the fault is the distribution of strain components, such as dilatation, rotation, shear, and others. Since it was quite difficult to get theoretical pictures to be compared with them, we carried out model experiments as stated in the same chapter. We obtained patterns of the strain components concerned, which were similar to the actual ones in their fundamental features (*cf.* Figs. 43 and 44).

The examination of the model should be made, on the other hand, with respect to such seismometrical aspects as shown in the right half of Fig. 52. The magnitude of the earthquake has been reported as 7.4, which means that the energy amounting to 10^{23} ergs has radiated from the origin. Taking the simplest way, we estimated that the variation of the strain energy associated with the fault prodution (Model B) amounted to as mush as 4×10^{22} ergs, approximately. This is of the same order with the seismic energy, though there exists slight difference between them.

We can expect that the total amount of the strain energy associated with the fault model is two or three times as large as that given above, provided we take the influences of dilatation, vertical movement of the earth's surface, etc. into account. Such agreement of both the sort of energy suggests that the fault movement as assumed previously can supply such a large quantity of wave energy, provided it took place very rapidly.

The fact that the hypocentre seismometrically determined is located just on the fault plane (lower part) supports the applicability of the model. This information refers to the discussion in Chapter IV. Fig. 51 illustrates a cross-sectional view of the hypocentral region thus inferred, in which we see an indication of inseparable relations between the fault and the hypocentres of the main- and aftershocks. Although we do not know exactly what this fact means, it would suggest something of importance.

As to the wave-forms, we have not many evidences for detailed discussion. The spectrum of the initial P-wave recorded at the Hongo station showed the maximum intensity at the period of 23 sec. According to the theory developed in Chapter V (Model C), the P-wave radiated from the fault plane will show the spectrum somewhat similar to that obtained from the seismograms. The maximum intensity of the theoretical spectrum occurs at the component whose wave-length is 1.2 times or more as long as the fault, so that it is expected, from the present model ($2L=30$ km), that the characteristic period becomes 11 sec. The period of the maximum spectral intensity depends upon the type of the origin force, and we are not so confident in applying the two-dimensional model to the actual case; however, we may not be greatly mistaken, in the present step of approximation, in reaching the conclusions above.

Another kind of aspect to be dealt with here is the systematic distribution of the push- and pull-sense of the initial P-wave. The Tango earthquake has resulted into the quadrant type of the pattern, the nodal lines of which are in N29°W and N61°E direction, respectively. With the aid of the studies in the last chapter, we can expect that the model exhibit the quadrant type of the push-pull distribution accompanied by the nodal lines, parallel and perpendicular to the fault. So that the proposed model does not contradict to the azimuthal effect of P-wave. The theory indicates also the S-wave from the fault to be of the distorted quadrant pattern for the period some ten sec, where the spectrum takes the maximum intensity. The lack of information about the characteristics of S-wave makes, however, the examination of the model from this side impossible. As H. Honda pointed out, the characteristics of S-wave are related so seriously with the force system at the origin[97] that the information from them would be very useful for the present purpose. It is highly desirable, therefore, that the observational data of S-wave should be accumulated to get more decisive evidence for the model.

The fact that the present model is in good harmony with all the aspects of the earthquake as derived from seismological and geodetic observations enables us to assume this sort of model for the case of the Tango earthquake. We have to remember, however, that the above

---

97) H. HONDA, *Sci. Rep., Tohoku Univ.*, [V] **9** (1957), 1.

discussion has been worked out on some assumptions. Remarks on the incompleteness of the theory being very necessary for further development of this research field, the writer would like here to give a brief description of it.

One cause of the incompleteness is the lack of discussion related to the vertical component of crustal deformations. It has been brought out by repeated levellings that the deformations are fairly systematic in their fundamental features, though they were sometimes overlapped by local disturbances probably caused by block structures of the crust[98]. According to Y. Otuka, there is a general tendency that the distribution of such deformations is closely related with the direction of fault movements[99]. The uplift and subsidence areas at the extremities of the fault were found more remarkably in the case of the North-Izu earthquake than those for the Tango earthquake. Although the present paper could not deal with the tendency theoretically, we would be able to investigate experimentally such a tendency by improving the technique of model experiments.

Another important assumption taken in the previous discussion is that the fault appears in a very short time. Discussion on the energy as well as on the spectrum of seismic waves is so closely related with the rapidity of stress change on the fault plane that it should be studied in more detail in the following section. The last and the most essential assumption for the model is related with strain accumulation in the crust, which becomes so large as to exceed the limit strength of rock. The mechanism of strain accumulation in the crust being one of the major projects in tectonophysics, the present writer can hardly make full discussion in this paper, and he would like only to examine the possibility of it on the basis of hypotheses so far proposed by a number of geophysicists (*cf.* Chapter VII).

3. Rapidity of fault production in the crust.

The rapidity of fault production in the crust seriously influences the foregoing discussion. Suppose the stress does not change so rapidly as is assumed in the last section, we could no longer expect high conversion efficiency of the strain energy into the seismic waves' one and the feature of the spectrum would also be different from that for the case of very rapid stress change. The alteration of such conditions might sometimes cause serious difficulties in accepting the model as a likely one.

---

[98] C. TSUBOI, *loc. cit.*, 6).

[99] Y. OTUKA, *Chishitsu-kôzô to sono Kenkyû* (1952), p.196 (in Japanese).

H. F. Reid has presented the elastic rebound theory by taking the assumption that the fracture is propagated in the strained crust with the velocity higher than that of the distortional wave but lower than the longitudinal one[100]. Unfortunately, since fracture production is very complicated in its nature, we have no direct information about that point, and consequently we can presume the rapidity only from a few bits of information obtained from macroseismic studies of great earthquakes.

In the case of the Tottori earthquake of 1944, seismologists found out a notable evidence related to fault production under a resident's house. The house stood just on the seismic fault accompanied by the said earthquake but did not fall down notwithstanding the remarkable deformation of its foundation caused by the fault movement. This fact suggested that the earth's movement in the said case was not very rapid in spite of its large relative movements on the opposite sides of the fault. Taking these kinds of evidence into consideration, T. Matuzawa presumed that the fault appeared in a certain duration of time, some ten seconds say[101]. Another notable evidence for presuming the rapidity was obtained from the oceanographic observation at Yokosuka, in the case of the Kwanto earthquake (1923). Judging from the rapid raise of the sea level recorded with the mareograph, we could infer that the crustal deformation (land upheaval) had appeared within a short time which could be regarded, in effect, as an instant on the recording paper[102].

It has been pointed out by some geophysicists, lately, that they found particular events which might be related with such phenomena as fracture propagation through the crust, on the seismograms of some great earthquakes. According to T. Usami who analysed the seismograms of the Bôsô-oki earthquake, for example, three remarkable phases were observed in the initial part of the records. After seismometrical analyses he came to the conclusion that these three had originated from different points lying on a straight line which passed through the hypocentral region from east to west. The origin times determined for them showed systematic differences from one another, which might be attributed to some unknown origin being propagated along the line with the velocity of 9.8 km/sec. S. Komura studied the seismograms of the Fukui earthquake (1948) from another standpoint and arrived at the conclusion that the earthquake might probably be originated from the fracture plane propagating through the earth with the velocity of 2.1 km/sec.[104]

---

[100] H. F. Reid, *loc. cit.*, 10).

[101] T. Matuzawa, *Jishin-gaku* (1950), p. 242 (in Japanese).

[102] *ditto.*

[103] T. Usami, *loc. cit.*, 9).

Although it is not possible to conclude definitely that all the destructive earthquakes were associated with those special effects, it might still be permissible for us, in the present step, to presume the rapidity of fault production for the Tango earthquake on the basis of those studies. From such a standpoint the following discussion will refer to the assumption that the fault production takes some ten seconds to finish the predominant part of the process.

Let us now consider that the stress change on the fault plane is expressed in the following way, that is,

$$\left.\begin{aligned} S(t)&=0 \ (t<0)\ , \\ &=(1-e^{-ct}) \ (t\geqq 0), \end{aligned}\right\} \qquad (100)$$

where, c is a time constant and the function is reduced to the unit step-function when c becomes infinity. When $c=0.5\ \text{sec}^{-1}$, for instance, the function indicates the stress change which approaches its final state within the first ten seconds (Fig. 53, curve(b)). Applying Fourier transform to $S(t)$, we get the spectra for stress change at the origin. Curves in the lower part of Fig. 53 are the spectra thus obtained, where c is taken as a parameter for the family of curves. In spite of the remarkable difference between the features of

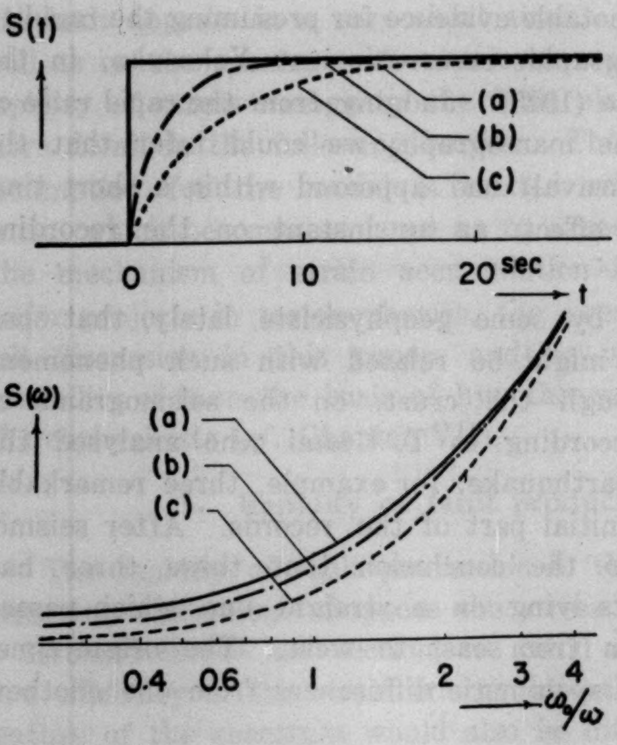

Fig. 53. Various modes of stress change and their spectra, (a) $c=\infty$, (b) $c=0.5\ \text{sec}^{-1}$, (c) $c=0.2\ \text{sec}^{-1}$.

---

[104] S. KOMURA, *loc. cit.*, 9).

spectra (a) and (b) at higher frequencies, they are similar with one another with respect to the range of lower frequency, such as $\omega_0/\omega > 0.7$ (ω_0 corresponds to the characteristic period (T_0) which is assumed as 20 sec). This sense of difference would not have, however, serious influence upon our previous discussion of the spectrum, in which we did not put much stress on the features of spectra at high frequencies.

Discussion about the efficiency would be very difficult to develop for the present model, therefore we shall study tentatively the wave generation from a spherical cavity as Sezawa and Kanai discussed[105]. Suppose we take the spherical model whch is equivalent to the fault model with respect to its characteristic period of spectrum (20 sec or so), we see from their result that the conversion efficiency for the gradual stress change ($c=0.5$ sec^{-1}) is about 60% of that for the step-like change. This decrease in the efficiency would not become an essential difficulty in accepting the fault model as a likely one in the present step of approximation.

4. Remarks on further application of the model to the other cases.

All through the discussion in the foregoing two sections, it became clear that the characteristics of the Tango earthquake can be explained well by taking the model of fault production as assumed in Fig. 52. In the next place, the writer would like to examine to what extent the present model is applicable to the other earthquakes.

As to the North-Izu earthquake, for instance, the application of the model may be justified by the similarity between the distribution of crustal deformations and the pattern of push-pull distribution[106]. This consideration is also supported by the results in the former chapters, which indicate that the change in the strain energy associated with the Tanna fault is approximately equal to the energy of seismic waves and that the focus is determined seismometrically at the bottom of the fault plane. Another support is obtained from the comparison of the observed wave-forms with the theory of wave radiation (*cf.* Chapter V), although such a comparison is possible only with respect to the characteristic period (T_0) of the spectrum of the initial P-wave. T_0 was given for the North-Izu earthquake (seismograms at the Hongo station) as 13 sec, which agreed well with the theory when the length of the fault was taken as 15 km (*cf*. Table IX). Under these considerations we may accept the model of fault production as a suitable one for the said case, too, though there still remains some uncertainty relating to the distribution of the vertical component of crustal deformations as well as to the process of fracture propagation in the crust.

---

[105] K. Sezawa and K. Kanai, *loc. cit.*, 56).

[106] H. Honda, *loc. cit.*, 8).

In the other cases of great earthquakes, however, we usually have no data for such a comparison. The only information available for the study is obtained from the examination of the push-pull sense of the initial motions, the distribution of which enables us to infer the direction of fault movement occurring at the origin[107]. This kind of study has been useful for understanding the nature of seismic active belts in relation to tectonic forces of the earth, but it is also an indisputable fact that the azimuthal effect gives merely a part of the information about the nature of seismic origins and that we would be more confident in accepting the results of analyses if we could carry out all the necessary examinations in a similar way to that of the previous section.

The result obtained from Chapter III would be useful for such an examination. The apparent density of strain accumulation around the seismic origin (see Fig. 26) falls in the range between 3×10^4 erg/c.c. and 3×10^2 erg/c.c., and the upper limit of the range for deep-focus earthquakes does not greatly differ from that for shallow earthquakes. This sense of distribution could be understood if it is supposed that deep-focus earthquakes are coused by fracture-like events in the earth.

Chapter VII.

Strain Accumulation in the Crust.

1. Introduction.

In the previous chapters we have been dealing with seismological and geodetic aspects of earthquakes in order to establish a reliable model of the origin. We remember that all the discussion concerned has been developed assuming strain accumulation in the earth. Since the previous conclusion is likely to be seriously affected by the assumption, we shall briefly discuss the strain accumulation and the related problems in this chapter.

---

107) J. H. HODGSON, *loc. cit.*, 83).

2. Mechanism of strain accumulation in the crust.

Strain accumulation is attributed nowadays to some tectonic forces in the earth, and several explanations have been provided for their mechanism. Most geophysicists agree that thermal effects are probably the most important one. From this standpoint, the earth is considered as a heat engine, which transforms thermal energy due to the temperature difference in the earth into mechanical work evident in faulting and other phenomena.

The geological implications of such phenomena lead to the so-called contraction hypothesis, which provides an explanation for the stress distribution in the "orogenetic shell."[108] According to H. Jeffreys, who assumes that the earth once has been a hot, liquid body and is in cooling stage at present, thermal effect due to cooling of the mantle results in the compressional and the tensile stresses working, respectively, in the uppermost layer and that lying below it. With the aid of this theory as well as of theories of stress analysis, we can find out a reasonable way to understand fundamental tendency of seismic activity in relation to the tectonic process of the earth, althongh there are some criticisms against it. According to J. H. Hodgson and others, for instance, the modes of faulting associated with many earthquakes have been estimated as transcurrent rather than normal or reversed, and this fact can hardly be explained by the theory.[109]

T. Matuzawa has presented another kind of hypothesis with the intention of studying the occurrence of great earthquakes in the upper part of the crust. He attributed the strain accumulation to the increasing pressure in a magma reservoir lying beneath the crust. The reservoir is subject to continuous supply of thermal energy, probably being transported from beneath by convection current in the subcrustal layer. Thermal energy accumulated in this part will cause, under a certain condition, phase transition of the rock, which will result into the increase of pressure at the boundary. Taking probable values for the constants he estimated the strain energy which is to be accumulated in the crust.[110] This hypothesis is advantageous of interpreting not only the occurrence of the main shock but also the tendency of aftershock occurrence and some other aspects of seismic activity.

---

[108] H. Jeffreys, *The Earth*, 3rd ed. (Cambridge 1952), p. 355.

[109] J. H. Hodgson, R. S. Storey and P. C. Bremner, *Bull. Geol. Soc. Amer.*, **63** (1952), 1354.

[110] T. Matuzawa, *Bull. Earthq. Res. Inst.*, **31** (1953), 179.
T. Matuzawa and H. Hasegawa, *ibid.*, **32** (1954), 231.

The contraction hypothesis looks useful for our understanding general features of seismic activity in the earth, whereas Matuzawa's theory has the advantage of explaining the more detailed mechanism of earthquake occurrence so for as shallow earthquakes are concerned. It might not be impossible to consider that both theories are not contradictory but consistent with one another giving explanation for the different sides of the earth's phenomenon, respectively. In either case, we may accept the assumption of strain accumulation in the crust as reasonable, in the present step.

3. Strain accumulation in the visco-elastic crust.

The above-mentioned discussion on strain accumulation assumes perfect elasticity of the crust. Although such an assumption may be taken as the first approximation, it is a well-known fact that the viscous or plastic properties of rocks sometimes play an importanl *rôle* in developing crustal deformation evident in folded strata. M. Ishimoto had raised, for instance, an objection to the elastic rebound theory under the consideration that the large amount of strain energy could not be accumulated in the crust because of the stress release due to the viscosity of rocks.[111] Such an effect would be a fatal obstacle to the proposed model, if it were remarkable, hence we shall refer to the writer's previous paper to examine how remarkable the viscous flow is.[112]

The paper deals with the deformation of the bottom surface of the crust which is subject to normal stress increasing with time(Fig.54). Such a model gives a simplified picture of Matuzawa's hypothesis, on the basis of which we are going to estimate the magnitude of the viscous flow of the crust.

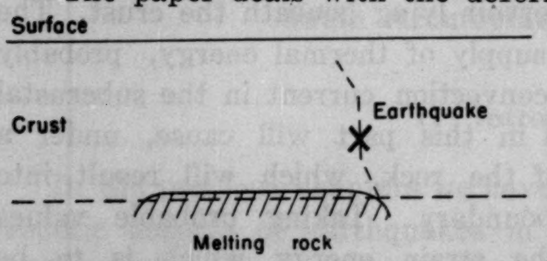

Fig. 54. Matuzawa's model of strain accumulation in the crust.

The increased pressure of the molten rock causes the deformation of the crust, which is accompanied by the volume increase of the reservoir, at the same time. The volume increase (ΔV) comes into effect partly due to the elastic deformation of the crust (ΔV_e) and partly, to the plastic flow (ΔV_p). Matuzawa assumes that such a volume increase is proportional to the thermal energy to be spent in the phase transition in the magma reservoir.

---

[111] M. ISHIMOTO, *Jishin to sono Kenkyû* (1935), p. 275 (in Japanese).

[112] K. KASAHARA, *Bull. Earthq. Res. Inst.*, **34** (1956), 157.

Meanwhile, the energy of earthquakes is supplied only from the strain energy due to the elastic deformation, therefore, it is only a part of the supplied thermal energy that contributes to the radiation of seismic energy. Denoting the part of the energy which contributes to ΔV_e and ΔV_p as E_e and E_p, respectively, we may take the following expression as the efficiency of strain accumulation.

$$H=\frac{E_e}{E_e+E_p}. \tag{101}$$

H is 1 when the crust is perfectly elastic, while it is very small when the majority of the crustal deformation is attributed to the plastic flow of rocks.

Mathematical investigation of the model indicates that H is a function of the viscosity (the relaxation time, τ) of the rock and of the duration time of strain accumulation, T. Suppose we take 10^{10} sec and 100 years as the probable values for τ and T, respectively, H will be 0.8~0.9; from which we might conclude that the viscosity has no serious influence on the strain accumulation.

4. Continuous observations of crustal deformation associated with strain accumulation in the crust.

We are of the opinion that the energy of earthquakes is supplied from the strain energy which is accumulated in the earth over long periods. It has been generally expected, therefore, that some deformations of the earth's surface will be observed when a part of the crust is subject to the stresses. Suppose we detect such evidences of strain accumulation, they would be useful for inferring the process that is occurring in the earth, which would provide, at the same time, the basis for the prediction of earthquake occurrence.

Although the geodetic observations of crustal deformation have been well developed, most of them are concerned with the comparison of observations made before and after the earthquake. Since it is difficult, or even impossible, to repeat levellings or triangulations frequently, the necessary information about the strain accumulation can not be obtained only by this means.

One of the way to make for the lack is the tide-gauge observation as has been proposed by S. Yamaguti in relation to the possibility of detecting the vertical movement of the land relative to the level of sea water.[113] The sea level being seriously affected by the oceanographic and other conditions, it is not always easy to detect to very small movements of the land.

We can not apply, however, tide-gauges to the observation at points distant from the sea-coast, so that we have to use instruments of other types, such as tiltmeters and extensometers, in those cases. Since we must observe changes taking place very gradually, the instrument would be useless if it were not stable over a long period of time. According to T. Hagiwara, who made effort to establish the reliable observation system, the instruments, which are in use at present, work so stably that they are able to give accurate information about the progress of the earth's deformations.[114]

We must remark here, also, the development of electronic apparata for geodetic observation, which bave accomplished remarkable development after the last war. One of them is known as the geodimeter, which transmits light signal to a distant reflector. It is possible to measure the distance between the projector and the reflector, very accurately.[115] Although the apparatus have not been brought into practical use for continuous observations yet, it will play an important *rôle* in this research field in future.

It is hardly likely that we would get satisfactory results from observations at few points. Since the crustal deformation can be observed only in a limited area around the epicentre, it might sometimes be missed by them. Geophysical stations for continuous observation are not densely distributed at present, hence it is strongly desired that we shall have more dense net-work in order to get clearer information about what occurs in the crust.

Concluding Summary.

General Introduction. Investigations on the nature of seismic origins are historically reviewed. In the earlier period of seismology, investigators assumed that waves were radiated from a point in the earth. The progress in theoretical and observational sides of seismology led us to improve the model of a point origin to a more complicated one. The model of a spherical origin has been proposed in order to interpret the results of seismological observations, while the studies of seismic energy and of crustal deformations have provided another basis in inferring the nature of seismic origins.

---

[113] *f.i.* S. YAMAGUTI, *Bull. Earthq. Res. Inst.*, **33** (1955), 27.

[114] T. HAGIWARA, *Continuous observation of crustal deformations, Monthly Meeting of E.R.I.*, (June 26, 1956),

[115] E. BERGSTRAND, *K. Svenska Velenskapsakademien*, **36** A (1948), No. 20, 11.

We are now on the step to look for a model by which we can explain all the seismological and the geodetic aspects of earthquakes, consistently. The main purpose of the present paper is to establish such a model and to examine the characteristics of it as closely as possible.

Chapter I. Wave-forms of the initial part of seismograms are regarded as useful information for the examination of the nature of seismic origins. It is no easy matter, however, to perform a complete analysis of them because they have complicated features. A modified method of spectral analysis is devised in order to deal with spectrum of waves easily. The method is based on multiplication procedure of the original wave-form by a weight function. By this procedure, it is possible to get the isolated wave-form, which is practically equivalent to the original in its spectral structure.

Some reduction for the influences of the seismograph's characteristics as well as other factors which may sometimes cause distortion of the spectrum is also discussed.

Chapter II. Analyses and discussion are carried out about the nature of explosion origins as inferred from the spectrum of seismic waves. It is shown that the larger the charge of explosives is, the longer becomes the period of the maximum spectral intensity. The spectra of seismic waves from an origin are nearly the same with each other, even if they are recorded at different stations. This fact leads us to a conclusion that it is the conditions of the origin, and not of the propagation paths', that have the most serious influence on the types of the spectra. Under such a consideration, we may presume the nature of the origin by comparing observational results with theory. Such a comparison enables us to estimate the apparent dimension of the explosion origin.

The explosion origin thus estimated was several times as large as that of the crushed region in its radius. This difference could not be attributed only to the errors in the analysis. In order to improve this point, another model is proposed as shown in Fig. 18.

Chapter III. We apply the proposed method to the records of natural earthquakes and estimate the dimension of their origins on the basis of the theoretical model of a spherical origin. A marked tendency has been noticed that the larger the magnitude of the earthquake is, the larger the dimension of the origin becomes. We also estimated the apparent density of strain energy being accumulated around the origins.

The densities thus estimated for various earthquakes are distributed in the range from 3×10^2 c.g.s. to 3×10^4 c.g.s.. The upper limit of the accumulation density has already been estimated as large as 2×10^3 c.g.s. or 2×10^4 c.g.s. by C. Tsuboi. It is interesting that the densities estimated from different bases agree with one another. We must remark another notable fact that the range of the density for deep-focus earthquakes does not greatly differ from that of shallow earthquakes. This might be understood as an evidence that the cause of both types of earthquakes are similar with one another.

Chapter IV. Crustal deformations are analysed for the purpose of obtaining information about earthquake origin from the geodetic point of view. Statistical investigation of the great earthquakes taking place in the Japan area suggests that the occurrence of crustal deformation is closely related to the magnitude and the focal depth of the earthquake. In the cases of some typical shallow earthquakes, such as the Tango earthquake that was accompanied by lateral faults, we see that the earth's deformation is distributed systematically.

We propose a simplified model of a lateral fault for the purpose of studying the notable tendency of horizontal displacements of triangulation points. Mathematical treatment of the model has proved satisfactory agreement of the theory with the observational data. The decrease in displacements with distance from the fault is explained theoretically. From the comparison we estimate the probable values for the depth and the amount of strain energy associated with the Gômura fault and others.

Model experiments were also carried out in order to make up for the lack of the theoretical study, which provided some interpretations of the complicated distribution of strain components at the ends of the fault.

Chapter V. Wave generation from a fault plane was studied for the purpose of studying the characteristics of waves in relation to the two-dimensional model of fault movement, which causes the rapid change (step-like) of shear so as to canncel the initial stress on the fracture plane. Numerical calculations were carried out on the basis of Sezawa's theory for the purpose of estimating the displacements at distant points. The calculation being made for the periodic excitation of different frequencies, some reduction was necessary for inferring the spectrum of waves due to step-like excitation. As a result of the calculation, it is shown that the maximum intensity of the spectrum (P-wave) will fall on the component whose wave-length is 1.2 times as long as the fault's length. Characteristics of S-wave are also discussed.

Applying the results to the case of the Tango earthquake, we found out that the observed characteristics of P-wave could be approximately explained by assuming the sudden occurrence of the fault plane in the same direction as that of the Gômura fault.

Chapter VI. The foregoing chapters have been dealing with the seismological and the geodetic aspects of earthquakes, separately. On the basis of those discussions, we propose a unified model for the occurrence of the Tango earthquake and examined whether or not it is consistent with all the accompanying phenomena. Geodetic observation provided for our discussion the information about crustal deformations, such as the distribution of horizontal displacements, dilatation, shear, etc., whereas, from seismological observations, the data of the energy of the earthquake, location of the origin, spectrum and azimuthal effect of the waves are obtained.

The proposed model of the origin is the sudden occurrence of a fault plane which is 30 km long and 15 km deep. The strike and the dip are assumed as N 30° W and 90°, respectively, and the stress change (shear) on the fault plane is taken as 3×10^7 c.g.s.. This is also a reasonable value for the limit of strength of the crust. The examination of the fault movement, as proposed in such a way, has proved that the model is acceptable for the said case, though there still remain some uncertainties coming from the approximated treatment of it. Supplementary discussion is also made about the fracture production in rocks as well as about further application of the similar model to the other earthquakes.

Chapter VII. All the discussion is on the assumption that the crust is subject to strain accumulation being so large as to cause fractures in a large scale. Since the assumption seriously affects the conclusions in those chapters, the last chapter is added in order to examine the possibility of strain accumulation.

Discussion is also undertaken about the viscosity of rocks which causes stress release in the crust. Estimation with respect to Matuzawa's model of strain accumulation showed that the energy dissipation due to the effect is not so remarkable as to result into the essential alteration of the conclusions.

We also make a short remark on continuous observation of crustal deformations as the useful means of getting information about the strain accumulation. Suppose the observation is carried out at numbers of points in the seismic active region, we would have reliable data for predicting the earthquake occurrence.

Acknowledgements.

The writer wishes to express his hearty thanks to Prof. Takahiro Hagiwara of this institute, who has given unfailing support to the writer throughout the course of this study. He is also thankful to Prof. Chuji Tsuboi and Dr. Tsuneji Rikitake for their kind advice and encouragement. The writer is obliged to the following organizations and the research groups, which kindly permitted him to use the records obtained by themselves. They are, the Seismological Division of this institute, the Seismological Division of the Japan Meteorological Agency, the Geological Survey of Japan, the Research Group for Explosion Seismology, the Seismic Exploration Group of Japan, and others. Lastly, the writer would like to thank Miss M. Ninomiya and Miss R. Iwaya, for their kind assistance in the preparation of the manuscript.

---

2. 震源の性状に関する地震学的及び測地学的研究 (二)

地震研究所 笠 原 慶 一

前報に引きつづき震源の性状に関する解析を行つた．

第5章． 断層運動によつて発生する弾性波の特性を，断層生成の諸条件との関連において調べた．本章においては二次元的な断層モデルを採用し，その面上で shear 歪力が急激に，例えば階段函数的に変化するものと考える．

焦点距離が断層面の長さに等しい楕円座標に関する波動方程式を取り扱い，歪力が断層面上で周期的に変化する場合の解を得る．更に数値計算によつて遠方の点の変位を求めると，それは震源力の周期及び観測点の方位の函数として与えられるから，これを用いて発生する弾性波のスペクトラムや押し引き分布の特性を推定することができる．

例えばP波の場合，最大スペクトル強度に対応する成分はその波長が断層の長さの約1.2倍であること，又波長がこの程度であるような成分は略々象限型の押し引き分布を示すことがわかつた．S波の特性はP波のそれに比べてやや複雑であるが，波長が断層と同程度である成分の場合は，やはり象限型に近い押し引き分布型式が現われるようである．

以上の結果を丹後地震の場合に適用すると，郷村断層に沿う長さ 30 km 程度の垂直面上において shear 歪力が急激に減少したとするわれわれのモデル（前報参照）は，地震波動の諸特性に関しても観測事実とよく調和することがわかる．更に附加的議論として，実際の歪力変化（つまり断層面の現われ方）か瞬間的でなくある有限時間をかけて行われる可能性，及びそれによつてスペクトラムやエネルギー放出効率がうけるべき影響の程度についても考察した．

第6章． 第3～5章の研究によつて得られた知識を基にして，丹後地震の震源特性に関する綜合的考察を試みた．モデルの適歪を判断する根拠としては，大別して測地学的な観測事実と地震学的なそれとがある．前者は例えば水平変動量や各種の歪成分の分布状況に関するものであり，後者に属するものとしては地震動のエネルギー，震源の位置，初動部のスペクトラム，押し引き分布の型式等が考えられる．

モデルとして，郷村断層に沿う，長さ 30km，深さ 15km，伏角 90° の辷り破壊面が短時間内に発生し，その面上において 3×10^7 c.g.s. 程度の shear 歪力変化が行われたと考えれば，上記の諸観測事実はすべて矛盾なく解釈できるし，「地殻の強さの上限」に関する従来の考え方とも調和する．勿論，これらの議論はかなり大胆な近似又は仮定の上に立つて行われたものであり，今後改善の余地も多いのであるが，第一近似として上記のモデルを丹後地震に対して採用することは許されることと思う．本章の後半においては，以上の議論でふれ得なかつたいくつかの要素，例えば垂直方向の地殻変動，破壊面が発生進行する速さ等について議論を進め，又同種のモデルを他の地震の場合に適用する可能性についても簡単に述べてある．

第7章． 以上の議論の基底となつているものは，地殻の強度限界を越える程度の著るしい歪の集積が，かなり広い範囲に亘つて行われるという仮定である．この問題は既に tectonophysics の分野で検討されて来ているので，提出されている代表的な仮説を引用しつつ歪集積の可能性を考察した．

ところで，歪集積の進行速度がどの程変であるかによつて，岩石の粘性流動が大きな影響をもち，歪エネルギーが有効に集積されなくなるおそれもあるので，松沢過程を例としてその影響の程度の見積りを試みた．普通考えられるような条件の下では，粘性流動の果す役割はそれ程大きなものでないようである．

一方，歪集積に伴つて地震発生の前にも緩漫な地殻変動が進行する筈であり，それの模様を多くの地点において連続的に観測することができれば，歪集積の物理的機構を明らかにし，ひいては大地震発生の予知を実現する上にも大きな貢献を果すことが期待される．その意味においてこの種の観測網の充実が要望される．

BULLETIN OF THE EARTHQUAKE
RESEARCH INSTITUTE
Vol. 36 (1958), pp. 55-64

3. *Calibration of an Electromagnetic Seismograph by Means of the Frequency Analysis*

By Tosimatu MATUMOTO,

Earthquake Research Institute.

(Read Nov. 22, 1955 and June 26, 1956.—Received Dec. 28, 1957.)

Abstract

The tapping test method for obtaining the response curve of an electromagnetic seismograph by the application of the theory of frequency analysis is described in this paper.

A slight tapping is applied to the pendulum, and the motion of the pendulum and the galvanometer activated by it are recorded at the same time. The spectra of both the recorded motions are calculated, and then the magnification, the frequency characteristics and the phase angle of the electromagnetic seismograph are reckoned.

This method enables us to get the response curve for both the amplitude and the phase angle for all frequency ranges and for all kinds of electromagnetic seismographs having arbitrary damping and arbitrary period both for the galvanometer and the pendulum without any shaking table or another special apparatus. This simple method with a high accuracy good enough for ordinary purposes would be very useful for the calibration of the electromagnetic seismograph in field work as well as in routine work.

1. Ever since Galitzin[1)] developed the first electromagnetic seismograph, valuable studies on this subject have been carried out by many authorities.[1)–8)]

[1)] B. GALITZIN, *Vorlesungen über Seismometrie* (*Leipzig*: *Teubner*).
[2)] J. COULOMB and G. GRENET, *Annales de Physique*, **11** (1935), 321-369.
[3)] G. SCHMERWITZ, *Annalen der Physik*, **5** (1939), 209-223.
[4)] J. ROYBNER, *Gerlands Beitr. z. Geophy.*, **55** (1939), 303-313.
[5)] F. T. WORRELL, *Bull. Seism. Soc. Amer.*, **32** (1942), 31-48.
[6)] S. K. CHAKRABARTY, *Bull. Seism. Soc. Amer.*, **39** (1949), 205-218.
[7)] K. TAZIME, *Zisin*, **7** (1954), 96-115.
[8)] J. P. EATON, *Bull. Seism. Soc. Amer.*, **47** (1957), 37-75.

In the use of electromagnetic seismographs, it is very important to know the characteristics of the seismograph exactly, but the method of obtaining these characteristics is not so simple. According to the ordinary theoretical method, we have to measure at least five constants to know the characteristics of the electromagnetic seismogragh as Coulomb and Grenet[2] have pointed out. This method may include a considerably large error of measurement because the characteristics of the electromagnetic seismograph are expressed by the product or some complicated form of these constants, and especially this error on the characteristics may become larger when some of these constants are expressed by the damping constants of the pendulum and the galvanometer, which is liable to include a comparatively large error of measurement.

The direct metheod applying the shaking table test gives us a considerably good accuracy of measurement, but the usual seismograph such as the Galitzin type in which the mass of the pendulum is 7 kg. in weight is too large to apply the shaking table test. Further, if the characteristics of the seismograph extend over a considerably long period, it is also difficult to apply this direct method. Therefore it is desirable to find some simple method which enables us to make the calibration for all kinds of seismographs and for all ranges of period.

In this paper, a simple method applying the theory of frequency analysis to the tapping test of the electromagnetic seismograph is offered. This method is applicable for all kinds of seismographs and for all ranges of period.

2. The block diagram of the electromagnetic seismograph is illustrated in Fig. 1, in which $F(t)$ means the ground movement while $P(t)$ and $G(t)$ represent respectively the motion of the pendulum and that of the galvanometer caused by $F(t)$.

Expressing the spectra of $F(t)$, $P(t)$ and $G(t)$ by $f(\omega)$, $p(\omega)$ and $g(\omega)$ respectively, we get

$$\left.\begin{matrix} F(t) \\ P(t) \\ G(t) \end{matrix}\right\} = \frac{1}{2\pi}\int_{-\infty}^{+\infty} \left\{\begin{matrix} f(\omega) \\ p(\omega) \\ g(\omega) \end{matrix}\right\} e^{i\omega t}\, dw \qquad (1)$$

and

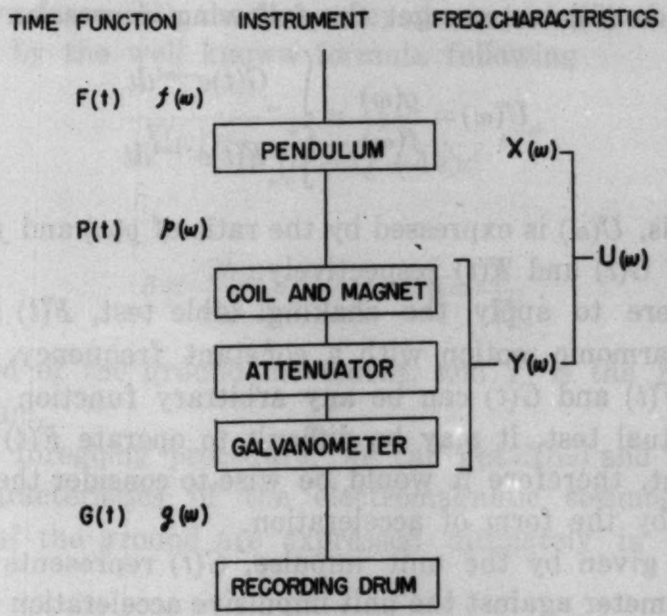
TIME FUNCTION
INSTRUMENT
FREQ.CHARACTRISTICS
F(t) f(ω)
PENDULUM
X(ω)
P(t) p(ω)
U(ω)
COIL AND MAGNET
ATTENUATOR
Y(ω)
GALVANOMETER
G(t) g(ω)
RECORDING DRUM

Fig. 1. The time functions, the frequency characteristics and the block diagram of the electromagnetic seismograph.

$$\left.\begin{matrix} f(\omega)\\ p(\omega)\\ g(\omega)\end{matrix}\right\}=\int_{-\infty}^{\infty}\left\{\begin{matrix}F(t)\\ P(t)\\ G(t)\end{matrix}\right\}e^{-i\omega t}dt \qquad (2)$$

We denote the frequency characteristics of the instrument as follows

$X(\omega)$: frequency characteristics of the pendulum against the ground movement.

$Y(\omega)$: frequency characteristics of the galvanometer against the motion of the pendulum.

$U(\omega)$: frequency characteristics of the galvanometer against the ground movement.

Then we get the following relations

$$P(t)=\frac{1}{2\pi}\int_{-\infty}^{\infty}X(\omega)f(\omega)e^{i\omega t}d\omega \qquad (3)$$

$$G(t)=\frac{1}{2\pi}\int_{-\infty}^{\infty}Y(\omega)p(\omega)e^{i\omega t}d\omega \qquad (4)$$

$$G(t)=\frac{1}{2\pi}\int_{-\infty}^{\infty}U(\omega)f(\omega)e^{i\omega t}d\omega \qquad (5)$$

The function $U(\omega)$ is the amplitude-frequency characteristics of the electromagnetic seismograph that we want to obtain. From equation

(1) and equation (5), we can get the following expression

$$U(\omega)=\frac{g(\omega)}{f(\omega)}=\frac{\int_{-\infty}^{\infty}G(t)e^{-i\omega t}dt}{\int_{-\infty}^{\infty}F(t)e^{-i\omega t}dt} \tag{6}$$

In other words, $U(\omega)$ is expressed by the ratio of $g(\omega)$ and $f(\omega)$ which are the spectra of $G(t)$ and $F(t)$ respectively.

If we were to apply the shaking table test, $F(t)$ and $G(t)$ must be a simple harmonic motion with a constant frequency, while in our present test $F(t)$ and $G(t)$ can be any arbitrary function of time.

In the actual test, it may be difficult to operate $F(t)$ by the form of displacement, therefore it would be wise to consider the case in which $F(t)$ is given by the form of acceleration.

If $F(t)$ is given by the unit impulse, $G(t)$ represents the response of the galvanometer against the unit impulsive acceleration of the ground, and $g(\omega)$ represents the acceleration-frequency characteristics of this seismograph.

If we get the acceleration-frequency characteristics, it will be easy to calculate the amplitude-frequency characteristics.

On the basis of the above theory, it would be preferable to adopt the following process to determine the magnification, the amplitude-frequency characteristics and the phase angle of the electromagnetic seismograph.

(1) When we want to record the corresponding $G(t)$ and $P(t)$ on a recording drum, we have to put an attenuator circuit by which we can control $G(t)$ to a suitable amplitude, keeping both the dampings of the pendulum and of the galvanometer in the original state.

(2) From the records of $P(t)$ and $G(t)$, we get the corresponding spectra $p(\omega)$ and $g(\omega)$, and therefore we get

$$Y(\omega)=\frac{g(\omega)}{p(\omega)}=\frac{\int_{-\infty}^{\infty}G(t)e^{-i\omega t}dt}{\int_{-\infty}^{\infty}P(t)e^{-i\omega t}dt} \tag{7}$$

(3) Although it is difficult to realise a perfect impulse, if the duration time of $F(t)$ is short enough compared to T_1 (the natural period of the pendulum) and T_2 (the natural period of the galvanometer), we can treat $F(t)$ as a perfect impulse in practice. If we calculate the damping constant of the pendulum h_1[9] from the recorded $P(t)$ which is activated

---

[9] *loc. cit.* 8)

by an impulsive force $F(t)$, the frequency characteristics of the pendulum $X(\omega)$ is given by the well known formula following

$$X(\omega)=\frac{1}{\sqrt{(u^2-1)^2+4h_1^2u^2}}e^{-i\delta} \tag{8}$$

where

$$\delta=\frac{2h_1u}{u^2-1}, \qquad u=\frac{T}{T_1}.$$

T is the period of the ground movement, and T_1 is the natural period of the pendulum.

(4) From the foregoing procedure, we can get $X(\omega)$ and $Y(\omega)$, then the frequency characteristics of the electromagnetic seismograph for the displacement of the ground are expressed ultimately in the following form.

$$U(\omega)=X(\omega)Y(\omega) \tag{9}$$

(5) If the force $F(t)$ is a perfect impulse, the spectrum $f(\omega)$ has zero phase shift through the whole frequency ranges[10].

In this case, the phase angle for the displacement of the ground $\theta(\omega)$ is expressed in the following form

$$\theta(\omega)=\arg g(\omega)-\pi \tag{10}$$

Table I.

	Transducer	Galvanometer
Name of the instrument	HES-H	HES-R-1
Natural period	1.0 sec.	1.2 sec.
Resistance of the coil	1,523 ohm	500 ohm
Shunt resistance of critical damping	1.400 ohm	1.800 ohm
Total flux of the magnet	1.0×10^5 maxwell	2.5×10^4maxwell
Sensitivity	*2.47×10^{-5} A/mm	0.70×10^{-8} A/mm
Weight of the mass	1×10^4 gram	0.251 gram
Moment of inertia	3.78×10^6 gram cm^2	

* The length of the optical lever is 100 cm.

3. As an example, a practical test of an electromagnetic seismograph will be described below.

---

[10] S. GOLDMAN, *Information Theory*, New York (1953,) 220.

The electromagnetic seismograph used in this measurement was the same kind of instrument which has been working in the seismological station of our institute at Mt. Tsukuba for the routine observation since May, 1956. The constants of this instrument are shown in Table 1. The HES–H transducer is a moving-coil type instrument employing a single magnet for transducing and damping.

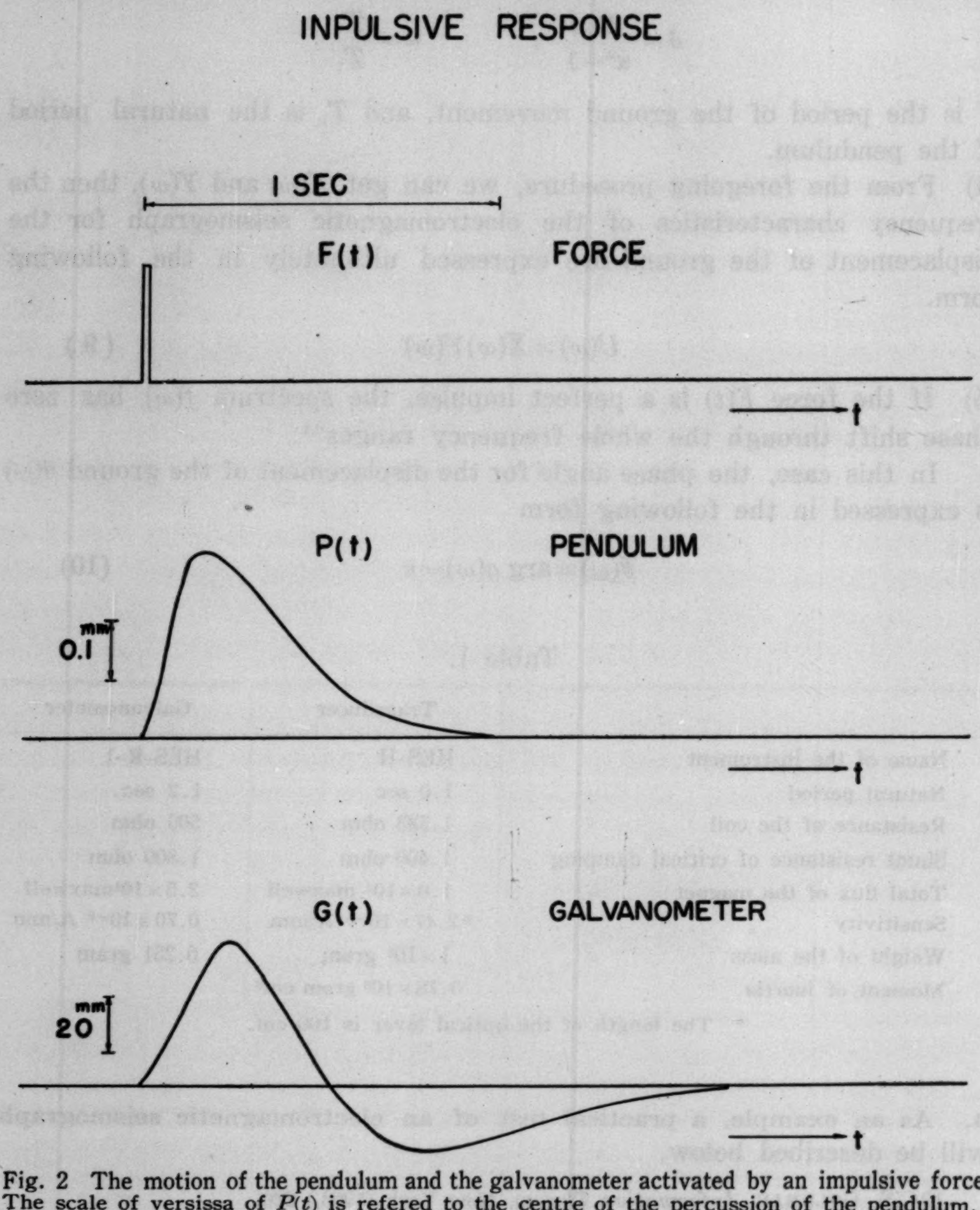

Fig. 2 The motion of the pendulum and the galvanometer activated by an impulsive force. The scale of versissa of $P(t)$ is refered to the centre of the percussion of the pendulum.

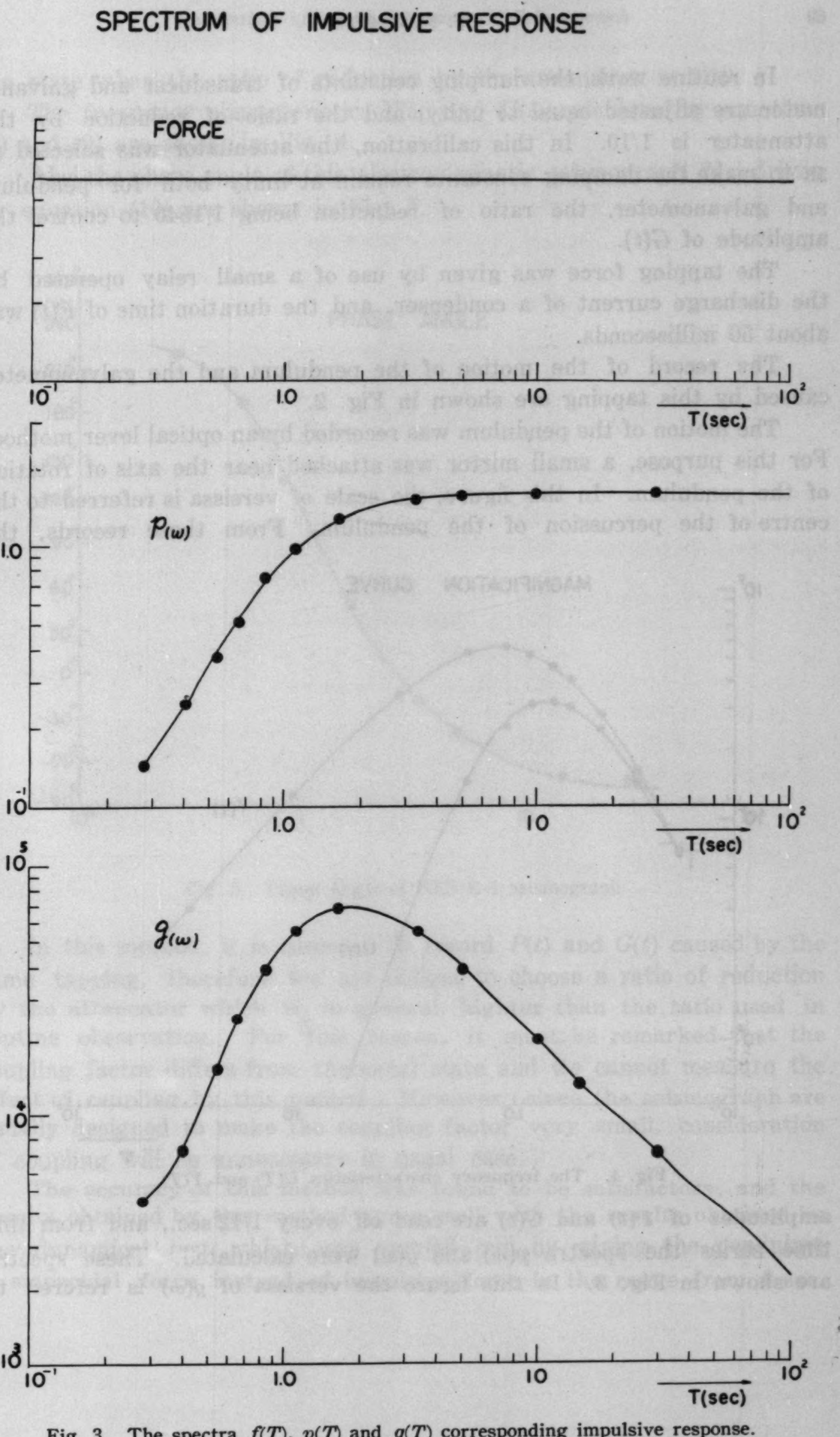

Fig. 3. The spectra $f(T)$, $p(T)$ and $g(T)$ corresponding impulsive response.

In routine work, the damping constants of transducer and galvanometer are adjusted equal to unity, and the ratio of reduction by the attenuator is 1/10. In this calibration, the attenuator was selected so as to make the damping constants remain at unity both for pendulum and galvanometer, the ratio of reduction being 1/1540 to control the amplitude of $G(t)$.

The tapping force was given by use of a small relay operated by the discharge current of a condenser, and the duration time of $F(t)$ was about 50 milliseconds.

The record of the motion of the pendulum and the galvanometer caused by this tapping are shown in Fig. 2.

The motion of the pendulum was recorded by an optical lever mothod. For this purpose, a small mirror was attached near the axis of rotation of the pendulum. In this figure, the scale of versissa is referred to the centre of the percussion of the pendulum. From these records, the amplitudes of $P(t)$ and $G(t)$ are read off every 1/12 sec., and from this time series the spectra $p(\omega)$ and $g(\omega)$ were calculated. These spectra are shown in Fig. 3. In this figure the versissa of $g(\omega)$ is refered to

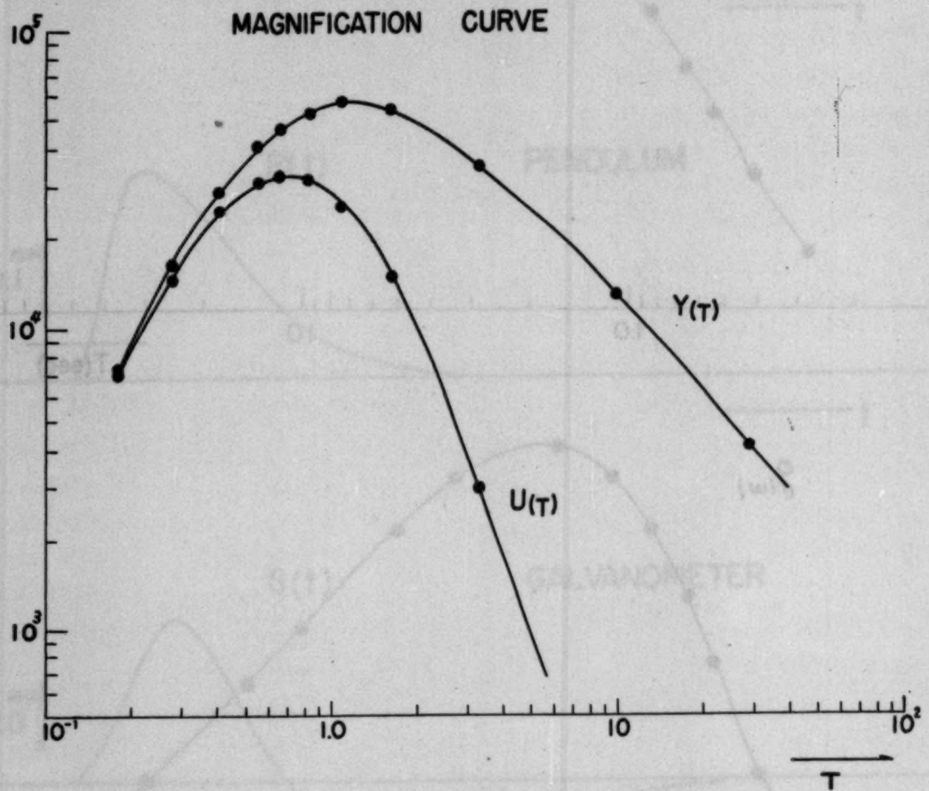

Fig. 4. The frequency characteristics $U(T)$ and $Y(T)$.

the state when the ratio of reduction by the attenuator is 1/10.

The frequency characteristics $Y(\omega)$ and $U(\omega)$ calculated by equations (8) and (9) are shown in Fig. 4.

Also the phase angle of this electromagnetic seismograph $\theta(\omega)$ driven by equation (10) are shown in Fig. 5.

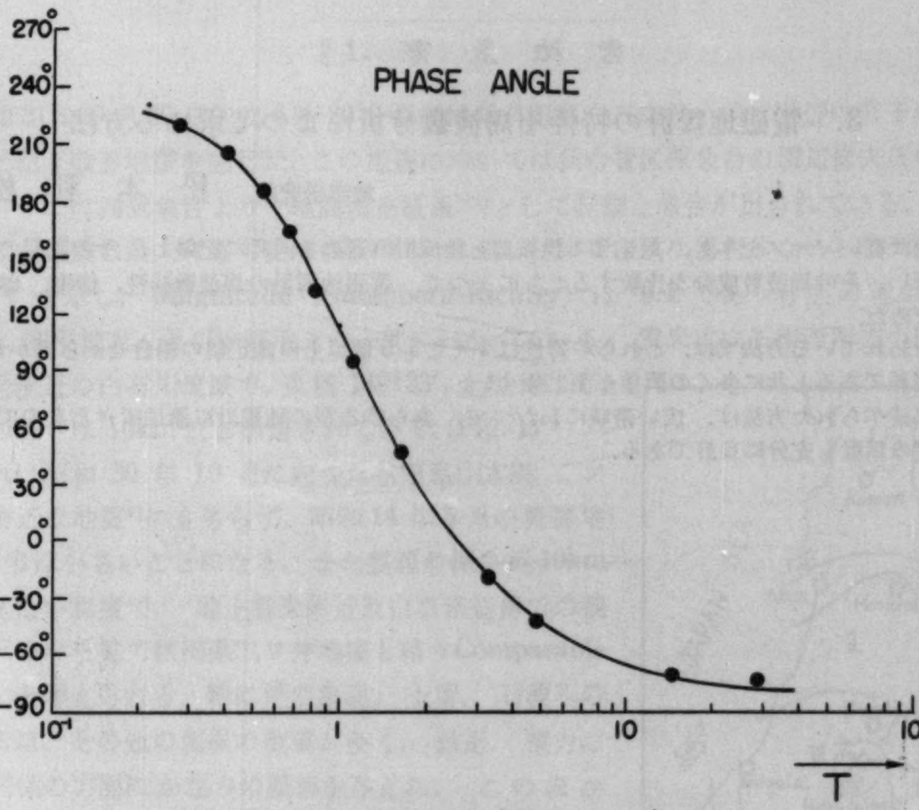

Fig. 5. Phase Angle of HES-R-1 seismograph

4. In this method, it is essential to record $P(t)$ and $G(t)$ caused by the same tapping, therefore we are obliged to choose a ratio of reduction by the attenuator which is, in general, highter than the ratio used in routine observation. For this reason, it must be remarked that the coupling factor differs from the usual state and we cannot measure the effect of coupling by this method. However, since the seismograph are usually designed to make the coupling factor very small, consideration of coupling will be unnecessary in usual case.

The accuracy of this method was found to be satisfactory, and the results obtained by this method agree well with the results obtained by the dynamical test which was carried out by giving the pendulum a sinusoidal force instead of impulsive force in the range from 4 sec.

to 0.3 sec.. Also these results agree well with the response calculated by the ordinary method based on the measurement of the period and the damping of the pendulum and the galvanometer[11]. In conclusion, the writer wishes to express his hearty thanks to Prof. T. Hagiwara who gave him valuable suggestions and advice about this study.

3. 電磁地震計の特性を周波数分析によつて求める方法

地震研究所　松本利松

換振器に軽いパルスを与え，対応する換振器と検流計の運動を同時に記録し，その記録の周波数分析を行い，その周波数成分を比較することによつて，電磁地震計の周波数特性，倍率，および位相角を求めた.

従来行われている方法では，これらの特性は少くとも5個以上の測定値の組合せから導かれるが，測定が繁雑であると共に多くの誤差が生じやすい.

ここに述べられた方法は，広い帯域にわたつて，あらゆる型の地震計に適用できるものであり．また測定の精度も充分に良好である.

---

[11] A description of this method is now being printed by T. Hagiwara.

地震研究所彙報
第36号(1958)65-70頁

4. 宮城県白石市附近の地震(1956年9月30日)と水準測量の結果

地震研究所　岡田　惇

(昭和31年12月18日発表—昭和32年12月28日受理)

§1. まえがき

昭和31年9月30日午前6時20分頃宮城県刈田郡白石市及小原村附近に若干の被害を伴つた稍々顕著地震を感じた．この地震については仙台管区気象台の渡辺偉夫氏の調査があり，すでに同気象台より“地震調査概報”[1]として詳細な報告が出されている．これによれば本地震の最大有感半径は 260 km に達し，白石市及小原村すなわち震央附近では震度 V を示し，Magnitude (Gutenberg-Richter) は 6.1 であり有感の地域は東北地方，関東地方，及び中部地方の一部にわたつている．震央は白石市西南方小原村南部材木岩附近の白石川流域で，東経 140°23′，北緯 38°57′，震源の深さは 10km 位と推定されている．(Fig. 1)

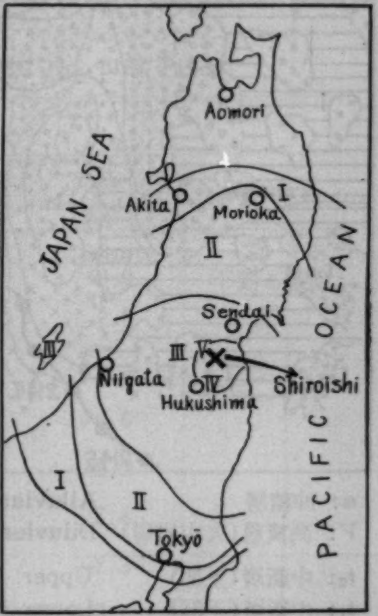

Fig. 1. Isoseismal map of Shiroishi Earthquake Sept. 30th, 1956 (after Sendai District M.O.)
白石地震の等震度分布図(仙台管区気象台)

これは昭和30年10月に起つた秋田県山本郡二ツ井町附近の地震[2]にも劣らず，昭和14年5月の男鹿地震[3]よりは小さいことになる．また震源の深さが 10km を超えない程度で，地上震央附近及白石市近傍での被害状況等から見て秋田県二ツ井地震と略々Comparable order と考えられる．特に壁の亀裂，土塀，石積みの塀，石垣，その他の垣根の倒壊が多く，鉄道，電力，工場関係の方面にかなりの被害を与えた．このほか各所に地割れ，崖崩れも多く，本震は勿論，余震も地鳴を伴うことが一つの特徴のようであつた．また震央附近には小原，鎌先温泉等二三の温泉が湧出しているが，これらの温泉や地下水には一時的異変を認められたのみで特筆する変化はなかつたようである．以上がこの地震についての概要であるが，秋田県二ツ井地震の場合と非常に類似する現象が多く，震源の深さが 10 km 位とすると，震央近傍において地質構造的な異変，例えば二ツ井地震のように測地学的[4]に見出される構造

---

[1] 仙台管区気象台“地震調査概報”宮城県阿武隈川下流域(白石-小原周辺) 昭和31年10月
[2] 島　悦三・柴野睦郎 Bull. Earthq. Res. Inst., **34** (1956), 112.
[3] 萩原尊礼 Bull. Earthq. Res. Inst., **17** (1939), 627.
[4] 宮村摂三・岡田　惇 Bull. Earthq. Res. Inst., **34** (1956), 373.

断層，或は震央附近の隆起のような現象が発生しているのではないかと考えられた．このように小区域に発生した地震による地殻変動の調査研究は過去においても数多く行はれてきた．幸なことにこの附近にも地理調査所水準点が南北に縦断していて，かつ2年前に，東京ー青森間の一等水準測量の改測が行われているので，白石市附近の検測を計画して，11月中旬より下旬にかけて現地の測量を行つた．

§2. 白石市附近の水準路線と地形及地質の概略

蔵王火山群及び山形県境奥羽背稜山脈に源を発した白石川は七ヵ宿村を東流し多くの支流を集めて次第に水量を増し材木岩の頸部を経て，本地震の震央と推定された小原村南部で北方に向きを変え，深い渓谷となつて再び東流して，阿武隈川の本流に合し大平洋に注いでいる．小原村附近の谷には小原，鎌先両温泉を始め，発電所もあり白石市附近の平地に達し，白石市市街東方で支流斎川と合流しているが，地理調査所の levelling route はこの斎川に沿つて南に延び，越河峠を経て福島県藤田方面に達している．この levelling route は東京ー青森を結ぶ main route で，筆者はその一部白石市を中心にした僅々24km，水準点13点について再測を行つた．又この levelling route を狭む地域の地質構造の概略は Fig.2 に見られるように西側には蔵王火山群の噴出物等で覆われ，東側にはいわゆる阿武隈高原と呼ばれる台地との接するやや複雑な地域である．levelling route は丁度この両地形の接する縁辺に位置して，大部分は浅い第四紀洪積層乃至は冲積層の deposite の上にある．又前述の白石川中流に

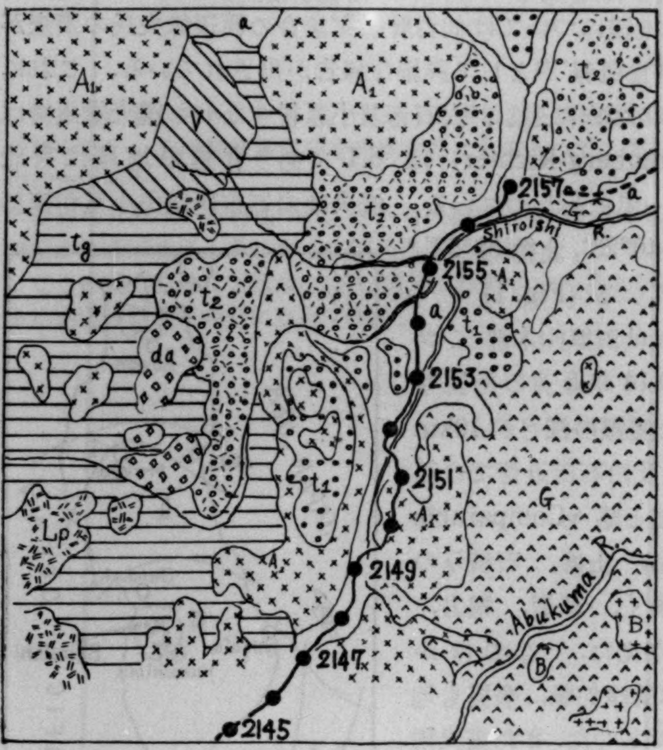

a:	冲積層	Alluvium
V:	洪積層（火山岩層）	Diluvium (Volcanic detritus)
t_2:	中新層（上部）	Upper Miocene
t_1:	中新層（下部）	Lower Miocene
t_g:	同　上（同上）	〃　〃
B:	玄武岩	Basalt
A_1,A_2:	安山岩及集塊岩	Andesite-agglomerate
da:	石英安山岩	Dacite
L_p:	石英粗面岩	Quartz Porphyry
G:	花崗岩	Granite

Fig. 2. Geological map (after Miyagi Pref.) and Levelling route (G.S.I.)

地質図（宮城県発行による）と水準路線（地理調査所）

おける左岸には，景勝地材木岩と呼ばれている，主として石英安山岩よりなる見事な柱状節理の発達した cliff でその落差は 200m にも及び，天然紀念物に指定されている．これに対する右岸には石英粗面岩の大露頭が突出して迫り，ここに一つの狭窄部を形成している．しかしこの地震で相当量の崩壊があり，Fig. 5～Fig. 11 に見られるように曾ての岩場の美しい松の眺めはすつかり損われ，かつ一時は白石川をせき止める危険にさらされたが，無事であつたようである．

§3. 測量とその結果

この地震が一年前の秋田県二ツ井地震[5]と略々同規模であることは前に述べたとおりであつて，その震害等の状況から見て震央附近には当然，地震に直接関係ある一次的な地殻変動が発生する公算は極めて大きいように考えられた．何故ならばそれは二ツ井地震においては地形上の観察は不可能であつたけれども震央附近を過ぎる levelling route の検測によつて，15cm 程度の地震に直接関係すると考えられた垂直変位が発見され[6]，これを測地学的断層と呼んだからである．かつこれは活動褶曲構造の研究上興味ある問題を提供した．しかし白石市附近では前にも述べたように Fig. 3 に示す levelling route

Table I. Results of Levelling Survey. (Assum. BM. No. 2157 Fixed)

水準測量の結果

BM. No.	Loc.	ΔH_1 (1954)	ΔH_2 (1956)	$\Sigma\delta h$ $(\Delta H_2-\Delta H_1)$	Remark
				mm	
2157	Miya	*m*	*m*	0.0	不動と仮定
		+ 0,1956	+ 0,1944		
2156				−1.2	
		+ 7,1072	+ 7,1088		
2155				+0.4	
		+ 8,9220	+ 8,9221		
2154	Shiroishi			+0.5	
		+ 4,3288	+ 4,3258		
2153				−2.5	
		+12,9795	+12,9766		
2152				−5.4	
		+13,1800	+13,1781		
2151	Saikawa			−7.3	
		+50,8566	+50,8602		
2150				−3.7	
		+16,7025	+16,7051		
2149				−1.1	
		+34,8480	+34,8492		
2148	Kosugo			+0.1	
		−29,4906	−29,4918		
2147				−1.1	
		−73,1297	−73,1298		
2146				−1.2	
		− 5,7300	− 5,7307		
2145	Fujita			−1.9	

ΔH_1 は 1954 年 G. S. I. 測量結果より．(ΔH_1; 1954, G. S. I. Levelling data)

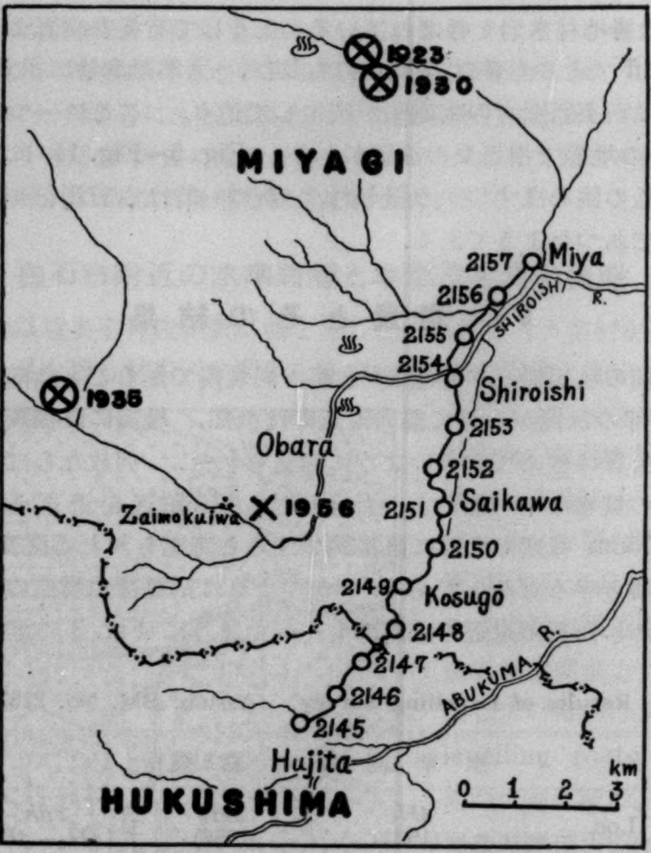
1923
1930
MIYAGI
2157
Miya
2156
SHIROISHI R.
2155
2154
Shiroishi
1935
2153
Obara
2152
2151
Saikawa
Zaimokuiwa
1956
2150
2149
Kosugō
2148
2147
ABUKUMA R.
2146
2145
Hujita
HUKUSHIMA
km
0 1 2 3

Fig. 3. Route map of G.S.I. Bench Marks near Shiroishi City

白石市附近の水準路線図

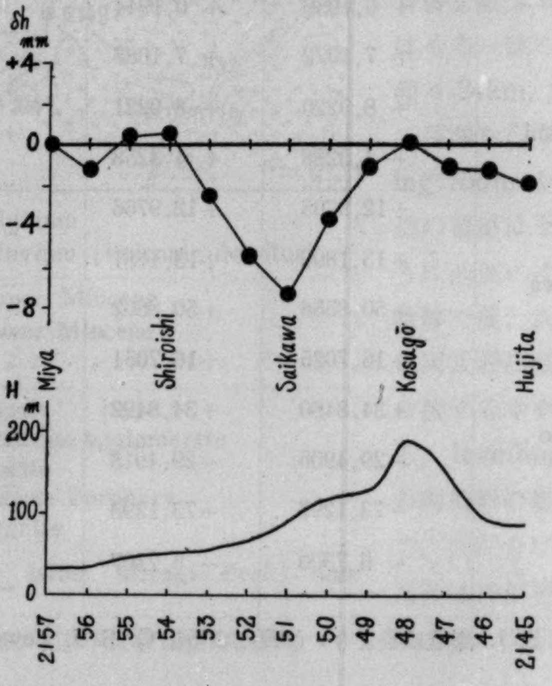

Fig. 4. Vertical displacement (upper) and true heights (lower) of Bench Marks in the neighbourhood of Shiroishi City.

について検測を行つた結果，1954年度に地理調査所で実施された結果との比較を白石市北方6km宮(B.M. No. 2157)を不動と仮定して，白石市を経て斎川，越河峠を越えて福島県藤田に至る13箇のBench Markの垂直変動量はTable I, 及びFig. 4に示したとおりである．ここでFig. 4の変動曲線からB.M. No. 2157を不動と仮定したとき，斎川附近において，約1cm未満の相対的な沈下を認めることが出来るがそのほか特別顕著な変化は表われているとは思えない．検測が行われたlevelling routeの経路，震央との相対的位置の関係に左右されて，一方的に解釈することは甚だ困難でもあり危険なことであるが，秋田二ツ井地震とはやや事情を異にしてる．一般に過去における日本の内陸に発生した地震の地殻変動の特徴として，垂直変位に関する限り，地質学的構造断層(或は測地学的地震断層)か又は，震央附近の限られた範囲における相対的な隆起の現象の何れかに帰するものであるが，此の地域ではlevelling routeが比較的震央に接近している割合には，異つた傾向を示していることに注目しなければならない．いわば蔵王火山群と阿武隈台地の縁辺に狭まれた部分の，震央に最も近いと思われる附近に，垂直変動の凹部が対応し．僅かな沈下が表われたと見るべきかも知れない．勿論水平方向の変動すなわち位置の水平変位は全く未知であつてむしろこの方が垂直変位を上回ることもあり得るのであるが，小地域の地震についてこの方面の研究は費用と困難を伴うので未だ殆んど充分に行われていない．従来阿武隈川下流附近には太平洋岸を含めて多数の地震が発生しており，これらの地震の相関性については良く知られていない．ただ今回の地震とやや関係のありそうなものは過去30年間数回あり，何れも蔵王火山周辺における局発性地震で鳴動を伴つている[7][8]．特に1935年6月下旬の七ヵ宿村より小原村にかけて起つた地震は続発生のものであつた．何れも火山活動とは一応無関係であるが，火山地帯周辺に発生する特別なものではなかろうかといはれている．若し白石川に沿つて上流に向い，東西に延びるlevelling routeを設けて調査することと，此の附近の三角点について水平位置の相対変位を測定することが出来るならば，或は地震と密接な関係ある地殻変動の実体を解明する有力な手がかりを得られるのではなかろうか．

§4. あとがき

地震による地上の被害状況や，観察された地震による地変と，計測された震度等から，地殻変動が生じたのではなかろうかと期待されたが，精密水準測量の結果では垂直変動に関する限り余り顕著なものは発見することができなかつた．ただしやや少量ではあつたが異つた様子を示す変動が認められた．特に地理調査所における前回の測量が，東京—青森間を結ぶMain routeとして2年前の1954年度に実施されて[9]，比較的短い

---

5) 島　悦三・柴野睦郎 *loc. cit., 2)*.
6) 宮村摂三・岡田　惇 *loc. cit., 3)*.
7) 加藤愛雄 Zisin, [i] **17** (1935) 473-484.
8) 田中館秀三 Zisin, [i] **17** (1935) 485-492.
9) 地理調査所　一等水準点検測成果集録 第二巻 昭和30年8月.

期間についての比較が得られたことは非常に有益であつた．1954年度以前の変化については水準点そのものの故障が大多数で，この附近の傾向を仔細に調べることができなかつた．今回の結果より僅少であるが震央近くで沈降の現象を示したのは，此の附近にしばしば発生する局発性地震に伴ふものか，或は別の暗示を意味するものか，それは残された問題であつて，地震計測より求められた震央域に比較的接近した地域に，地震に関係あるかと思われる凹部が表われていることは事実であり注目に値する．

終りに此の調査に御指導を賜つた地震研究所長那須信治教授，並びに宮村摂三助教授に厚く御礼を申上げる．出張に際し種々御助力下さつた実川顕技官，仙台管区気象台渡辺偉夫技官に感謝する．又現地においては宮城県土木部の方々に多大の御援助を戴いた．ここに謝意を表したい．

---

4. *Shiroishi Earthquake of Sept. 30th, 1956, and Precise Levelling Resurvey of its Epicentral Area, Miyagi Prefecture.*

By Atsushi OKADA,

Earthquake Research Institute.

A severe earthquake occurred on Sept. 30th 1956, in the vicinity of Shiroishi City in Miyagi Prefecture, North eastern Japan. (Fig 5) The intensity and magnitude of the earthquake were *V* (J.M.A. intensity scale) and 6.1 (Gutenberg-Richter magnitude) respectively. The earthquake was felt in an area of about 260 km in maximum radius, with the epicenter located in the southern part of Obara village near Shiroishi City. (Fig. 2 and Fig. 3) Landslides and some damage to houses and other constructions were caused by the earthquake in the epicentral area. (Photographs)

With the object of finding out only vertical crustal displacement caused by the earthquake, a levelling resurvey of the G. S. I. bench marks was carried out by the auther on the route running for about 24 km through the epicentral area. (Fig. 3) The results of the survey are shown in Table I and Fig. 4. Fig. 4 shows that the epicentral area underwent a little downward movement (less than 1 cm) during 1954–1956.

The present earthquake differs in this respect from the past inland earthquakes of Japan, in most of which the epicentral area except for alluvial subsidences showed an upheaval movement with or without faulting.

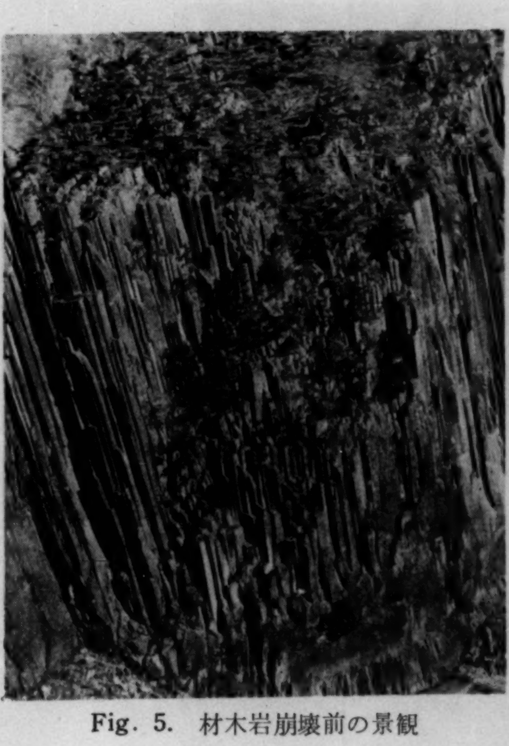

Fig. 5. 材木岩崩壊前の景観

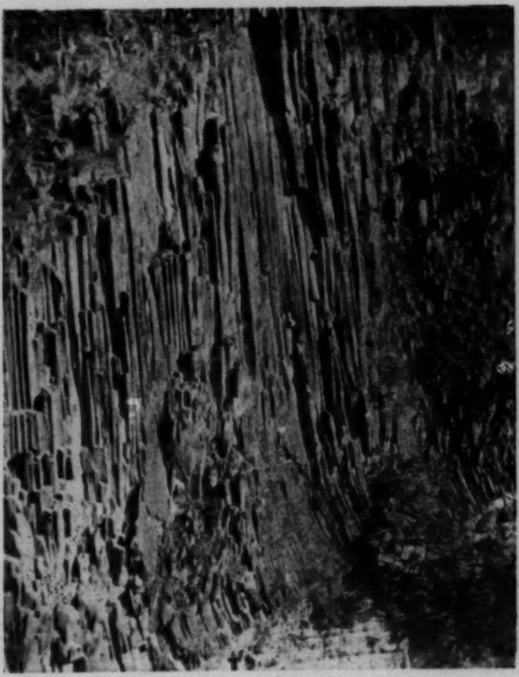

Fig. 6. 材木岩崩壊前の景観

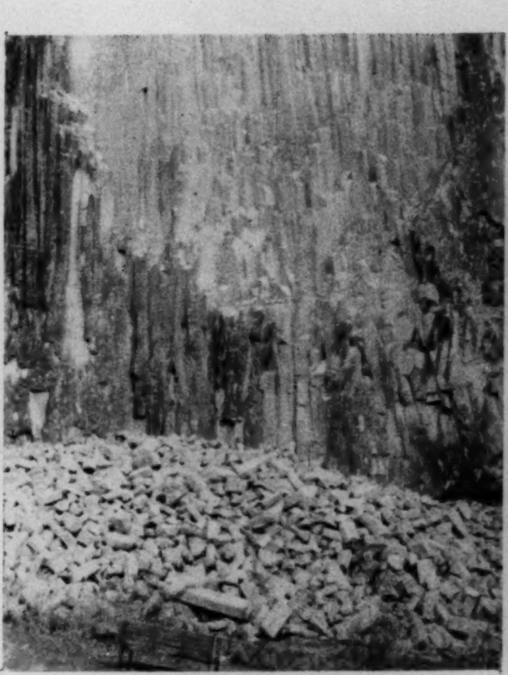

Fig. 7. 地震による崩壊

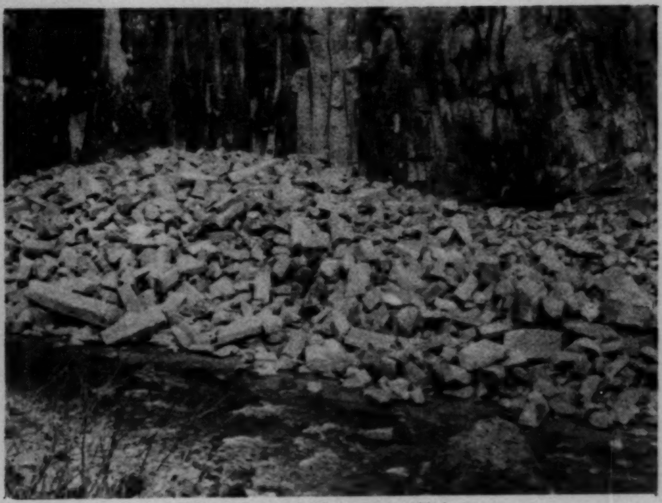

Fig. 8. 地震による崩壊

（震研彙報 第三十六号 図版 岡田）

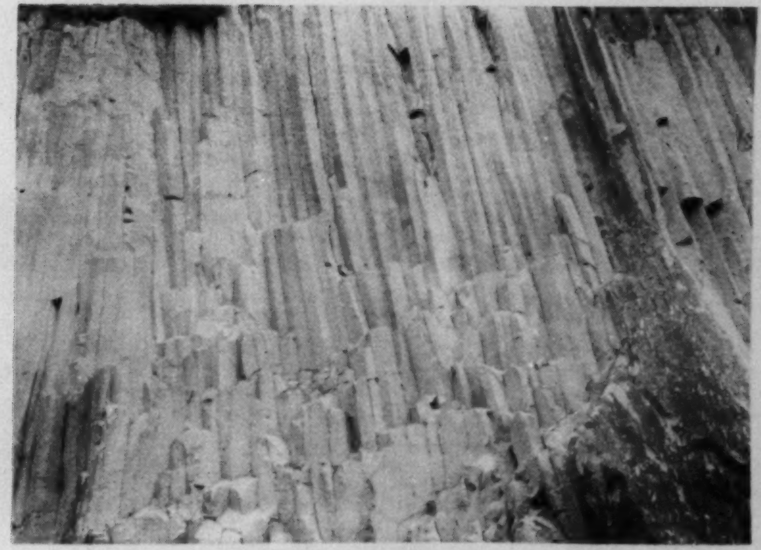

Fig. 9.　崩壊面

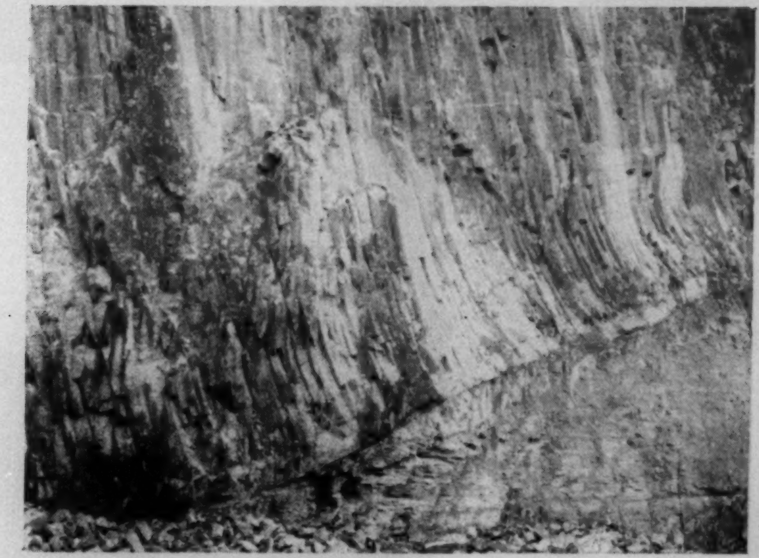

Fig. 10.　同　上

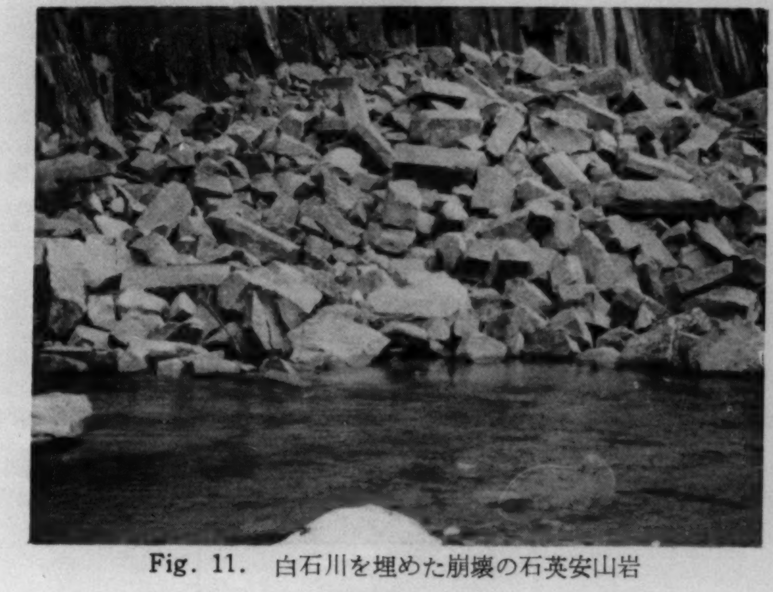

Fig. 11.　白石川を埋めた崩壊の石英安山岩

（震研彙報　第三十六号　図版　岡田）

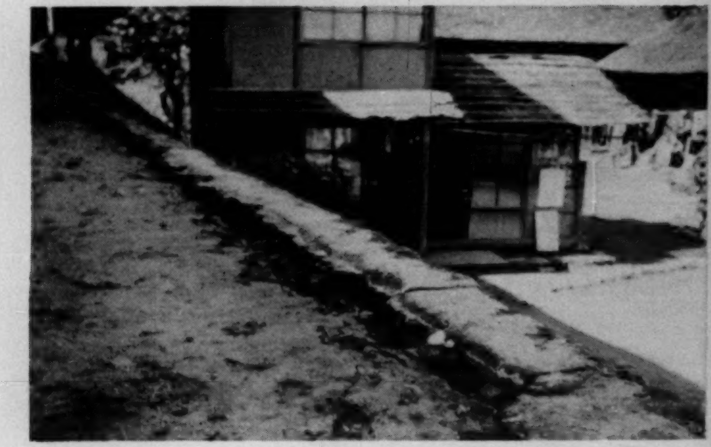

Fig. 12. 白石市内における亀裂

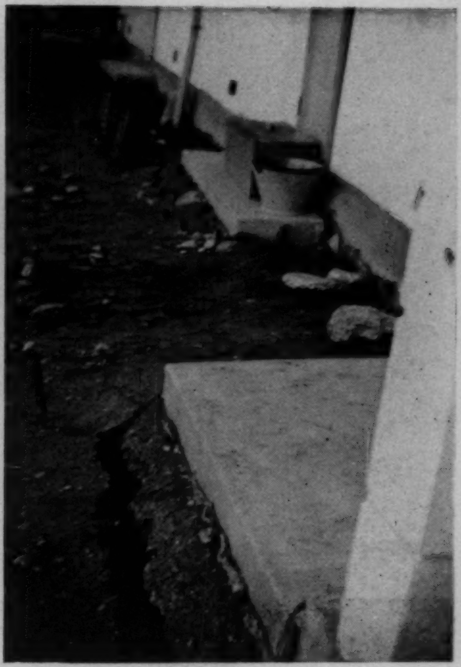

Fig. 13. 建物附近の地割れ
（市営アパート）

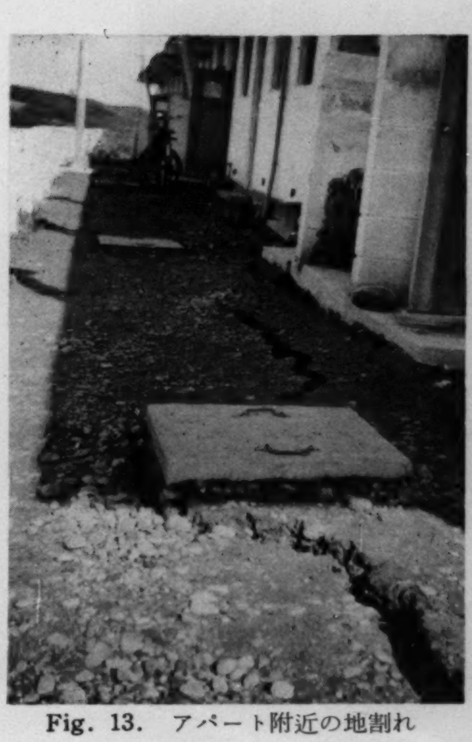

Fig. 13. アパート附近の地割れ

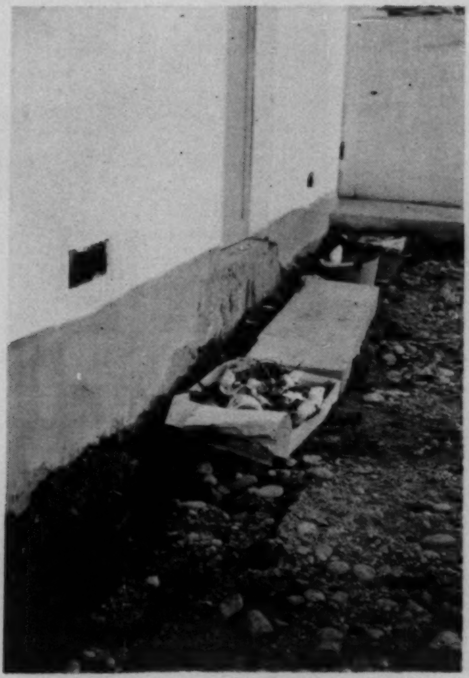

Fig. 14. アパート基礎の破壊

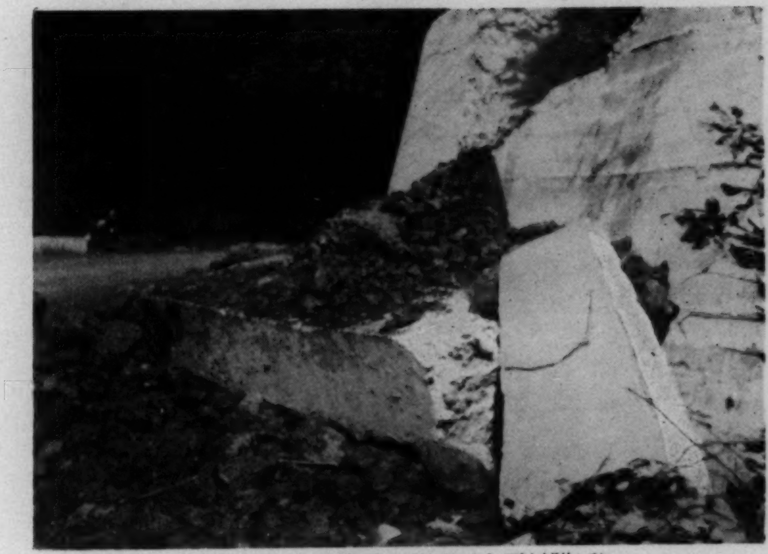

Fig. 16. 土砂止築堤の崩壊（小原村附近）

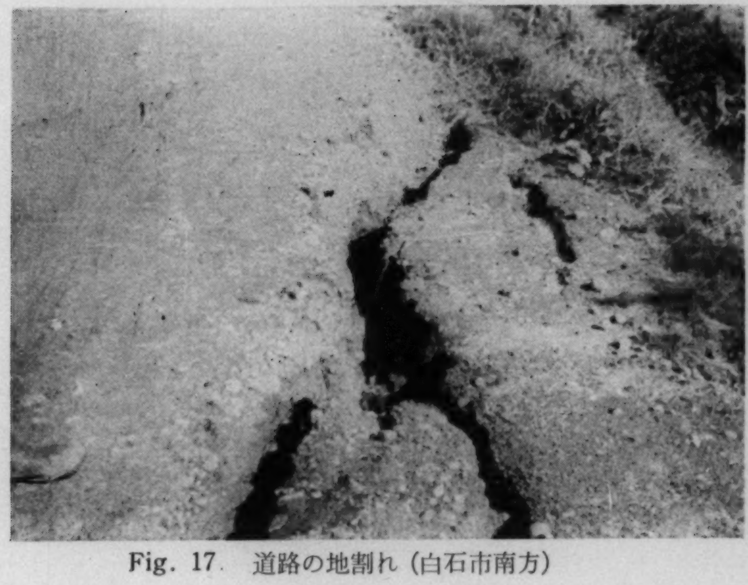

Fig. 17 道路の地割れ（白石市南方）

（震研彙報 第三十六号 図版 岡田）

昭和33年5月5日印刷
昭和33年5月10日発行

東京都文京区本富士町一番地
東京大学構内
編纂兼
発行者　東京大学地震研究所

東京都千代田区富士見町一丁目十番地
印刷者　笠井康頼

東京都千代田区富士見町一丁目十番地
印刷所　株式会社　国際文献印刷社

売捌所
東京都中央区日本橋通二丁目六番地
丸善株式会社

Sold by Maruzen Co., Ltd., Nihonbashi-dôri, Chûô-ku, Tôkyô.
Price of this copy: 232 Yen. (Postage exclusive.)

BULLETIN OF

THE EARTHQUAKE RESEARCH INSTITUTE

UNIVERSITY OF TOKYO

Vol. 36, Part 1. March, 1958.

Contents.

Papers and Reports.

Page

1. T. RIKITAKE, I. YOKOYAMA, S. UYEDA, T. YUKUTAKE and E. NAKAGAWA, The Anomalous Behaviour of Geomagnetic Variations of Short Period in Japan and Its Relation to the Subterranean Structure. The 7th report. (in English).... 1
2. K. KASAHARA, The Nature of Seismic Origins as Inferred from Seismological and Geodetic Observations (2). (in English)........ 21
3. T. MATUMOTO, Calibration of an Electromagnetic Seismograph by Means of the Frequency Analysis. (in English)........ 55
4. A. OKADA, Shiroishi Earthquake of Sept. 30th, 1956, and Precise Levelling Re-survey of its Epicentral Area, Miyagi Prefecture. (in Japanese)........ 65

(For the papers written in Japanese or in occidental languages, the abstracts are given in occidental languages or in Japanese respectively.)

BULLETIN OF THE EARTHQUAKE RESEARCH INSTITUTE,
UNIVERSITY OF TOKYO. Vol. 36, Part 2. June, 1958.

東京大學
地震研究所彙報

第 36 號　第 2 冊

昭和 33 年 6 月

目　次

論文及報告

頁

5. 近地地震波動のスペクトル的研究 (1) (英文) …… 安芸敬一・辻浦賢・堀実・後藤健一 71
6. 火山の噴火とその周辺の地殻変動との関係 (英文) …… 茂木清夫 99
7. ¹⁴C による地球化学的研究 (II) 火山噴出物の年代および泥炭の沈積速度について (英文) …… 島誠・南英一 135
8. 電磁地震計の倍率その他について (英文) …… 萩原尊礼 139
9. 鉄筋コンクリート造建物の振動実験 (英文) …… 金井清・岸上冬彦・那須信治・河角広 165
10. 建物の動揺，弾性振動 第 1 報 (起振機による振動実験) (英文) …… 金井清・田中貞二・鈴木富三郎 183
11. 建物の動揺，弾性振動 第 2 報 (地震観測) (英文) …… 金井清・田中貞二・鈴木富三郎 201
12. 1894 年の庄内地震の研究 (邦文) …… 岸上冬彦 227
13. 木造家屋の耐震性 (第 2 報) (自然地震の観測) (邦文) …… 鈴木正治 235

所　報

(The titles in occidental languages are given on the back cover.)

地震研究所彙報は，年4回定期に（ただし，第1号より第6号までは不定期に，第7号は3冊として刊行された），彙報別冊は不定期に刊行される．

この彙報に載せちれた論文及び報告についての責任は，すべてその著者のみにある．

この彙報についての照会通信は，すべて東京大学地震研究所長にあてられたい．

The Bulletin is published quarterly. (Vols. 1–6 were published at irregular intervals and Vol. 7 consisted of three parts.)

Supplementary Volume is published at irregular interval.

The authors of the papers alone are responsible for the statements and opinions contained in their respective papers.

All communications relating to this Bulletin should be addressed to the Director of the Earthquake Research Institute, University of Tokyo, Japan.

Earthquake Research Institute, University of Tokyo
Address:
No. 1, Motofuji-cho, Bunkyo-ku,
Tokyo Metropolis, Japan.
Telephone: 92-3161-Extension 6506
Cable address: ZISINKEN, TOKYO.

東京大学地震研究所
所在地
東京都文京区本富士町一番地
電話 小石川 92—3161（代）構内 6506
電略 ブンケウ トウダイ チシン

BULLETIN OF THE EARTHQUAKE
RESEARCH INSTITUTE
Vol. 36 (1958), pp. 71-98

5. *Spectral Study of Near Earthquake Waves (1).*

By Keiiti AKI, Masaru TSUJIURA, Minoru HORI and Kenichi GOTÔ,

Earthquake Research Institute.

(Read January 28, 1958.—Received March 31, 1958.)

1. Introduction

Many studies have been made of complicated seismograms of near earthquakes from the viewpoint of "phase", but we do not yet have any satisfactory knowledge about the nature of the waves prevailing over various portions of such seismograms. For instance, the vibrations following the initial *P* wave called preliminary tremors are believed by some to be the mixture of waves which started from the origin at the same time as the initial *P* wave and travelled along a number of different paths, while others believe that they are secondary waves, whether surface waves or local surface vibrations, generated at some places by the incidence of primary waves coming from the origin. Also, it is not impossible to presume that they are primary waves which have travelled along the same path as the initial *P* wave, and are due to the events which occurred after the initial breakdown at the origin of earthquake.

The question of this kind may be asked about every portion of a near earthquake seismogram, especially about the origin of its coda portion. The reason why those questions can not yet be settled seems to be owing to the lack of an appropriate method of dealing with such complicated waves.

Recently one of the present writers, K. Aki[1] (1957), proposed a useful method of revealing the nature of these complicated waves, and applied it successfully to microtremors in the city area. Since in the method the relation between the spatial spectrum and the frequency spectrum of waves plays an important part, it is necessary to assume the waves in question as stationary in space and time at least within the range to be studied. This assumption represents quite an opposite extremity when compared with that underlying the ordinary "phase" method. An earthquake wave as a whole is certainly not stationary in time, but it may be possible to divide the wave into consecutive portions, within each of which the wave can be safely assumed as stationary.

---

[1] K. AKI, *Bull. Earthq. Res. Inst.*, **35** (1957), 415–456.

The present paper is a preliminary report in which an application of the spectral method is attempted for seismic waves of near earthquakes in order to give an answer to the above question.

A tripartite system of seismometers were set up at Kamakura, in Kanagawa Prefecture. The vibrations of three seismometers caused by earthquakes are recorded simultaneously, by the use of a frequency modulation, on a magnetic tape. The analyses according to the method are applied to the vibrations, reproduced afterwards in our laboratory, with the aid of filters and a correlation computer.

2. Method of Analysis

Our method may be divided into two steps; first a filtration by a resonator having an assigned frequency f_0 is applied to ground vibrations recorded by three seismometers of the tripartite system; secondly, the correlation coefficient is computed between each pair of the filtered vibrations.

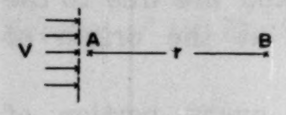

Fig. 1.

Suppose that two seismometers are placed as shown in Fig. 1 r meter apart from each other, and that a plane wave having velocity V and direction parallel to AB are passed through the place, the correlation coefficient corresponding to a particular frequency f_0 of the resonator will take the form,

$$\rho(r, f_0) = \cos\left(2\pi \frac{r f_0}{V}\right). \tag{1}$$

This equation shows that we can determine the value of velocity V by computing the correlation for various frequencies.

It was shown by Aki (1957) that Eq. 1 also holds for a dispersive wave only by the substitution of $V(f)$, velocity as a function of frequency, for the constant V.

Further, it was shown that if the wave is composed of partial waves having different velocities V_n's, the corresponding correlation coefficient will take the form

$$\rho(r, f_0) = \sum_n \frac{P_n(f_0)}{P(f_0)} \cos\left(2\pi \frac{r f_0}{V_n}\right) \tag{2}$$

where $P(f_0)$ and $P_n(f_0)$ are the power of the composite wave and that of the nth partial wave respectively.

If we do not know the direction of propagation of the wave in question, we need at least three seismometers in order to determine its direction and velocity. Supposing that a plane wave is propagated through the tripartite system as shown in Fig. 2, we shall have correlation coefficients for three pairs of seismometers as follows,

$$\left.\begin{aligned} \rho_{12}(r,f_0)&=\cos\left(2\pi\frac{r_{12}\cos(\theta_0-\theta_{12})}{V}f_0\right)\\ \rho_{23}(r,f_0)&=\cos\left(2\pi\frac{r_{23}\cos(\theta_0-\theta_{23})}{V}f_0\right)\\ \rho_{31}(r,f_0)&=\cos\left(2\pi\frac{r_{31}\cos(\theta_0-\theta_{31})}{V}f_0\right)\end{aligned}\right\}. \tag{3}$$

Hereafter we shall call these correlation coefficients as functions of resonator frequency f_0 simply " correlation curves ". Introducing a " characteristic frequency " f^*, which is defined by

$$\rho(r,f_0)=\cos\left(2\pi\frac{f_0}{f^*}\right) \tag{4}$$

and which can be at once found by the inspection of correlation curve obtained, we can write the apparent velocities along the three lines as

$$\left.\begin{aligned} V_{12}&=\frac{V}{\cos(\theta_0-\theta_{12})}=r_{12}f_{12}{}^*\\ V_{23}&=\frac{V}{\cos(\theta_0-\theta_{23})}=r_{23}f_{23}{}^*\\ V_{31}&=\frac{V}{\cos(\theta_0-\theta_{31})}=r_{31}f_{31}{}^*\end{aligned}\right\}. \tag{5}$$

If the values of f_{12}^*, f_{23}^* and f_{31}^* are found from the correlation curves, the velocity V and azimuthal angle θ_0 of wave propagation will be determined by the use of a graphical mothod as shown in Fig. 3 or that in Fig. 4. In both figures *OP* is the velocity vector giving the direction and velocity of wave.

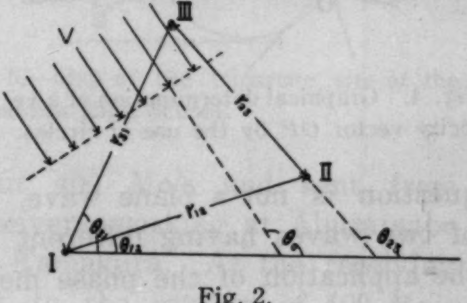

Fig. 2.

Here should be noted two essential differences between the direction determination by the present method and that by the ordinary " phase " method.

In the latter method, by observing the arrival times of a particular phase at three points, we get the apparent velocities

$$
\begin{aligned}
V_{12}&=r_{12}/(t_1-t_2)\\
V_{23}&=r_{23}/(t_2-t_3)\\
V_{31}&=r_{31}/(t_3-t_1)
\end{aligned}
\qquad (6)
$$

From these equations and Eq. 5, it can be seen that the values of apparent velocities obtained by the spectral method cannot be negative, while those determined by the phase method can be negative as well as positive. This means that the spectral method cannot give us the polarity of velocity vector, but the phase method can.

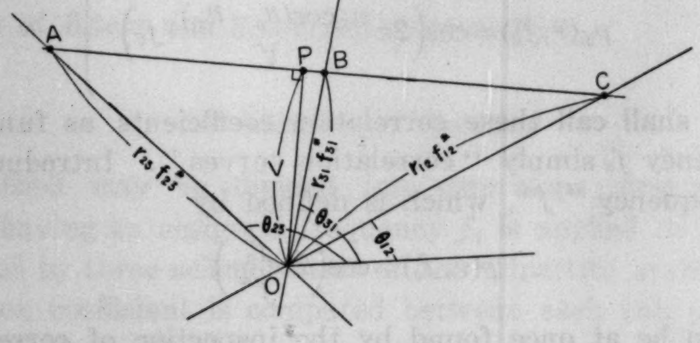

Fig. 3. Graphical determination of a velocity rector (*OP*).

The other essential difference between the two methods is that the three apparent velocities are obtained independently of one another in the case of the spectral method, while those obtained by the phase method are dependent as seen from Eq. 6. In other words, by the use of the phase method we always get a definite velocity and direction even if the wave in question is not a plane wave. For instance, if the wave is a mixture of two waves having different velocities and directions of propagation, the application of the phase method, if possible at all, will yield a single direction and a single value of velocity which differ from those of the two component waves. On the other hand, in the spectral method, by examining the correlation curves and finding the two characteristic fre-

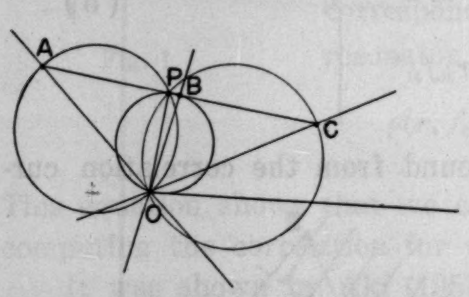

Fig. 4. Graphical determination of a velocity vector *OP* by the use of circles.

quencies corresponding to the two component waves from each of the curves, we can obtain velocity vectors for both waves, even though we cannot determine the polarity of vectors.

As we are using information involved in waves having a certain range of frequency, it is preferable that the frequency spectrum of the wave is flat over the range to be analysed. If the prevailing frequencies of wave have a narrow range, longer spans of tripartite should be taken. The choice of length of span also depends on the velocity value of wave to be studied and may be determined by the following relation

$$\frac{r\Delta f}{V} \approx 1 \qquad (7)$$

where Δf is the range of frequency over which the wave has enough power to be analysed.

3. Observation and Analyses

For the purpose stated in the preceding sections, we set up a tripartite system of seismometers in the grounds of Kamakura High School in August 1957 and made observations for about a month. Seismometers were placed in caves which were dug into a cliff of sandstone behind the school. A map of the tripartite site is shown in Fig. 5. The seismometers used are moving coil type transducers sensitive to vertical motion, and have free frequency of about 3cps.

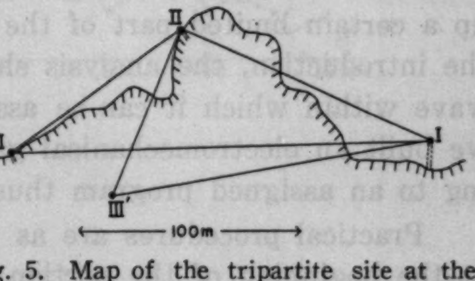

Fig. 5. Map of the tripartite site at the Kamakura High School.

Signals coming from the seismometers are sent to amplifiers through wires, and after appropriate amplification, are frequency modulated by carriers of audiofrequency.

The modulated signals are again frequency-modulated by carriers of about 400 Mc/s and sent from transmitters as radio waves to the receivers working at Aburatsubo which is located about 19 km apart from Kamakura. At the receiving station, after demodulation with respect to the carriers of 400 Mc/s seismometer signals are recorded on a magnetic tape having two tracks, in such a way that the signal modulated by the carrier of 2800 cps and that by one of two carriers having frequency 800 cps are recorded on one of the tracks, and the signal modulated by the remaining carrier of 800 cps on the other.

In fact, for the present purpose we do not need the wireless part in the above arrangements. The use of this part in this study is merely due to the circumstance that the present observation is made as a part of a comprehensive study on seismicity of the Southern Kanto District conducted by Assoc. Prof. S. Miyamura of our Institute, and that the apparatus used is the UHF radio telerecording seismograph, RTS-II, made by S. Miyamura and M. Tsujiura[2] (1957).

The recording was made by using an endless reel having a very simple structure. The tape enclosed in the reel works as long as 7 minutes for a speed of 7.5 inches per second.

During the period of observation, the taperecorder is continuously in action waiting for an earthquake, and when one takes place, it is made to stop by means of a delayed trigger circuit after recording of waves.

The record of earthquake motions stored in the endless magnetic tape are brought to the laboratory, and analysed by the apparatus mentioned before. The filter used for this analysis is of phase shift type and its resonance frequency covers the range from 3.5 cps to 20 cps. Explanation of this filter and also of our correlation computer were given in the paper of K. Aki (1957) referred to before. Besides, in the analysis of an earthquake wave, we need an apparatus which can pick up a certain limited part of the seismogram, because as mentioned in the introduction, the analysis should be applied to the portion of the wave within which it can be assumed as stationary. For this purpose, we built an electromechanical gate which is opened and closed according to an assigned program thus controlling the operation of computer.

Practical procedures are as follows: at first we set the gate to open at the beginning of the portion of the seismogram to be studied and to close at its end; a pair of seismic signals, which are reproduced from the tape recorder and demodulated, are put into a pair of filters which are adjusted to have the same and assigned resonance frequency f_0 and Q value; after the filtration both signals are put into the correlation computer which works under the control of the gate; the result of computation is shown on the decatron indicators; and the same operation as above is applied to the other two pairs of signals.

---

[2] S. Miyamura and M. Tsujiura, *Bull. Earthq. Res. Inst.*, **35** (1957) 381-394.

Repeating the above procedures for various frequencies of the filter, we can obtain a set of three correlation curves, which indicate the characteristics of the wave portion in question in the way explained in the preceding section.

4. Interpretation of Actual Correlation Curves

As shown in Eq. 1, for the wave portion having a single definite velocity the correlation curve becomes a cosine function of the resonator frequency. The correlation curves obtained by actual earthquake wave parts, however, do not take such a simple form, but almost always indicate that they are composed of partial waves having different velocities in spite of the circumstance that the time intervals of the portion into which the waves are divided are taken as short as 1.5 to 3 seconds.

Typical examples of the curves are shown in Fig. 6a and Fig. 6b.

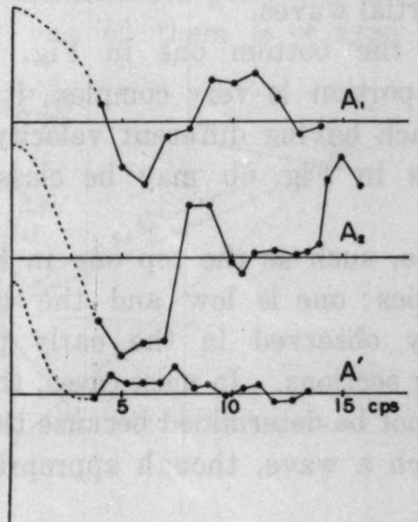

Fig. 6a. Typical correlation curves for wave portions having no component waves of high velocity.

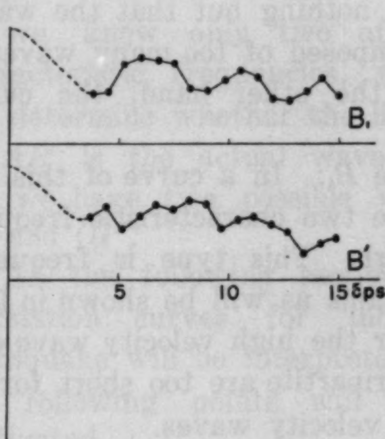

Fig. 6b. Typical correlation curves for wave portions involving high velocity waves.

There is a marked difference between the curves in Fig. 6a and those in Fig. 6b. Each of the latter curves are shifted upward from the zeroline, suggesting that the wave portion concerned has a partial wave of very high velocity. On the other hand the former curves do not indicate such a shift and run on the negative side as much as on the positive.

Type A_1: Of the curves in Fig. 6a, the top one has a nearly sinusoidal form, even if the absolute values of the maximum and minimum are considerably lower than unity, and we can learn from them a single characteristic frequency f^*, referred to in Section 2. This type of curve is specified by A_1.

Type A_2: Sometimes, we can find two characteristic frequencies from a single curve. The second one in Fig. 6a is an example of this type. As can be seen from Eq. 2, the correlation curve for a wave consisting of two partial waves takes the form,

$$\rho(r, f_0) = \frac{P_1(f_0)}{P(f_0)} \cos\left(2\pi \frac{f_0}{f_1^*}\right) + \frac{P_2(f_0)}{P(f_0)} \cos\left(2\pi \frac{f_0}{f_2^*}\right) \quad (8)$$

$$P(f_0) = P_1(f_0) + P_2(f_0) \ .$$

Therefore, if $P_1(f_0)$ and $P_2(f_0)$ vary with f_0 only slightly, we can obtain from the correlation curve the value of characteristic frequency and the fraction of power for each of the partial waves.

Type A': From such a curve as the bottom one in Fig. 6a, we can say nothing but that the wave portion is very complex, it is possibly composed of too many waves each having different velocity.

On the other hand, the curves in Fig. 6b may be classified as follows.

Type B_1: In a curve of this type, such as the top one in Fig. 6b, there are two characteristic frequencies; one is low and the other is very high. This type is frequently observed in the early parts of seismograms as will be shown in later sections. In most cases, the value of f^* for the high velocity wave cannot be determined because the spans of our tripartite are too short for such a wave, though appropriate for the low velocity waves.

Type B': From a curve such as the bottom one in Fig. 6b the characteristic frequencies can not be found for both low and high velocity waves, but the fraction of power for the high velocity wave can be estimated approximately by the inspection of the curve.

All of the correlation curves obtained can be classified into the above five types. The next step will be then to find velocity vectors by means of a graphical method such as shown in Fig. 3 or Fig. 4. If the wave portion investigated is an ideal plane wave, the points A, B and C in Fig. 3 should lie on a straight line which indicates the wave front, or the three circles in Fig. 4 should intersect at a point P. On the other hand, if the wave is not unidirectional, the points in Fig. 3 will not lie on a straight line, nor will the circles in Fig. 4 intersect at a point.

In an actual earthquake wave, some of the wave portions are fairly well unidirectional, while others show departures from the ideal plane wave. The degree of departure from the ideal plane wave may be measured roughly by the area of hatched domain surrounded by three arcs such as shown in Fig. 7. If the wave portion is perfectly unidirectional this domain is reduced to a point.

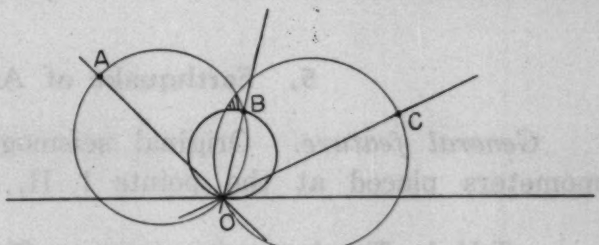

Fig. 7. The degree of departure from the ideal plane wave may be measured roughly by the area of hatched domain.

It happens, though not often, that for a particular wave portion the three correlation curves corresponding to three seismometer pairs can not be classified as the same type; for instance, one of them is of type A', while the other two are both of type A_1. As can be seen in Fig. 8, if we know only two of three characteristic frequencies, we can not determine whether the line AB or AB' is the actual wave front, and we have two possible vectors, OP and OP'.

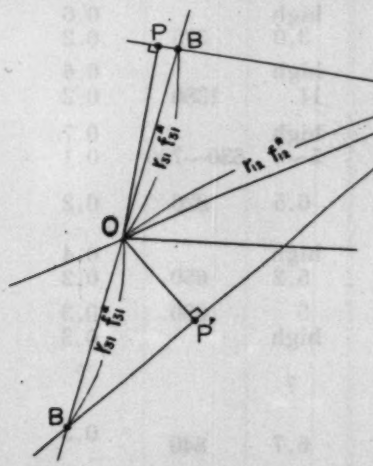

Fig. 8. Possible two velocity vectors OP and OP'.

In the following sections, the correlation curves for individual earthquake will be interpreted, and the following points will be investigated.

1. *General features* The general features of correlation curves are described with reference to the original seismograms from which the curves are reduced.

2. *High velocity waves* The value of velocity and the fraction of power for the high velocity waves are investigated.

3. *Velocity vectors of low velocity waves.* Velocity vectors are derived for low velocity waves whenever possible. If a wave portion is not unidirectional, the degree of departure from the ideal plane wave will be measured roughly by the area of domain surrounded by arcs

such as shown in Fig. 7. When we can get only two of three characteristic frequencies for a particular wave portion, two possible vectors are shown with question marks as in Figs. 12, 16, and 20.

It should be noted here again that we can not determine the polarity of velocity vectors in any case only by the spectral method. Our velocity vectors will be plotted on a half plane instead of a full plane.

5. Earthquake of Aug. 11, 1957.

General feature. Original seismograms, obtained from the seismometers placed at the points I, II, and III in Fig. 5, are shown in Fig. 9. The analysis is made of ten portions into which the seismograms are divided as shown in Fig. 9; each portion covers 3 seconds. Correlation curves from them are shown in Fig. 10. At first sight, it can be seen that none of their forms is simply sinusoidal as is expected for an unidirectional wave having a single definite velocity. The curves for the earlier portions of the seismogram are of the types B_1 and B', while for the later portions the types A_1, A_2 and A' are predominant.

Tabl. 1. The characteristic frequency f^*, apparent velocity V along each line, and ratio of power borne by component waves.

	I—III			II—III			I—II		
Wave portion	f^* (cps)	V (mps)	Power ratio	f^* (cps)	V (mps)	Power ratio	f^* (cps)	V (mps)	Power ratio
1	70 10	13,600 1,950	0.7 0.2	high		∼1.0	high		0.8
2	5.4 high	1,050	0.4 0.2	high 6.2	590	0.4 0.4	high 3.0	375	0.6 0.2
3	high 13	2,530	0.4 0.1	high 6.0	570	0.5 0.1	high 11	1380	0.6 0.2
4	39 2∼3	7,600 400∼600	0.8 0.1	high 5.4	520	0.3 0.2	high 5∼6	630∼750	0.7 0.1
5	3	590	0.2	5.2	500	0.2	6.5	820	0.2
6	3.7	720	0.3	?		?	high 5.2	650	0.4 0.2
7	3	590	0.2	6	570	0.2	5 high	630	0.3 0.3
8	?		?	4	380	0.1	?		?
9	?		?	3	290	0.1	6.7	840	0.3
10	7	1380	0.2	5	480	0.1	2∼4 12	250∼500 1,500	0.3 0.2

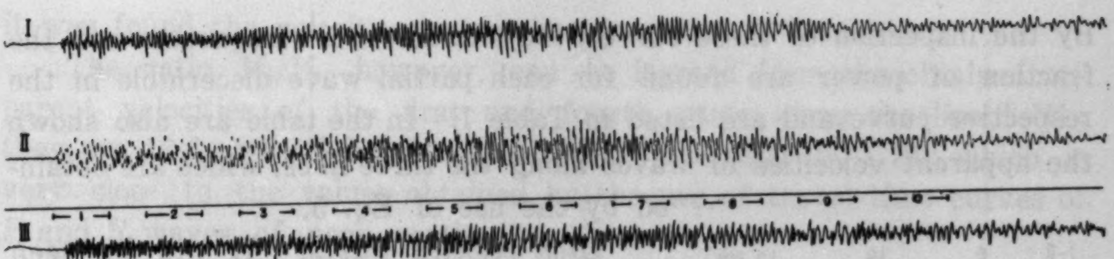

Fig. 9. Seismograms of the earthquake of Aug. 11, 1957.

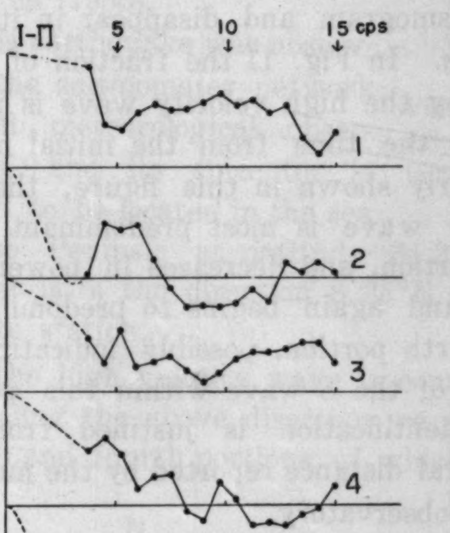

Fig. 10a.

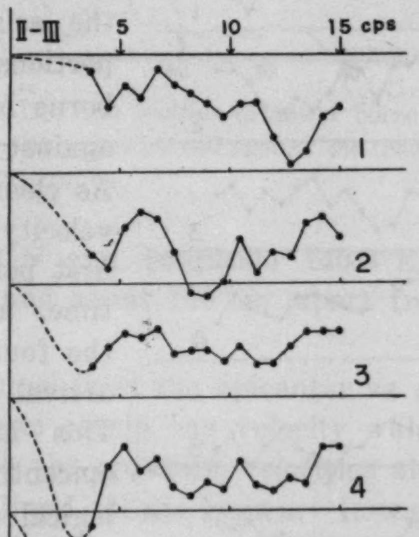

Fig. 10b.

By the inspection of these curves, the characteristic frequency and the fraction of power are found for each partial wave discernible in the respective curve and are listed in Table I. In the table are also shown the apparent velocities of waves along the three lines, which are obtained by the use of Eq. 5.

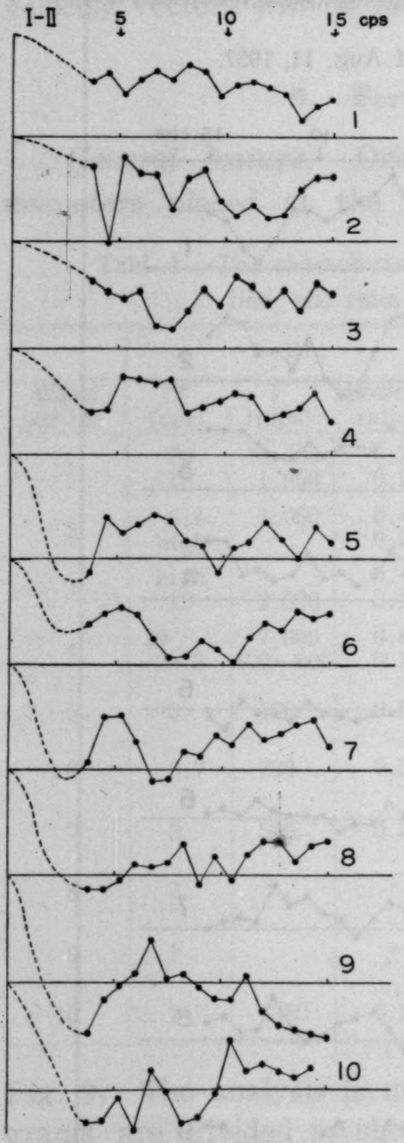

Fig. 10c.

High velocity waves. It can be seen from Table I that the high velocity wave is predominant in the earlier portions of the seismogram and disappear in its coda portions. In Fig. 11 the fraction of power borne by the high velocity wave is plotted against the time from the initial motion. As clearly shown in this figure, the high velocity wave is most predominant in the first portion, and decreases in power with time, and again begins to predominate in the fourth portion, possibly indicating the arrival of the *S* wave within this portion. This identification is justified from the epicentral distance reported by the meteorological observatory,

On the other hand, in the portions following the fifth portion the high velocity wave almost disappears. It is interesting to observe that these portions are relatively larger in amplitude than the preceding portions as shown in the seismograms.

The velocity of high velocity wave is often too high to be determined from the present analysis; this is partly owing to the lack of power in the waves in their range of frequency high than 15 cps and partly due to too short a length of span being taken for such waves.

This velocity, as well as direction of propagation, may be deduced from the arrival times of initial motion. Although this attempt also failed, because the arrival times for three seismometers coincide with each other within the range of error caused by the vagueness of the initial motion itself, it was found the velocity can not be lower than 5 kmps.

The ratio V_p/V_s, however, can be learned from the obtained apparent velocities of the first and fourth parts along the line I–III; they are 13.6 and 7.6 kmps respectively. The ratio is 1.79, which is very close to the values obtained by the use of travel time curves of P and S waves of near earthquakes, by Sagisaka (1931), Honda (1931) and Sagisaka and Takehama (1935).

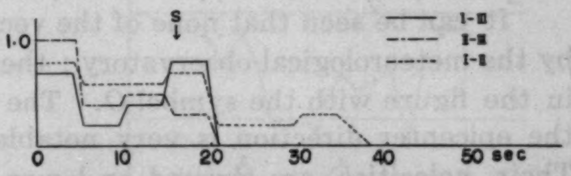

Fig. 11. The fraction of power borne by high velocity waves plotted against the time from the initial motion.

This earthquake was observed by the seismometer network of local meteorological observatories, and its epicenter is reported to be located in the sea off Boso Peninsla at latitude 34.2°N and longitude 140.3°E. This epicenter is in the direction S 35°E and about 150 km apart from our tripartite station.

If the high velocity wave is coming from the epicenter as a plane wave, using the above direction we can obtain the velocity values for the first and fourth portions, of which the apparent velocities along the line I–III are known. It was found that the velocity of the first portion is 7.4 kmps and that of the fourth 4.1 kmps, reasonable ones for P and S wave refracted critically at the Mohorovicic discontinuity.

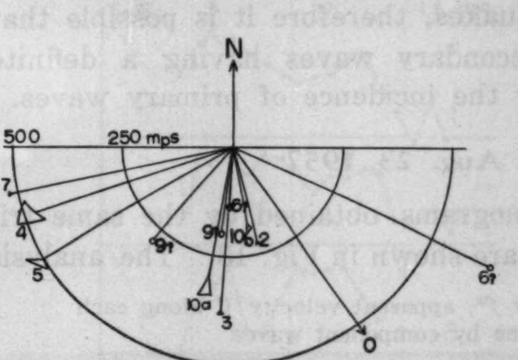

Fig. 12. Velocity vectors for low velocity waves.

Velocity vectors of low velocity waves. The velocity vectors of low velocity waves are obtained by the graphical method as illustrated in Fig. 4 and Fig. 7, and shown in Fig. 12. The area of domain surrounded by three arcs roughly measures the degree of departure from the ideal plane wave as referred to in the preceding section. The number attached to each vector indicates the number of the wave portion. For the sixth and nineth portions, only two of three characteristic frequencies are found, and two possible vectors with question marks are shown for each of them in Fig. 12. We could not find the vector for the first portion and for the eighth which are of the type B' and A' respectively.

Fig. 12 shows that the directions of low velocity waves can be grouped into two ; one is nearly N–S direction, and the other is nearly N 70°E–S 70°W. The portions 4, 5 and 7 belong to the latter, and their velocities are around 500 mps. On the other hand, the portions 2, 3, 10a, 10b and possibly 6 and 9 point to the N–S direction, and the velocity value ranges from 150 mps to 400 mps.

It can be seen that none of the vectors point to the epicenter reported by the meteorological observatory ; the direction of the epicenter is shown in the figure with the symbol *O*. The departure of their directions from the epicenter direction is very notable, but is not impossible to explain. Their velocities are around or lower than 500 mps, and the ranges of frequency is from 3 cps to 15 cps, so that their wave lengths are less than two hundred meters. Those waves must be generated at a very shallow part of the crust by the incidence of primary waves coming from the origin of earthquake, and have travelled through the shallow part to the observation point. Thus the topographical and geological heterogeneities over the very shallow part of earth's crust may cause notable refraction and scattering of the waves in the horizontal plane.

As will be seen in the following sections, the low velocity wave having direction of propagation nearly N–S and velocity value around 350 mps exists also in other earthquakes, therefore it is possible that there is a certain place at which secondary waves having a definite character are always generated after the incidence of primary waves.

6. Earthquake of Aug. 23, 1957

General features. Original seismograms obtained by the same tripartite station as the preceding one are shown in Fig. 13. The analysis

Table 2. The characteristic frequency f^*, apparent velocity V along each line, and ratio of power borne by component waves.

	I—III			II—III			I—II		
Wave portion	f^* (cps)	V (mps)	Power ratio	f^* (cps)	V (mps)	Power ratio	f^* (cps)	V (mps)	Power ratio
1.	high		∼1.0	high 5.5	530	0.8 0.2	high 6	750	0.6 0.3
2.	60 6.5	11,700 1,270	0.8 0.2	high		∼1.0	66	8,300	0.8
3.	high		0.4	high		0.5	high		0.6
4.	60 5	11,700 980	0.4 0.3	high 5.5	530	0.7 0.2	high		0.4
5.	9.5	1,850	0.4	5.5	530	0.4	9.0	1,130	0.4

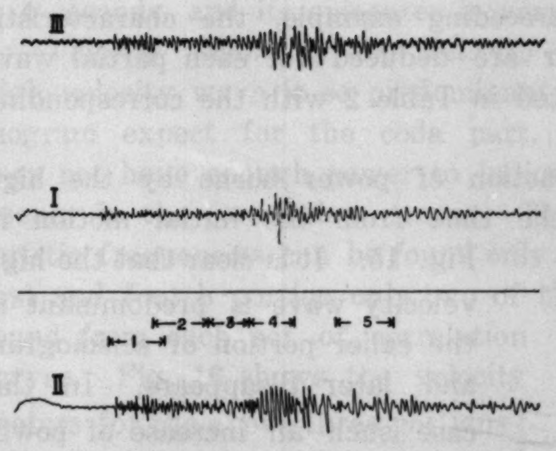

Fig. 13. Seismograms of the earthquake of Aug. 23, 1957.

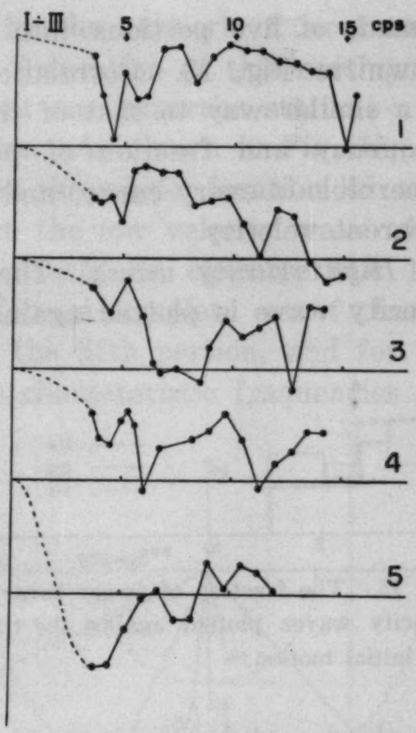

Fig. 14a.

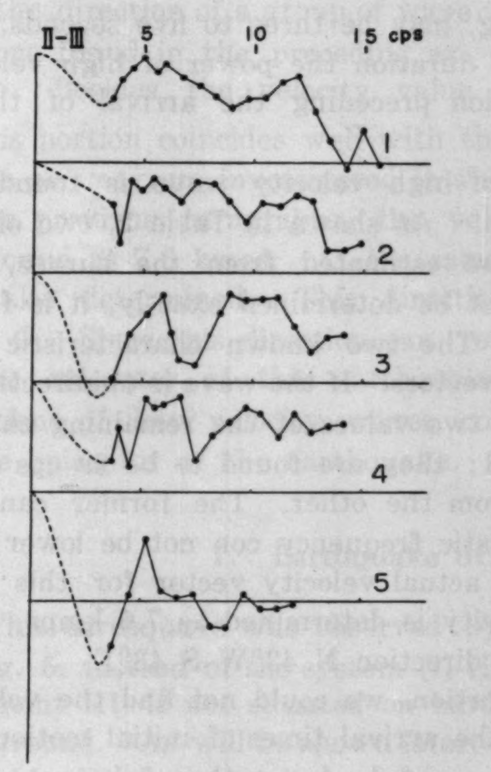

Fig. 14b.

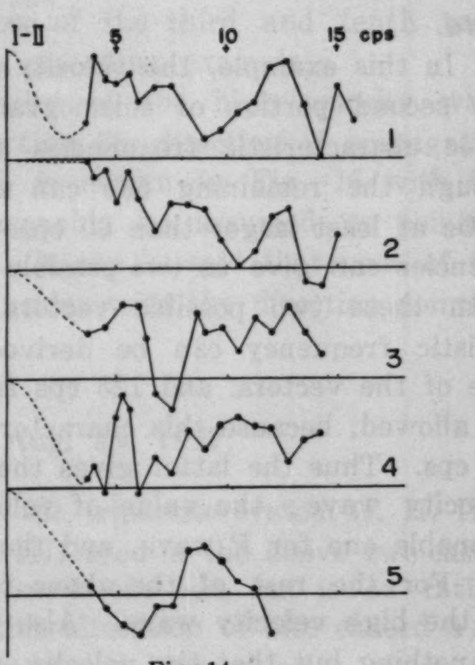

Fig. 14c.

is made of five portions into which the seismograms are divided as shown in Fig. 13. Correlation curves for them ares hown in Fig. 14. In a similar way to that of the preceding example, the characteristic frequency and fraction of power are deduced for each partial wave discernible in every curve, and listed in Table 2 with the corresponding apparent velocity.

High velocity waves. The fraction of power borne by the high velocity wave is plotted against the time from the initial motion in Fig. 15. It is clear that the high velocity wave is predominant in the ealier portion of seismogram and later disappears. In this case such an increase of power at the arrival of the S wave as observed in the preceding example can not be seen; the arrival of the S wave is found in the third part by the inspection of the original seismograms. This fact may be explained by supposing that the duration of event at the origin of earthquake is considerably long, may be three to five seconds, and therefore in the case of short P–S duration the power of high velocity wave can not decrease in the portion preceding the arrival of the S wave.

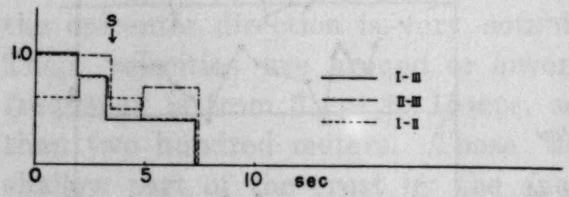

Fig. 15. The fraction of power borne by high velocity waves plotted against the time from the initial motion.

In this example, the velocity of high velocity wave is found for the second portion of seismogram. As shown in Table 2, two of the three characteristic frequencies are estimated from the curves, and though the remaining one can not be determined exactly, it is found to be at least larger than 60 cps. The two known characteristic frequencies can give us two possible vectors. If the wave is unidirectional, from these two possible vectors two values of the remaining characteristic frequency can be derived; they are found to be 29 cps from one of the vectors, and 123 cps from the other. The former can not be allowed, because this characteristic frequency con not be lower than 60 cps. Thus the latter gives the actual velocity vector for this high velocity wave; the value of velocity is determined as 7.6 kmps, a reasonable one for P wave, and the direction N 43°W–S 43°E.

For the rest of the above portion, we could not find the velocity of the high velocity wave. Also the arrival times of initial motion tell us nothing but that the velocity can not be lower than 5 kmps.

This earthquake was not registered by the network of local meteorological observatories. The observed *P–S* duration of this earthquake is 4 seconds, and its epicenter is very near our tripartite station.

Velocity vectors of low velocity waves. As shown in Fig. 15, the high velocity wave is so predominant over the whole duration of seismogram expect for the coda part, that the low velocity wave often does not have enough power to indicate clearly its characteristic frequency in the correlation curves. Therefore, a complete set of characteristic frequencies can be found only for the fifth portion, and for the first and fourth portion only two of three characteristic frequencies are found from each set of correlation curves. Fig. 16 shows the velocity vectors for the above three portions; one vector for the fifth portion and two possible vectors for each of the first and fourth portions.

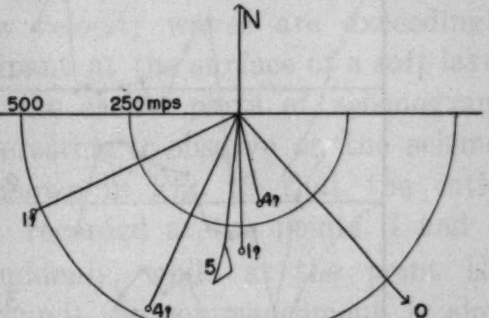

Fig. 16. Velocity vectors for low velocity waves.

It is remarkable that the direction of propagation of the fifth wave portion is nearly N–S, which was also the direction of a group of wave portions found in the preceding example. Besides, the velocity value of this portion coincides well with those of the third and tenth parts of the seismogram investigated in the preceding example.

In previous paragraphs, the velocity of the high velocity wave was found as 7.6 kmps. At the same time its direction of propagation was also determined. This direction is shown in Fig. 16 with the mark *O*. Since this direction can reasonably be assumed as pointing to the epicenter of this earthquake, it can be said that none of the directions of low velocity waves coincides with the direction pointing to the epicenter of the earthquake.

7. Earthquake of Aug. 25, 1957.

This earthquake was observed by the tripartite system (I, II, III′) in Fig. 5, instead of the system (I, II, III) used in the above two cases. The point III′ is not situated on hard sandstone bed, but is on rather soft ground. As will be shown later, this alteration of site caused a remarkable decrease in fraction of power of the high velocity wave for

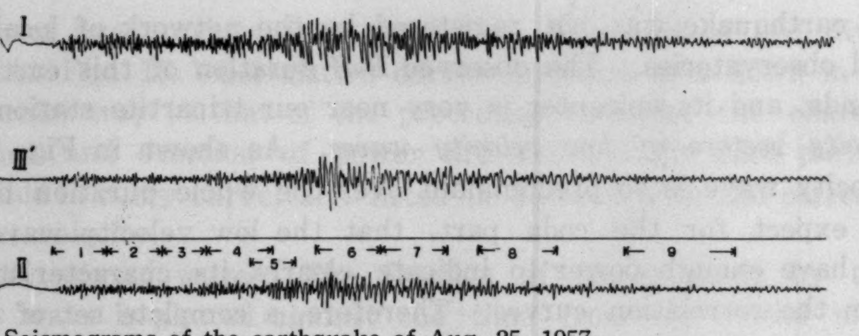

Fig. 17. Seismograms of the earthquake of Aug. 25, 1957.

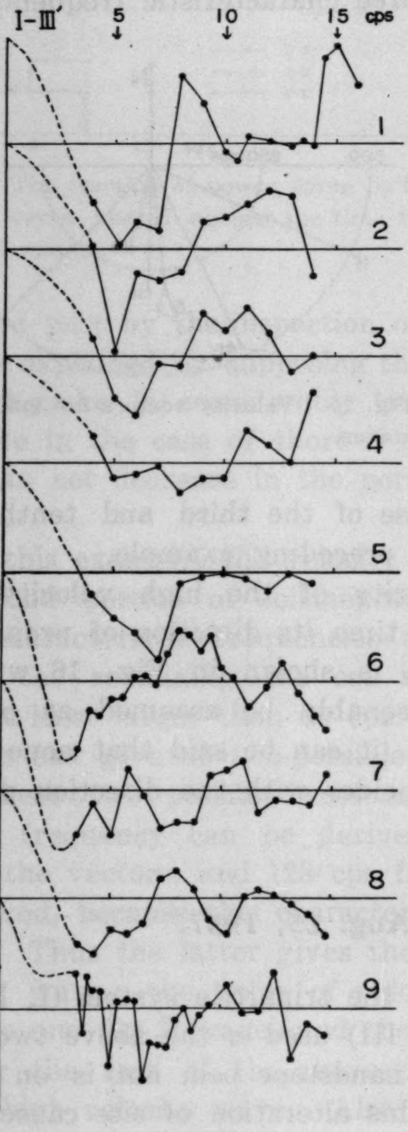

Fig. 18a.

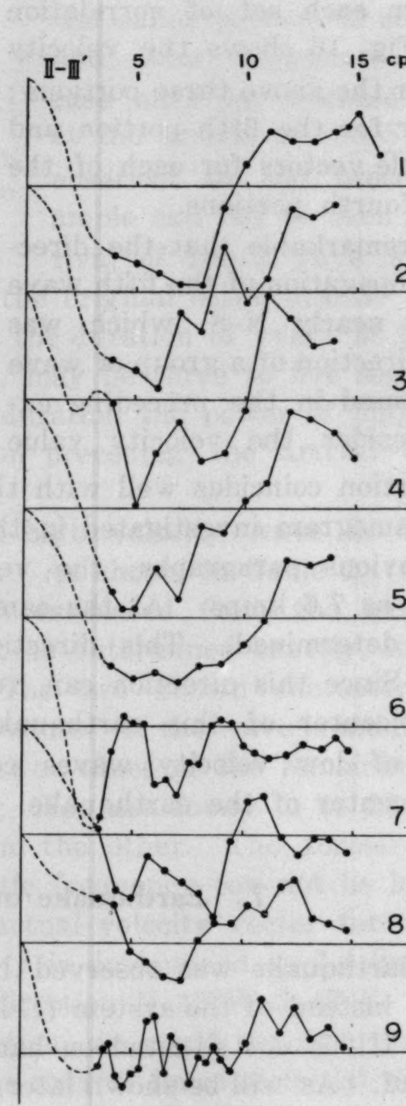

Fig. 18b.

the seismometer pairs (I III′) and (II III′).

General features. Original seismograms are shown in Fig. 17. Each of them are divided into nine portions, as shown in the figure. Correlation curves are obtained for these portions and shown in Fig. 18. It can be seen that the forms of curves for the seismometer pair (I, II) resemble those found in the preceding examples, except that near 10 cps an abnormal negative value of correlation coefficient is observed, which may be due to a local abnormal vibration at the place. While, in all of the curves for the seismometer pairs (I, III′) and (II, III′) the high velocity wave is not discernible. This fact shows that low velocity waves are exceedingly predominant at the surface of a soft layer even in the earlier parts of seismogram. It is interesting to observe on the seismograms shown in Fig. 18 that the intial motions recorded at the points, I and II begin suddenly, while at the point III′ (soft ground) the commencement is slow and vague.

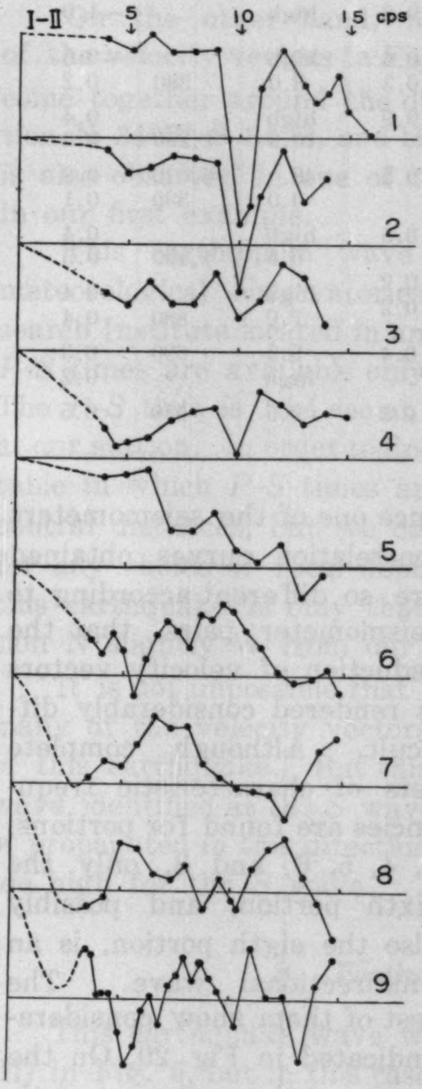

Fig. 18c.

In a similar way as in the preceding examples, the characteristic frequency and fraction of power are found for each partial wave discernible in every curves and listed in Table 3 with the corresponding apparent velecity.

High velocity waves. The fraction of power borne by the high velocity wave found in the curves for the seismometer pair (I, II) is plotted against the time from the initial motion in Fig. 19. It can be seen that the high velocity wave is most predominant in the first portion after which it gradually decrease in power and again predominates in the fifth portion which is identified as the S wave on the original seismograms. In the portions following the fifth, the high velocity wave is, if not absent, feeble.

In this case, the velocity of the high velocity wave could not be determined except that the apparent velocity of the wave portion identified as the S wave along the line (I II) is estimated as 6.0 kmps.

Table 3. The characteristic frequency f^*, apparent velocity V along each line, and ratio power borne by component waves.

	I—III			II—III			I—II		
wave portion	f^* (cps)	V (mps)	Power ratio	f^* (cps)	V (mps)	Power ratio	f^* (cps)	V (mps)	Power ratio
1.	8.0 12.0	1,170 1,760	0.4 0.4	13.0	1,020	0.6	high		~1.0
2.	11.5	1,690	0.6	12.0	940	0.8	high		~1.0
3.	10.0	1,470	0.5	12.0 3.5	940 280	0.6 0.3	high 3.0	 380	~0.6 0.2
4.	16.0	2,350	0.2	12.0	940	0.9	high 10.0	 1,250	0.4 0.2
5.	10.0	1,470	0.4	13.0	1,020	0.5	48. 3.0	6,010 380	0.9 0.1
6.	8.0	1,170	0.6	4.5	350	0.5	high 9.5	 1,190	0.4 0.3
7.	5.5	810	0.2	11.0 6.0	870 470	0.2 0.2	high 7.0	 880	0.4 0.4
8.	8.0	1,170	0.5	12.0	940	0.4	5.5	690	0.3
9.	low 11	2,600	0.3 0.1	low		0.2	high 3.5	 440	0.2 0.5

Velocity vectors of low velocity waves. Since one of the seismometers is placed on a soft ground, the type of correlation curves obtained are so different according to seismometer pairs, that the reduction of velocity vectors is rendered considerably difficult. Although complete sets of characteristic frequencies are found for portions, 3, 4, 5, 6, and 8, only the sixth portion, and possibly also the eigth portion, is an unidirectional wave. The rest of them show considerable departure from the ideal plane wave as indicated in Fig. 20. On the other hand, for the portions, 1, 2, and 7, only two of three characteristic

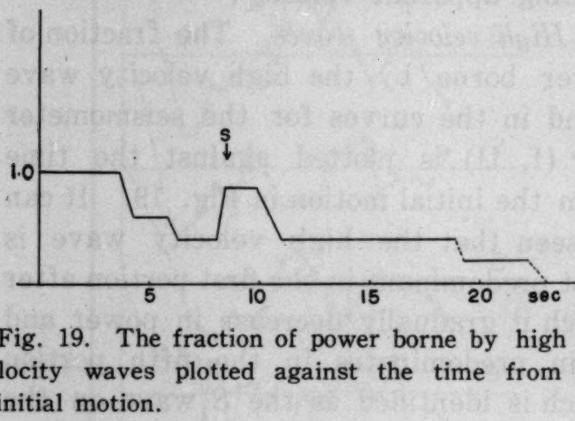

Fig. 19. The fraction of power borne by high velocity waves plotted against the time from the initial motion.

frequencies are obtained and two possible vectors are shown for each of them.

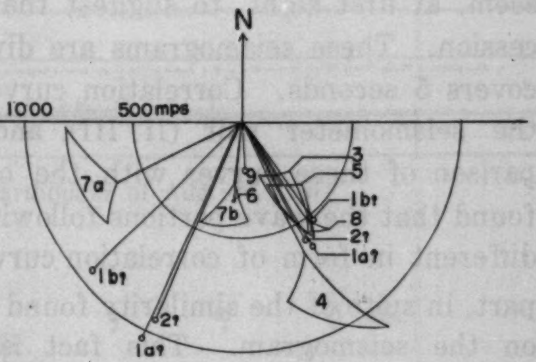

Fig. 20. Velocity vectors for low velocity waves.

The velocity vector of the sixth portion, found as unidirectional, has nearly the same direction and velocity value as those for the fifth wave portion of Earthq. of Aug. 23, the third and tenth portion of Earthq. of Aug. 11.

On the other hand, many of the velocity vectors in Fig. 20 come together around the direction N 34°W–S 34°E, and their velocity value are about 500 mps, which is also observed in one of the two groups of low velocity waves found in our first example.

This earthquake wave was recorded at five stations ; three local meteorological observatories and two stations of the Earthquake Research Institute located in and near Kanto district. Of the five stations, *P–S* times are available only at two ; Tsukuba and Matsushiro stations. The *P–S* time is 13.4 sec at Tsukuba and 20.9 at Matsushiro ; it is 9 sec at our station. In order to find the epicenter, we used Sagisaka-Takehana's table in which *P–S* times are given for various focal depths and epicentral distances, but we could not determine a well defined epicenter for any choice of focal depth. What we can say about the epicenter of this earthquake is only that it lies in the land area, possibly in a direction N slightly W from our tripartite station.

It is not impossible that the direction N 34 W–S 34 E, around which many of the velocity vectors come together, is pointing to the epicenter of this earthquake. But this seems unlikely, because if the high velocity wave identified as the *S* wave, of which an apparent velocity is known, is propagated in this direction, its velocity should exceed 5 kmps, perhaps too high for the *S* wave.

8. Earthquake of Aug. 29, 1957.

This earthquake wave was recorded by the tripartite system (I II III) in Fig. 5, but in this case the vibration of seismometer at the point I was not recorded well on the magnetic tape. Therefore, the velocity vectors could not be obtained for this earthquake.

General features. In Fig. 21 are shown original seismograms, which seem, at first sight, to suggest that there was two earthquakes in succession. These seismograms are divided into twenty six portions; each covers 5 seconds. Correlation curves for these portions are obtained for the seismometer pair (II III), and shown in Fig. 22. From the comparison of these curves with the original seismograms in Fig. 21, it is found that the wave portions following the initial motion are remarkably different in form of correlation curve from those following the fifteenth part, in spite of the similarity found between them in general appearance on the seismogram. This fact is clearly indicated in Fig. 23, which shows the fraction of power borne by high velocity wave. The high velocity wave is predominant over the portions from the first to the sixth, while hardly discernible in the portions after the fifteenth portion. The former wave portions may be bodily waves coming from underneath the crust, while the latter may be surface waves. Between these two main wave groups, we can find wave portions having a single low velocity such as the seventh and eighth portions, as well as those being comparatively rich in power of high velocity wave such as the nineth, eleventh, and thirteenth portions, each followed by wave portions being not so rich in it.

Taking into account the results obtained in the preceding example, let us examine whether the whole seismogram is due to two earthquakes which occurred in succession or due to one single earthquake. If the former is the case, the portions from the first to the nineth must be considered as caused by the earlier earthquake, aud the remaining portions as caused by the later one, because in the tenth portion contains a considerable amount of high velocity wave, which is not prevailing in the coda portions of earthquakes hitherto analysed. Then, the general appearances of the original seismogram suggests that the S wave of this earlier earthquake may be found in the first portion or the second. Thus we must have for this earthquake an unusual seismogram, in which the duration of high velocity wave is too long for the short P–S duration.

It seems more natural to suppose that the seismogram is due to a single earthquake; the portions from the first to the sixth are the P wave, the one or all of the nineth, eleventh and thirteenth is the S wave, and the portions following the fifteenth are surface waves. Then this earthquake must be considered as a rather distant and comparatively

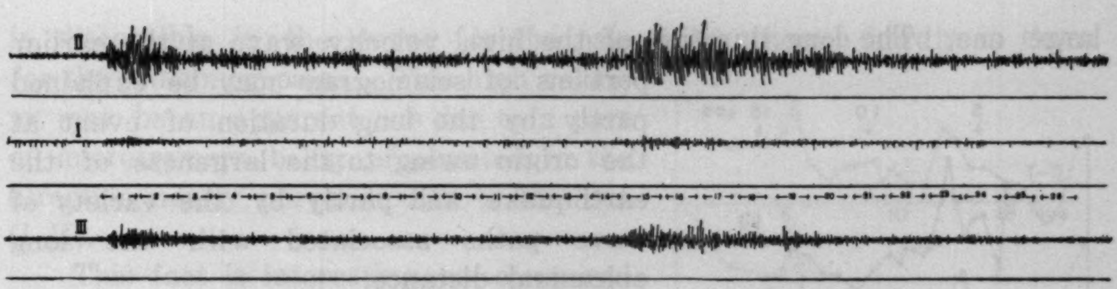

Fig. 21. Seismograms of the earthquake of Aug. 29, 1957.

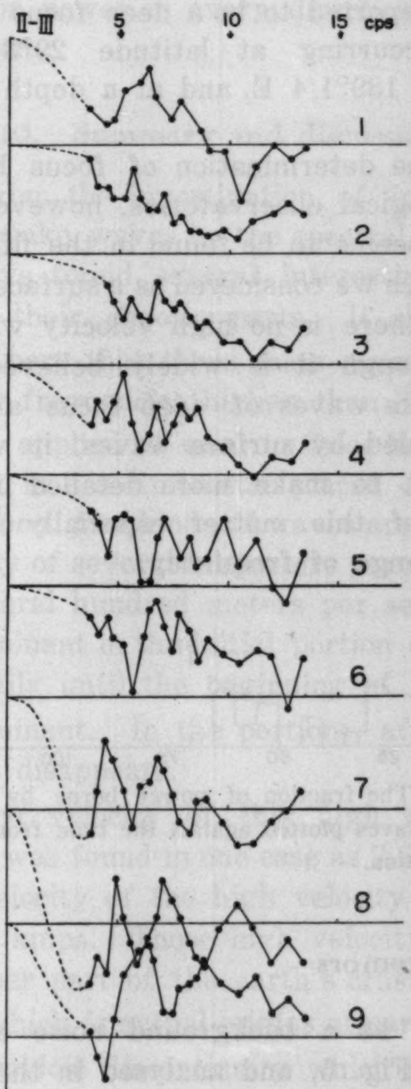

Fig. 22a.

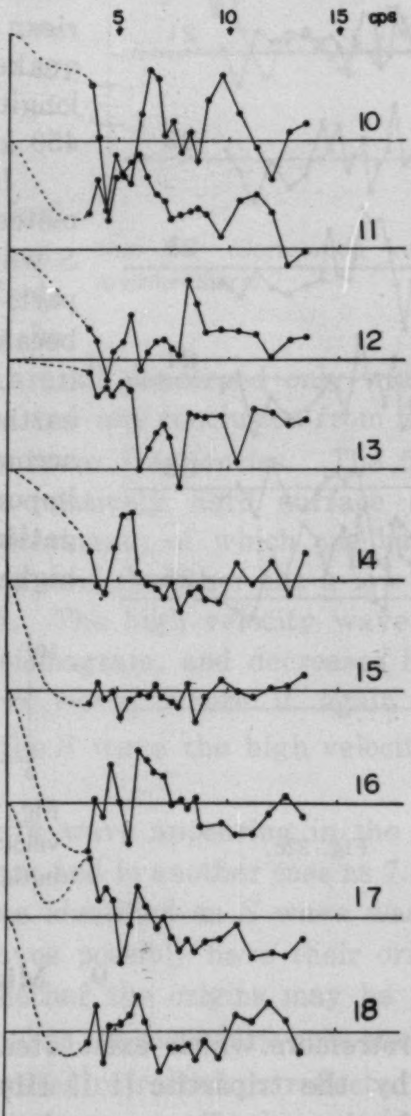

Fig. 22b.

large one. The long duration of the high velocity wave at the earlier portions of seismogram may be explained partly by the long duration of event at the origin owing to the largeness of the earthquake, and partly by the variety of wave paths associated with the long epicentral distance.

In fact, this was due to a single earthquake, which according to the observation network of local meteorological observatories, is reported to be a deep focus earthquake occurring at latitude 29°3/4 N, longitude 139°1/4 E, and at a depth about 450 km.

In the determination of focus by the meteorological observatories, however, the *S* wave seems to be found in the fifteenth part, which we considered as a surface wave because there is no high velocity wave in it. Although it is widely believed that earthquake waves of deep focus are not accompanied by surface waves, it will be important to make more detailed investigations of this matter especially in the higher range of frequency.

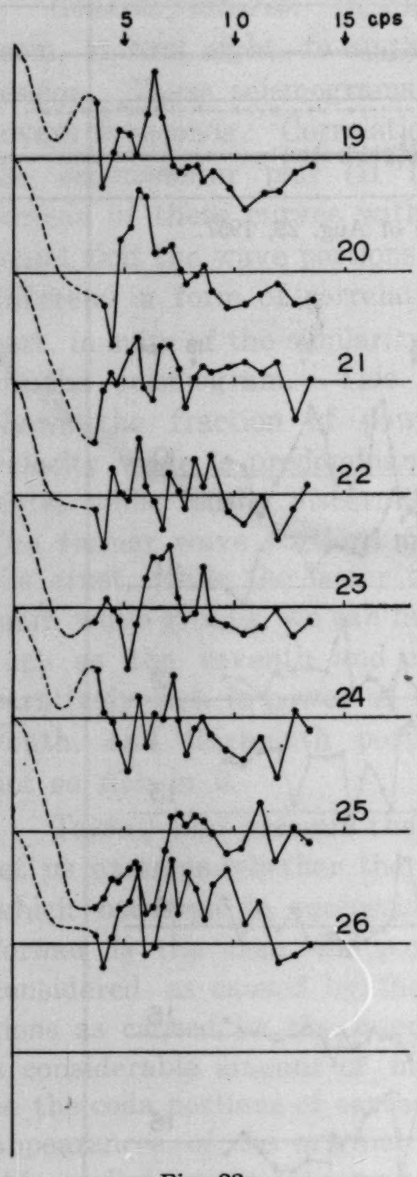

Fig. 22c.

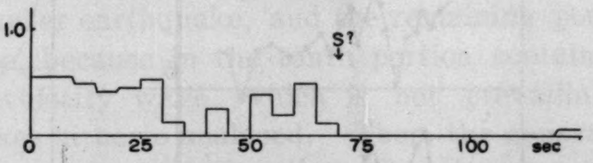

Fig. 23. The fraction of power borne by high velocity waves plotted against the time from the initial motion.

9. Microtremors

Microtremors which exist steadily as a background noise are recorded by the tripartite (I II III) in Fig. 5, and analysed in the same way as in the preceding examples. Fig. 24 shows correlation curves for the three seismometer pairs. We can see that the high velocity wave is discernible in the curve for the pair (I II), though hardly in those for the remaining pairs. This high velocity may be an apparent one due to a part of microtremors being propagated in the direction nearly perpendicular to the line (I II).

This fact is interesting as compared with the nature of microtremors in the city area. Microtremors observed at Hongo, in Tokyo, by Aki (1957) have almost uniform power in every direction of propagation.

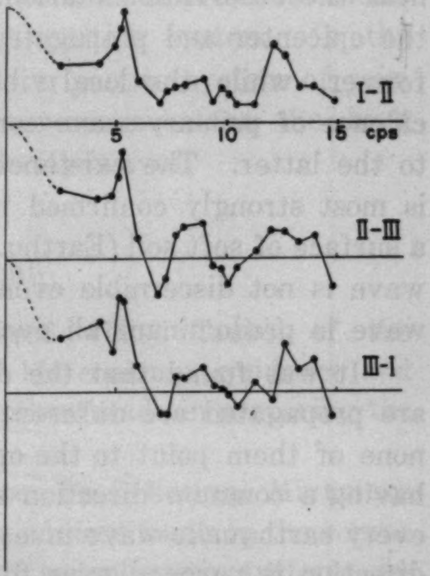

Fig. 24. Correlation curves for microtremors.

10. Summary and discussion

From the investigation of individual earthquake waves by the spectral method, we have found several interesting facts about their chaotic parts. It should be noted here that those facts revealed are all concerned only with wave having frequencies higher than 3 cps, and any conclusion from them can not be applied at once to those having lower frequencies. The first fact is that in a seismometer placed on a relatively hard surface such as sandstone, two kinds of waves are predominant; of which one has a high velocity of several kilometers per second, and the other has a low velocity of several hundred meters per second. The high velocity wave is most predominant in the initial portion of seismogram, and decreases in power gradually until the beginning of the *S* wave, where it again become predominant. In the portions, after the *S* wave the high velocity wave almost disappears.

The velocity of this high velocity wave appearing in the *P–S* interval was found in one case as 7.6 kmps, and in another case as 7.4 kmps. The velocity of the high velocity wave identified as *S* wave was found as 4.1 kmps. Those high velocity waves possibly have their origins at a deeper part of the earth's crust, whether the origins may be primary ones which is actual origins of earthquakes, or secondary ones such as the Mohorovičić discontinuity which generates refracted or reflected waves.

On the other hand, the low velocity waves must be considered as originating at the shallow part of crust. They may be classified into two groups according to whether the origins are near the epicenters or near the observation station. A surface wave that is generated around the epicenter and propagated from there to the station belongs to the former, while the local vibration of surface layer generated by the incidence of primary wave coming from the origin of earthquake belongs to the latter. The existence of a low velocity wave of the latter type is most strongly confirmed in the record of a seismometer placed on a surface of soft soil (Earthq. of Aug. 25.). In this case, the high velocity wave is not discernible even in the initial portion, and the low velocity wave is predominant all over the seismograms.

It was found that the directions along which the low velocity waves are propagated are different among wave portions of a seismogram, and none of them point to the origin of earthquake. Further, wave portions having a common direction and a common value of velocity are found in every earthquake wave investigated. It is interesting that this common direction is perpendicular to the coast line near the observation station.

It is expected that the duration of the high velocity wave has some bearing upon the duration of event at the earthquake origin. No conclusion, however, can be drawn here because the number of records obtained is insufficient. It is also expected that the study along this line will make possible a sound estimation of energy of chaotic earthquake waves based on the investigation of separate powers carried by waves of different types. We hope that these important problems will be solved by applying the present method to a tripartite system having longer spans and determining the exact values of velocity and fraction of power for high velocity waves which are discernible in every portion of seismogram.

The present study is essentially a preliminary one in which are presented suggestions of several interesting problems solvable by the spectral method rather than conclusions to those problems.

The lengths of spans of the tripartite system should be chosen as appropriate to the waves to be studied. Those chosen in the present investigation are too small for the high velocity waves but appropriate for the low velocity waves in the range of frequencies as investigated in the present study.

Though it is not so easy to expand the range of frequency to the lower side, this expansion is necessary for the fuller understanding of earthquake waves, especially of the surface waves.

In order to draw conclusions about the nature of chaotic parts of earthquake waves, we are preparing for a further study of near earthquake waves, with improvements in equipment and an appropriate choice of both the place and the length of span of tripartite system. In the next attempt, we are going to use a double tripartite system of seismometers, in which one tripartite having longer spans is for the high velocity waves and the other for the low velocity waves.

11. Acknowledgement.

The writers express their thanks to Prof. Chuji Tsuboi of the Geophysical Institute, Tokoy University for his constant guidance and encouragement as well as his valuable suggestions made in preparing the manuscript.

The writers' thanks are also due to Assoc. Prof. Setumi Miyamura of our Institute for his kind help and valuable advices made in the course of investigation, especially in the operation of seismograph systems developed by him without which the present work could not be carried out.

---

5. 近地地震波動のスペクトル的研究 (1)

地震研究所
安芸敬一
辻浦賢
堀実
後藤健一

近地地震波動は一般に極めて複雑であつて，その任意の部分の波としての性質を明らかにするには，これまでの走時解析を用いる位相的な立場からの研究だけでは不充分だと思われる．この論文では，前に著者の一人が微動の解析に用いた方法，即わち波動を時間的にフーリエ分解し，分解された成分波について空間相関をしらべるという方法を，近地地震波に応用した．

地震波の記録には，宮村・辻浦の極超短波無線地震計RTS II を用い，3 cps の上下動地震計3台を鎌倉高校の裏庭に設置した．地震波形は無線によつて油壺に送られ，そこで2-track のテープレコーダーに記録された．解析は研究室においてデカトロン相関器と位相ロ波器を用いて行われた．

8月一杯の観測で解析されうる地震記録が4組得られた．数は少ないが次のような興味深い事実が明らかにされた．但し次の事実は周波数範囲 3cps から 15cps の間の地震波動について得られたものである．

1. Sandstone のような比較的固い地表上に地震計をおいて記録した波動には2種類の波，1つは数粁毎秒の伝播速度をもつ速い波，1つは数百米毎秒の伝播速度をもつ遅い波が現われる，速い波は記象の最初の部分に最も卓越し，その後次第に減少して，S波の到来する時間にまた著しくなる．S波のあとは速い波の含まれる割合は殆んど零になる．

2. p～s間に表われる速い波の伝播速度は，ある地震の場合に 7.6 kmps，他の地震で 7.4 kmps

であつた．S波のところに表われる速い波の伝播速度は 4.1 kmps であつた．

3. 遅い波は，震央付近で発生し観測点まで伝播して来た表面波か，あるいは震源から直接くる波によつて観測点近くの地表に 2次的に生じた局地的振動の一種であろう．この後者の型の波の存在は，比較的やわらかい表土上に地震計をおいたとき (8月25日の地震)，もつとも著しく認められた．こういう表土の上におかれた地震計の記録には速い波の占める割合がP波の初めから，尾部に到るまで殆んど零であつた．

4. 遅い波の伝播方向は一般に真の震源の方向からはずれており，そのなかにはどの地震にも共通に，同じ伝播速度と方向をもつ波が見出された．速度の大きさは，350 mps，方向は南北に近く，その方向が観測点近傍の海岸線と直角になつていることは興味深い．

5. この研究では三点観測の span が，速い波の速度をもれなく決めるのに充分な程長くなかつたので，その性質をくわしく調べられなかつた．近い将来，大きい三角点と小さい三角点とを併用して，速い波と遅い波について一層くわしい研究をする予定である．

BULLETIN OF THE EARTHQUAKE
RESEARCH INSTITUTE
Vol. 36 (1958), pp. 99-134

6. *Relations between the Eruptions of Various Volcanoes and the Deformations of the Ground Surfaces around them.*

By Kiyoo MOGI,

Earthquake Research Institute.

(Read Feb. 28, 1956 and Feb. 25, 1958.—Received March 31, 1958.)

Introduction

It is well known that on the occasions of the great volcanic eruptions the enormous volume of substance which constitutes the earth's crust moves up to the earth's surface as lava flow and fragmental ejecta. Of course, the ejection of lava is always accompanied with the movements of the substances in the earth's crust, and it causes the deformation of the earth's surface. The changes of the state in the earth's crust seem to have a close relation to the mechanism of volcanic eruption. From this point of view, the various types of deformation are investigated in this paper.

In fact, the remarkable deformation of the earth's crust around the volcanoes has been observed by the precise surveys. F. Ōmori[1] investigated for the first time the vertical displacement of the ground surface around the Usu Volcano before and after the 1910 eruption by precise levellings. And in the 1914 eruption[2] of the

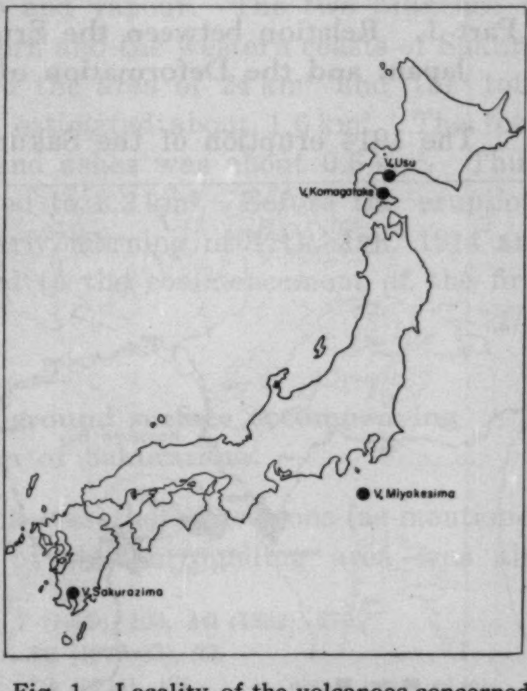

Fig. 1. Locality of the volcanoes concerned with the present discussion, in Japan.

---

[1] F. ŌMORI, *Bull. Imp. Earthq. Inv. Com.*, **5** (1911–13), Nos. (1, 2), **9** (1920), No. 2.
[2] F. ŌMORI, *Bull. Imp. Earthq. Inv. Com.*, **8** (1914–19), Nos. (1–6).

Sakurazima Volcano he observed the remarkable depression over the wide surrounding area. Thereafter the precise levellings or triangulations were always executed before and after notable volcanic eruptions in Japan. However, for other districts we have not the data of the survey, except for the Kilauea Volcano, Hawaii.

Thus the feature of the crustal deformation seems to have been obtained nearly sufficiently, but the physical meaning of these notable results has not yet been discussed. The writer investigated the characteristics of the crustal deformation around volcanoes and discussed the mechanism of these phenomena. This paper is composed of the following parts ;

Part 1. Relation between the Eruptions of the Sakurazima Volcano, Japan, and the Deformation of the Ground Surface around It
Part 2. The Deformations of the Ground Surface around the Kilauea Volcano, Hawaii, accompanied by the 1924 Eruption
Part 3. Relations between the Deformations of the Ground Surface around the Volcanoes and Other Volcanic Phenomena

Part 1. Relation between the Eruptions of the Sakurazima Volcano, Japan, and the Deformation of the Ground Surface around It.

The 1914 eruption of the Sakurazima Volcano is one of the greatest eruptions in recent years. The volume of ejecta amounted to about 2.2 km^3, and the deformation of the ground surface was very remarkable. The results of precise survey on the deformation were obtained by F. Ōmori and the circular depression of the coast along Kagosima Bay was measured by him. He resurveyed these area in 1915 and 1919,

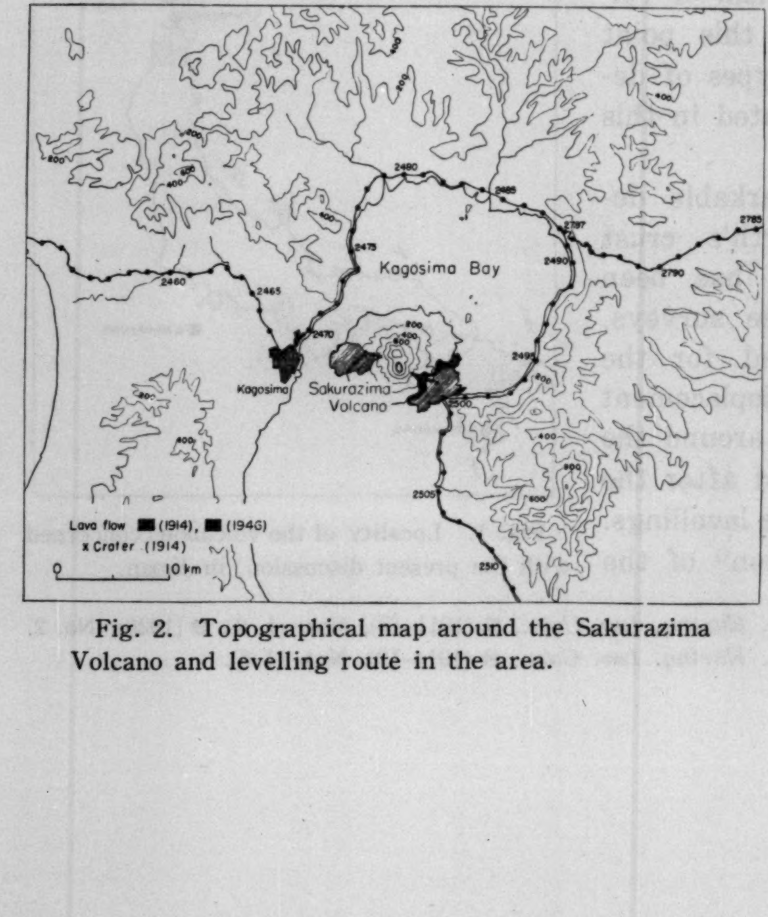

Fig. 2. Topographical map around the Sakurazima Volcano and levelling route in the area.

and found the subsided area recovering. Thereafter, resurveys were carried out in 1932, 1946 and 1957. These results have been discussed by C. Tsuboi[3], N. Miyabe[4] and Y. Harada[5], from the stand point of tilting of land blocks, and T. Minakami and A. Okada[6] recently.

The writer investigated the character of the ground deformation and discussed the mechanism of deformation and its volcanological significance.

§1. The 1914 great eruption[7].

The Sakurazima Volcano is a andesitic volcano situated in Kagoshima Bay, Southern Kyūshū. The volcano consists of three cones ; Kita-Dake, Naka-Dake and Minami-Dake, of which the southern one (Minami-Dake) is active up to the present time.

On the 12th, Jan. 1914, the eruption took place from the two opposite flanks of the Minami-Dake. The numerous newly opened craters are arranged along a line through the centre of the Minami-Dake crater, in an ESE and WNW direction. The outbursts were very vigorous with ejection of lava fragments, pumices and vapour. The two branches of the lava streams flowed to the eastern and the western coasts of Sakurazima Island respectively and covered the area of 24 km^2 and the total volume of the lava of out-flow was estimated about 1.6 km^3. The total volume of lava fragments, pumices and ashes was about 0.6 km^3. Thus, the total sum of the ejecta amounted to 2.2 km^3. Before the eruption, felt earthquakes occured on the early morning of 11th, Jan. 1914 and the number of earthquakes increased to the commencement of the first eruption and thereafter decreased.

§2. The deformation of the ground surface accompanying the 1914 eruption of Sakurazima.

The 1914 eruption of Sakurazima was the largest one (as mentioned above) and the ground deformation of the surrounding area was also very remarkable. The subsidence of the coast of Sakurazima Island and the coast of Kagosima Bay were observed and also the tide gage at Kagoshima harbour recorded the changes of sea level. The deformation of the ground surface around the Sakurazima Volcano was surveyed quantitatively by means of the precise levelling and triangulation.

---

[3] C. TSUBOI, *Bull. Earthq. Res. Inst* , **7** (1929), 103. **10** (1932), 570.
C. TSUBOI, *Jap. Jour. Astr. Geophys.* **10** (1932–33), 93.

[4] N. MIYABE, *Bull. Earthq. Res. Inst.*, **12** (1934), 471.

[5] Y. HARADA, *Bull. Geogr. Surv. Inst.*, **1** (1950), 1.

[6] T. MINAKAMI and A. OKADA, *Bull. Volcan. Soc. Jap.*, **1** (1957), 65.
A. OKADA, *Bull. Volcan. Soc. Jap.*, **2** (1957), 53.

[7] F. ŌMORI, *loc. cit.* 2)

The surveys were executed in 1895 before the eruption and in June 1914 after the eruption, and these results of the precise surveys by F. Ōmori are indicated in Fig. 3 and Table 1. The deformation seems to have occured suddenly at the time of the 1914 eruption, considering the records of tide gage at Kagosima. Within the Sakurazima Island, although several triangulation points close to the craters were destroyed by the violent explosion, the vertical and the horizontal displacements were obtained by triangulation.

From the results of levelling and triangulation, the following characteristics of the deformation of the ground surface were clarified.

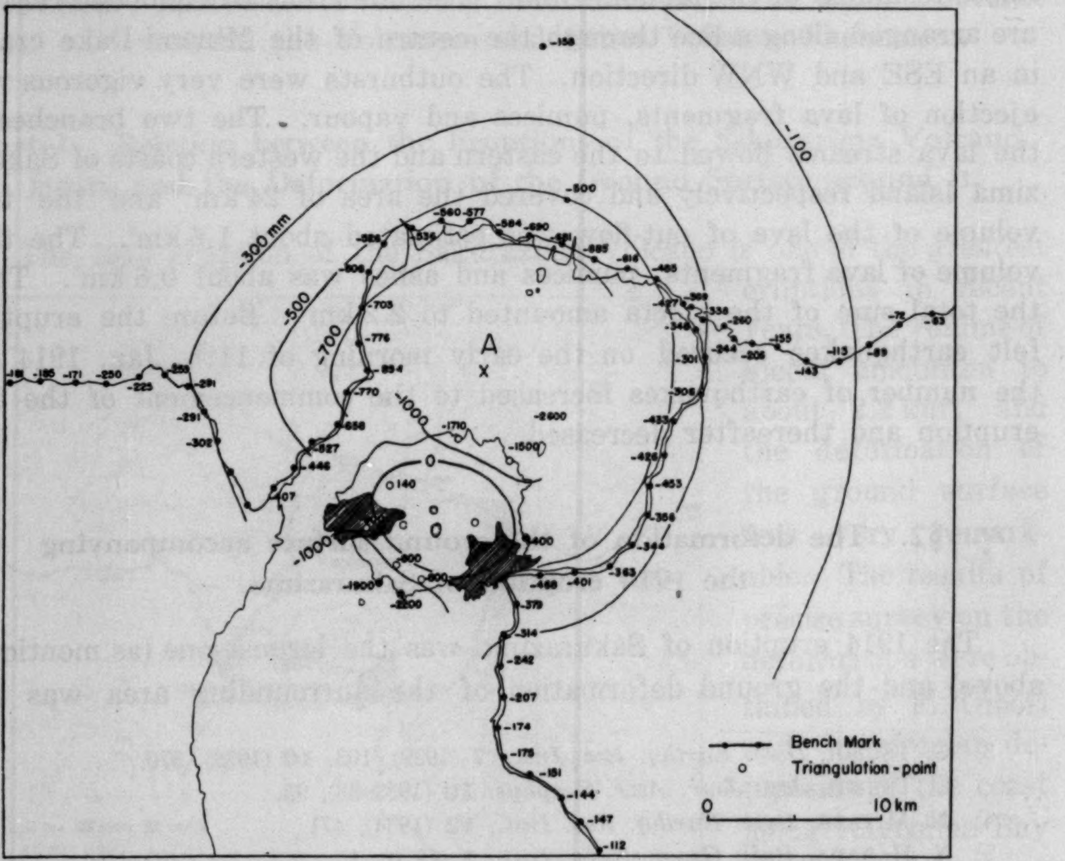
-100
-300 mm
-500
-700
-1000
0
A
x
-158
-500
-181
-185
-171
-250
-225
-250
-291
-291
-302
-586
-560
-577
-536
-584
-690
-681
-685
-616
-465
-506
-703
-776
-854
-770
-658
-627
-446
-07
-1710
-2600
-1500
140
-1000
-800
-800
-1900
-2200
400
-427
-369
-338
-260
-346
-244
-205
-155
-143
-113
-89
-72
-83
-301
-306
-433
-426
-453
-356
-344
-363
-401
-468
-379
-314
-242
-207
-174
-175
-151
-144
-147
-112
Bench Mark
Triangulation-point
0
10 km

Fig. 3. Vertical displacements of the ground surface around the Sakurazima Volcano before and after the 1914 great eruption. (after F. Ōmori) (A): centre of depression.

Table 1.

B. M.	Vertical displacement Δh (1895—1914)	Distance from the centre of dipression d	B. M.	Vertical displacement Δh (1895—1914)	Distance from the centre of dipression d
2464	−291 *mm*	17.0 *km*	2488	−427 *mm*	11.9 *km*
2465	−291	16.2	(2797)	−369	12.15
2466	−302	15.75	2489	−348	12.1
2467	−301	15.3	2490	−301	12.5
2468	−306	15.3	2491	−306	12.3
2469	−407	13.5	2492	−433	10.95
2470	−446	12·45	2493	−426	11.05
2471	−527	10.4	2494	−453	11.0
2472	−658	8.7	2495	−356	12.0
2473	−770	7.85	2496	−344	12.4
2474	−894	6.7	2497	−363	12.5
2475	−776	7.75	2498	−401	11.6
2476	−703	8.25	2499	−468	11.2
2477	−608	9.15	2501	−379	12.6
2478	−526	9.85	2502	−314	13.95
2479	−536	9.7	2503	−242	15.8
2480	−560	9.55			
2481	−577	9.3	2797	−369	12.15
2482	−684	8.5	2796	−338	12.5
2483	−690	8.55	2795	−260	13.75
2484	−681	8.95	2794	−244	14.15
2485	−685	9.15	2793	−206	15.4
2486	−616	10.05	2792	−155	17.25
2487	−485	11.1	2791	−143	18.8

(1) The limited area close to the crater was upheaved locally and the maximum vertical displacement amounted to several metres. The value of tilting of the ground surface which was calculated from the results of triangulation amounted to $10^{-2} \sim 10^{-3}$.

(2) The circular wide area which subsided at the time of the explosion was not near the active crater of the Sakurazima Volcano, but in the Kagosima Bay 10 km north from the present crater. It is remarkable that the contours of equal depression are typically circular and concentric (Fig. 5). The maximum depression did not exceed 2 m and tilting of the ground surface was less than 10^{-4}.

The two types of deformation of the ground surface are very different as mentioned above.

The deformation of the ground surface accompanied by the volcanic eruption seems to have occured by the movement of the substances or the changes of the pressure in the depth of the earth's crust. The magnitude of the deformed area is affected by the depth of origin causing the deformation of the ground surface. Thus the above mentioned upheavals of the ground surface which extended to the limited area close to the crater were caused by the shallow origin, that is the upward forces near the surface accompanied by the out-flow of lava from a deep source. On the other hand, the origin of the depression extending to the wide surrounding area seems to be deeper. The position of the origin of the deformation is estimated by means of the application of the elasticity theory, in the following section.

§3. The mechanism of the deformation of the ground surface at the time of the eruption.

For the purpose of the estimation of the position of the origin of the depression, the following model of the mechanism of the deformation is assumed; (1) the earth's crust is a ideal semi-infinite elastic body and (2) the deformation of the earth's crust is caused by the sperical source with hydro-static pressure in the earth's crust.

With respect to the assumption (1), the sudden deformation of the earth's crust at the time of the eruption seems to be elastic in the first approximation, although the earth's crust is a visco-elastic body in a long time deformation. It is the writer's opinion that the assumed spherical origin (2) seems to harmonize well with the idea of the magma resevoir under the earth's surface.

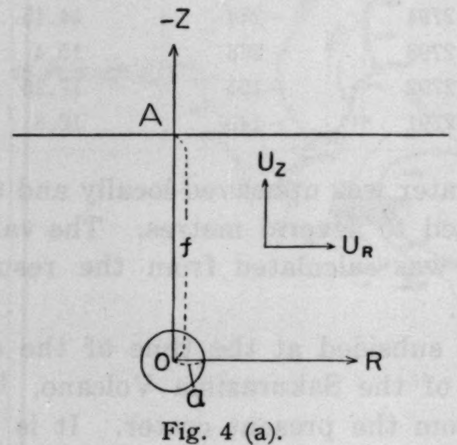

Fig. 4 (a).

According to the elasticity theory, the calculated deformation of the semi-infinite elastic body which is caused by the change of the hydrostatic pressure in a small sphere in the semi-infinite elastic solid is as follows[8]. (Fig. 4.)

---

8) N. YAMAKAWA, *Zisin* (*Jour. Seis. Soc. Japan*), **[ii] 8** (1955), 84.

$$\left.\begin{aligned} U_R &= -\frac{a^3P}{4\mu}\frac{R}{\{(Z+2f)^2+R^2\}^{5/2}}\cdot(5Z^2+14fZ+8f^2-R^2) \\ &\quad +\frac{a^3P}{4\mu}\left[\frac{R}{(Z^2+R^2)^{3/2}}+\frac{R}{\{(Z+2f)^2+R^2\}^{3/2}}\right] \\ U_Z &= \frac{a^3P}{4\mu}\frac{1}{\{(Z+2f)^2+R^2\}^{5/2}}\cdot(7Z^3+38fZ^2+68f^2Z+40f^3+4fR^2+ZR^2) \\ &\quad +\frac{a^3P}{4\mu}\left[\frac{R}{(Z^2+R^2)^{3/2}}+\frac{Z+2f}{\{(Z+2f)^2+R^2\}^{3/2}}\right] \end{aligned}\right\} \tag{1}$$

where

U_R: displacement in the radial direction (R-axis direction)
U_Z: displacement in the direction vertical to the surface
a: radius of the sphere with the hydrostatic pressure
P: change of the hydro-static pressure in the sphere
f: depth of the centre of the sphere from the surface
$\mu(=\lambda)$: Lame's constant

The equations (1) are first aproximation for the case of $a/f \ll 1$. If, take $Z=-f$, the surface deformation is obtained as follows,

$$\left.\begin{aligned} \Delta d &= \frac{3a^3P}{4\mu}\frac{d}{(f^2+d^2)^{3/2}} \\ \Delta h &= \frac{3a^3P}{4\mu}\frac{f}{(f^2+d^2)^{3/2}} \end{aligned}\right\} \tag{2}$$

in which $d\ (\equiv R)$: radial distance on the surface from the point A.
Δd: displacement in the direction of R-axis on the surface
Δh: vertical displacement on the surface.

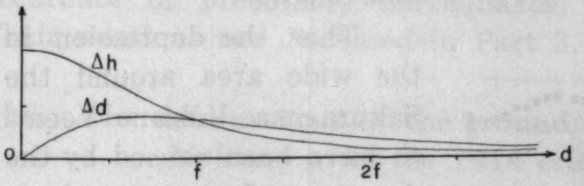

Fig. 4 (b). Calculated curves of the vertical displacement (Δh) and of the horizontal displacement (Δd), versus the radial distance (d).

Thus, if the radius of a sphere is relatively small, the form of the deformation curves is a function of the depth only and the values of displacements depends on P, a and μ.

Comparing the actual deformation by the precise survey with the calculated one, the agreement is surprising when the depth of a sphere is (10±1) km. (Fig. 5) But, we can not obtain uniquely the radius of a sphere and the change of pressure. Fig. 6 is another expression of the relation between the calculation and the observation. The curve

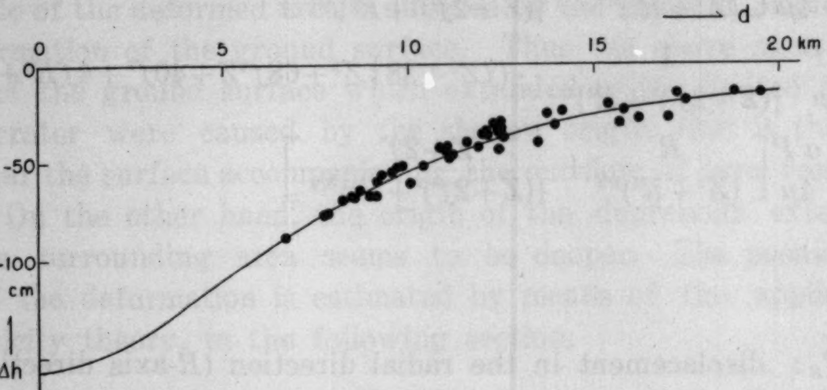

Fig. 5. Relation between the vertical displacements (*Δh*) of bench marks and the displace distances (*d*) from the centre of depression (*A*) to bench marks. The curve is calculated result for the case of the depth 10 km of the spherical origin.

(II) in Fig. 6 shows the vertical displacements of bench marks expected from the calculation along the levelling route and it is completely similar with the variation of the actual displacements of bench marks (III). Therefore, it is possible to explain the deformation of the ground surface by the theoretical results of the deformation of a uniform earth's crust, although the curve (III) has been discussed as a tilting movement of land blocks.

Thus the depression in the wide area around the Sakurazima Volcano seems to have been caused by the decrease of pressure in a spherical origin at the depth of 10 km and the sphere corresponds perhaps to the magma reservoir and the decrease of pressure seems

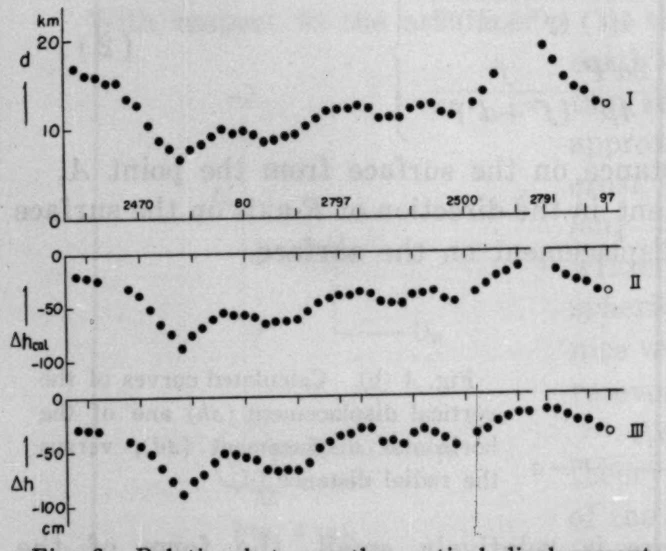

Fig. 6. Relation between the vertical displacement (*Δh*) and the radial distance (*d*). (I): radial distance (*d*) of bench mark from the centre of depression. (II): calculated vertical displacement (*Δh* cal) at the station of the radial distance (*d*). (III): observed vertical displacement of bench mark.

to be due to the out-flow or intrusion of lava at the time of the eruption.

On the other hand, the deformation of the limited area close to the crater which seems to have been caused by the upward movement of magma and the out-flow of the lava is conspicuous and complicated, accompanying the fracture of the ground. According to the results of triangulation, the lands of both sides of the fissure lines moved to the out-ward and the upward direction, represented in Fig. 7.

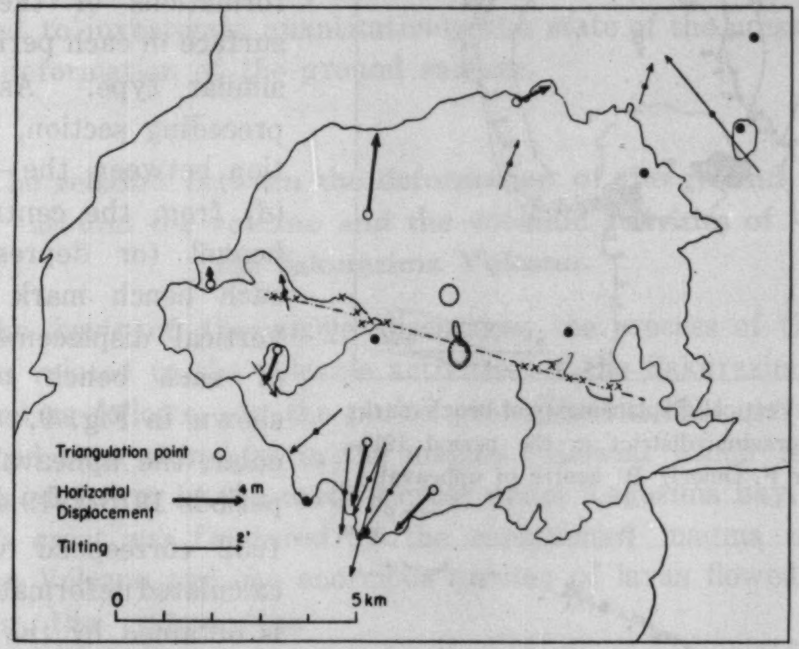

Fig. 7. Horizontal displacements of triangulation points (after F. Ōmori) and tilting of the ground surface calculated from the vertical displacements of triangulation points, in the Sakurazima Island. Chain line is a line of newly opened fissure. (the 1914 eruption)

The deformation related directly to the opening of the craters, the occurence of precursory earthquakes, and other volcanic phenomena. Their relations are discussed in Part 3.

§4. The deformations of the ground surface around the Sakurazima Volcano after the 1914 eruption (1914-1946).

Succeeding the precise levelling of 1914, resurveys were carried out in 1915, 1919[9], 1932[10] and 1946[11]. In the period from Aug. 1914 to Feb. 1915, the depression proceeded still. Therefore, the subsided area began to rise in the period from 1915 to 1919 and the upheaval continued to 1946. The deformations of the ground surface in each period are of similar type. As in the preceding section, the relation between the distances (*d*) from the centre of upheaval (or depression) to each bench mark and the vertical displacements (Δh) of each bench mark are shown in Fig. 9. In particular, the upheavals in the periods 1915–1919 and 1919–1932 correspond with the calculated deformation which is obtained by the increase of the pressure of the spherical origin of 10 km depth, like one at the time of the 1914 eruption. And the horizontal position of centres of the deformations agreed nearly with the centre of the depression of the 1914 eruption. The deformation in the period 1932–1946 is of a little different type from the other. It is noticeable that in this period the sudden subsidence corresponding to the 1946 eruption[12] might have occured in addition to the succeeding upheaval.

---

[9] F. Ōmori, *loc. cit.* 2)
[10] N. Miyabe, *loc. cit.* 4)
[11] Y. Harada, *loc. cit.* 5)

Thus, the above rising process of the ground sur-

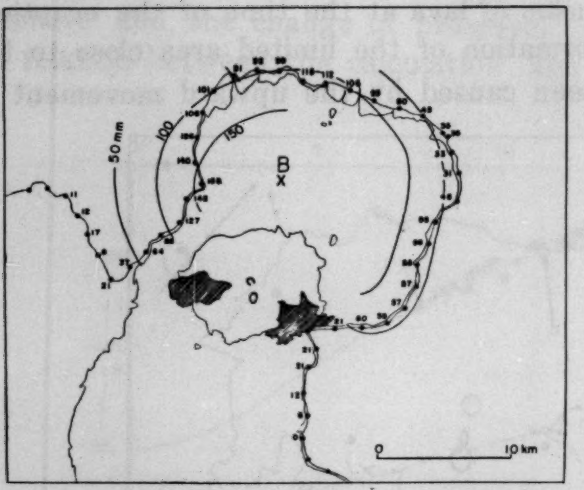

Fig. 8. Vertical displacements of bench marks in the Sakurazima district in the period 1915–1919. (after F. Ōmori) B: centre of upheaval.

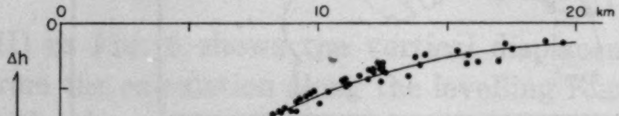

Fig. 9. Relation between the vertical displacements (Δh) of bench marks and the radial distance (*d*) of bench marks from the centre of depression (or upheaval) in each period.

face around the volcano suggests the increase of the pressure in the lava reservoir after the 1914 eruption.

However, the slow movements of the earth's crust seem to be not elastic only, but to include a plastic deformation. Therefore, it is very complicated to investigate quantitatively the state of the pressure origin from the deformation of the ground surface.

§ 5. The relation between the deformation of the ground surface around the volcano and the volcanic activities of the Sakurazima Volcano.

On the basis of the above discussion, the process of the ground movements related to the volcanic activities of the Sakurazima Volcano is explained as follows. In the period preceding the 1914 eruption, high pressure had been stored up in the magma reservoir which is situated at a depth of 10 km in the earth's crust under Kagosima Bay. In 1914, the earth's crust was fractured by the compressed magma under the Sakurazima Volcano and the enormous volume of lavas flowed out suddenly from the craters (the 1914 great eruption). As the result of the out-flow of lava, the pressure in the magma reservoir decreased and the wide area around the volcano subsided remarkably. After the eruption, the rising of the area took place and succeeded to the 1946 eruption. This fact shows that the pressure in the magma reservoir increased gradually and at last the next out-flow of lava occured in 1946.

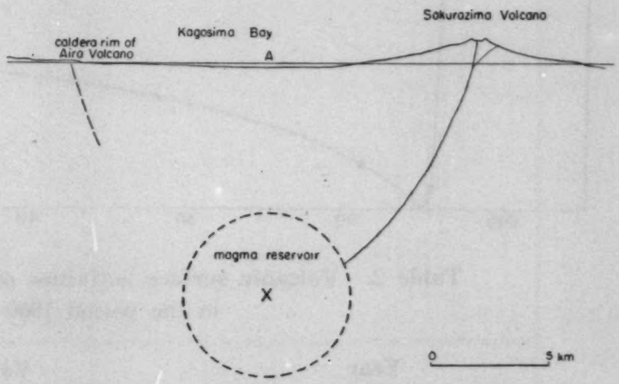

Fig. 10. Profile of the Sakurazima district.

It is quite interesting that the position of the magma reservoir which was obtained from the ground deformation is directly below the centre of the Aira caldera at the rim of which the Sakurazima Volcano stands. This indicates the close relation between the active Sakurazima Volcano and the Aira Volcano[13] which was active in the geological age. (Fig. 11)

---

[12] T. HAGIWARA *et. al.*, *Bull. Earthq. Res. Inst.*, **24** (1946), 143.

[13] T. MATSUMOTO, *Jap. Jour. Geol. and Geog.*, **19** (1943), Special No.

How are the surface activities of the volcano related to the ground movements around the volcano? The relation between the volume of the subsidence or upheaval of the wide surrounding area as mentioned above and the eruptive activities at the Sakurazima crater is shown in Fig. 12. It is obvious that the surface volcanic activities are affected greatly by the increase of the pressure in the magma reservior.

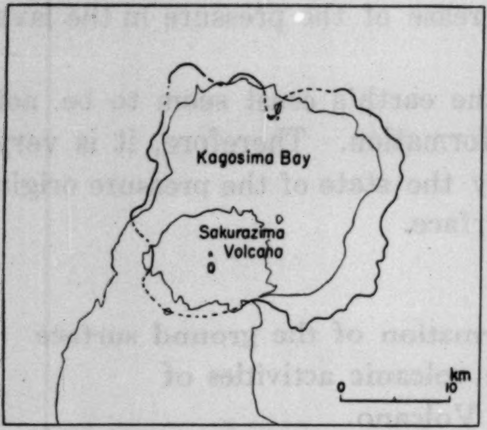

Fig. 11. Aira Caldera (after T. Matsumoto).

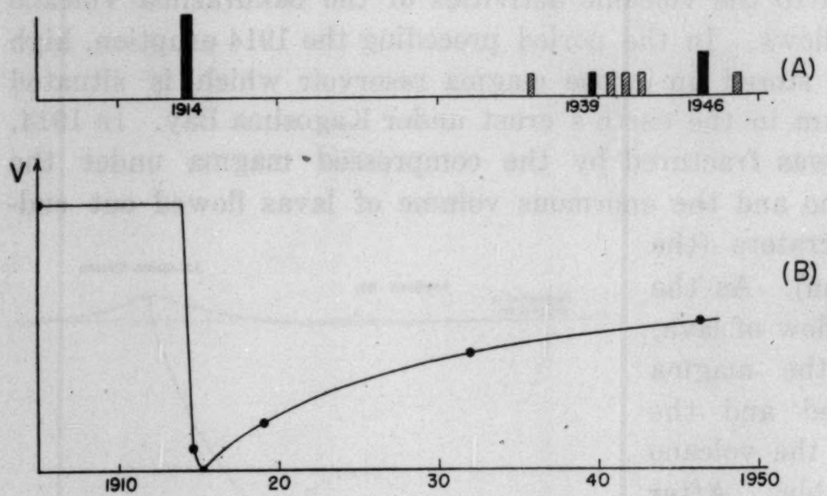

Fig. 12. Relation between the volcanic eruptions of the Sakurazima Volcano and the volume of the depression (or upheaval) in its surrounding area.

Table 2. Volcanic surface activities of the Sakurazima Volcano in the period 1900–1950[14].

Year	Valcanic Activities
1914 (Jan.–June)	Great eruption with outflow of an enormous volume of lavas
1935 (Sept.)	A small explosion (at summit crater)
1939 (Oct.)	A small flank eruption (with nuée ardent)
1940 (April–June)	Small explosions
1941 (April–June)	Small explosions
1942 (July)	Small explosions
1943–1944	Black vapour
1946 (March–June)	Great eruption with outflow of lavas
1948 (July)	Small exploisons
1950 (June–Sept.)	Small explosions

In the above discussion, we investigated mainly the deformation of the ground surface with the wide extent which seems to have been caused by the deep source. On the other hand, the deformation of the limited area near the crater is also remarkable and related to the other volcanic phenomena, but the writer will discuss this subject in the later part.

Part 2. The Deformations of the Ground Surface around the Kilauea Volcano, Hawaii, accompanied by the 1924 Eruption.

The Kilauea Volcano is a shield volcano in Hawaii Island and has erupted frequently at the rift zone on the flanks of the mountain. The 1924 eruption[15)] is noticeable for the explosive eruption from the central crater (Halemaumau) and the remarkable deformation of the ground surface accompanying the volcanic activity. In this paper, the remarkable deformations of the ground surface around the crater are investigated on the basis of the precise surveys, in relation to the volcanic activity of 1924.

The 1924 eruption was investigated by various methods, namely the continuous observation of tilting of the ground surface at the volcano observatory, the measurement of the depths of the crater bottom, the seismometric observation, the precise levelling and triangulation of the surrounding area, etc. This study is due to these investigations, especially the interesting results of the precise surveys by R. M. Wilson.

§1. Analysis of the results of levelling survey.

The levellings on the surrounding area of the Kilauea crater were executed in 1912, 1921 and 1927. The net of levelling routes covers the area around the crater and is connected to a tide gage at Hilo by a levelling route from the Volcano House to Hilo, in order to obtain the absolute value of vertical displacement. (Fig. 13 (a), (b)).

The vertical displacements of the area in the periods 1912–1921 and 1921–1927 by R. M. Wilson[16)] are shown in Fig. 14 and 15 respectively. The depression of the ground surface seems to have taken place suddenly at the time of the 1924 eruption, because the continuous tilt observation

---

14) H. TSUYA and T. MINAKAMI, *Bull. Earthq. Res. Inst.*, **18** (1940), 318. Geophysical Review, (monthly Journal by the Central Meteorological. Observatory)

15) T. A. JAGGER, Origin and Development of Crater (1947)

16) R. M. WILSON, *Univ. Hawaii Res. Publ.*, No. 10 (1935).

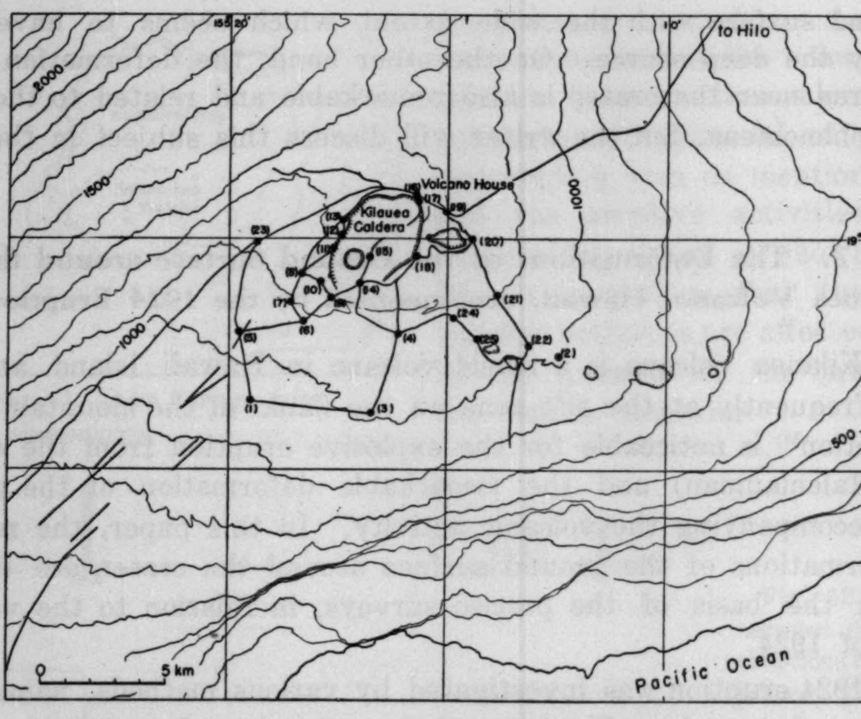
155°20'
155°10'
to Hilo
2000
1500
1000
Volcano House
Kilauea Caldera
19°25'
1000
500
20'
0
5 km
Pacific Ocean

Fig. 13 (a). Topographical map around the Kilauea crater and levelling routes and triangulation points in the district.

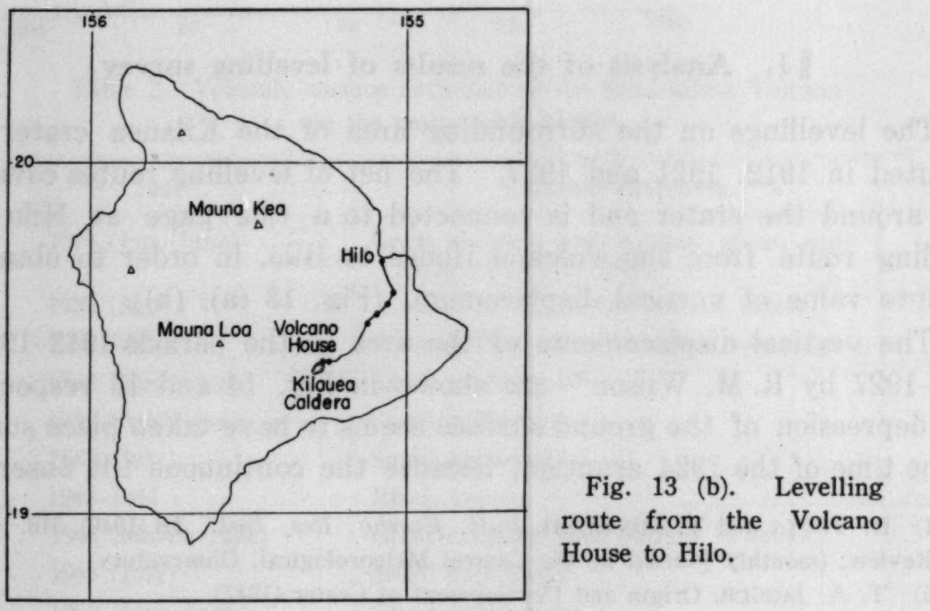
156
155
20
19
Mauna Kea
Hilo
Mauna Loa
Volcano House
Kilauea Caldera

Fig. 13 (b). Levelling route from the Volcano House to Hilo.

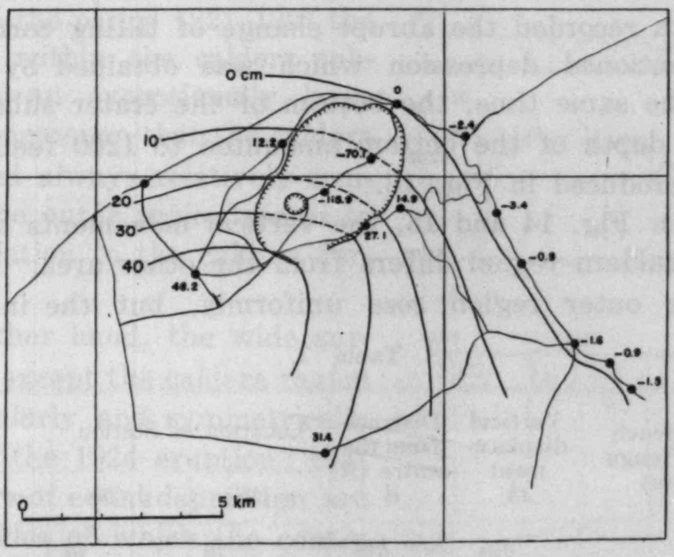
0 cm
10
20
30
40
0
-2.4
12.2
-70.7
-115.9
14.9
27.1
-3.4
-0.9
48.2
-1.6
-0.9
-1.5
31.4
0
5 km

Fig. 14. Vertical displacements of the ground surface around the Kilauea crater in the period 1912–1921. (after R. M. Wilson)

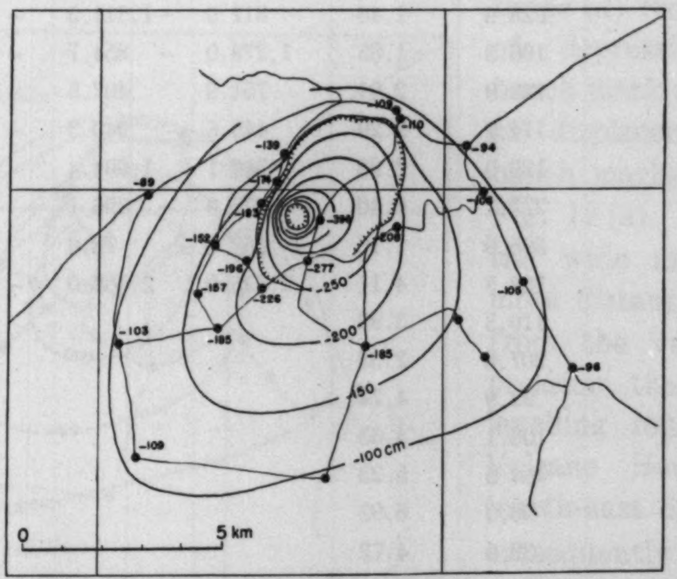
-109
-110
-139
-94
-174
-89
-106
-193
-394
-152
-208
-196
-277
-250
-157
-226
-106
-103
-185
-200
-185
-96
-150
-109
-100 cm
0
5 km

Fig. 15. Vertical displacements of the ground surface around the Kilauea crater in the period 1921–1927. (after R. M. Wilson)

of the ground surface at the volcano observatory at the rim of the Kilauea Caldera recorded the abrupt change of tilting corresponding to the above mentioned depression which was obtained by the levelling survey. At the same time, the bottom of the crater subsided and the change of the depth of the bottom amounted to 1200 feet. These records17) are reproduced in Fig. 16.

As seen in Fig. 14 and 15, the vertical movements of the ground surface in the caldera region differs from the other area. In the period 1912–1921, the outer region rose uniformly, but the inner region of

Table 3.

No.	Station of Bench Mark and Triangulation Point	Vertical displacement Δh	Distance from the centre (A) d	Location of Station		Horizontal displacement	
				x (W)	y (N)	u (W)	v (N)
		cm	*km*	*m*	*m*	*cm*	*cm*
1	Koae	108.5	6.55	4,069.1	-5,664.7	0	0
2	Puu Huluhulu		8.14	-8,227.5	-3,882.8	0	0
3	Ohale	93.3	5.12	- 766.3	-6,170.4	- 6.1	22.9
4	Ahua Kamokukolau	184.7	2.32	-1,851.7	-3,035.5	16.5	107.3
5	Aa	102.7	5.46	4,531.2	-2,930.3	- 21.0	3.7
6	Nose	184.7	2.90	1,905.3	-2,534.4	- 77.1	32.9
7	Cone Peak	157.0	3.08	2,430.0	-1,666.3	- 78.0	6.1
8	Pali	152.4	2.65	2,000.4	521.8	- 79.3	- 3.7
9	Sand Hill	225.9	1.46	812.0	-1,511.5	- 74.4	52.1
10	Cracks	196.3	1.85	1,278.0	- 854.7	- 98.5	10.7
11	South Rim	182.9	2.01	751.3	407.5	-115.8	- 43.0
12	North Rim	174.3	2.29	445.6	940.3	- 81.4	- 66.1
13	Uwekahuna	139.0	2.83	319.1	1,604.4	- 57.3	- 43.0
14	Spit	277.1	0.40	- 178.9	- 896.1	1.2	96.3
15	Begger	395.9	1.16	662.0	78.6	132.3	31.1
16	Observatory	108.5	4.11	2,635.0	2,468.0	- 4.6	5.8
17		110.3	3.93				
18		207.6	2.38				
19		93.9	4.74				
20		106.1	4.63				
21		104.5	5.23				
22		96.0	6.92				
23		89.6	4.72				
24		150.	3.74				
25		125.	4.75				

---

17) R. H. FINCH and T. A. JAGGER, *Bull. Seism. Soc. Am.*, **19** (1929), 38.

the caldera subsided remarkably. Thereafter, in the period 1921–1927 the bench marks within the caldera subsided also in an exceptionally large way. The phenomenon that the caldera region subsided always relatively compared with the outer region seems to have some relation to the caldera formation.

On the other hand, the wide surrounding area except the caldera region subsided circularly and symmetrically at the time of the 1924 eruption; that is, the contours of equal depression are concentric circles of which the centre is situated at the station (*A*) near the crater, as shown in Fig. 17. Moreover the distribution of tilting of the ground surface was obtained from the results of levelling (Fig. 18) and the vectors of tilting concentrate also on the above centre of the depression. And the relation between the distanec (*d*) from the centre of depression to each bench mark and the vertical displacements (Δh) of bench marks is shown in Fig. 19 (a). However, on the wide area which is more distant than 10 km from the centre of depression, there is only one levelling route from the Volcano House to Hilo (north-east direction) and consequently it is insufficient in order to know the areal deformation. Therefore, the circular

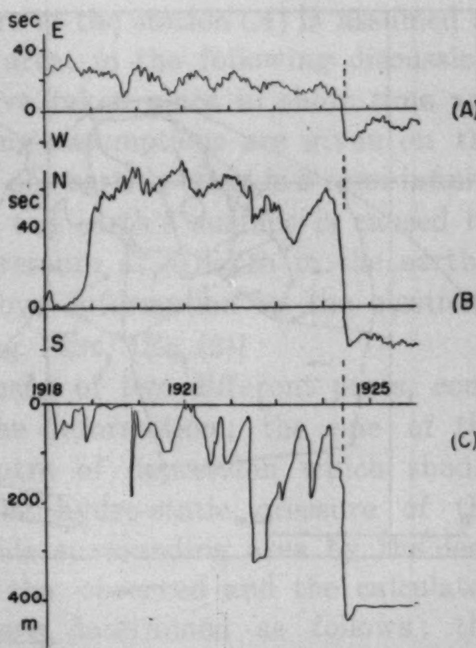

Fig. 16. (A): Tilting records in EW direction at the Observatory. (B): in NS direction. (C): Change of the depth of the crater bottom. (after T. A. Jagger and R. H. Finch)

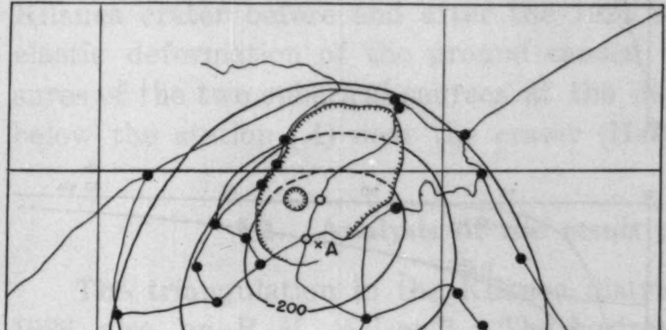

Fig. 17. Contours of equal depression around the crater, excluding the caldera region. (1921–1927) (A): Centre of depression.

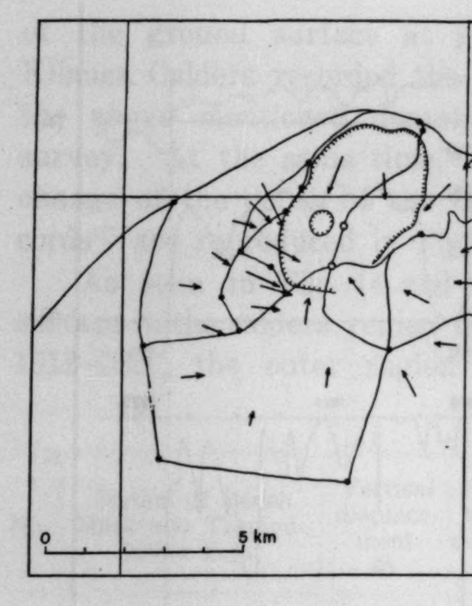

Fig. 18. Tilting of the ground surface calculated from the results of levelling survey (1921–1927).

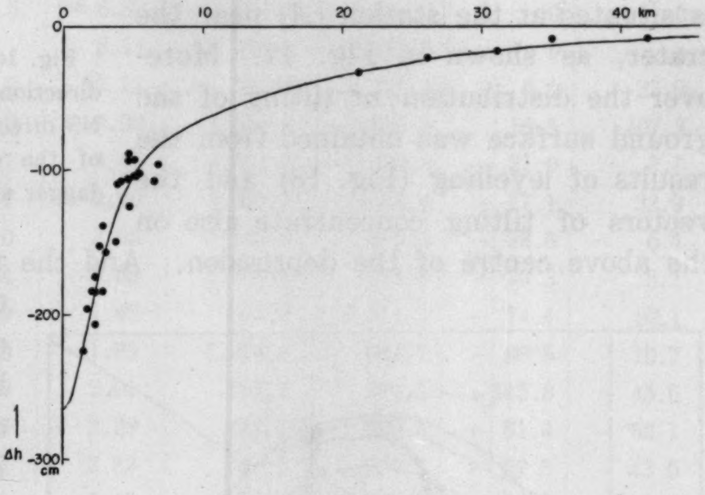

Fig. 19 (a). Relation between the vertical displacement (Δh) of bench marks and radial distances (d) of bench marks from the centre of depression, in the 1924 eruption. Curve is the calculated result of the vertical displacements versus the radial distance (d).

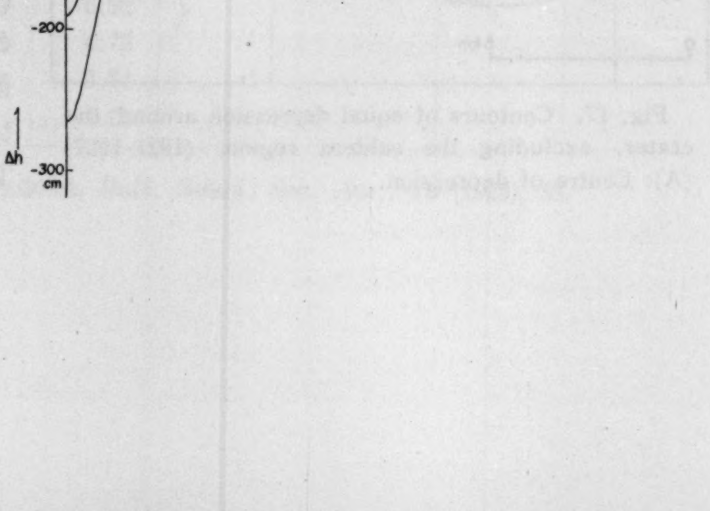

Fig. 19 (b). Calculated vertical deformation curves for the cases of the depth 3.5 km and 25 km, and the superposed deformation curve.

symmetrical deformation with its centre at the station (A) is assumed to be also true in the case of the distant area, in the following discussion.

Considering the depression to have taken place in short time and to be a circular symmetry, the following assumptions are given on the ground deformation, as in Part 1. ; (1) the earth's crust is a semi-infinite elastic solid and (2) the deformation of the earth's surface is caused by a spherical source with hydro-static pressure at a depth in the earth's crust. The calculated result of the above deformation by the elasticity theory has been shown in the preceding Part. [Eq (2)]

The observed depression may consist of two different parts, compared with the theoretical results of the deformation ; the one of the relatively limited area close to the centre of depression which should have been caused by the decrease of the hydro-static pressure of the shallow source and the other of the wide surrounding area by the deep source. By the comparison between the observed and the calculated values, the depths of two sources were determined as follows ; the shallower 3.5 ± 1 km and the deeper 25 ± 5 km, as shown in Fig. 19 (a) (b). The superposition of the above mentioned solutions which are non-linear is impossible mathematically, but the mutual effects of the two boundary conditions seem to be negligible, because the depths of the two sources are very different from each other, and therefore the superposed solution will be applicable in the present case.

Thus, the circular depression of the ground surface around the Kilauea crater before and after the 1924 eruption is explained as the elastic deformation of the ground caused by the decreases of the pressures of the two spherical sources at the depths 3.5 ± 1 km and 25 ± 5 km below the station (A) near the crater (Halemaumau).

§ 2. Analysis of the result of triangulation.

The triangulation in the Kilauea district was executed in 1922 and 1926 also by R. M. Wilson[18]. The horizontal relative displacements of triangulation points in the period 1922–1926 are shown in Fig. 20, but the triangulation points, Koae (1) and Puu Huluhulu (2), were fixed as the base points. The deformation also seems to have taken place suddenly at the time of the 1924 eruption, like the above mentioned depression. The vectors of the horizontal displacements concentrate on a station near the crater and are larger in the near vicinity of this

---

[18] R. M. Wilson, *loc. cit.* 16)

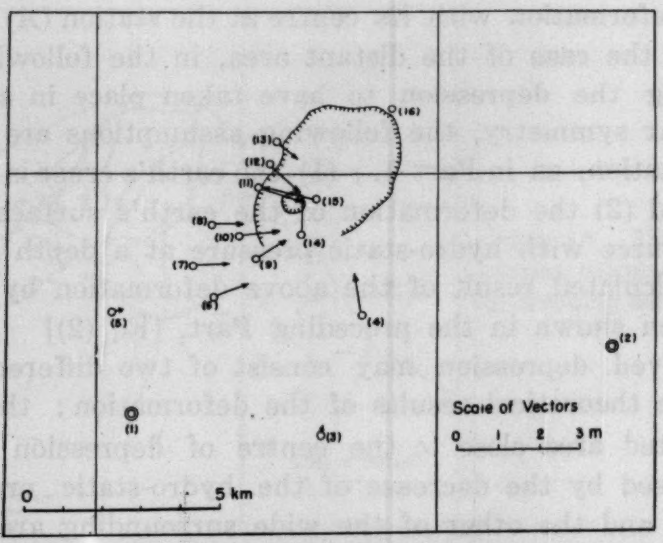

Fig. 20. Relative horizontal displacements of triangulation points around the Kilauea crater in the period 1922–1926, fixed station (1) and (2). (after R. M. Wilson)

station, like the vectors of tilting. As will be discussed in the next section, it seems that the horizontal deformations correspond to the above mentioned vertical one.

In order to the make clear the characteristics of the deformation, the two-dimensional strain on the ground surface caused by the horizontal deformation is calculated by means of C. Tsuboi's method[19]. If we take X and Y axes in the directions of west and north respectively and represent by u and v the westward and northward conponent of displacement of a triangulation point, then the dilatation, the rotation and the maximum shear are given as follows.

$$\text{Dilatation} \qquad \varDelta=\left(\frac{\partial u}{\partial x}+\frac{\partial v}{\partial y}\right)$$

$$\text{Rotation} \qquad \varpi=\frac{1}{2}\left(\frac{\partial v}{\partial x}-\frac{\partial u}{\partial x}\right) \qquad (3)$$

$$\text{Maximum Shear} \quad \varSigma=\sqrt{\left(\frac{\partial u}{\partial x}-\frac{\partial v}{\partial y}\right)^2+\left(\frac{\partial u}{\partial y}+\frac{\partial v}{\partial x}\right)^2}$$

The distributions of $\varDelta$, ϖ and $\varSigma$ are shown in Fig. 21 (a), (b) and (c) respectively. From the results, the following characteristics are noticeable.

(1) The contours of the equal dilatation and maximum shear are

---

[19] C. Tsuboi, *Jap. Jour. Astr. Geophs.*, **10** (1932–33), 93.

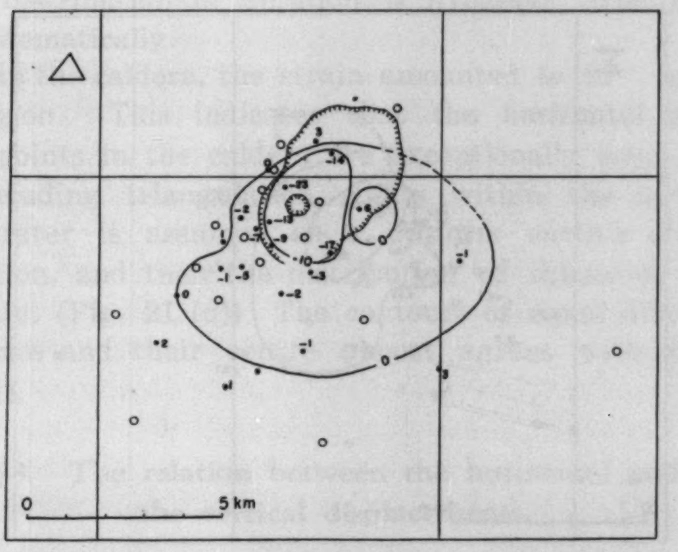
△
3
-14
0
-23
-2
-13
-6
1
-7
-9
-17
0
-1
-10
-1
-3
-3
0
-2
2
-1
0
3
1
0
5 km

Fig. 21 (a).

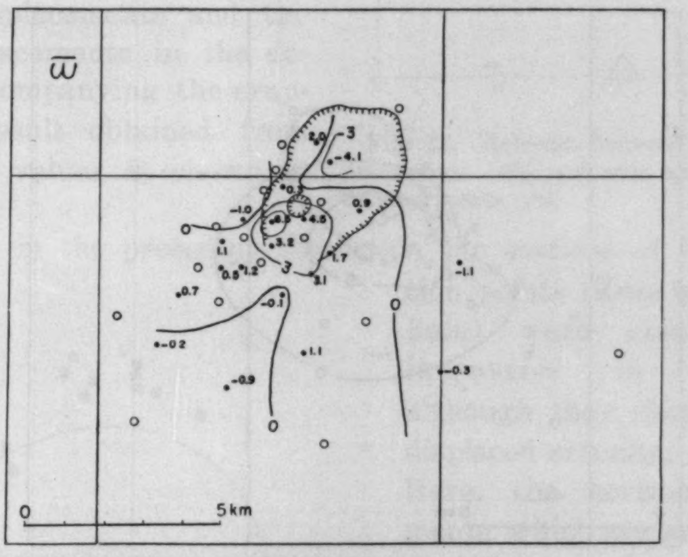
$\overline{\omega}$
2.0
-3
-4.1
0.3
0.9
-1.0
4.5
3.2
1.1
1.7
0.5
1.2
3
3.1
-1.1
0.7
-0.1
0
-0.2
1.1
-0.3
-0.9
0
0
5 km

Fig. 21 (b).

Fig. 21 (a) (b). Two dimensional strain of the ground surface around the Kilauea crater;

(a): Dilatation in 10^{-4}

(b): Rotation in 10^{-4}

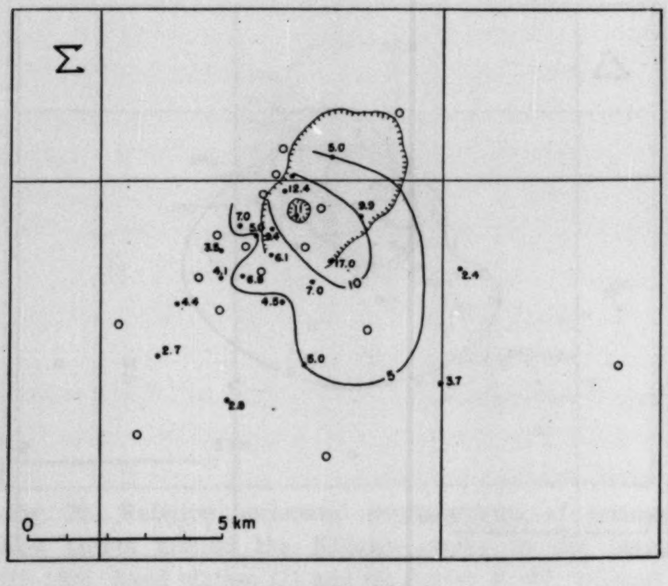
Σ
5.0
12.4
9.9
7.0
5.0
3.4
3.5
6.1
17.0
4.1
6.8
7.0
10
2.4
4.4
4.5
2.7
5.0
5
3.7
2.8
0
5 km

Fig. 21 (c).

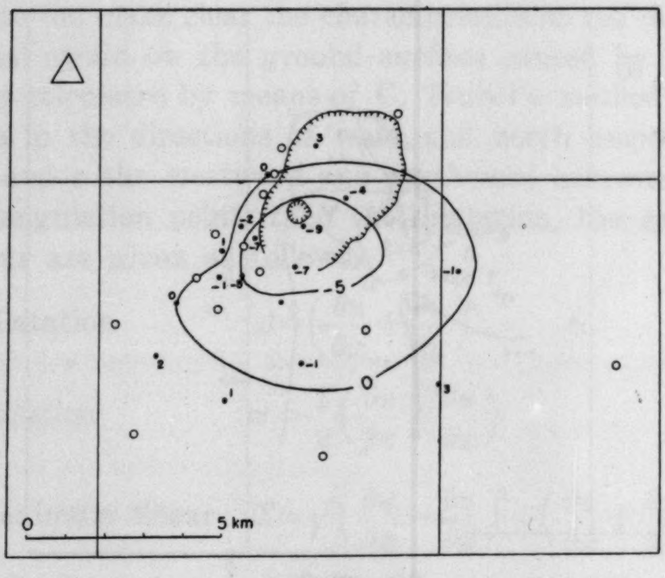
△
3
-4
-2
-9
1
-7
-7
-1
-1 -5
-5
2
-1
0
1
3
0
5 km

Fig. 21 (d).

Fig. 21 (c) (d). Two dimensional strain of the ground surface around the Kilauea crater;
(c): Maximum shear in 10^{-4}
(d): Dilatation, excluding the caldera region, in 10^{-4}

nearly concentric.

(2) The distribution of rotation is irregular, namely the area did not rotate systematically.

(3) Within the caldera, the strain amounted to 10^{-3}, against 10^{-4} on the outer region. This indicates that the horizontal movements of triangulation points in the caldera are exceptionally large.

Thus, excluding triangulation points within the caldera, the area around the crater is assumed as a uniform earth's crust, as in the preceding section, and then the distribution of dilatation on the area calculated again. (Fig. 21 (d)) The contours of equal dilatation are also concentric circles and their centre almost agrees with the centre of depression. (*A*).

§3. The relation between the horizontal and the vertical displacements.

As the stations of triangulation points coincide completely with a large part of bench marks of levellings, we can discuss sufficiently the relation between the horizontal displacements and the vertical displacements in the deformation accompanying the eruption. The result obtained from the measured values is shown in Fig. 22.

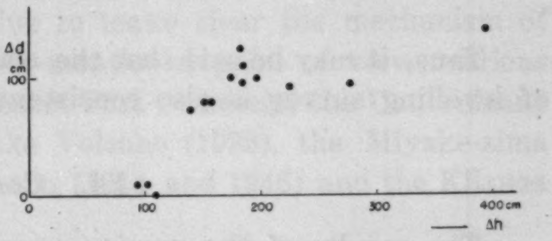

Fig. 22. Relation between the vertical displacements (Δh) and the relative horizontal displacements (Δd).

However, in the preceding discussion the stations of two triangulation points (Koae and Puu Huluhulu) were assumed to be immovable in the period, although they should have been displaced actually, more or less. Here, the horizontal displacements which are presumed from the theoretical result of the model of deformation obtained by levelling survey are assumed as displacements of the two stations. By this assumption, the absolute displacement of

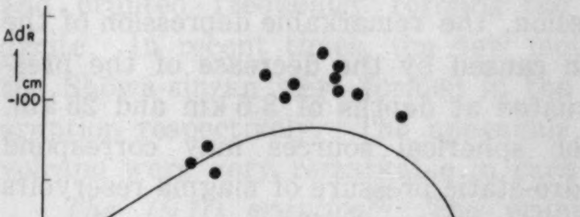

Fig. 23. Relation between the vertical displacements (Δh) and the radial components ($\Delta d_R'$) of horizontal displacements.

Curves show a theoretical result for the elastic model obtained from the result of levelling survey.

other triangulation points are estimated. The difference between the relative deformation and the absolute one obtained by the above procedure is not much qualitatively. Next, the relation between the radial component and the vertical displacement is shown in Fig. 23, and the relation between the radial component ($\Delta d'_R$) of the horizontal displacement and the radial distance (d) of the triangulation point from the centre of depression (A) is shown in Fig. 24. At the same time the calculated curve for the horizontal displacement of the model of deformation determined from the result of levelling are shown in Fig. 23 and 24, respectively.

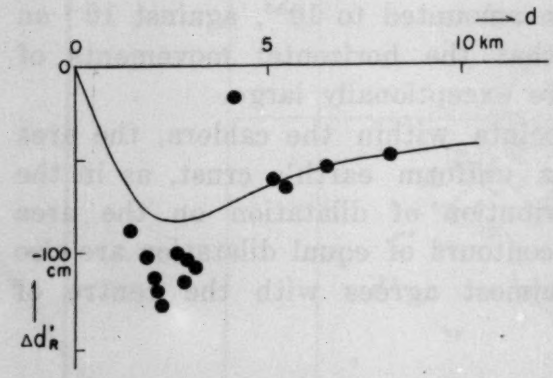

Fig. 24. Relation between the radial components of horizontal displacements ($\Delta d_R'$) and the radial distances (d) of the triangulation points from the centre (A). Curve is a theoretical result for the model.

Thus, it may be said that the elastic model obtained from the result of levelling survey is also consistent with the result of triangulation.

§4. Conclusion.

The results of the precise surveys by R. M. Wilson on the deformation of the ground surface at the time of the 1924 eruption are very interesting because of the large scale of the deformation itself and also for the reason that triangulation and levelling were executed simultaneously and independently.

According to the above discussion, the remarkable depression of the ground surface seems to have been caused by the decrease of the pressure of two spherical sources situated at depths of 3.5 km and 25 km. The changes of the pressure of the spherical sources may correspond perhaps to the decrease of the hydro-static pressure of magma reservoirs below the area and may have been caused by the intrusion or the extrusion of magma from the reservoirs. The sudden subsidence of the crater bottom before and after the 1924 eruption (Fig. 16) also suggests the above conclusion.

On the other hand, the volume of extruding lavas from the crater (Halemaumau) is relatively little. Therefore, the depression seems to be caused not by the out-flow of lavas from the crater, but by the intrusion of magma or the invisible out-flow of lavas from the rift zone under the sea. Thus, it may be concluded that the volcanic activity in 1924 took place on a large scale under the earth's surface rather than on the surface.

Part 3. Relations between the Deformations of the Ground Surface around the Volcanoes and Other Volcanic Phenomena.

As mentioned in the preceding Parts, both the eruptions of the Sakurazima Volcano (1914) and of the Kilauea Volcano (1924) were accompanied by typical enormous depression. However, there are various types of the ground surface deformation. For example, at the time of the eruption of the Usu Volcano, a remarkable upheaval of the ground surface took place, in particular more than 100 m at the limited area close to the crater and on the other hand, the depression around it was of no account.

Thus the study of the physical meaning of such various types of ground deformation will give a clue to make clear the mechanism of the volcanic eruption. From the above-mentioned point of view, various eruptions are investigated in the present Part; namely, the Usu Volcano (1910 and 1943–1945), the Komagatake Volcano (1929), the Miyake-sima Volcano (1940), the Sakurazima Volcano (1914 and 1946) and the Kilauea Volcano (1924).

§ 1. The 1910 and the 1943–1945 eruptions of the Usu Volcano.

The Usu Volcano stands at the rim of the Tōya caldera (Tōya Lake) and erupted frequently forming the lava domes or the cript domes of dacite. In recent times, the new mountains of the Yosomi-yama and the Shōwa-sinzan were formed in the 1910 eruption and the 1943–1945 eruption respectively. The upheavals of the ground surface around the volcano were very remarkable in each case.

The 1910 eruption[20] The eruption commenced from the newly opened fissure on the north flank of the mountain on July 25, 1910 and the abundant volcanic detritus of various sizes which were not dedived from fresh lavas were ejected, but the out-flow of lava did not occur. Thereafter the limited area of the ground surface near the craters was upheaved largely and the rising amounted to about 100 m.

---

[20] F. Ōmori, *loc. cit.* 1)

The phenomenon seems to have been caused by the uplift of the cript dome of very viscous lava. Preceding the eruption, a large number of earthquakes was felt in a wide area around the volcano and the radius of area of sensible motion of the strongest earthquake on July 24 amounted to about 60 km in NE direction and 140 km in SW direction.

The levelling surveys were executed repeatedly in 1905, 1911, 1912 and 1919[21]. The changes of level of bench marks before and after the 1910 eruption are shown in Fig. 26. The area around the craters was upheaved remarkably,

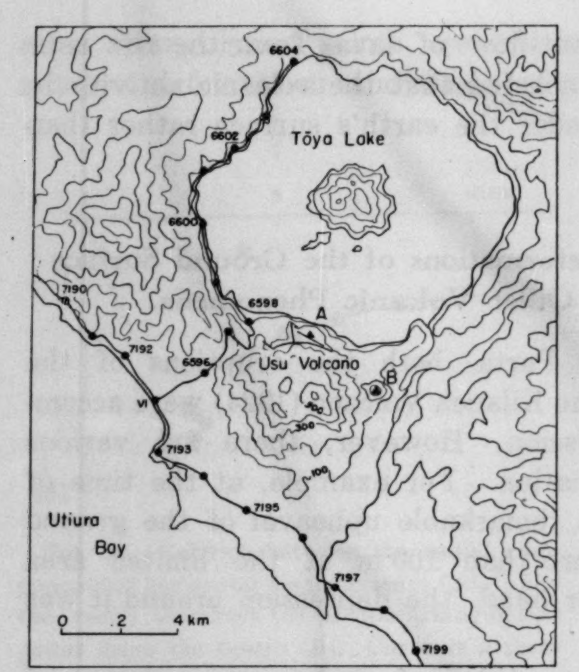
6604
6602
Tōya Lake
6600
7190
6598
A
7192
6596
Usu Volcano
B
VI
400
300
7193
100
7195
Utiura
Bay
7197
0 2 4 km
7199

Fig. 25. Topographical map around the Volcano Usu and the levelling route in the district. A: new mountain (1910) B: new mountain (1943–45).

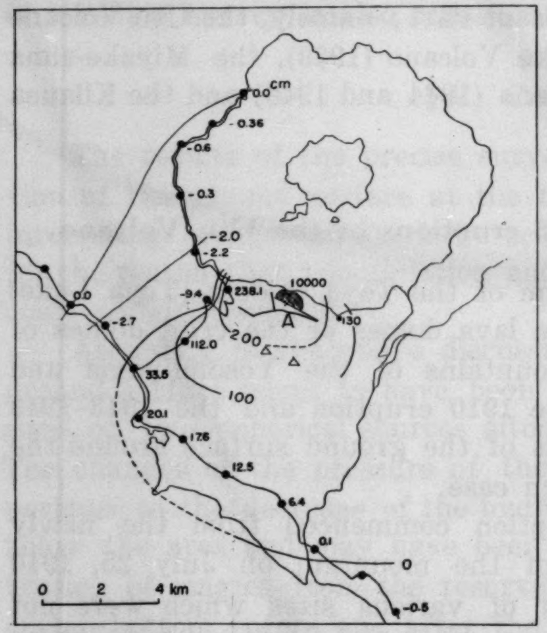
0.0 cm
-0.36
-0.6
-0.3
-2.0
-2.2
0.0
-9.4
238.1
10000
A
-2.7
130
112.0
200
33.5
100
20.1
17.6
12.5
6.4
0.1
0
0 2 4 km
-0.5

Fig. 26. Vertical displacements of bench marks and contours of equal vertical displacement around the Volcano Usu, before and after the 1910 eruption (1905–1919). (after F. Ōmori) A: new mountain.

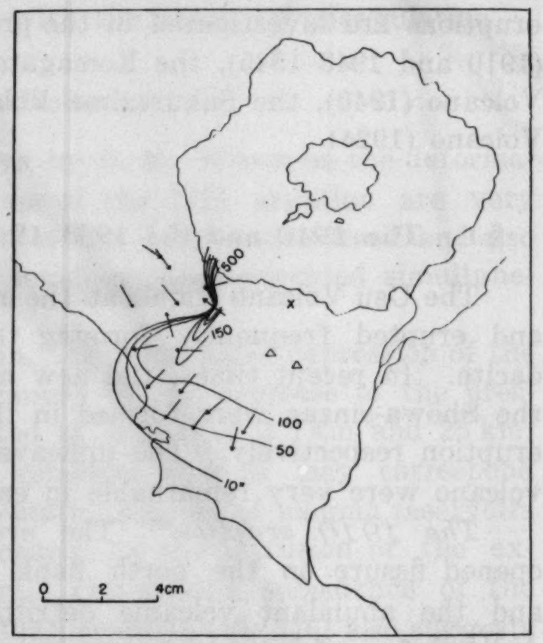
500
X
150
100
50
10"
0 2 4cm

Fig. 27. Tilting of the ground surface calculated from the results of levelling survey (1910 eruption).

---

[21] F. Ōmori, *loc. cit.* 1)

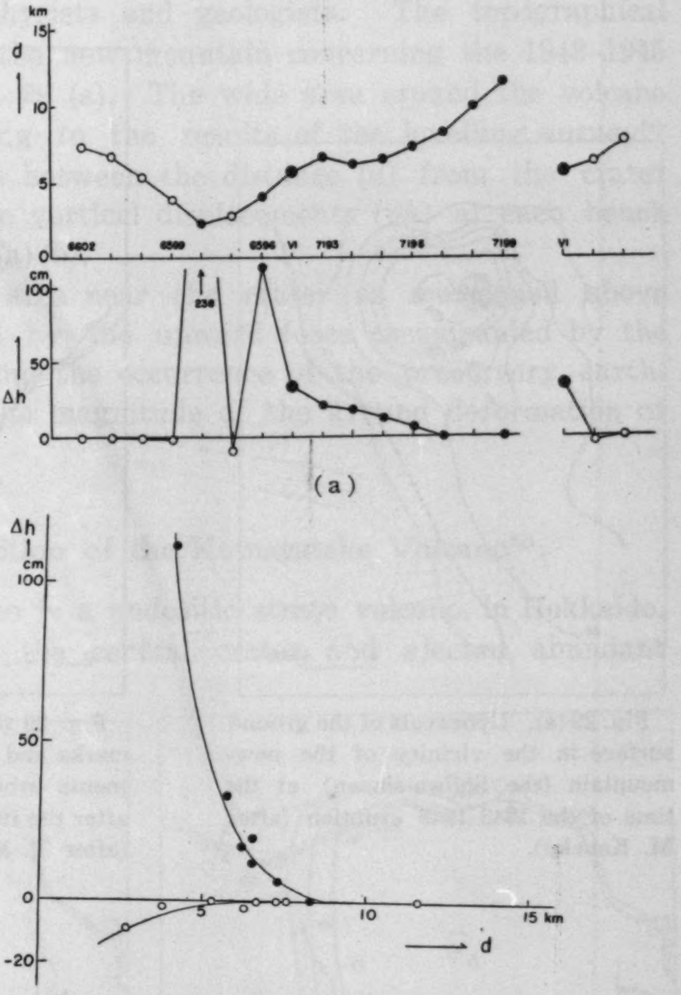

(a)

(b)

Fig. 28. (a)(b) Relation between the vertical displacements (Δh) of bench marks and the radial distances (d) of bench marks from the centre of craters, in the 1910 eruption. open circle: depression, closed circle: upheaval.

with the exception of a small amount of depression of the western region. Fig. 27 is the distribution of tilting of the ground surface around the volcano which was calculated from the results of the levelling survey. The discontinuous boundary between the depression and the upheaval is conspicuous and it suggests the formation of a fault under the ground surface. The relation between the distances (d) from the centre of craters to bench marks and the vertical displacement (Δh) is shown in Fig. 28 (a) (b). It is remarkable that the branches of upheaval and of depression in Fig. 28 (b) are symmetrical.

The 1943–1945 eruption[22] The eruption forming the new mountain of the Shōwa-sinzan was a most famous one in recent years. The precursory earthquakes began to occure from Dec. 28, 1943. The strongest earthquake of Jan. 5, 1944 was felt as far as over 20 km from the volcano. After that, eruptions took place at the area of the east flank of the mountain in June, 1944. Successively, the area was upheaved remarkably by the intrusion of lava and lastly the lava dome extruded to a height of 300 m from the ground surface. The process of development of lava dome was investigated

---

[22] T. Minakami, T. Ishikawa, and K. Yagi, *Bull. Volcanologique*, [ii], **11**, (1951), 45.

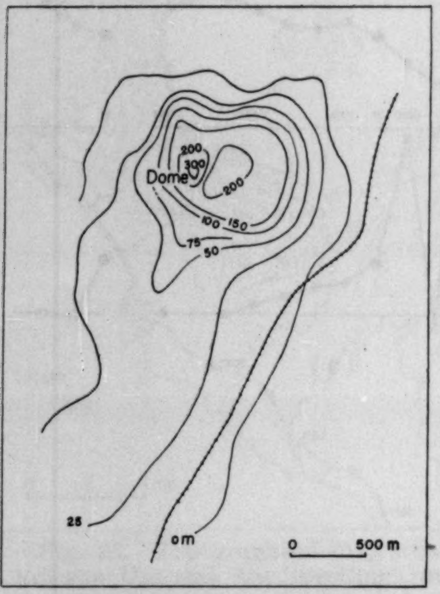
Dome
300
300
200
200
150
100
75
50
25
0 m
0
500 m

Fig. 29 (a). Upheavals of the ground surface in the vicinity of the new-mountain (the Shōwa-sinzan), at the time of the 1943–1945 eruption (after M. Kaneko).

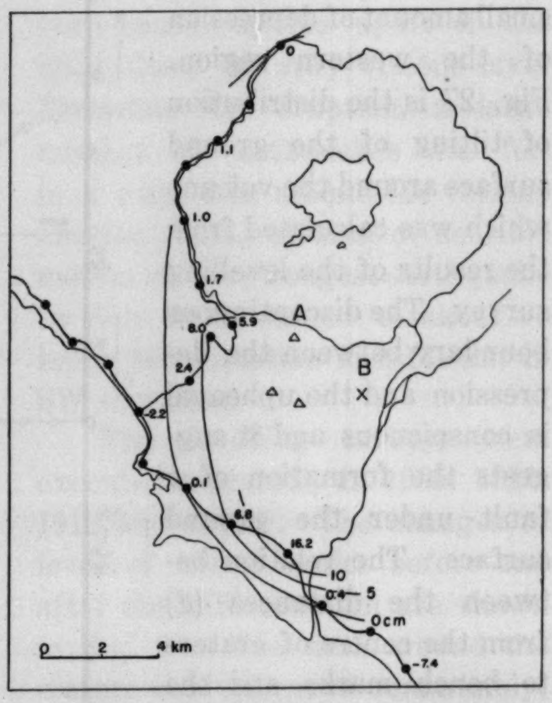
0
1.1
1.0
1.7
5.9
8.0
2.4
-2.2
A
B
0.1
6.8
16.2
10
0.4
5
0 cm
-7.4
0
2
4 km

Fig. 29 (b). Vertical displacements of bench marks and contours of equal vertical displacements around the Volcano Usu before and after the 1943–1945 eruption. B: new mountain (after T. Minakami and A. Okada)

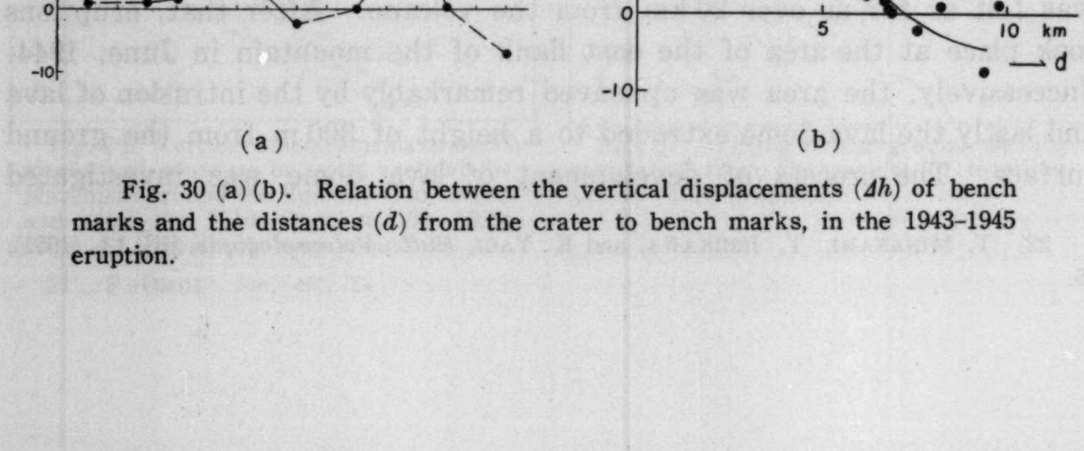

Fig. 30 (a) (b). Relation between the vertical displacements (Δh) of bench marks and the distances (d) from the crater to bench marks, in the 1943–1945 eruption.

particularly by many geophysists and geologists. The topographical change[23] in the vicinity of the new mountain concerning the 1943-1945 eruption are shown in Fig. 29 (a). The wide area around the volcano was upheaved also, according to the results of the levelling survey[24] in Fig. 29 (b). The relation between the distance (*d*) from the crater to the bench marks and the vertical displacements (Δh) at each bench mark are shown in Fig. 30 (a) (b),

These upheavals of the area near the crater as mentioned above seem to have been caused by the upward force accompanied by the uplift of the viscous lava, and the occurrence of the precursory earthquakes have reference to the magnitude of the ground deformation of this type.

§ 2. The 1929 eruption of the Komagatake Volcano[25].

The Komagatake Volcano is a andesitic strato volcano, in Hokkaido. In June 1929, it erupted at the central crater and ejected abundant

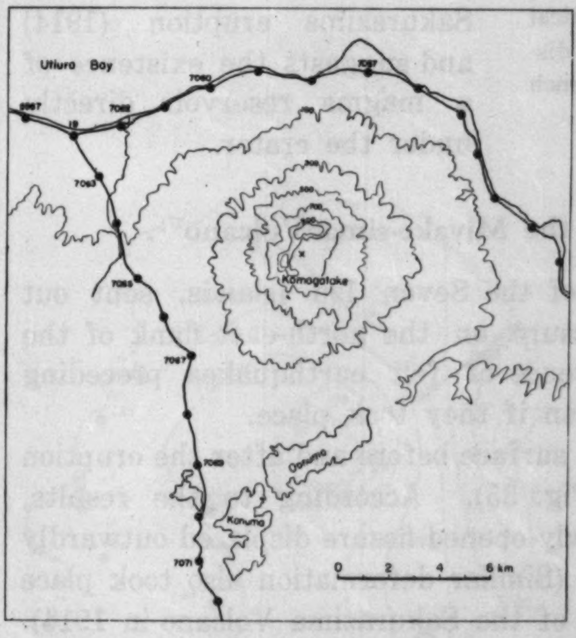
Utiura Bay
7087
7080
6967
7082
19
7063
7065
7067
7069
7071
100
300
500
700
Komagatake
Oonuma
Konuma
0
2
4
6 km

Fig. 31. Topographical map around the Komagatake Volcano and levelling route in the district.

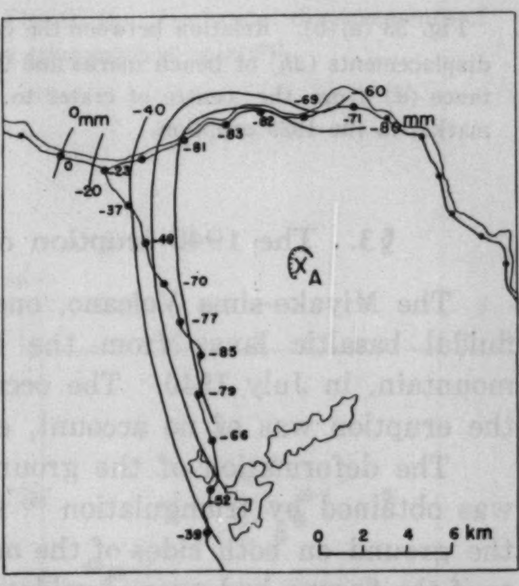
0mm
-40
-60
-69
-71
-80 mm
-81
-83
-82
0
-23
-20
-37
-40
-70
-77
-85
-79
-66
-52
-39
A
0
2
4
6 km

Fig. 32. Vertical displacements of bench marks and contours of equal depression around the Komagatake Volcano, before and after the 1929 eruption (after C. Tsuboi and the Land Surv. Depart.)

---

23) M. KANEKO, *Report Geol. Survey. Jap.*, 136 (1950).

24) T. MINAKAMI, *et. al.*, *loc. cit.* 22).

25) H. TSUYA, *et. al.*, *Bull. Earthq. Res. Inst.*, **8** (1930), 239.

pumices and ashes, but did not send out lavas. Precursory earthquakes were not felt at all by habitants near the volcano.

According to the results of the levelling survey[26] before and after the eruption, the area at the foot of the mountain subsided circular-symmetrically (Fig. 32). The relation between the distances (*d*) from the crater to bench marks and vertical displacements of bench marks (*Δh*) are shown in Fig. 33 (a) (*b*). The depression is the same type as in the case of the Sakurazima eruption (1914) and suggests the existence of a magma reservoir directly under the crater.

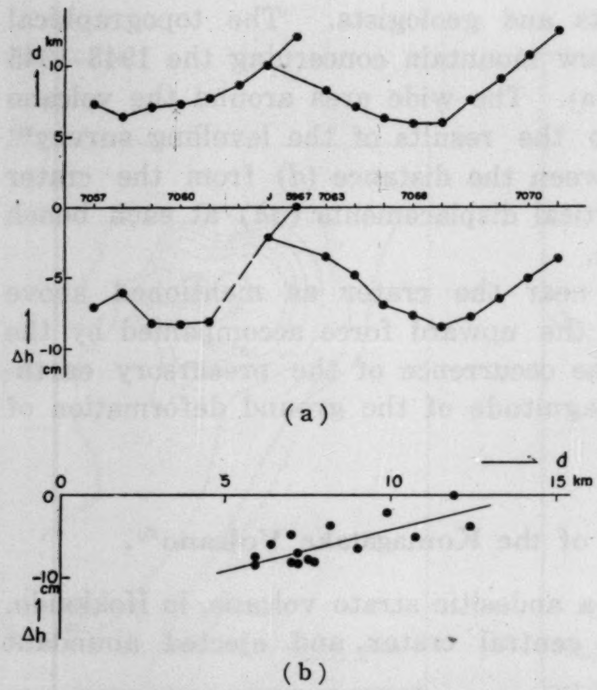

(a) (b)

Fig. 33 (a) (b). Relation between the vertical displacements (*Δh*) of bench marks and the distance (*d*) from the centre of crater to bench marks, in the 1929 eruption.

§3. The 1940 eruption of the Miyake-sima Volcano[27].

The Miyake-sima Volcano, one of the Seven Izu Islands, sent out fluidal basaltic lavas from the fissure on the north-east flank of the mountain, in July 1940. The occurence of felt earthquakes preceding the eruption was of no account, even if they took place.

The deformation of the ground surface before and after the eruption was obtained by triangulation [28] (Fig. 35). According to the results, the ground on both sides of the newly-opened fissure displaced outwardly as if the fissure had opened wider. (Similar deformation also took place at the time of the fissure eruption of the Sakurazima Volcano in 1914). The area around the caldera subsided and this seems to suggest that the magma reservoir is situated below the caldera. But, the accuracy

---

[26] C. TSUBOI, *Bull. Earthq. Res. Inst.*, **8** (1930), 298.

[27] H. TSUYA, *et. al.*, *Bull. Earthq. Res. Inst.*, **19** (1941), 260.

[28] *Bull. Earthq. Res. Inst.*, **19** (1941), 544.
S. OMOTE, *ibid.* **20** (1942), 127.

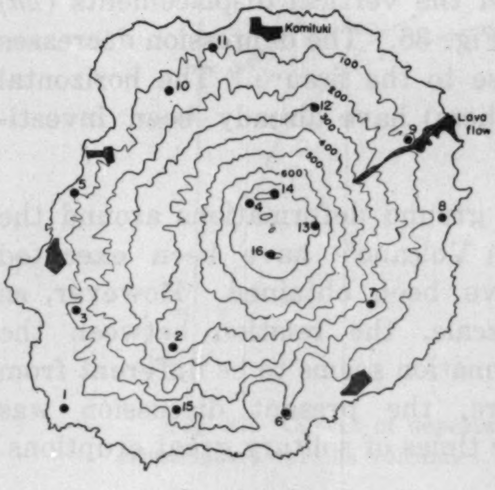
Komituki
Lava flow
100
200
300
400
500
600
1
2
3
4
5
6
7
8
9
10
11
12
13
14
15
16
0 1 2 3 4 km

Fig. 34. Topographical map of the Miyakesima Volcano.

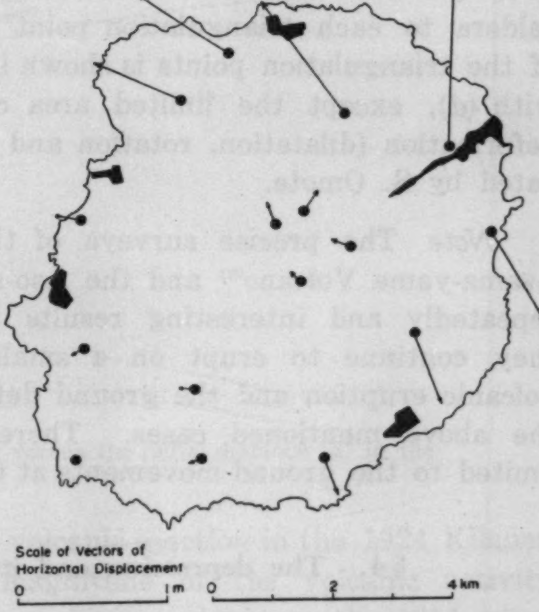
Scale of Vectors of Horizontal Displacement
0 1m
0 2 4 km

Fig. 35 (a). Horizontal displacements of the triangulation points[28].

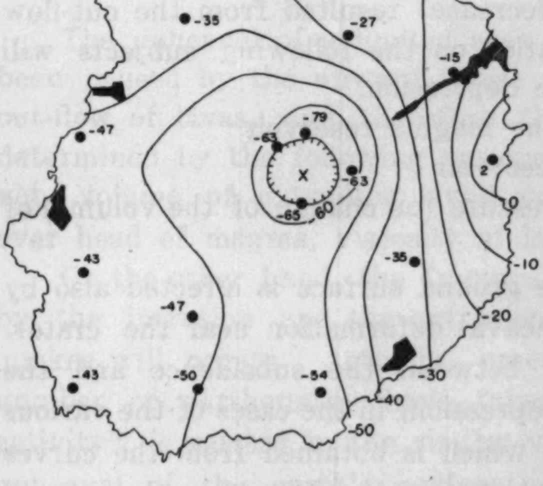
-31
-35
-27
-15
-47
-79
-63
-63
-65
60
2
0
-10
-43
-47
-35
-20
-43
-50
-54
-30
-40
-50
0 2 4 km

Fig. 35 (b). Vertical displacements before and after the 1940 eruption[8]. (in cm)

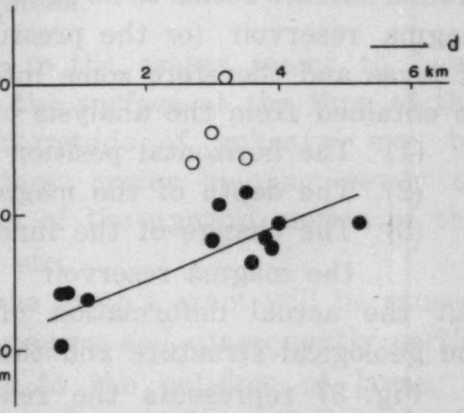

Fig. 36. Relation between the vertical displacements of the triangulation points and the distances (*d*) of triangulation points from the centre of caldera. (open circle: triangulation points close to the fissure).

of vertical displacements by triangulation is insufficient to discuss quantitatively. The relation between the distances (d) from the centre of the caldera to each triangulation point and the vertical displacements (Δh) of the triangulation points is shown in Fig. 36. The depression decreases with (d), except the limited area close to the fissure. The horizontal deformation (dilatation, rotation and others) have already been investigated by S. Omote.

Note The precise surveys of the ground deformations around the Asama-yama Volcano[29] and the Aso-san Volcano[30] have been executed repeatedly and interesting results have been obtained. However, as they continue to erupt on a small scale, the relation between the volcanic eruption and the ground deformation seems to be different from the above mentioned cases. Therefore, the present discussion was limited to the ground movements at the times of solitary great eruptions.

§4. The depression and its volcanological meaning.

As the eruptions are essentially the phenomena of out-flow of lavas from a depth in the earth's crust, the depression of the ground surface related to the deep sources seems to be clue to make clear the mechanical changes of the inner state of the earth's crust before and after the eruption.

As mentioned in the preceding discussion, the depression of the ground surface seems to be caused by the decrease of the volume of the magma reservoir (or the pressure decrease) resulted from the out-flow of lavas and therefore some information on the following subjects will be obtained from the analysis of the depression.

(1) The horizontal position of the magma reservoir
(2) The depth of the magma reservoir
(3) The change of the inner pressure (or change of the volume) of the magma reservoir

But the actual deformation of the ground surface is affected also by the geological structure and the upheaval deformation near the crater.

Fig. 37 represents the relation between the subsidence and the radial distance from the centre of depression, in the cases of the various eruptions. The volume of subsidence which is obtained from the curves corresponds to the magnitude of volcanic activities under the ground

---

[29] T. MINAKAMI, *Bull. Volcanologique*, **[ii]**, **18** (1956), 65.

[30] K. YOSHIKAWA, *Zisin* (*Jour. Seis. Soc. Japan*) **[ii]**, **7** (1954), 151.

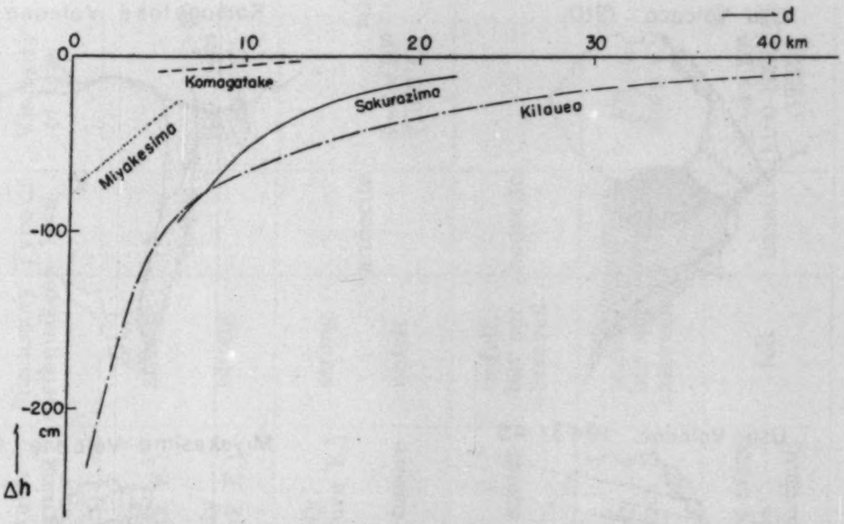

Fig. 37. Curves of depression versus the radial distance (*d*) in the eruptions of various volcanoes.

surface. For example, although the volcanic ejection in the 1924 Kilauea eruption was relatively small, the magnitude of the volcanic activity under the ground surface might have been as large as the 1914 great eruption of the Sakurazima Volcano. It has been supposed that the enormous volume of magma extruded perhaps from the east zone in the sea bottom[31], but we could not observe it.

§5. The upheaval around the crater and the other volcanic phenomena.

The upheaval of a limited area close to the crater seems to have been caused by the upward forces near the surface at the time of the out-flow of lavas, and therefore the magnitude of upheaval may be determined by the following various factors; crater opening newly or not, volume of extruding lavas, velocity of the upward motion of the over head of magma, viscosity of lavas, etc.

On the other hand, the fracture of the earth's crust will be caused by the intrusion and the extrusion of magma and consequently earthquakes will occure. Actually, preceding to the out-flow of lavas, a number of earthquakes have taken place frequently, and the seismic activity[32] is related to the similar various factors, as the case of the upheaval of the earth's surface near the crater (volume of extruding

---

31) G. A. MACDONALD, *Catalogue. Active Volc. World, Part* 3 (1955), 27.

32) T. MINAKAMI, *et. al., loc. cit.* 22)

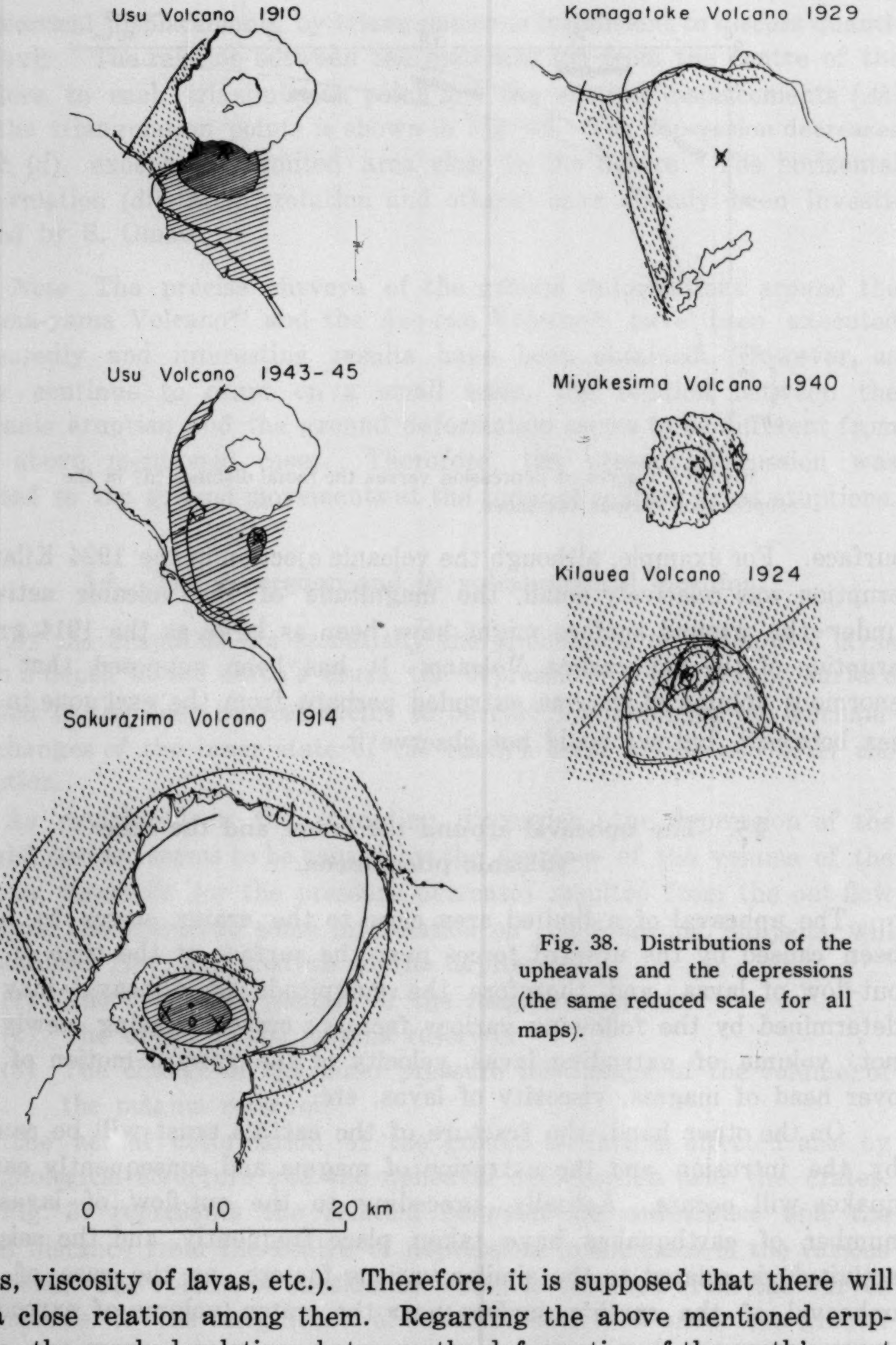
Usu Volcano 1910
Komagatoke Volcano 1929
Usu Volcano 1943-45
Miyakesima Volcano 1940
Kilauea Volcano 1924
Sakurazima Volcano 1914
0
10
20 km

Fig. 38. Distributions of the upheavals and the depressions (the same reduced scale for all maps).

lavas, viscosity of lavas, etc.). Therefore, it is supposed that there will be a close relation among them. Regarding the above mentioned eruptions, the marked relations between the deformation of the earth's crust and the other volcanic phenomena are listed in Table 4.

Table 4.

Volcano	Year	Ground surface deformation			Volume of ejecta	Crater opening	Precursory earthquakes	Type of lava	Viscosity of lava
		Volume of depression	Volume of upheaval	Maximum upheaval					
		km^3	*km*^{3}	*m*	*km*^{3}				
Usu	1910	0.0	—	~100	—	newly (flank E.)	strong	dacite	10^{11}—10^{12} (1000°C)[33]
	1943 -45	—	0.18	~300 (200)*	—	newly (flank E.)	strong		
Sakurazima	1914	0.7	~0.1	~ 10	2.2	newly (fissure E.)	strong	andecite	$3\sim6\times10^{6}$ (1000°C)[34]
	1946	—	—	—	0.08	old fissure	unfelt		
Komagatake	1929	0.03	—	—	0.05[35]	old crater	unfelt, but not observed.	andecite	—
Miyakesima	1940	0.08?	0.00	0.02	0.02[36]	newly (fissure E.)	unfelt, but not observed.	basalt	7×10^{5} (1000°C)[37]
Kilauea	1924	1.5 (0.3)**	0.00	0.00	0.0002[38]	active crater (Halemaumau)	felt	basalt	$2\sim4\times10^{4}$ (1100–1050°C) (1952)[39]

* Upheaval of the old layer (the roof mountain).

** Volume of depression in the circular region of radius of 5 km of which the central is the crater.

---

[33] T. Minakami, *et. al., loc. cit.* 22)
[34] T. Hagiwara, *et. al., loc. cit.* 12)
[35] H. Tsuya, *et. al., loc. cit.* 25)
[36] H. Tsuya, *et. al., loc. cit.* 27)
[37] T. Hagiwara, *Bull. Earthq. Res. Inst.*, **19** (1941), 299.
[38] G. A. Macdonald, *loc. cit.* 31)
[39] G. A. Macdonald, *U. S. Geol. Survey Bull.*, 1021-B (1955), 15.

Summary and Acknowledgment

The various deformations of the ground surface around the volcano before and after the eruptions were investigated, on the basis of the results of the precise levellings and triangulations. According to the above investigation, there are two types of ground deformation ; one is the circular depression of the wide area which is concerned with the change of the state of the magma reservoir and the other is the upheaval of the limited area near the crater which is caused by the extrusion of lavas. The two types of ground deformation will take place more or less in all cases of eruptions, but their magnitudes seem to depend on the characters of the eruption. The remarkable relation between the ground deformation and the other volcanic phenomena was obtained in this paper. Moreover the writer discussed the mechanism of the eruption owing to the investigation of the ground deformation, particularly in the Sakurazima eruption (1914) and the Kilauera eruption (1924).

In conclusion, the writer wishes to express his sincere thanks to Prof. T. Minakami who gave him much advice and encouragement.

---

6. 火山の噴火とその周辺の地殻変動との関係

地震研究所 茂木清夫

噴火の際に火山周辺の地殻が著しく変動することは，古く1910年の有珠山の噴火の場合に大森博士によつて精密水準測量が行われて以来，主な噴火について同様の測量が実施されて，次第に明らかになつて来た．これらの火山周辺の地殻変動に関する研究は必ずしも少なくないけれども，火山の噴火の機構との関係としてその火山学的意味を吟味したものはほとんど見られない．本論文ではこれまでに得られた測量の結果を調べて地殻変動の特性及び，噴火現象との関係を明らかにすることを試みた．

第1部では桜島の大正3年の大噴火及びその後の火山活動に関係した地殻変動を論じ，第2部でKilauea 火山の1924年噴火の際の大規模な沈降を解析してその機構を考察した．第3部に於いて，その他の諸火山の噴火を加えて，地殻変動の一般的な特性を論じ，噴火に関係する他の諸現象，例えば火山性地震の発生などとの密接な関係を明らかにした．これらの結論を要約すると次の様になる．噴火に関係した地殻変動には2つの type があつて，その発生機構を異にし，この両者が重なつて現れるのが一般である．その一つは火口の近傍の比較的狭い地域に起る隆起であつて，有珠山の場合の様に極めて著しい場合がある．これは溶岩が地下から流出する過程に於いて地殻上層を押し上げることによつて起つたものと考えられ，その大きさは溶岩の粘性や火口形成の状況等に関係するものである．もう一つの変動は一般に更に広い地域に一様に起る沈降で，これは地下に存在すると考えられる溶岩溜の容積が，噴火の際の溶岩の流出の結果急激に減少するために起つたものと推定される．例えば大正3年の桜島の噴火の際に起つた鹿児島湾岸一帯の沈降は火口の北方 10 km 深さ 10 km の溶岩溜の状態の変化によつて起つたと考えられ，この溶岩溜の位置が古いアイラ火山の直下に存在することは興味ある事である．またこの様な沈降の規模は地下に於ける活動の規模を推定するのに役立つと考えられる．例えば1924年の Kilauea 火山の噴火では火口からの溶岩の噴出は微々たるものであつたが，地下活動は桜島の大噴火に匹敵する規模のものであつたと推定される．

BULLETIN OF THE EARTHQUAKE
RESEARCH INSTITUTE
Vol. 36 (1958), pp. 135-138

7. *On the Geochemical Study of Carbon 14. (II). Agedating of Volcanic Product and the Rate of Peat Sedimentation.*

BY Makoto SHIMA and Eiiti MINAMI,
Earthquacke Research Institute.

(Read April 23, 1957.—Received March 31, 1958.)

1. Introduction.

In part I of this study[1], the age dating method with carbon 14 was applied to Ozegahara peat. An over-all view of the counting system is shown in Fig. 1, and Fig. 2 is an end-on view of the assembly in place with the door of the shield. The peat layer was about 4.8 m thick and contains layers of volcanic products ; the vertical section at Naka-

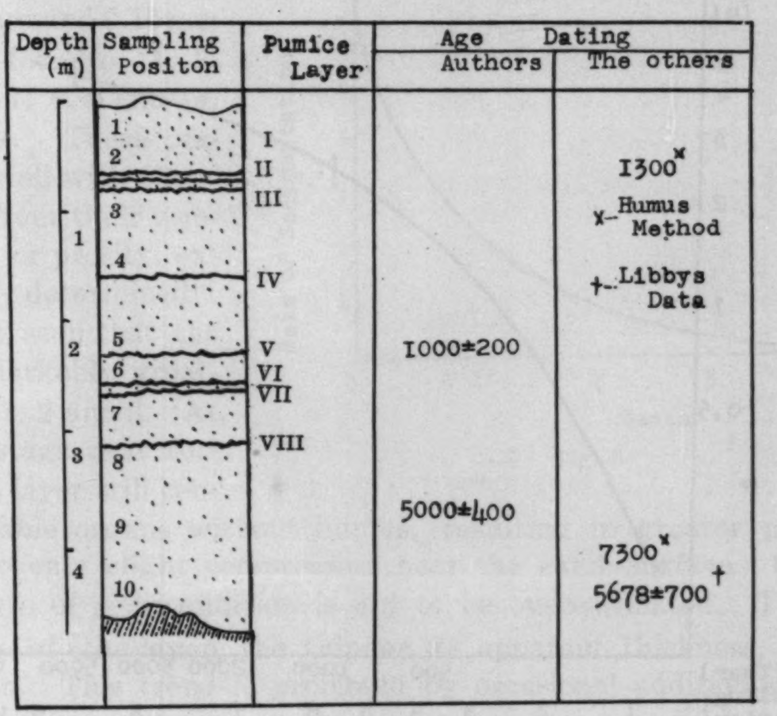
Depth (m)
Sampling Positon
Pumice Layer
Age Dating
Authors
The others
1
2
3
4
1
2
3
4
5
6
7
8
9
10
I
II
III
IV
V
VI
VII
VIII
1000±200
5000±400
1300ˣ
×-- Humus Method
+-- Libbys Data
7300ˣ
5678±700⁺

Fig. 3

---

[1] M. SHIMA, *Bull. Chem. Soc. Japan*, **29** (1956), 443.

tashiro is shown in Fig. 3. Results of age dating are also summarised in Fig. 3.

In Fig. 3 are also tabulated the ages calculated by Sakaguchi[2] from the rate of humus. A value of 5678±700 was obtained at Chicago University[3]; which made use the carbon 14 method on the request of the Ozegahara scientific research committee. This value being in an approximate agreement with the authors' results, the age of the layers of volcanic product was estimated on the basis of the authors experimental results on the age of peat and the rate of sedimentation.

2. Results and Discussion.

When the depth of the sediments was plotted against its age, a curve was obtained as shown in Fig. 4. Since the age of the samples used for age dating was known, it was plotted along the horizontal axis.

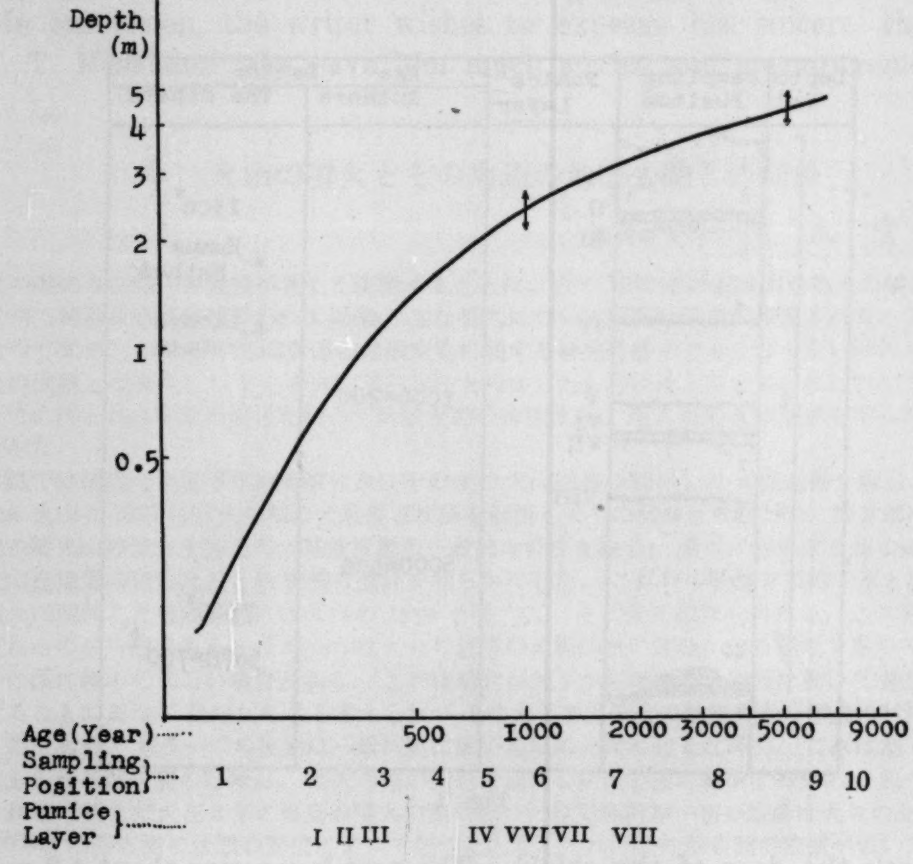

Fig. 4

---

[2] Ozegahara Scientific Research Committee, *Ozegahra*, 63 (1952), 841.

[3] *ibid.*

It was assumed that no significant change took place in the rate of sedimentation and the external condition for formation of layers, including compression of the volcanic product layer.

The age of formation of samples No. 2, 3, 4, 5, 6, 7, 8, 9, and 10 are approximately estimated as 250, 400, 580, 780, 1100, 1700, 3200, 6000, and 7800 years ago, respectively. On the basis of these values, the layers of volcanic product II and III seem to have sedimented about 300 years ago and those IV and V about 1000 years ago. When compared with the results on the rate of humus, (II, III, 1300 years ago, the peat layer at 4.8m depth, 7300 years ago) the present results for old layers agree well but new ones do not.

The rate of sedimentation was then estimated with the aid of the data in Fig, 4, for the layers from which the samples were collected. The approximate values are shown in Fig. 5; they are 5.5 mm, 3.6mm, 2.2 mm, 1.4 mm, 0.98 mm, 0.53 mm, 0.33 mm, 0.18 mm, 0.15 mm and 0.15mm per year, for No. 1, 2, 3, 4, 5, 6, 7, 8, 9 and 10, respectively. These values agree well with those calculated from their compressibility or prosity, experimentally determined[4]. It is clearly seen that the rate is remarkably greater for No. 1, 2 and 3. At the initial stage peat formation, the layer still contains vegetable organs without humus, resulting in greater prosity; it is subject to only slight compression near the earth-surface. Hence the apparent rate of sedimentation is apt to be overestimated. The deeper the location of the layer, the thinner its apparent thickness, owing to coalnifization. This trend is promoted by occasional addition of volcanic products.

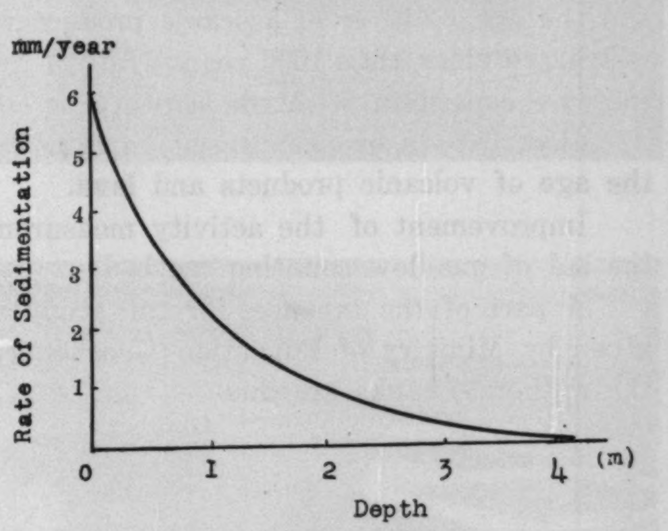

Fig. 5

According to the results on the rate of humus of organic substance, it is indicated that 5700 years passed between the formation of II and III layers and that of the deepest layer. This suggests that a layer as thick as 3.6 m was deposited within this period. Thus the mean rate of sedimentation is 0.78 mm per year, much greater than that (0.07 mm per year) for shallower layers than one meter. This does not agree with the common conception that the thickness of a layer decreases with time.

---

[4] N. YAMAGATA, Details of this will be published in the near future.

Although the carbon 14 dating method can provide only approximate values for samples as old as 1000 years, the authors' result appears to be more easily interpreted by the conventional concept about sedimentation.

3. Conclusion.

The age of various peat layers at Ozegahara and their rate of sedimentation were discussed with the aid of carbon 14 dating method and the age of layer of volcanic product was also estimated. For these which are older than 1000 years, (fairly) resonable results were obtained, that are consistent with the porosity or compressibility of the layers.

Closer study on each specimen is now in progress with reference to the age of volcanic products and lava.

Improvement of the activity measurement is also being tried with the aid of gas-flow counting method.

A part of the expenses for this study was defrayed from the grant given by Ministry of Education (Geochemical study of Volcanos) to which the authors' thanks are due.

---

7. ^{14}C による地球化学的研究 (II)

火山噴出物の年代および泥炭の沈積速度について

地震研究所 島 誠
南 英一

尾瀬ヶ原泥炭層の年代決定に引続き，泥炭層の中に 8 層の火山噴出物があるので，これの年代を定めた．^{14}C による年代決定法と腐植速度からの計算を照合した．次いで，泥炭層の沈積速度を ^{14}C による年代から計算した．泥炭層の垂直方向の存在位置により，沈積速度は変化する．即ち上部と下部では異なつた結果を示した．

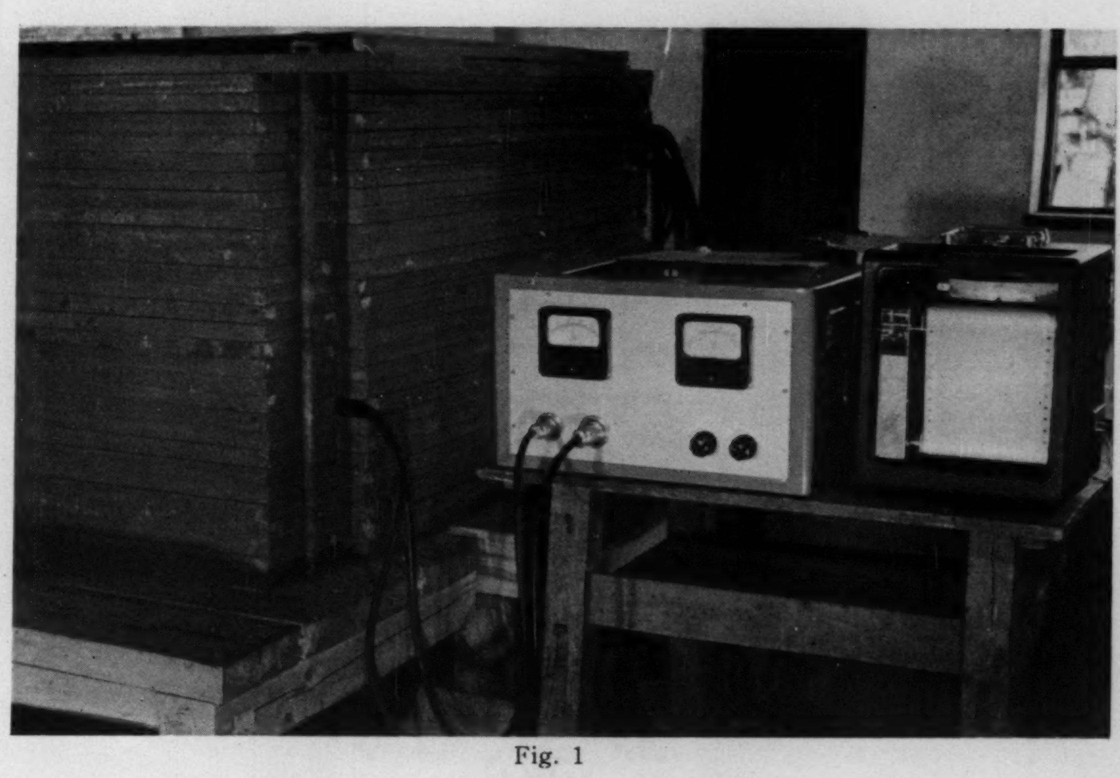

Fig. 1

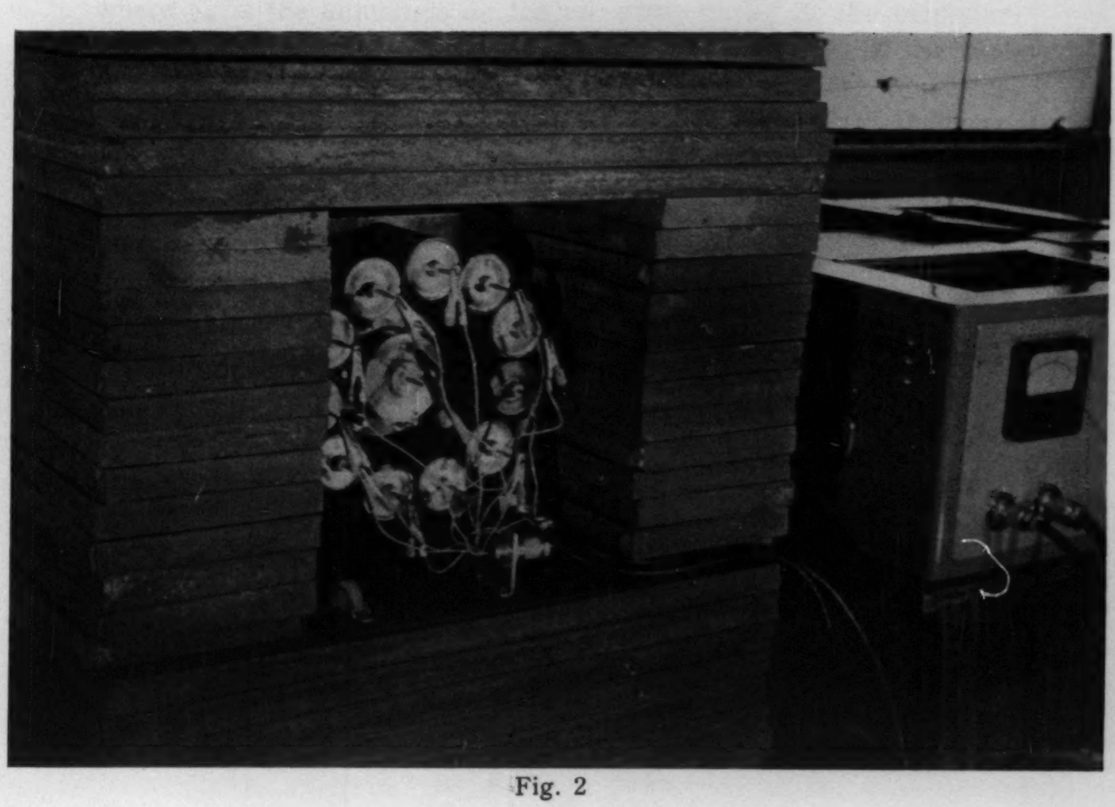

Fig. 2

（震研彙報 第三十六号 図版 島・南）

BULLETIN OF THE EARTHQUAKE
RESEARCH INSTITUTE
Vol. 36 (1958), pp. 139-164

8. *A Note on the Theory of the Electromagnetic Seismograph.*

By Takahiro HAGIWARA,

Earthquake Research Institute.

(Read October 23, 1956.—Received March 31, 1958.)

Abstract

An attempt was made to derive the expressions for the theory of the electromagnetic seismograph in a more convenient form for practical use.

The magnification of the electromagnetic seismograph of the moving coil type was found to be expressed in the following form.

$$\frac{y_m}{x_m}=Q\cdot f$$

$$Q=MH\frac{2\pi}{T_1}\left(\frac{2\pi}{T_2}\right)^2 S_1S_2\mu_1\frac{1}{Z_{11}}$$

where y_m is the amplitude on the recording drum, x_m the maximum amplitude of the simple harmonic motion of the ground, M the mass of the pendulum of the transducer, H the distance between the center of gravity and the axis of rotation of the pendulum, T_1 the transducer period, T_2 the galvanometer period, S_1 the sensitivity of the transducer when regarded as a sort of galvanometer (angular deflection of the pendulum when unit direct current is given to the transducer coil), and S_2 the sensitivity of the galvanometer (displacement of the light spot on the recording drum when unit direct current is given to the galvanometer coil). μ_1, the attenuation factor newly defined here, expresses the ratio of the current through the galvanometer coil and the current through the transducer coil when the galvanometer is cramped, and Z_{11} is the resistance of the transducer coil plus its external damping resistance. f, the period response of the seismograph, is given as a function of h_1, h_2, T_2/T_1, σ, and T_ω/T_1, where h_1 is the damping constant of the transducer, h_2 the damping constant of the galvanometer, σ the coupling factor, and T_ω the period of the ground motion.

The coupling factor σ was found to be expressed in the following form.

$$\sigma^2=\frac{(h_1-h_{01})(h_2-h_{02})}{h_1h_2}\frac{Z_{22}}{Z_{11}}\mu_1^2$$

where h_1 is the damping constant of the transducer while h_{01} is the same constant when the circuit is open and hence no current passes through the coil. h_2 and h_{02} are the analogous quantities for the galvanometer. Z_{11} is the resistance of the transducer coil plus its external damping resistance. Z_{22} is the analogous quantity for the galvanometer.

It should be noticed that the above expression for σ does not contain the mass or the moment of inertia of the pendulum as well as of the galvanometer. This means that we can never avoid the reaction of the galvanometer against the transducer simply by using a heavy mass as the pendulum. When no additional damping device is attached to the pendulum, the only way to make σ small is to reduce the attenuation factor μ_1. If the transducer has no additional damping device and the damping is caused simply by the current through the coil, then $h_1 \gg h_{01}$, and for the galvanometer also $h_2 \gg h_{02}$. The seismograph is designed, in many cases, so that $Z_{11} \approx Z_{22}$. In such a case, σ is approximately equal to μ_1.

Numerical calculation for the period response of the seismograph, of which the result is indicated in Fig. 3~20, shows that if we make $\sigma < 1/3$ the reaction of the galvanometer will be neglected even in the case when T_1 coincides with T_2 and the reaction of the galvanometer is expected to be most effective.

1. Introduction

Since the first investigation of Galitzin, the theory of the electromagnetic seismograph of the moving-coil type has been developed by Wenner, Coulomb and Grenet, Schmerwitz, Eaton and other investigators. The historical outline of the development is stated in Eaton's paper[1].

Tazime also investigated theoretically the coupling factor, which is a standard of the reaction of the galvanometer on the pendulum, replacing mechanical quantities by electrical ones[2]. Although the theory of the electromagnetic seismograph has been almost completed by these investigators, the author faced the necessity of writing the mathematical expression in a more understandable form for the convenience of designing and calibrating the seismograph. When the electromagnetic seismograph is treated mathematically, we used to consider simply the shunt resistance between the transducer and the galvanometer. However, as Neumann[3] pointed out, it is necessary in routine seismological observation to control the magnification of the seismograph from time to time, because the microseisms predominate in Winter while they become quiet in Summer except when a typhoon or cyclone appears, and therefore the seismograph must have an attenuation circuit reducing the magnification to a desired value keeping the damping constants of both the transducer and the galvanometer unchanged. Then it would be more practical to consider an attenuation circuit rather than the simple shunt resistance at the start of the mathematical treatment of the electromagnetic seismograph. In this paper, the attenuation factor was defined as the ratio of the current through the galvanometer coil and the current through the transducer coil when the electromotive force is given simply to the transducer coil. Introducing such a new quantity, and guided by the previous investigators, an attempt was made to find out the mathematical formulae in convenient form for the design and calibration of the electromagnetic seismograph.

---

[1] **Eaton**, J. P., *Bul. Seism. Soc. America*, **47** (1957), 37–75.

[2] **Tazime**, K., *Jour. Fac. Sci. Hokkaido Univ.*, [**vii**], **1** (1957), 55–67.

[3] **Neumann**, F., *Trans. American Geophys. Union*, **37** (1956), 483–490.

2. Formulae for computing the magnification of the elertromagnetic seismograph

We consider the attenuation circuit of T-type inserted between the transducer and the galvanometer as shown in Fig. 1. The circuit diagram shows that

R_1 is the resistance of the transducer coil;
I_1 is the current through the transducer coil;
R_2 is the resistance of the galvanometer;
I_2 is the current through the galvanometer coil;
X_1, X_2, and X_3 are the resistances of the T-type attenuator;
V_1 is the electromotive force induced in the transducer coil; and
V_2 is the electromotive force induced in the galvanometer coil.

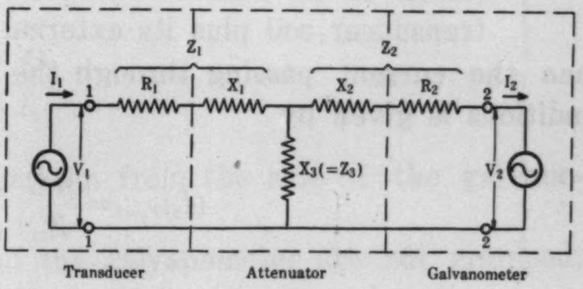

Fig. 1.

V_1 is given by

$$V_1 = G\frac{d\theta}{dt} \tag{1}$$

where

θ is the angular deflection of the pendulum of the transducer;

t is the time; and

G is the electrodynamical constant of the transducer.

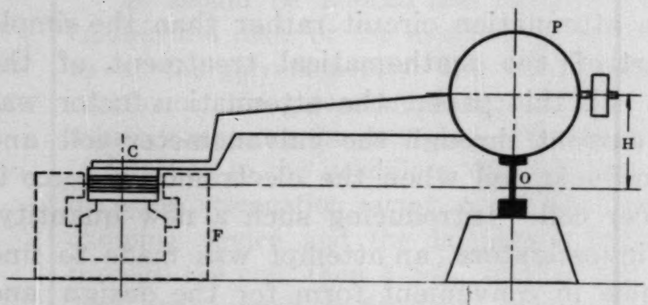

Fig. 2.

For the arrangement as shown in Fig. 2, G is the circumference times the number of turns of the coil, times the field strength of the magnet, times the distance from the coil and the axis of rotation of the pendulum. If the galvanometer is cramped and no electromotive force is induced in the galvanometer coil, then

$$(I_1)_{V_2=0}=\frac{V_1}{Z_{11}}=\frac{G}{Z_{11}}\frac{d\theta}{dt} \qquad (2)$$

where

Z_{11} is the resistance measured from the terminals 11 when the terminals 22 are shorted and corresponds to the resistance of the transducer coil plus its external damping resistance.

Then the current passing through the galvanometer under the same conditions is given by

$$(I_2)_{V_2=0}=\frac{\mu_1 G}{Z_{11}}\frac{d\theta}{dt} \qquad (3)$$

where μ_1 is the attenuation factor defined as in the following.

$$\mu_1=\left(\frac{I_2}{I_1}\right)_{V_2=0} \qquad (4)$$

The suffix $V_2=0$ in the above expressions means that the terminals 22 in the diagram are shorted.

When the galvanometer is not cramped the motion of the coil will generates the electromotive force which is given by

$$V_2 = -g\frac{d\phi}{dt} \qquad (5)$$

where

ϕ is the angular deflection of the galvanometer ; and

g is the electrodynamical constant of the galvanometer and is given by the product of the area, the number of turns of the coil, and the field strength of the magnet.

If the transducer coil is cramped and no electromotive force is induced in it, then the current through the galvanometer coil is given by

$$(I_2)_{V_1=0} = \frac{V_2}{Z_{22}} = -\frac{g}{Z_{22}}\frac{d\phi}{dt} \qquad (6)$$

where

Z_{22} is the resistance measured from the terminals 22 when the terminals 11 are shorted and corresponds to the resistance of the galvanometer coil plus its external damping resistance.

The suffix $V_1=0$ in the above expression means that the terminals 11 are shorted. Then the current passing through the transducer coil under the same condition is given by

$$(I_1)_{V_1=0} = -\frac{\mu_2 g}{Z_{22}}\frac{d\phi}{dt} \qquad (7)$$

where μ_2 is defined as

$$\mu_2 = \left(\frac{I_1}{I_2}\right)_{V_1=0} \qquad (8)$$

μ_2 is a sort of attenuation factor seen from the side of the galvanometer.

When both the transducer and the galvanometer are not cramped, the current passing through both the coils is therefore given by

$$\left.\begin{aligned} I_1 &= (I_1)_{V_2=0} + (I_1)_{V_1=0} \\ &= \frac{G}{Z_{11}}\frac{d\theta}{dt} - \frac{\mu_2 g}{Z_{22}}\frac{d\phi}{dt} \end{aligned}\right\} \qquad (9)$$

$$\left.\begin{aligned} I_2 &= (I_2)_{V_2=0} + (I_2)_{V_1=0} \\ &= \frac{\mu_1 G}{Z_{11}}\frac{d\theta}{dt} - \frac{g}{Z_{22}}\frac{d\phi}{dt} \end{aligned}\right\} \qquad (10)$$

The equation of motion for the transducer and the galvanometer are written according to Wenner's notations as follows:

$$K\frac{d^2\theta}{dt^2}+D\frac{d\theta}{dt}+U\theta=-MH\frac{d^2x}{dt^2}-GI_1\,, \tag{11}$$

$$k\frac{d^2\phi}{dt^2}+d\,\frac{d\phi}{dt}+u\phi=gI_2 \tag{12}$$

where

K is the moment of inertia of the pendulum about the axis of the rotation;
D is the coefficient of the damping of the pendulum, including all forms of damping when the electric circuit is open;
U is the coefficient of the restitutive force;
M is the mass of the pendulum;
H is the distance between the center of gravity and the axis of rotation of the pendulum;
x is the displacement of the ground;
k is the moment of inertia of the moving system of the galvanometer;
d is the coefficient of the damping of the galvanometer with the circuit open; and
u is the coefficient of the restitutive force of the galvanometer.

Putting (9) into (11), and (10) into (12), we obtain

$$K\frac{d^2\theta}{dt^2}+\left[D+\frac{G^2}{Z_{11}}\right]\frac{d\theta}{dt}+U\theta=-MH\frac{d^2x}{dt^2}+\frac{\mu_2 Gg}{Z_{22}}\frac{d\phi}{dt} \tag{13}$$

$$k\frac{d^2\phi}{dt^2}+\left[d+\frac{g^2}{Z_{22}}\right]\frac{d\phi}{dt}+u\phi=\frac{\mu_1 Gg}{Z_{11}}\frac{d\theta}{dt} \tag{14}$$

or

$$\frac{d^2\theta}{dt^2}+2\varepsilon_1\frac{d\theta}{dt}+n_1^2\theta=-\frac{MH}{K}\frac{d^2x}{dt^2}+2\sigma_1\varepsilon_1\frac{d\phi}{dt} \tag{15}$$

$$\frac{d^2\phi}{dt^2}+2\varepsilon_2\frac{d\phi}{dt}+n_2^2\phi=2\sigma_2\varepsilon_2\frac{d\theta}{dt} \tag{16}$$

where

$$\left.\begin{aligned} 2\varepsilon_1 &= \frac{D}{K}+\frac{G^2}{KZ_{11}} \\ 2\varepsilon_2 &= \frac{d}{k}+\frac{g^2}{kZ_{22}} \\ 2\sigma_1\varepsilon_1 &= \frac{\mu_2 Gg}{KZ_{22}} \\ 2\sigma_2\varepsilon_2 &= \frac{\mu_1 Gg}{kZ_{11}} \end{aligned}\right\} \tag{17}$$

We obtain the following equation, eliminating θ from (15) and (16).

$$\frac{d^4\phi}{dt^4}+m\frac{d^3\phi}{dt^3}+n\frac{d^2\phi}{dt^2}+o\frac{d\phi}{dt}+p\phi=-q\frac{d^3x}{dt^3} \tag{18}$$

where

$$\left.\begin{aligned} m &= 2(\varepsilon_1+\varepsilon_2) \\ n &= n_1^2+n_2^2+4\varepsilon_1\varepsilon_2(1-\sigma^2) \\ o &= 2(\varepsilon_1 n_2^2+\varepsilon_2 n_1^2) \\ p &= n_1^2 n_2^2 \\ q &= \frac{MHGg\mu_1}{KkZ_{11}} \end{aligned}\right\} \tag{19}$$

and

$$\sigma^2=\sigma_1\sigma_2 \tag{20}$$

σ, which is called the coupling factor, expresses the largeness of the reaction of the galvanometer.

If the motion of the ground is assumed to be a simple harmonic, with amplitude x_m, angular velocity ω, and phase angle α,

$$x=x_m e^{j\alpha}e^{j\omega t} \tag{21}$$

where j is $\sqrt{-1}$. If we limit the case to the stationary state, we can put

$$\phi=\phi_m e^{j\beta}e^{j\omega t} \tag{22}$$

where ϕ_m is the amplitude in angle, and β the phase angle of the motion of the galvanometer. Putting (21) and (22) into (18), we obtain

$$(\omega^4-j\omega^3 m-\omega^2 n+j\omega o+p)\phi_m e^{j\beta}e^{j\omega t}=j\omega^3 q x_m e^{j\alpha}e^{j\omega t} \tag{23}$$

Hence

$$\frac{\phi_m}{x_m}e^{j(\beta-\alpha)}=\frac{j\omega^3 q}{\omega^4-j\omega^3 m-\omega^2 n+j\omega o+p} \tag{24}$$

The right hand side of equation (24) is of complex form and the absolute value gives the amplitude ratio ϕ_m/x_m, and the quotient, the imaginary part divided by the real part, gives tan $(\beta-\alpha)$, namely,

$$\begin{aligned}\frac{\phi_m}{x_m}&=\frac{q\omega^3}{\sqrt{(\omega^4-\omega^2 n+p)^2+(-\omega^3 m+\omega_0)^2}}\\&=\frac{q\omega^3}{\sqrt{[\omega^4-\{n_1^2+n_2^2+4\varepsilon_1\varepsilon_2(1-\sigma^2)\}\omega^2+n_1^2 n_2^2]^2+[-2(\varepsilon_1+\varepsilon_2)\omega^3+2(\varepsilon_1 n_2^2+\varepsilon_2 n_1^2)\omega]^2}}\end{aligned} \tag{25}$$

$$\begin{aligned}\tan(\beta-\alpha)&=\frac{\omega^4-\omega^2 n+p}{-\omega^3 m+\omega o}\\&=\frac{\omega^4-\{n_1^2+n_2^2+4\varepsilon_1\varepsilon_2(1-\sigma^2)\}\omega^2+n_1^2 n_2^2}{-2(\varepsilon_1+\varepsilon_2)\omega^3+2(\varepsilon_1 n_2^2+\varepsilon_2 n_1^2)\omega}\end{aligned} \tag{26}$$

The equations (25) and (26) can be written in the following form.

$$\frac{\phi_m}{x_m}=\frac{q}{n_1}f(h_1, h_2, \nu, \sigma, u_1) \tag{27}$$

$$\begin{aligned}&f(h_1, h_2, \nu, \sigma, u_1)\\&=\frac{u_1}{\sqrt{\left[1-\left\{\left(1+\frac{1}{\nu^2}\right)+4h_1h_2\frac{1}{\nu}(1-\sigma^2)\right\}u_1^2+\frac{1}{\nu^2}u_1^4\right]^2+\left[-2\left(h_1+\frac{1}{\nu}h_2\right)u_1+2\left(\frac{1}{\nu}h_1+h_2\right)\frac{1}{\nu}u_1^3\right]^2}}\end{aligned} \tag{28}$$

$$\tan(\beta-\alpha)=\frac{1-\left\{\left(1+\frac{1}{\nu^2}\right)+4h_1h_2\frac{1}{\nu}(1-\sigma^2)\right\}u_1^2+\frac{1}{\nu^2}u_1^4}{-2\left(h_1+\frac{1}{\nu}h_2\right)u_1+2\left(\frac{1}{\nu}h_1+h_2\right)\frac{1}{\nu}u_1^3} \tag{29}$$

where

$h_1=\frac{\varepsilon_1}{n_1}$ (damping constant of the transducer)

$h_2=\frac{\varepsilon_2}{n_2}$ (damping constant of the galvanometer)

$\nu=\frac{n_1}{n_2}=\frac{T_2}{T_1}$

$u_1=\frac{n_1}{\omega}=\frac{T_\omega}{T_1}$

T_ω=period of the ground motion
T_1=period of the transducer
T_2=period of the galvanometer

If we consider the deflection of the light spot on the recording drum as in the usual case,

$$y_m=L\phi_m \tag{30}$$

where

y_m is the amplitude on the recording drum;
L is the length of optical lever, that is, twice the distance between the mirror of galvanometer and the recording drum.

If we use y_m in place of ϕ_m, the equation (27) can be written as follows:

$$\left.\begin{aligned}\frac{y_m}{x_m}&=Q\cdot f(h_1, h_2, \nu, \sigma, u_1)\\ Q&=\frac{qL}{n_1}\end{aligned}\right\} \tag{31}$$

Here f is the amplitude characteristics and $\beta-\alpha$ is the phase characteristics of the seismograph and both of them are the function of h_1, h_2, ν, σ, and u_1. y_m/x_m is the actual magnification of the seismograph.

Next the method of obtaining the quantity qL/n_1 will be examined. We can regard the transducer as a sort of galvanometer because if the electric current is given to the coil of the transducer the pendulum is deflected. We can measure the deflection of the pendulum just like a galvanometer if we attach a mirror near the axis of rotation of the pendulum and put a lamp scale at a suitable distance. If the deflection angle of the pendulum is θ when the direct current I is given to the coil,

$$n_1^2\theta=\frac{G}{K}I \tag{32}$$

G/n_1^2K is therefore the deflection angle of the pendulum when unit direct current passes through the transducer coil.

If the deflection angle of the galvanometer is ϕ when the direct current i passes through the galvanometer coil,

$$n_2^2\phi=\frac{g}{k}i \tag{33}$$

If we denote the displacement of the light spot on the recording drum by y, since $y=\phi L$,

$$n_2^2y=\frac{gL}{k}i \tag{34}$$

gL/n_2^2k is therefore the displacement of the light spot on the recording drum when unit direct current passes through the galvanometer coil. The ampere sensitivity of a galvanometer in ordinary use is just the inverse of gL/n_2^2k. If we use such measurable quantities, Q can be written in the following form:

$$\left.\begin{aligned} Q&=\frac{MHGg\mu_1L}{KkZ_{11}n_1}\\ &=MHn_1n_2^2\frac{G}{n_1^2K}\,\frac{gL}{n_2^2k}\,\mu_1\frac{1}{Z_{11}} \end{aligned}\right\} \tag{35}$$

$$\left.\begin{aligned} &=MH\,\frac{2\pi}{T_1}\left(\frac{2\pi}{T_2}\right)^2S_1S_2\mu_1\frac{1}{Z_{11}}\\ S_1&=\frac{G}{n_1^2K}\\ S_2&=\frac{gL}{n_2^2k} \end{aligned}\right\} \tag{36}$$

Since μ_1 and Z_{11} can be computed if the values of resistance of the electric circuit are known, all terms of the right hand side of equation (36) are measurable quantities. Since Q is proportional to μ_1, we can easily reduce to magnification of the seismograph to a desired value by reducing the value of μ_1 without changing any other state.

3. Expression for σ

From equations (17) and (20),

$$\left.\begin{aligned}\sigma^2&=\sigma_1\sigma_2\\&=\frac{(Gg)^2\mu_1\mu_2}{2\varepsilon_1 2\varepsilon_2 KkZ_{11}Z_{22}}\end{aligned}\right\}\qquad(37)$$

From equation (17),

$$\left.\begin{aligned}h_1&=\frac{\varepsilon_1}{n_1}\\&=h_{01}+\frac{G^2}{2n_1KZ_{11}}\end{aligned}\right\}\qquad(38)$$

$$\left.\begin{aligned}h_2&=\frac{\varepsilon_2}{n_2}\\&=h_{02}+\frac{g^2}{2n_2kZ_{22}}\end{aligned}\right\}\qquad(39)$$

where

$$h_{01}=\frac{D}{2n_1K}$$

$$h_{02}=\frac{d}{2n_2k}$$

h_{01} is the damping constant of the transducer when the circuit is open and no current passes through the coil. h_{02} is the analogous quantity to the galvanometer. From (38) and (39),

$$\frac{G^2}{2n_1KZ_{11}}=h_1-h_{01}\qquad(40)$$

$$\frac{g^2}{2n_2kZ_{22}}=h_2-h_{02}\qquad(41)$$

Therefore

$$\left.\begin{aligned}\sigma^2&=\frac{n_1}{\varepsilon_1}\frac{n_2}{\varepsilon_2}\frac{G^2}{2n_1KZ_{11}}\frac{g^2}{2n_2kZ_{22}}\mu_1\mu_2\\&=\frac{(h_1-h_{01})(h_2-h_{02})}{h_1h_2}\mu_1\mu_2\end{aligned}\right\}\qquad(42)$$

The last equation shows that σ is a dimensionless quantity and $0 \leqq \sigma \leqq 1$ because $0 \leqq \mu_1 \leqq 1$ and $0 \leqq \mu_2 \leqq 1$.

If we regard the circuit as a four-terminal network with terminals 11 and 22 as shown in Fig. 1 and denote its four parameters by

$$\begin{bmatrix} A & B \\ C & D \end{bmatrix},$$

then we have the well-known formulae written as follows.

$$\begin{bmatrix} V_1 \\ I_1 \end{bmatrix} = \begin{bmatrix} A & B \\ C & D \end{bmatrix} \begin{bmatrix} V_2 \\ I_2 \end{bmatrix}, \tag{43}$$

$$\begin{bmatrix} V_2 \\ I_2 \end{bmatrix} = \begin{bmatrix} D & B \\ C & A \end{bmatrix} \begin{bmatrix} V_1 \\ I_1 \end{bmatrix}, \tag{44}$$

and

$$\begin{vmatrix} A & B \\ C & D \end{vmatrix} = 1 . \tag{45}$$

Therefore

$$\left.\begin{aligned} \mu_1 &= \left(\frac{I_2}{I_1}\right)_{V_2=0} = \frac{1}{D} \\ \mu_2 &= \left(\frac{I_1}{I_2}\right)_{V_1=0} = \frac{1}{A} \\ Z_{11} &= \left(\frac{V_1}{I_1}\right)_{V_2=0} = \frac{B}{D} \\ Z_{22} &= \left(\frac{V_2}{I_2}\right)_{V_1=0} = \frac{B}{A} \end{aligned}\right\} . \tag{46}$$

Hence

$$\frac{\mu_2}{\mu_1} = \frac{D}{A} = \frac{Z_{22}}{Z_{11}} . \tag{47}$$

Hence

$$\mu_2 = \frac{\mu_1 Z_{22}}{Z_{11}} . \tag{48}$$

Equation (42) can be therefore written as follows.

$$\sigma^2 = \frac{(h_1-h_{01})(h_2-h_{02})}{h_1 h_2} \frac{Z_{22}}{Z_{11}} \mu_1^2 . \tag{49}$$

The interesting fact is that the above expression for σ does not contain the inertia term of the pendulum as well as of the galvanometer. This means that σ is independent of the inertia of the pendulum and the galvanometer but depends on the damping constants and the constants

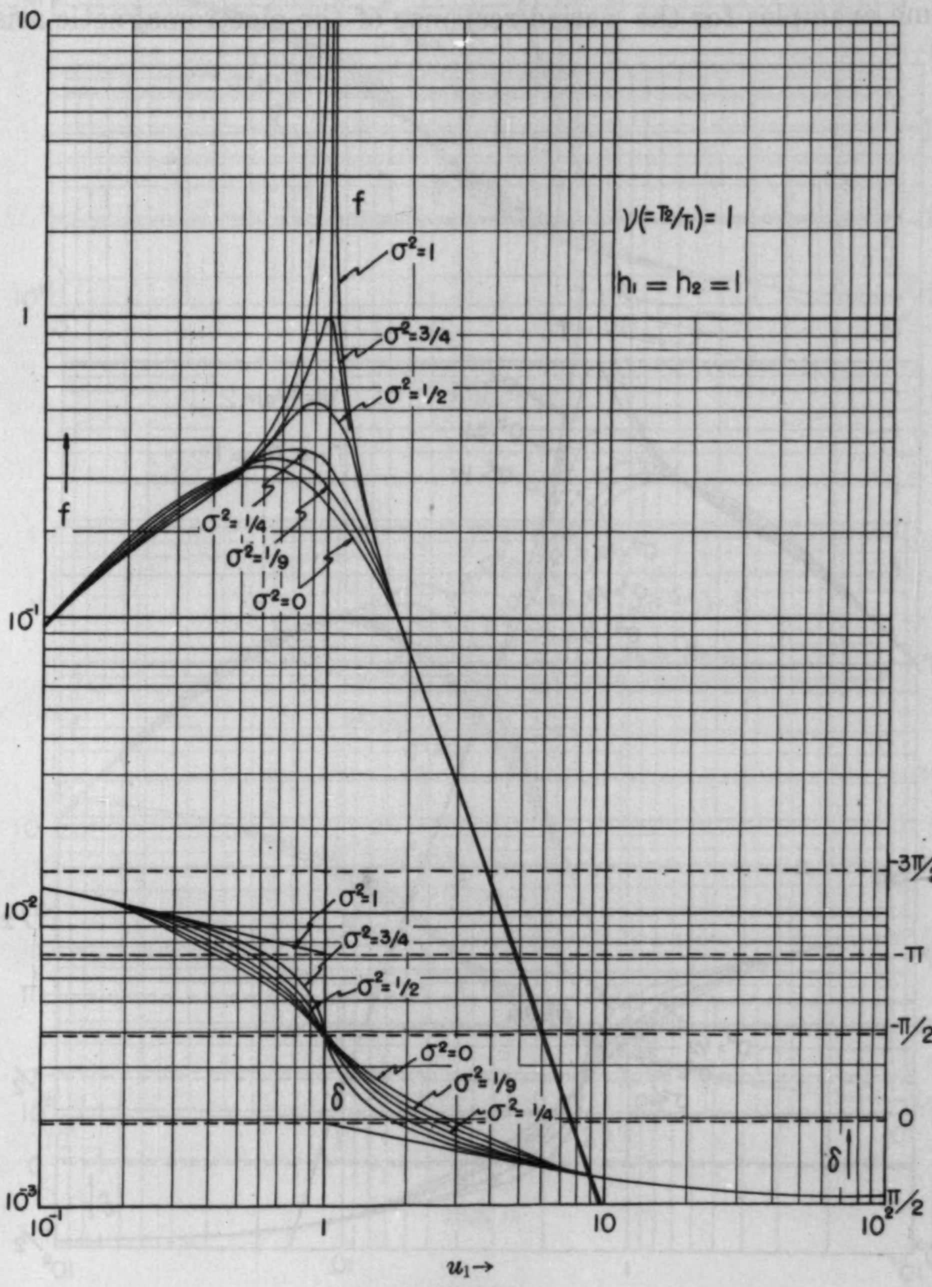

Fig. 3.

of the electrical circuit. We can never avoid the reaction of the galvanometer on the pendulum simply by adopting a heavy mass as the pendulum. If any additional damping device is not provided for the pendulum, the only way to avoid the reaction of the galvanometer is to decrease the attenuation factor of the circuit.

4. Effect of σ on the period responce

Some examples for the period response of the electromagnetic seismo-

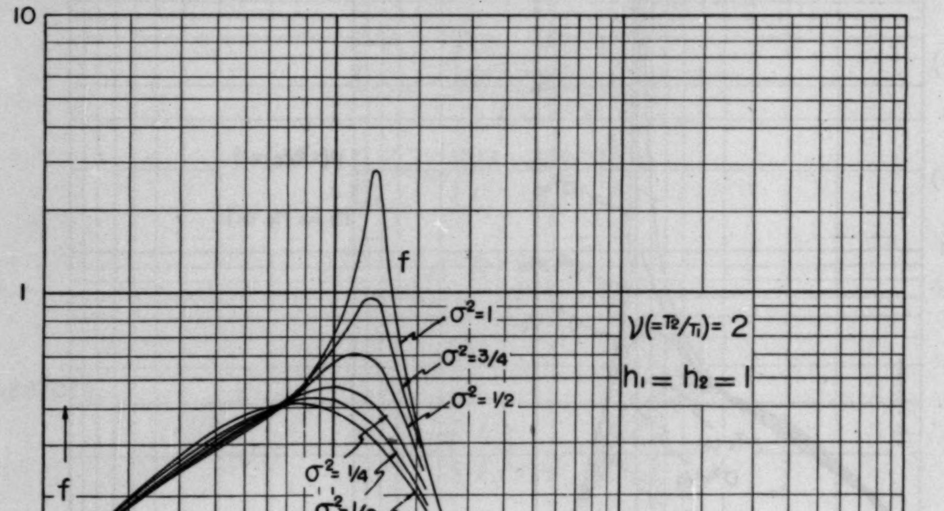

Fig. 4.

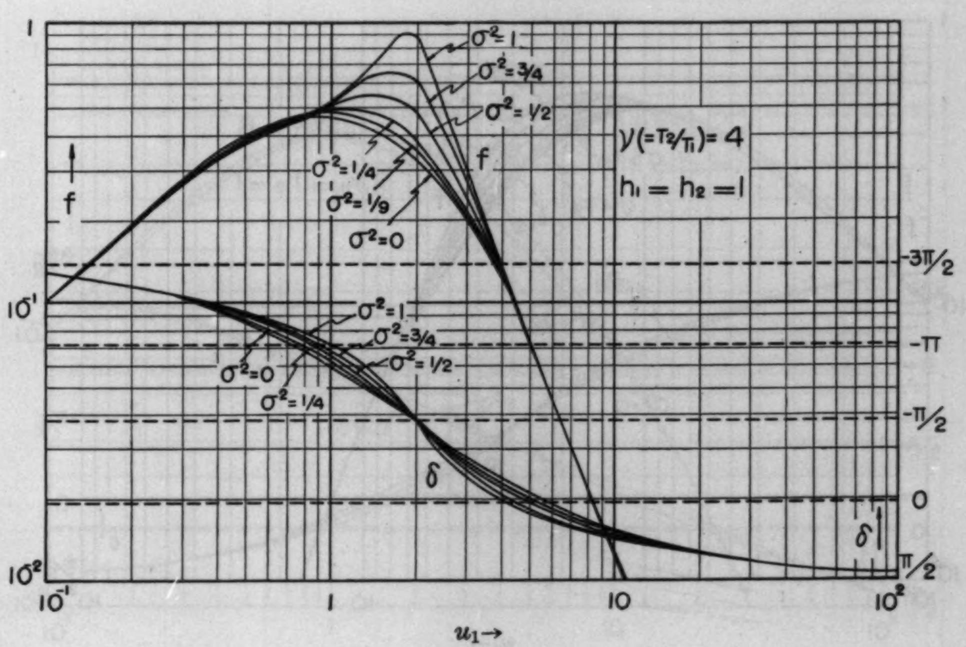
1
10^{-1}
10^{-2}
10^{-1}
1
10
10^{2}
$u_1 \rightarrow$
f
f
$\sigma^2=1$
$\sigma^2=3/4$
$\sigma^2=1/2$
$\sigma^2=1/4$
$\sigma^2=1/9$
$\sigma^2=0$
$\nu(=T_2/T_1)=4$
$h_1=h_2=1$
$-3\pi/2$
$-\pi$
$-\pi/2$
0
$\pi/2$
$\sigma^2=1$
$\sigma^2=3/4$
$\sigma^2=1/2$
$\sigma^2=0$
$\sigma^2=1/4$
δ
δ

Fig. 5.

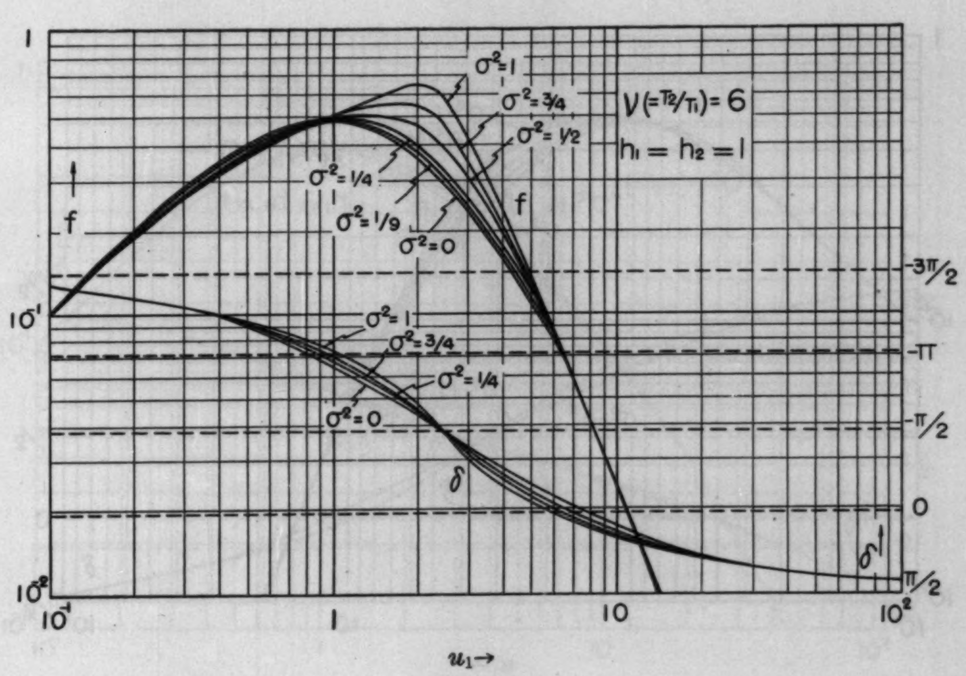
1
10^{-1}
10^{-2}
10^{-1}
1
10
10^{2}
$u_1 \rightarrow$
f
f
$\sigma^2=1$
$\sigma^2=3/4$
$\sigma^2=1/2$
$\sigma^2=1/4$
$\sigma^2=1/9$
$\sigma^2=0$
$\nu(=T_2/T_1)=6$
$h_1=h_2=1$
$-3\pi/2$
$-\pi$
$-\pi/2$
0
$\pi/2$
$\sigma^2=1$
$\sigma^2=3/4$
$\sigma^2=1/4$
$\sigma^2=0$
δ
δ

Fig. 6.

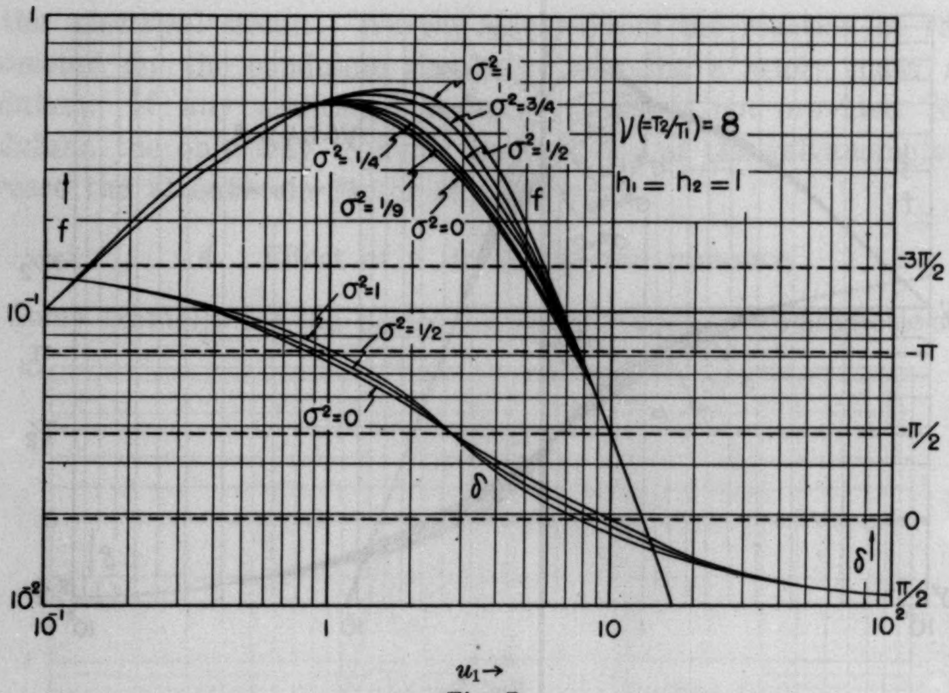
1
10^{-1}
10^{-2}
f
$\sigma^2=1$
$\sigma^2=3/4$
$\sigma^2=1/2$
$\sigma^2=1/4$
$\sigma^2=1/9$
$\sigma^2=0$
$\nu(=T_2/T_1)=8$
$h_1=h_2=1$
$\sigma^2=1$
$\sigma^2=1/2$
$\sigma^2=0$
δ
$-3\pi/2$
$-\pi$
$-\pi/2$
0
$\pi/2$
δ
10^{-1}
1
10
10^{2}
u_1→

Fig. 7.

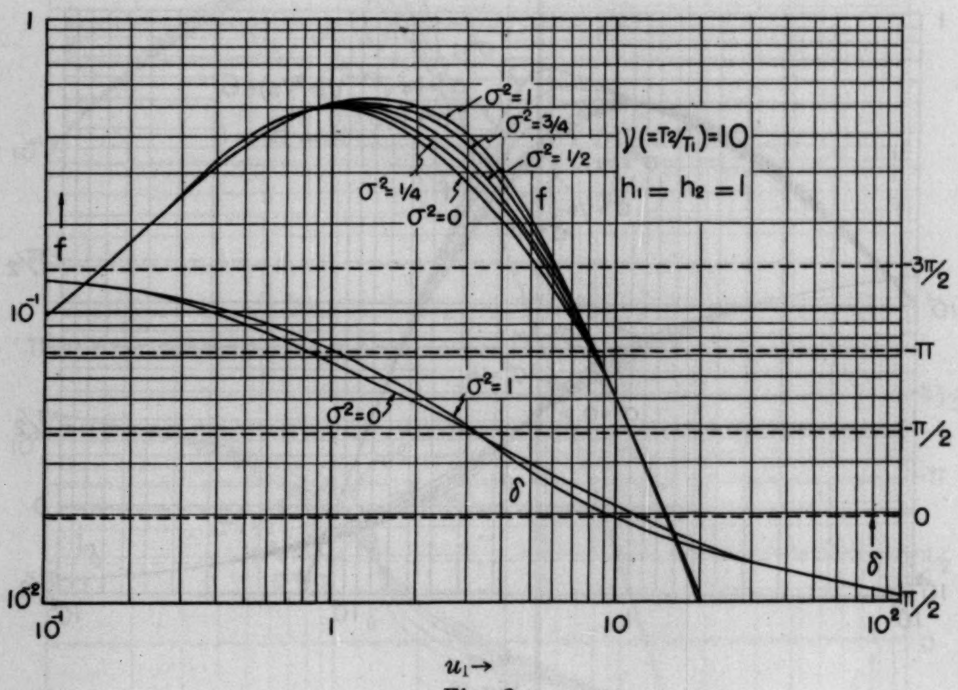
1
10^{-1}
10^{-2}
f
$\sigma^2=1$
$\sigma^2=3/4$
$\sigma^2=1/2$
$\sigma^2=1/4$
$\sigma^2=0$
$\nu(=T_2/T_1)=10$
$h_1=h_2=1$
$\sigma^2=0$
$\sigma^2=1$
δ
$-3\pi/2$
$-\pi$
$-\pi/2$
0
$\pi/2$
δ
10^{-1}
1
10
10^{2}
u_1→

Fig. 8.

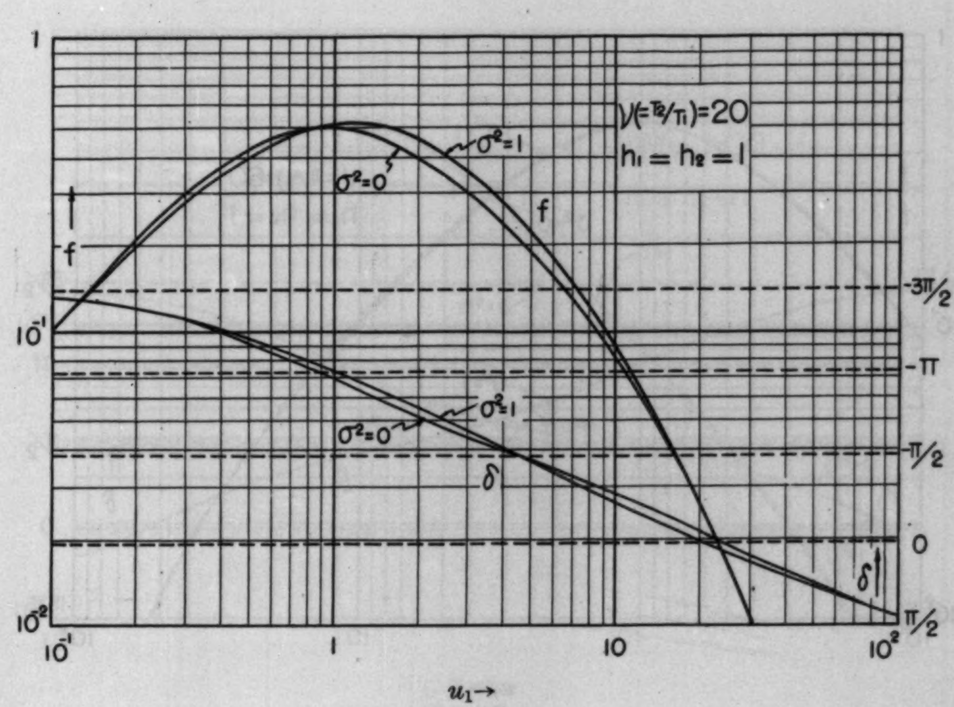
1
10^{-1}
10^{-2}
f
$\nu(=T_2/T_1)=20$
$h_1 = h_2 = 1$
$\sigma^2=1$
$\sigma^2=0$
f
$\sigma^2=1$
$\sigma^2=0$
δ
$-3\pi/2$
$-\pi$
$-\pi/2$
0
$\pi/2$
δ
10^{-1}
1
10
10^2
$u_1\rightarrow$

Fig. 9.

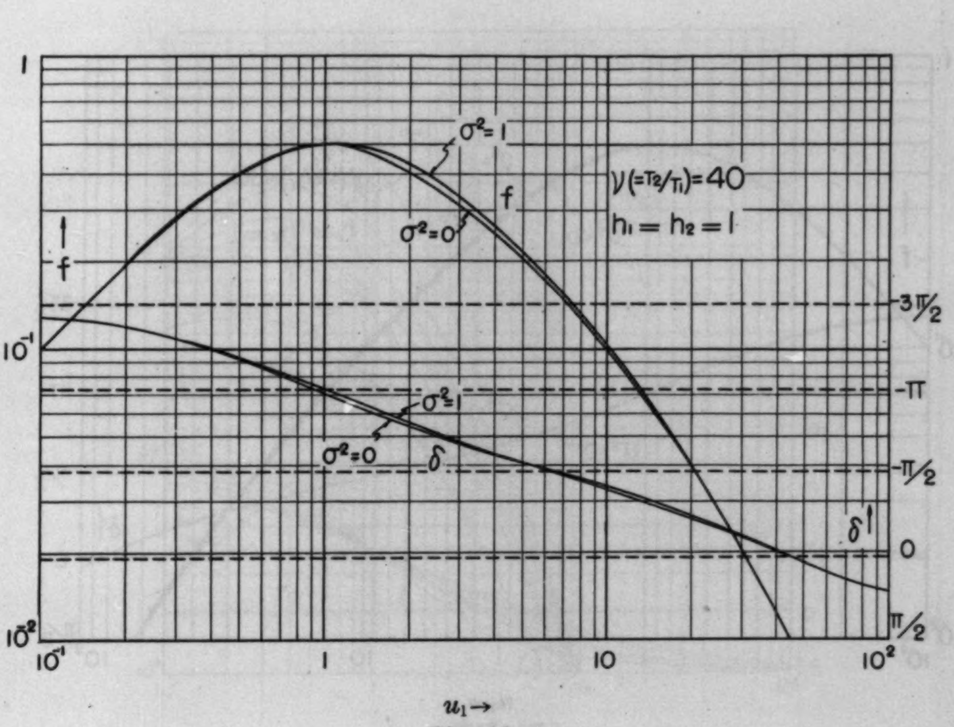
1
10^{-1}
10^{-2}
f
$\nu(=T_2/T_1)=40$
$h_1 = h_2 = 1$
$\sigma^2=1$
$\sigma^2=0$
f
$\sigma^2=1$
$\sigma^2=0$
δ
$-3\pi/2$
$-\pi$
$-\pi/2$
0
$\pi/2$
δ
10^{-1}
1
10
10^2
$u_1\rightarrow$

Fig. 10

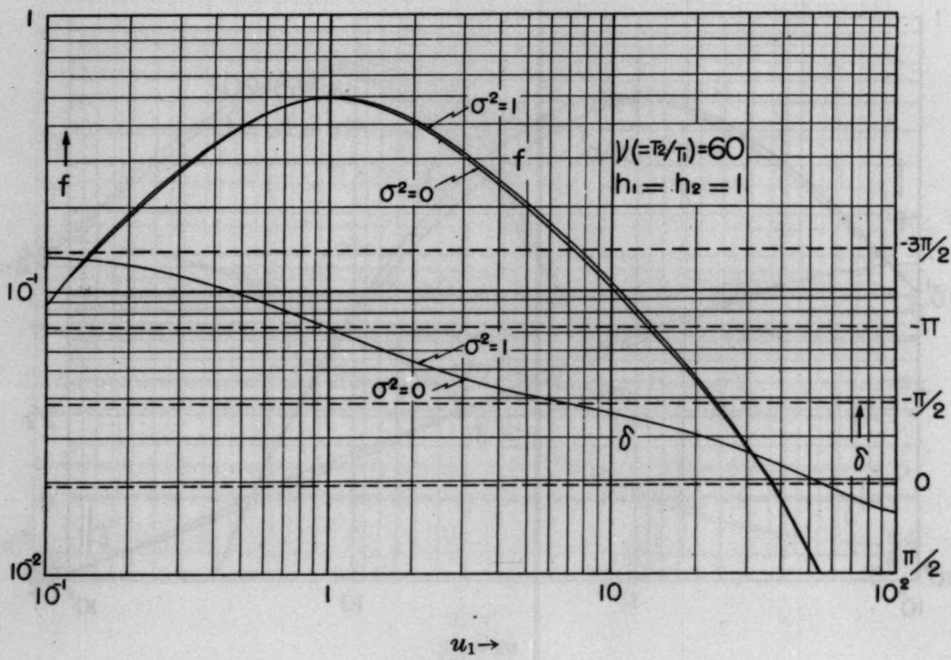
1
f
10^{-1}
10^{-2}
10^{-1}
1
10
10^2
u_1→
$\sigma^2=1$
$\sigma^2=0$
f
$\nu(=\tau_2/\tau_1)=60$
$h_1=h_2=1$
$\sigma^2=1$
$\sigma^2=0$
δ
δ
$-3\pi/2$
$-\pi$
$-\pi/2$
0
$\pi/2$

Fig. 11.

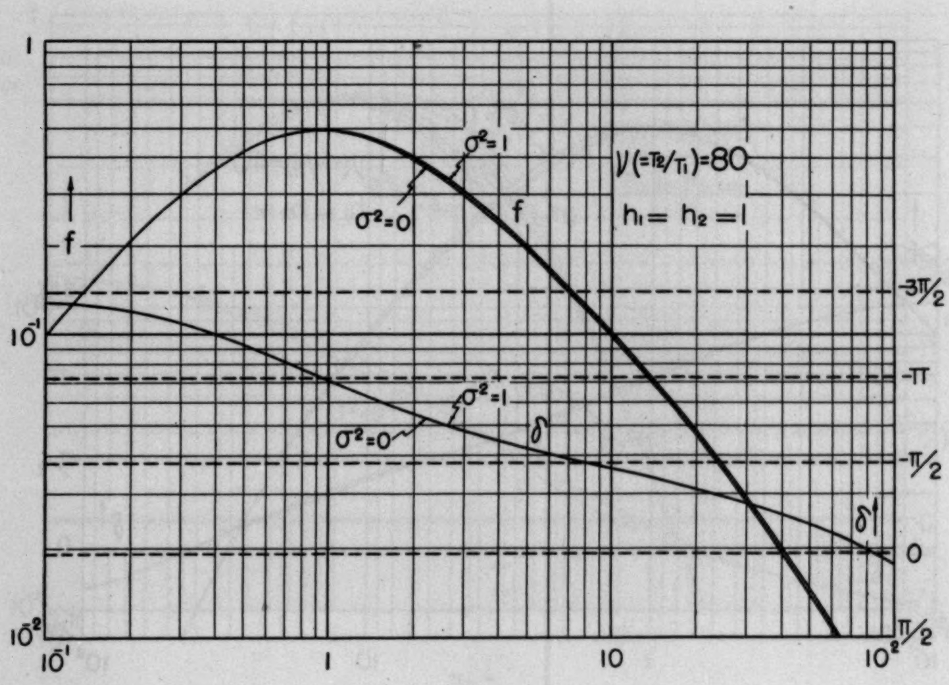
1
f
10^{-1}
10^{-2}
10^{-1}
1
10
10^2
u_1→
$\sigma^2=1$
$\sigma^2=0$
f
$\nu(=\tau_2/\tau_1)=80$
$h_1=h_2=1$
$\sigma^2=1$
$\sigma^2=0$
δ
δ
$-3\pi/2$
$-\pi$
$-\pi/2$
0
$\pi/2$

Fig. 12.

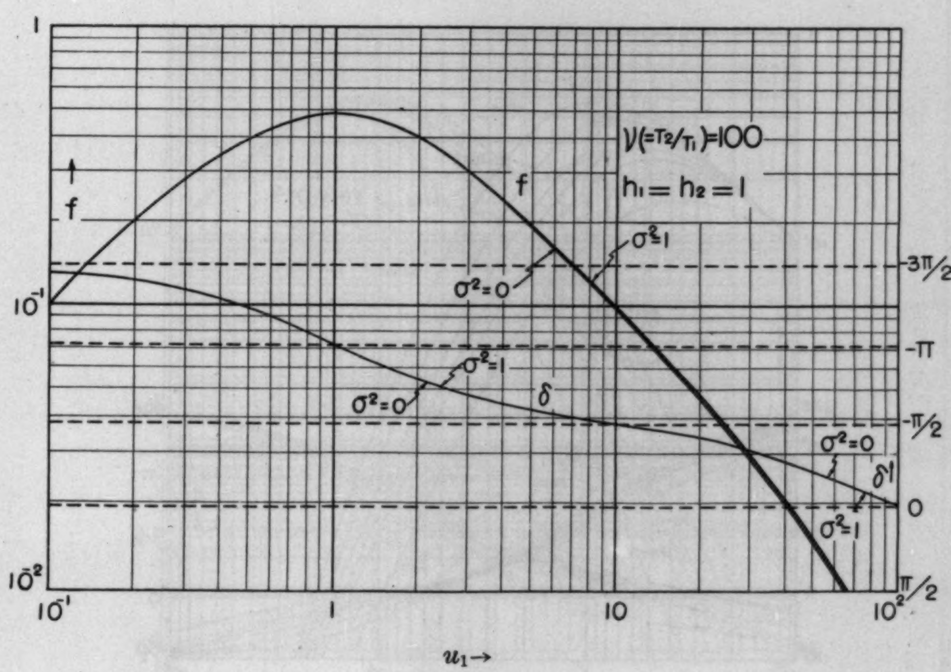
1
f
10^{-1}
10^{-2}
10^{-1}
1
10
10^{2}
$u_1 \rightarrow$
$\nu(=T_2/T_1)=100$
$h_1=h_2=1$
f
$\sigma^2=1$
$\sigma^2=0$
$\sigma^2=1$
$\sigma^2=0$
δ
$\sigma^2=0$
δ
$\sigma^2=1$
$-3\pi/2$
$-\pi$
$-\pi/2$
0
$\pi/2$

Fig. 13.

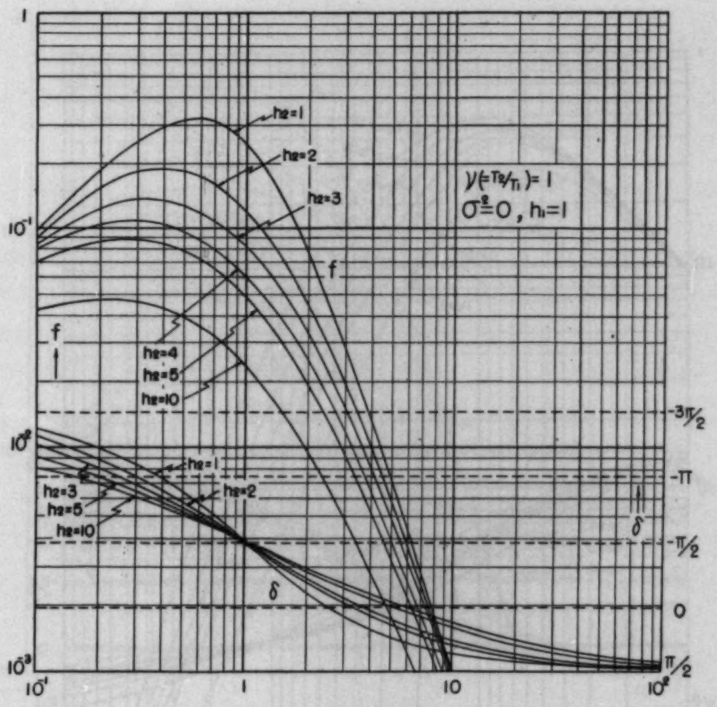
1
10^{-1}
f
10^{-2}
10^{-3}
10^{-1}
1
10
10^{2}
$u_1 \rightarrow$
$\nu(=T_2/T_1)=1$
$\sigma^2=0$, $h_1=1$
$h_2=1$
$h_2=2$
$h_2=3$
f
$h_2=4$
$h_2=5$
$h_2=10$
$h_2=1$
$h_2=2$
$h_2=3$
$h_2=5$
$h_2=10$
δ
δ
$-3\pi/2$
$-\pi$
$-\pi/2$
0
$\pi/2$

Fig. 14.

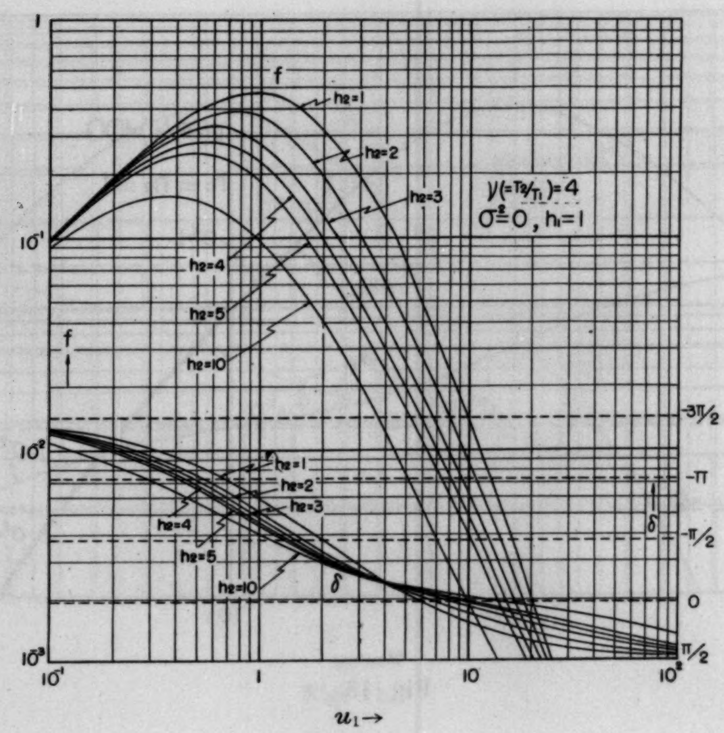
1
10⁻¹
10⁻²
10⁻³
10⁻¹
1
10
10²
u_1→
f
f ↑
h2=1
h2=2
h2=3
h2=4
h2=5
h2=10
γ(=T2/T1)=4
σ=0, h1=1
-3π/2
-π
-π/2
0
π/2
δ ↑
δ

Fig. 15.

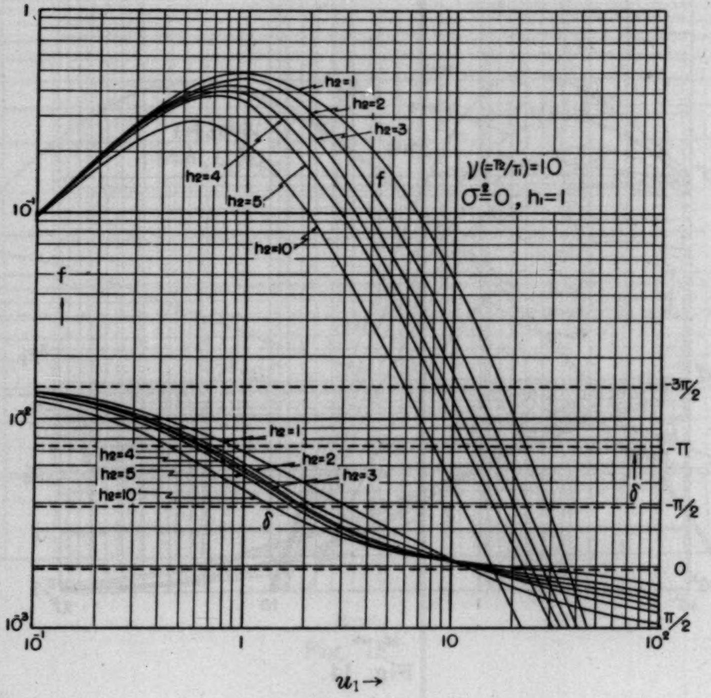
1
10⁻¹
10⁻²
10⁻³
10⁻¹
1
10
10²
u_1→
f
f ↑
h2=1
h2=2
h2=3
h2=4
h2=5
h2=10
γ(=T2/T1)=10
σ=0, h1=1
-3π/2
-π
-π/2
0
π/2
δ ↑
δ

Fig. 16.

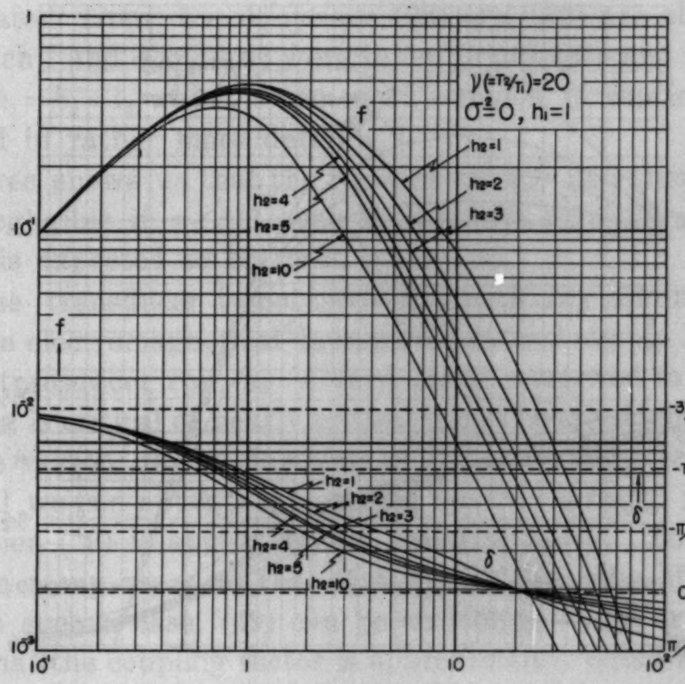

1
$\nu(=T_2/T_1)=20$
$\sigma^2=0,\ h_1=1$
f
$h_2=1$
$h_2=2$
$h_2=3$
$h_2=4$
$h_2=5$
$h_2=10$
10^{-1}
10^{-2}
10^{-3}
-3π/2
-π
-π/2
0
π/2
δ
10^{-1}
1
10
10^{2}
$u_1\rightarrow$

Fig. 17.

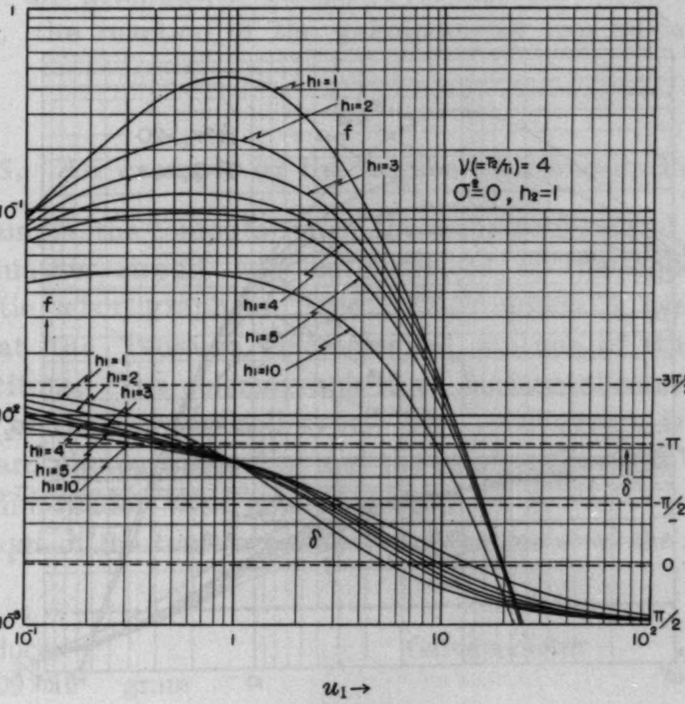

1
$\nu(=T_2/T_1)=4$
$\sigma^2=0,\ h_2=1$
f
$h_1=1$
$h_1=2$
$h_1=3$
$h_1=4$
$h_1=5$
$h_1=10$
10^{-1}
10^{-2}
10^{-3}
-3π/2
-π
-π/2
0
π/2
δ
10^{-1}
1
10
10^{2}
$u_1\rightarrow$

Fig. 18.

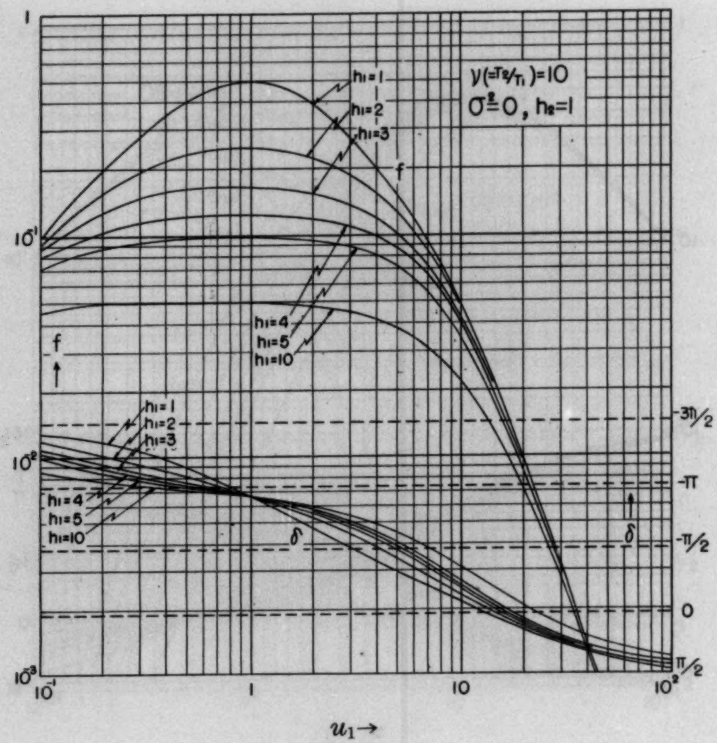
1
10⁻¹
10⁻²
10⁻³
ν(=T₂/T₁)=10
σ²=0, h₂=1
h₁=1
h₁=2
h₁=3
f
h₁=4
h₁=5
h₁=10
f
h₁=1
h₁=2
h₁=3
h₁=4
h₁=5
h₁=10
δ
δ
-3π/2
-π
-π/2
0
π/2
10⁻¹
1
10
10²
u₁→

Fig. 19.

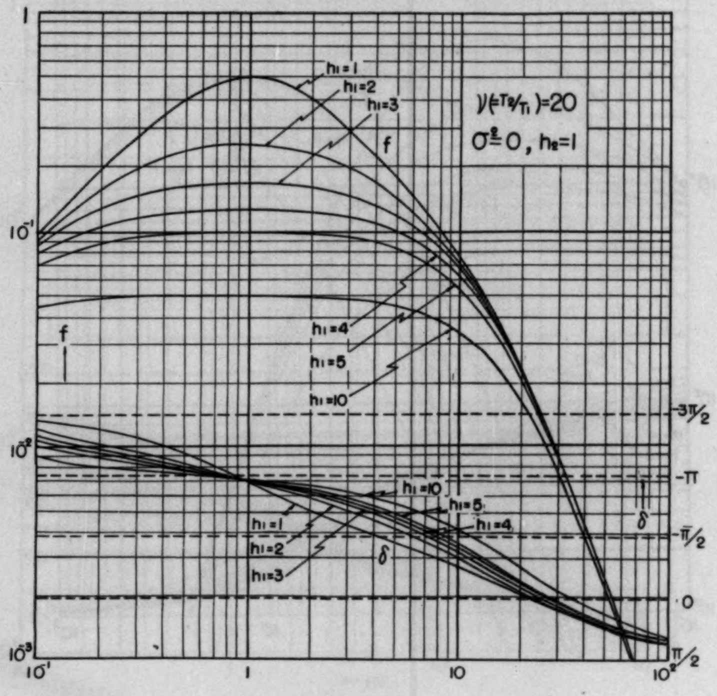
1
10⁻¹
10⁻²
10⁻³
ν(=T₂/T₁)=20
σ²=0, h₂=1
h₁=1
h₁=2
h₁=3
f
h₁=4
h₁=5
h₁=10
f
h₁=10
h₁=5
h₁=4
h₁=1
h₁=2
h₁=3
δ
δ
-3π/2
-π
-π/2
0
π/2
10⁻¹
1
10
10²
u₁→

Fig. 20.

graph calculated from the equations (28) and (29) are shown in Figs. 3~20, in which f and $\delta(=\beta-\alpha)$ were taken in ordinate and u_1 in abscissa. The case for $h_1=h_2=1$, which is the most common in routine observation was indicated in rather more detail.

The figures shows us that the reaction of the galvanometer becomes practically negligible if $\sigma<1/3$ even in the case when T_1 equals T_2 and the reaction is expected to be most influential.

When the transducer is not provided with any additional damping device and the electromagnetical damping is caused simply by the current through the transducer coil, h_{01} is very small compared to unity, so that if the damping is critical or nearly critical it can be considered that $h_1 \gg h_{01}$. For the same reason, if the damping of the galvanometer is critical or nearly critical we can put $h_2 \gg h_{02}$. Hence the first term of the right hand side of equation (49) is approximately equal to unity. The seismograph is designed in many cases so that $Z_{11} \approx Z_{22}$ for the sake of matching resistances. In such a case, (49) can be written as $\sigma^2 \approx \mu_1^2$ or $\sigma \approx \mu_1$, so that we can say that the coupling factor is approximately equal to the attenuation factor. This means that when the additional damping device is not provided for the transducer, if we select the attenuation factor less than 1/3 inserting an attenuation circuit between the transducer and the galvanometer, the reaction of the galvanometer can be left out of consideration.

5. An example of the numerical computation

As an example, the computation of the magnification and the resistances of the attenuation circuit will be indicated in the following for the electromagnetic seismograph of Type HES-H which is used for routine observation at the Tsukuba seismological station of the Earthquake Research Institute. The seismograph is of horizontal component and the transducer is of the moving coil type. The seismogram is registered on 35 mm standard photographic film and the reading is made after that by means of a film-reader with enlarging ratio of 8.

The constants of the transducer and the galvanometer of the seismograph are as follows :

	Transducer			Galvanometer	
M	1.09×10^4	gram			
H	5.0	cm			
T_1	1.00	sec	T_2	1.10	sec

$2\pi/T_1$	6.28		$(2\pi/T_2)^2$	3.26×10	
S_1	2.02×10^2	radian/unit current in c.g.s. e.m.u.	S_2	1.43×10^8	cm/unit current in c.g.s. e.m.u.
R_1	1520	ohm	R_2	500	ohm
Ω_1 (external damping resistance)	1400	ohm	Ω_2 (external damping resistanace)	1800	ohm
h_1	1.0		h_2	1.0	
h_{01}	0.0		h_{02}	0.0	

The following numericals are computed for the case $\mu_1=1/10$ using the above constants.

$$Z_{11}=R_1+\Omega_1=2920\ \text{ohm}=2.92\times10^{12}\ \text{c.g.s. e.m.u.}$$

$$Z_{22}=R_2+\Omega_2=2300\ \text{ohm}$$

$$\left\{\begin{aligned} A&=\frac{1}{\mu_1}\frac{Z_{11}}{Z_{22}}=12.70\\ B&=\frac{1}{\mu_1}Z_{11}=29{,}200\\ C&=\frac{AD-1}{B}=4.315\times10^{-3}\\ D&=\frac{1}{\mu_1}=10 \end{aligned}\right.$$

For the T-type network,

$$\left\{\begin{aligned} Z_1&=\frac{A-1}{C}=2710\ \text{ohm}\\ Z_2&=\frac{D-1}{C}=2090\ \text{ohm}\\ Z_3&=\frac{1}{C}=232\ \text{ohm} \end{aligned}\right.$$

Hence,

$$X_1=Z_1-R_1=1190\ \text{ohm},$$

$$X_2=Z_2-R_2=1590\ \text{ohm},$$

$$X_3=Z_3=232\ \text{ohm}.$$

And

$$\sigma=\sqrt{\frac{(h_1-h_{01})(h_2-h_{02})}{h_1h_2}\frac{Z_{22}}{Z_{11}}}\,\mu_1=0.089\,,$$

$$Q=1.09\cdot10^4\times5.0\times6.28\times3.26\cdot10\times2.02\cdot10^2\times1.43\cdot10^8\times10^{-1}\times\frac{1}{2.92\cdot10^{12}}$$

$$=11{,}040$$

Maximum value of f is obtained as 0.330 from the period response curves when $h_1=h_2=1$ and $T_2/T_1=1.1$. Hence the maximum magnification of the seismograph becomes ;

$V_{\max}$ (on the recording film)$=Q\cdot f_{\max}=11{,}040\times0.330=3{,}640$
$V_{\max}$ (on the film-reader)$=3{,}640\times8=29{,}100$

---

8. 電磁地震計の倍率その他について

地震研究所　萩原尊禮

直結式電磁地震計の理論は，Galitzin 以後 Wenner, Coulomb と Grenet, Schmerwitz, Eaton, 田治米などの研究者により進められ，ほぼ完成の域に達した．しかし，実際に地震計を設計したり，検定したりする場合になると，必要な公式がもう少し便利な形で表現されていることが望ましくなる．本文では，こういうことを考慮して，電磁地震計の理論式をできるだけ理解しやすく且つ簡単に測定できる量を使つて表わすことを試みた．

従来は，電磁地震計を理論的に取扱う場合に，換振器と電流計を結ぶ回路に一つのシャント抵抗を置くものとして出発したが，実際の観測では時により倍率を変化させる必要を生じるので，換振器と電流計の減衰常数を変えることなく倍率だけを変化できるアテニュエーター回路を初めから考えに入れて出発した方が便利である．本文では，電磁地震計の倍率を決める式を次のような形で表現した．

$$\frac{y_m}{x_m}=Q\cdot f$$

$$Q=MH\frac{2\pi}{T_1}\left(\frac{2\pi}{T_2}\right)^2 S_1S_2\mu_1\frac{1}{Z_{11}}$$

ここに，y_m は記録ドラム上の振動振幅，x_m は正弦波形をした地面の変位振幅，M は換振器の振子の質量，H は振子の重心と回転軸の間の距離，T_1 は換振器の自然周期，T_2 は電流計の自然周期，S_1 は振子のコイルに単位電流を与えた場合の振子のふれの角（これは，振子の回転軸付近に小さな鏡を取付け，ランプスケールを使つて，電流計の感度検定と全く同じ操作で測定すれば求められる），S_2 は電流計のコイルに単位電流を与えた場合の記録ドラム上の光点の変位（ふつう電流計のアンペア感度と称されているものは，S_2 の逆数に相当する）である．μ_1 はここに新しく定義したもので，電流計をクランプしておいて換振器のコイルに起電力を与えた場合に電流計を流れる電流と換振器を流れる電流の比を表わす．即ち，換振器の電流の μ_1 倍が電流計に分流するわけである．μ_1 を attenuation factor と称することにする．Z_{11} は換振器のコイルの抵抗とその外部減衰抵抗（換振器に所定の減衰を起させる外部抵抗）との和である．f はこの地震計の周期特性であつて，h_1（換振器の減衰常数），h_2（電流計の減衰常数），T_2/T_1（電流計と換振器の自然周期の比），σ (coupling factor)，及び T_ω/T_1（地面の周期と換振器の周期の比）の函数で表わされる．

σ については次の式で表現した．

$$\sigma^2=\frac{(h_1-h_{01})(h_2-h_{02})}{h_1h_2}\,\frac{Z_{22}}{Z_{11}}\,\mu_1^2$$

ここに，h_{01} は換振器の外部抵抗を取去りコイルに電流が流れないようにした場合の換振器の減衰常数であつて，特別にダンパーを取付けてなければほとんど零に近い値を取る．h_{02} は電流計に対する同じ意味の値である．Z_{22} は電流計のコイルの抵抗とその外部減衰抵抗との和である．σ は電流計の運動が振子の運動に及ぼす影響の度合を示す量であつて，$0\leqq\sigma\leqq1$ の値を取り，$\sigma=0$ のとき

は影響は無く，$\sigma=1$ のとき影響が最も大きい．換振器が特別にダンパーを備えていない場合は，$h_1 \geqq h_{01}$ であり，電流計についても $h_2 \geqq h_{02}$ である．また，ふつうの場合は，Z_{11} と Z_{22} とはとびはなれて違つた値を取ることはなく，$Z_{11} \approx Z_{22}$ のように設計されている．従つて，近似的には $\sigma \approx \mu_1$ と見てさしつかえない場合が多い．即ち，σ は近似的には attenuation factor そのものにほぼ等しいと見てもよい．このように考えると σ の物理的意味がかなりはつきりしてくる．

本文の終りに振幅特性 f と位相特性 δ の図を示してある．σ の影響の最も大きいのは $T_1=T_2$ の場合であるが，この場合でも $\sigma<1/3$ であれば，電流計の反作用の影響は実際上ほとんど無視してよいことがわかる．従つて，特別にダンパーを取付けず，減衰をコイルの電流の作用だけに頼る場合でも，attenuator により attenuation factor をある程度小さくすれば，電流計の反作用を無視できることになる．

注目すべきことは，上に示した σ の表現に，振子や電流計の慣性が含まれていないことである．これは，振子の質量を如何に大きくしても，ただそれだけでは，電流計の反作用の影響を小さくすることは決してできないということを意味している．特別にダンパーを取付けない場合は，attenuation factor を小さくするということが，電流計の反作用から免れる唯一の道である．もつとも，振子の質量を大きくすれば，それに比例して地震計の倍率は大きくすることができるから，あらかじめ決められた倍率を得るためには attenuation factor を充分小さくできることになるから，こういう意味では振子の質量を大きくすることが電流計の反作用を小さくすることにはなる．

最後に，倍率，σ，μ_1 などを望む値にするための attenuator の抵抗値の決め方などについて実例を示した．実際に地震計測に従事する方々の参考になれば幸である．

BULLETIN OF THE EARTHQUAKE
RESEARCH INSTITUTE
Vol. 36 (1958), pp. 165-182

9. *Vibration of a Reinforced Concrete Building moved with Vibration Generators.*

By Kiyoshi KANAI, Fuyuhiko KISHINOUYE, Nobuji NASU
and Hirosi KAWASUMI,

Earthquake Research Institute.

(Read Nov. 16, 1954. — Received March 31, 1958)

The building was constructed in Marunouchi, Tokyo, a short time before the Tokyo-Yokohama earthquake of 1923 and demolished in 1953. Its height was 27.7m and six storied, total floor area 1460m^2. At the great earthquake, fissures were formed in a screen wall at entresol and in a wall at porch. The width of the fissures became gradually smaller as their positions grew higher and higher, and over the 4th floor no fissures were found. Before demolishing the building was investigated for constructional conditions; not only vibration measurements, but measurement of the deflection of the floor by loading, study of corrosion of steel in cement and other experiments were carried out.

Measurements of vibration of the building

Two vibration generators were used for this investigation. One consisted of 3 wheels with two horizontal axes (property of the Earthquake Research Institute), and the other a horizontal wheel with a vertical axis and more powerful than the first (property of the Building Research Institute). The former excited vibrational force in one direction, but the latter generated revolving force.

The 3 wheel vibration generator was set on the 6th floor or 3rd

Table 1. Vibration generators.

Type	Eccentric mass	Eccentric radius	Eccentric Moment
Horiz. axes (E. R. I.)	40×1+20×2=80 kg	15 cm	21.7 kg.m.
		31	34.4
Vert. axis (B. R. I.)	176.9		136.6

floor. The direction of the axes was changed in the direction of beam, or in the direction of girder to change the direction of the vibration of the building. In some cases, the generator was put near the end of the floor to give the building torsional vibrations.

Instruments used for the measurements of vibrations

Nine vibrographs were prepared for the measurements, and the number of the instruments used was changed to answer the need of

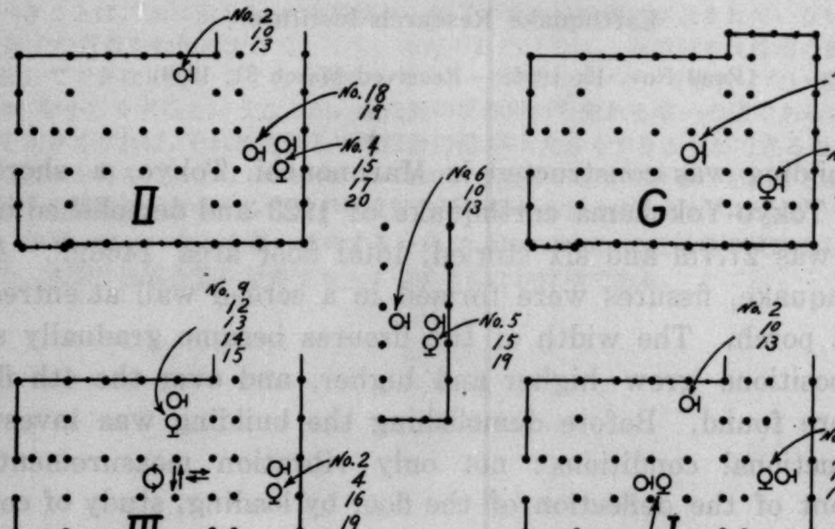
No.2 10 13
No.18 19
No.4 15 17 20
II
No.6 10 13
No.5 15 17
G
No.6 10 13
No.5 15 19
No.9 12 13 14 15
No.2 4 16 19 21
III
No.2 10 13
No.4 15 16 17
I
No.19~23
No.9 12
No.2 3 14
VI
No.2~12
No.1
No.7 8 11
No.11
No.7 8 11 16 20
No.7 8 11
No.7 8 11
No.14
IV
No.9 12
No.2 3 14
R
No.9 12
No.2 3 14 22
V

Fig. 1. Arrangement of the vibrographs on each floor at each No. of experiment.

the observation conditions. Type of the vibration generator, positions of the generator and vibrographs at each of the measurements are shown in Table 3. and Fig. 1.

Results of the observations

The relation between amplitude and period was studied, and the results are shown in Figs. 14∼37.

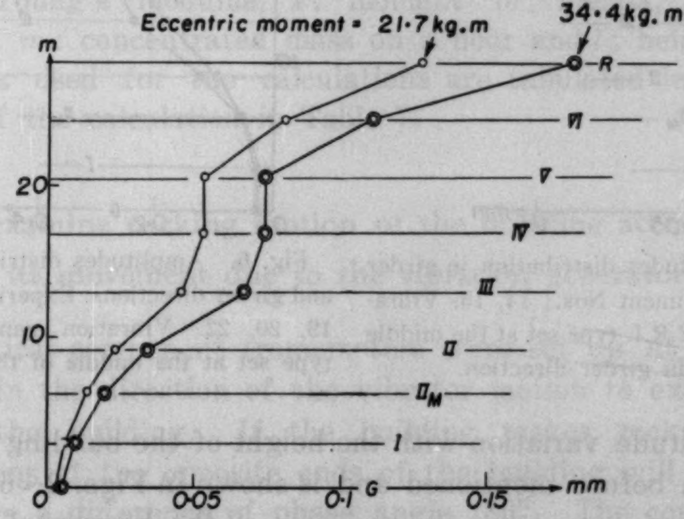

Fig. 2 Amplitudes distribution in beam direction. Experiment Nos.; 2, 6. Vibration generator; E.R.I. type set at the middle of the 6th-floor. Vibration direction; beam.

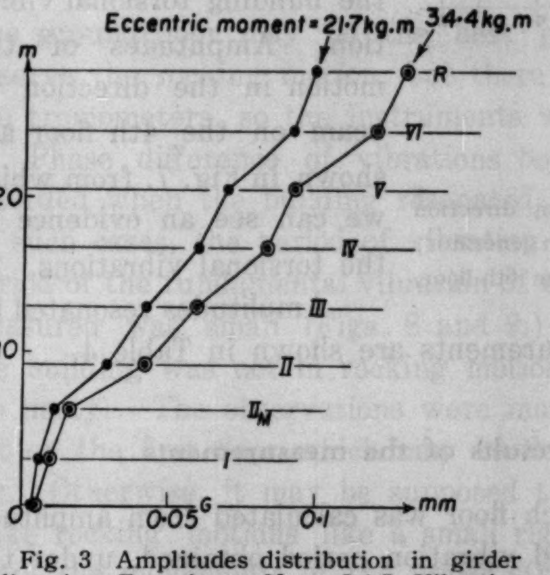

Fig. 3 Amplitudes distribution in girder direction. Experiment Nos.; 3,4,5. Vibration generator; E.R.I. type set at the middle of the 6th-floor. Vibration direction; girder.

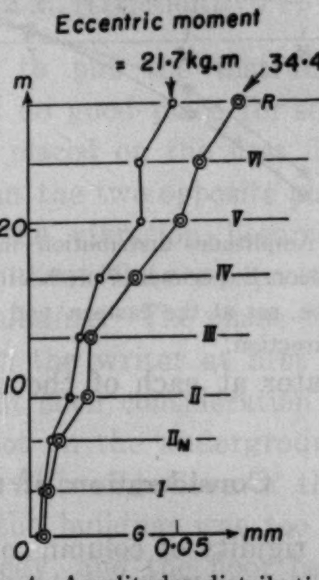

Fig. 4 Amplitudes distribution in beam direction. Experiment Nos.; 12 13. Vibration generator; E.R.I. type set at the middle of the 3rd-floor. Vibration direction; beam.

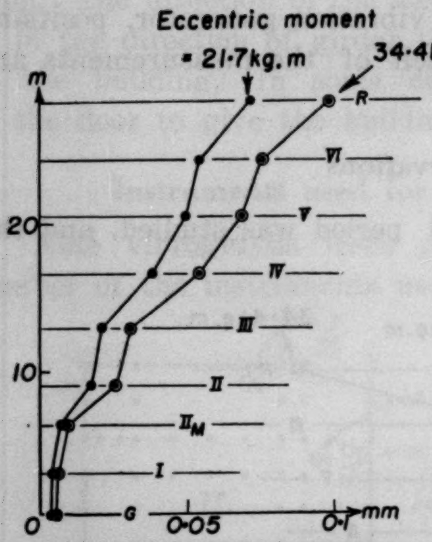

Fig. 5 Amplitudes distribution in girder direction. Experiment Nos.; 14, 15. Vibration generator; E.R.I. type set at the middle of the 3rd-floor in girder direction.

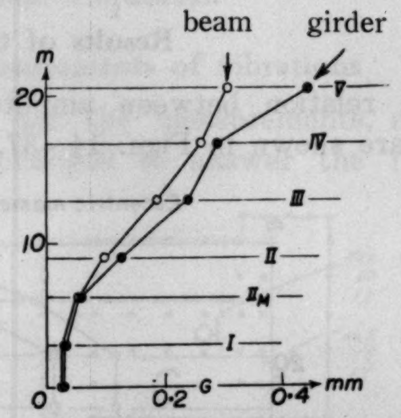

Fig. 6. Amplitudes distribution in beam and girder directions. Experiment Nos.; 17, 19, 20, 22. Vibration generator; B.R.I. type set at the middle of the 3rd-floor.

The amplitude variation with the height of the building was obtained from the data before mentioned and is shown in Figs. 2∼6. Sometimes the horizontal axes vibrator was driven at the eastern end on the 6th floor to give the building torsional vibration. Amplitudes of the motion in the direction of beam on the 4th floor are shown in Fig. 7. from which we can see an evidence of the torsional vibrations. Amplitudes resonated by the vibrator at each of the measurements are shown in Table 4.

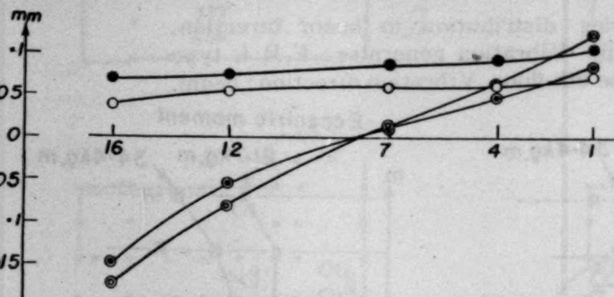

Fig. 7 Amplitudes distribution in beam direction on the 4th-floor. Experiment No.; 8. Vibration generator; E. R. I. type, set at the eastern end of the 6th-floor, in beam direction.

Consideration of the results of the measurements

The rigidity of columns on each floor was calculated from amplitude variation according to height and vibration period obtained, under the following assumptions: the feet of columns are fixed, the joints between floor and columns are rigid, the floor and girder are rigidly connected, the loads on the floor are concentrated, and the dissipation of the vibration energy of the building to the ground is negligible. The formula of K. Kanai was adopted to express relation between period, amplitude and mechanical properties of the building.

$$E_sI_s=\frac{1}{12}\left(\frac{2\pi}{T}\right)^2\frac{l_s^3}{y_s-y_{s-1}}\sum_{r=s}^{n}m_ry_r\ ,\ (s=1,\ 2,\ \cdots,\ n) \qquad (1)$$

where E: Young's modulus, I: moment of inertia, y: horizontal displacement, m: concentrated mass on a floor and l: height of column.

The data used for the calculations are tabulated in Table 6, and the results of the calculation in Table 7.

Test to examine rocking motion of the building accompanying its movement due to the vibration generator

Two vertical component tromometers were set up at the ends of the building in the direction of the vibrator motion to examine rocking motions of the building. If the building makes rocking vibration, vertical motions at the opposite ends of the building will be opposite in phase, or have a difference of phase angle 180°. The constants of the vertical tromometers used for the experiment were as follows:

$$T(\text{period})=3.0\ \text{sec.},\ v(\text{damping})=2.2,\ r(\text{friction})=0\ .$$

The ground floor may be the best place to put the instruments to observe the rocking motion, but there was no good place for setting up the tromometers, so the instruments were placed on the first floor.

Phase difference of vibrations between the two opposite places was recorded when the building resonated and the vibration became large. In such cases, the period of vibration was about 0.4 sec., probably the period of the fundamental vibration of the building. The phase difference measured was small (Figs. 8 and 9.) Then the writer at first deduced the building was not in rocking motion, but such consideration may be too hasty. The observations were made not on the underground floor, but on the first floor which may be flexed with vibrations of the building. Otherwise, it may be supposed that the building was too large to make rocking motions like a small rigid body, and the floor bended to adapt the movements of the upper structure and to the deformation of the ground.

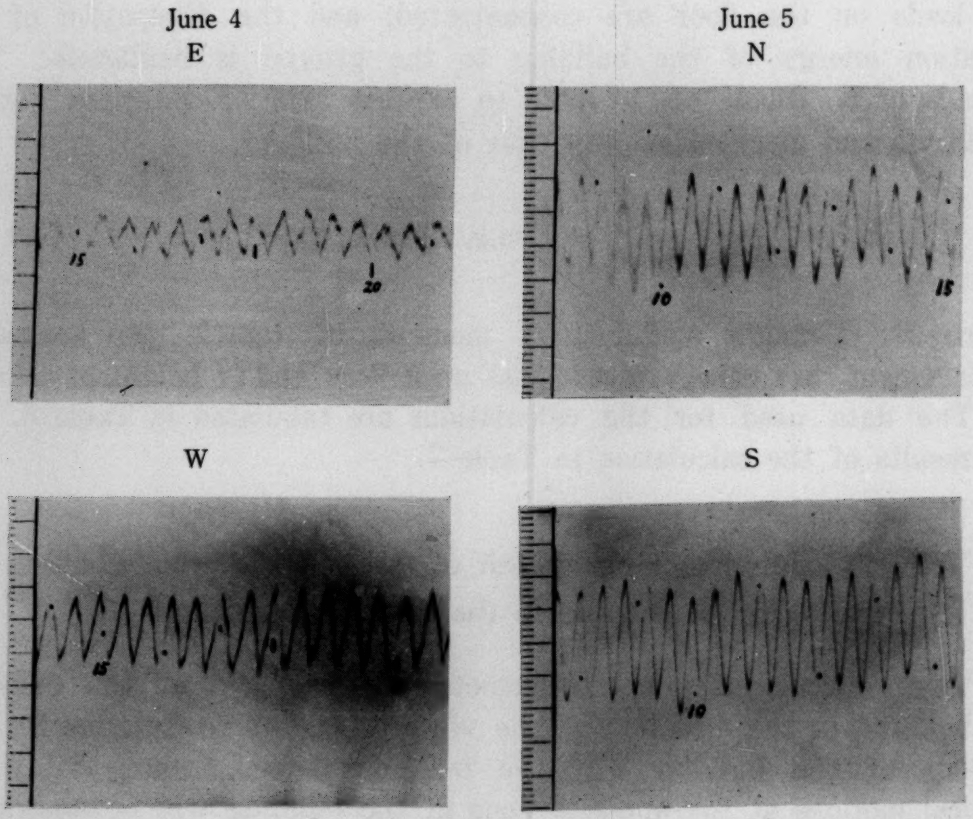

Fig. 8

Further the rocking motions were checked with two electromagnetic transducers and a 3 element electromagnetic oscillograph. On the ground floor horizontal component motion of the building was recorded side by side with vertical component. When the horizontal motion in the direction of beam was in resonance, the vertical component became in phase with them in rocking motions as shown in Figs. 10 and 12. When the building was moved in the direction of girder at first horizontal motions were observed with vertical motions as before, secondly vertical motions at the two ends of the building were recorded (Figs. 11, 12 and 13). In these cases rocking motion could not be found.

In this studies K. Kanai and N. Nasu were assigned the measurements of vibrations, F, Kishinouye, H. Kawasumi and E. Sima those of rocking motions, and the results were compiled by F. Kishinouye.

We wish to express our hearty thanks to Mr. Kyoji Nakagawa of the Building Research Institute, Dr. T. Naito of the Waseda University and Dr. R. Takahasi of our Institute with whose aid the studies were made.

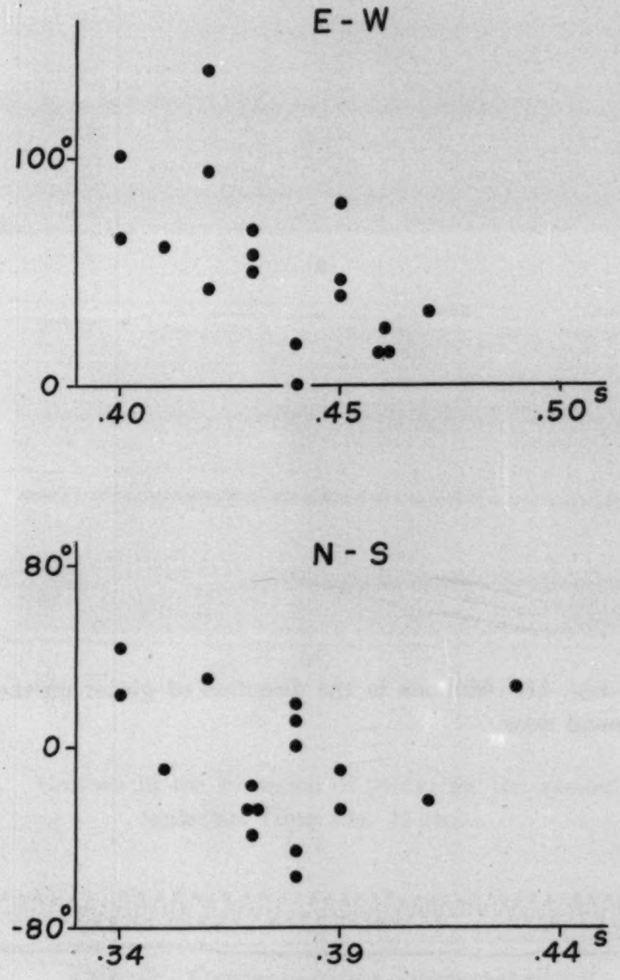

Fig. 9. Phase diffenence of vertical vibrations at two places.

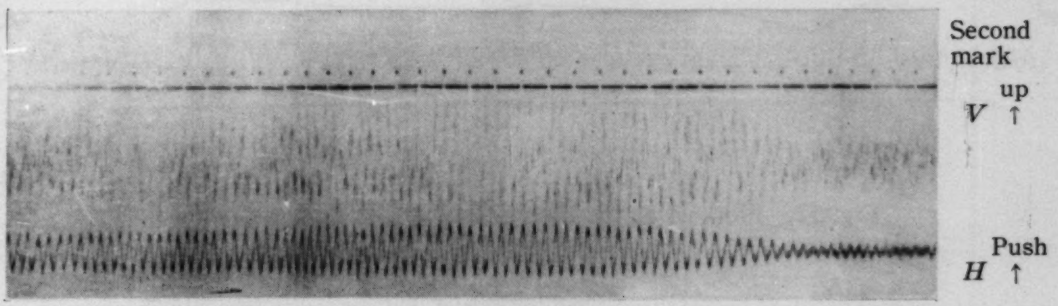

Fig. 10. Motions in the direction of beam on the ground floor. Horizontal and vertical transducers were set at opposite ends of the building in beam direction.

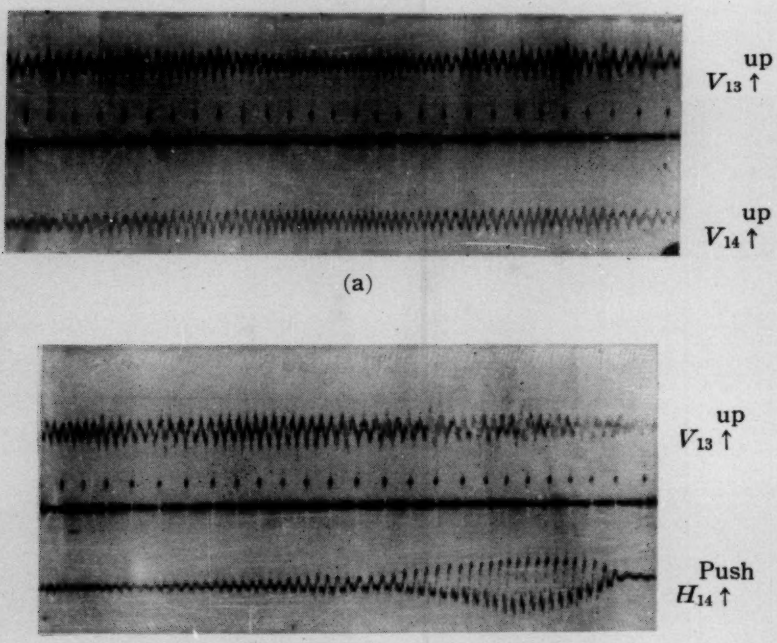

(a)

(b)

Fig. 11. Motions in the direction of girder on the ground floor.

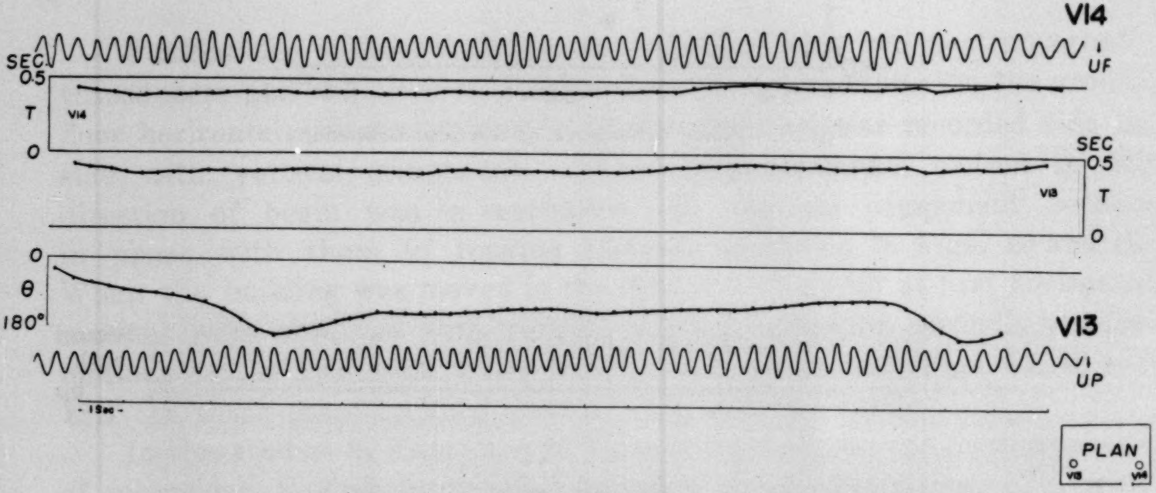

Fig. 12. Motions in the direction of girder on the ground floor. (enlarged from Fig. 11,(a))

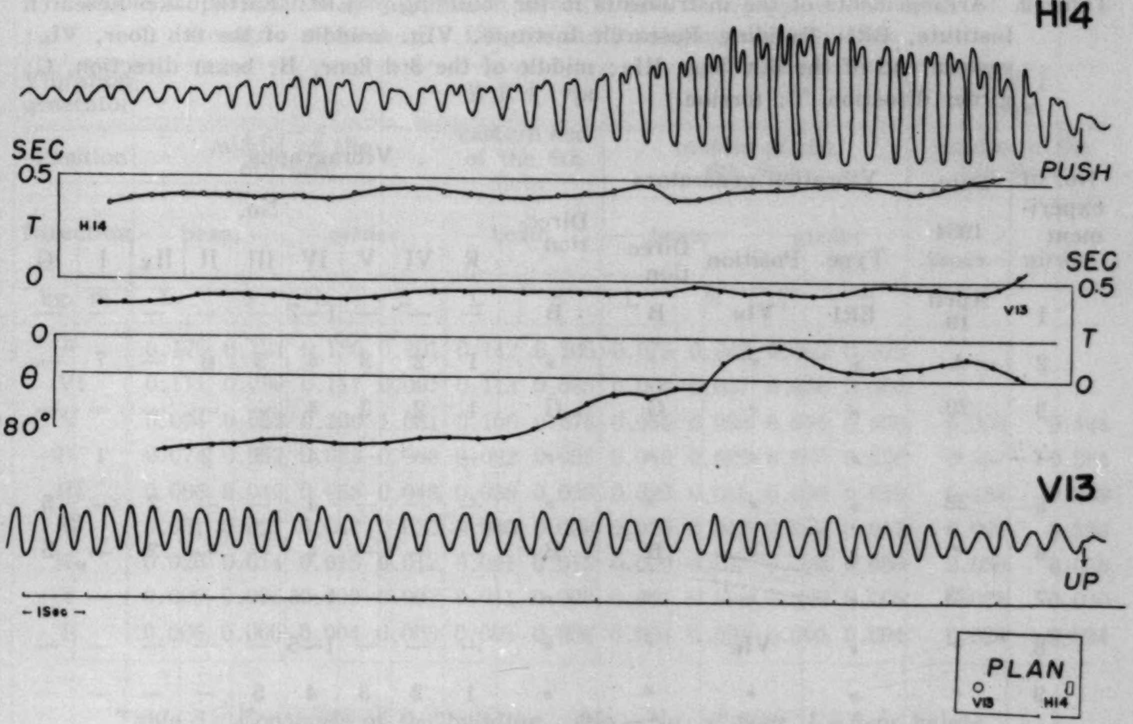

Fig. 13. Motions in the direction of girder on the ground floor. (enlarged from Fig. 12,(b))

Table 2. Constants of the vibrographs.

No. of vibrograph	Self-vibration period (sec)	Damping ratio	Magnification
1	1.0	13:1	120
2	〃	〃	130
3	〃	〃	150
4	〃	〃	200
5	〃	〃	180
6	〃	〃	175
7	〃	〃	180
8	5.0	〃	20
9	〃	〃	18

Table 3. Arrangements of the instruments in the building. (ERI: Earthquake Research Institute, BRI: Building Research Institute, $\mathrm{VI_M}$: middle of the 6th floor, $\mathrm{VI_E}$: eastern end of the 6th floor, $\mathrm{III_M}$: middle of the 3rd floor, B: beam direction, G: girder direction, T: torsion.)

No. of experiment	Date. 1954	Vibration generators			Vibragraphs									
					Direction	No.								
		Type	Position	Direction		R	VI	V	IV	III	II	$\mathrm{II_M}$	I	G
1	April 19	ERI	$\mathrm{VI_M}$	B	B	—	—	—	1∼7	—	—	—	—	—
2	〃	〃	〃	〃	〃	1	2	3	4	5	6	—	7	—
3	20	〃	〃	G	G	1	2	3	4	—	—	—	—	—
4	〃	〃	〃	〃	〃	—	—	—	4	3	2	—	1	—
5	22	〃	〃	〃	〃	—	—	—	4	—	—	2	—	5
6	〃	〃	〃	B	B	—	—	—	4	—	—	2	—	5
7	23	〃	〃	〃	〃	—	—	—	1∼5	—	—	—	—	—
8	〃	〃	$\mathrm{VI_E}$	〃	〃	—	—	—	1∼5	—	—	—	—	—
9	〃	〃	〃	〃	〃	1	2	3	4	5	—	—	—	—
10	24	〃	〃	〃	〃	—	—	—	4	—	3	2	1	5
11	〃	〃	〃	〃	〃 G	— —	— —	— —	4 1∼5	— —	— —	— —	— —	— —
12	25	〃	$\mathrm{III_M}$	〃	B	1	2	3	4	5	—	—	—	—
13	〃	〃	〃	〃	〃	—	—	—	—	5	3	2	1	4
14	27	〃	〃	G	G	1	2	3	4	5	—	—	—	—
15	〃	〃	〃	〃	〃	—	—	—	—	5	3	2	1	4
16	June 3	BRI	$\mathrm{III_M}$	T	B G	— —	— —	— —	1 2	3 4	— —	— —	5 —	— —
17	〃	〃	〃	〃	B G	— —	— —	— —	— —	— —	1 2	— —	— 5	3 4
18	4	〃	〃	〃	B	—	—	—	—	—	1∼5 8,9	— —	— —	— —
18′	〃	ERI	〃	B	B	—	—	—	—	—	1∼5 8,9	— —	— —	— —
19	〃	BRI	〃	T	B G	— —	— —	— —	— —	8 9	— —	1 2	3 4	— —
19′	〃	ERI	〃	G	B G	— —	— —	— —	— —	8 9	— 5	1 2	3 4	— —
20	5	BRI	〃	T	B G	— —	— —	— —	8 9	— —	1 2	— —	3 4	— —
21	〃	〃	〃	〃	B G	— —	— —	— —	— —	8 9	— —	— —	3 4	— —
21′	〃	ERI	〃	B	B G	— —	— —	— —	— —	8 9	— —	— —	3 4	— —
22	〃	BRI	〃	T	B G	— —	— —	8 9	— —	— —	— —	— —	3 4	— —
23	〃	〃	〃	〃	B G	— —	— —	— —	— —	— —	— —	— —	3 4	— —

Table 4. Resonance Amplitudes in mm. (L and S represent the cases of the eccentric moment of 2.17kg.m and 3.44kg.m, respectively.)

Vibration generator	E R I type										B R I type	
Position	middle of the 6th floor				eastern end of the 6th floor		middle of the 6th floor				middle of the 6th floor	
Direction	beam		girder		beam		beam		girder		beam	girder
kg. m	L	S	L	S	L	S	L	S	L	S		
R	0.175	0.124	0.130	0.101	0.142	0.105	0.075	0.048	0.102	0.075		
VI	0.111	0.080	0.117	0.091	0.113	0.085	0.060	0.037	0.078	0.056		
V	0.074	0.052	0.100	1.081	0.106	0.076	0.055	0.036	0.070	0.050	0.308	0.444
IV	0.074	0.052	0.083	0.063	0.082	0.055	0.040	0.025	0.055	0.038	0.257	0.284
III	0.066	0.045	0.063	0.048	0.056	0.036	0.025	0.015	0.030	0.019	0.184	0.238
II	0.031	0.023	0.042	0.032	0.040	0.028	0.020	0.013	0.026	0.017	0.098	0.124
II_M	0.020	0.014	0.015	0.012	0.021	0.015	0.009	0.007	0.009	0.006	0.055	0.055
I	0.009	0.006	0.009	0.007	0.011	0.008	0.006	0.004	0.006	0.005	0.028	0.030
B	0.006	0.005	0.004	0.003	0.005	0.004	0.004	0.003	0.005	0.004	0.024	0.024

Table 5. Constants of the building. (No.=No. of floor, l_s=floor height, m_s=concentrated mass.)

No.	G	I	II	III	IV	V	VI
l_s(m)	2.97	6.15	3.79	3.19	3.79	3.79	3.94
m_s(ton)	1100	297	192	184	184	175	288

Table 6. The values of effective stiffness of all vertical members of the building, EI calculated by equation (1). (L=eccentric moment of 34.4kg.m., S=21.7kg.m.)

EI $\times 10^{-18}$ C.G.S.	ERI type								BRI type	
	middle of the 6th-floor				middle of the 3rd-floor				middle of the 3rd-floor	
	beam direction		girder		beam		girder		beam	girder
	L	S	L	S	L	S	L	S		
E_6I_6	0.6	0.6	1.8	1.9	1.2	1.1	0.8	0.8		
E_5I_5	1.1	1.2	1.9	2.6	4.8	15.2	3.3	3.3		
E_4I_4	∞	∞	2.5	1.9	2.1	1.8	2.3	2.1	3.1	1.0
E_3I_3	7.4	6.5	2.6	2.7	2.5	2.4	1.6	1.6	2.9	4.6
E_2I_2	1.9	2.3	2.8	2.9	8.1	12.9	11.4	16.0	3.0	2.2
E_1I_1	14.2	14.0	8.4	8.8	13.7	13.7	10.8	12.6	17.9	13.1
E_0I_0	12.7	29.1	6.8	6.8	12.0	15.5	26.4	18.7	39.8	25.5

Explanation of notations in Figs. 14~37;

Exp.=Experiment number

Type=Type of the vibration generator (eccentric moment)

Position=Position of the vibration generator

Vibration=Vibration direction of the vibration generator

Measurement=Measurement direction of vibrographs

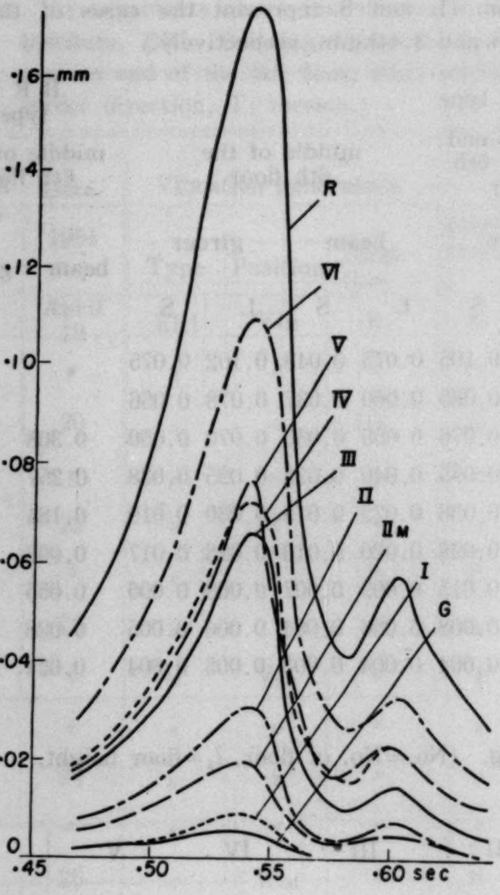

Fig. 14. Exps.; 2, 6
Type; ERI (34.4kg.m.)
Position; middle of the 6th-floot
Vibration; beam
Measurement; beam.

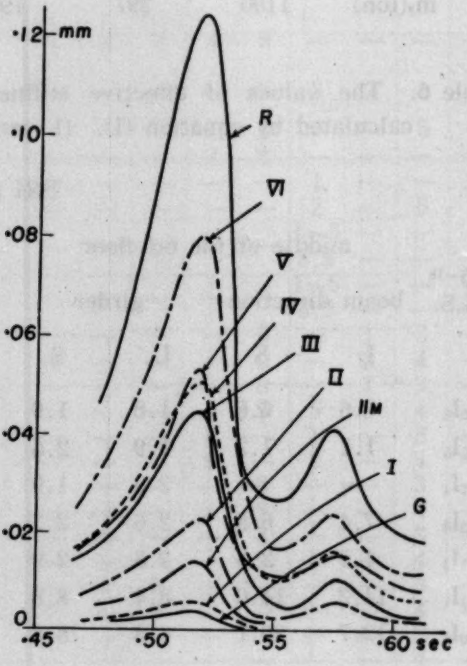

Fig. 15. Exps.; 2, 6
Type; ERI (21.7kg.m.)
Position; middle of the 6th-floor
Vibration; beam
Measurement; beam.

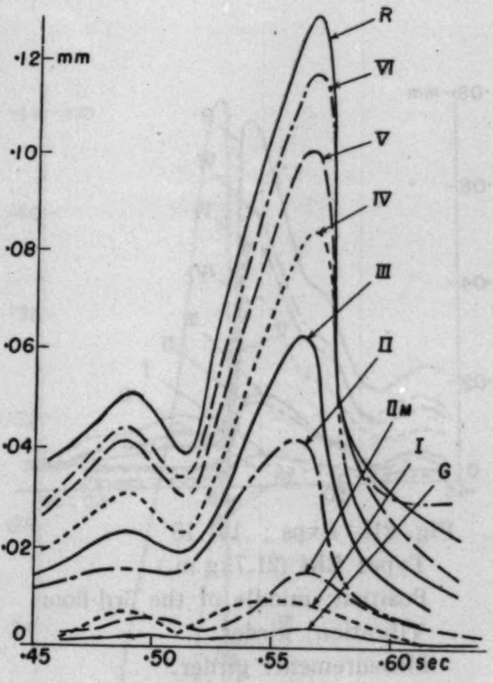

Fig. 16. Exps.; 3, 4, 5
Type; ERI (34.4kg.m.)
Position; middle of the 6th-floor
Vibration; girder
Measurement; girder.

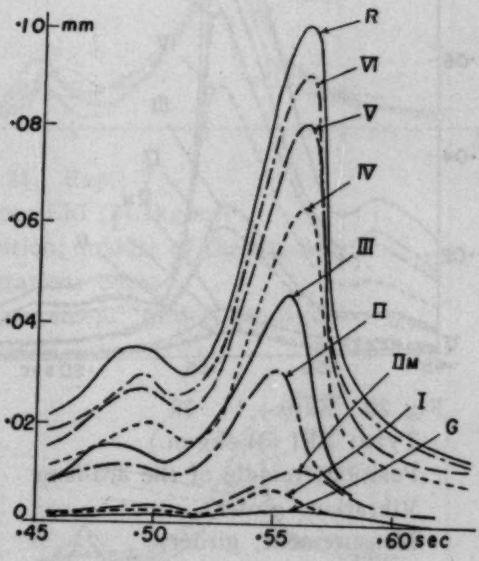

Fig. 17. Exps.; 3, 4, 5
Type; ERI (21.7kg.m.)
Position; middle of the 6th-floor.
Vibration; girder
Measurement; girder.

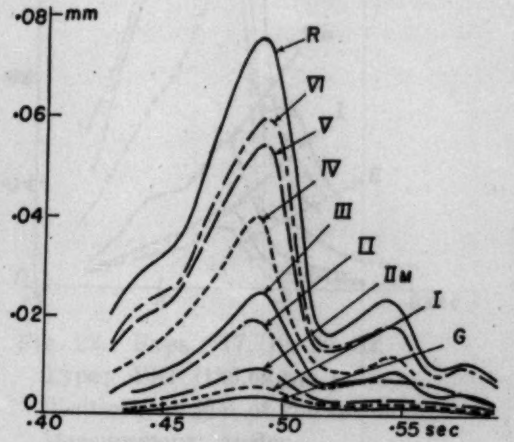

Fig. 18. Exps.; 12, 13
Type; ERI (34.4kg.m.)
Position; middle of the 3rd-floor
Vibration; beam
Measurement; beam.

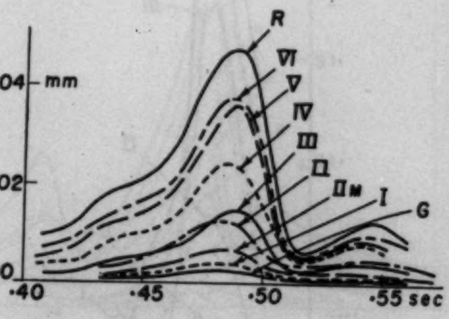

Fig. 19. Exps.; 12, 13
Type; ERI (21.7kg.m.)
Position; middle of the 3rd-floor
Vibration; beam
Measurement; beam.

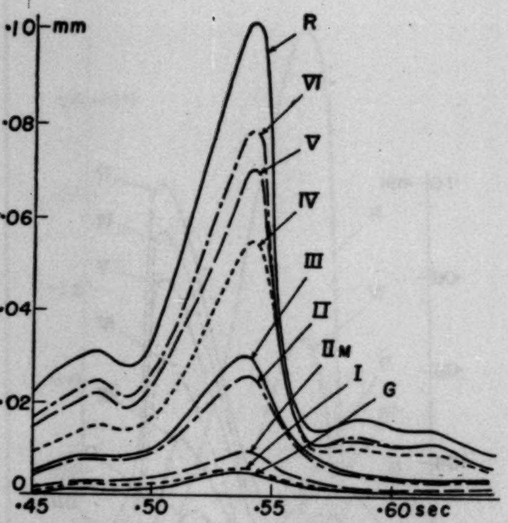

Fig. 20. Exps.; 14, 15
Type; ERI (34.4kg.m.)
Position; middle of the 3rd-floor
Vibration; girder
Measurement; girder.

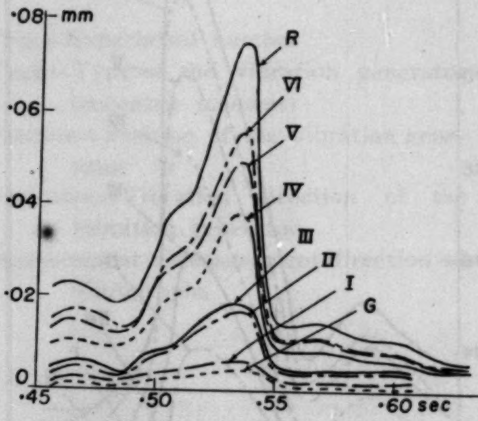

Fig. 21. Exps.; 14, 15
Type; ERI (21.7kg.m.)
Position; middle of the 3rd-floor
Vibration; girder
Measurement; girder.

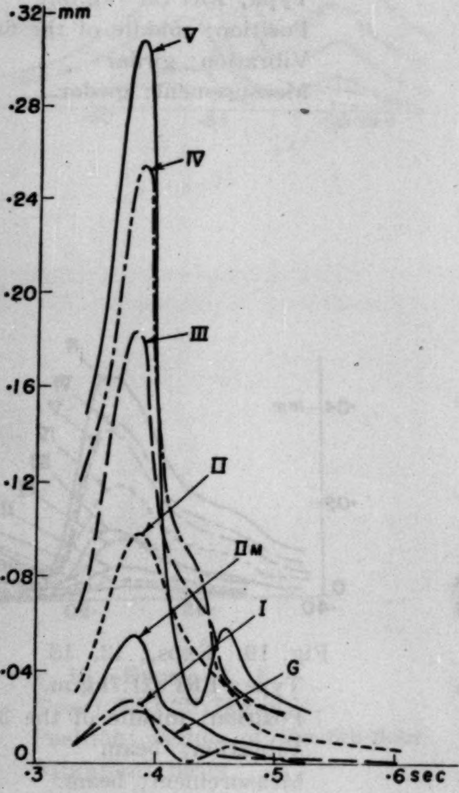

Fig. 22. Exps.; 17, 19, 20, 22
Type; ERI (136.6kg.m.)
Position; middle of the 3rd-floor
Measurement; beam.

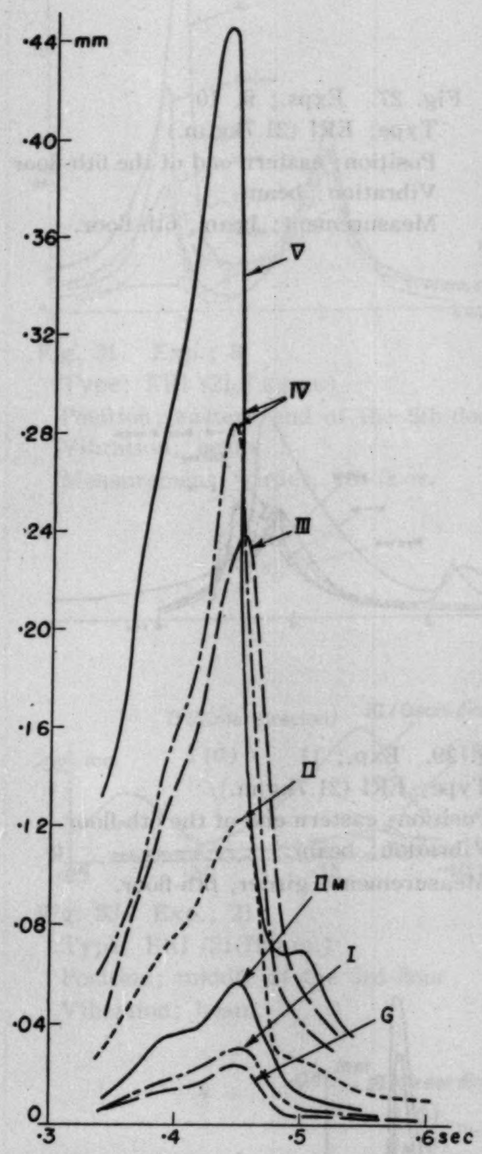

Fig. 23. Exps.; 17, 19, 20, 22
Type; BRI (136.6kg.m.)
Position; middle of the 3rd-floor
Measurement; girder.

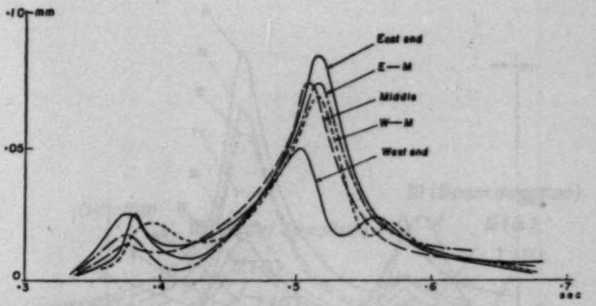

Fig. 24. Exp.; 7
Type; ERI (34.4kg.m.)
Position; middle of the 6th-floor
Vibration; beam
Measurement; girder, 4th-floor.

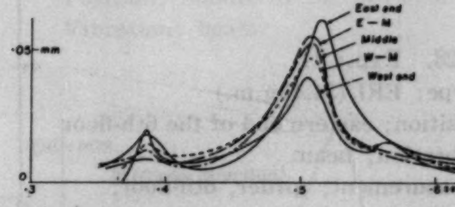

Fig. 25. Exp.; 7
Type; ERI (21.7 kg.m.)
Position; middle of the 6th-floor
Vibration; beam
Measurement; girder, 4th-floor.

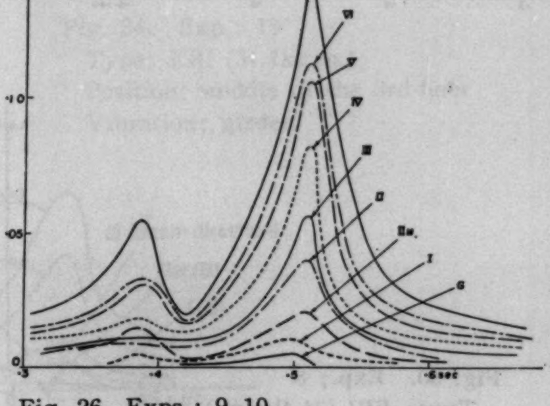

Fig. 26. Exps.; 9, 10
Type; ERI (34.4kg.m.)
Position; eastern end of the 6th-floor
Vibration; beam
Measurement; beam, 6th-floor.

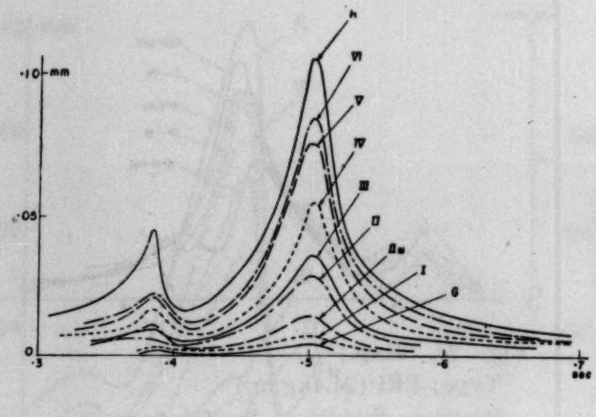

Fig. 27. Exps.; 9, 10
Type; ERI (21.7kg.m.)
Position; eastern end of the 6th-floor
Vibration; beam
Measurement; beam, 6th-floor.

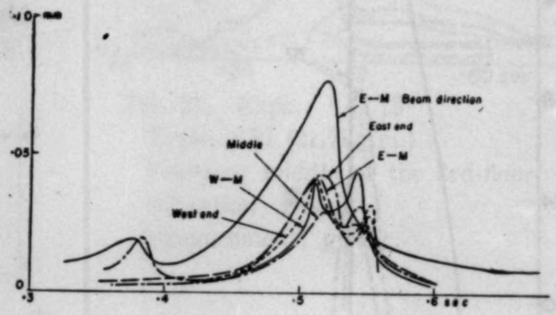

Fig. 28. Exp.; 11
Type; ERI (34.4kg.m.)
Position; eastern end of the 6th-floor
Vibration; beam
Measurement; girder, 6th-floor.

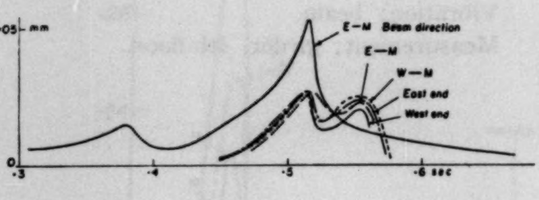

Fig. 29. Exp.; 11
Type; ERI (21.7kg.m.)
Position; eastern end of the 6th-floor
Vibration; beam
Measurement; girder, 6th-floor.

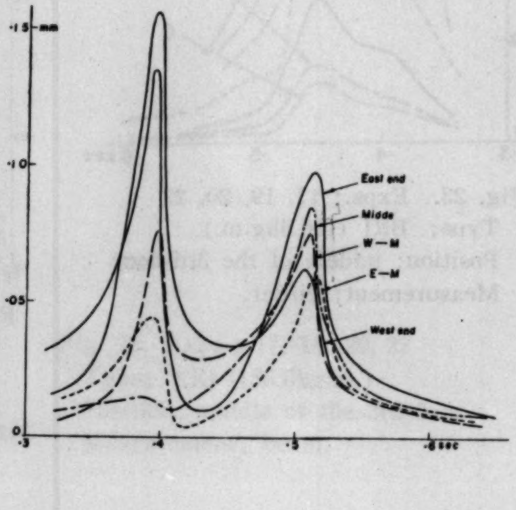

Fig. 30. Exp.; 8
Type; ERI (34.4kg.m.)
Position; eastern end of the 6th-floor
Vibration; beam
Measurement; girder, 4th-floor.

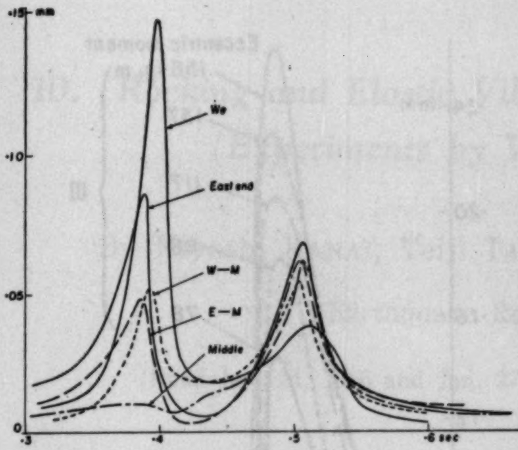

Fig. 31. Exp.; 8
Type; ERI (21.7 kg.m.)
Position; eastern end of the 6th-floor
Vibration; beam
Measurement; girder, 4th-floor.

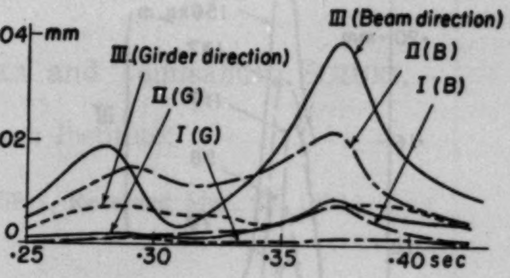

Fig. 32. Exp.; 21′
Type; ERI (34.4kg.m.)
Position; middle of the 3rd-floor
Vibration; beam.

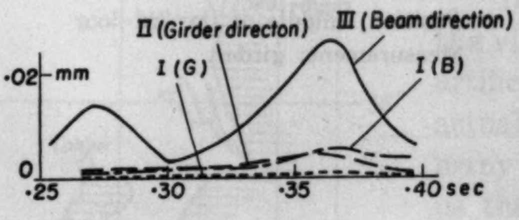

Fig. 33. Exp.; 21′
Type; ERI (21.7kg.m.)
Position; middle of the 3rd-floor
Vibration; beam.

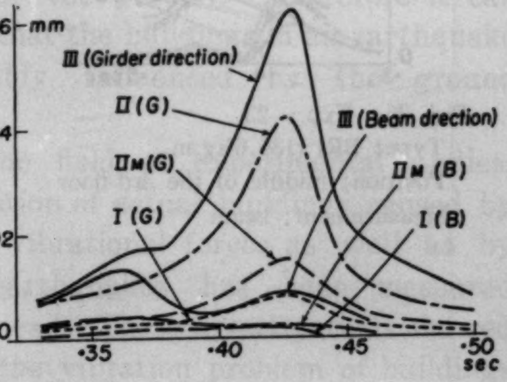

Fig. 34. Exp.; 19′
Type; ERI (34.4kg.m.)
Position; middle of the 3rd-floor
Vibration; girder.

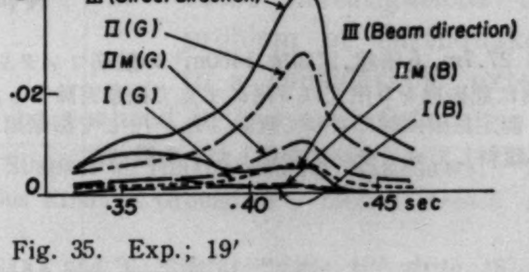

Fig. 35. Exp.; 19′
Type; ERI (21.7kg.m.)
Position; middle of the 3rd-floor
Vibration; girder.

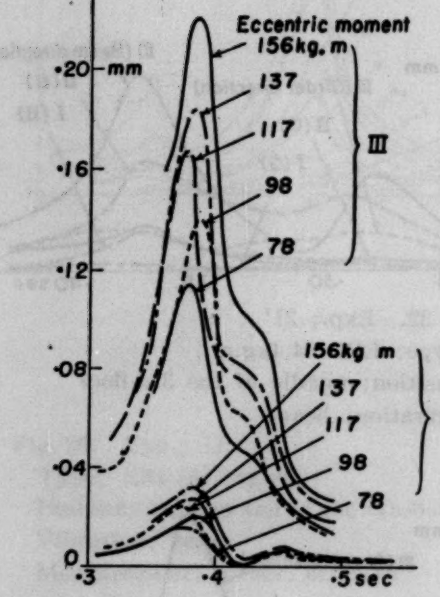

Fig. 36. Exp.; 23
Type; BRI (136.6kg.m.)
Position; middle of the 3rd-floor
Measurement; beam.

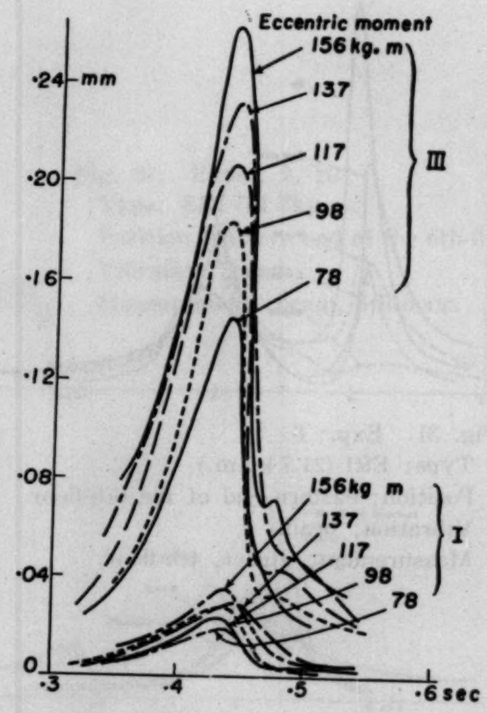

Fig. 37. Exp.; 23
Type; BRI (136kg.m.)
Position; middle of the 3rd-floor
Measurement; girder.

9. 鉄筋コンクリート造建物の振動実験

地震研究所
金井清
岸上冬彦
那須信治
河角広

東京丸ノ内にあつた高さ 27.7m, 6階建,床面積 1460m^2 の鉄筋コンクリート造の建物が 1953年に取こわされた．こわす前に起振機を6階又は3階にすえて振動実験をした．その実験につかつた計器については表に示し，測定結果は図によつて表わした．そして振動周期については計算値と比較し，振動に伴つて建物が傾斜してロッキングを起したかを調べた．

BULLETIN OF THE EARTHQUAKE
RESEARCH INSTITUTE
Vol. 36 (1958), pp. 183-199

10. *Rocking and Elastic Vibrations of Actual Building. I.*
(*Experiments by Vibration Generator*).

By Kiyoshi KANAI, Teiji TANAKA and Tomisaburo SUZUKI,
Earthquake Research Institute.

(Read Jan. 24, 1956 and Jan. 27, 1958. — Received Mar. 31, 1958.)

1. Introduction

The property of building vibration varies according to the ground property even if the same vibrational force acts on buildings of the same structure, and the property of earthquake motion depends on the nature of the ground. Therefore it can be said that the buildings in an earthquake are doubly influenced by the ground property.

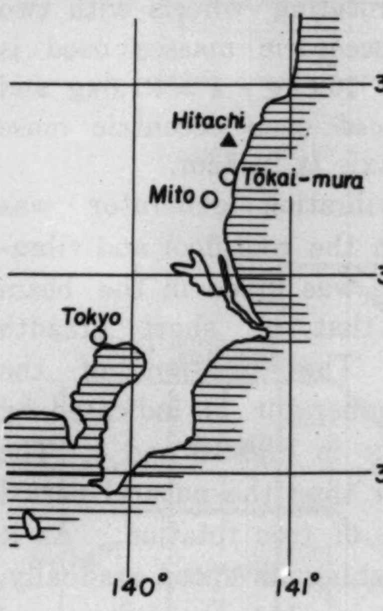

Fig. 1.

In the field of experimental studies, the vibration of actual buildings caused by artificial vibrational forces as well as by actual earthquakes has been measured many times.[1] These investigations showed us that the vibration problem of buildings in a destructive earthquake is very complex and many subjects concerning this problem remain to be treated.

Nevertheless it can be said that, since these investigations threw light on the problem of earthquake-proof construction to a considerable extent, its remarkable developement will be realized in the near future.

---

[1] K. KANAI, T. SUZUKI, T. HISADA and K. NAKAGAWA, "Vibration Experiments in the Buildings on Various Kinds of Ground. I", *Report Archit. Inst. Japan*, **33** (1955), 185.

K. KANAI, T. TANAKA and T. SUZUKI, "*ditto*. II", *ditto*, 187.

K. KANAI and T. SUZUKI, "Relation between the Property of Building Vibration and the Nature of Ground", *Bull. Earthq. Res. Inst.*, **31** (1953), 305: Part II, *ditto*, **33** (1955), 109: Part III, *ditto*, **34** (1956), 61.

With a view of gaining further insight into the problem just mentioned, we tried the investigation of the vibration problem of actual buildings standing on rock and on crushed stone. We carried out the experiments on the buildings by means of a vibration generator.

The buildings submitted to these experiments are three-storied reinforced concrete apartment-houses, located at Hitachi Mine site, Ibaraki prefecture. One building called No. 14 house stands on crushed stone with six meter concrete piles. Another building called No. 6 house stands directly on fresh rock.

2. The case of No. 14 house

(i) Method of experiments.

Figs. 2~5 are the photographs and the rough sketches of the plane view, side view and parts of foundation of No. 14 house. The vibration generator used in this case consists of three rotating wheels with two horizontal axes. The total weight of the eccentric masses used is $5.4\text{kg} \times 2 + 10.8\text{kg} \times 1 = 21.6\text{kg}$ and the length of each eccentric mass from the axis is 21.5cm.

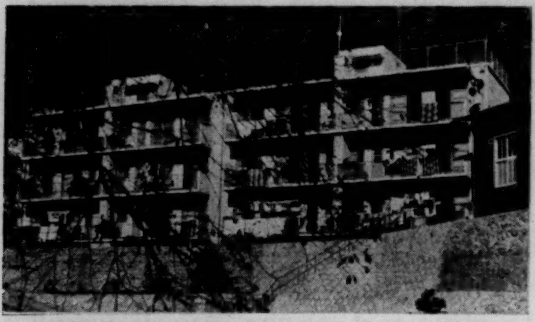

Fig. 2. Photograph of No. 14 house.

The vibration generator was installed on the roof-floor and vibrational force was given in the beam direction, that is, short breadth direction. The position of the vibration generator is indicated by the mark × in Figs. 3 and 4. The vibration generator was driven manually faster than the natural period of a test building and then set free in a state of free rotation. As it keeps on running for quite a long time diminishing its speed gradually, it can be considered as the first approximation that the vibrational force acted on a test building for each period is sinusoidal.

Four horizontal component vibrographs and two vertical component vibrographs were used. The former have a mechanical magnification system with smoked paper for recording, and the latter have an electromagnetic magnification system with smoked paper for recording. The constants of these are shown in Tables 1 and 2 respectively. The positions of the horizontal and vertical vibrographs are indicated by marks ○ and ● in Figs. 3 and 4, respectively. The number of vibrographs used at each position are shown in Table 3 and 4.

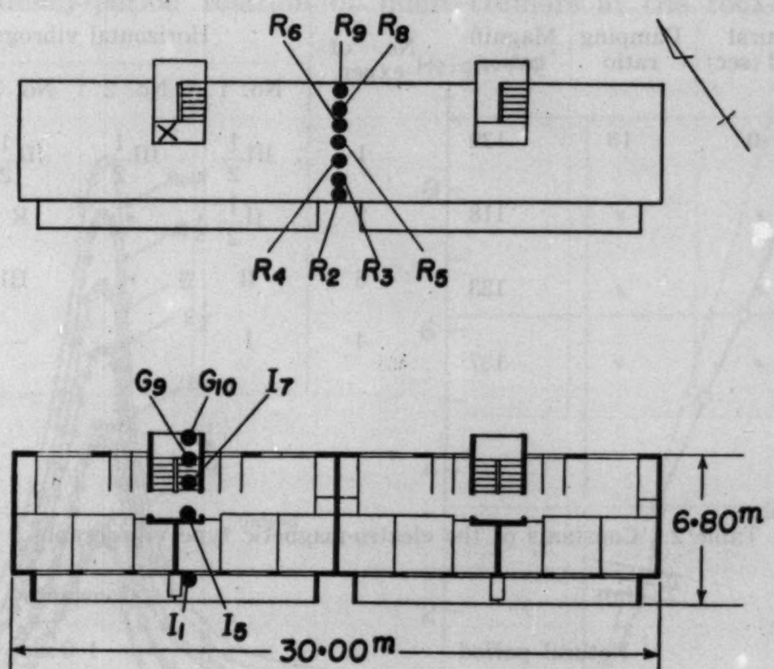
R6
R9
R8
R4
R2
R3
R5
G9
G10
I7
I1
I5
6·80m
30·00m

Fig. 3. Sketch of the plane view of No. 14 house.

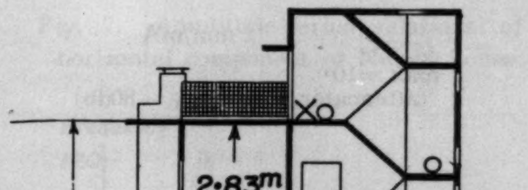
2·83m
9·04m
2·73m
2·73m
0·75m
5·50m
1·30m
0·87m

Fig. 4. Sketch of the side view of No. 14 house.

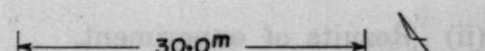
30·0m
6·8m
1·4m
6·0m
5·9m

Fig. 5. Sketch of the foundation parts of No. 14 house.

Table 1. Constants of the mechanical type vibrographs.

No.	Natural period (sec)	Damping ratio	Magnification
1	1.0	13	139
2	〃	〃	118
3	〃	〃	123
4	〃	〃	137

Table 3. Locations of the mechanical type vibrographs.

No. of exper.	Horizontal vibrographs			
	No. 1	No. 2	No. 3	No. 4
1	III$\frac{1}{2}$	III$\frac{1}{2}$	III$\frac{1}{2}$	III$\frac{1}{2}$
2	II$\frac{1}{2}$	〃	R	—
3	II	〃	III	I$\frac{1}{2}$
4	I	—	—	G

Table 2. Constants of the electro-magnetic type vibrographs.

Unit		Constants
Transducer	Natural period	1.0 sec
	Damping ratio (electro-magnetic)	10
Amplifier	Conductance between input and output	28 mho
Recorder (smoke writing type)	Natural period	0.045 sec
	Sensitivity	2 mm/mA
Overall magnification		max.$=10^5$ (attenuater, 2db step, -80db)

(ii) Results of experiment.

The representative records are illustrated in Fig. 6. The relation between the amplitudes of horizontal component and the vibration periods at each position is shown in Fig. 7. The vibrational force produced by the vibration generator is represented by $f=m(4\pi^2/T^2)r$, where m=eccentric mass, r=radius, T=period. Therefore, the observed values represent the amplitudes corresponding to the applied force which changes according to frequency. This makes theoretical consideration rather complicated. So the values are converted into the amplitudes, supposing that the constant force of 5.5×10^6 dyne, that is, force corresponding to the period of 0.18 sec, acts regardless of period.

From Fig. 7, it is found that the resonance period of the beam direction of No. 14 house was 0.182 sec, and we obtain the value of the fraction of critical damping of No. 14 house in h, that is, $h=0.032$.2) The frequency-period relation of micro-tremors at the roof-floor of this

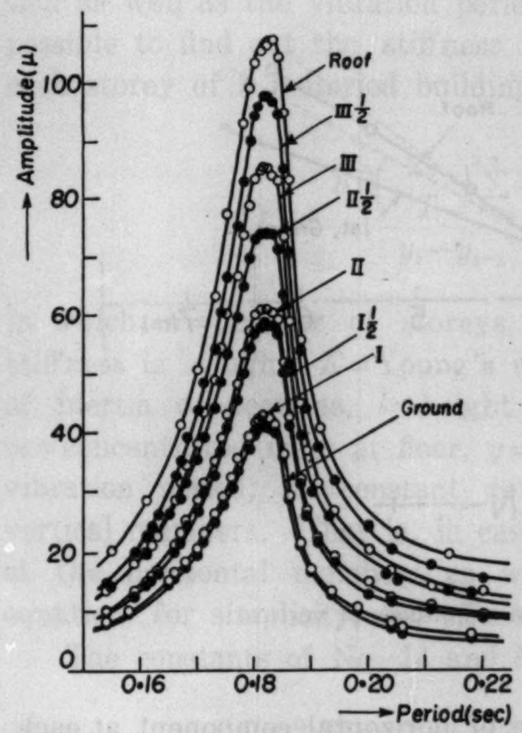

Fig. 7. Amplitude-period relations of horizontal component of No. 14 house.

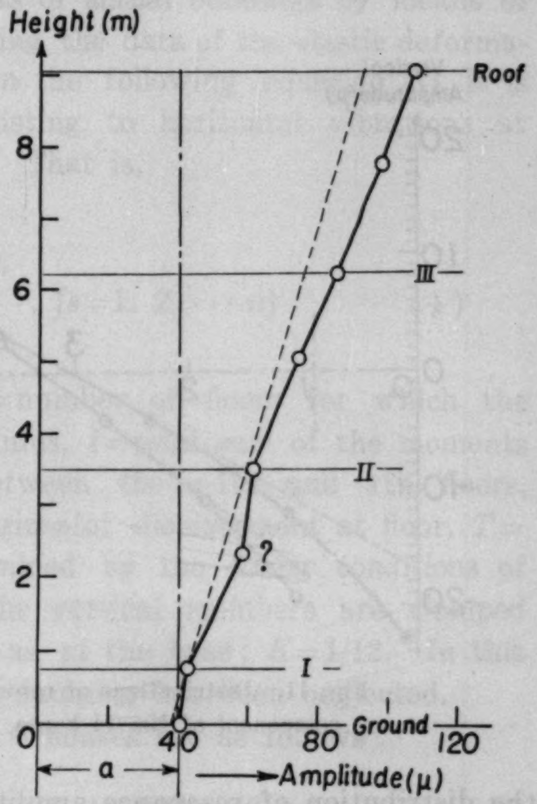

Fig. 8. Amplitude distribution of horizontal component of No. 14 house.

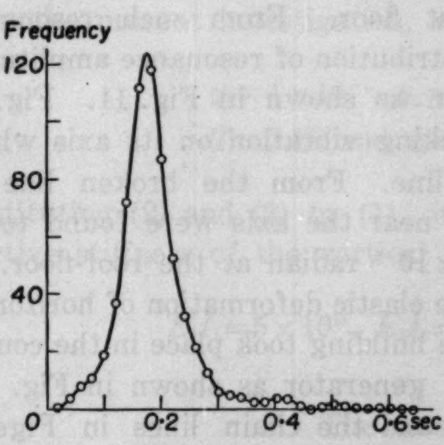

Fig. 9. Frequency-period relation of micro-tremors.

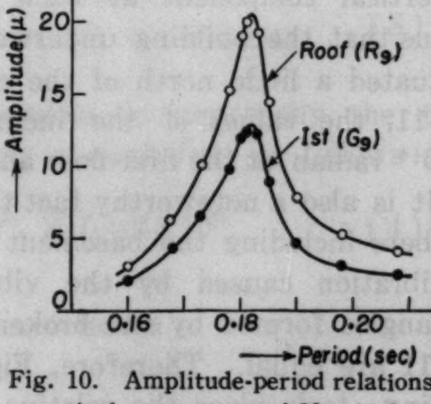

Fig. 10. Amplitude-period relations of vertical component of No. 14 house.

---

2) $h=\{(1/T_2)^2-(1/T_1)^2\}T_0^2/4$, in which T_1, T_2 and T_0 are the periods of resonance curve at $1/\sqrt{2}$ times resonance amplitude and resonance period

house is illustrated in Fig. 9. Figs. 7 and 9 tell us that the predominant period of micro-tremors at the top of a building coincides fairly with the resonance period of the same building. From Fig. 7, we obtain the distribution of resonance amplitude of horizontal component at each position as shown in Fig. 8. Next, Fig. 10 shows the examples of the relation between the amplitudes of vertical component and vibration periods at the roof-floor and at the first floor. From such resonance curves as in Fig. 10, we obtain the distribution of resonance amplitudes of vertical component at each position as shown in Fig. 11. Fig. 11 tells us that the building underwent rocking vibration on its axis which is situated a little north of the center line. From the broken line in Fig. 11, the values of the inclination near the axis were found to be 6×10^{-6} radian at the first-floor and 7.5×10^{-6} radian at the roof-floor.

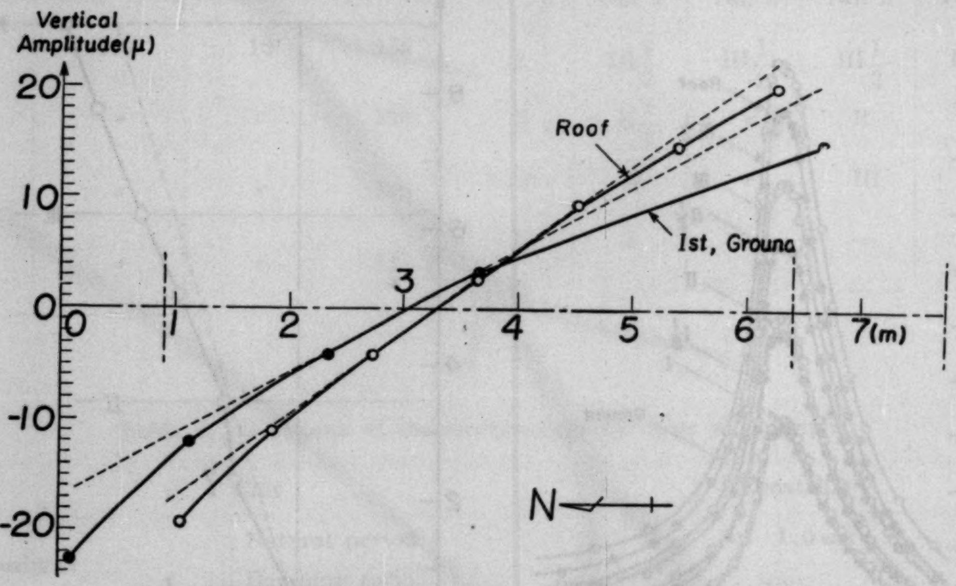

Fig. 11. Distributions of resonance amplitudes of vertical component of No. 14 house.

It is also a noteworthy fact that the elastic deformation of horizontal members including the basement of the building took place in the course of vibration caused by the vibration generator as shown in Fig. 11. The angles formed by the broken lines and the chain lines in Figs. 8 and 11 are equal. Therefore, Figs. 8 and 11 tell us that there, in the building, took place the relative displacement at the foundation to the ground, a, the rocking vibration of the angle θ together with the elastic deformation corresponding to the displacement between the broken line and the full line, in the course of the vibration caused by the vibration generator.

In case of vibrational experiments of actual buildings by means of the vibration generator, by substituting the data of the elastic deformation as well as the vibration period in the following equation (1), it is possible to find out the stiffness resisting to horizontal vibrations at each storey of a n-storied building.[3] That is,

$$E_sI_s = \frac{Kl_s^3\left(\dfrac{2\pi}{T}\right)^2 \sum\limits_{r=s}^{n} m_r y_r}{y_s - y_{s-1}}, \quad [s=1,\ 2,\ \cdots\ n] \tag{1}$$

in which, n=number of storeys, s=number of floors for which the stiffness is sought, E=Young's modulus, I=total sum of the moments of inertia of sections, l=height between the s-1th and sth floors, m=concentrated mass at floor, y=horizontal displacement at floor, T=vibration period, K=constant determined by the fixing conditions of vertical members. That is, in case the vertical members are clamped at the horizontal members as well as at the base; $K=1/12$. In this equation, for simplicity, the effect of damping has been neglected.

The constants of No. 14 and No. 6 houses are as follows:

$$\begin{aligned} &l_1=2.73\times10^2,\ l_2=2.73\times10^2,\ l_3=2.83\times10^2, \\ &m_1=m_2=m_3=3.3\times10^8. \qquad \text{(C. G. S. unit)} \end{aligned} \tag{2}$$

From the present investigation, we obtained the following data:

$$\begin{aligned} &y_1=4\times10^{-4},\ y_2=9\times10^{-4},\ y_3=15\times10^{-4} \\ &T=0.18 \text{ and } K=1/12. \qquad \text{(C. G. S. unit)} \end{aligned} \tag{3}$$

Substituting (2) and (3) in (1), it is possible to get easily the total effective stiffness of the vertical members of each floor as follows:

$$E_1I_1=5\times10^{18},\ E_2I_2=3\times10^{18},\ E_3I_3=2\times10^{18}. \tag{4}$$

3. The case of No. 6 house

(i). Method of experiments.

---

[3] K. KANAI, "A Method of Determining the Stiffness of Each Storey of a n-storied Building", *Bull. Earthq. Res. Inst.*, **28** (1950), 161.

Figs. 12∼15 are the photograph and the rough sketches of the plane view, side view and parts of foundation of No. 6 house.

Fig. 12. Photograph of No. 6 house.

The vibration generator used in this case consists of two rotating wheels with two horizontal axes. The total weight of the eccentric masses used is 1.4kg × 2 = 2.8kg and the length of each eccentric mass from the axis is 21.5cm. The vibration generator was installed on the roof-floor and vibrational force was given in the beam direction, that is, short breadth direction. The position of the vibration generator is indicated by the mark × in Figs. 13 and 14. The vibration generator was driven by A.C. motor of 1/2HP faster than the natural period of a test-building and then set free in a state of free rotation. For the first approximation, the vibrational force acted on a test-building for each period may be considered sinusoidal.

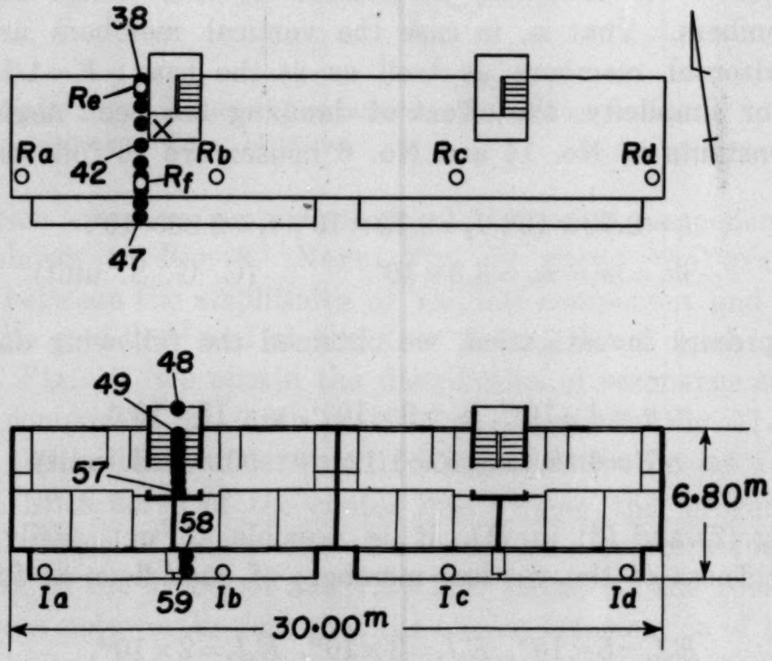

Fig. 13. Sketch of the plane view of No. 6 house.

Six horizontal and two vertical component electro-magnetic type vibrographs and one mechanical magnification type vibrograph were used. The electro-magnetic type vibrographs were used in combination

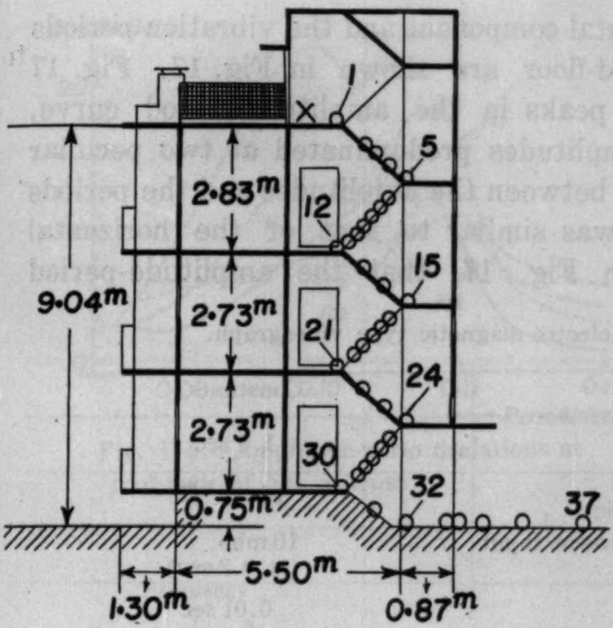

Fig. 14. Sketch of the side view of No. 6 house.

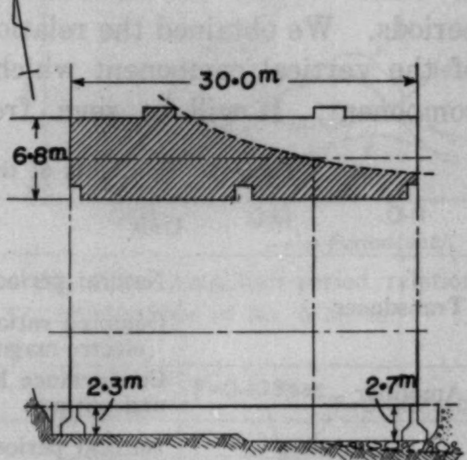

Fig. 15. Sketch of the foundation parts of No. 6 house.

with a six-element oscillograh, and a mechanical type vibrograph used as the standard was combined with smoked paper recording apparatus. The constants of vibrographs are shown in Table 5.

The positions of the horizontal and vertical vibrographs are indicated by marks ○ and ● in Figs. 13 and 14, respectively. The locations of the vibrographs are shown in Table 6.

Observation on the stairs was made in order to measure the vibration of horizontal component at the parts between each floor. Only a few measurements of vertical component were made on the south side of the building, because the rooms on that side had Japanese mats on the floor.

(ii) Results of experiment.

Table 4. Locations of the electromagnetic type vibrographs.

No. of exper.	Vertical vibrographs	
	No. 1	No. 2
1	G_9	G_9
2	G_{10}	〃
3	I_7	〃
4	I_5	〃
5	I_1	〃
6	R_9	〃
7	R_3	R_2
8	R_4	〃
9	R_5	〃
10	R_6	〃
11	R_8	〃
12	R_9	〃
13	R_2	〃

The representative records are illustrated in Fig. 16. The relations between the amplitudes of horizontal component and the vibration periods at the roof-floor and the ground-floor are shown in Fig. 17. Fig. 17 shows plainly that there are two peaks in the amplitude-period curve, in other words, the vibration amplitudes predominated at two peculiar periods. We obtained the relation between the amplitudes and the periods of the vertical component which was similar to that of the horizontal component. It will be seen from Fig. 17, that the amplitude-period

Table 5. Constants of the electro-magnetic type vibrograph.

Unit		Constants
Transducer	Natural period	1.0 sec
	Damping ratio (electro-magnetic)	10
Amplifier	Conductance between input and output	10 mho (at 0.2 sec)
Oscillograph	Natural period	0.01 sec
	Sensitivity	14 mm/mA
Overall magnification		1.5×10^5 (attenuater, 2db step, −80db)
Overall period characteristics		Displacement type (in a period range between 0.05 sec and 1.0 sec.)

Table 6. Locations of the vibrographs.

No. of exper.	Vertical vibrographs		Horizontal vibrographs			
	V_1	V_2	H_3	H_4	H_5	H_6
1	5	5	5	5	5	5
2	38	47	〃	1	12	15
3	39	46	〃	21	24	30
4	40	45	〃	32	33	34
5	41	44	〃	35	36	37
6	42	43	R_d	R_c	R_b	R_a
7	49	59	I_d	I_c	I_b	I_a
8	〃	〃	〃	〃	〃	〃
9	51	58	28	26	4	2
10	49	38	23	22	10	7
11	53	55	20	17	14	13
12	50	52	25	31	3	11
13	54	56	27	29	6	8
14	48	57	18	19	9	16
15	R_e	R_f	R_e(B)	R_e(G)	R_f(B)	R_f(G)
16	R_e	R_e	R_e	R_e	R_e	R_e

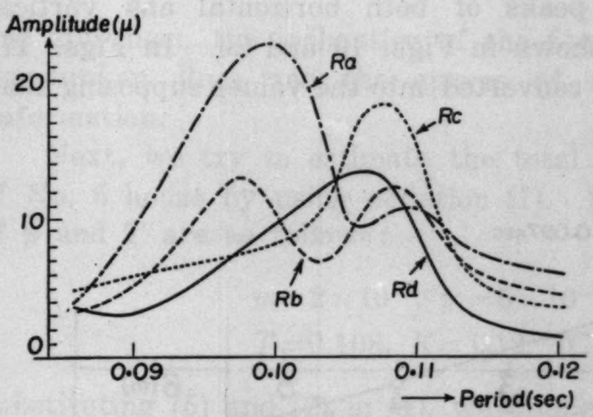

Fig. 17a. Amplitude-perio drelations at roof-floor of No. 6 house.

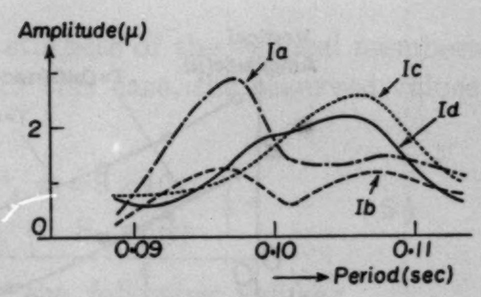

Fig. 17b. Amplitude-period relations at first-floor of No. 6 house.

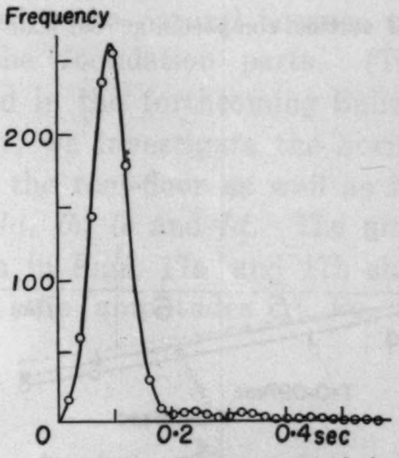

Fig. 18. Frequency-period relation of micro-tremors.

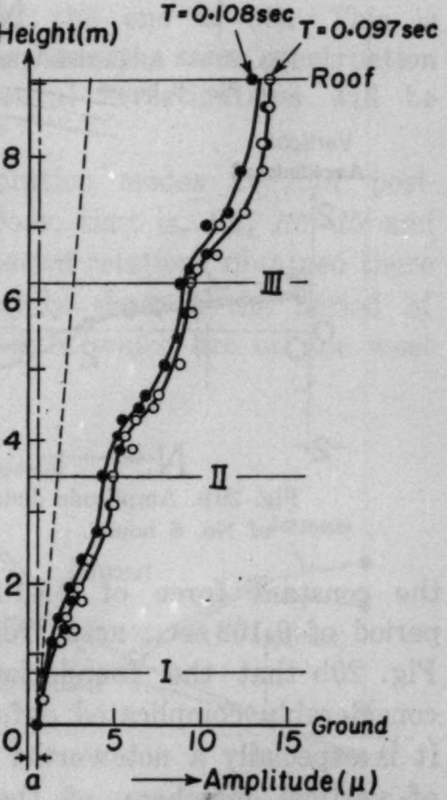

Fig. 19. Amplitude distributions of horizontal component of No. 6 house.

relation of No. 6 house is very complex, and then it is too difficult to obtain the value of *h* of No. 6 house. Therefore, in next time, we will estimate it by adopting various means. The frequency-period relation of micro-tremors at the roof-floor of this house is illustrated in Fig. 18. It is found from Figs. 17 and 18 that the frequency-period relation of micro-tremors at the top of No. 6 house differs from the amplitude-period relation of sinusoidal-forced oscillation of the house and the peak in the former curve nearly coincides with one of the peaks in the latter curve. The amplitude distribution of two peaks of both horizontal and vertical components of each position is shown in Figs. 19 and 20. In Figs. 17, 19 and 20, the amplitudes were converted into the values supposing that the constant force of 2×10^8 dyne, that is, force corresponding to the period of 0.108 sec., acted regardless of period. It will be seen from Fig. 20b that the foundation beam of the No. 6 house was given a considerably complicated deformation by the horizontal vibrational force. It is especially a noteworthy result that the type of bending oscillation of vertical members of the house has appeared so clearly in such experiments as shown in Fig. 19.

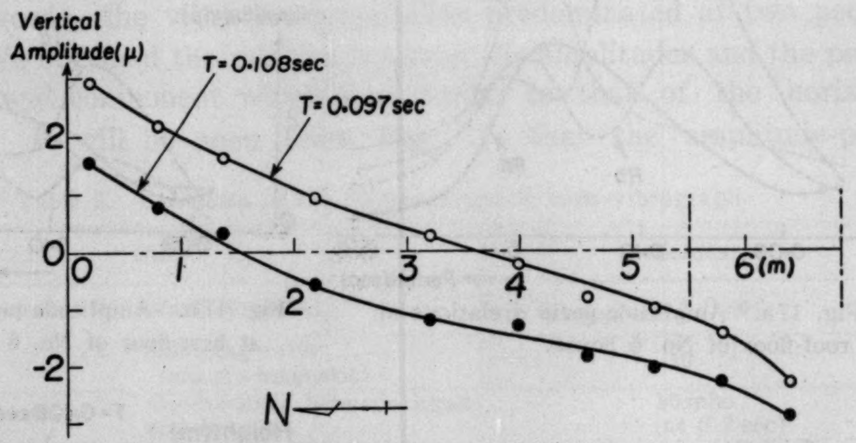

Fig. 20a. Amplitude distributions of vertical component at roof-floor of No. 6 house.

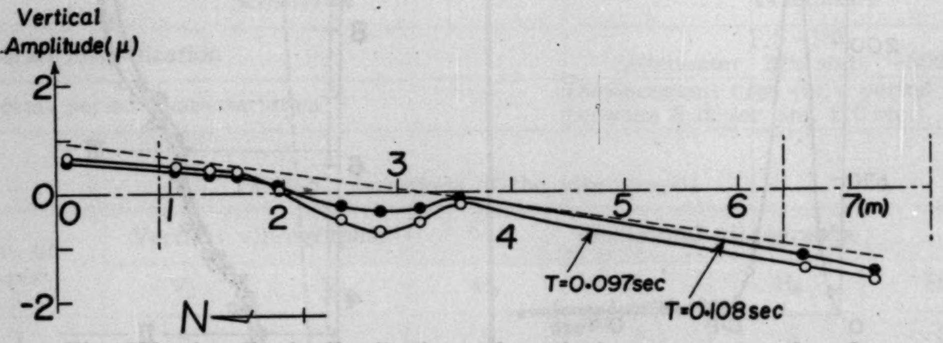

Fig. 20b. Amplitude distributions of vertical component at first-floor of No. 6 house.

At any rate, Figs. 19 and 20 show that in No. 6 house, that is, a house standing on the rock, there also took place the relative displacement at the foundation to the ground, rocking vibration and elastic deformation in the course of the sinusoidal forced oscillation. Roughly speaking, the angles formed by the broken lines and the chain lines in Figs. 19

and 20b mean the inclination of the foundation, and the values between the broken lines and the curves of full line correspond to elastic deformation.

Next, we try to estimate the total stiffness of the vertical members of No. 6 house by using equation (1). In this case, the observed values of y and T are as follows:

$$\left.\begin{array}{l} y_1=2\times10^{-4},\ y_2=5\times10^{-4},\ y_3=8\times10^{-4} \\ T=0.108,\ K=1/12\quad \text{(C. G. S. unit)} \end{array}\right\} \tag{5}$$

Substituting (5) and (2) in (1), we obtain the following values:

$$E_1I_1=18\times10^{18},\ E_2I_2=10\times10^{18},\ E_3I_3=7\times10^{18}\quad \text{(C. G. S. unit)} \tag{6}$$

The each value in (6) are about 1/3 of the one in (4). This is considered to be natural because two houses have the same construction except the foundation parts. (The theoretical investigations will be presented in the forthcoming Bulletin.)

Next, we investigate the horizontal vibration modes at four positions on the roof-floor as well as the first-floor, that is, *Ra*, *Rb*, *Rc* and *Rd* and *Ia*, *Ib*, *Ic* and *Id*. The amplitude-period relations obtained there as shown in Figs. 17a and 17b show us plainly that at the period of 0.097 sec the amplitudes at *Ra*, *Rb*, *Ia* and *Id* which are on the west side grew large, on the other hand, at the period of 0.108 sec the amplitudes at *Rc*, *Rd*, *Ic* and *Id* on east side predominated. The amplitude distributions at the moment when the horizontal amplitude of each position at the roof-floor and the first-floor became maximum are shown

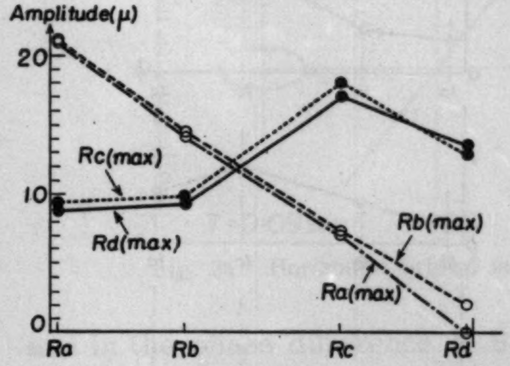

Fig. 21 a. Amplitude distributions at the moment when the horizontal amplitude of each position at the roof-floor of No. 6 house became maximum.

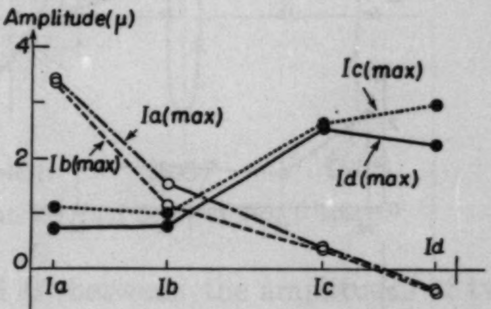

Fig. 21 b. Amplitude distributions at the moment when the horizontal amplitude of each position at the first-floor of No. 6 house became maximum.

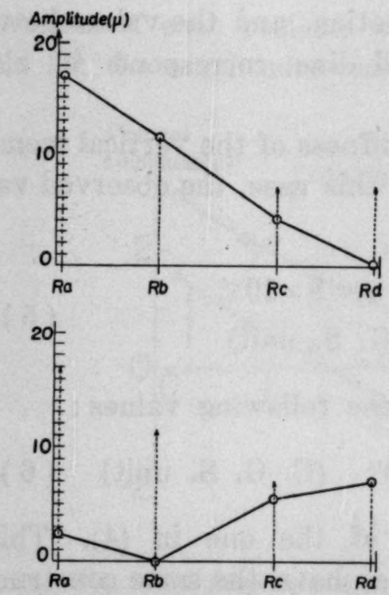

Fig. 22a. Horizontal amplitude distributions at the moments within 1/4 cycle of vibration, including the moment when the amplitude of position *Rb* (roof-floor) of No. 6 house became maximum.

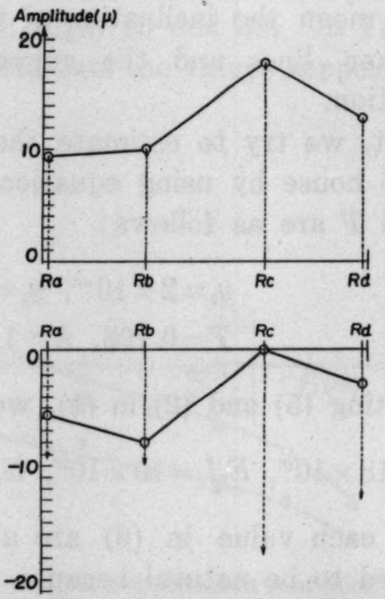

Fig. 22b. Horizontal amplitude distributions at the moments within 1/4 cycle of vibration, including the moment when the amplitude of position *Rc*(roof-floor) of No. 6 house became maximum.

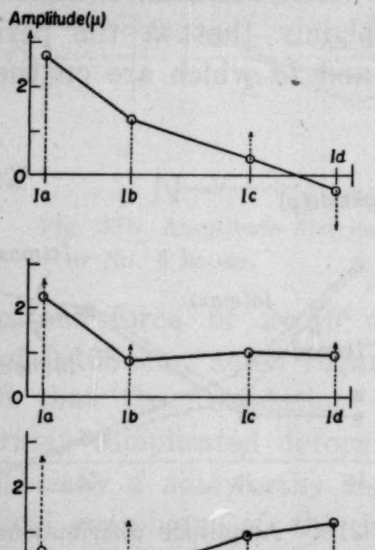

Fig. 22c. Horizontal amplitude distributions at the moments within 1/4 cycle of vibration, including the moment when the amplitude of position Ib (first-floor) of No. 6 house became maximum.

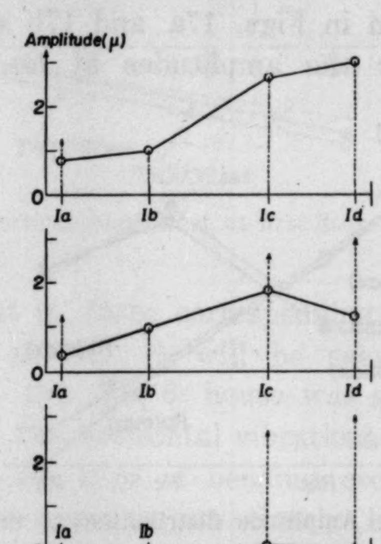

Fig. 22d. Horizontal amplitude distributions at the moments within 1/4 cycle of vibration, including the moment when the amplitude of position Ic (first-floor) of No. 6 house became maximum.

in Figs. 21a and 21b, respectively. From Figs. 21a and 21b, it will be seen that the mode of the horizontal vibration of which the amplitudes at c and d became maximum is approximatelу parallel to the long breadth direction of the house, on the other hand, that of the vibration of which the amplitudes at a and b became maximum is the horizontal vibration on a axis lying near the east end of the house. Figs. 22a, 22b, 22c and 22d show the horizontal amplitude distributions along the long breadth direction of the house at peculiar moments within 1/4 cycle of vibration, including the moment when the amplitudes of *Rb*, *Rc*, *Ib* and *Ic* became maxima, respectively. The amplitude-period relations of both the beam and girder directions observed simultaneously and the figures of horizontal orbital motions at *Re* are shown in Figs. 23 and 24, respectively. It is found from Figs. 23 and 24 that No. 6 house vibrated in the beam direction at the long period of vibration, and in the phase difference of 90° and 0° between the amplitudes of two directions at the time of predominant vibrations of 0.108 sec and 0.098 sec periods, respectively. It seems to be natural to consider that the values of the proper periods of rocking and elastic vibrations of No. 6 house are near to each other, and the vibrations of the periods of 0.108 sec and 0.098 sec correspond to the vibrations of the beam and the diagonal directions, respectively.

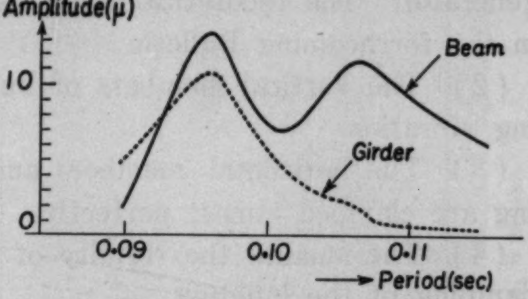

Fig. 23. Amplitude-period relation of both the beam and girder directions of No. 6 house observed simultaneously.

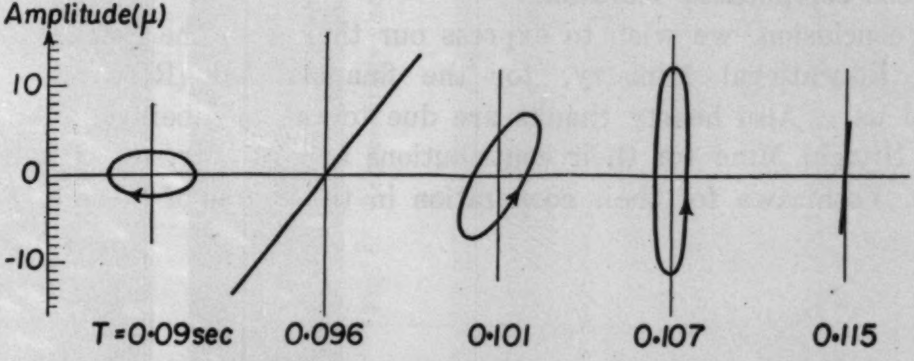

Fig. 24. Horizontal orbital motions at Re (roof-floor) of No. 6 house.

4. Conclusion

The results of experiments using a vibration generator made in two buildings of the same structure standing on ground of different properties, that is, rock and crushed stone, proved the following more evidently than ever.

(1) In the buildings there take place the relative displacement at the foundation to the ground and rocking vibration together with elastic deformation, in the course of the vibration caused by a vibration generator. The theoretical investigations of this subject will be presented in the forthcoming Bulletin.

(2) The vertical members of buildings perform almost perfect bending vibration.

(3) The horizontal members and the vertical members of the building are clamped almost perfectly.

(4) The smaller the rigidity of the ground, the greater the vibration damping of the building.

(5) In general, the longest proper period of the building corresponds to the resonance period of rocking vibration.

(6) In the case of the ununiform property of ground, the building undergoes complicated vibration.

In conclusion, we wish to express our thanks to the Science Section of the Educational Ministry, for the financial aid (Research Funds) granted us. Also hearty thanks are due to the members of Motoyama Office, Hitachi Mine for their contributions and to Mr. K. Osada and Miss S. Yoshizawa for their cooperation in the course of these investigations.

---

10. 建物の動揺，弾性振動　第1報　(起振機による振動実験)

地震研究所
金井　清
田中貞二
鈴木富三郎

茨城県日立鉱山の岩盤上並びに砕石上に建つ2棟の3階建鉄筋コンクリート造アパートについて，起振機による振動実験を行つて，次の事柄を明かにした．

なお，本実験では同時に6ケの振動計を使い，記録紙の速度も早くしたので，振動型についての，相当にたちいつた議論ができた．

(i) 建物は，振動の際に，基礎と地面との間で相対水平変位と傾斜運動をしながら，各部材に弾性変形を生ずる．

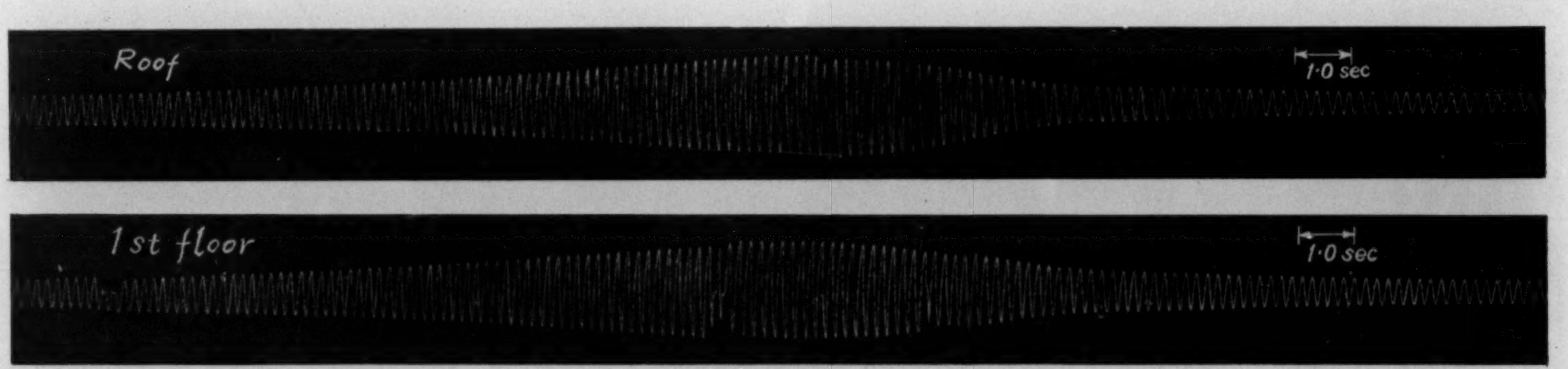

Fig. 6. Representative records of No. 14 house.

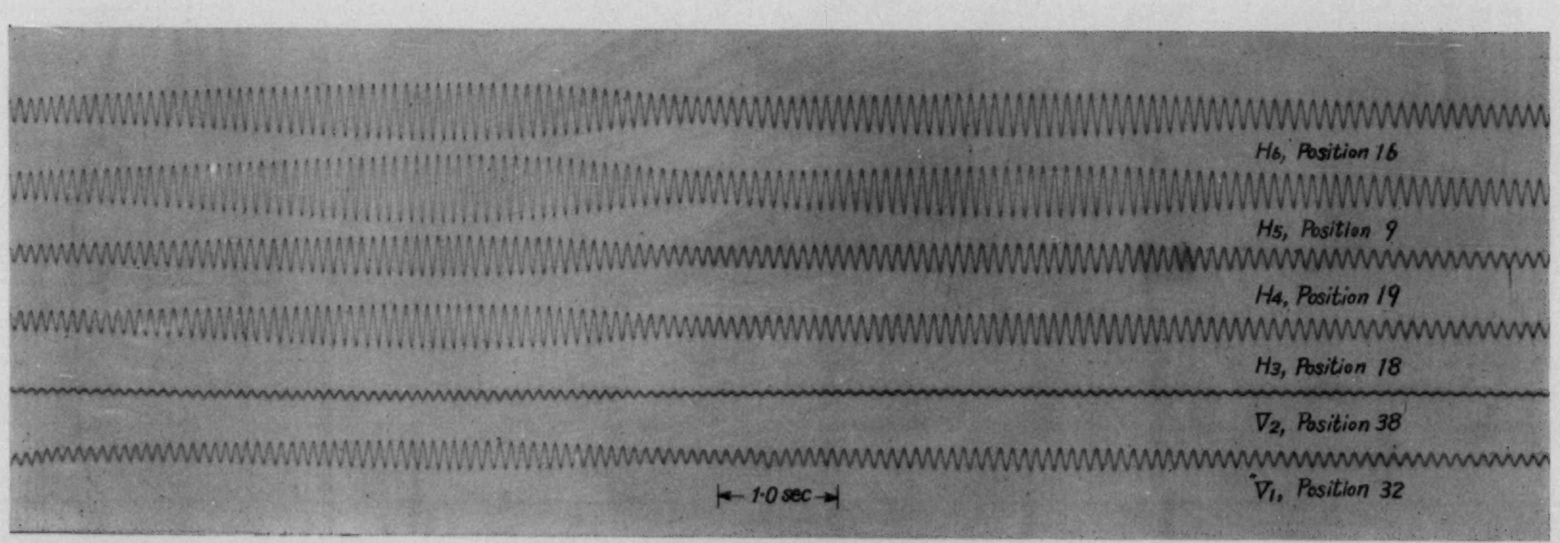

Fig. 16. Representative records of No. 6 house.

(ii) 縦架材と横架材は完全固定の状態に近い.

(iii) 縦架材は両端固定の屈曲振動をする.

(iv) 一般に，建物の固有周期としては，動揺振動の周期があらわれやすい.

(v) 数多くの建物について， このような実験を行つた後でなければ決定的なことは言えないが，少くとも，本実験の結果だけからみると， 基礎梁にも弾性変形が起り， 特に，地盤が均質でない場合には基礎梁の変形の様子が非常に複雑である.

BULLETIN OF THE EARTHQUAKE
RESEARCH INSTITUTE
Vol. 36 (1958), pp. 201-226

11. *Rocking and Elastic Vibrations of Actual Building. II. (Observation of Earthquake Motion).*

By Kiyoshi KANAI, Teiji TANAKA and Tomisaburo SUZUKI,

Earthquake Research Institute.

(Read Nov. 27, 1956 and July 16, 1957. — Received Mar. 31, 1958.)

1. Introduction

The property of earthquake-motion at a building varies according to the ground property on which the building stands. Therefore the value of earthquake force, which has to be taken into consideration in designing earthquake proof construction, depends on the ground property. In order to make the estimation of such a value more clearly, we made a simultaneous observation by installing seismographs both on the basements and the roof-floors of two buildings of the same structure standing on different ground properties, that is, one standing directly on the rock and the other on the crushed stone with concrete piles. These buildings are in Hitachi Mine site, Ibaraki prefecture.

The results of the vibration tests by means of a vibration generator at the buildings have already been given in the previous paper.[2]

2. Observations of earthquake motion

Four horizontal seismographs were installed on the roof-floors and on the ground-floors of two buildings. The component of beam direction (short length direction) of earthquakemotion was observed. The constants of seismographs used in the comparative observation are shown in Table 1.

The rough sketches of the buildings and positions of the seismographs installed are shown in Figs. 1 and 2.

Four recording drums of the seismographs were started automatically

---

[1] K. KANAI and T. SUZUKI, "Relation between the Property of Building Vibration and the Nature of Ground", *Bull. Earthq. Res. Inst.*, **31** (1953), 305: Part II, *ditto*, **33** (1955), 109: Part III, *ditto*, **34** (1956), 61.

[2] K. KANAI, T. TANAKA and T. SUZUKI, "Rocking and Elastic Vibrations of Actual Building. I", *ditto*, **36** (1958), 183

at the same time by means of a starter. The starter has a horizontal component pendulum with a period of 0.3 sec, which starts when earthquakes were greater than 0.5 gals in acceleration, that is, twice the amplitude of usual micro-tremor, and stops automatically after a three-minute running record.[3] The driving speed of recording papers was 1.05 cm/sec. The period of observations of earthquake motion was about one year, from February, 1956 to March, 1957.

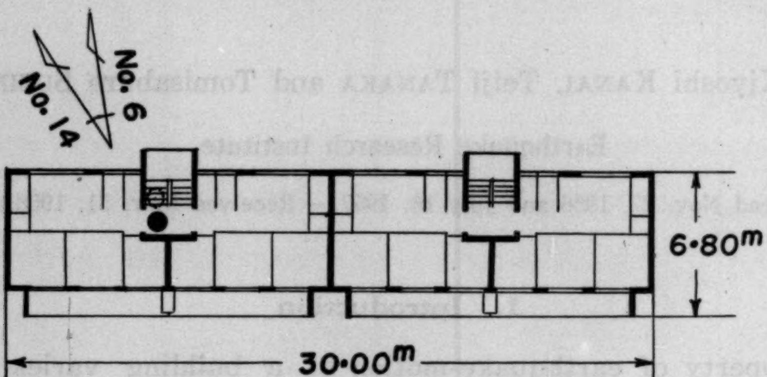

Fig. 1a. Sketch of the plane view.

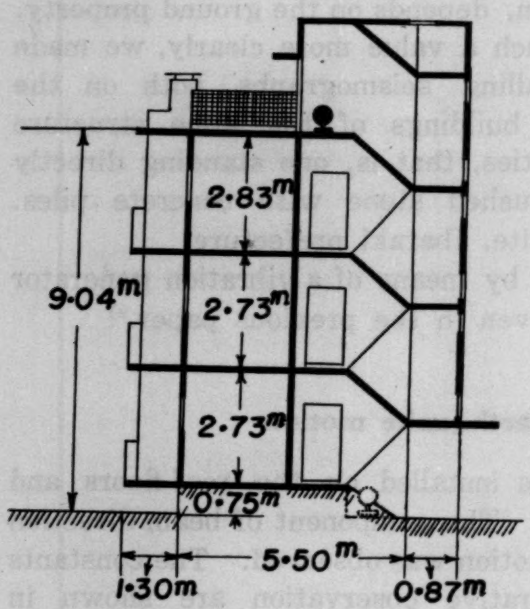

Fig. 1b. Sketch of the side view.

The number of earthquakes, recorded during the period was 110, among which 43 earthquakes were recorded satisfactorily. All the records of earthquakes treated here had been started before the main shocks began. The position of the origins of those earthquakes and the observation position are shown in Table 5.

Fig. 3, illustrates the epicenters of earthquakes treated here.

3. Results of observations

The representative seismograms observed simultaneously at those

---

[3] T. TANAKA and K. KANAI, "A New Starter for Observations of Earthquakes", *Monthly Meeting of the Earthq. Res. Inst.*, (Dec. 1955).

Table 1. Constants of seismographs.

No. of seismograph	Natural period (sec)	Damping ratio	Magnification	Position	Direction
1	1.0	13	200	No. 6 roof	beam
2	〃	〃	210	No. 6 ground	〃
3	〃	〃	190	No. 14 roof	〃
4	〃	〃	180	No. 14 ground	〃

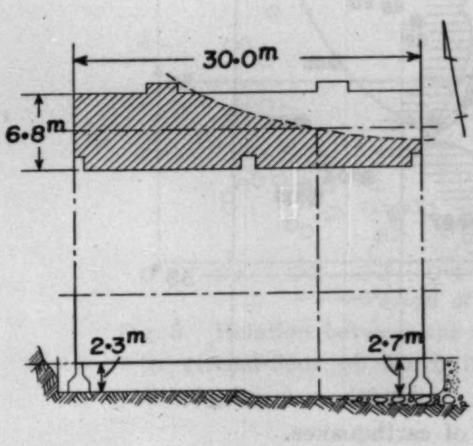

Fig. 2a. Foundation parts of No. 6 house.

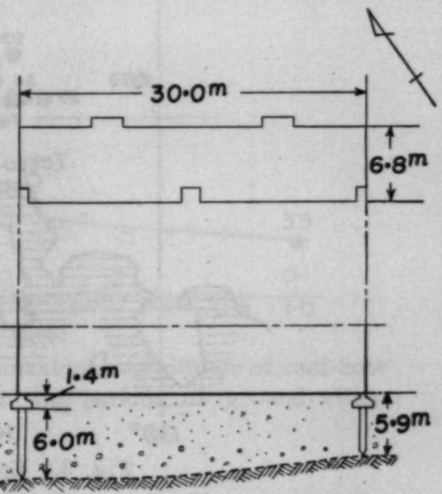

Fig. 2b. Foundation parts of No. 14 house.

positions are illustrated in Fig. 4.

As the constants of every seismograph were almost equal, we are able to know easily the difference of earthquake motions at those positions by merely looking at Fig. 4. That is to say, from Fig. 4, the amplitudes on the ground-floor of No. 6 house standing on the rock are smaller than those of No. 14 house standing on the crushed stone. On the other hand, the amplitude ratios of the roof-floor to the ground-floor of No. 6 house are larger than those of No. 14 house. The precise discussions will appear in the successive paragraphs.

(i) Period characteristics of earthquake-motion

Table 6 gives the values of the maximum amplitude of buildings observed at the roof-floor, the amplitudes and the periods at the ground-floor in the time when the amplitude of roof-floor became maximum and the amplitude ratios of the roof-floor to the ground-floor mentioned above,

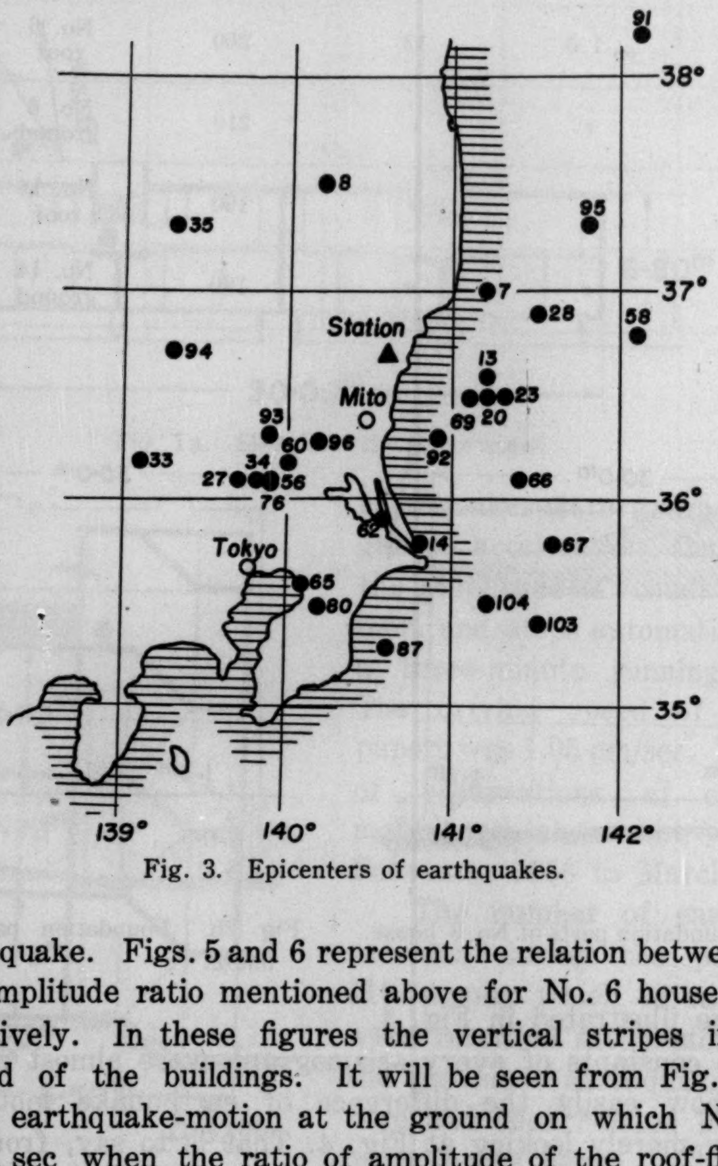

Fig. 3. Epicenters of earthquakes.

for each earthquake. Figs. 5 and 6 represent the relation between the period and the amplitude ratio mentioned above for No. 6 house and No. 14 house respectively. In these figures the vertical stripes indicate the natural period of the buildings. It will be seen from Fig. 5 that the period of the earthquake-motion at the ground on which No. 6 house stands is 0.1 sec when the ratio of amplitude of the roof-floor to that of the ground-floor becomes maximum. The maximum value of the ratio is about 9.5. On the other hand, from Fig. 6 it is found that this ratio for No. 14 house becomes maximum at the period of 0.2 sec and the value is 4.5.

Figs. 5 and 6 tell us that the magnification of amplitude in building at the time of earthquakes is maximum when the period of the earthquake motion at the ground nearly corresponds to the natural period of the building. It seems that the principal cause that the amplitude ratio of roof-floor to ground-floor varies even when the period of the ground vibration is the same is correlated to the succession number of the earthquake-motion of the same period.[4]

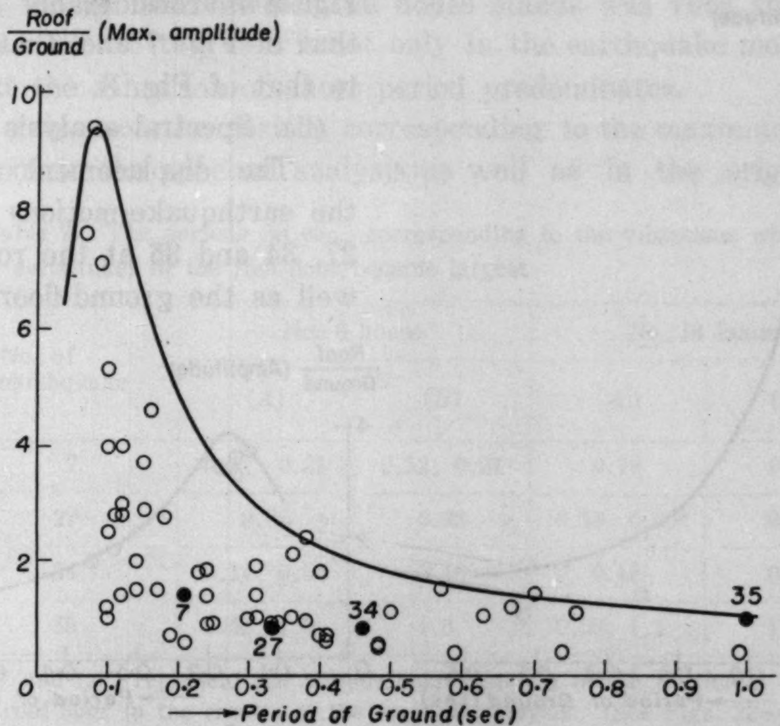

Fig. 5. Relation between the ratios of maximum amplitude of roof-floor to ground-floor of No. 6 house and the periods of ground vibration, for each earthquake.

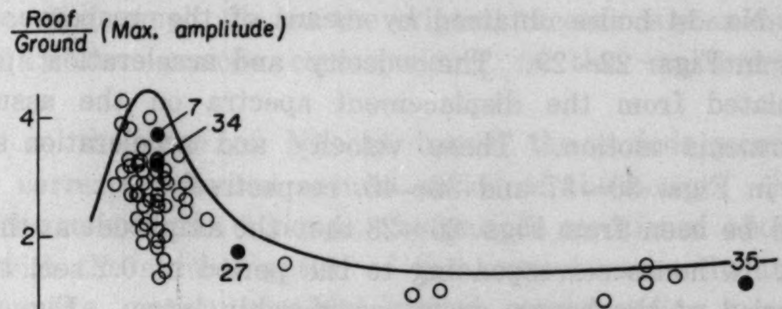

Fig. 6. Relation between the ratios of maximum amplitude of roof-floor to ground-floor of No. 14 house and the periods of ground vibration, for each earthquake.

---

[4] K. Kanai, K. Osada and S. Yoshizawa, "Observational Study of Earthquake Motion in the Depth of the Ground. IV", *Bull. Earthq. Res. Inst.*, **31** (1953), 233, Fig. 12.

Figs. 7 and 8 show the amplitude ratios of the roof-floor to the ground-floor concerning each wave of No. 35 earthquake at No. 6 house and No. 14 house, respectively. It will be seen that the envelope of Fig. 5 is considerably similar to that of Fig. 7 and that of Fig. 6 to that of Fig. 8.

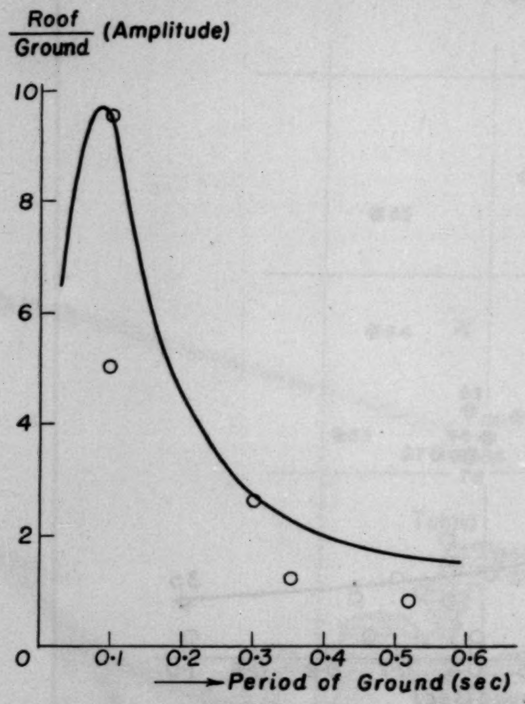

Fig. 7. Amplitude ratios of roof-floor to ground-floor for each wave of No. 35 earthquake at No. 6 house.

(ii) Spectral analysis

The displacement spectra of the earthquake-motions of Nos. 7, 27, 34 and 35 at the roof-floor as well as the ground-floor in No. 6 house and No. 14 house obtained by means of the response computer[5] are shown in Figs. 22～29. The velocity and acceleration spectra have been calculated from the displacement spectra on the assumption of simple harmonic motion. These velocity and acceleration spectra are presented in Figs. 30～37 and 38～45, respectively.

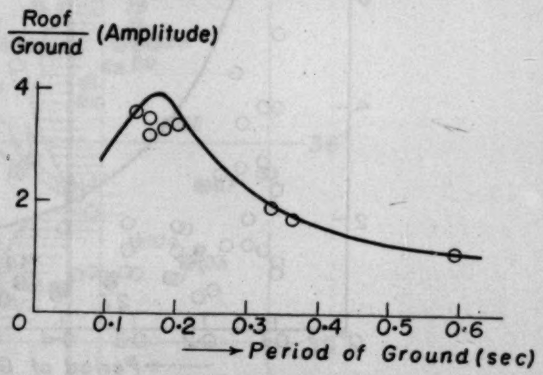

Fig. 8. Amplitude ratios of roof-floor to ground-floor for each wave of No. 35 earthquake at No. 14 house.

It will be seen from Figs. 26～28 that the amplitude at the roof-floor in the No. 14 house corresponding to the period of 0.2 sec, that is, the natural period of the house, grew considerably large. Figs. 25 and 29 show that, in the special case of No. 35 earthquake, the roof amplitude corresponding to 0.2 sec natural period of No. 14 house, appears rather modest because the amplitudes corresponding to 0.5 sec as well as 1.0 sec are extremely large.

In the case of No. 6 house, the absolute amplitude at the roof hardly grew large, in spite of the fact that the roof amplitude corresponding to 0.1 sec of the natural period of the house was magnified considerably. This is because the absolute amplitude of the period mentioned above at the ground on which the house stands was very small.

---

[5] R. TAKAHASI, "A Response Computer Preliminary Report", Proc. 3rd Japan National Congr. *Applied Mech.*, (1953), 373.

Figs. 22～25 tell us it is not only in the earthquake motion on fresh rock that the vibration of short period predominates.

The values of the periods corresponding to the maximum amplitudes at the roof in the spectral analysis as well as in the original records are shown in Table 2. It will be seen from Table 2 that the periods, when the roof amplitude in the original records is maximum coincide mostly with the periods corresponding to the maximum value of spectrum.

Table 2. The periods (in sec.) corresponding to the vibrations when the amplitudes of the roof-floor became largest.

No. of earthquake	No. 6 house		No. 14 house	
	(*A*)	(*B*)	(*A'*)	(*B'*)
7	0.1, 0.21	0.12, 0.21	0.18	0.17
27	0.35	0.33	0.19, 0.39	0.28
34	0.14, 0.55	0.46	0.18	0.16
35	0.52, 1.0	1.0	0.55, 1.1	1.0

(*A*) and (*A'*) represent the periods corresponding to the maximum amplitudes at the roof-floor in the results of the spectral analysis. (See Figs. 22～29.)

(*B*) and (*B'*) represent the periods corresponding to the maximum amplitudes at the roof-floor in the original records.

And, in the case of No. 14 house, the periods mentioned above generally correspond to the natural period of the house. On the other hand, in the case of No. 6 house, the periods mentioned above scarecely coincide with the natural period of the house because the amplitudes of the earthquake motion of short period corresponding to the natural period of the house were rather small.

Figs. 9～16 show the amplitude ratio of the roof-floor to the ground-floor in each house which were obtained from the results of spectral analysis of Figs. 22～29.

In the case of No. 6 house, the phenomena of excitement of free oscillation of the house are clearly seen from the amplitude ratio of the roof-floor to the ground-floor shown in Figs. 9～12, though they are not

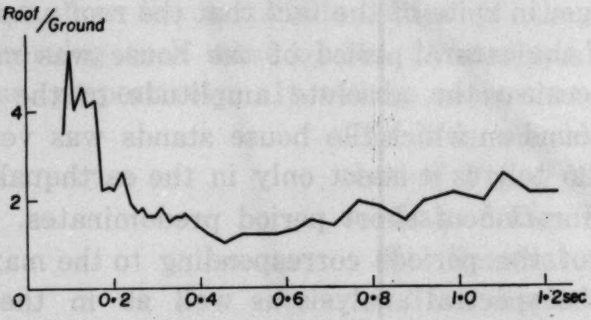

Fig. 9. Amplitude ratio of No. 7 earthquake at No. 6 house.

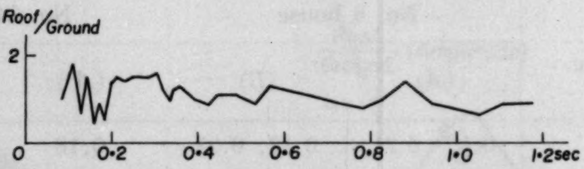

Fig. 10. Amplitude ratio of No. 27 earthquake at No. 6 house.

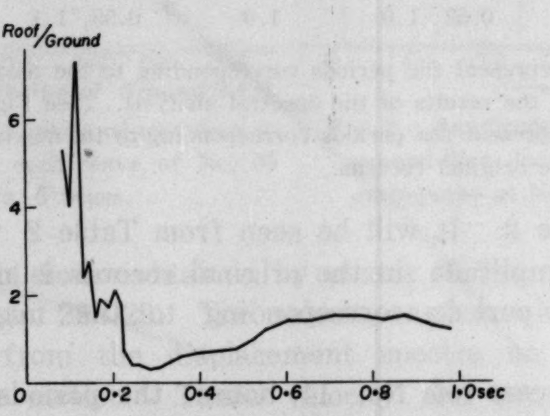

Fig. 11. Amplitude ratio of No. 34 earthquake at No. 6 house.

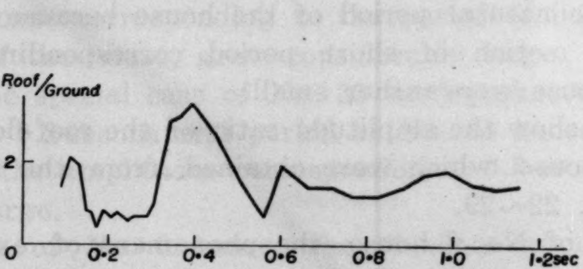

Fig. 12. Amplitude ratio of No. 35 earthquake at No. 6 house.

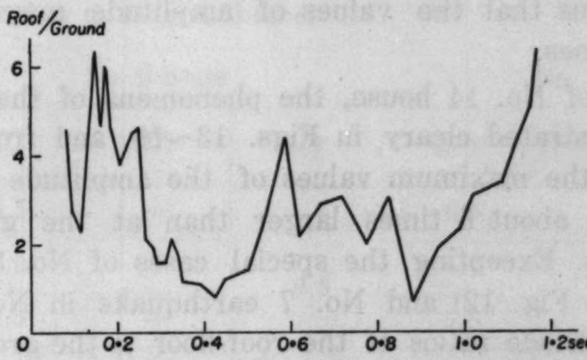

Fig. 13. Amplitude ratio of No. 7 earthquake at No. 14 house.

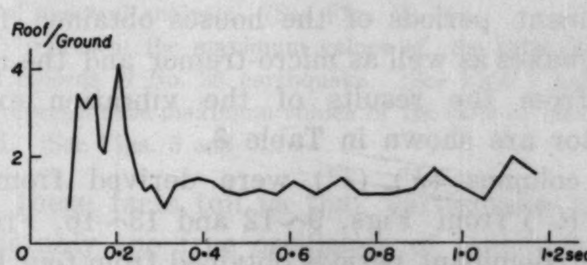

Fig. 14. Amplitude ratio of No. 27 earthquake at No. 14 house.

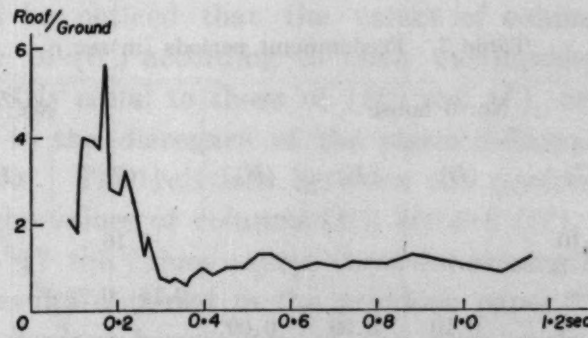

Fig. 15. Amplitude ratio of No. 34 earthquake at No. 14 house.

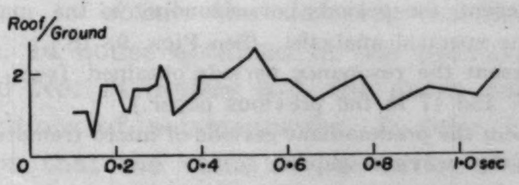

Fig. 16. Amplitude ratio of No. 35 earthquake at No. 14 house.

manifested by the results of the spectral analysis in Figs. 22~25. Figs. 9~12 tell us that the values of amplitude magnification at the roof exceed 7 times.

In the case of No. 14 house, the phenomena of the amplitude magnification are illustrated cleary in Figs. 13~16, and from Figs. 13~16 we know that the maximum values of the amplitude magnification at the roof become about 6 times larger than at the ground on which the house stands. Excepting the special cases of No. 35 earthquake in No. 6 house (see Fig. 12) and No. 7 earthquake in No. 14 house (see Fig. 13), the amplitude ratios of the roof-floor to the ground floor became nearly unity when the period of earthquake motion exceeded the natural periods of the houses.

The predominant periods of the houses obtained from the analysis of natural earthquakes as well as micro-tremor and the natural periods of them obtained from the results of the vibration experiments using vibration generator are shown in Table 3.

In Table 3, columns (*F*), (*F'*) were derived from Figs. 5, 6 and columns (*C*) and (*C'*) from Figs. 9~12 and 13~16. From Table 3, it is found that the predominant periods obtained from four kinds of examinations, that is, the observations of earthquakes and micro-tremors and the artificial vibration experiments, are nearly equal to each other. In

Table 3. Predominant periods (in sec.).

No. of earthquake	No. 6 house				No. 14 house			
	(*C*)	(*D*)	(*E*)	(*F*)	(*C'*)	(*D'*)	(*E'*)	(*F'*)
7	0.10	0.10	0.09	0.09	0.16	0.18	0.18	0.16
27	—				0.15, 0.20			
34	0.11				0.17			
35	0.11, 0.4				—			

(*C*) and (*C'*) represent the periods corresponding to the maximum ratios of roof to ground from the spectral analysis. (See Figs. 9~16.)

(*D*) and (*D'*) represent the resonance periods obtained from the vibration experiment. (See Figs. 7 and 17 in the previous paper.)

(*E*) and (*E'*) represent the predominant periods of micro-tremors at the roof-floor. (See Figs. 9 and 18 in the previous paper.)

(*F*) and (*F'*) represent the periods when the ratios of roof to ground became maximmum. (See Figs. 5, 7 and 6, 8.)

Table 4. The largest values of the amplitude ratios of the roof-floor to the ground-floor.

No. of earthquake	No. 6 house			No. 14 house		
	(G)	(H)	(I)	(G')	(H')	(I')
7	5.5	—	9.5	6.5	—	4.5
27	2.0	—		4.0	—	
34	7.5	—		5.5	—	
35	3.5	9.5		2.5	4.0	

(G) and (G') represent the maximum values of the ratio of roof to ground from the results of spectral analysis. (See Figs. 9～16.)

(H) and (H') represent the maximum values of the ratio of roof to ground from the original records of No. 35 earthquake. (See Figs. 7 and 8.)

(I) and (I') represent the maximum values of the ratio of maximum amplitudes of roof to ground. (See Figs. 5 and 6.)

the other words, these facts tell us that earthquake and micro-tremor will excite considerably the free oscillation of buildings.

(iii) Vibrational damping of building

The largest values of the amplitude ratio of the roof-floor to the ground-floor obtained from Figs. 9～16 and Figs. 5～8 are shown in Table 4. It will be noticed that the values of column (G) somewhat differ from those of (G') according to each earthquake while those of (H) and (I) are nearly equal to those of (H') and (I'), respectively. This seems to be due to the disregard of the phase difference in the results in spectral analysis. The relations between the predominant periods of the ground and the values of columns (H), (I) and (H'), (I') are shown in Fig. 17. In Fig. 17 the values except those concerning No. 6 and No. 14 houses are the results obtained in the previous paper.[6] As the present houses and the previous houses are of the same style but of different height, in Fig. 17 the reduction of the effect of height has been made for the present houses.

Next, we try to obtain the damping coefficient of No. 6 house using that of No. 14 house obtained in the previous paper.[7]

As No. 6 and No. 14 houses are the same both in the upper construction and positions of seismographs, it may be considered as the first approximation that the value of the ratio of $9.5/4.5=2.1$ in (I) and

---

[6] *loc. cit.*, 1), Part III, 77, Fig. 16.

[7] loc. cit., 2), 188.

(I') columns of Table 4 is inversely proportional to the value of the ratio of h of No. 14 house to the h of No. 6 house, in which h is the fraction of critical damping.

After the above consideration, we obtain the value of h of No. 6 house in the following:

$$h_6 = h_{14} \times (4.5/9.5) = 0.032 \times 0.47 = 0.015 .$$

In spite of that the value of h of No. 6 house is about half of that of No. 14 house, there appeared only a little difference between the amplitude ratios of the roof to the ground concerning No. 6 and No. 14 houses obtained after spectral analysis as seen in the columns (G) and (G') of Table 4. The facts mentioned above may be explained as follows:

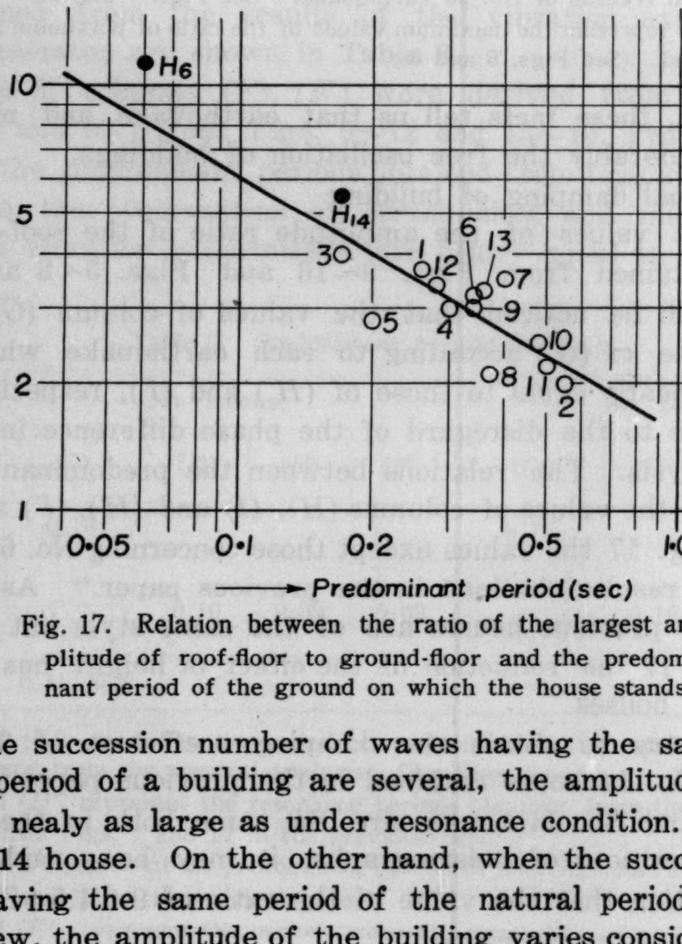

Fig. 17. Relation between the ratio of the largest amplitude of roof-floor to ground-floor and the predominant period of the ground on which the house stands.

When the succession number of waves having the same period of the natural period of a building are several, the amplitude of the building grow up nealy as large as under resonance condition. This is the case of No. 14 house. On the other hand, when the succession number of waves having the same period of the natural period of a building are only a few, the amplitude of the building varies considerably according to the succession number. As the waves of the period smaller than about 0.1 sec happen infrequently in earthquake motion, No. 6 house is the case under this condition, and the results are shown in the column (*G*) of Table 4 and Fig. 5.

(iv) Vibration characteristic of ground

Figs. 18∼21 give the ratios between the amplitudes at the ground-floor of No. 14 and No.6 houses obtained from Figs. 22∼29. It will be seen in Figs. 18∼21 that the ratio mentioned above takes the maximum value at the period of about 0.2 sec in general. As the amplitude ratio of the roof-floor to the ground-floor at the period of about 0.2 sec is notquite so large as shown in Figs. 9∼12 and 16, the above mentioned fact seems to have no relation to the natural period of the houses. It is natural that the period of about 0.2 sec is considered the natural period of the ground on which No. 14 house stands. In the case of No. 14 house, it may be considered that the natural periods of the house and the ground

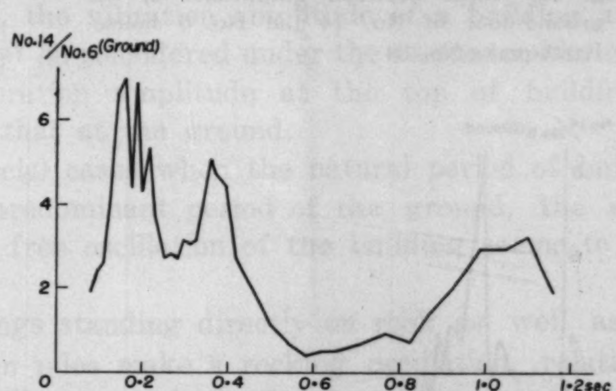

Fig. 18. Ratio between amplitudes at the ground-floor of No. 14 and No. 6 houses. Earthquake No. 7.

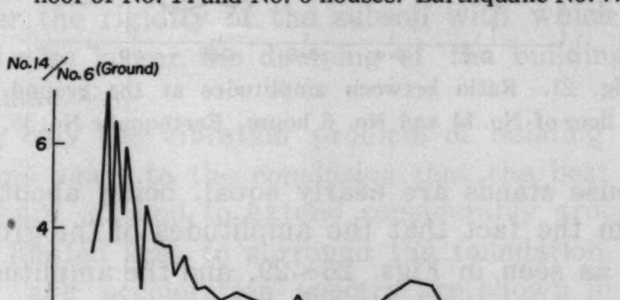

Fig. 19. Ratio between amplitudes at the ground-floor of No. 14 and No. 6 houses. Earthquake No. 27.

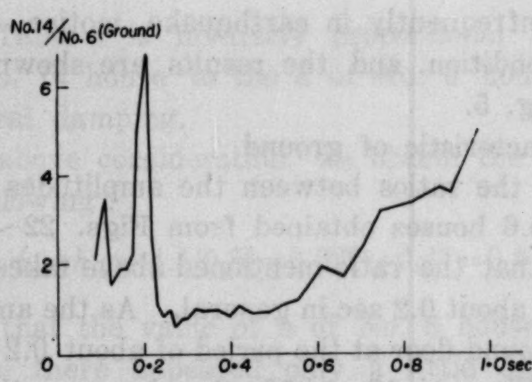

Fig. 20. Ratio between amplitudes at the ground-floor of No. 14 and No. 6 house Earthquake No. 34.

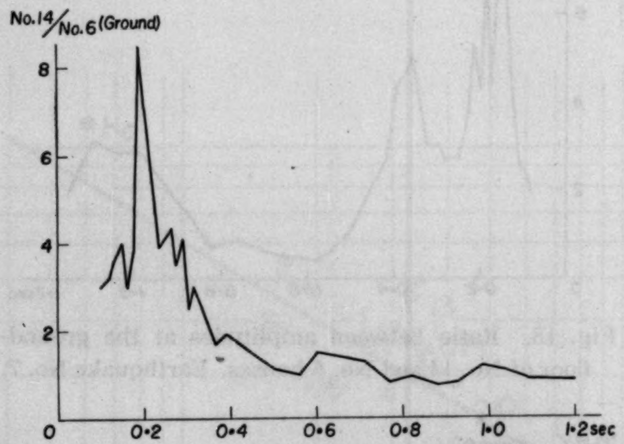

Fig. 21. Ratio between amplitudes at the ground-floor of No. 14 and No. 6 house. Earthquake No. 35.

on which the house stands are nearly equal, being about 0.2 sec. This is presumed from the fact that the amplitudes of the ground are largest at about 0.2 sec as seen in Figs. 26~29, and the amplitude ratios of the roof to the ground take the largest value at about 0.2 sec as shown in Figs. 13~16.

On the other hand, in the case of No. 6 house, the amplitude ratio of the roof to the ground is the largest at about 0.1 sec as shown in Figs. 9~12, and the amplitude of the ground itself is not so large at about 0.1 sec as shown in Figs. 22~25. Roughly speaking, the amplitude at the ground takes a large value at 0.4~0.6 sec, and this feature may be considered to be the vibration characteristics of the ground itself.[8]

Let A, ρ and v be the maximum amplitudes, density and velocity of S-waves at the ground on which the houses stand and suffixes 6 and 14 represent the house numbers.

---

[8] K. KANAI, Monthly Meeting, Earthq. Res. Inst., (May, 1958).

Considering $A_{14}/A_6=\rho_6 V_6/\rho_{14} V_{14}(\equiv 7)$ and assuming $\rho_6=\rho_{14}$ as well as adopting the equation $v_{14}=4\times 6.6/0.2=132\ m/s$ (thickness $=6.6$ m, period $=0.2$ sec), we obtain $v_6(\equiv$ base rock$)=132\times 7=924\ m/s$.⁹⁾

4. Conclusion

The results of the comparative observation of earthquakes made at reinforced concrete buildings standing on rock and on crushed stone, proved the following quite evidently.

(1) In general, the vibration amplitude of a building at the time of an earthquake must be considered under the resonance-like condition, that is to say, the vibration amplitude at the top of building is several times as large as that at the ground.

(2) In the special cases when the natural period of building is much smaller than the predominant period of the ground, the effect of the excitement of the free oscillation of the building seems to be negligibly small.

(3) The buildings standing directly on rock as well as on crushed stone with 2 or 3m piles make a rocking oscillation, relative horizontal movement against the ground at the basement together with elastic deformation of the members at the time of earthquake.

(4) The smaller the rigidity of the subsoil with which the foundation is surrounded, the larger the damping of the building vibration in case of an earthquake.

(5) Concerning only the vibration problem of building in case of an earthquake we come again to the conclusion that the best condition for buildings is for hard ground to extend considerably around a building and soft soil of a limited area to surround the foundation. (For reference the velocity and acceleration spectra are shown in Figs. 30~37 and 38~45, respectively.)

In conclusion, we wish to express our thanks to the Science Section of the Educational Ministry, for the financial aid granted us. Also thanks are due to the members of Motoyama-office, Hitachi Mine and Prof. R. Takahasi and Mr. I. Aida, for their cooperation in tho course of these investigations and to Mr. K. Osada and Miss S. Yoshizawa for the valuable assistance they offered in these investigations.

---

9) K. KANAI, "The Result of Observation of Wave Velocity in the Ground", *Bull. Earthq. Res. Inst.*, **29** (1951), 503.

Table 5. The origins of earthquakes and the locations of seismographs.

No. of earthquake	Time of occurrence	Origin			No. 6 house		No. 14 house	
		°*N*	°*E*	*D* (in km)	roof	ground	roof	ground
1	1956 II				○	○	○	○
2	〃 〃 27				○	○	○	○
3	〃 III				○	○	○	○
4	〃 〃				—	—	○	○
5	〃 III 30				—	—	○	○
6	〃 IV 1				—	—	○	○
7	〃 〃 2	37.0	141.2	40~50	○	○	○	○
8	〃 〃 12	37.5	140.2	very shallow	—	—	○	○
9	〃 〃 12				—	—	○	○
13	〃 〃 25	36.6	141.2	about 40	○	○	○	○
14	〃 〃 26	35.8	140.8	about 30	○	○	○	○
15	〃 〃				—	—	○	○
17	〃 IV 29				○	○	○	○
18	〃 V				○	○	○	○
20	〃 〃 15	36.5	141.2	about 30	○	○	×	—
22	〃 〃 17				○	○	—	○
23	〃 〃 18	36.5	141.3	about 40	○	○	×	○
24	〃 〃				—	—	○	○
25					○	○	○	○
26					—	—	○	○
27	〃 VI 6	36.1	139.7	about 90	○	○	○	○
28	〃 〃 10	39.9	141.5	40~50	○	○	○	○

(to be continued.)

(Table 5. continued.)

No. of earth-quake	Time of occurrence	Origin			No. 6 house		No. 14 house	
		°*N*	°*E*	*D* (in km)	roof	ground	roof	ground
29	1956 VI 18				—	—	○	○
30	〃 〃				—	—	○	○
32	〃 〃 23				—	—	○	○
33	〃 〃 26	36.2	139.1	about 160	○	○	○	○
34	〃 〃 26	36.1	139.8	about 60	○	○	○	○
35	〃 〃 29	37.3	139.3	about 20	○	○	○	○
36	〃 VII				—	—	○	○
37	〃 〃				○	○	○	○
38	〃 〃				○	○	○	○
39	〃 〃				○	○	○	○
40	〃 〃				—	○	○	○
41	〃 〃				○	—	○	○
42	〃 〃				○	○	○	○
43	〃 〃				○	○	○	○
44	〃 〃				○	○	○	○
45	〃 〃				○	○	○	○
46	〃 〃				—	○	○	○
47	〃 〃				○	—	○	○
48	〃 〃				○	—	○	○
49	〃 〃				○	○	○	○
50	〃 〃				—	—	○	○
51	〃 〃				○	○	○	○
52	〃 〃				○	—	○	○
53	〃 〃				○	○	○	○

(to be continued.)

(Table 5. continued.)

No. of earthquake	Time of occurrence	Origin			No. 6 house		No. 14 house	
		°N	°E	D (in km)	roof	ground	roof	ground
54	1956 VII				○	○	○	○
55	〃 〃 28				○	○	—	—
56	〃 〃 30	36.1	139.9	about 50	○	○	—	○
57	〃 〃				○	○	○	○
58	〃 VIII 2	36.8	142.1	40	○	○	○	○
59	〃 〃				—	—	○	○
60	〃 〃 8	36.2	140.0	60～70	—	○	○	○
61	1956 VIII				—	—	○	○
62	〃 〃	35.9	140.6	about 40	○	○	○	○
63	〃 〃 15				○	—	○	○
65	〃 〃 16	35.6	140.1	about 70	○	○	○	○
66	〃 〃 20	36.1	141.4	20～30	○	○	○	○
67	〃 〃 24	35.8	141.6	about 60	○	○	○	○
68	〃 〃				—	—	○	○
69	〃 〃 30	36.5	141.1	about 60	○	○	○	○
70	〃 IX				○	—	○	○
71	〃 〃				○	○	○	○
72	〃 〃				○	○	○	○
73	〃 〃				—	—	○	○
74	〃 〃				○	—	○	○
75	〃 〃 24				○	—	○	○
76	〃 〃 24	36.1	139.9	about 70	○	—	○	○
77	〃 〃				○	—	○	○
78	〃 〃 26				○	○	○	○
80	〃 X 8	35.5	140.2	about 80	○	—	○	○

(to be continued.)

(Table 5. continued.)

No. of earth-quake	Time of occurrence	Origin			No. 6 house		No. 14 house	
		°*N*	°*E*	*D* (in km)	roof	ground	roof	ground
81	1956 X 11	44.5	150.5	about 100	○	○	○	○
85	〃 〃 17	36.8	142.3	about 40	○	○	○	○
87	〃 〃 14	35.3	140.6	about 40	—	○	○	○
88	〃 XI 16	36.8	140.7	about 100	—	○	○	○
89	〃 〃 〃				—	○	○	○
90	〃 〃 17				—	○	○	○
91	〃 〃 21	38.3	142.1	about 70	—	○	○	○
92	〃 〃 26	36.3	140.9	about 40	○	○	×	○
93	〃 XII 7	36.3	139.9	60	○	○	×	○
94	〃 〃 10	36.7	139.3	20	○	○	○	○
95	〃 〃 13	37.3	141.8	about 40	○	○	—	○
96	〃 〃 14	36.3	140.2	about 50	○	○	○	○
98	〃 〃 22	33.8	139.6	about 20	○	○	○	○
100	〃 〃 26	36.3	141.0	shallow	○	○	○	○
103	〃 〃 9	35.4	141.5	about 40	○	○	○	○
104	〃 〃 17	35.5	141.2	about 10	○	○	×	○
105	〃 〃 19				○	○	—	○
106	〃 〃 20				○	○	—	○
107	〃 〃 21	37.1	141.0	about 70	○	○	—	○
108	〃 〃 〃	36.6	141.0	about 50	○	○	—	○
109	〃 〃 24				○	○	○	○
110	〃 〃 〃				○	○	○	○

Table 6. The values of the amplitudes (in micron) and the periods (sec) of the largest vibrations.

No. of earthquake	No. 6 house				No. 14 house			
	amplitude		period	roof / ground	amplitude		period	roof / ground
	roof	ground	ground		roof	ground	ground	
1	5.5	6.0	0.33	0.9	22	9	0.21	2.5
2	25	2.6	0.08	9.4	45	16	0.13	2.7
3	6.0	5.5	0.76	1.1	13	16	0.80	0.8
4	—	—	—	—	8.2	3.9	0.18	2.1
5	12	1.6	0.07	7.6	32	11	0.21	2.9
6	—	—	—	—	20	8.9	0.18	2.2
7	9.8	7.0	0.21	1.4	48	13	0.17	3.7
8	—	—	—	—	40	13	0.18	3.1
9	—	—	—	—	22	7	0.14	3.1
13	14	12	0.41	1.2	55	22	0.18	2.5
14	21	20	0.64	1.1	60	19	0.15	3.1
15	—	—	—	—	12	3.1	0.14	3.9
17	7.5	1.1	0.09	7.1	18	4.6	0.13	3.8
18	4.8	1.2	0.10	4.0	12	5.3	0.24	2.2
20	11	13	0.30	1.0	—	—	—	—
22	13	3.1	0.15	3.7	—	—	—	—
23	110	63	0.23	1.8	—	167	0.25	—
24	—	—	—	—	31	13	0.17	2.7
25	7.5	7.0	0.50	1.1	6.5	7.0	0.53	0.9
26	—	—	—	—	13	4.4	0.15	2.9
27	19	22	0.33	0.9	71	42	0.29	1.7
28	6.5	4.8	0.31	1.4	19	5.5	0.20	3.4
29	—	—	—	—	20	6.0	0.17	3.3
30	—	—	—	—	13	3.1	0.12	4.3
32	—	—	—	—	27	9.0	0.16	3.0
33	8.0	3.8	0.36	2.1	23	8.0	0.14	2.9
34	9.0	11	0.46	0.8	25	8.0	0.16	3.2
35	38	40	1.0	1.0	50	45	1.0	1.1
36	—	—	—	—	42	14	0.18	3.1
37	11	1.9	0.21	5.8	34	11	0.18	3.1
38	2.3	3.1	0.19	0.7	13	5.0	0.17	2.5
39	1.0	0.7	0.17	1.5	4.2	1.4	0.18	3.0
40	—	8.3	0.39	—	26	18	0.18	1.4
41	1.0	—	—	—	3.2	1.4	0.17	2.3

(to be continued.)

(Table 6. continued.)

No. of earthquake	No. 6 house				No. 14 house			
	amplitude		period	roof/ground	amplitude		period	roof/ground
	roof	ground	ground		roof	ground	ground	
42	1.0	0.7	0.14	1.5	8.7	3.3	0.14	2.6
43	3.4	2.4	0.12	1.4	22	8.6	0.17	2.5
44	4.3	2.1	0.14	2.0	13	4.5	0.14	2.9
45	2.0	0.7	0.11	2.8	5.3	2.8	0.15	1.9
46	—	2.6	0.11	—	22	10	0.15	2.2
47	0.5	—	—	—	4.7	1.9	0.17	2.5
48	0.3	—	—	—	2.6	1.4	0.17	1.9
49	2.5	2.1	0.10	1.2	30	9.2	0.17	3.3
50	—	—	—	—	12	3.3	0.15	3.5
51	2.0	1.4	0.12	1.4	10	4.7	0.17	2.2
52	7.5	—	—	—	16	5.0	0.16	3.2
53	2.0	0.5	0.12	4.0	6.6	3.1	0.18	2.1
54	120	26	0.17	4.6	—	42	0.18	—
55	5.0	1.0	0.10	5.3	—	—	—	—
56	23	8.1	0.12	2.8	—	27	0.17	—
57	11	11	0.10	1.0	14	11	0.17	1.3
58	4.8	1.9	0.10	2.5	7.6	3.1	0.17	2.5
59	—	—	—	—	12	3.1	0.16	4.0
60	—	1.7	0.18	—	22	9.2	0.18	2.4
61	—	—	—	—	7.9	2.5	0.13	3.2
62	9.0	4.8	0.31	1.9	28	11	0.17	2.7
63	3.4	—	—	—	14	4.7	0.11	2.9
65	4.0	1.4	0.15	2.9	30	11	0.17	2.7
66	1.5	2.6	0.21	0.6	18	8.9	0.18	2.0
67	5.5	2.9	0.24	1.9	11	6.4	0.18	1.6
68	—	—	—	—	2.4	0.8	0.17	2.9
69	2.3	1.7	0.24	1.4	5.3	1.9	0.14	2.7
70	0.5	—	—	—	5.0	1.9	0.17	2.6
71	2.8	1.0	0.12	3.0	27	9.7	0.17	2.8
72	3.0	1.2	0.18	2.5	16	4.7	0.13	3.4
73	—	—	—	—	9.2	3.6	0.13	2.6
74	5.0	—	—	—	28	9.4	0.16	2.9
75	3.5	—	—	—	3.4	1.9	0.17	1.8
76	2.3	—	—	—	3.5	2.5	0.18	1.4
77	0.5	—	—	—	2.6	0.8	0.15	3.1

(to be continued.)

(Table 6. continued.)

No. of earthquake	No. 6 house				No. 14 house			
	amplitude		period	roof/ground	amplitude		period	roof/ground
	roof	ground	ground		roof	ground	ground	
78	—	—	—	—	30	12	0.17	2.5
80	8.3	—	—	—	57	21	0.20	2.7
81	11	4.5	0.38	2.4	22	22	0.57	1.0
85	6.5	8.3	0.33	0.8	18	8.6	0.15	2.1
87	—	9.8	0.47	—	26	11	0.21	2.4
88	—	7.1	0.24	—	27	10	0.14	2.7
89	—	5.7	0.38	—	20	6.1	0.14	3.2
90	—	8.6	0.31	—	24	7.5	0.14	3.2
91	—	27	1.04	—	33	24	0.86	1.4
92	33	77	0.74	0.4	—	33	0.46	—
93	24	27	0.34	0.9	—	31	0.19	—
94	4.5	5.2	0.25	0.9	32	11	0.18	2.9
95	5.0	11	0.48	0.5	—	11	0.17	—
96	5.5	11	0.48	0.5	14	9.2	0.35	1.5
98	8.5	5.7	0.57	1.5	6.6	5.3	0.90	1.2
100	3.8	4.0	0.36	1.0	23	7.2	0.12	3.1
103	21	15	0.70	1.4	22	20	0.86	1.1
104	22	37	0.41	0.6	—	27	0.17	—
105	56	30	0.40	1.8	—	22	0.34	—
106	30	26	0.67	1.2	—	16	0.13	—
107	7.5	7.6	0.40	1.0	—	19	0.16	—
108	9.0	13	0.40	0.7	—	14	0.54	—
109	2.5	2.4	0.31	1.0	9.5	3.6	0.16	2.6
110	3.0	3.3	0.24	0.9	18	6.9	0.15	2.5

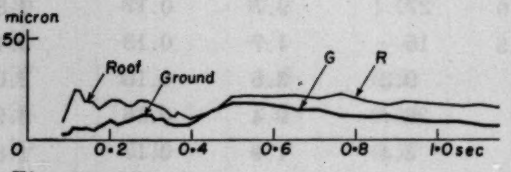

Fig. 22. Displacement spectra of No. 7 earthquake at No. 6 house.

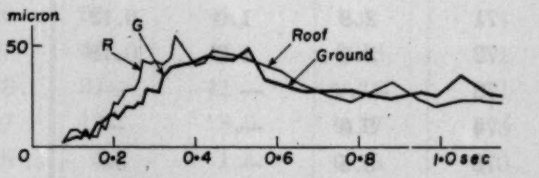

Fig. 23. Displacement spectra of No. 27 earthquake at No. 6 house.

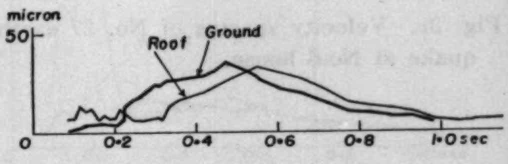

Fig. 24. Displacement spectra of No. 34 earthquake at No. 6 house.

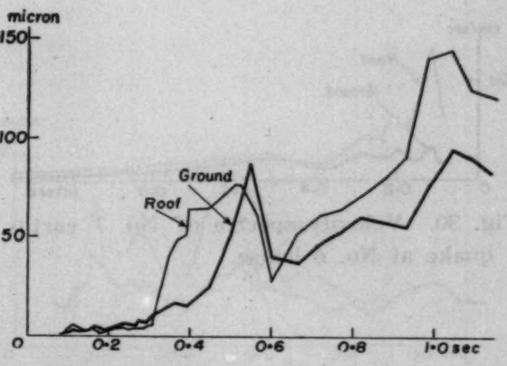

Fig. 25. Displacement spectra of No. 35 earthquake at No. 6 house.

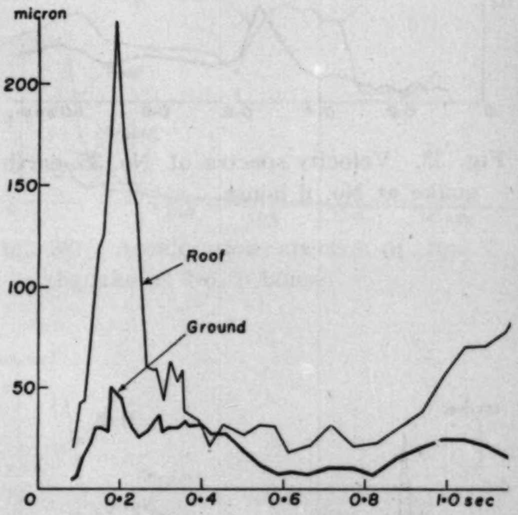

Fig. 26. Displacement spectra of No. 7 earthquake at No. 14 house.

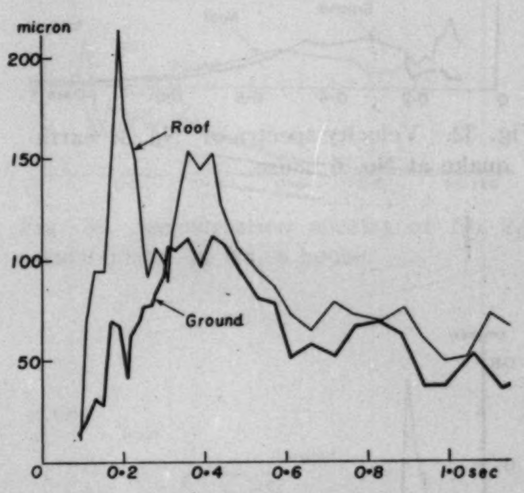

Fig. 27. Displacement spectra of No. 27 earthquake at No. 14 house.

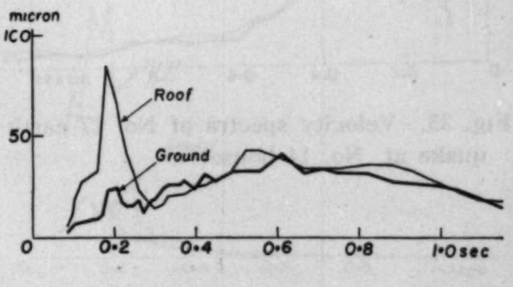

Fig. 28. Displacement spectra of No. 34 earthquake at No. 14 house.

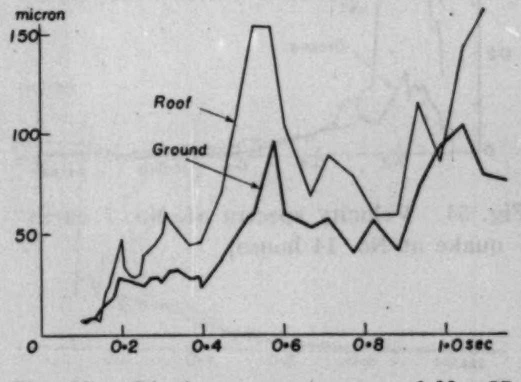

Fig. 29. Displacement spectra of No. 35. earthquake at No. 14 house.

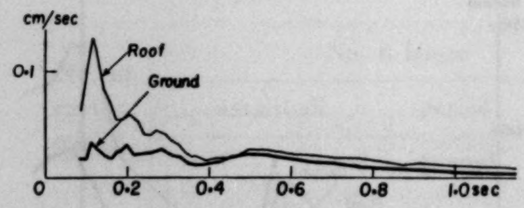

Fig. 30. Velocity spectra of No. 7 earthquake at No. 6 house.

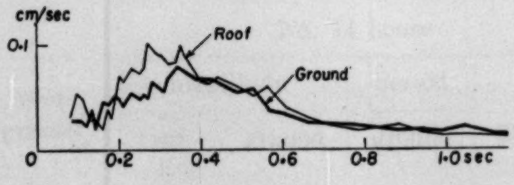

Fig. 31. Velocity spectra of No. 27 earthquake at No.6 house.

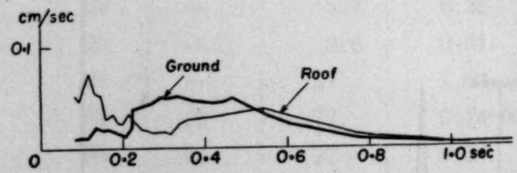

Fig. 32. Velocity spectra of No. 34 earthquake at No. 6 house.

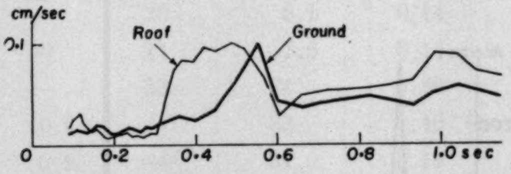

Fig. 33. Velocity spectra of No. 35 earthquake at No. 6 house.

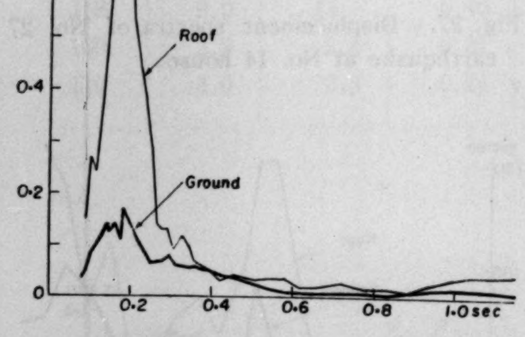

Fig. 34. Velocity spectra of No. 7 earthquake at No. 14 house.

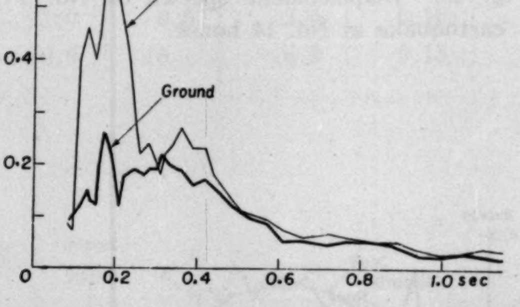

Fig. 35. Velocity spectra of No. 27 earthquake at No. 14 house.

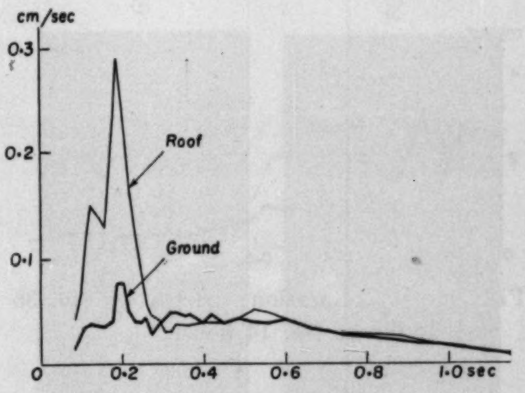

Fig. 36. Velocity spectra of No. 34 earthquake at No. 14 house.

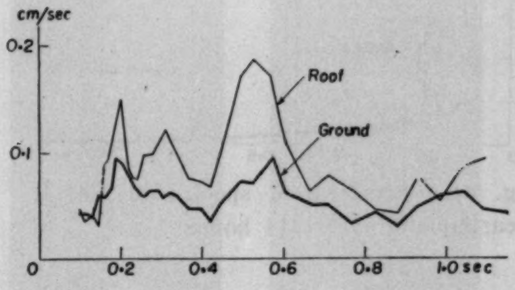

Fig. 37. Velocity spectra of No. 35 earthquake at No. 14 house.

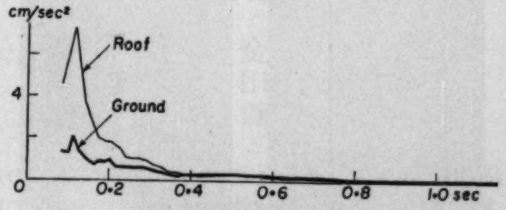

Fig. 38. Acceleration spectra of No. 7 earthquake at No. 6 house.

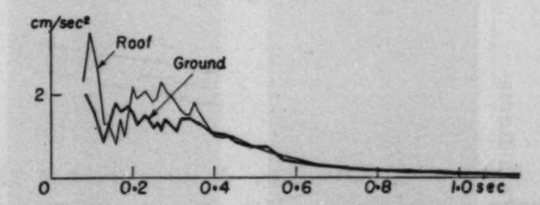

Fig. 39. Acceleration spectra of No. 27 earthquake at No. 6 house.

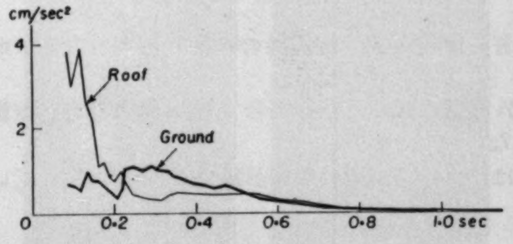

Fig. 40. Acceleration spectra of No. 34 earthquake at No. 6 house.

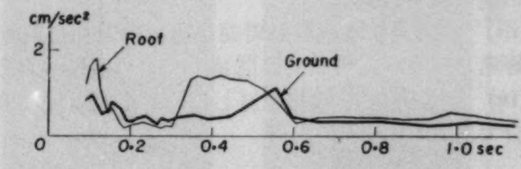

Fig. 41. Acceleration spectra of No. 35 earthquake at No. 6 house.

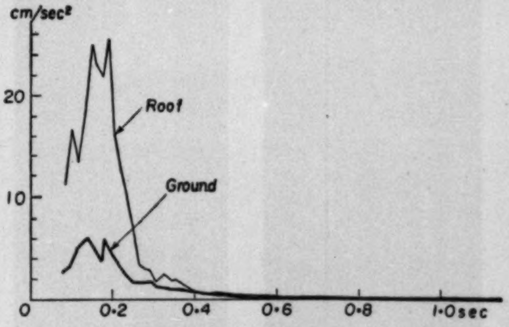

Fig. 42. Acceleration spectra of No. 7 earthquake at No. 14 house.

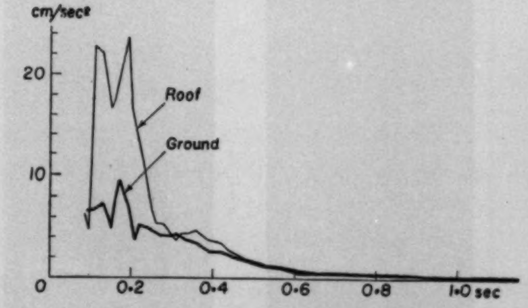

Fig. 43. Acceleration spectra of No. 27 earthquake at No. 14 house.

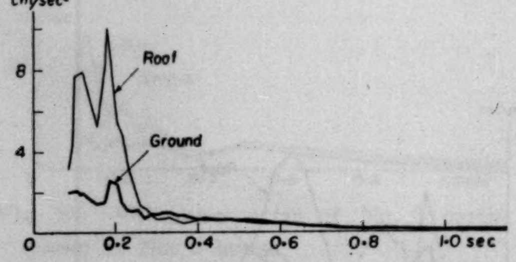

Fig. 44. Acceleration spectra of No. 34 earthquake at No. 14 house.

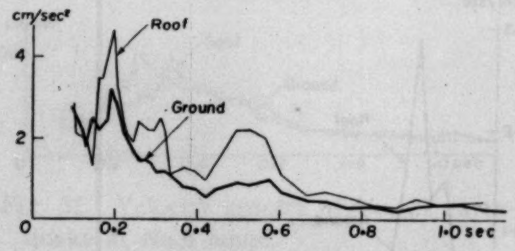

Fig. 45. Acceleration spectra of No. 35 earthquake at No. 14 house.

11. 建物の動揺，弾性振動 第2報 (地震観測)

地震研究所 金井　清
田中貞二
鈴木富三郎

茨城県日立鉱山の岩盤上，砕石上に建つ2棟の3階建鉄筋コンクリート造アパートについての起振機による振動実験の結果は，第1報で報告した. 本研究は，それらの建物の屋上並びに地階で地震観測を行つたものである. 100個に余る地震について，いろいろな方法で解析を行つた結果，次の事柄がわかつた.

(i) 一般に，地震時の建物振動では，自己振動が誘発されやすく，上部では土地の振幅の数倍になる.

(ii) 建物の振動増巾度は地盤が硬い程大きい. 言い換えると，地震時の建物の振動減衰性は地盤が硬い程小さい.

(iii) 地震動の卓越震動周期と建物の固有周期とが非常に離れている場合でも，建物の自己振動は誘発されるが，耐震的に問題にするほどにはならない.

(iv) 要するに，建物に対して最も不利な地震動は，大振巾の地動周期が建物の固有周期に近い場合である.

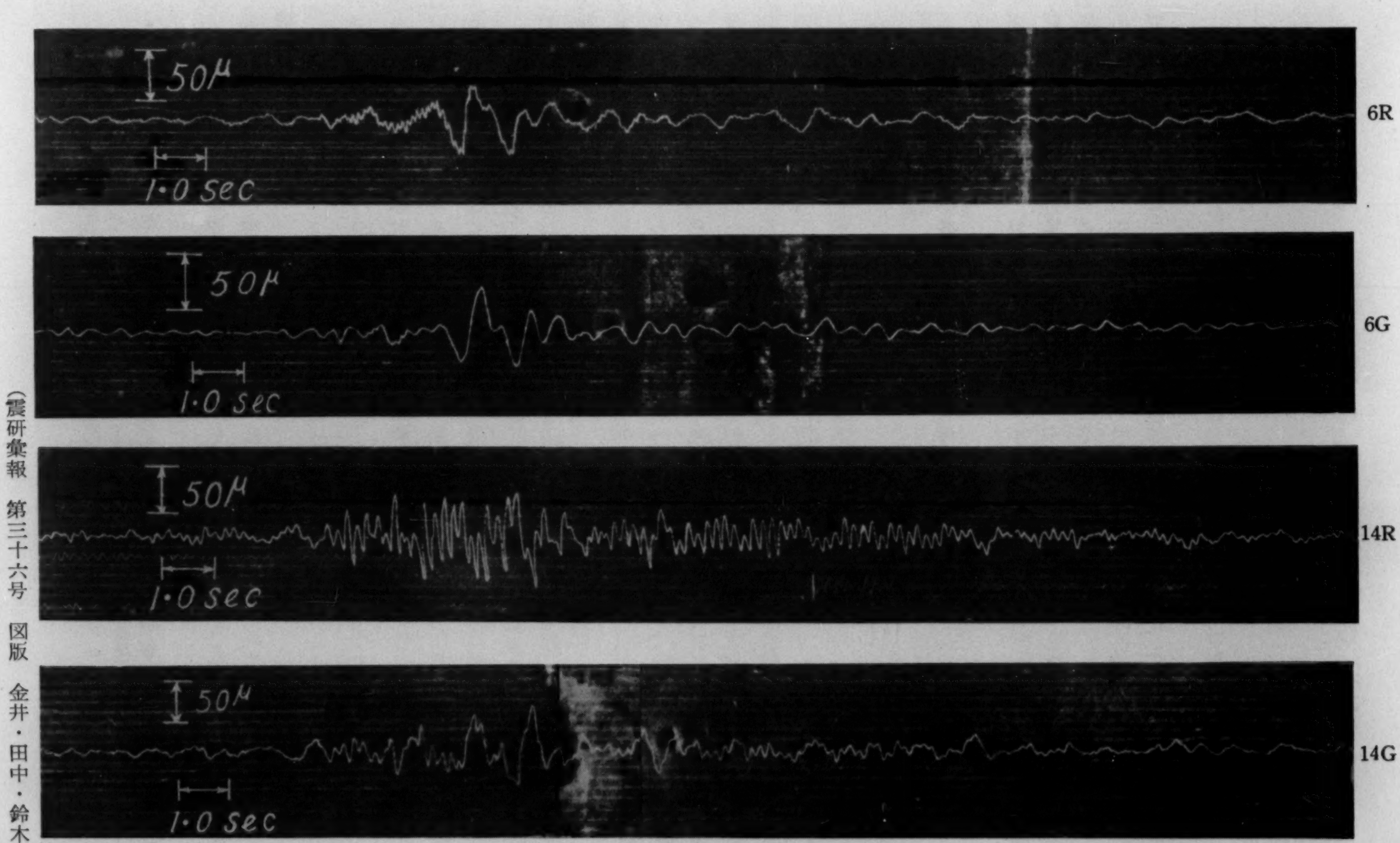

Fig. 4. Representative seismograms.

地震研究所彙報
第36号(1958)227-233頁

12. 1894年の庄内地震の研究

地震研究所　岸上冬彦

(昭和32年10月22日発表—昭和33年3月31日受理)

1894 (明治 27) 年10月22日の庄内地震は，山形県の北西部，庄内平野に起り，特に酒田で災害が大きかつたので酒田地震ともいわれる．当時の地震の調査報告としては震災予防調査会報告に出たもの[1]がよく知られている．

酒田市図書館には当時の町村役場の震害記録，救済に関する対策，新聞，絵画（この頃まだ写真は数少ない）が保存されている．その中にその年の 12 月に鶴岡で発行された単行本が2冊ある．

1. 東京今村次郎助纂，両羽震災取調所編
   悲愴惨怛　両羽地震誌
2. 鶴栖舎主人述
   東西田川飽海三郡甲午大地震記

この2冊には酒田市内の震災について前にのべたものより詳しく書かれているので，これらを参考にしてこの地震を調べなおした．しかし，被害家屋の数などは大森氏の報告[1]と多少違う．この点については，大森氏の方が後で発表され，公式の報告によつたものであるから地震直後のものより確かなものと考え，ここでは大森氏の報告の数によつた．その他家屋の構造も変わり，地震の調査方法も現在とちがうので，わからない点が少なくないが，この地震については余りよく知られてないので調べた．これが震災予防に役に立てば幸である．

この地震は 1894 年 10 月 22 日 17 時 34 分頃に起り，潰家 3,858，死者 726，負傷者 1,060，焼失家屋 2,148 で，震央は 39.2°N, 139.5°E (酒田の北西，日本海中) と報告されているが，小藤氏は最上川下流の新堀から北東方の生石にむけて断層を見出し，当時の考えとしてこの断層が地震を起したと考えた．現代の考えでは，最上川下流に震央のあつた地震が起り，それによつて地表に断層ができたとし，そのころは地震観測所の数が少なく震源位置決定の精度が悪かつたので，日本海に震央がきめられたのであろう．

被害分布について

地震当時のすべての報告には激震区域を最上川の下流域と，その支流赤川の最上川へ合流する地点附近との2個所にとり，更にその2つの区域をつないでいる．しかし各町村に

---

[1] 大森　房吉「山形県下地震調査に関する報告」震災予防調査会報告 **3** (1895), 79～106.
小藤文次郎「庄内地震に関する地質学上調査報告」同上 **8** (1899), 1～22.
中村達太郎・辰野金吾「山形県下震災被害建築調査報告」同上 **7** (1895), 4～14.

ついて全潰家屋数の全戸数に対する比を第１図に示すように，庄内平野の冲積地一体で被害が大きい．これが地震当時の激震区域図とちがうのは古い報告は川岸近くに生じた地面の割目を重く見たためと考えられる．赤川の下流，黒森附近では地割れが甚しく，その為に家屋の倒れたものが多かつたと書かれてある．

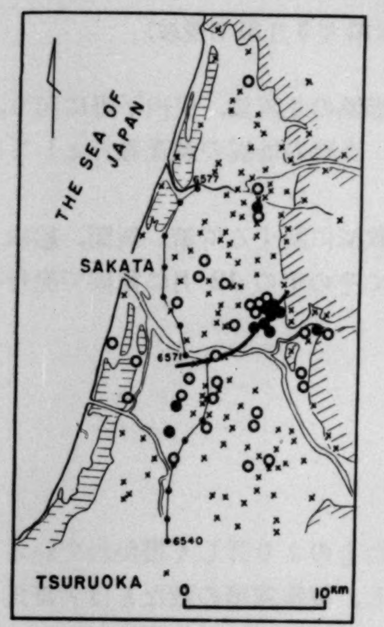
THE SEA OF JAPAN
SAKATA
TSURUOKA
657
6540
0
10km

Fig. 1. Damage ratio of wooden houses.
● >80%, ○ 79–40%, × <39%
Thick line shows the earthquake fault. Thin line shows levelling route and small spots bench marks.

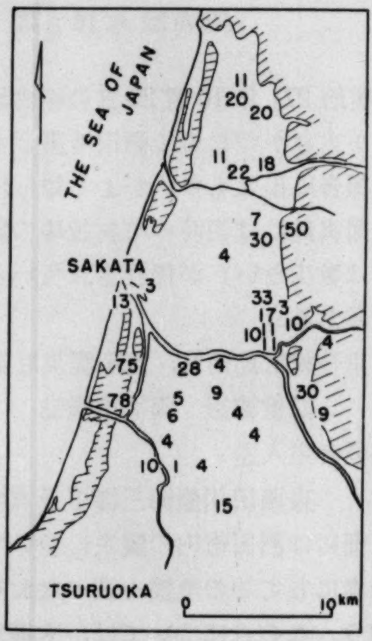
THE SEA OF JAPAN
SAKATA
TSURUOKA
11
20
20
11
22
18
7
30
50
4
33
3
17
10
10
11
4
13
3
75
28
4
9
30
78
5
6
4
4
9
4
10
1
4
15
0
10km

Fig. 2. Damage of plaster-walled warehouses.
(percentage to the total houses)

次に木造家屋と土蔵とは地盤の硬軟によつて震害率がちがうという近頃の学説について調べてみた．土蔵については被害数が書かれてあるばかりで，その総数がわからないので被害率が出せない．そこで各町村における土蔵の総数はそこの家屋の総数に比例し，家屋の総数は木造家屋の総数に等しいと仮定して，土蔵の全潰数の全潰家屋数に対する百分率を以て土蔵の被害を表わすこととした．第２図に示すように家屋の被害の少ない所，特に山地において土蔵の震害が比較的多い．このことは構造物の震害は地盤の硬軟によるという説，いいかえれば地盤の固有振動周期と地震動の周期とが一致した場合に構造物が共振して大きくゆれて破損するという説のよい実例であろう．しかし前にものべたように黒森附近の家屋は地震動によるばかりでなく，地割れや地盤の不同沈下によつて倒れたと考えるべきであろう．即ち地割れが大きく数が多いことで黒森附近を激震地とは考えることはできない．

この地震の震源地は最上川の北岸の断層の現われ，その上家屋の被害の多かつた地点をとるべきであろう．

酒田市の被害

酒田の震火災について前にのべた2冊の本により詳しくみた．地震当時と現在とでは仁井田川下流の最上川と合流する辺りは地形が変つている．洪水予防のため最上川の流路を直線的にし船場町附近まで埋立てた．明治15年につくられた酒田の地図を大正年間の初めの地図と比べて，当時の地形を推定して地図をかき，その上に震災の分布図をかいた．

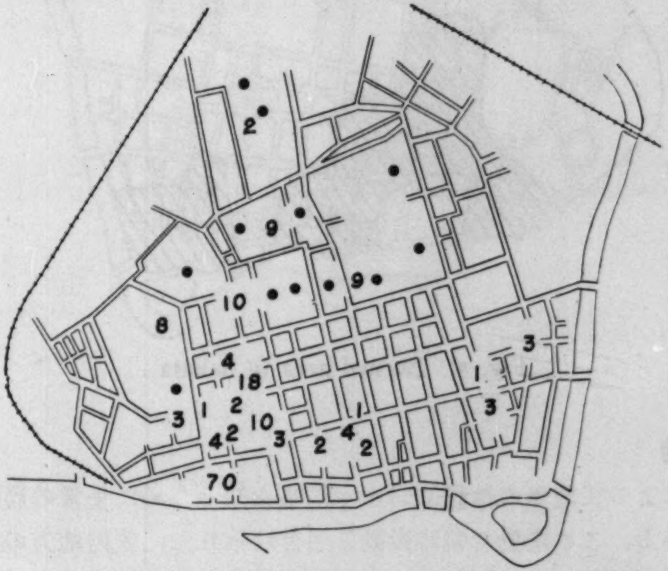

Fig. 3.　Number of victims in each street in Sakata.
Black dots shows the site of collapsed temples.

余り詳しいことは書いてないが，町別の死者の数を見ると，船場町が最も多く70人，その他，伝馬町18，秋田町10，今町10，寺町9，上台町4，桜小路3，上小路2，下小路4，上荒町2，下荒町1，下中町1，本町七丁目3，同四丁目1，染屋小路2，利右衞門小路4，下袋小路2，上内町3，給人町3，外野町1，南千日堂前2，鍛冶町1であつた．

この数字を見ると，震災による人命の損失は船場町から今町附近が多い，この中には地震によつて起された火災によつて死んだ人を含めているであろうが，実際船場町附近では地震が強かつたので家が潰れ，火事も多く出たのであろう．当時の酒田町としては北部から東部にかけて町はずれにあつた多くの寺の建物が殆ど皆地震で倒されたことから見て，酒田の地震が大きかつたと推定される．

次に火災について調べる．焼けた町を地図にかけば第4図となる．人命の損失数の分布とよくあう．近頃の地震の際にも地盤の悪い地域に震災が大きく火事の発生も多い．東京，豊岡，峰山，鳥取など地震火災の例に見られる．

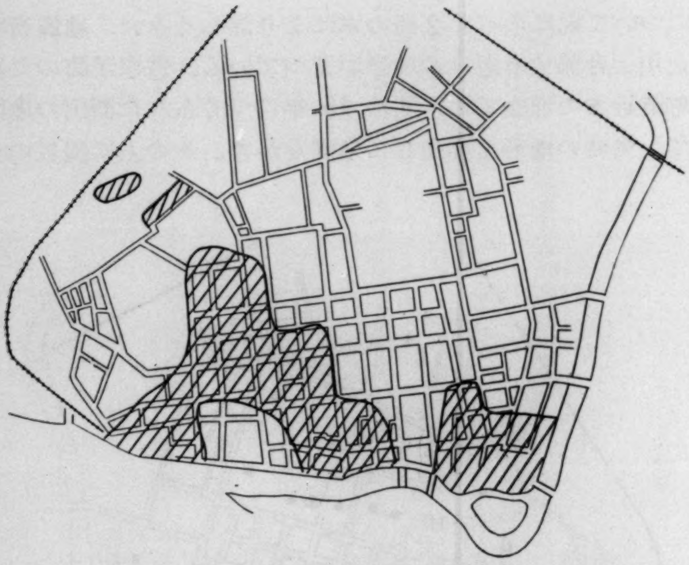

Fig. 4. Burned area in Sakata.

震害と常時微動

最近金井清氏によつて地盤の地震に対する性質を知るために平常の周期1秒以内の地盤振動が測られている．この振動を常時微動と名付けられた．庄内地方の測定結果[2]から得られた地盤種別判定試案とこの地震の被害とを比較してみる．

庄内平野は地盤種別では第4種の所が多く，震害の大きかつたことをよく説明する．鶴岡市の南方に行くにつれ堅い地盤となつて第2種，第1種となり震害も次第に小さくなつた．この震害分布は震源からの距離が遠くなつたばかりでなく地盤の硬軟に影響された所が多いと考える．

酒田市については地盤種別を判定された地点の数が多いので，前にのせた第3図と比べると今町は第3種で地震の被害の大きかつたこととよくあう．その他の常時微動の測定点の地盤種別も震害とあうが，市街の南部の測候所と第三中学校とは敷地が隣あつているのに測候所は第4種，三中は第1種又は第2種と判定されていることは，その差が大き過ぎる．三中は新しく埋立て砂地であること，測候所は高い風力塔があつて，これがゆれて常時微動に影響を与えるかも知れない．其の後，山形大学の志田勇氏に周期約4秒の脈動をこの2個所で比較することを依頼した．その結果は三中の方が測候所より振巾で0.7～0.8であつたという，このことは常時微動による判定と傾向は同じであるが，更に詳しく調べたい問題である．

---

2)　金井清・那須信治・新井信夫・鈴木富三郎・森下利三「常時微動による地盤調査結果」庄内地方の地盤基本調査報告第2報 (1956), 20.
金井清・那須信治・田中貞二・長田甲斐男「常時微動の測定結果 (庄内地方)」地震研究所彙報 **35** (1957) 149～162.

地震断層と精密水準測量結果

前述のようにこの地震のとき最上川の下流北岸に北東方に向け約 10 km の長さの断層ができた，この断層の存在を確めようと水準測量の結果を探した．一等水準線路が鶴岡から酒田を経て北に走つている．その結果は第 5 図に示す．最初の測量は 1901 年で，次は 1934 年であるから，この地震後の地殻変動を示すものであるが，2 回の測量の時間差 33 年間に最上川をこえる新堀附近で約 10 cm 酒田側が下がつた．この位置は地震断層と報告されたものとよく一致している．地震断層は地震の前にも後にも変動を続けていることが多いから，以上の結果は地震断層を確めたと考えられる．

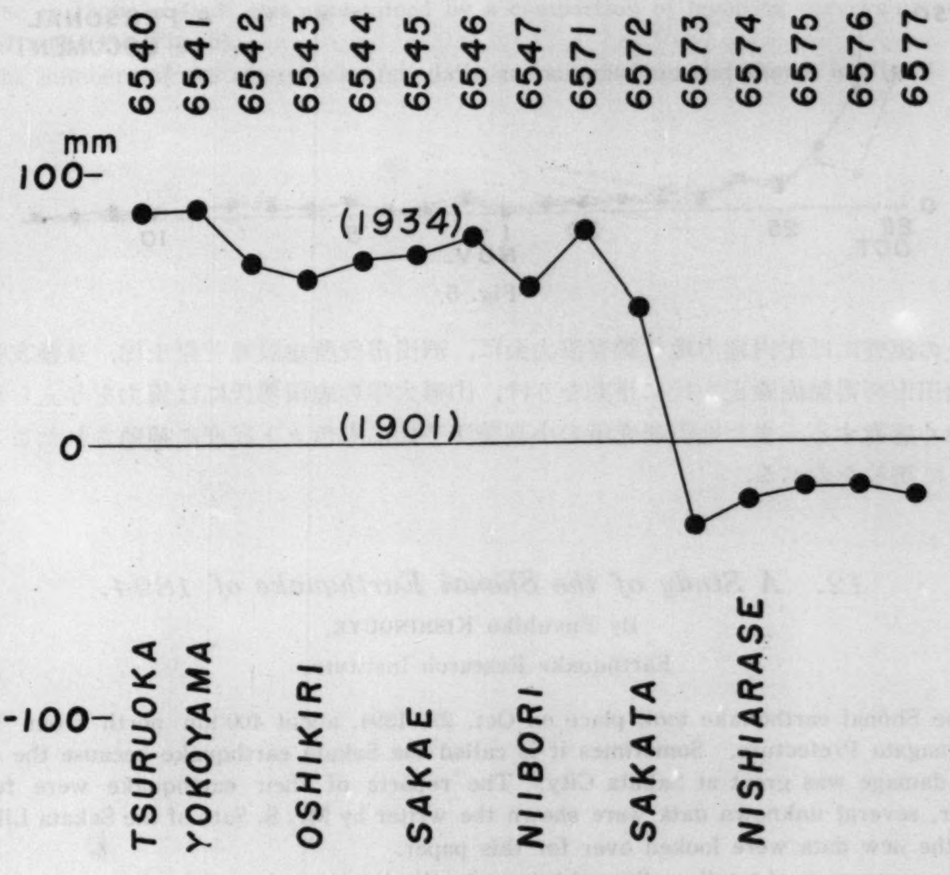

Fig. 5.　Relevelling in 1934.
Numerals on the top signify the bench mark numbers.

余震について

この地震の場合にも余震の起つた時刻をかき残してあるので，その毎日の回数を図に示す．この図を見ると地震の回数の多いのは大地震後 3 日間で，回数のへり方はおよそ一様で速い．このことはこの地震が局部的のものであつたことと，いいかえれば規模の余り大きい地震でなかつたことを示すのであろう．

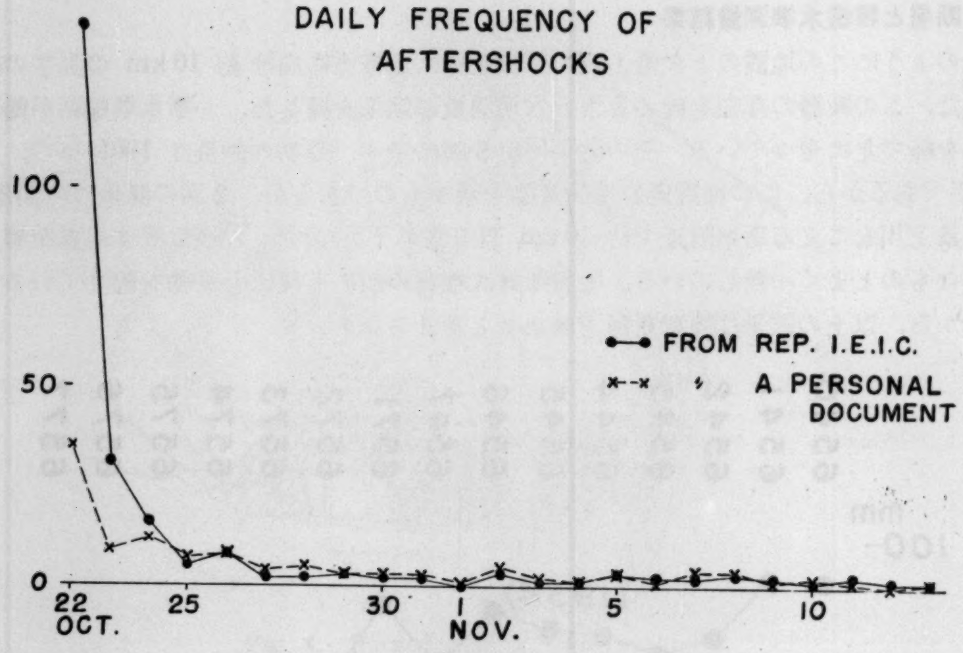

Fig. 6.

以上の調査には庄内地方地盤調査協力会に，酒田市役所建設課菅原士郎，斎藤友弥の両氏，酒田市図書館佐藤正吉氏に援助をうけ，山形大学の志田勇氏には協力を与えられたことを深く感謝する．また地震研究所の小高美江子氏にも色々と研究に補助されたことにつきここに御礼をのべる．

12. A Study of the Shōnai Earthquake of 1894.

By Fuyuhiko KISHINOUYE,
Earthquake Research Institute.

The Shōnai earthquake took place on Oct. 22, 1894, about 400 km north from Tokyo in Yamagata Prefecture. Sometimes it is called the Sakata earthquake because the earthquake damage was great at Sakata City. The reports of their earthquake were few in number, several unknown data were shown the writer by Mr. S. Sato of the Sakata Library. Then the new data were looked over for this paper.

The percentage of totally collapsed houses to the total number of houses was calculated for every village and town (Fig. 1). The damage to houses was great in the Shonai alluvial plain. A fault was found on the northern bank of the Mogami river, and it was considered at that time as the orgin of the earthquake. In old reports the meizoseismal area extended to the confluence of the Mogami and Aka rivers from the fault line. But now, the confluence area may be excluded from the meizoseismal area, because the violence of the earthquake there was considered from earth fissures caused at the earthquake. The fissures might be produced from the condition of surface soil, not of the earthquake motion. Then the epicentre of the earthquake was deduced to be near the fault.

The damage ratios of plaster-walled warehouses to the total number of houses are shown in Fig. 2. It is considered that the damage to plaster-walled houses is greater in a hilly region than in an alluvial plain, and the distribution of damage is opposite to the case of wooden houses which fall down more readily in an alluvial plain than a hilly region. The damage caused by this earthquake supports the above theory.

Damage at Sakata was studied in detail. Fig. 3 shown the number of lives lost and positions of totally collapsed temples, and Fig. 4 the area of burned street. At most great earthquakes in Japan fire took place on the soft ground where wooden houses were severely damaged. This earthquake was no exception in this respect.

Recently microtremors were observed at many places near Sakata by Dr. K. Kanai to classify the subsoil condition. His results were compared and found to agree with the earthquake damage.

The earthquake fault was ascertained by a comparison of levelling surveys carried out in 1901 and 1934 (Fig. 5).

The numbers of the aftershocks felt daily are summed up and shown in Fig. 6.

地震研究所彙報
第36号(1958)235-250頁

13. 木造家屋の耐震性（第2報）

（自然地震の観測）

地震研究所　鈴木正治

（昭和31年6月26日発表—昭和33年3月31日受理）

1. 緒　言

従来構造物の耐震性の研究を目的としてなされた地震動の観測には，大抵は変位地震計又は加速度地震計が使用され，これ等の地震計は通常構造物の床上及びこれに近接せる地上に設置観測された．坪井，宮村[1]等は直接家屋の歪の観測を行い，重要なる研究報告をされている．木造家屋の耐震性に関する研究結果の内，自然地震を木造家屋で観測した代表的なものは，宮村[2]，金井[3]及び斎田[4]等によるものをあげることが出来る．

これ等の観測に用いた家屋と地盤との関係は，斎田の場合は，沖積層の比較的軟弱地盤上に建つ古い二階建店舗，ローム層の良好なる地盤上に建つ比較的新しい二階建住宅である．宮村の場合は，ローム層上の比較的柔構造の旧い一階建教室である．又金井の場合は良好なる地盤上の貼石・モルタルぬり等の木構造の短周期の建物及び神殿造の住居のような柔構造の建物である．

上記建物に於ける震動観測結果を要約すれば次の如きものである．

(i) 卓越振動周期　建物の震動（加速度）[5]観測記象から周期とその頻度の関係を求めると，建物に卓越振動周期が存在し，その値は建物に強制力を与える地震動（地上）の周期及びその加速度の大きさによつて多少異る値を示し，なおそれは，その建物を人工的加力による建物の自由振動及び強制振動の実験結果より得られた建物の固有振動周期と一致した．

又建物の歪[6]震動についてその波動群の平均周期とその頻度との関係を求めると，卓越周期が存在し，その値は地震により多少異るが，これらの平均値は，記象を高橋，伏見[7]の方法によつて求めた建物の自己振動周期と殆んど一致することがわかつた．

今市地震の余震の観測結果[8]によれば，建物の歪震動の卓越周期は，剛構造の建物では地上の加速度の卓越周期と殆んど一致し，柔構造の建物では二つの卓越周期が存在するものと，一つの卓越周期のものがある．この二つの卓越周期が存在する場合，小さい周期は地上の卓越周期に，他の一つは人工的に加えた強制振動の共振周期にそれぞれ一致するこ

---

1) 坪井忠二・宮村摂三　震研彙報 **20** (1942), 291～295; **21** (1943), 216～230.
2) 前出　1).
3) 金井　清・鈴木富三郎　震研彙報 **28** (1950), 465～470.
4) 斎田時太郎　日本学術振興会「第**14**小委員会（耐震構造）」報告，第1号.
5) 前出　4).
6) 前出　1).
7) 高橋浩一郎　理研彙報 **14** (1935), 255～271.
8) 前出　3).

とがわかつた．

(ii) 最大加速度　階上と地上の震動の加速度比を比較すると[9]，軟弱地盤上の店舗では，0.8～3.4で，建物の方向（間口，奥行）により多少の差違がある．又ローム層上の住宅では1.3～4.1倍で，建物の間口方向の比率が平均して約2倍大きな値が観測された．この方向による比率の差違は，その建物の自己振動周期，その減衰率及び地上地震動の周期等の関係により差違を生ずるものと考えられるのであるが，店舗の場合は建物の自己振動周期の長い方向，住宅では短い周期の方向がそれぞれ比率が大きい．これらの比率の大きい方向は著者の考えではそれぞれの建物の地上地震動の卓越振動周期に近い周期を有する方向のようである．

(iii) 加速度又は歪と周期　建物の震動加速度とその周期の関係[10]を，比較的震度の大きい二つの地震について調べた結果によれば，建物の二階の震動加速度の振巾とその周期は大体に於て直線的な関係で，振巾の増加に伴い周期は増加する．これ等の関係は人工的に加えた強制振動による振巾，周期の関係と殆んど同じ傾向にあることが認められた．

又歪振動の群の最大歪振巾とその平均周期との関係[11]について多くの地震について求めると，歪振巾が増加すると平均周期も増加の傾向にあることがわかり，これ等の関係を$T=KA^n$（Tは群の平均周期，Aは群の最大歪振巾，nは常数）と置き，K, nを最小二乗法によつて決定している．

(iv) 加速度振巾比と周期[12]　階上と地上の震動加速度振巾比とその周期との関係，即ち共振曲線より極大振巾比を与える地上の震動周期は建物を人工的に振動せしめて得られた共振周期の値と殆んど一致することがわかつた．

(v) 歪の振巾分布とその周期[13]　歪の振巾と周期との関係を求めると，その極大値を与える周期は，柔構造の場合には二つ，剛構造は一つ存在し，前者の場合の一つの極大値を与える周期は地上地震動の加速度の最大値の周期に，他の一つは人工的に与えた強制振動による共振周期に殆んど一致する．又後者の場合には強制振動による共振周期又は地上の地震動の加速度の最大値の周期と殆んど一致することがわかつた．

その他建物の自己振動周期，減衰率[14]を高橋，伏見の方法によって求め，建物の歪振動の解析がなされている．

本研究の目的は，従来多くの人々によつてなされた研究事項を，前報告において使用した実験家屋を用い，地震動の観測をなし，そこで得られた結果と比較検討し，更に実験家屋と類似体（単一質量系振子）の震動観測も併せ行い，その振動特性と実際の建物との比較を行い，耐震構造研究の基礎的な資料を求めんとするものである．

---

9) 前出 4).
10) 前出 3).
11) 前出 1).
12) 前出 4).
13) 前出 3).
14) 前出 1).
15) 鈴木正治・荘司良也　震研彙報 **20** (1956), 381～400.

2. 測定器及び地震動の観測方法

観測に使用した測定器は変位地震計2台，加速度地震計1台，家屋歪計2台及び類似体(固有周期，減衰係数可変の振動計) 2台で，これらの測定器の諸常数は第1表の如きものである．

第 1 表　観測期間中の測定器の常数

観測期間			天井 (変位)			地上(変位又は加速度)				歪	類似体 (A)			類似体 (B)		
年	月	日	周期 T_n	減衰比 v	倍率 V	周期 T_n	減衰比 v	倍率 V	感度 s	倍率 V	周期 T_n	減衰比 v	倍率 V	周期 T_n	減衰比 v	倍率 V
			sec.			sec.			min/gal		sec.			sec.		
30	12	18	1.0	10	57.0	1.0	11	54.0		128	0.160	1.27	46.0			
〃	〃	29	〃	〃	〃	〃	〃	〃		〃	0.200	1.25	43.0			
31	1	10	〃	〃	36.8	〃	10	36.0		〃	〃	〃	〃			
〃	〃	18	〃	〃	〃	〃	〃	〃		〃	0.212	1.22	〃			
〃	3	20	〃	〃	〃	〃	〃	40.0		92	0.186	〃	44.0			
〃	4	18	〃	〃	〃	〃	〃	〃		〃	0.225	〃	37.0			
〃	5	05	〃	〃	22.5	〃	〃	〃		55	0.256	〃	28.0			
〃	〃	27	〃	〃	〃	〃	〃	〃		〃	0.221	〃	33.0			
〃	6	06	〃	〃	〃	〃	〃	〃		〃	〃	1.40	〃			
〃	〃	10	〃	〃	〃	〃	〃	〃		〃	〃	1.22	〃			
〃	〃	30	〃	〃	〃	〃	〃	〃		〃	0.300	1.25	〃			
〃	7	29	〃	〃	〃	〃	〃	〃		〃	0.193	1.27	33.3	0.48	1.20	50
〃	8	31	〃	〃	〃	0.13	13		0.29	〃	0.317	1.25	22.5	〃	〃	〃
〃	9	30	〃	〃	〃	〃	〃		〃	〃	〃	1.90	〃	〃	〃	〃
〃	10	13	〃	〃	〃	〃	〃		〃	〃	〃	1.25	〃	〃	〃	〃
〃	11	6	〃	〃	〃	〃	〃		〃	〃	〃	〃	〃	〃	〃	〃
振子型式			剪断振動型			剪断振動型					逆立振子型			逆立振子型		
質量 kg			14.6			14.6					1.77			4.27		
慣性能率 g-cm²											2.3×10^5			2.8×10^6		

変位地震計は天井及び地上に設置し，家屋の歪計は A (玄関)，B (物置) の場所において，それぞれ地上約 70cm の高さの柱の位置と地上との相対変位を記録せしめるように，類似体は地上に設置した．第1図はこれら測定器の家屋におけるる平面上の位置を示す．

測定器は総て東西方向の地震動を観測せしめた．なお歪計と類似体はその記録の比較に便ならしめるため，同一の記録用ドラムに記録するようにした．

測定器の総ての記録用ドラムはワーレン電動機により駆動され，その記録紙速度は2mm毎秒とした．No. 23 以後の地震観測には田中，金井[16]による地震動の初期に作動する記

---

[16] 田中貞二・金井　清　地震研究所談話会 (昭和 30 年 12 月)

録用ドラム起動装置の使用により記録紙速度を最初の5倍にすることが出来た．

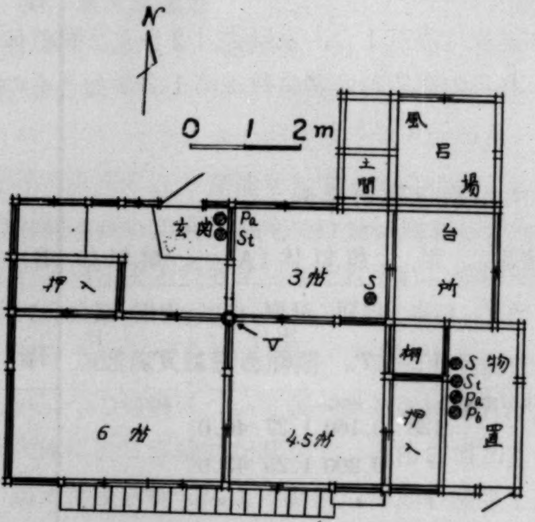
N
0 1 2m
風呂場
土間
台所
玄関
Pa
St
押入
3帖
S
V
棚
S
St
Pa
Pb
物置
6帖
4.5帖
押入

Fig. 1. Plan view of the wooden house. V: vibrator, P_a, P_b: pendulum, S: displacement or acceleration seismograph, S_t: strain-graph.

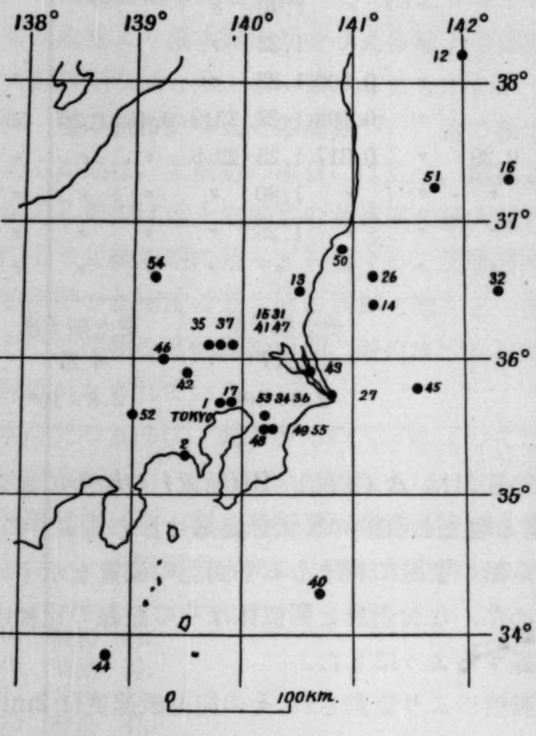
138°
139°
140°
141°
142°
38°
37°
36°
35°
34°
12
16
51
50
26
32
14
54
13
15 31
41 47
35 37
46
43
42
27
45
17
1
53 34 36
52
TOKYO
49 55
48
2
40
44
0
100KM.

Fig. 3. The epicenters of earthqukes.

類似体の固有周期，減衰率の値を如何にするかが問題となるが，その固有周期は0.16 sec. より始め家屋の固有周期を含むように変化した．即ち必要な記録を観測し終ると適宜その値を変化するようにした．減衰率は二三の地震観測以外はなるべく家屋の減衰率附近の値を選んだ．観測期間中の類似体の固有周期，減衰比は第1表に示す．第2図は家屋の天井，歪，及び類似体の自由振動の記録を示したものである．

東京都地盤調査のための地震動観測に際し，宮村[17]は構造物の類似体を兼ねた数種類の固有周期の地震計を使用した．その際の振子の減衰比は通常地震観測時の値であつた．多くの人々によつて測定された木造家屋の減衰比は大抵1.1～2程度のもので，一般に地震の観測時の値に比較して小さいものである．類似体の減衰率が通常の地震観測時の値であれは，類似体の地上地震動による震動周期は一般に，地上地震動の周期に似る事は想像されることである．そこで類似体の減衰率は木造家屋に存在するようなものを選ぶことにした．

天井，地上，歪及び類似体2成分，合計五要素を約一年間観測し，この期間中観測し得た地震中で東京に於ける有感地震の震度は次の如くであつた．震度 IV: 2回，III: 3回，其の他 II，I は合計 30 余回であつた．

第2表は観測し得た地震の発震時，震央其の他の事項で，気象庁地震観測課の報告によるものである．

第3図は第2表の地震の震央位置を示し，なお図中の数字は地震番号を示す．

---

[17] 地震研究所地盤研究会　震研彙報 **33** (1955), 513.

第 2 表　観測された地震

地震	発	震	時			震	央		深さ
番号	年	月	日	時	分	φ	λ	地名	(km)
1	30	12	21	02	30	35.7°	139.8°	東京附近	約 60
2	〃	〃	〃	05	00	35.3	139.5	神奈川県南部	約 40
3	〃	〃	31	04	27			東京附近	
4	31	1	5	14	06	32.3	138.5	八丈島南西沖	
5	〃	〃	7	07	25	38.4	142.5	牡鹿半島東方沖	
6	〃	〃	10	23	51			茨城県南西部	
7	〃	〃	11	15	39	32.6	139.3	八丈島南西沖	約 280
8	〃	〃	18	04	24			房総半島南東沖	
9	〃	〃	30	05	42			房総半島東方沖	
10	〃	2	1	23	18			Marianas	
11	〃	〃	2	04	22			東京附近	
12	〃	〃	4	05	12	37.8	142.0	金華山南東沖	約 60
13	〃	〃	〃	18	58	36.5	140.5	茨城県中部	約 40
14	〃	〃	9	19	19	36.4	141.2	茨城県東方沖	約 60
15	〃	〃	10	06	55	36.1	139.9	茨城県南西沖	約 60
16	〃	〃	〃	09	02	37.3	142.4	福島県東方沖	約 60
17	〃	〃	14	09	53	35.7	139.9	江戸川下流	約 50
18	〃	〃	14	23	12			関東地方南部	
19	〃	〃	18	16	34	29.9	138.5	鳥島西方沖	約 480
20	〃	〃	20	02	06			茨城県，群馬県境	
21	〃	〃	21	23	19			茨城県南西部	
22	〃	4	1	04	11			千葉県北部	
23	〃	〃	2						
24	〃	〃	12	11	32			神奈川県南部	
25	〃	〃	〃	15	17			千葉県北部	
26	〃	〃	25	02	25	36.6	141.2	茨城県	約 40
27	〃	〃	26	20	38	$35.{}^{3}/_{4}$	140.8	銚子附近	約 30
28	〃	〃	30	16	40			関東中部	
29	〃	5	12	19	05			福島県地域	
30	〃	〃	13	05	33			茨城県南西部	
31	〃	〃	16	00	47	36.1	139.9	〃	約 50
32	〃	〃	18	08	00	36.5	141.3	茨城県東方沖	約 40
33	〃	〃	24	12	08			群馬県，栃木県境	
34	〃	6	5	04	09	35.6	140.2	千葉県中部	60～80
35	〃	〃	6	04	56	36.1	139.7	埼玉県，茨城県境	約 90
36	〃	〃	10	05	05	35.6	140.2	千葉県中部	約 80
37	〃	〃	26	07	00	36.1	139.8	茨城県南西部	約 60
38	〃	7	7	16	37	35.4	139.0	神奈川県西部	約 10

(続く)

第 2 表（続き）

地震	発	震	時		震		央	深さ
番号	年	月	日	時	分	φ	λ	地名	km
39	31	7	16	15	28	38.5°	137.3/4°	相川北北西沖	約 30
40	〃	〃	24	23	01	34.3	140.7	房総半島南東沖	約 40
41	〃	〃	30	07	03	36.1	139.9	茨城県南西部	約 50
42	〃	8	5	10	57	35.9	139.5	埼玉県東部	約 90
43	〃	〃	10	00	14	35.9	140.6	千葉県，茨城県境	約 40
44	〃	〃	13	01	59	33.8	138.8	伊豆半島南方沖	約 70
45	〃	〃	24	07	05	35.8	141.6	銚子沖	約 60
46	〃	〃	31	23	48	36.0	139.3	埼玉県中部	約 120
47	〃	9	24	21	01	36.1	139.9	茨城県南西部	約 70
48	〃	〃	30	08	21	35.5	140.2	千葉県中部	約 70
49	〃	〃	30	09	03	35.5	140.25	〃	約 60
50	〃	10	14	09	31	36.8	140.9	茨城県東岸沖	約 90
51	〃	〃	15	06	05	37.25	141.75	福島県東方沖	約 40
52	〃	〃	29	02	40	35.6	139.0	山梨県東部	約 20
53	〃	11	4	14	37	35.6	140.2	千葉県中部	約 80
54	〃	〃	5	11	38	36.7	139.2	群馬県東部	約 10
55	〃	〃	5	17	09	35.5	140.25	千葉県中部	約 60

第4図〜第6図は観測された地震の記象例で，比較的震度の大きいものである．なお昭和 31 年4月以降に記録紙速度が大きくなつた時に観測し得たものについては次の機会に掲載の予定である．

3. 家屋及び類似体の最大振巾と地上地震動との関係

第3表は各地震における家屋の天井の振巾が最大のとき，家屋の歪，類似体及び地上の振巾，周期等の値を示すものである．

第7図〜第8図は第3表に示した各要素の震動振巾の地上地震動振巾に対する割合，即ち振巾比と地上地震動周期との関係を示したものである．又これ等の図中の実線は単一質量系の振子の支持点に単位振巾の正弦波振動を与えた時，定常状態における，絶対系及び運動系の座標に対する振子の位置を示す[18]．

天井の振巾比は 7.2〜1.0 であつて，その最大値を与える地上の震動周期は 0.2 sec. 附近で，この値は家屋の振巾が小さい時の家屋の固有振動周期の値と殆んど等しい．

家屋の歪振巾の地上地震動振巾に対する振巾比は 2.1〜0.02 であつて，天井と同様に，その最大値を与える周期の値は家屋の固有周期と殆んど一致し，地上の周期が相当に大き

---

[18] 例えば，坪井忠二　振動論によれば，

$$F=\frac{u\sqrt{u^2+4h^2}}{\sqrt{(u^2-1)^2+4h^2u^2}}\ (\text{絶対系}),\quad F_a=\frac{1}{\sqrt{(u^2-1)^2+4h^2u^2}}\ (\text{運動系}).$$

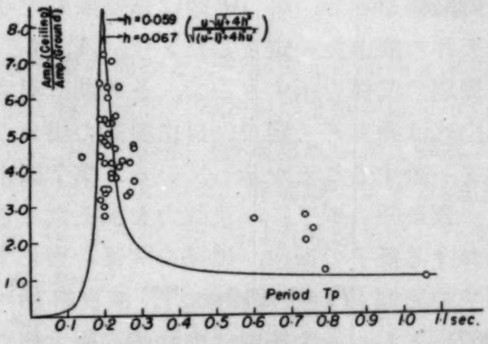

Fig. 7. Relation between the maximum amplitude ratio and the period of the earthquake motion on the ground.
(Representation of
$u\sqrt{u^2+4h^2}/\sqrt{(u^2-1)^2+4h^2u^2}$)

くなると（遠震の場合），その値は零に近くなる．この場合家屋の振巾は地上の震動振巾に殆んど等しくなり，家屋は地面と一体となつて振動し，即ち家屋は剛体のような運動をしていることを意味する．

歪の観測は．地上で変位震動計で観測を行つた期間において，*A* 点 (No. 8～No. 21)，*B* 点 (No. 22～No. 45) で行つたもので，二点の同時観測ではない．これらの点の振巾比は夫々 0.14～0.49 及び 2.09～0.60 となり，*B* 点は *A* 点の約 3.5 倍となる．この二点の振巾比の相違は家屋の構造上より生ずるものと，二点が同時観測によらない即ち地上地震動の性質とによることが一応は考慮される事である．そこで *A*, *B* 二点の観測期間中の天井の振巾比の平均を求めて見ると 4.1 及び 4.7 となるから，この振巾比の相違を地上地震動の性質によるものと考えこれを考慮して上記二点の振巾比の平均を修正すると，その倍率は 2.9 となる．この値は実に家屋に人工的に自由振動又は強制振動を与えた時に，天井における振巾を一定値としたときの二点の振巾比と殆んど一致する．この事実は二点 *A*, *B* の剛性比を示すものであろう．

第9図は家屋の自由振動による天井と *A*, *B*

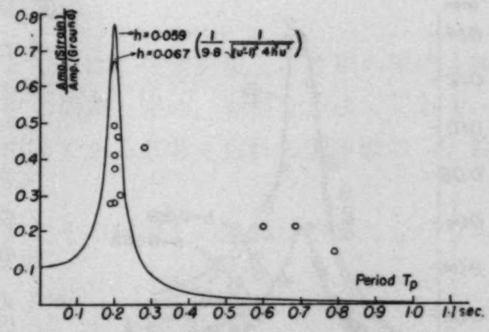

Fig. 8a. Relation between the maximum amplitude ratio and the period of the earthquake motion on the ground.
(Representation of
$1/9.8\sqrt{(u^2-1)^2+4h^2u^2}$)

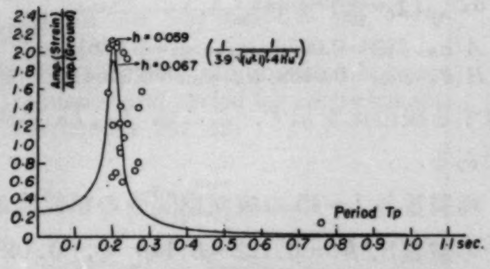

Fig. 8b. Relation between the maximum amplitude ratio and the period of the earthquake motion on the ground.
(Representation of
$1/3.9\sqrt{(u^2-1)^2+4h^2u^2}$)

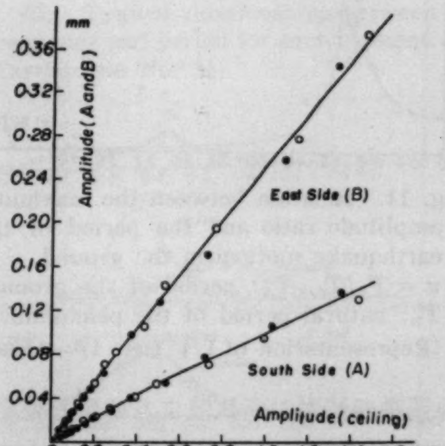

Fig. 9. Comparison of the amplitude between *A* and *B* in the case of free vibration.

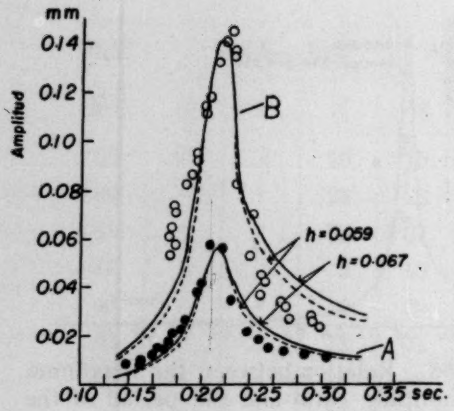

Fig. 10. Comparison of amplitude between A and B in the case of forced vibration. (Representation of $\alpha_h \Big/ \sqrt{\left(1-\frac{1}{u^2}\right)^2+4h^2\frac{1}{u^2}}$), $A(\alpha_{h=0\cdot067}=0.0076,\ \alpha_{h=0\cdot059}=0.066)$, $B(\alpha_{h=0\cdot067}=0.0189,\ \alpha_{h=0\cdot059}=0.0164)$.

二点の振巾の関係を示し，第 10 図は強制振動を与えた場合，天井の振巾を一定としたとき，A, B 二点の振巾，周期の関係を示すもので，各周期に対する二点の振巾比は殆んど一定で，自由振動の場合の比率と殆んど一致することを示している．第7図中の曲線は単一質量系の振子に，正弦力を加えたとき定常状態における振子の振巾，周期の関係を表わすもので，振子の周期 (T_n=0.212 sec.)，減衰率 (h=0.059, 0.067) とし，極大振巾は実験値の極大値に一致せしめた．図に示す如く家屋の振動は単一質量系の振子の振動とは完全には一致しないことを示す．さてここにおける h の値は，極大振巾の $1/\sqrt{2}$ の振巾を与える二つの周期の値と，極大振巾を与える周期から前報告において述べた方法で求めた．

第 11 図は類似体 (A) の各周期比 ($u=T_p/T_n$) に対する振巾比を示す．ここに T_p, T_n は夫々地上地震動の周期及び類似体の固有振動周期である．

地震番号 1〜45 の観測期間中の類似体の固有周期は第 1 表の如く T_n = 0.16〜0.32 sec. その減衰比 h = 0.122〜0.149 で，0.149, 0.140 の二つの場合以外は 0.122〜0.127 であつた．

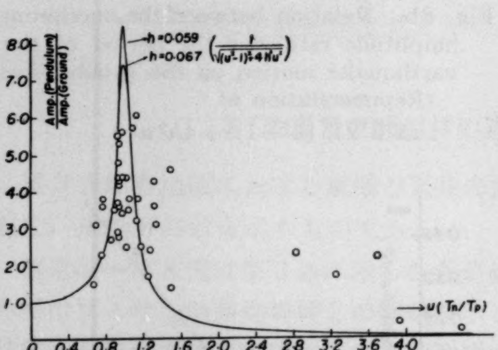

Fig. 11. Relation between the maximum amplitude ratio and the period of the earthquake motion on the ground. $u=T_p/T_n$, T_p: period of the ground, T_n: natural period of the pendulum. (Representation of $1/\sqrt{(u^2-1)^2+4h^2u^2}$)

振巾比は地上の震動周期と類似体の固有周期及びその減衰係数により相異なる値を示すことは当然なことであるが，一般に固有周期，減衰係数が一定の振子の場合と同様，周期比と振巾比の関係を図示すると第 11 図の如くなり，周期比が 1 附近において振巾比が最大となり，斯様な場合でも家屋歪における周期—振巾比の関係と類似な傾向にあることを示している．

第 6 図〜第 8 図及び第 11 図において，同一の地上震動周期に対する各要素の振巾比の分布の要因としては種々考えられるが，地上の地震動の波形の正弦波よりの歪の程度はその一つの大きな要素と考えられる．尚家屋の天井，歪及び類似体等の各要素に最大振巾を与えた地上の震動周期の大部分は，0.15 sec.〜0.27 sec. である．

4. 周期と頻度との関係

各要素の周期とその頻度との関係を求める方法としては，先ず記象上の波動の相続く極大値と極小値間の時間差の2倍を以てその震動振巾の周期と定め，斯様な方法で記象を，適宜に定めた時間（各地震につき比較的大きな振巾時であると考えられる主要動の 20 秒間をとつた）につき，各周期に対する集計を行つた.

第 12 図～第 39 図は各地震毎に，各要素の周期とその頻度との関係を示したものであ

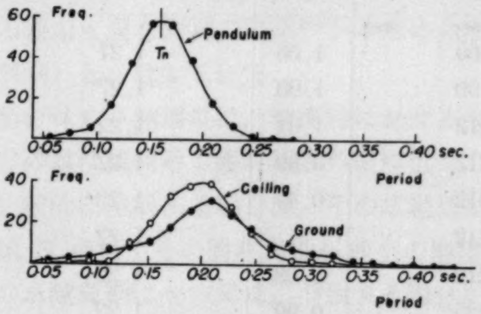

Fig. 12. Typical relationships between frequency and period for each element. (Earthquake No. 2)

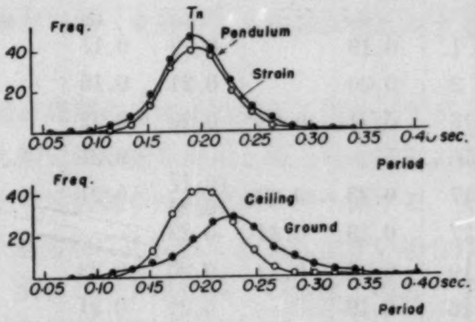

Fig. 13. Typical relationships between frequency and period for each element. (Earthquake No. 42)

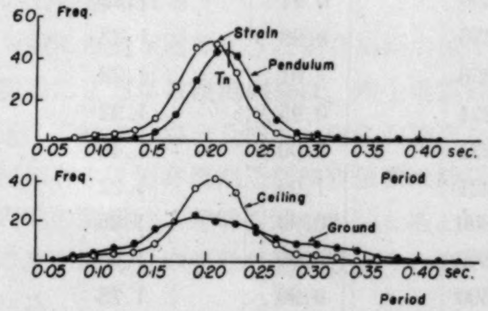

Fig. 14. Typical relationships between frequency and period for each element. (Earthquake No. 35)

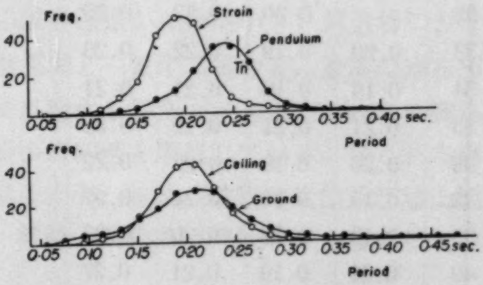

Fig. 15. Typical relationships between frequency and period for each element. (Earthquake No. 31)

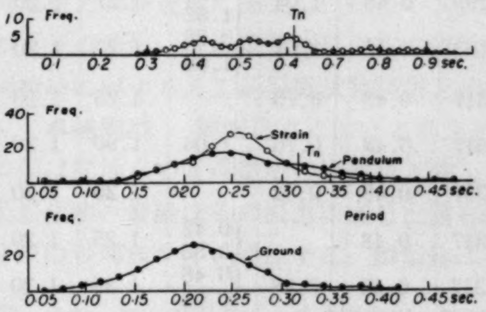

Fig. 16. Typical relationships between frequency and period for each element. (Earthquake No. 48)

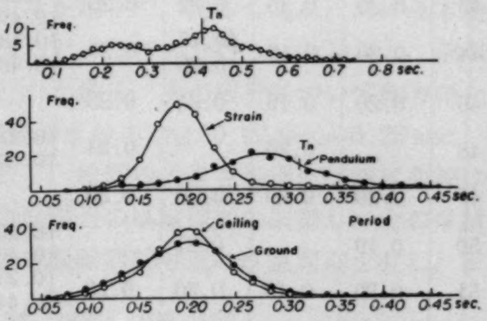

Fig. 17. Typical relationships between frequency and period for each element. (Earthquake No. 51)

る．これらの曲線の極大値を与える周期をその地震の各要素の卓越振動周期と決めることにする．第 4 表は第12図〜第39図の各図より求めた卓越振動周期を一括して示したも

第 4 表　観測された卓越振動周期及び類似体の固有周期 (T_n)，減衰比 (v)

地震番号	天井	歪	地上	類似体		類似体		周期比		減衰比	
				A	B	A	B	A	B	A	B
	T_p	T_p	T_p	T_p	T_p	T_n	T_n	T_p/T_n	T_p/T_n	v	v
	sec.	sec.	sec.	sec.	sec.	sec.	sec.				
1	0.19		0.22	0.17		0.160		1.06		1.27	
2	0.20		0.21	0.16		0.160		1.00		1.27	
15	0.24	0.23	0.20	0.22		0.212		1.04		1.22	
16				0.21		0.212		0.99		1.22	
17	0.23	0.23	0.17 0.26	0.21		0.212		0.99		1.22	
17	0.19	0.24	0.22			0.212				1.22	
19	0.22	0.22	0.20	0.23		0.212		1.08		1.22	
26	0.19		0.21	0.21		0.225		0.99		1.22	
27	0.22	0.22	0.21	0.21		0.225		0.99		1.22	
28	0.20	0.19	0.22	0.22		0.225		1.04		1.22	
31	0.20	0.19	0.21	0.24		0.256		0.94		1.22	
32		0.20	0.23	0.25		0.256		0.98		1.22	
33	0.20	0.19	0.22	0.26		0.256		1.01		1.22	
34	0.19	0.19	0.21	0.21		0.221		0.95		1.22	
35	0.21	0.21	0.19	0.22		0.221		1.00		1.40	
36	0.20	0.19	0.22	0.22		0.221		1.00		1.22	
38	0.19	0.18	0.22	0.27		0.300		0.90		1.25	
39	0.19	0.18	0.20	0.27		0.300		0.90		1.25	
40	0.21	0.19	0.21	0.27		0.300		0.90		1.25	
41	0.20	0.19	0.20	0.19		0.193		0.99		1.27	
42	0.20	0.20	0.23	0.20		0.193		1.04		1.27	
43	0.20	0.20	0.22	0.20	0.22 0.49	0.193	0.48	1.04	0.46 1.02	1.27	1.20
44	0.20	0.19	0.17 0.26	0.20	0.18 0.48	0.193	0.48	1.04	0.38 1.00	1.27	1.20
46	0.20	0.19	0.21	0.23		0.317	0.48	0.73		1.25	1.20
48		0.26		0.24	0.42 0.60	0.317	0.48	0.76	1.06	1.90	1.20
49	0.20	0.20	0.20	0.26		0.317	0.48	0.82		1.25	1.20
50	0.19		0.21		0.20 0.40	0.317	0.48		0.42 0.83	1.25	1.20
51	0.20	0.19	0.20	0.28	0.23 0.44	0.317	0.48	0.88	0.48 0.92	1.25	1.20
53	0.24		0.21								
平均	0.20	0.20	0.21		0.21 0.46		0.48	0.96	0.44 0.97		

のである.

家屋，類似体の強制力となる地上の地震動の卓越周期は 0.19 sec.～0.23 sec. で，加速度振巾の場合もこれらの値と殆んど同様な値で，それらの平均値は，同一地点において観測された常時微動による地上の卓越周期19)の値と全く一致している.

家屋の天井における卓越周期は 0.19 sec.～0.24 sec. で，又歪の場合は天井の値と殆んど同様で，これらの値は地上の震動周期に支配されることは勿論，その振巾の大小により影響をうける. 即ち地上の振巾の大きいものほど卓越周期は大となる. これは前報告における振巾と固有周期の関係20)から求めた家屋の固有周期（家屋のある振動振巾に対する固有周期）と一致している.

類似体の卓越周期は，観測時における夫々の固有周期の値により異なる値を示すが，それらの値は観測時の固有周期の値に近く，若しも類似体の固有周期と地上の地震動の周期が比較的に差異ある場合は，その卓越周期は地上の地震動の卓越周期の方へ偏する. 又類似体 B の如くその固有周期が地上の地震動の卓越周期に比較して相当に大きい場合は，その卓越周期は一つ又は二つ生ずる場合がある. 前者の場合は勿論その値はその固有周期に殆んど一致し，後者の場合は，その一つは類似体の固有周期に，他の一つは地上の地震動の卓越周期に殆んど一致するようである. 斯様な事実は斎田21)，金井等22)の研究報告においても見られる.

一般に木造家屋のような固有周期の値で，その減衰係数が比較的小さい構造物における地震動による卓越振動周期は，地上地震動の卓越周期と一致する場合と，家屋の固有周期附近に卓越する場合及びこの両者が適当な割合で卓越する場合とがある. これらの関係は家屋の有する固有周期及び減衰係数に接近した振子の特性と類似している. 又これら両卓越周期の関係は，建物の固有周期と地上地震周期の大小，建物の減衰の状態及び地上地震動の波形即ちその波形の正弦波よりの歪の程度，相続く振動の持続性等によるものと考えられる.

5. 結　言

関東地方及び近傍に発生した地震の変位，加速度を地上で，又この地点における木造家屋の天井の変位，柱の歪及び類似体の運動を観測した. これより得られた結果と，前報告の同建物に対する人工的振動試験結果と比較を行つた結果，次の項目について知り得た.

1. 卓越周期　観測地点における地上の地震動の卓越周期は 0.19 sec.～0.23 sec. で，この値は同地点の常時微動の観測値と殆んど一致し，地震の大きさが増せば頻度曲線は多少平坦化す. 家屋はその振巾に応じた固有振動周期附近の卓越周期で振動し，その卓越周期は振巾の増加に伴い増加する. 類似体はその固有振動周期附近に卓越周期を有し，家屋

---

19)　金井　清・田中貞二・長田甲斐男　震研彙報 **35** (1957), 109～133.
20)　前出　15).
21)　前出　4). 15. 第 11 図
22)　前出　3). 468. 第 7 図

第3表　最大振巾及び其の周期

地震番号	天井 振巾 (mm)	天井 周期 (sec.)	地上 振巾 (mm)	地上 加速度 (gal)	地上 周期 (sec.)	類似体 振巾 (mm)	類似体 周期 (sec.)	歪 振巾 (mm)	歪 周期 (sec.)	振巾比 天井/地上	振巾比 類似体/地上	振巾比 歪/地上
1	0.140	0.17	0.034		0.24	0.048	0.15			4.1	1.4	
2	0.768	0.22	0.260		0.20	0.500	0.16			3.0	1.7	
3	0.154	0.18	0.035		0.19	0.148	0.20			4.4	4.2	
4	0.056	0.21	0.013		0.14	0.040	0.19			4.4	3.1	
5	0.094	0.74	0.035		0.74	0.076	0.20			2.7	2.2	
6	0.059	0.18	0.011		0.19	0.040	0.19			5.4	3.6	
7	0.124	0.22	0.025		0.21	0.094	0.20			5.0	3.8	
8	0.051	0.19	0.011		0.28	0.047	0.19	0.0047	0.19	4.6	4.3	0.43
9	0.081	0.19	0.017		0.20	0.082	0.20	0.0070	0.19	4.8	4.8	0.41
10	0.089	0.10	0.086		1.06	0.017	0.20			1.0	0.2	
11	0.043	0.19	0.008		0.20	0.035	0.20	0.0039	0.19	5.4	4.4	0.49
12	0.035	0.20	0.010		0.19	0.038	0.20	0.0031	0.19	3.2	3.5	0.28
13	0.099	0.19	0.028		0.20	0.078	0.20	0.0078	0.17	3.5	2.8	0.28
14	0.116	0.19	0.044		0.60	0.101	0.20	0.0094	0.18	2.6	2.3	0.21
15	1.92	0.25	0.556		0.21			0.2540	0.23	3.5		0.46
16	0.229	0.79	0.194		0.79			0.0266	0.20	1.2		0.14
17			0.905		0.22			0.356	0.28			0.39
18	0.070	0.19				0.096	0.20	0.0070	0.19			
19	0.669	0.22	0.328		0.69	0.540	0.23	0.0704	0.23	2.0	1.7	0.21
20	0.048	0.19	0.013		0.28	0.047	0.21			3.7	3.6	
21	0.064	0.19	0.019		0.20	0.082	0.20	0.0070	0.19	3.4	4.3	0.37
22												
23												
24	0.157	0.21	0.041		0.22	0.104	0.21	0.046	0.21	3.8	2.5	1.12
25	0.109	0.19	0.023		0.28	0.106	0.18	0.036	0.20	4.7	4.6	1.57
26	0.098	0.20	0.014		0.22	0.049	0.22			7.0	3.4	
27	1.51	0.23	0.394		0.23	1.05	0.23	0.236	0.23	3.8	2.5	0.60
28	0.140	0.21	0.030		0.21	0.11	0.22	0.024	0.22	4.7	3.7	0.70
29	0.088		0.013		0.24	0.071	0.21	0.025	0.21	6.8	5.5	1.92
30	0.133	0.19	0.032		0.27	0.105	0.21	0.045	0.21	4.2	3.3	1.40
31	0.279	0.21	0.071		0.22	0.189	0.24	0.068	0.24	3.9	2.7	0.96
32			0.045		0.24	0.132	0.24	0.055	0.24		2.9	1.22
33	0.226	0.21	0.054		0.20	0.207	0.24	0.058	0.24	4.2	3.8	1.07
34	0.153	0.20	0.021		0.20	0.114	0.21	0.042	0.21	7.2	5.3	2.08
35	1.31	0.24	0.388		0.27	0.871	0.25	0.313	0.25	3.4	2.2	0.80
36	0.229	0.20	0.043		0.21	0.178	0.19	0.090	0.19	5.3	4.4	2.09
37	0.204	0.21	0.049		0.22	0.171	0.21	0.044	0.21	4.2	3.5	0.91

（続く）

第　3　表　(続き)

地震番号	天井		地上			類似体		歪		振巾比		
	振巾 (mm)	周期 (sec.)	振巾 (mm)	加速度 (gal)	周期 (sec.)	振巾 (mm)	周期 (sec.)	振巾 (mm)	周期 (sec.)	$\frac{\text{天井}}{\text{地上}}$	$\frac{\text{類似体}}{\text{地上}}$	$\frac{\text{歪}}{\text{地上}}$
38	0.394	0.21	0.085		0.23	0.196	0.25	0.091	0.25	4.6	2.3	1.07
39	0.159		0.060		0.20	0.090	0.30	0.040	0.30	2.7	1.5	0.66
40	0.231	0.21	0.042		0.23	0.153	0.28	0.085	0.28	5.5	3.6	2.00
41	0.226	0.19	0.040		0.19	0.225	0.19	0.082	0.19	6.4	5.6	2.05
42	0.257	0.21	0.054		0.22	0.337	0.18	0.077	0.18	5.3	6.2	1.41
43	0.300	0.22	0.050		0.21	0.285	0.21	0.106	0.21	6.0	5.7	2.06
44	0.586	0.76	0.261		0.76	0.105	0.19	0.034	0.19	2.3	0.4	0.13
45	0.099	0.23	0.030		0.26	0.094	0.24	0.022	0.24	3.3	3.1	0.73
46	0.342	0.24		7.0	0.25	0.750	0.32	0.064	0.24	0.049	0.105	0.009
47	0.080	0.20		2.3	0.24	0.057	0.28	0.031	0.24	0.035	0.025	0.013
48				132.0	0.21	2.43	0.25	0.955	0.31		0.018	0.007
49	0.320	0.22		3.4	0.17	0.063	0.22	0.086	0.23	0.095	0.018	0.025
50	0.378	0.23		8.1	0.20					0.047		
51	0.276	0.23		4.9	0.23	0.208	0.30	0.058	0.24	0.056	0.043	0.019
52	0.332	0.23		4.5	0.23					0.074		
53	1.82	0.26		77.2	0.19					0.023		
54	0.085	0.21		2.1	0.22					0.041		
55	0.149	0.22		3.4	0.19					0.044		
平均	No. 1～21	0.20			0.21		0.20		0.20	3.6	3.1	0.33
	No. 22～45	0.21			0.23		0.22		0.22	4.7	3.6	1.26
	No. 1～45	0.21			0.22		0.21		0.22	4.2	3.3	
	No. 46～55	0.23			0.21		0.27		0.25	0.052	0.042	0.015
	No. 1～55	0.21			0.22		0.22		0.22			

備考：1. No. 46～55 の振巾比の単位：mm/gal.
　　　2. 遠震は平均周期の集計より除く。

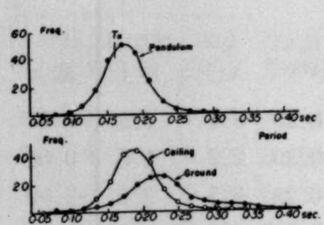

Fig. 18. Earthquake No. 1

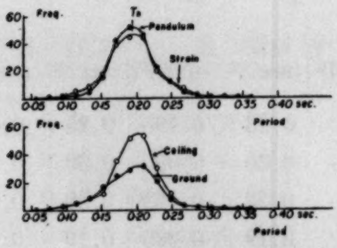

Fig. 19. Earthquake No. 41

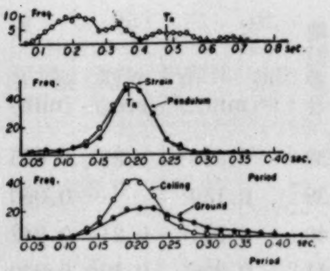

Fig. 20. Earthquake No. 43

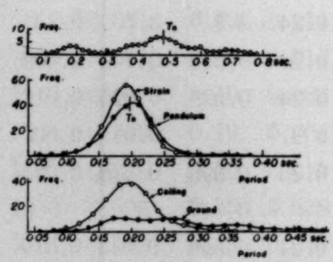

Fig.2 1. Earthquake No. 44

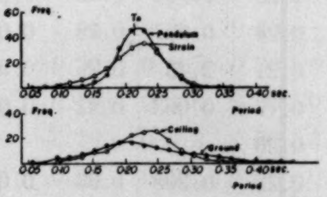

Fig. 22. Earthquake No. 15

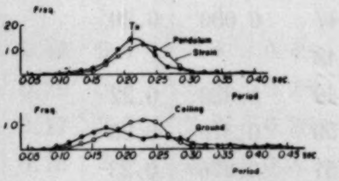

Fig. 23. Earthquake No. 17

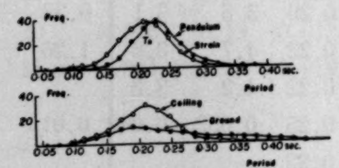

Fig. 24. Earthquake No. 19

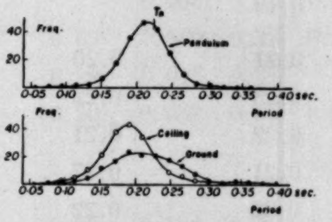

Fig. 25. Earthquake No. 26

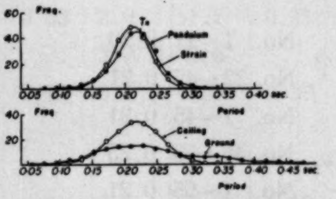

Fig. 26. Earthquake No. 27

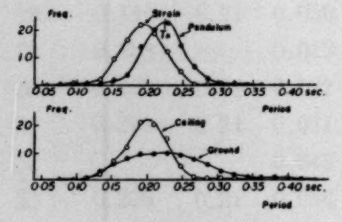

Fig. 27. Earthquake No. 28

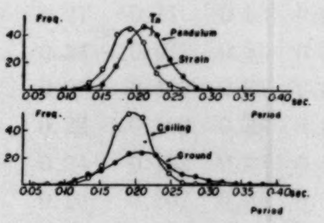

Fig. 28. Earthquake No. 34

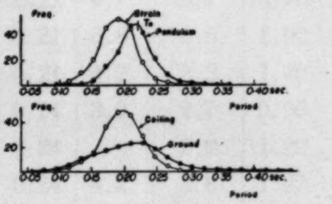

Fig. 29. Earthquake No. 36

Figs. 18∼29. Relation between frequency and period for each element.

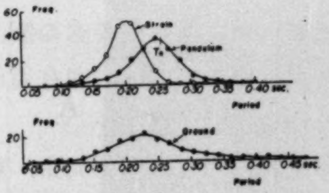

Fig. 30. Earthquake No. 32

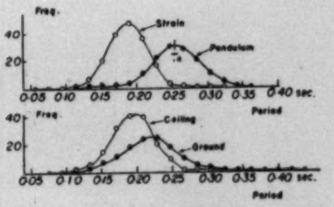

Fig. 31. Earthquake No. 33

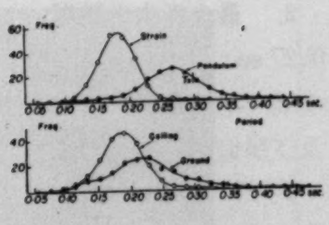

Fig. 32. Earthquake No. 38

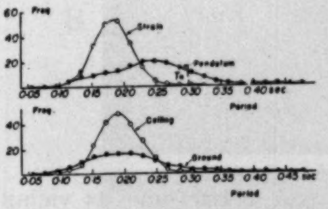

Fig. 33. Earthquake No. 39

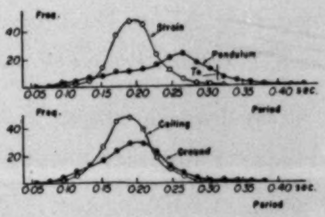

Fig. 34. Earthquake No. 40

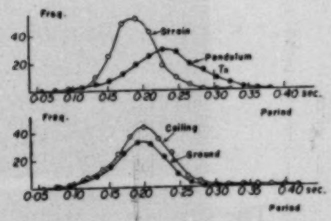

Fig. 35. Earthquake No. 46

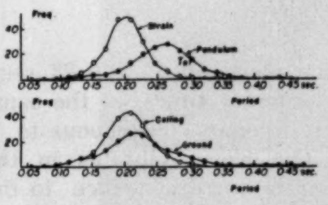

Fig. 36. Earthquake No. 49

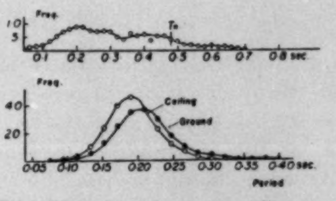

Fig. 37. Earthquake No. 50

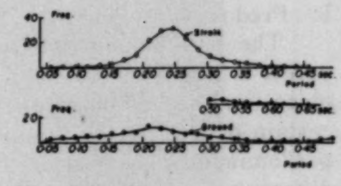

Fig. 38. Earthquake No. 17

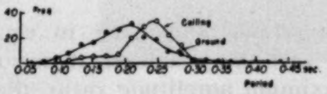

Fig. 39. Earthquake No. 53

Figs. 30~39. Relation between frequency and period for each element.

と類似の振動特性を示すが，家屋のように振巾の増加に伴う卓越周期の増加は認められない．

2.　最大振巾と周期　各要素に最大振巾を与えた地上の地震動の周期は 0.19 sec.～0.27 sec. で，この値は地上地震動の卓越周期と一致する．家屋，類似体の各要素の振巾の地上地震動振巾に対する振巾比の極大値を与える周期は，振巾に応じた家屋の固有周期及び類似体の夫々の固有周期と一致することが認められる．

終りに臨み本研究に当り終始御指導，激励を賜わつた東京大学教授西村源六郎先生，東京大学地震研究所金井清先生，建設省建築研究所久田俊彦博士，中川恭次氏に感謝の意を表し，又種々御助力を頂いた荘司良也君に御礼を述べる．なおこの実験，観測費は主として文部省科学試験研究費によるものである．

---

13. *Aseismic Properties of a Wooden House. Part 2.*
(*Observation of Earthquakes*)

By Masazi SUZUKI,
Earthquake Research Institute.

The displacement and acceleration of earthquakes in the Kanto district and its vicinity were observed on the ground simultaneously with the displacement of a ceiling, the strain on a pillar of a wooden house and the vibration characteristics of a pendulum at the same place. These experiments were held to compare the results with those of a previous paper in which were described the vibration characteristics of the same house when vibrated by means of artificial force. The results of the present experiment can be summarized as follows:

1. Predominant Period:

The predominant period of the earthquake at the observation place was 0.19-0.23 sec., which is nearly equal to that of the micro-tremors observed at ordinary times at the same place, and the relationship between the period and its frequency becomes conspicuous to a certain degree as the amplitude of the earthquake increases. The house vibrates in the predominant period near the natural frequency which occured in correspondence to the different amplitude of vibration and the predominant period increases as the amplitude increases.

The pendulum has similar vibration characteristics to those of the house, and the predominant period can be observed near its natural period of frequency, but does not tend to increase with an increase in the amplitude as was the case with the house.

2. Maximum Amplitude and its Period

The period of earthquake on the ground that caused the maximum amplitude to each element mentioned above was 0.19-0.27 sec., which is in accord with the predominant period of the earthquake on the ground. The period that gives a maximum amplitude ratio, that is, the ratio of each element of the house and of the pendulum to the earthquake on the ground was observed to concur with the natural periods of the house and of the pendulum respectively.

In conclusion, we express sincere thanks to Prof. G. Nishimura, Faculty of Engineering, Dr. K. Kanai, Earthquake Research Institute of Tokyo University, Dr. T. Hisada and Mr. K. Nakagawa, Architectural Research Institute of the Ministry of Construction for their kind guidance and encouragement given us, and also to Mr. R. Shoji for his valuable assistance during this work. Moreover, we wish to acknowledge the fact that part of these experiments was carried out by grant from the scientific experiment and research fund of the Education Ministry.

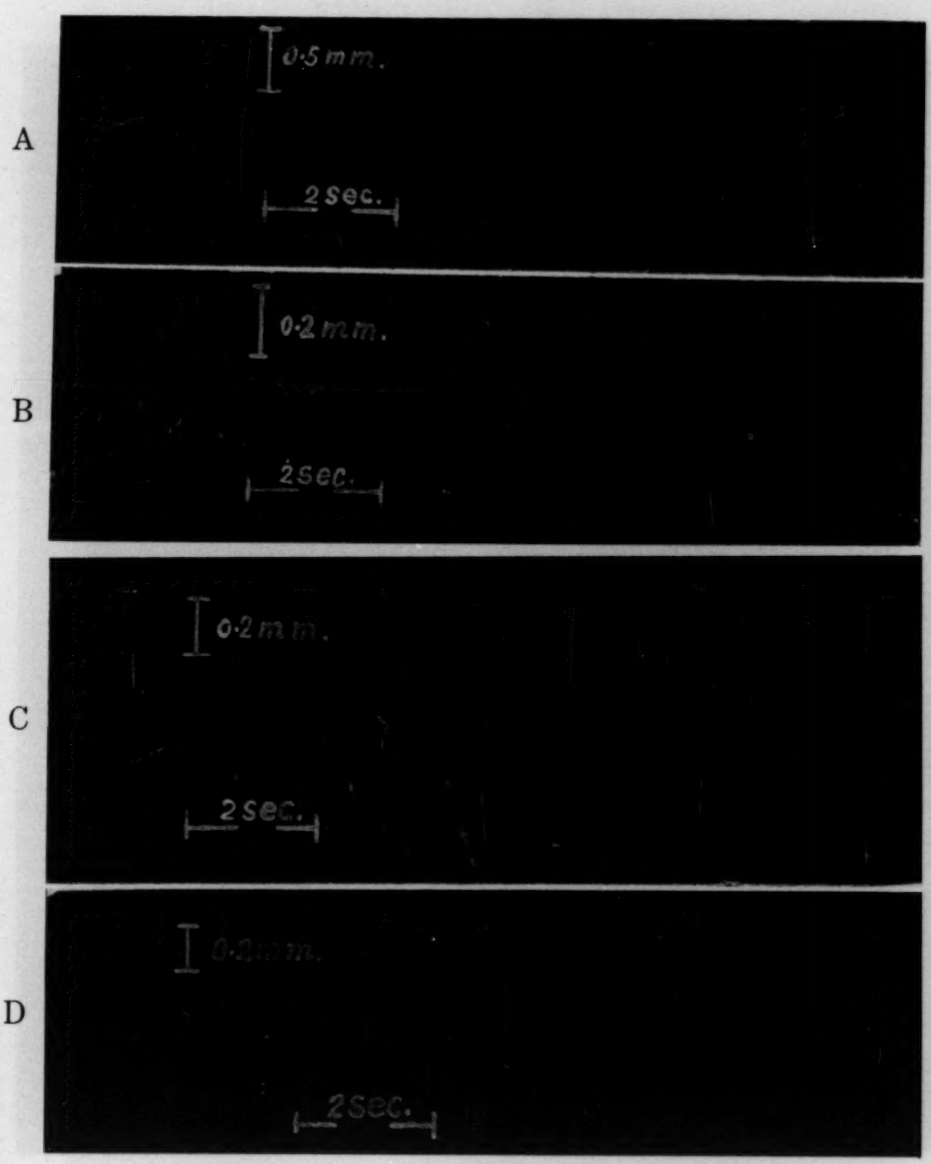

Fig. 2. Records of free vibration of the test house and pendulum.
A: Ceiling. B: Strain. C: Pendulum ($T_n = 0.186$ sec.).
D: Pendulum ($T_n = 0.30$ sec.).

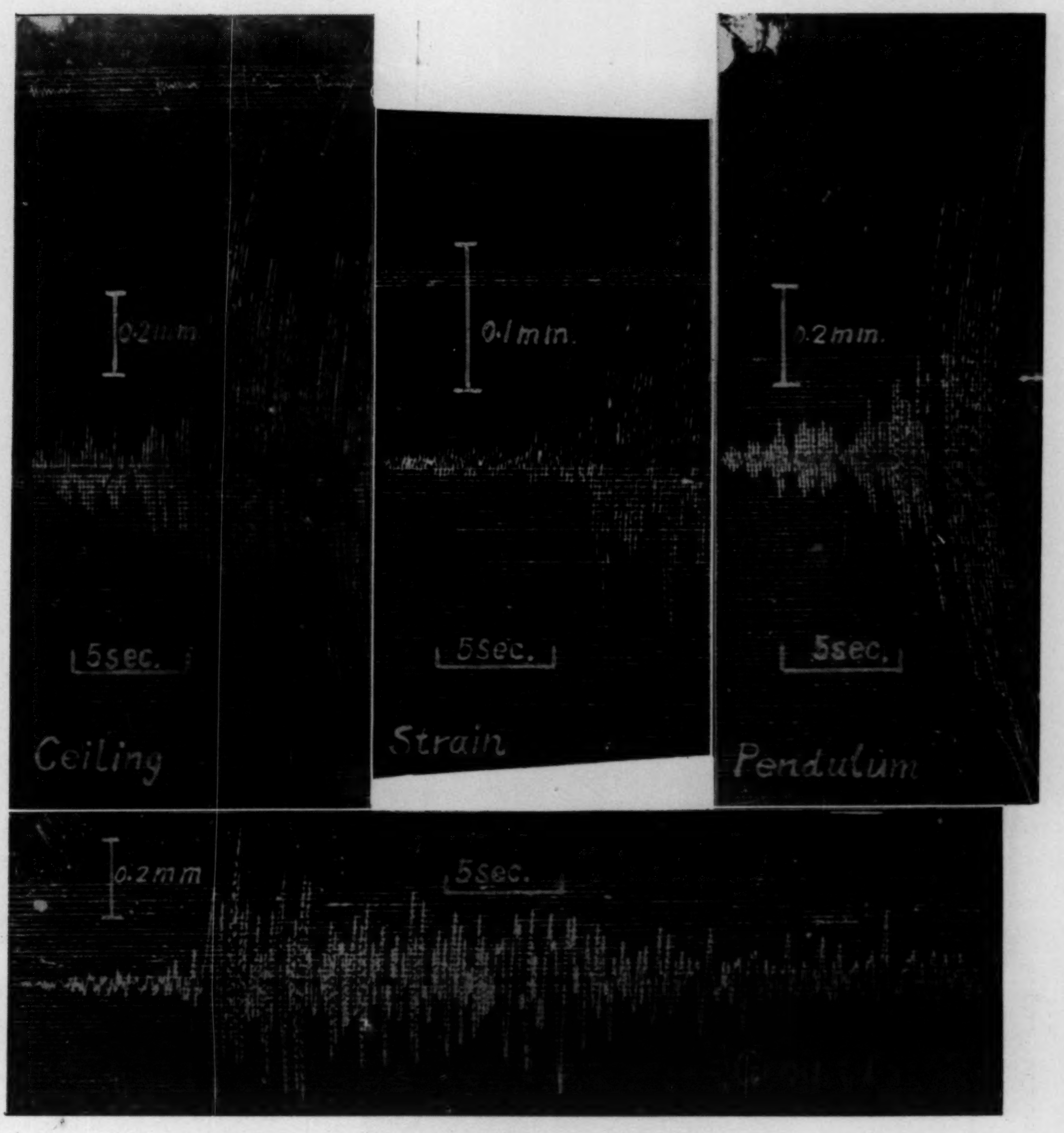

Fig. 4. The representative seismograms.
(Earthquake No. 15) Original × 1.4

（震研彙報 第三十六号 図版 鈴木）

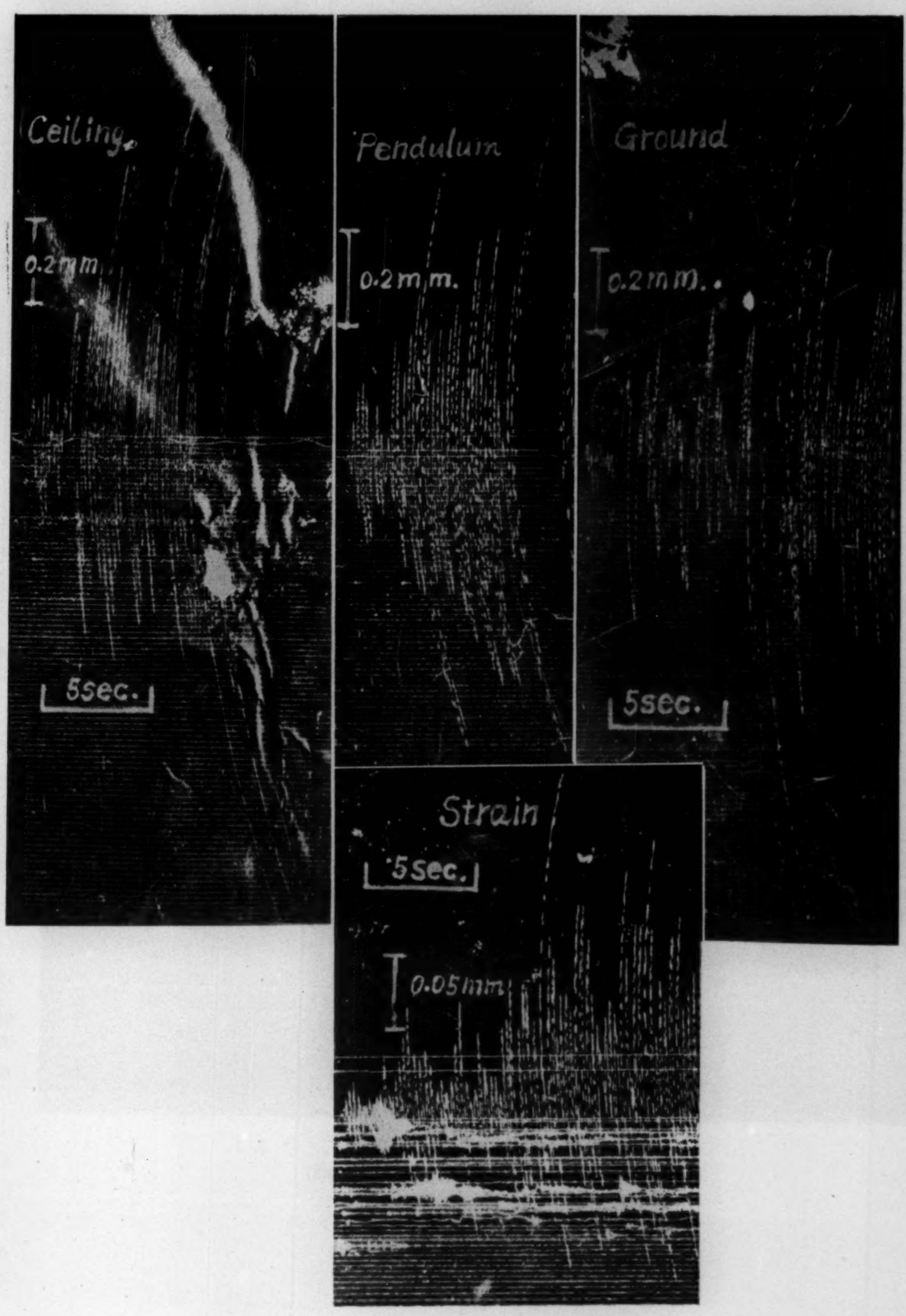

Fig. 5. The representative seismograms.
(Earthquake No. 17) Original × 1.4

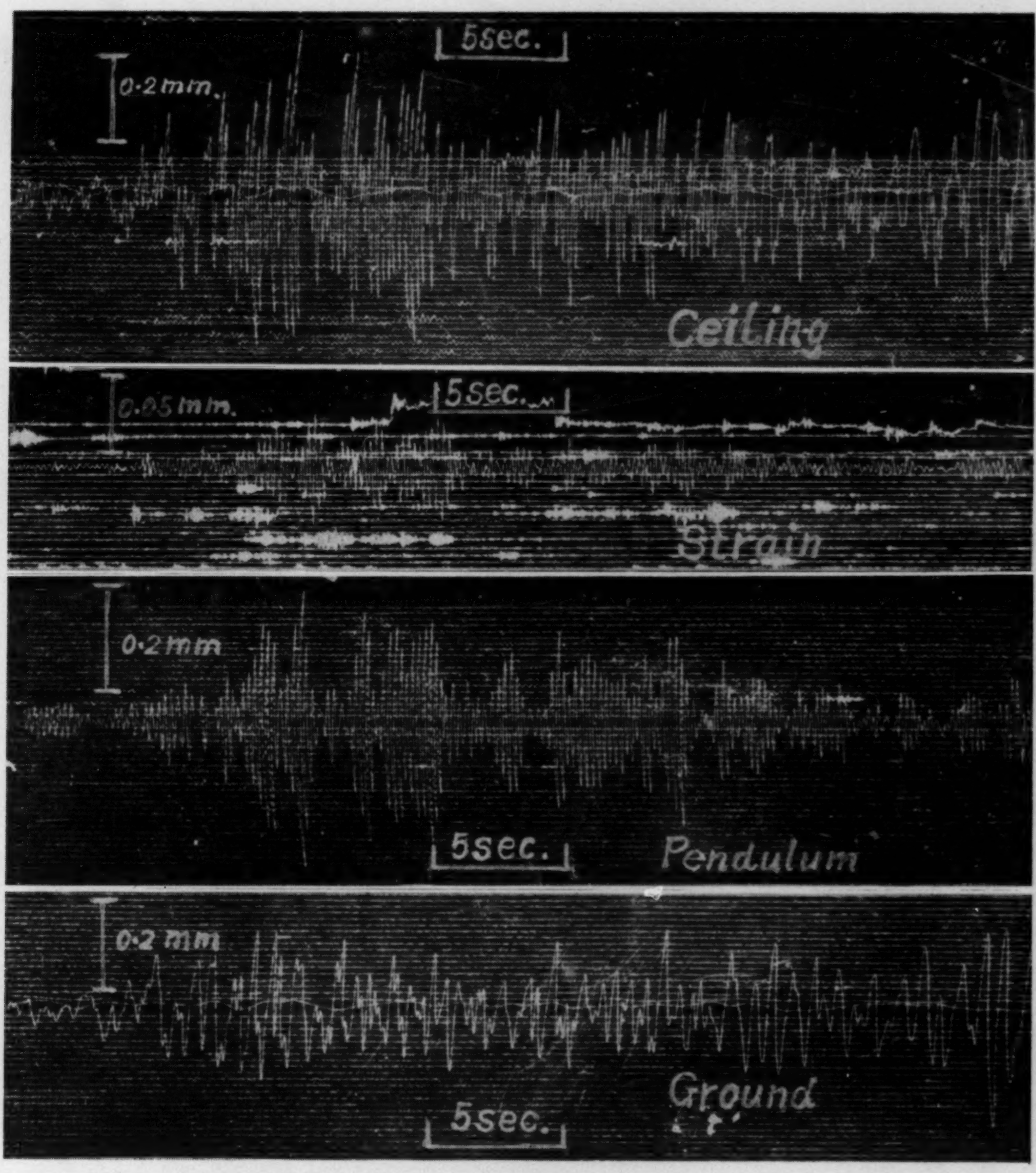

Fig. 6. The representative seismograms.
(Earthquake No. 19) Original × 1.4

（震研彙報 第三十六号 図版 鈴木）

―――所　報―――

◎談話会記事

第 351 回談話会（昭和 33 年 1 月 28 日）

1. 東京都隅田川，神田川，石神井川の水質について
   野口喜三雄
   小野記彦
   杉村行勇
   広川秀夫
2. 近地地震波動の複雑な部分のスペクトル的研究（序報）
   安芸敬一
   堀　実
   辻浦　賢
   後藤健一
3. 土地の脈動と颱風
   岸上冬彦
   小高美江子

第 352 回談話会（昭和 33 年 2 月 25 日）

1. 三原山の噴火にともなう地磁気偏角の変化
   行武　毅
   （力武所員紹介）
   棚岡　巖
   （力武所員紹介）
2. 火山の噴火とその周辺の地殻変動との関係（続報）
   茂木清夫
3. 山形市における土地脈動の三点観測
   岸上冬彦
   志田　勇
   （岸上所員紹介）
   高橋　弘
4. 実在建物の振動実験
   （多数点同時測定の場合）
   金井　清
   田中貞二
   鈴木富三郎
5. 建物の動揺振動と弾性振動
   金井　清
   吉沢静代

第 353 回談話会（昭和 33 年 3 月 25 日）

1. 阿蘇外輪山産の玄武岩について
   松本幡郎
   （森本所員紹介）
2. 最大振巾と震央距離との関係について
   吉山良一
3. 酒田市に於ける土地の脈動の三点観測（続報）
   岸上冬彦
   志田　勇
   （岸上所員紹介）
   高橋　弘

第 354 回談話会（昭和 33 年 4 月 22 日）

1. 古記録による大地震の調査（第 2 報）
   （安政の江戸地震）
   佐山　守
2. 関東地震後の地震活動について
   （その 2）
   浅野周三

3. 庄内平野に於ける土地脈動の三点観測
岸上冬彦
志田勇
（岸上所員紹介）
高橋弘

4. 中部地方における古地磁気学的研究 第1報
（諏訪湖周辺の火成岩類による地質年代に関する研究）
百瀬寛一
小林国夫
（力武所員紹介）
山田哲夫
（力武所員紹介）

5. 北部フオッサ・マグナの構造についての一私見（ムラサメ帯について）
小林国夫
（森本所員紹介）

6. 小諸附近に分布する浅間火山軽石の粒度組成
津屋弘逵
村井勇
細谷与七

第355回談話会（昭和33年5月27日）

1. 脈動をおこす気象条件について（序報）
三東哲夫

2. 地球熱学（第1報）
上田誠也
行武毅
（力武所員紹介）
棚岡巖
（力武所員紹介）

3. プロトン磁力計の試作
（研究組織代表者） 力武常次

4. 一様な磁場中におかれた球の電磁流体振動（続報）
力武常次

5. 電気鉄道列車による地盤振動
金井清
那須信治
田中貞二
森下利三

6. 地下における地震動の研究 第8報
（土地の固有震動の誘起の問題）
金井清
吉沢静代

7. 浅間火山の活動と同火山に発生する地震の研究（続報）
水上武
茂木清夫
内堀貞雄
平賀士郎
宮崎務

8. 三宅島火山の活動性に関する一調査
附話 三宅島北方の群発地震
水上武
平賀士郎
伊東喜久子

9. 第2回 鉢田爆破地震動の観測（其の1）
地震動観測結果
爆破地震動研究グループ
代表者 松沢武雄

10. 第2回 鉢田爆破地震動の観測（其の2）
東北及び関東地方の地殻構造
松沢武雄
松本利松
浅野周三

昭和33年7月15日印刷
昭和33年7月20日発行

東京都文京区本富士町一番地
東京大学構内
編纂兼
発行者　東京大学地震研究所

東京都千代田区富士見町一丁目十番地
印刷者　笠井康頼

東京都千代田区富士見町一丁目十番地
印刷所　株式会社　国際文献印刷社

売捌所
東京都中央区日本橋通二丁目六番地
丸善株式会社

Sold by Maruzen Co., Ltd., Nihonbashi-dôri, Chûô-ku, Tôkyô.
Price of this copy: 580 Yen. (Postage exclusive.)

BULLETIN OF

THE EARTHQUAKE RESEARCH INSTITUTE

UNIVERSITY OF TOKYO

Vol. 36, Part 2. June, 1958.

Contents.

Papers and Reports.

Page

5. K. AKI, M. TSUJIURA, M. HORI and K. GOTÔ, Spectral Study of Near Earthquake Waves (1). (in English) 71
6. K. MOGI, Relations between the Eruptions of Various Volcanoes and the Deformations of the Ground Surfaces around them. (in English) 99
7. M. SHIMA and E. MINAMI, On the Geochemical Study of Carbon 14. (II). Age-dating of Volcanic Product and the Rate of Peat Sedimentation. (in English) 135
8. T. HAGIWARA, A Note on the Theory of the Electromagnetic Seismograph. (in English) 139
9. K. KANAI, F. KISHINOUYE, N. NASU and H. KAWASUMI, Vibration of a Reinforced Concrete Building moved with Vibration Generators. (in English) 165
10. K. KANAI, T. TANAKA and T. SUZUKI, Rocking and Elastic Vibrations of Actual Building. I. (Experiments by Vibration Generator). (in English) 183
11. K. KANAI, T. TANAKA and T. SUZUKI, Rocking and Elastic Vibrations of Actual Building. II. (Observation of Earthquake Motion). (in English) 201
12. F. KISHINOUYE, A Study of the Shōnai Earthquake of 1894. (in Japanese) 227
13. T. SUZUKI, Aseismic Properties of a Wooden House. Part 2. (Observation of Earthquakes) (in Japanese) 235

Institute Notes

(For the papers written in Japanese or in occidental languages, the abstracts are given in occidental languages or in Japanese respectively.)

BULLETIN OF THE EARTHQUAKE RESEARCH INSTITUTE,
UNIVERSITY OF TOKYO. Vol. 36, Part 3. September, 1958.

東京大學
地震研究所彙報

第36號　第3册

昭和33年9月

目次

論文及報告

頁
14. 地球熱学（第1報）日本に於ける地殻内熱流量についての序報（英文）……上田誠也・行武毅・棚岡巌 251
15. 地震動の振幅と周期の関係（英文）……金井清・吉沢静代 275
16. 強震動に関する1つの考察（英文）……金井清 295
17. 砂層の中を伝わる波の波形について（英文）……表俊一郎・小牧昭三・中島直吉（旧姓 小林） 311
18. 大爆破による北関東地方の地殻構造について　其の1　観測報告（英文）……爆破地震動研究グループ 329
19. 大爆破による北関東地方の地殻構造について　其の2　地下構造（英文）……宇佐美竜夫・三雲健・嶋悦三・玉城逸夫・浅野周三・浅田敏・松沢武雄 349
20. 自動水準式振動計（英文）……金井清・田中貞二 359
21. 山形県天童・山形・上ノ山地方の斜長石石英粗面岩及びその関係岩類に関する地質学的考察（英文）……市村毅 369
22. 茨城県筑波地方産変質堆積岩の重鉱物（英文）……市村毅 395
23. 小諸附近に分布する浅間火山軽石の粒度組成（邦文）……津屋弘逵・村井勇・細谷与七 413
24. プロトン磁力計の試作研究（邦文）……文部省科学試験研究費研究班（代表者 力武常次） 433

(The titles in occidental languages are given on the back cover.)

地震研究所彙報は，年4回定期に（ただし，第1号より第6号までは不定期に，第7号は3冊として刊行された），彙報別冊は不定期に刊行される．

この彙報に載せられた論文及び報告についての責任は，すべてその著者のみにある．

この彙報についての照会通信は，すべて東京大学地震研究所長にあてられたい．

The Bulletin is published quarterly. (Vols. 1–6 were published at irregular intervals and Vol. 7 consisted of three parts.)
Supplementary Volume is published at irregular interval.

The authors of the papers alone are responsible for the statements and opinions contained in their respective papers.

All communications relating to this Bulletin should be addressed to the Director of the Earthquake Research Institute, University of Tokyo, Japan.

Earthquake Research Institute, University of Tokyo
Address:
No. 1, Motofuji-cho, Bunkyo-ku,
Tokyo Metropolis, Japan.
Telephone: 92-3161-Extension 6506
Cable address: ZISINKEN, TOKYO.

東京大学地震研究所
所在地
東京都文京区本富士町一番地
電話　小石川 92—3161（代）構内 6506
電略　ブンケウ　トウダイ　ヂシン

BULLETIN OF THE EARTHQUAKE
RESEARCH INSTITUTE
Vol. 36 (1958), pp. 251-273

14. *Studies of the Thermal State of the Earth. The First Paper: Preliminary Report of Terrestrial Heat Flow in Japan.*

By Seiya UYEDA, Takesi YUKUTAKE and Iwao TANAOKA,

Earthquake Research Institute.

(Read May 27, 1958.—Received June 30, 1958.)

Summary

Determination of terrestrial heat flow in Japan has been attempted for the first time. Geothermal gradient, uncorrected, in the Sasago tunnel, Yamanasi Prefecture, central Japan, is $2.°71 C/100\,m$ and the mean thermal conductivity of the rocks penetrated by the tunnel is 7.61×10^{-3} *cal/cm sec °C*, giving the amount of heat flow of 2.06×10^{-6} *cal/cm² sec*. This and a few other preliminary results indicate that heat flow in Japan is greater than the global average determined so far, *i.e.* 1.2×10^{-6} *cal/cm² sec*. It seems, however, in spite of the active seismicity and volcanism of the Japanese Islands, unlikely that the order of magnitude of heat flow is different from the global average, except in areas close to active volcanoes.

1. Introduction

Importance of terrestrial heat flow in geophysics has been recognized for many years and its measurements have been practised in various parts of the world[1]. It seems to be an established fact that, while thermal gradients range from 5 to $70°C/km$, the amount of heat flow measured at various places of various geological environments falls within a small range, *i.e.* 1.2×10^{-6} *cal/cm² sec* $\pm 50\,\%$. As for the possible relation between the heat flow and the local state of the earth's crust, past or present, very little has been made definite[2],[3]. It may, however, be anticipated that where physical and chemical processes in the crust are active the amount of heat flow should be also greater, because the energy source originating these processes should mainly be the heat flowing out of the interior. This inference makes the determination of heat flow in Japan considerably significant, since the Japanese Islands are placed in one of the regions where igneous and seismic activities are most remakable in the world. To the author's knowledge, however, measurement of terrestrial heat flow has never been attempted in Japan. We are intending to perform a series of such measurements at as many localities as possible in Japan, so that overall thermal regime as well as local thermal anomalies of this geologically and geophysically active region can be clarified. In the present paper, a few preliminary results of thermal measurements set out along the above mentioned line will be reported.

---

[1] F. BIRCH, *Geophysics*, **19** (1954), 645.

[2] F. BIRCH, *Bull. Geol. Soc. Amer.*, **61** (1950), 567.

[3] E. C. BULLARD, A. E. MAXWELL and R. REVELLE, *Advances in Geophys.*, Academic Press Inc., **3** (1956), 153.

Fig. 1 shows the localities where the geothermal gradient has been determined, so far, without any topographic correction. Although there are many other places where the geothermal gradient was determined, in the past, there seems to be very little possibility of obtaining rock samples of which the thermal conductivity should be measured. In our studies, the temperature measurements are conducted by measuring the thermal variation of electrical resistance of pre-calibrated thermistors sealed in a pressure- and water-tight container. When calibration is made satisfactorily, it is easy to measure the temperature with an accuracy of 0.°1*C*, by an ordinary Wheatstone bridge.

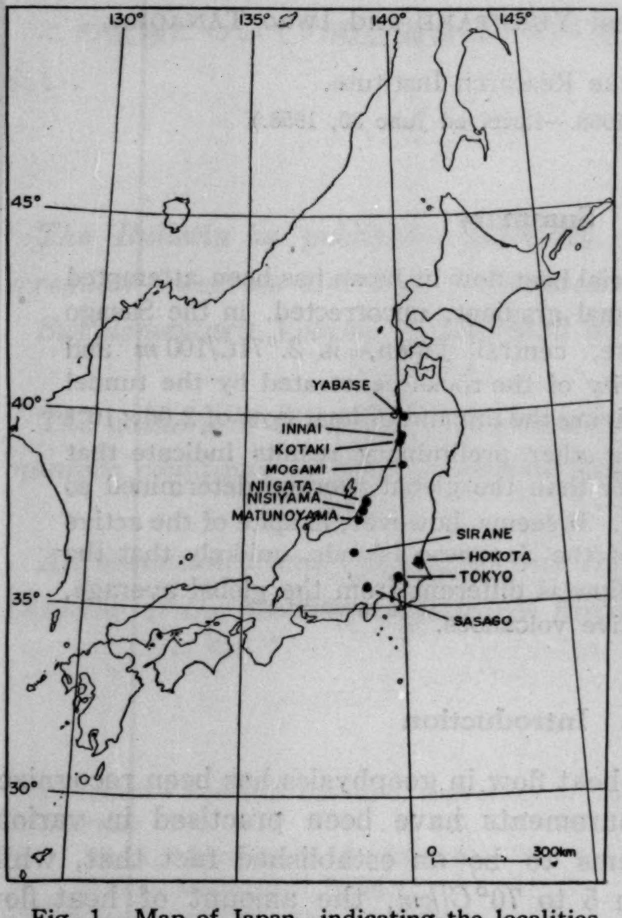

Fig. 1. Map of Japan, indicating the localities where the geothermal gradient have been determined.

The measurement of thermal conductivity of rocks has been made by the divided-bar method. The apparatus used, being very similar to that of Benfield[4], is illustrated in Figs. 2 and 3. For the temperature measurements at the points A, B, C, D, E, F and G, alumel-chromel thermo-junctions, 0.2 *mm* in diameter, are used. Thermo-electric characteristics of the individual junctions were ascertained to be close to each other, *i.e.* to a few *microvolts* at the temperatures concerned (<150°*C*).

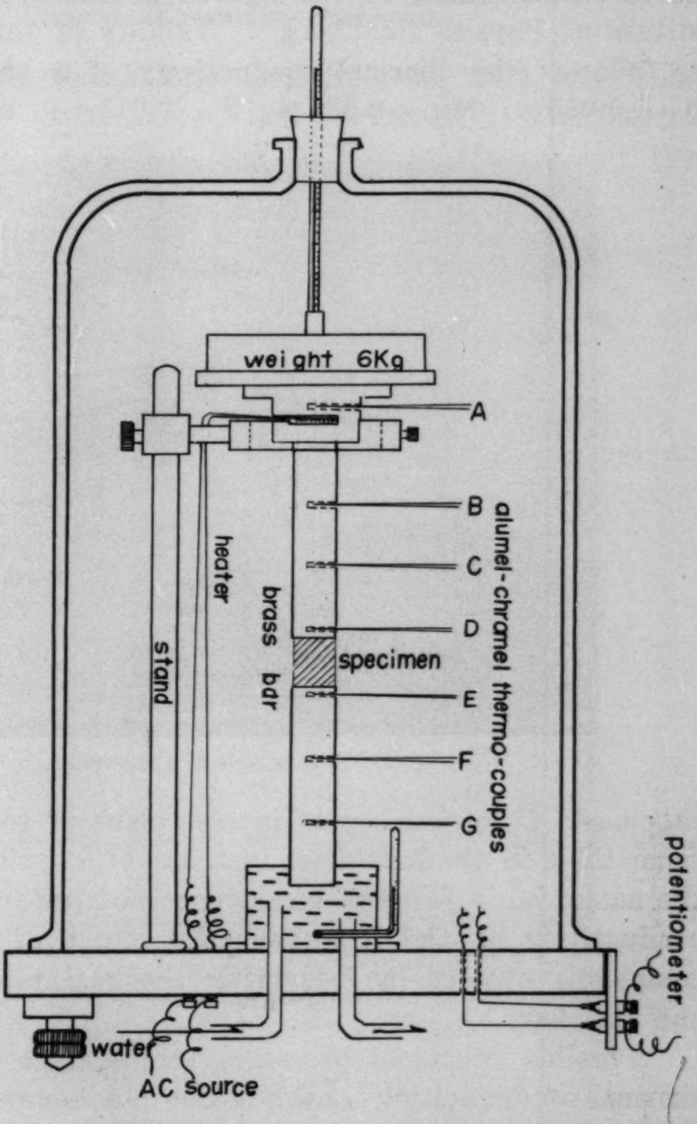

Fig. 2. Divided-bar device for measurement of thermal conductivity of rocks.

The rock specimens were cut in a form of disk, of which the diameter is one *inch*. Both surfaces of the disk were carefully made parallel by polish: Mr. T. Watanabe of the Earthquake Research Institute, Tokyo University has kindly undertaken the work of polishing. Results of thickness measurement by a micrometer indicated that the maximum difference in thickness measured at various parts of a disk never exceeds 1/50 *mm*.

To eliminate the inevitable inter-surface temperature drops between the sample and the brass bars, measurements were made on disks of different thickness. Mixture of vaseline and glycerin was used to improve the thermal

---

4) A. E. BENFIELD, *Proc. Roy. Soc.* A, **173** (1939), 428.

contact at the interfaces. Examples of actual measurements will be shown in Fig. 7.

The thermal conductivity of the brass (yellow) bars was assumed, tentatively in the present preliminary report, to be 0.218 *cal/cm sec °C* at 20°*C*, according to the figures in Table 4*g*–2 of the American Institute of Physics Handbook⁵⁾. Validity of this value has been checked as follows: the thermal conductivity of a bar of chemically pure iron (C···0.015 %, Mn···0.085 %, S···0.011 %) was measured to be 0.161 *cal/cm sec °C* by putting it in the place of rock specimen, whereas the same table in the American Institute of Physics Handbook gives exactly the same value for the conductivity of pure iron. In determining the conductivity of the iron bar, the effect of interface drop has been completely avoided by measuring the real temperature gradient within the iron bar.

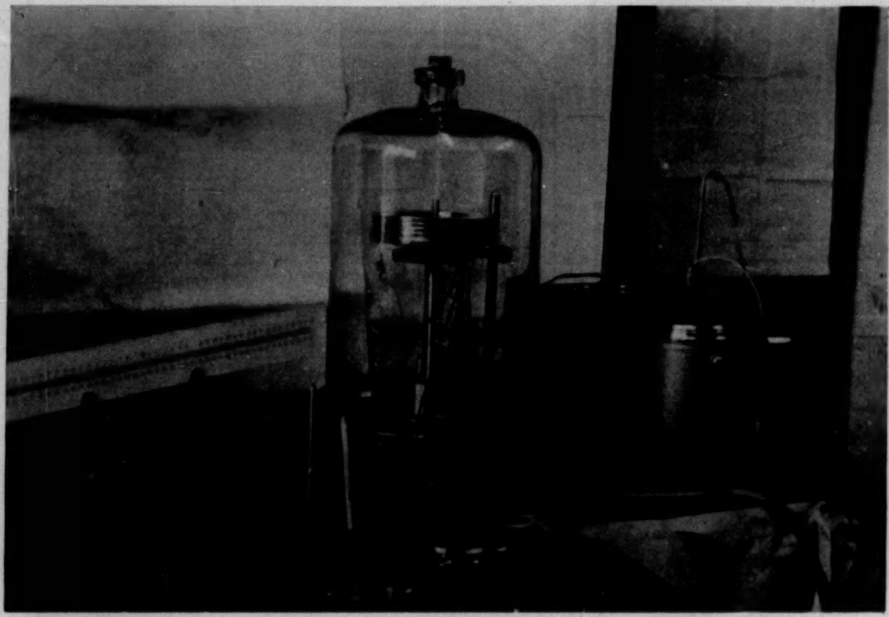

Fig. 3. Photograph of the divided-bar apparatus.

Possible effects of pressure, temperature and water content on the thermal conductivity6),7), have not been adequately taken into account. In most cases dealt within the present study, these effects may be considered as negligible in view of the accuracy of the conductivity measure-

---

5) W. E. FORSYTHE and R. L. POWELL, *Amer. Inst. Phys. Handbook*, Mcgrawhill (1957).

6) F. BIRCH, *Handbook of Physical Constants*, Geol. Soc. Amer. Sp. Papers No. 36 (1954).

7) F. BIRCH and H. CLARK, *Amer. Journ. Sci.*, **238** (1940), 529.

ment at the present stage. Care was taken, however, to keep the mean temperature of specimens during measurement close to their temperature *in situ*. It is planned to deal with these various corrections in future studies.

2. Sasago Tunnel, Yamanasi Prefecture

The late Professor A. Tanakadate measured, in 1902, the rock temperature in the Sasago tunnel, Yamanasi Prefecture[8]. The Sasago tunnel is a railway tunnel connecting (Fig. 4) Sasago Village, on the

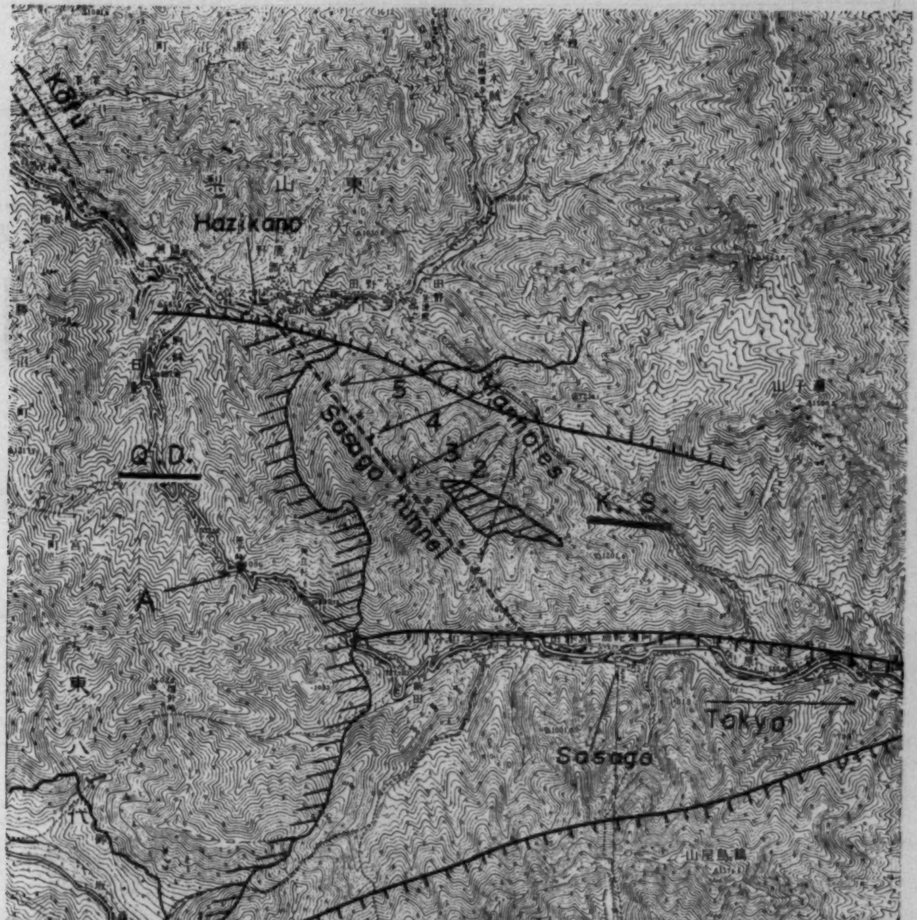

Fig. 4. Map of the Sasago-tunnel. Unhatched part between the faults and the hatched part show the areas where the Kobotoke Series and the quartz-diorite are exposed.

---

[8] A. Tanakadate, *Rep. Imp. Earthq. Invest. Committ.*, **45** (1903), 17.

Table I. Results of temperature measurement in the Sasago Tunnel, after A. Tanakadate[8].

(Table 1 continued)

date	distance from south-east portal	No. 1 960 *m*	No. 2 1707 *m*	No. 3 2323 *m*	No. 4 2933 *m*	No. 5 3693 *m*
May	18, 1902		19.4		18.1	
	19		19.5		18.1	
	20		19.5		18.0	
	21		19.1		18.0	
	22		19.0		18.0	
	23		19.0			
	24					
	25		19.5		18.0	
	26		19.5		18.0	
	27		19.5		18.0	
	28		19.5		18.0	
	29		19.5		18.0	
	30		19.5			
	31				17.4	
June	1	18.0			17.6	
	2	18.0			17.8	
	3	17.9			17.8	
	4	17.8			18.0	
	5	17.8			18.1	
	6					
	7	18.0		19.4		
	8	17.9		19.2		
	9	17.9		19.2		
	10	17.9				
	11	17.9				
	12	17.9				
	13	17.9				
	14	17.9				
	15	18.0				
	16	17.8				
	17					
	18					
	19			18.7		
	20			18.7		
	21			18.7		
	22			18.6		
August	22		20.1		18.4	
	23		20.1			
	24		20.1			
	25					
	26		20.1			
	27		20.1			
	28		20.1			
	29		20.1			
	30		20.1			
	31		20.1			
September	2		20.0			
	3		20.0			
	4		20.0			
	5		20.0			
	6		20.0			
	18				18.3	
	19				18.3	
	20				18.2	
	21				18.2	
	22				18.2	
	24				18.5	
	25				18.4	
	26				18.2	
	27				18.1	
	28				18.1	
	30				18.3	
October	1				18.0	
	2				18.0	
	3				18.0	
	4				18.1	
	5				18.3	

June	23			18.6		
	24			18.6		
July	2					13.5
	3					13.4
	4					13.4
	5					13.3
	6					13.2
	7					
	8					12.5
	9					12.5
	10					12.5
	11					12.5
	12					12.4
	13					13.4
	25		20.8			16.4
	26		20.8			16.4
	27		20.8			16.4
	28		20.7			16.4
	29		20.7			16.4
	30		20.7			16.4
August	1	19.7				16.4
	2	19.7				16.4
	3	19.6				16.4
	4	19.6				16.4
	5	19.6				16.3
	6					
	7	19.4				16.3
	8	19.4				16.2
	9	19.4				16.2
	10	19.4				16.3
	11	19.4				16.0
	12	19.5				16.2
	13					
	14		20.4			16.5
	15		20.3			16.5
	16		20.3			16.5
	17		20.2			16.5
	18		20.1			16.4
	19					
	20		20.1		18.5	
	21		20.1		18.5	
October	7				18.0	
	8				17.9	
	9				17.9	
	10				17.9	
	11				18.0	
	12				18.1	
	14			19.5		
	15			19.3		
	16			19.0		
	17			19.0		
	18			19.0		
	19			19.4		
	21			19.4		
	22			19.0		
	23			18.9		
	24			18.6		
	25			18.6		
	26			18.6		
	28			18.4		
	29			18.3		
	30			18.1		
	31			18.0		
November	1			17.9		
	2			17.8		
	3					
	4			17.5		
	5			17.6		
	6			17.7		
	7			17.7		
	8			17.7		
	9			17.7		
Mean temperature		18.7	20.1	18.7	18.1	15.3
Mean surface temperature		10.0	10.0	10.0	10.0	10.0
Depth (*m*)		302	412	479	320	137
ΔT (°C)/Δh (100 *m*)		2.88	2.45	1.82	2.53	3.86

(to be continued)

south-east side, with Hazikano Village on the north-west. It was driven from both ends between 1896 and 1902 and its length from portal to portal is 4647 *m*. There are five large manholes at distances from the east-south portal 960 *m*, 1707 *m*, 2323 *m*, 2933 *m* and 3693 *m*. The measurement of the rock temperature in the tunnel was conducted in the dynamite-storeroom in these large manholes by automatic recording thermometers, concurrently with the completion of the construction. The thermometers were placed in small holes drilled horizontally on the wall of the dynamite-storeroom. The length and width of the small holes were about five *feet* and one *foot*. The results of the temperature measurement are reproduced in Table 1. The measured mean temperature profile and the topographic section of the tunnel are reproduced in Fig. 5. The isothermal contours are due to A. Tanakadate, too.

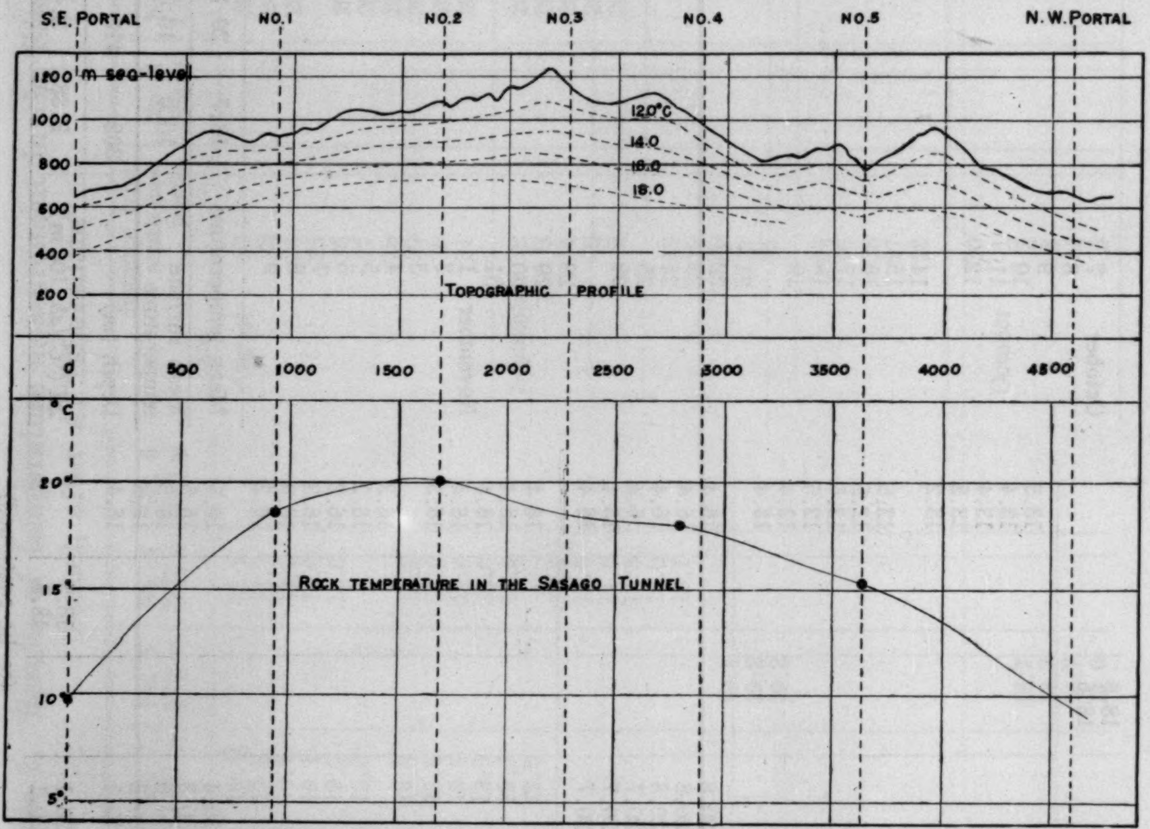

Fig. 5. Topographic profile and the temperature profile of the Sasago-tunnel, after A. Tanakadate.

The outline geology of the district is as follows: as the geological map in Fig. 4 shows, folded beds of sandstone and clayslate of Kobotoke

Series which is probably of Cretaceous age are dominently exposed in the area. These sedimentary rocks were intruded by stocks of the Misaka quartz-diorite of the middle Tertiary age and were metamorphosed to hornfels near the contact.

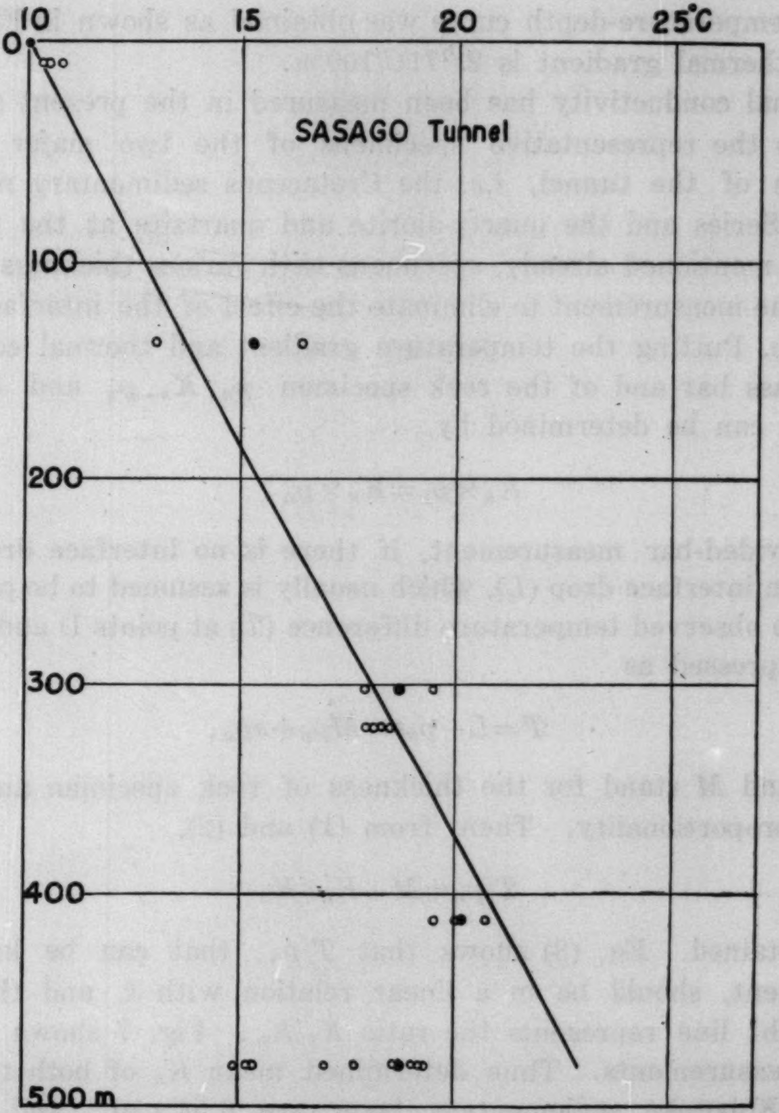

Fig. 6. Temperature-depth curve of the Sasago-tunnel, after A. Tanakadate.

Now the annual mean surface temperature was determined to be 10.°0*C* based on the results of continuous measurement of temperature in a cave, about 10 *m* deep and 1 *m* wide, at the highest point of the high-way at the Sasago-pass (point A in Fig. 4), and in a shaft, 30 *m* deep, at the north-west portal of the tunnel. Both measurements gave the mean annual temperature 10.°3C and 9.°7C respectively. As the amplitude of annual variation of the surface soil was considered to be less than 0.°5C, the mean surface temperature was taken to be 10.°0C everywhere tentatively.

The temperature-depth curve was obtained as shown in Fig. 6. The mean geothermal gradient is 2.°71$C/100\,m$.

Thermal conductivity has been measured in the present study with regards to the representative specimens of the two major geological formations of the tunnel, *i.e.* the Cretaceous sedimentary rock, called Kobotoke Series and the quartz-diorite and quartzite at the north-west part. As mentioned already, specimens with various thickness have been used for the measurement to eliminate the effect of the interface temperature drop. Putting the temperature gradient and thermal conductivity of the brass bar and of the rock specimen p_B, K_B, p_R and K_R respectively, K_R can be determined by

$$K_B\times p_B=K_R\times p_R\ , \qquad (1)$$

in the divided-bar measurement, if there is no interface drop. When there is an interface drop (L), which usually is assumed to be proportional to p_B[9], the observed temperature difference (T) at points D and E (Fig. 2) can be expressed as

$$T=L+p_Rs=Mp_B+sp_R\ , \qquad (2)$$

where s and M stand for the thickness of rock specimen and the constant of proportionality. Then, from (1) and (2),

$$T/p_B=M+K_Bs/K_R \qquad (3)$$

can be obtained. Eq. (3) shows that T/p_B, that can be known from measurement, should be in a linear relation with s, and the slope of the straight line represents the ratio K_B/K_R. Fig. 7 shows the results of the measurements. Thus determined mean K_R of both the diorites and the Kobotoke sediementary layer are 6.54×10^{-3} and 8.67×10^{-3} $cal/cm\,sec\,°C$. Taking the mean of these two values the approximate value of the heat flow at the Sasago tunnel is estimated to be 2.06×10^{-6} $cal/cm^2\,sec$. This value is considered as giving, though no topographic corrections have been made, the rough value of heat flow in the area.

---

[9] A. E. BENFIELD, *loc. cit.*

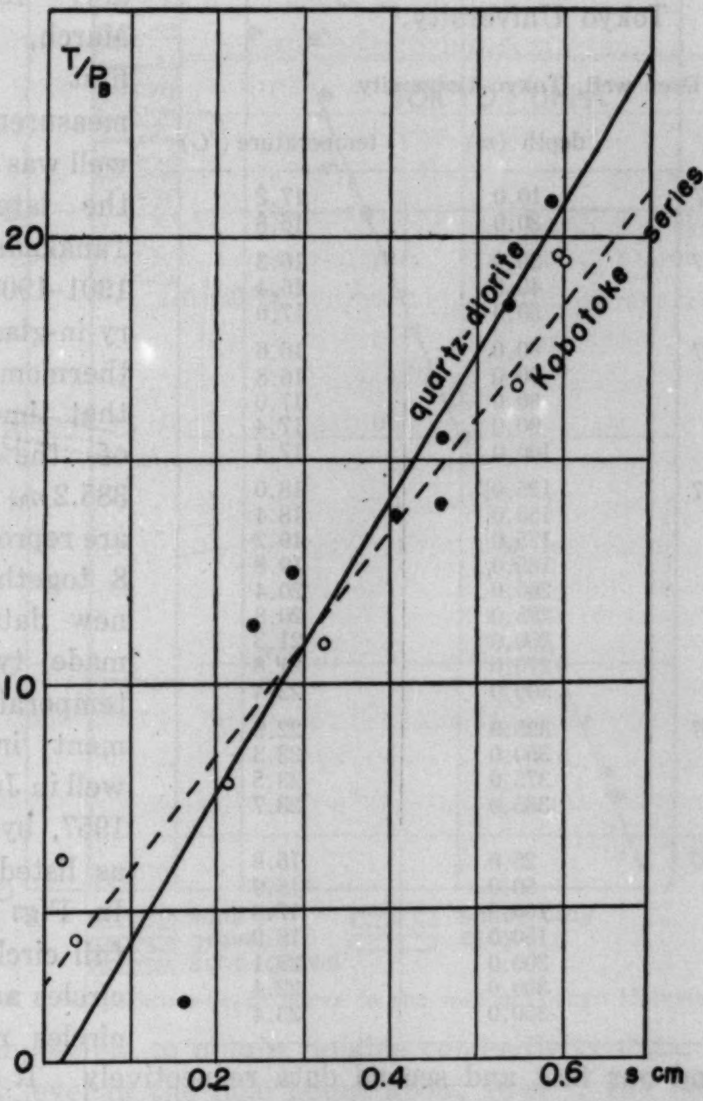

Fig. 7. Examples of conductivity measurement: specimens are the Kobotoke Series hornfels (hollow circles) and the quartz-diorite (full circles).
ordinate.... ratio of temperature drop between *D* and *E* (Fig. 2) to temperature gradient in brass-bars.
abscissa.... thickness of specimen.

3. Deep-well in Tokyo University, Tokyo

The deep well in Tokyo University was drilled under the sponsorship of Shinsai Yobo Chosakai (Imperial Earthquake Investigation Com-

Table 2. Temperature in the deep-well, Tokyo University.

Deep well, Tokyo University		
date	depth (m)	temperature (°C)
June 1, 1957	10.0	17.2
	20.0	16.8
June 2, 1957	30.0	16.3
	40.0	16.4
	50.0	17.0
June 3, 1957	60.0	16.6
	70.0	16.8
	80.0	17.0
	90.0	17.4
	100.0	17.4
June 4, 1957	125.0	18.0
	150.0	18.4
	175.0	19.2
	185.0	19.8
	200.0	20.4
	225.0	20.8
	250.0	21.3
	275.0	21.8
	300.0	22.4
June 5, 1957	325.0	22.9
	350.0	23.3
	375.0	23.5
	385.0	23.7
July 15, 1957	25.0	16.6
	50.0	16.9
	100.0	17.8
	150.0	18.9
	200.0	20.1
	300.0	22.4
	350.0	23.4

mittee) from 17 February, 1894, to 28 March, 1898. The first temperature measurement in the well was conducted by the late Prof. A. Tanakadate during 1901–1903, by mercury-in-glass maximum thermometers[10]. At that time, the depth of the well was 385.2 m. His results are reproduced in Fig. 8 together with our new data. We have made two series of temperature measurement in the same well in June and July, 1957, by thermistors, as listed in Table 2. In Fig. 8, the large full circles, small full circles and the double circles represent Tanakadate's and our first and second data respectively. It appears to be notable that the data taken at times about 50 years apart coincide almost perfectly. The mean geothermal gradient is $2.^{\circ}2\,C/100\,m$.

The geological column disclosed at the time of drilling is as shown in Fig. 8[11]. Tokyo area belongs geologically to the Kanto Structural Basin, where the ground has subsided since late Miocene. Most of the sand, clay and gravel penetrated by the well are probably the Quaternary marine sediments.

As the specimens now available are all dried sand, clay or gravel-sand, their water content *in situ* can not be assessed with certainty, it

---

[10] A. TANAKADATE, *loc. cit.*

[11] N. YAMAZAKI, *Rep. Imp. Earthq. Invest. Committ.*, **20** (1898), 4.

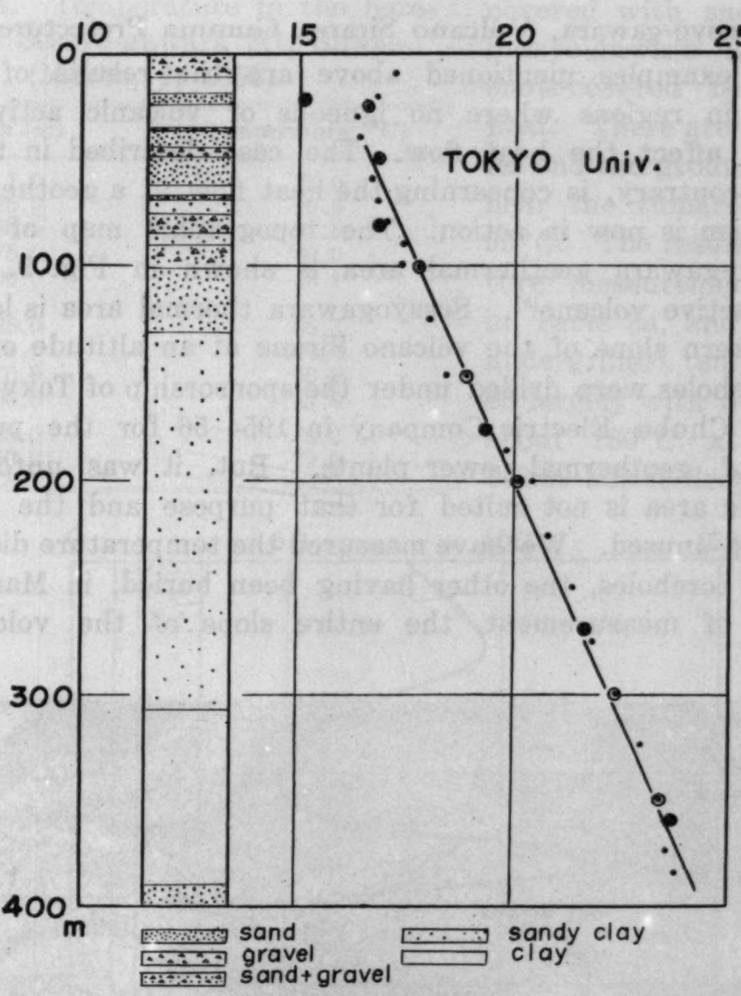

Fig. 8. Temperature-depth curve in the well at Tokyo University.

seems to be impossible to obtain reliable conductivity data. The underground water level in the hole being about 10 *m*[12], the beds are likely in a completely soaked state. Only for trial, we made disks of the clay taken at 255 *m* ~ 276 *m* by a press for the conductivity measurement. The weight applied for the press were 50 *kg* (two disks) and 100 *kg* (one disk) *per* 0.78 $inch^2$ (9.87 kg/cm^2 and 19.7 kg/cm^2) respectively. The preliminary measurement was conducted in dry state and gave the conductivity 1.99×10^{-3} *cal/cm sec°C*. Effects of the pressure and water content on the thermal conductivity of such specimens will be studied in the future. The present provisional value of thermal conductivity leads to the provisional heat flow in the well of 0.44×10^{-6} $cal/cm^2\ sec$, which is rather small. Of course this value can not be very plausible.

---

[12] K. MAEDA, *Zisin*, **6** (1934), 275.

4. Sessyo-gawara, Volcano Sirane, Gumma Prefecture

The two examples mentioned above are the results of thermal measurement in regions where no igneous or volcanic activities are considered to affect the heat flow. The case described in this paragraph, on the contrary, is concerning the heat flow at a geothermal area where volcanism is now in action. The topographic map of the area around Sessyo-gawara geothermal area is shown in Fig. 9. Volcano Sirane is an active volcano¹³⁾. Sessyogawara thermal area is located on the south-eastern slope of the volcano Sirane at an altitude of 1600 *m*. Two deep boreholes were drilled under the sponsorship of Tokyo Electric Company and Chubu Electric Company in 1954–56 for the purpose of development of geothermal power plants. But, it was unfortunately found that the area is not suited for that purpose and the boreholes have been left unused. We have measured the temperature distribution in one of the boreholes, the other having been buried, in March, 1958. At the time of measurement, the entire slope of the volcano was

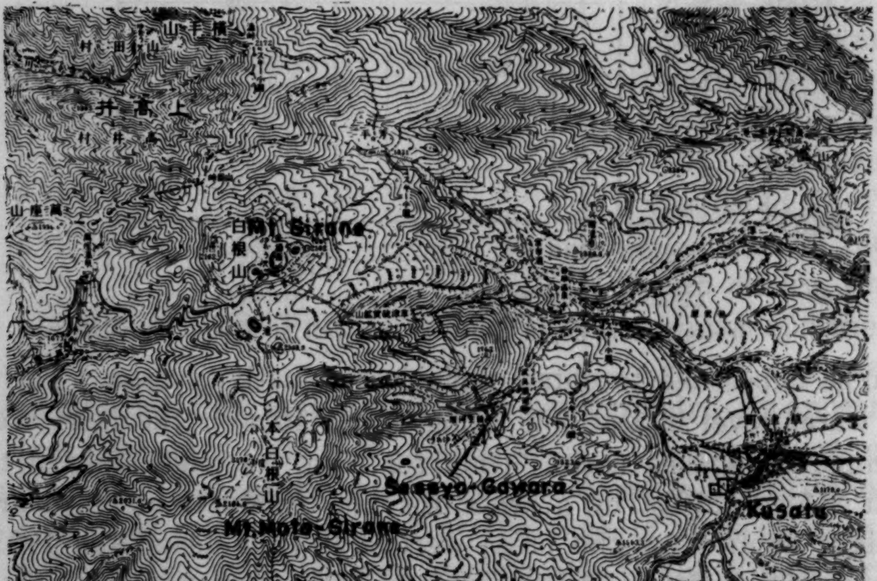

Fig. 9. Map around the Sessyo-gawara geothermal area.

---

13) T. MINAKAMI, K. MATUSITA and S. UTIBORI, *Bull. Earthq. Res. Inst.*, **20** (1942), 505.

covered with snow. But, the Sessyo-gawara area was not snow-covered because of the heat. There are many fumaroles and the ground temperature near the fumaroles was about 90°*C*. The results of temperature measurement are shown in Table 3a, and Fig. 10: the underground temperature varied largely with depth reaching about 130°*C* at a depth of 140 *m* but it dropped to about

Table 3a. Temperature in the borehole at Sessyo-gawara Mt. Sirane. (March, 4, 1958).

depth (*m*)	temperature (°*C*)
1.0	78.0
25.0	90.5
50.0	91.8
75.0	60.0
100.0	48.1
125.0	66.3
150.0	130.0
170.0	59.8
200.0	68.6
225.0	76.2
250.0	79.0

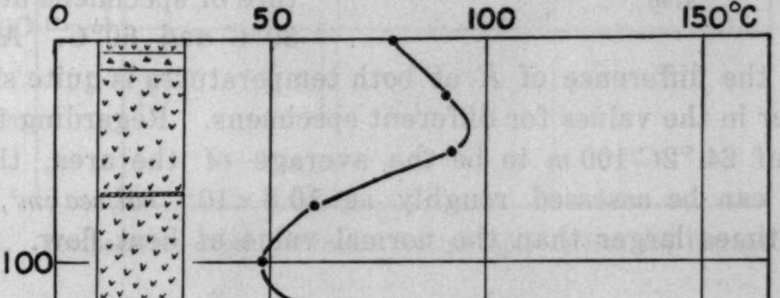

Fig. 10. Temperature-depth curve in the borehole at the Sessyo-gawara.

60°C at 170 m. Below 170 m, the gradient was approximately constant down to 250 m, *i.e.* 24.°2C/100 m. This value is about 10 times as large as those at the previous two localities. The large fluctuations in temperature above 170 m may be considered as caused by contacting of the borehole with the veins carrying the hot vapour. The thermal conductivities of 10 core samples from various depths have been measured. In this case, the measurements were conducted by keeping the mean temperature of specimens at both about 30°C and 60°C. As listed in Table 3b, the difference of K at both temperatures is quite smaller than the scatter in the values for different specimens. Regarding the thermal gradient of 24.°2C/100 m to be the average of the area, the value of heat flow can be assessed roughly as 10.8×10^{-6} *cal/sec cm*², which is about 10 times larger than the normal value of heat flow.

Table 3b. Thermal conductivity of andesites in the borehole at Sessyo-gawara.

depth (m)	K(10^{-3}*cal/cm sec°C*)	mean temerature at measurement
165–168	3.91	60°C
168–181	4.19	30
168–181	4.70	60
218–222	6.23	30
253–260	3.35	30
mean	4.48	

5. Borehole in Hokota, Ibaragi Prefecture

In August, 1957 the Research Group for Explosion Seismology made an explosion in specially drilled boreholes in the site of a disused airfield at Hokota, Ibaragi Prefecture. On that occasion the Research Group for Explosion Seismology kindly drilled an additional borehole, about 70 m deep, at the authors' request, at a distance of about 400 m from the explosion point. The drilling was made on 20 August, and the temperature measurement was repeated on 20 and 26, August and on 11, October, 1957. The results shown in Fig. 11 show that the temperature in the hole was about 19.°5C just after the drilling and became about 14.°5C after a week and changed no more thereafter. This may indicate that the temperature was first governed mainly by the temperature of water circulating in the operation of drilling and settled fairly rapidly. There seems to be no significant downward increase of temperature in the hole. These facts are probably due to natural circulation of underground water. In fact, the bed penetrated by the hole is loose sand filled with water.

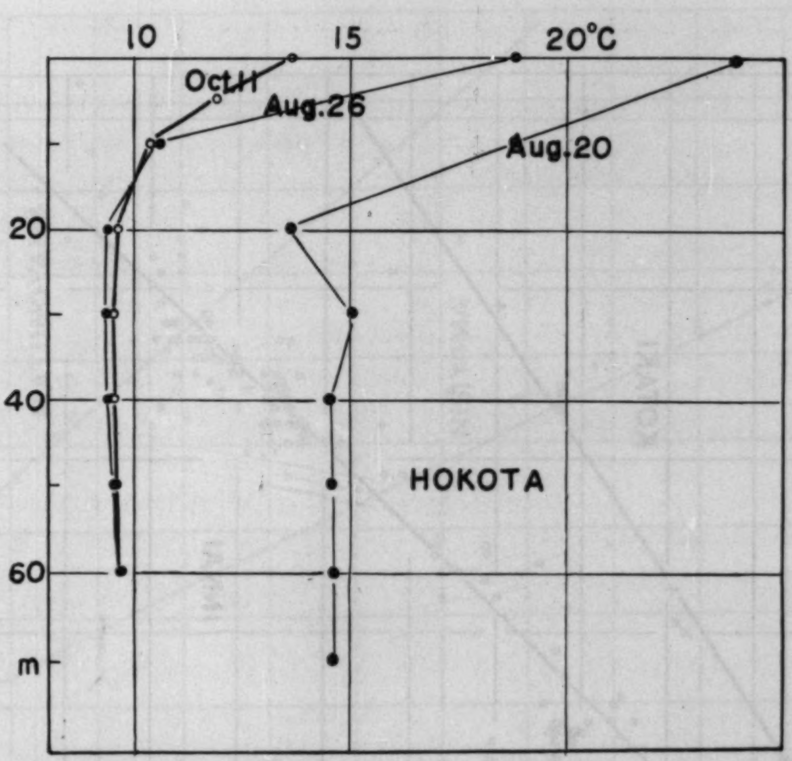

Fig. 11. Temperature-depth curves in the borehole at Hokota, Ibaragi Pref.

6. Temperatures in Oil-wells

There are many oil-fields in Akita, Yamagata and Niigata Prefectures in north-eastern Honsyu. Through the kindness of the Teikoku Oil Company, we had an opportunity of examining the records of the bottom temperatures, taken by the Company for many years, of many of the oil-wells in nine oil-fields and one gas-field (Fig. 1). The temperature measurements, according to the concerned in the Company, were made at various occasions: mostly about 20 *hours* after stopping of drawing of oil or water and normally only at the bottom of the wells by means of either a maximum mercury-in-glass thermometer or an "Amerada" type gas thermometer.

We have plotted all the available data against depth for each oil-field as shown in Figs. 12–17. Considering the above stated conditions of measurement, the individual points in the figures are not to be regarded as very significant. But the ensemble of the data in each figure may represent the approximate mean temperature distribution under each oil-field. Of course, when the number of data is small as

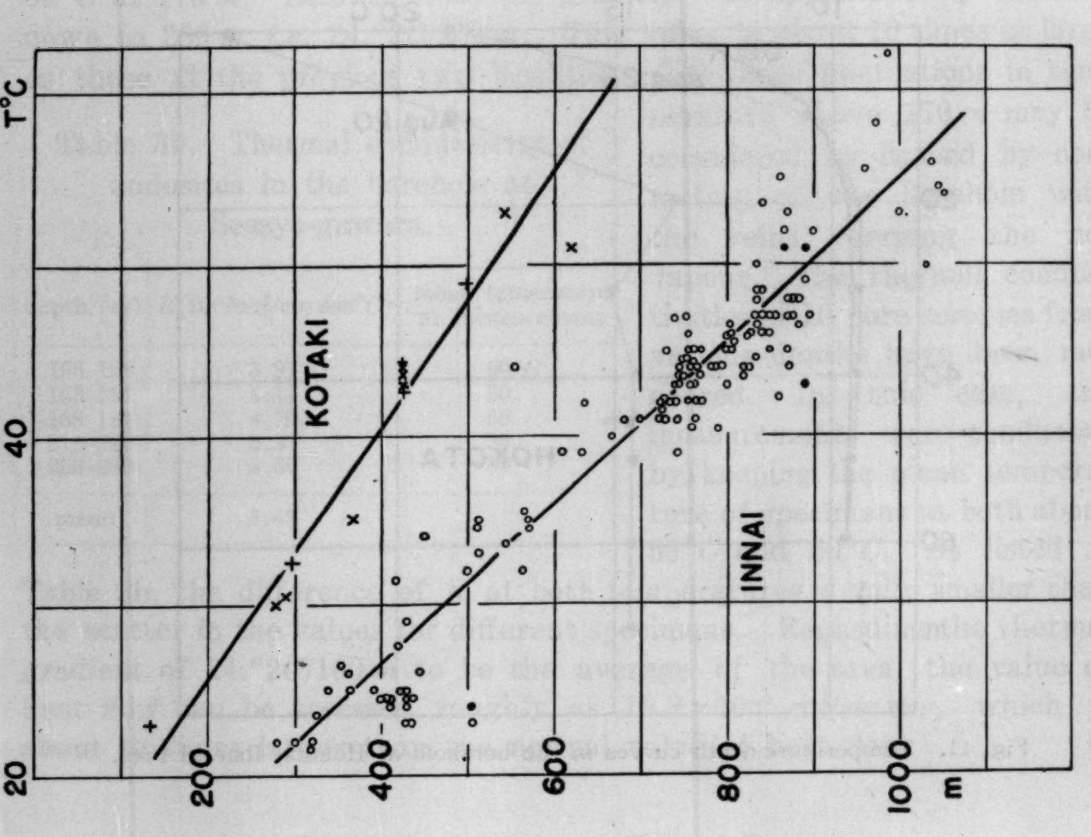

Fig. 13. Temperature-depth curve in oil-wells at the Innai and Kotaki oil-fields.

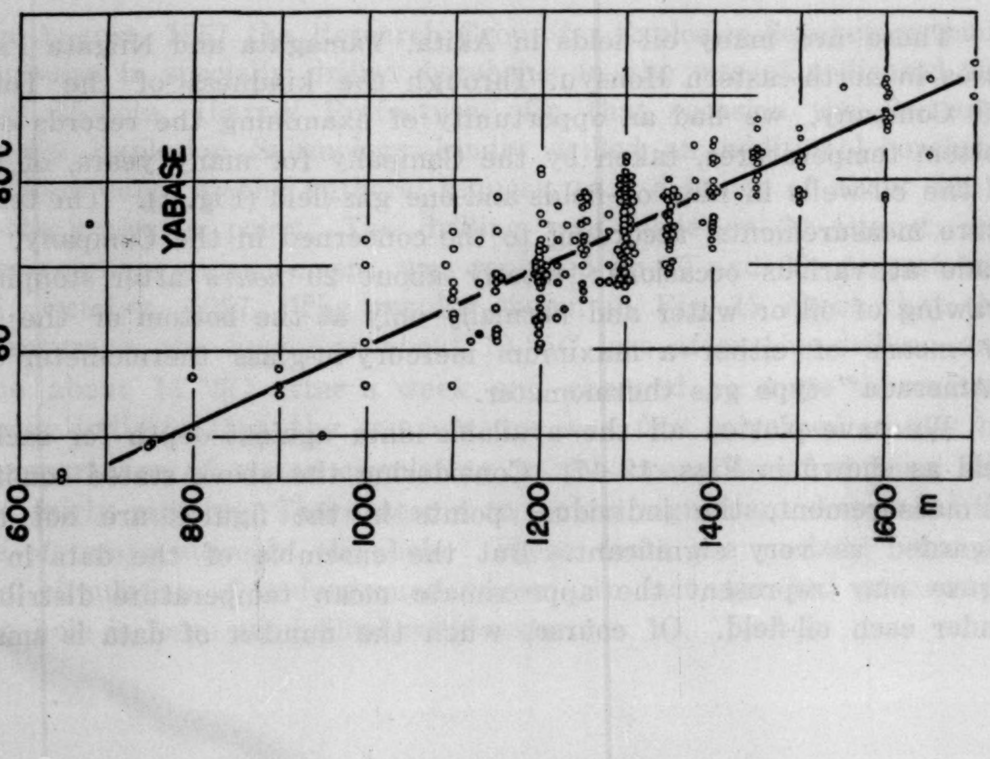

Fig. 12. Temperature-depth curve in oil-wells at the Yabase oil-field.

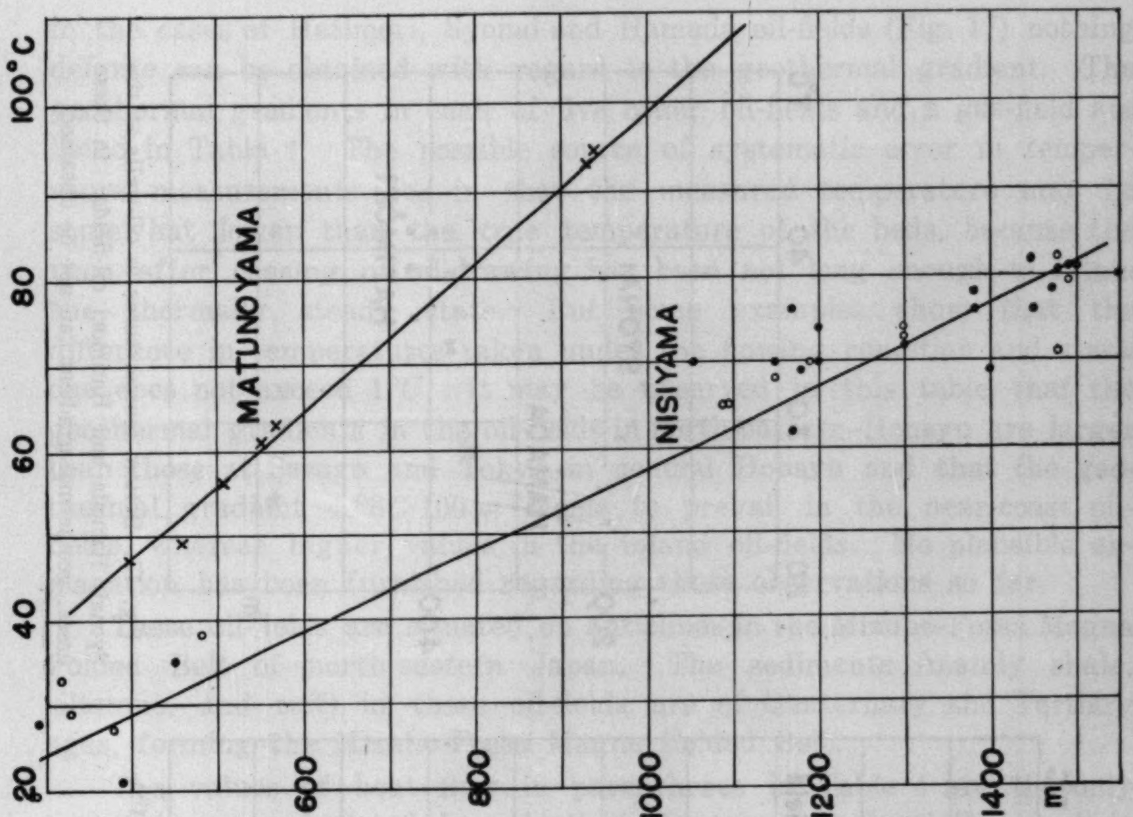

Fig. 15. Temperature-depth curves in oil-wells at the Nisiyama and Matunoyama oil-fields.

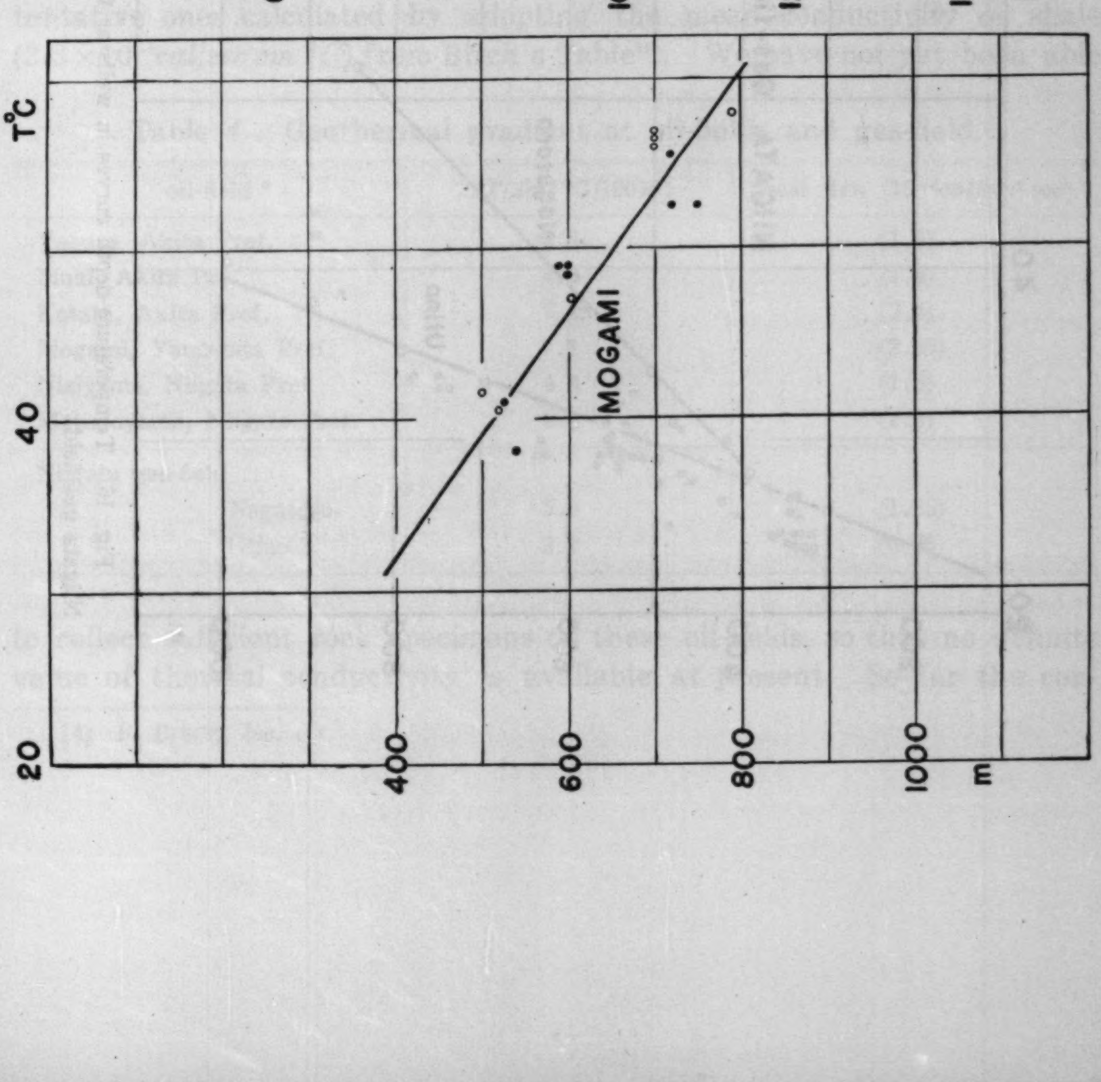

Fig. 14. Temperature-depth curve in oil-wells at the Mogami oil-field.

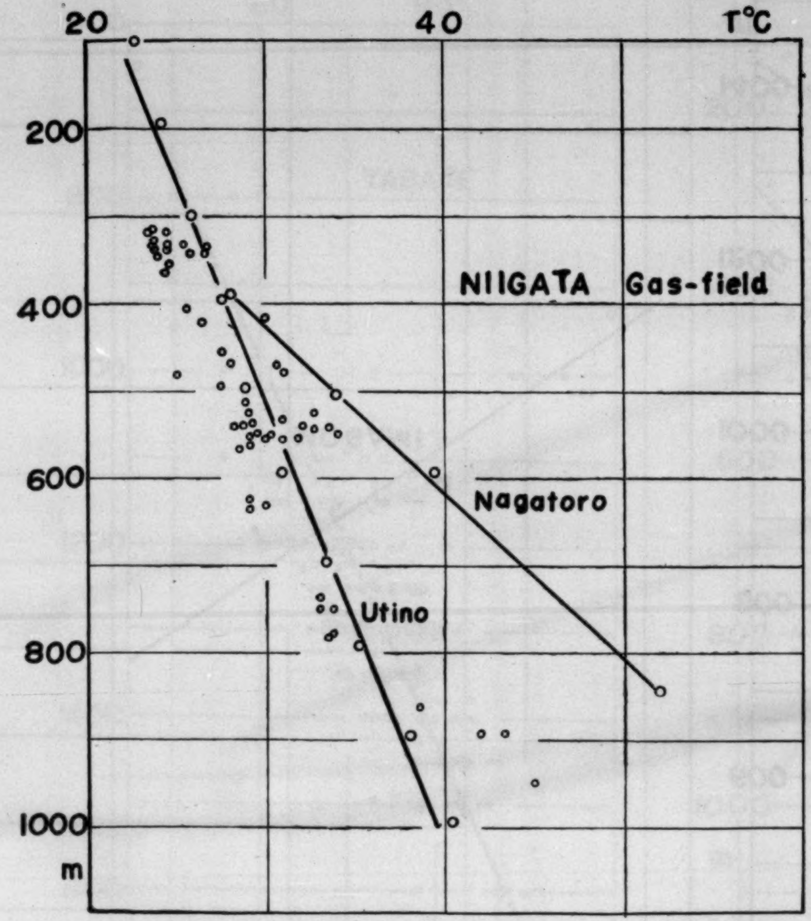

Fig. 16. Temperature-depth curves in wells at the Niigata gas-field.

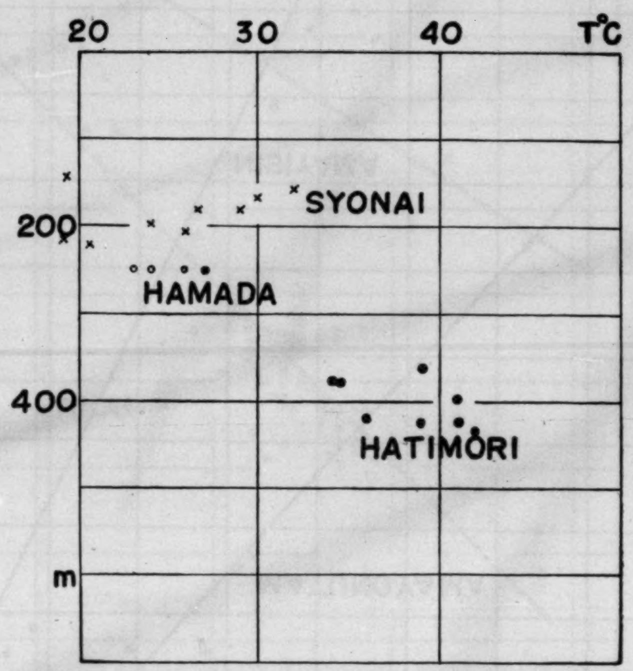

Fig. 17. Bottom temperatures in oil-wells at the Syonai, Hamada and Hatimori oil-fields. In these cases, geothermal gradient can not be obtained.

in the cases of Hatimori, Syonai and Hamada oil-fields (Fig. 17) nothing definite can be obtained with regard to the geothermal gradient. The geothermal gradients in each of five other oil-fields and a gas-field are listed in Table 4. The possible source of systematic error in temperature measurements lies in that the measured temperature may be somewhat lower than the true temperature of the beds, because the time after ceasing of oil-drawing has been not long enough to attain the thermally steady state. But some examples show that the difference in temperatures taken under the flowing condition and static one does not exceed 1°*C*. It may be observed in this table that the geothermal gradients in the oil-fields in north-eastern Honsyu are larger than those at Sasago and Tokyo in central Honsyu and that the geothermal gradient 4.°8*C*/100 *m* seems to prevail in the near-coast oil-fields, whereas higher values in the inland oil-fields. No plausible explanation has been furnished regarding these observations so far.

These oil-fields are situated on anticlines in the Mizuho-Fossa Magna Folded Belt of north-eastern Japan. The sediments (mainly shale, siltstone, and tuff) in these oil-fields are of Quaternary and Tertiary ages, forming the Mizuho-Fossa Magna Folded Belt.

The values of heat flow in parentheses in Table 4 are the only tentative ones calculated by adopting the mean conductivity of shale (3.3×10^{-3} *cal/sec cm °C*) from Birch's Table[14]. We have not yet been able to collect sufficient rock specimens of these oil-fields, so that no definite value of thermal conductivity is available at present. So far the con-

Table 4. Geothermal gradient at oil-fields and gas-field.

oil-field	$\Delta T/\Delta h$ (°C/100m)	heat flow (10^{-6} *cal/cm² sec*)
Yabase, Akita Pref.	4.8	(1.6)
Innai, Akita Pref.	4.8	(1.6)
Kotaki, Akita Pref.	7.25	(2.4)
Mogami, Yamagata Pref.	7.1	(2.35)
Nisiyama, Niigata Pref.	4.8	(1.6)
Matunoyama, Niigata Pref.	8.5	(2.8)
Niigata gas-field		
Nagatoro	5.0	(1.65)
Utino	2.0	(0.66)

---

[14] F. **Birch**, *loc. cit.*

ductivity measurement has been made of a specimen of shale sampled at a depth 1624–1626 m at the Yabase oil-field. The result gave its conductivity in dry state as $3.35\times10^{-3}\,cal/sec\,cm\,C^{\circ}$. (It may be added here that T. Iki[15] reported in 1927 the results of temperature measurements, by a thermo-junction, of two oil-wells in Akita prefecture. The geothermal gradients were obtained as $4.^{\circ}31C/100\,m$ and $5.^{\circ}78C/100\,m$.)

7. Conclusion

Preliminary result indicated that the terrestrial heat flow at the Sasago tunnel, Yamanashi Prefecture, Central Japan is $2.06\times10^{-6}\,cal/cm^2\,sec$. This value is certainly greater than the "normal" one that is $1.2\times10^{-6}\,cal/cm^2\,sec$. The geothermal gradients in oil-fields in northeastern Honsyu are large, say $4.^{\circ}92C/100\,m$ on the average, indicating that the heat flow will be also large. Exact amount of heat flow in these oil-fields has not yet been obtained because of lack in relevant conductivity data. In order to establish that the average heat flow in Japan is significantly larger than in normal parts of the world, however, it is necessary to increase the number of determinations and to apply various corrections to both observed geothermal gradients and thermal conductivities. The conclusion that may be drawn from the present preliminary results will, therefore, be that the heat flow in Japan may be larger than the "normal" value but is not as large as ten times or hundred times as the latter, except in volcanic area.

We thank Dr. T. Rikitake, under whose direction the present study has been taken up, for his constant valuable advice.

We should also like to express our thanks to Prof. T. Nagata for his constant encouragement and interest. The authors are grateful to Prof. T. Matuzawa and the staffs of the Tokyo Electric Company, Kusatsu Yuo Company, Research Group for Explosion Seismology and Teikoku Oil Company for their kind advice and help in obtaining the underground temperatures. We are indebted to Prof. H. Kuno, Drs. M. Yamazaki and A. Sugimura for their advice from geological point of view. Our sincere thanks are also due to Mr. T. Watanabe for the elaborate preparation of rock specimens used for the thermal conductivity measurements. We acknowledge the kind co-operation of Mr. S. Yugeta of Kyoritsu-sha Company in the construction of the apparatus for the same measurement.

---

[15] T. IKI, *Bull. Earthq. Res. Inst.*, **2** (1927), 109.

14. 地球熱学（第１報）

日本に於ける地殻内熱流量についての序報

地震研究所 上田誠也
行武毅
棚岡巖

本邦に於いては，地殻内熱流量についての研究が全くなされていないので，今回これを試みた．地球内部からの熱エネルギーが，あらゆる地殻内の現象のエネルギー源であることから考えれば，本邦の如き地震，火山活動の活潑な地域での熱流量を知ることは重要なことである．まだ序報の段階であるが，得られた結果は次の如くである．本邦といえども火山の極く近傍以外の場所での熱流量は，世界各地で従来測定された値と同じく，10^{-6} cal/sec cm^2 の桁である．しかし，本報の結果によれば，本邦での値はやや大きいようである．以後測定の数および精度を増して行く予定である．

Specific measurement has been made for specimen of shale sampled at a depth 1624–1627 m at the [illegible]. The result gave its conductivity in dry state as [illegible] cal/cm sec °C. It may be added here that T. [illegible] (1962) [illegible] the results of temperature measurements by [illegible] wells in Akita prefecture. The geothermal gradients were obtained as [illegible]/100 m and 5.°780/100 m.

Preliminary [illegible]. The [illegible] heat flow [illegible] $\times 10^{-6}$ cal/cm² sec. This value is certainly greater than the "normal" one that is 1.2×10^{-6} cal/cm² sec. The geothermal gradients at oil-fields in north-eastern Honshu are large, say [illegible]/100 m on the average, indicating that the heat flow will be also large. Exact amount of heat flow in these oil-fields has not yet been obtained because of lack in relevant conductivity data. In order to establish that the average heat flow in Japan is significantly larger than in normal parts of the world, however, it is necessary to increase the number of determinations and to apply various corrections to both observed geothermal gradients and thermal conductivities. The conclusion that may be drawn from the present preliminary results will, therefore, be that the heat flow in Japan may be larger than the "normal" value but is not as large as ten times or hundred times of the latter, except in volcanic area.

We thank Dr. T. Rikitake, under whose direction the present study has been taken up, for his constant valuable advice.

We should also like to express our thanks to Prof. T. Nagata for his constant encouragement and interest. The authors are grateful to Prof. [illegible] and the staffs of the Tokyo Electric Company, [illegible] Company, Research Group for Explosion Seismology and Teikoku Oil Company for their kind advice and help in obtaining the underground temperatures. We are indebted to Prof. H. Kuno, Drs. M. [illegible] and A. [illegible] for their advice from geological point of view. Our sincere thanks are also due to Mr. T. Watanabe for the elaborate preparation of rock specimens used for the thermal conductivity measurements. We acknowledge the kind co-operation of Mr. S. [illegible] of [illegible] Company in the construction of the apparatus for the same measurement.

[illegible] T. [illegible], Bull. [illegible] Survey, [illegible] (1957), [illegible]

BULLETIN OF THE EARTHQUAKE
RESEARCH INSTITUTE
Vol. 36 (1958), pp. 275-293

15. *The Amplitude and the Period of Earthquake Motions. II.*

By Kiyoshi KANAI and Shizuyo YOSHIZAWA,

Earthquake Research Institute.

(Read June 25, Nov. 26, 1957 and June 24, 1948.—Received June 30, 1958.)

1. Introduction

It goes without saying that a seismogram is a record of wave motions at ground surface transmitted from the point of origin of the earthquake through the earth's crust as a vibration system and, in general, is recorded by means of the pendulum of a vibration system. That is to say, when $O(T)$, $C(T)$, $G(T)$, and $I(T)$ represent vibration characteristics of the point of origin, the earth's crust, the ground and the seismograph, respectively, the wave form of seismogram $R(T)$ can be written as follows:

$$R(T)=O(T).C(T).G(T).I(T)\,. \qquad (1)$$

In order to study analytically the mechanism of earthquake generation as well as the nature of the earth's crust, it is desirable to use a seismogram in which the effect of $G(T)$ is negligible, because of much complication of the geological conditions of the ground near the surface. The ground underneath Hitachi Mine (Ibaraki prefecture), where we have been making observations for more ten years, has a very good condition in this respect.

In the previous paper¹⁾, we obtained the relation between the amplitude and the period of earthquake motions, that is,

$$A \propto T^2\,, \qquad (2)$$

by using the initial motion of P-waves observed at Hitachi Mine, in consideration of the fact that the change degree of wave form on the way of propagation would be the smallest in the initial motion of P-waves. And, in the same paper, we entered into the discussion of the mechanism of earthquake generation by using the above formula.

---

1) K. KANAI, K. OSADA and S. YOSHIZAWA, "The Relation between the Amplitude and the Period of Earthquake Motion", *Bull. Earthq. Res. Inst.*, **31** (1953), 45.

In this paper, we are going to examine the relation between the amplitude and the period of earthquake motions using the results of spectral analysis of seismograms obtained 300 m underground in Hitachi Mine.

2. Spectral analysis of seismograms

The constants of the seismograph used in the present investigation are as follows: type = inverted pendulum, natural period of pendulum = 1.0 sec, mechanical magnification = 204~440, damping ratio = 13 : 1, recording system = scratching smoked rotating-paper, driving = 6 watt motor for electric clock use, recording speed = 2 mm per sec.

Table 2 shows the positions of the origin of the earthquakes treated herein which were obtained by the Japan Meteorological Agency, Tokyo,

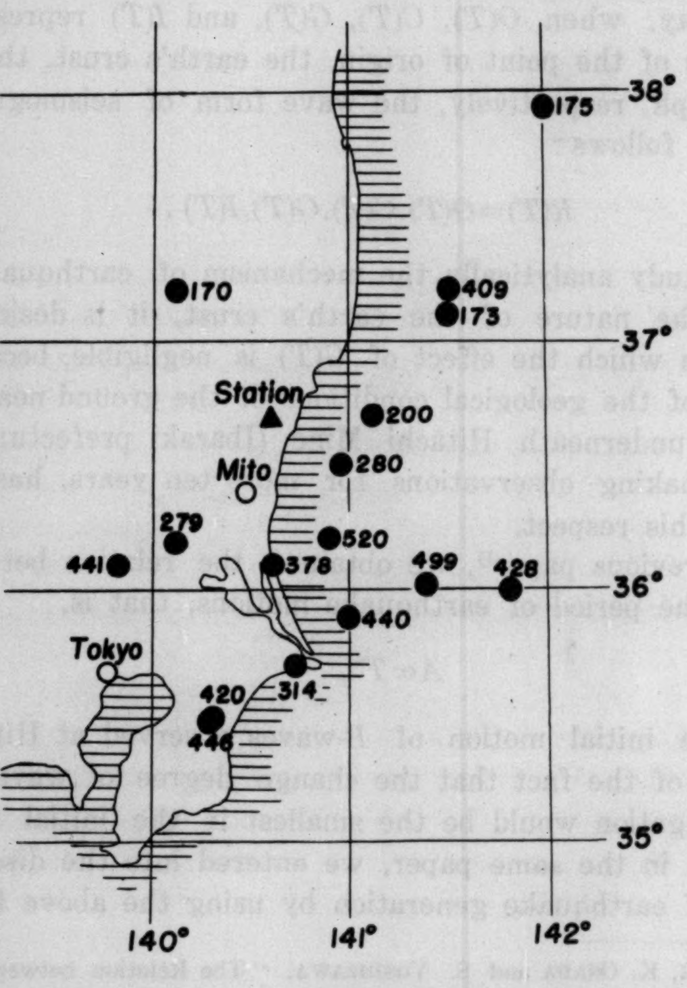
38°
175
170
409
173
37°
Station
200
Mito
280
279
520
441
378
499
428
36°
440
Tokyo
314
420
446
35°
140°
141°
142°

Fig. 1. The positions of the observing station and the epicenters.

and the duration of preliminary tremors observed at Hitachi Mine. The positions of the observing station and the epicenters written in the third column in Table 2 are shown in Fig. 1.

The displacement spectra of the earthquake motions obtained, from the photographs enlarged 3∼5 times the seismograms, by means of the response computer[2] are shown in Figs. 5∼20. The broken lines in Figs. 5∼20 represent the results which have been reduced to the results of spectral analysis for the seismograms with regard to vibration characteristics of the seismograph.

As we have seen from Figs. 5∼20 that there is a peak in every displacement-period relation, we try to find whether or not there exists a systematic relation between the maximum values of displacement spectra and the periods corresponding to the above mentioned values.

(i) First, the reduction of the amplitude of seismic waves according to hypocentral distance will be performed by the following formula:

$$A=\frac{A_0}{x}e^{-kx/T^2}, \qquad (3)$$

where

$$k=\frac{2\pi^2\xi}{\rho v^3}, \qquad (4)$$

in which, the following notations are employed, that is, x = hypocentral distance, A=amplitude at distance x, A_0=amplitude at origin, T=period of waves, ξ=viscous coefficient, ρ=density, v=velocity. If we adopt the value of damping factor $k=5\times10^{-8}$ C. G. S.[3], the amplitude of seismic waves at a spot 100 km away from the hypocenter may be written, based on equation (3), as follows:

$$A_{\Delta=100}=A\frac{x}{100}e^{(x-100)\times0.005/T^2}, \qquad (3')$$

in which, A is the amplitude at observation station and x is the hypocentral distance of the station in km.

---

[2] R. Takahasi, "A Response Computer, Preliminary Report", Proc. 3rd Japan National Cogr. *Applied Mech.*, (1953), 373.

[3] K. Sezawa and K. Kanai, "Viscosity Distribution within the Earth. Preliminary Notes", *Bull. Earthq. Res. Inst.*, **18** (1940), 169.

A. Kubotera, "Damping and Dispersion of Seismic Body-wave in the Earth's Crust", *Journ. Seism., Soc., Japan,* [ii], **5**, No. 3 (1952), 9, (in Japanese).

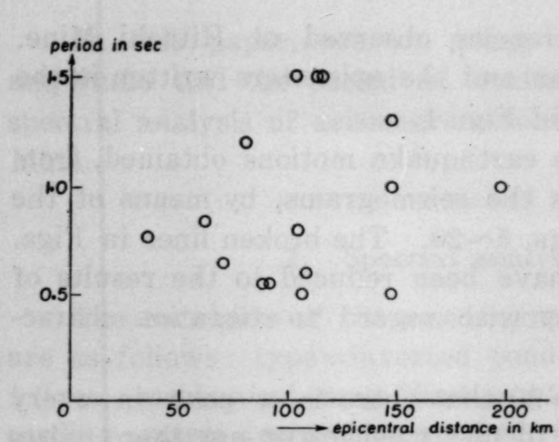

Fig. 2. Variations of the periods corresponding to the maximum amplitudes in Figs. 5∼20 with the epicentral distances.

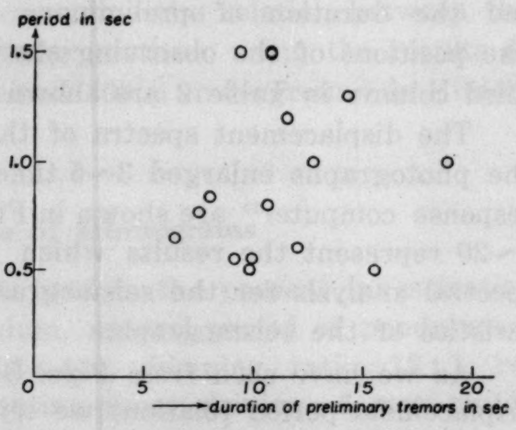

Fig. 3. Variations of the periods corresponding to the maximum amplitudes in Figs. 5∼20 with the duration of preliminary tremors observed at Hitachi Mine.

(ii) Figs. 2 and 3 show the variations of the periods corresponding to the maximum amplitudes in Figs. 5∼20 with the epicentral distances and the duration of preliminary tremors observed at Hitachi Mine. The only conclusion drawn from Figs. 2 and 3 is, that there is a scarcely recognizable relationship between the period of waves and epicentral distance and that is the same as the other results[4]. Therefore, in the present investigation, the reduction of the period of seismic waves according to hypocentral distance will be left out of consideration.

(iii) As the observations were made concerning only one component of seismic waves as shown in Table 1, the resultant amplitude will be calculated by assuming them to be *S*-waves.

The relation between the maximum values of displacement which are given by three kinds of reduction mentioned above to the results of spectral analysis shown in Figs. 5∼20, and the periods corresponding to them is shown in Fig. 4. From Fig. 4, the empirical formula concerning the relation of maximum displacement to the period of seismic waves may be written as follows:

$$A_{m\cdot s}=53T_m^{2.56} \qquad (5)$$

in which, units of $A_{m\cdot s}$ and T_m are micron and sec, respectively.

---

[4] B. GUTENBERG and C. F. RICHTER, "Earthquake Magnitude, Intensity, Energy, and Acceleration", *Bull. Seism. Soc. Amer.*, **32** (1942), 163.
A. E. JONES, "Empirical Studies of Some of the Seismic Phenomena of Hawaii", *ditto*, **28** (1938), 313.

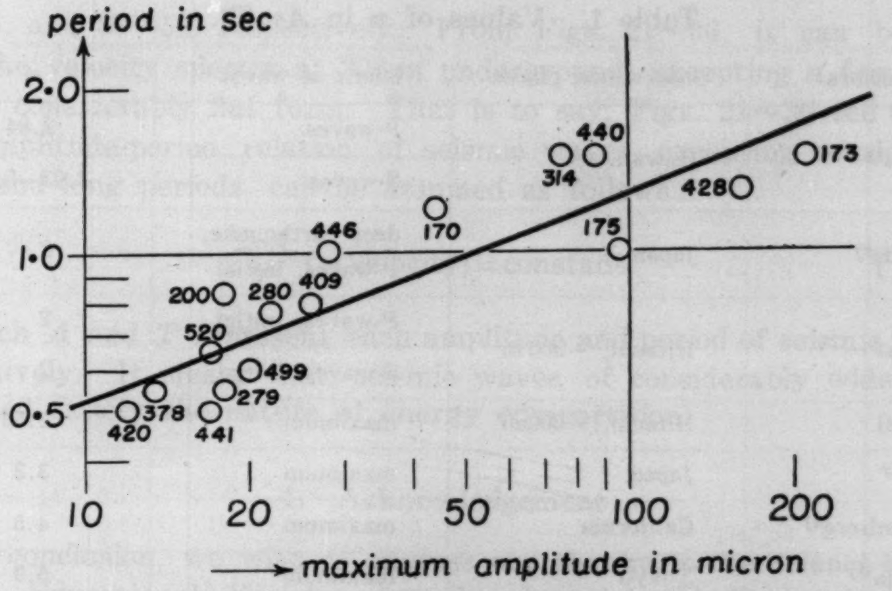

Fig. 4. Relation between the maximum values of displacement which are given by three kinds of reduction to the results of spectral analysis shown in Figs. 5∼20, and the periods corresponding to them.

3. Discussion

If we express the relation of the amplitude to the period of seismic waves as follows:

$$A \propto T^n , \qquad (6)$$

the values of n which have already been obtained by many authors can be tabulated as in Table 1. In Table 1, the results of magnitde-period relation of earthquakes are converted into the amplitude-period relation, using the original relation in which magnitude is proportional to the logarithm of amplitude.

It will be seen in Table 1 that the values of n in the first seven cases are considerably different from those of the last two cases, that is, n of the former takes 2∼3, while that of the latter becomes twice their value.

Now, we try to find the reason of such a large difference.

(a) The periods in the first seven cases were obtained from seismograms directly or after having made some analyses on seismograms, but in the last two cases, the periods were obtained after having made complicated calculations including the assumption $\alpha=(2\pi/T)^2A$, in which α

Table 1. Values of n in $A \propto T^n$.

Authors	Observation places	Kinds of waves	n
Jones⁵⁾	Hawaii	P-waves	2.94
		S-waves	2.93∼3.02
Honda⁶⁾	Japan	deep earthquake, P-waves, initial	2
Kanai⁷⁾	Hitachi, −300 m	P-waves, initial	2
		S-waves, initial	2
Kanai	Hitachi, −300 m	maximum	2.56
Aki⁸⁾	Japan	maximum	3.3
Gutenberg⁹⁾	California	maximum	4.5
Asada¹⁰⁾	Tokyo	maximum	5.9

and A represent the maximum acceleration and displacement of an earthquake motion.

(b) In the first seven cases either the seismographs of comparatively long period have been used or the reduction of the vibration characteristics of seismographs has been carried out; on the other hand, in the last two cases, the results obtained by using the seismographs of comparatively short period have been utilized.

At any rate, from the above considerations only, we can scarcely get the satisfactory answer to the present problem. But, these considerations will serve in the investigations of the mechanism of wave generation at the point of origin of an earthquake, in future.

Next, velocities and accelerations have been calculated from the displacements shown in Figs. 5∼20, on the assumption of simple harmonic motion. These velocity and acceleration spectra are presented in Figs.

---

5) A. E. JONES, *loc. cit.*, 4).

6) H. HONDA and H. ITO, "On the Period of the P-waves and the Magnitude of the Earthquake", *Geophys. Mag.*, **13** (1939), 155.

7) K. KANAI, K. OSADA and S. YOSHIZAWA, *loc. cit.*, 1).

8) K. AKI, "Correlogram Analysis of Seismograms", *Journ. Seism. Soc., Japan*, [ii], **8**, No. 2 (1955), 99, (in Japanese).

9) B. GUTENBERG and C. F. RICHTER, *loc. cit.*, 4).

10) T. ASADA, "On the Relation between the Predominant Period and the Maximum Amplitude of Earthquake-Motions", *Journ. Seism. Soc., Japan*, [ii], **6**, No. 2 (1953), 1, (in Japanese).

21～36, and 37～52, respectively. From Figs. 21～36, it can be seen that the velocity spectra at 300 m underground, excepting a few cases, take a considerably flat form. That is to say, Figs. 21～36 tell us that the amplitude-period relation of seismic waves, excepting considerably short and long periods, can be assumed as follows:

$$\frac{2\pi A}{T}(\equiv\text{velocity})=\text{constant} \tag{7}$$

in which A and T represent each amplitude and period of seismic waves, respectively. It means that, seismic waves of considerably wide range of period satisfy the nature of energy equipartition.

4. Acknowledgement

In conclusion, we wish to express our thanks to the Science Section of the Educational Ministry, for the financial aid (Research Funds) granted us. Also thanks are due to the members of Motoyama Office, Hitachi Mine, Prof. R. Takahasi and Mr. I. Aida for their help, and to Messrs. T. Tanaka, T, Suzuki and K. Osada for their cooperation, in the course of these investigations.

Table 2.

Earthquake No.	Date	Origin			Duration of preliminary tremor in sec	Observation direction
		°N	°E	Depth (km)		
170	1951 I 26	37.2	140.1	shallow	11.5	EW
173	〃 II 3	37.1	141.5	40～50	10.8	〃
175	〃 IV 5	37.9	142.0	70	18.8	〃
200	1952 III 10	36.7	141.1	40	8.0	〃
279	〃 VII 28	36.2	140.1	55	9.1	〃
280	〃 VIII 9	36.5	140.9	0～10	7.5	〃
314	〃 IX 14	35.7	140.7	30	10.8	〃
378	〃 XI 18	36.1	140.6	60	9.9	NS
409	〃 XII 11	37.2	141.5	30	10.6	EW
420	〃 〃 25	35.5	140.3	50	15.5	〃
428	1954 I 14	36.0	141.8	60	14.3	〃
440	〃 〃 22	35.9	141.0	60	9.4	NS
441	〃 〃 26	36.1	139.9	40	9.8	EW
446	〃 II 3	35.5	140.3	50	12.7	〃
499	〃 IV 10	36.0	141.4	20	12.0	NS
520	〃 V 20	36.2	140.9	40～30	6.4	EW

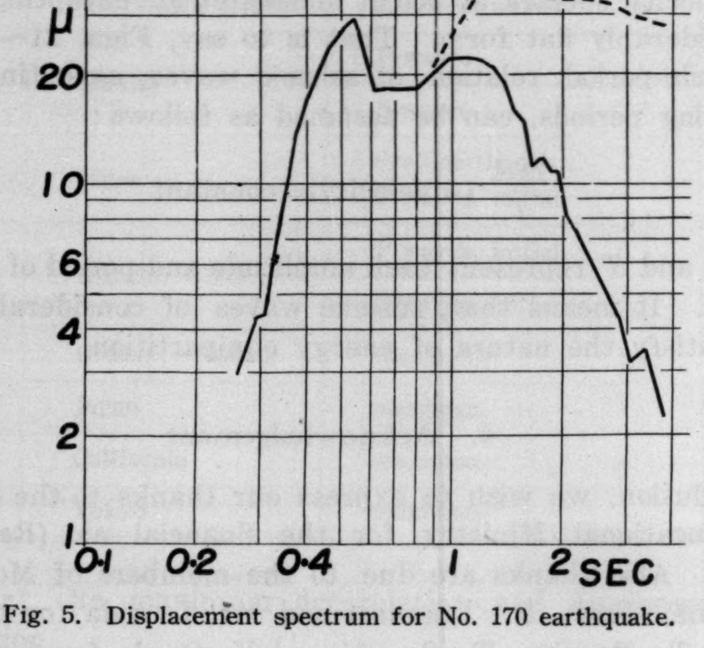

Fig. 5. Displacement spectrum for No. 170 earthquake.

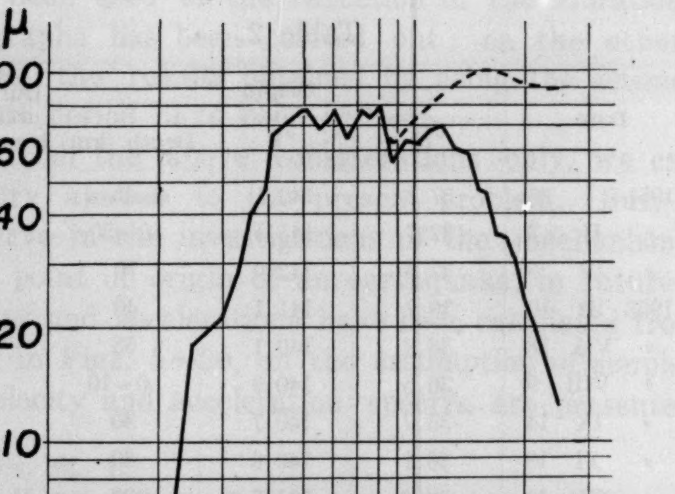

Fig. 6. Displacement spectrum for No. 173 earthquake.

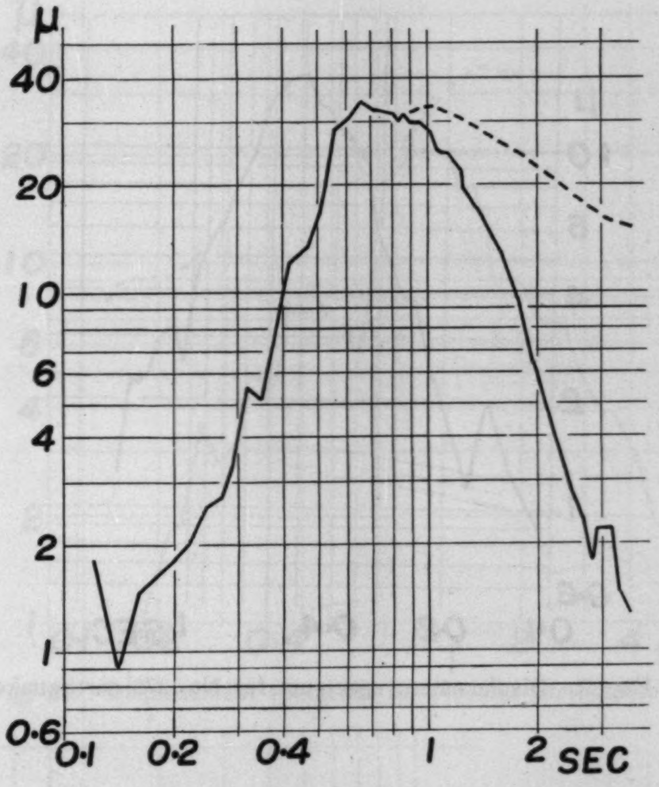

Fig. 7. Displacement spectrum for No. 175 earthquake.

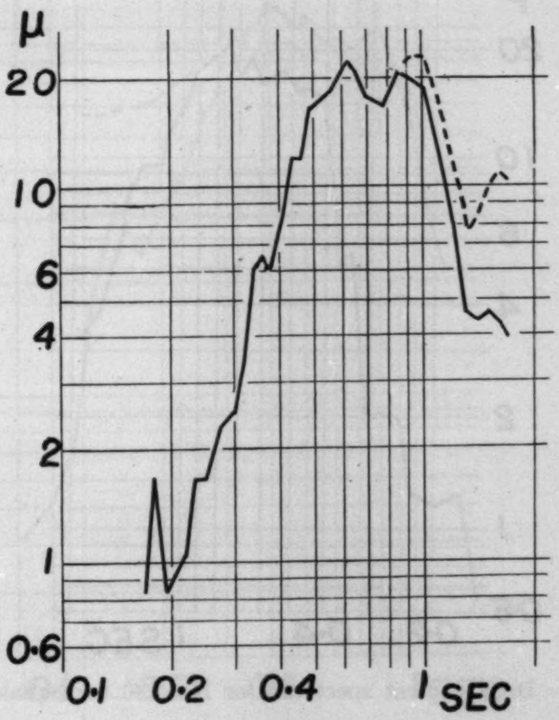

Fig. 8. Displacement sprectrum for No. 200 earthquake.

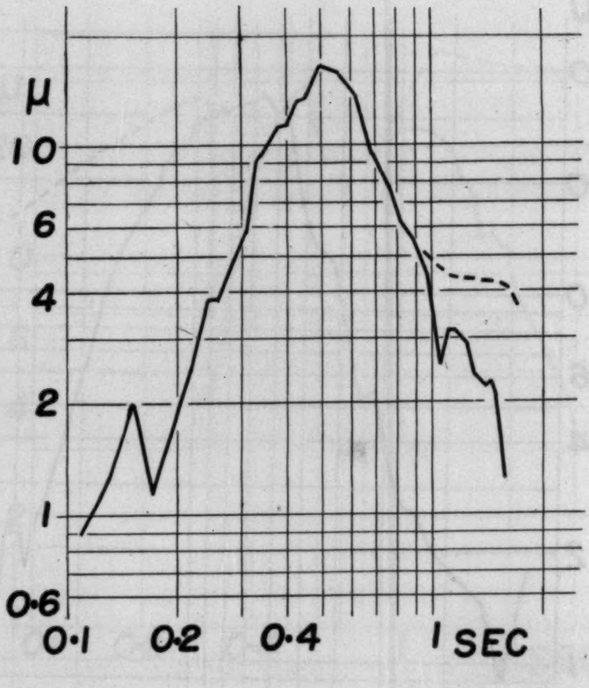

Fig. 9. Displacement spectrum for No. 279 earthquake.

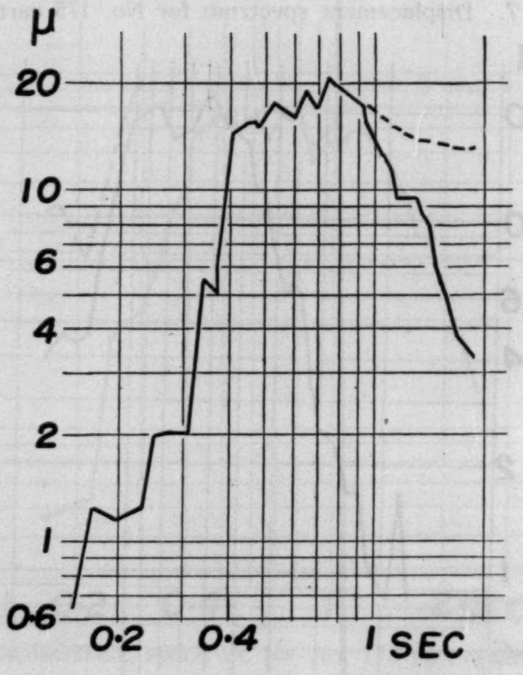

Fig. 10. Displacement spectrum for No. 280 earthquake.

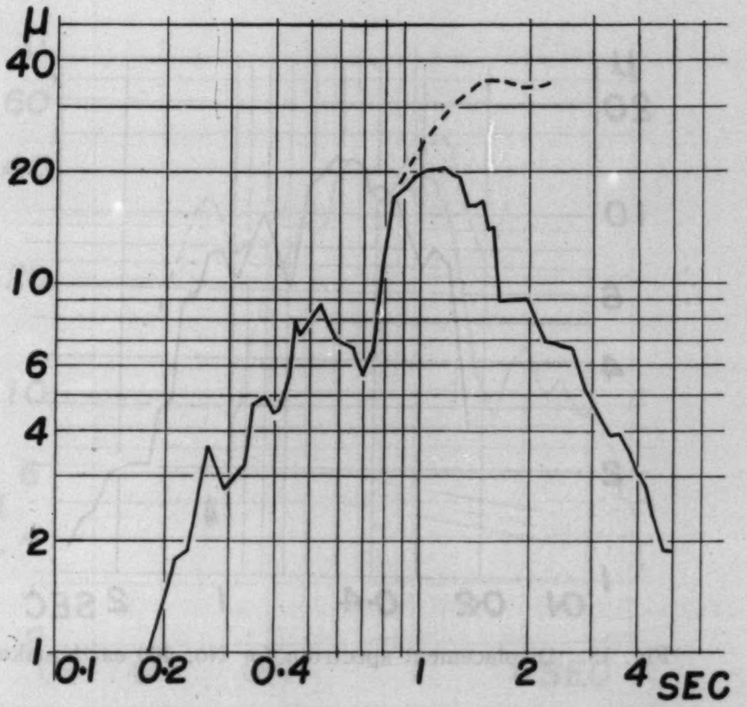

Fig. 11. Displacement spectrum for No. 314 earthquake.

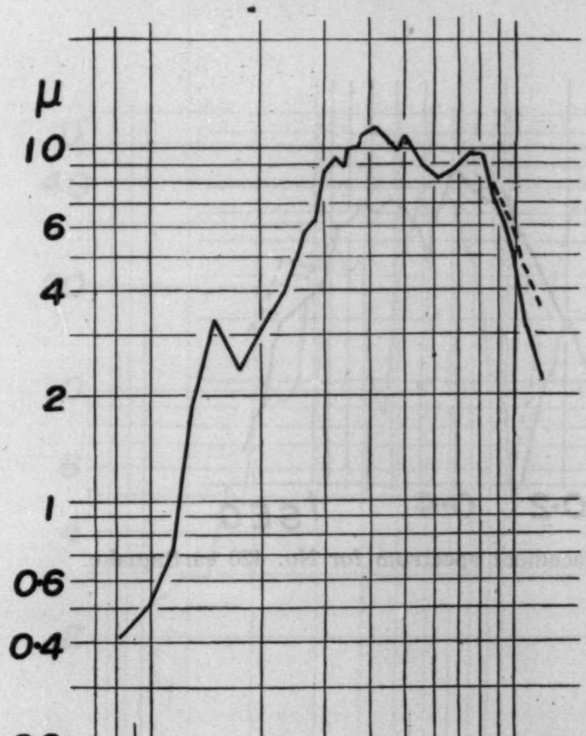

Fig. 12. Displacement spectrum for No. 378 earthquake.

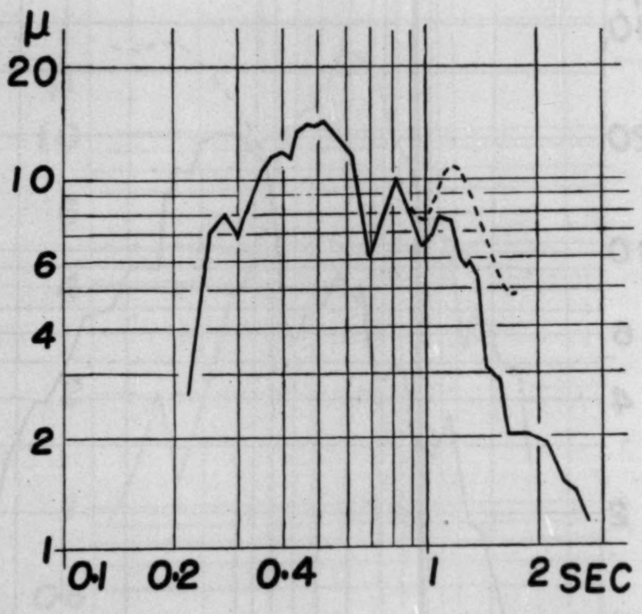

Fig. 13. Displacement spectrum for No. 409 earthquake.

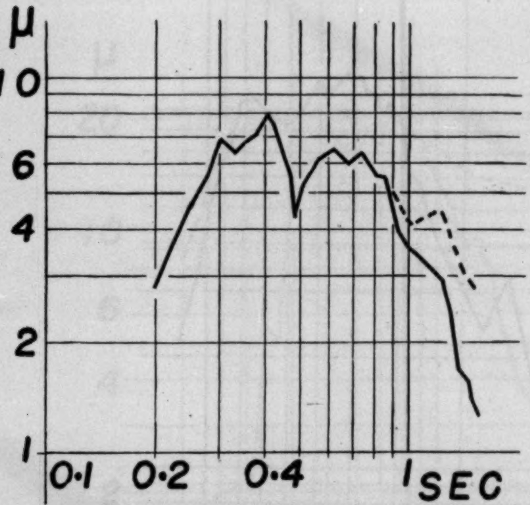

Fig. 14. Displacement spectrum for No. 420 earthquake.

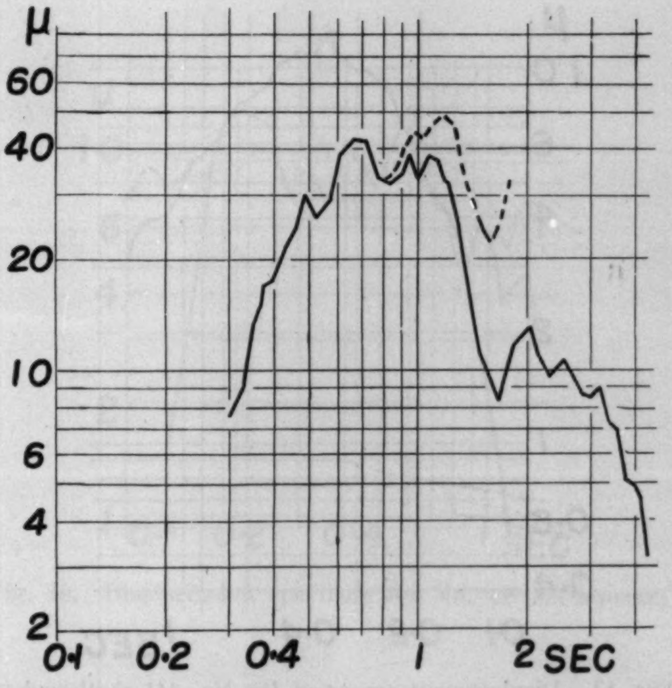

Fig. 15. Displacement spectrum for No. 428 earthquake.

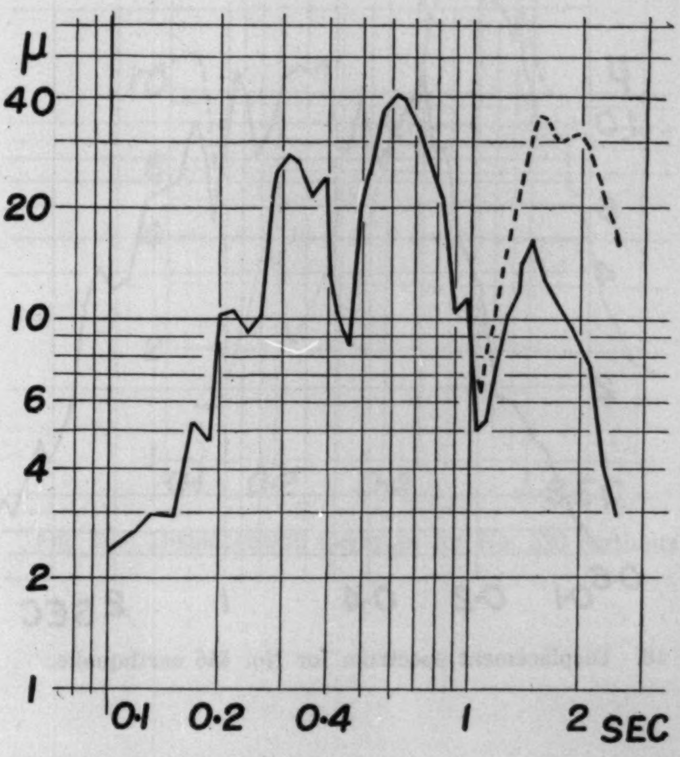

Fig. 16. Displacement spectrum for No. 440 earthquake.

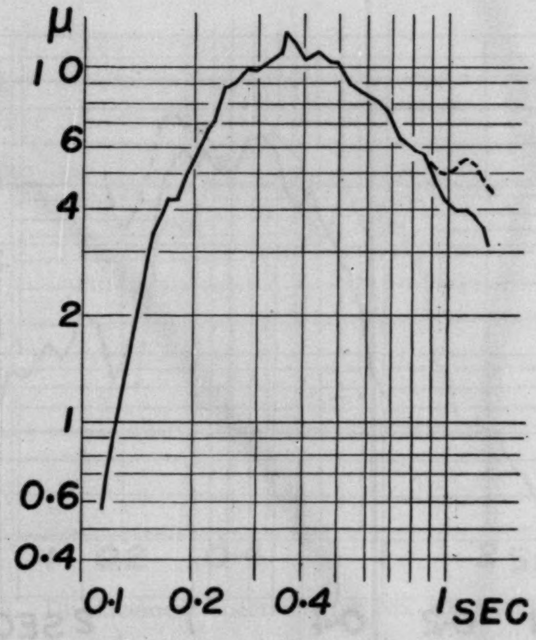

Fig. 17. Displacement spectrum for No. 441 earthquake.

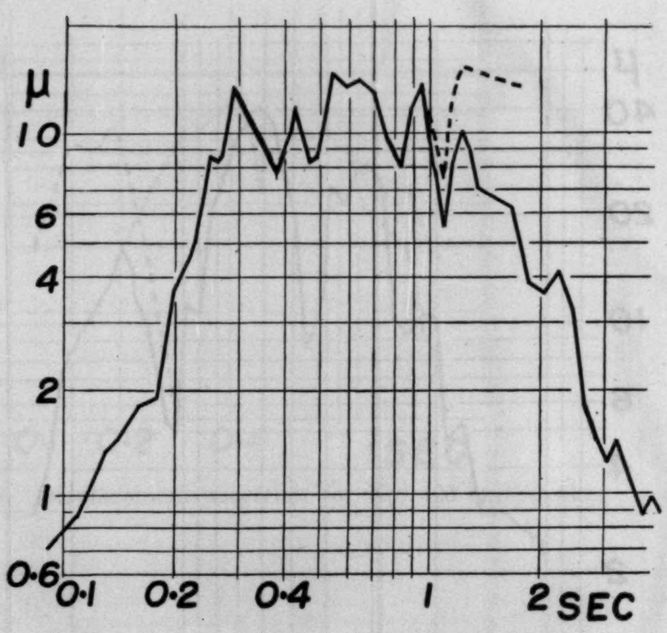

Fig. 18. Displacement spectrum for No. 446 earthquake.

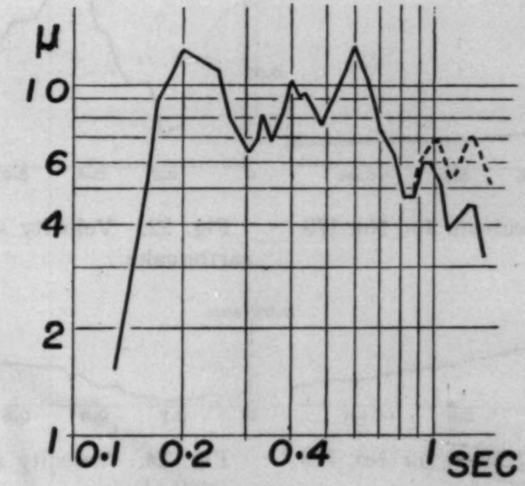

Fig. 19. Displacement spectrum for No. 499 earthquake.

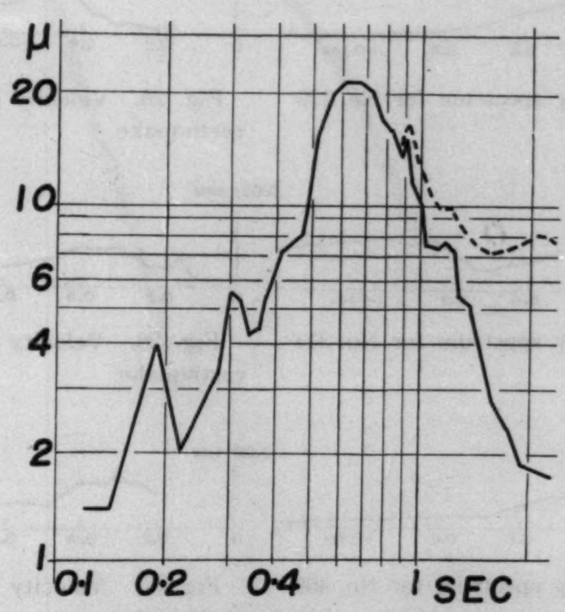

Fig. 20. Displacement spectrum for No. 520 earthquake.

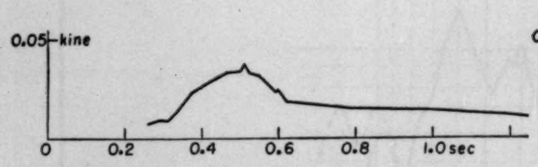

Fig. 21. Velocity spectrum for No. 170 earthquake.

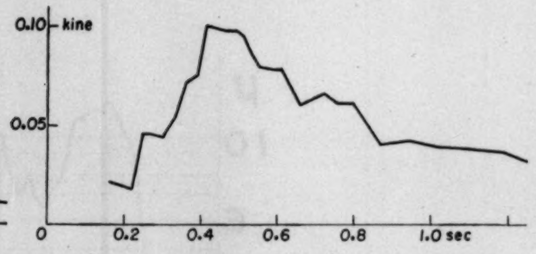

Fig. 22. Velocity spectrum for No. 173 earthquake.

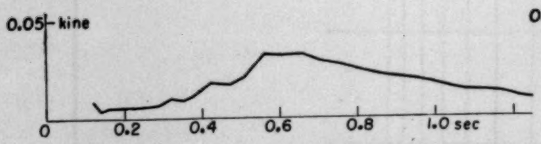

Fig. 23. Velocity spectrum for No. 175 earthquake.

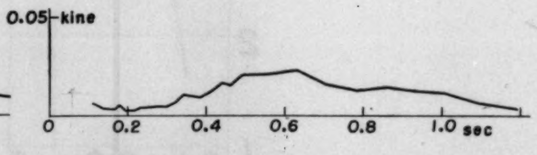

Fig. 24. Velocity spectrum for No. 200 earthquake.

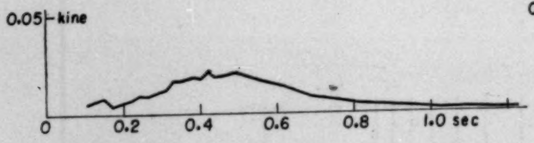

Fig. 25. Velocity spectrum for No. 279 earthquake.

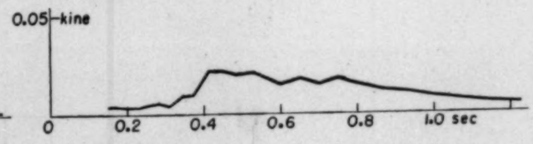

Fig. 26. Velocity spectrum for No. 280 earthquake.

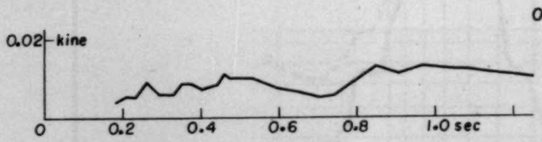

Fig. 27. Velocity spectrum for No. 314 earthquake.

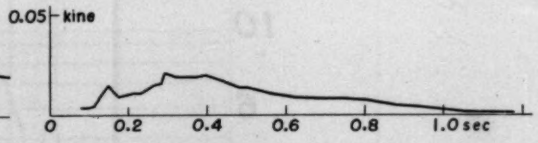

Fig. 28. Velocity spectrum for No. 378 earthquake.

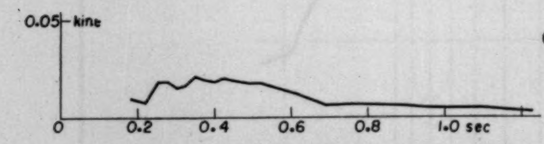

Fig. 29. Velocity spectrum for No. 409 earthquake.

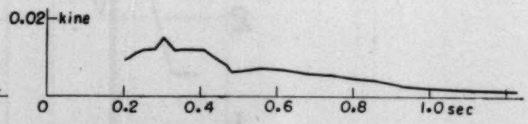

Fig. 30. Velocity spectrum for No. 420 earthquake.

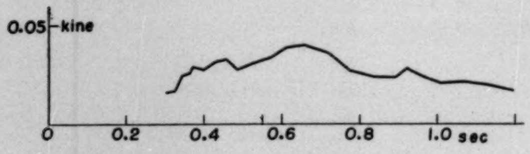

Fig. 31. Velocity spectrum for No. 428 earthquake.

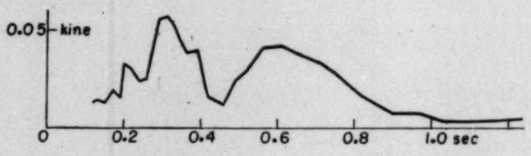

Fig. 32. Velocity spectrum for No. 440 earthquake

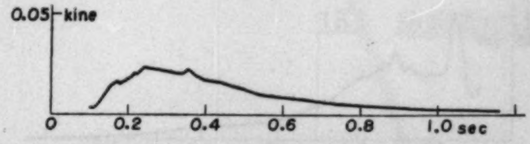

Fig. 33. Velocity spectrum for No. 441 earthquake.

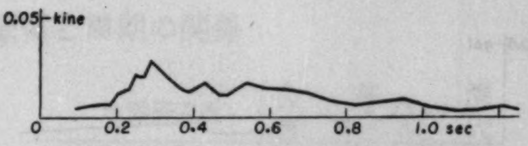

Fig. 34. Velocity spectrum for No. 446 earthquake.

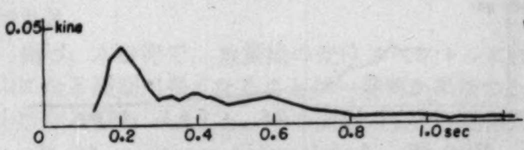

Fig. 35. Velocity spectrum for No. 499 earthquake.

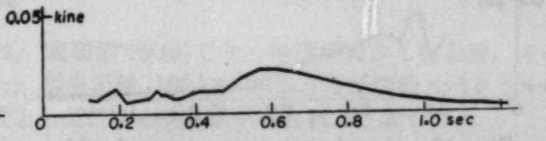

Fig. 36. Velocity spectrum for No. 520 earthquake.

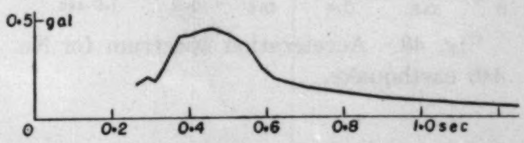

Fig. 37. Acceleration spectrum for No. 170 earthquake.

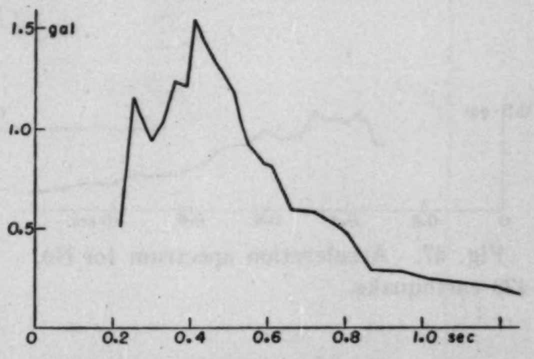

Fig. 38. Acceleration spectrum for No. 173 earthquake.

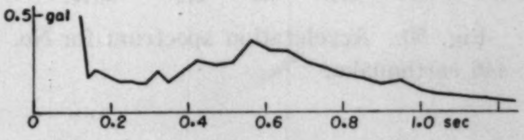

Fig. 39. Acceleration spectrum for No. 175 earthquake.

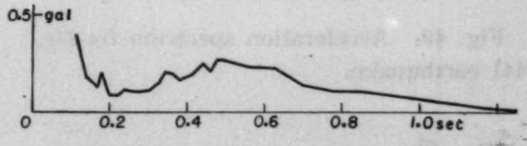

Fig. 40. Acceleration spectrum for No. 200 earthquake.

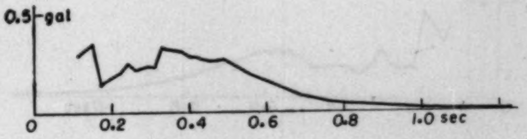

Fig. 41. Acceleration spectrum for No. 279 earthquake.

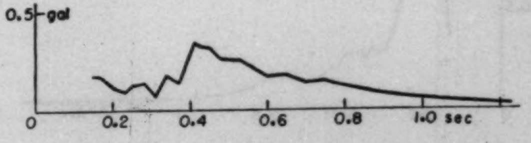

Fig. 42. Acceleration spectrum for No. 280 earthquake.

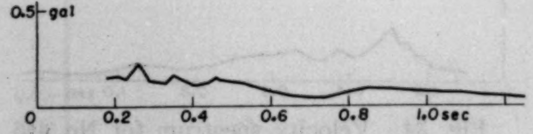

Fig. 43. Acceleration spectrum for No. 314 earthquake.

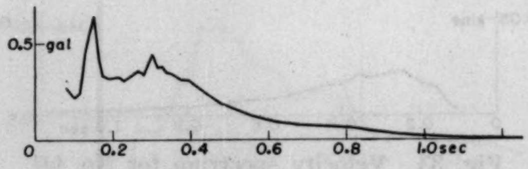

Fig. 44. Acceleration spectrum for No. 378 earthquake.

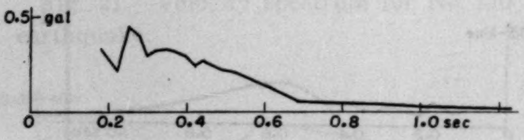

Fig. 45. Acceleration spectrum for No. 409 earthquake.

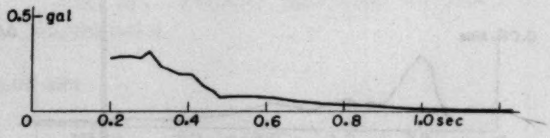

Fig. 46. Acceleration spectrum for No. 420 earthquake.

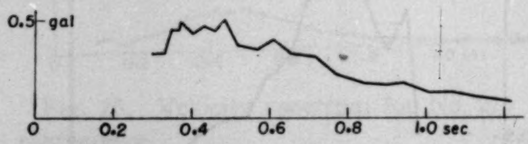

Fig. 47. Acceleration spectrum for No. 428 earthquake.

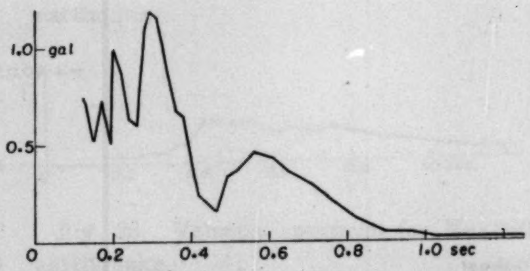

Fig. 48. Acceleration spectrum for No. 440 earthquake.

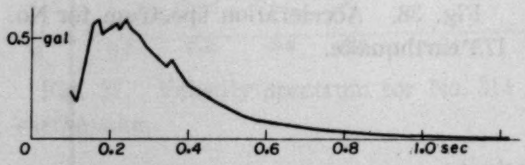

Fig. 49. Acceleration spectrum for No. 441 earthquake.

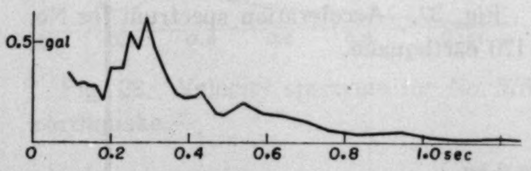

Fig. 50. Acceleration spectrum for No. 446 earthquake.

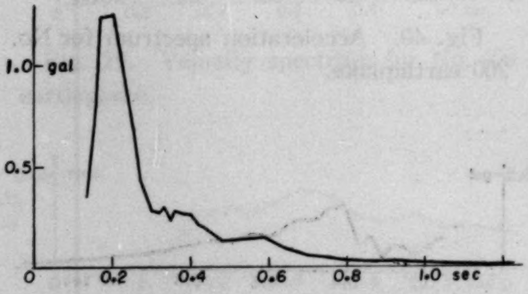

Fig. 51. Acceleration spectrum for No. 499 earthquake.

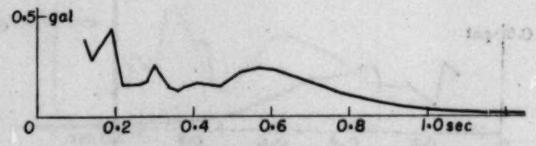

Fig. 52. Acceleration spectrum for No. 520 earthquake.

15. 地震動の振幅と周期の関係

地震研究所 金井　清
吉沢静代

地震動は，普通，いわゆる地盤の影響で非常に複雑な波形になり，その本性を調べるのが困難である．そこで，地盤による地震動の変調をできるだけ避けようとして，日立鉱山の坑内で地震観測を始めてから，10 年以上になる．今回の報告は，その期間に，地下 300 m で得られた地震記象の中から比較的満足な記録をしたものをえらんで周期解析を行い，振幅と周期の関係をしらべた結果である．

先づ，本研究で，地震動の変位スペクトルには，或周期で山ができ，地震が大きくなる程，その山になる周期が長くなることが一層明かになつた．震央距離 100 km における地震動スペクトルの山になる振幅 $A_{m\cdot s}$ と，その周期 T_mとの関係式として，次の実験式が得られた．即ち，

$$A_{m\cdot s}=53T_m^{2.56}\ \text{ミクロン} \qquad (1)$$

次に，地震動に含まれる各周期の波を単弦振動として，変位スペクトルから速度スペクトルを作つてみると，かなり広い範囲の周期にわたつて，速度スペクトルがほぼ一定であることがわかつた．即ち，地震動は，工学的に問題になりそうな周期の範囲内では，大体，勢力の等分配の法則を満足させていると考えてよいことがわかつたわけである．

15. 地震動の[illegible]と[illegible]の関係

金井 清

[illegible]

[illegible]

[illegible]

Fig. 47. Acceleration spectrum for No. [illegible] earthquake.

Fig. 48. Acceleration spectrum for No. [illegible] earthquake.

Fig. 49. Acceleration spectrum for No. [illegible] earthquake.

Fig. 50. Acceleration spectrum for No. [illegible] earthquake.

Fig. 51. Acceleration spectrum for No. [illegible] earthquake.

Fig. 52. Acceleration spectrum for No. [illegible] earthquake.

Bulletin of the Earthquake Research Institute
Vol. 36 (1958), pp. 295-310

16. *A Study of Strong Earthquake Motions.*

By Kiyoshi KANAI,

Earthquake Research Institute.

(Read Nov. 26, 1957.—Received June 30, 1958.)

1. Introduction

The following empirical formula[1] of the amplitude-period relation of earthquake motions has been obtained from the statistical treatment of the results of spectral analysis of a large number of seismograms which had been recorded deep in the ground where the influence of the vibration characteristics of the ground is very slight. That is

$$A_{m\cdot s}=53T_m^{2.56} \tag{1}$$

in which $A_{m\cdot s}$ and T_m represent, respectively, the maximum value of displacement spectrum at the spot of 100 km hypocentral distance in micron and the corresponding period in sec. On the other hand, from the previous paper[2] and others, the amplitude-period relation of seismic waves excepting considerably short and long periods can be assumed as follows:

$$\frac{2\pi A}{T}(\equiv\text{velocity})=\text{constant} \tag{2}$$

in which A and T represent each amplitude and period of seismic waves, respectively. This means that seismic waves of a considerably wide range of period satisfy the nature of energy equipartition. Fig. 1 shows the schematic figures of the above mentioned relation.

In the present investigation, we assume that, concerning an earthquake, A_m in Fig. 1 depends on epicentral distance while T_m in the same figure is independent of epicentral distance. That is to say, the value of A_m at a spot of 100 km epicentral distance corresponds to $A_{m\cdot s}$ in (1).

In this paper, we deal with the relation of the magnitude of an earthquake to its period by using the relations expressed by (1) and (2), and we try to find whether or not we can expect these studied results to provide information about waves in destructive earthquakes.

---

[1] K. KANAI and S. YOSHIZAWA, "The Amplitude and the Period of Earthquake Motions. II", *Bull. Earthq. Res. Inst.*, **36** (1958), 275.

[2] *ditto* 1).

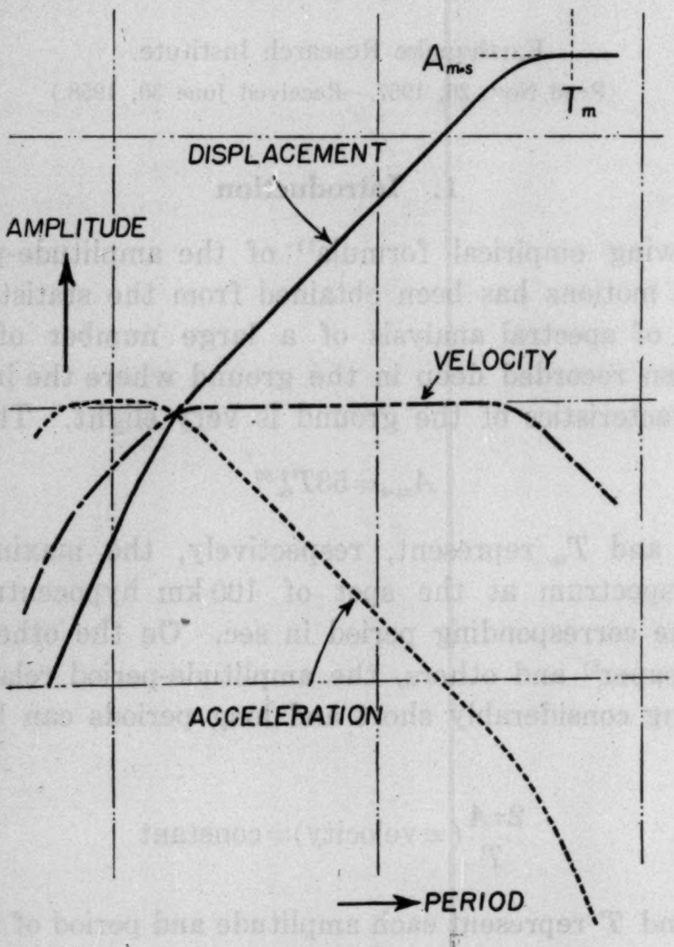

Fig. 1.

2. The case of the Kwanto earthquake of 1923

There are some records of the destructive earthquakes, including that of the Kwanto earthquake of 1923, in Japan, but none of them was successful. They are either incomplete or unreliable.

Now, we try to examine what characteristics of the waves may be expected in an earthquake motion having the same characteristics as the Kwanto earthquake, by using the relations of (1) and (2), and compare the results mentioned above with the analytical results obtained from the incomplete seismogram of the Kwanto earthquake which was recorded at Tokyo.

In the present case, the following formula as the expression of the relation among magnitude M, epicentral distance $\varDelta$ and maximum amplitude A is adopted. That is

$$\log A_m = M - 1.73 \log \varDelta + 0.83^{3)} \qquad (3)$$

in which, $\varDelta$ and A_m are measured in km and micron, respectively. Equating the common logarithm of (1) to the special case of (3) in which $\varDelta = 100$ km, we get

$$\log T_m = 0.39M - 1.70\ . \qquad (4)$$

From (3) and (4), we arrive at the relation,

$$\log \frac{A_m}{T_m} = 0.61M - 1.73 \log \varDelta + 2.53\ . \qquad (5)$$

If equipartition of energy is applicable to the seismic waves, that is to say,

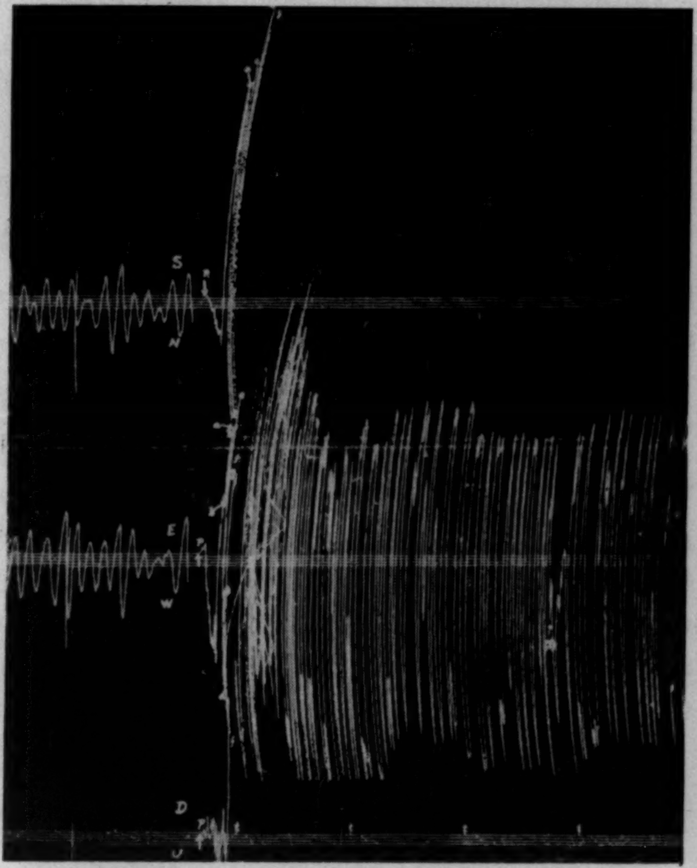

Fig. 2. Seismogram of the Kwanto earthquake.

$$\frac{A_m}{T_m}\left(\equiv\frac{A}{T}\right) = \text{constant} \qquad (6)$$

amplitude A measured in cm which corresponds to each period T of seismic waves can be expressed by

$$A = 10^{0.61M - 1.73 \log \varDelta - 1.47} T\ . \qquad (7)$$

And then, acceleration α measured in gal can be written as follows:

$$\alpha = \frac{(2\pi)^2 \cdot 10^{0.61M - 1.73 \log \varDelta - 1.47}}{T}\ . \qquad (8)$$

---

3) C. TSUBOI, "Determination of the Gutenberg-Richter Magnitude of Earthquakes occuring in and near Japan", *Journ. Seism. Soc. Japan*, [ii], **7**, No. 3 (1954), 185.

By means of (7) and (8), the values of displacement and acceleration in the cases, $T=0.3$ sec and 1.35 sec, besides the conditions $M=7.9$ and $\Delta=90$, which correspond to the values in Tokyo at the time of the Kwanto earthquake, are calculated. (The periods of 1.35 sec and 0.3 sec have been demonstrated to be the predominant waves of the Kwanto earthquake in Tokyo by Imamura⁴⁾ and Ishimoto⁵⁾, respectively.) The results of them are as follows:

$$\left.\begin{array}{lll} T=1.35\text{ sec}\ ; & A=1.23\text{ cm}\ , & \alpha=27\text{ gal}\ , \\ T=0.3\text{ sec}\ ; & A=0.27\text{ cm}\ , & \alpha=120\text{ gal}\ . \end{array}\right\} \quad (9)$$

On the other hand, the values estimated from seismogram by Imamura and Ishimoto are as follows:

$$\left.\begin{array}{lll} T=1.35\text{ sec}\ ; & A=4.43\text{ cm}\ , & \alpha=100\text{ gal}\ , \\ T=0.3\text{ sec}\ ; & A=0.6\sim0.8\text{ cm}\ , & \alpha=250\sim300\text{ gal}\ . \end{array}\right\} \quad (10)$$

Therefore, (9) and (10) tell us that the values estimated from seismograms are 2.5∼4 times larger than those derived from the empirical formula. Then it may be said that the calculated values are in comparative agreement with the estimated values as taking into consideration the vibration characteristics of the ground⁶⁾, because (1) has been obtained from the seismograms at −300 m underground.

3. The case of strong earthquakes in U.S.A.

In this chapter, we compare the values of the strong motion seismograms obtained in U.S.A. as well as the results of their spectral analysis with the values derived from the empirical formulae.

Now, magnitude M, epicentral distance of the observation places Δ and other factors of the earthquake treated here are shown in Table 1. (Among the earthquakes of which the spectral analysis has been carried out⁷⁾ all of the earthquakes whose magnitude has been presented⁸⁾

---

4) A. **IMAMURA**, "Report of the Investigation of the Kwanto Earthquake", *Rep. Imper. Earthq. Inv. Comm.*, No. 100 A (1925), 27, (in Japanese).

5) M. **ISHIMOTO**, Kokin-Shoin, Tokyo, (1925), 113, (in Japanese).

6) K. **KANAI**, "Semi-empirical Formula for the Seismic Characteristics of the Ground", *Bull. Earthq. Res. Inst.*, **35** (1957), 309.

7) J. L. **ALFORD**, G. W. **HOUSNER** and R. R. **MARTEL**, "Spectrum Analysis of Strong-Motion Earthquakes", *1st Tech. Rep. Office Nav. Res., Cotr. N6onr-244, Task Order 25, Project Design.* NR-081-095 (1951).

8) B. **GUTENBERG** and C. F. **RICHTER**, "Seismicity of the Earth", *Princeton University Press* (1954).

Table 1.

No.	Date	Epicenter	M	Location	Epicentral distance in km ($\varDelta$)
1	X, 3, '41	40¾N, 125W	6.4	Ferndale, Calif.	67
2	II, 9, '41	40½N, 125¼W	6.6	〃	86
3	IX, 12, '38	40¼N, 125W	5.5	〃	65
4	XII, 30, '34	32¼N, 115½W	6.5	El Centro, Calif.	61
5	V, 19, '40	32.7N, 115½W	6.7	〃	22
6	III, 11, '33	33.6N, 118W	6.25	Los Angeles, Subway	55
				Vernon, Calif.	48
7	X, 2, '33	33.8N, 118.1W	5.4	Los Angeles, Subway	37
				Vernon, Calif.	31

are treated here.)

In this case, we adopt the following formula as the expression of the relation among magnitude M, epicentral distance $\varDelta$ and maximum vibration amplitude A_m. That is

$$\log A_m = M - 3\log\varDelta + 2.92\text{[9)]} \qquad (11)$$

where $\varDelta$ and A_m measured in km and micron, respectively. Equating the common logarithm of (1) to the special case of (11) in which $\varDelta =$ 100 km, we get

$$\log T_m = 0.39M - 1.88\ . \qquad (12)$$

From (11) and (12), we arrive at the relation,

$$\log\frac{A_m}{T_m} = 0.61M - 3\log\varDelta + 4.80\ . \qquad (13)$$

If equipartition of energy is applicable to the seismic waves, amplitude A measured in cm which corresponds to each period T of seismic waves can be expressed by

$$A = 10^{0.61M - 3\log\varDelta + 0.80}\cdot T\ . \qquad (14)$$

---

9) B. GUTENBERG and C. F. RICHTER, "Earthquake Magnitude, Intensity, Energy and Acceleration", *Bull. Seism. Soc. Amer.*, **32** (1942), 163.

And then, acceleration α measured in gal can be written as follows:

$$\alpha=\frac{(2\pi)^2\cdot 10^{0.61M-3\log\Delta+0.80}}{T}. \tag{15}$$

Substituting the values of M and Δ of Table 1 in (15), the accelerations correspond to the periods of Column 3 in Table 2 are calculated. The results of them are shown in Column 5 in Table 2.

Table 2.

No.	Observation			Calculation	
	Maximum acceleration in gal	Predominant period in sec	Ratio of maximum velocity to constant velocity	Acceleration corresponding to τ in gal	α_0/α_c
	α_0	τ	m	α_c	
1	120	0.3	4	22	5
2	70	0.3	4	14	5
3	90	0.2	4	10	9
4	140	0.5	4	20	7
5	300	0.5	4?	300	1
6	50	0.65	2	15	3
6′	150	0.3	2?	41	4
7	50	0.6	2	16	3
7′	110	0.35	3	47	2

It will be seen from Table 2 that the values of the maximum acceleration observed are several times larger than those calculated. The reason of the difference mentioned above can be explained in the same way pointed out in the former chapter, that is, equation (1) has been obtained from the seismograms at -300 m underground and the seismograms treated here are the records of the motions magnified due to the vibration characteristics of ground. If the above explanation is true, the value of α_0/α_c (α_0=observed acceleration, α_c=calculated acceleration) in any earthquake at a place must be definite.

Hereafter, we examine the values of α_0/α_c shown in Table 2 in order to know whether the above explanation is true or not.

The full lines in Figs. 3∼11 show the velocity spectra in the cases of zero damping of the analyzer[10]. It will be seen from Figs. 3∼11 that, in many cases, every velocity takes comparatively the same value throughout every period excepting around period τ (τ is the period correspond to the maximum acceleration.) That is to say, it may be said that the strong earthquake motion at bed rock satisfies the energy equipartition, and at ground surface the amplitude is magnified considerably according to the vibration characteristics of the ground. (Only for reference, the acceleration spectra are shown in Figs. 12～20.) The values of magnification in Column 4 in Table 2 represent the ratios between velocity corresponding to period τ and assumed constant velocity which is represented by broken lines in Figs. 3～11. In each case, the values in Columns 4 and 6 in Table 2 seem somewhat different but the calculated values can be corrected easily by adjusting epicentral distance.

---

[10] *loc. cit.*, 7).

(i) In the cases of Ferndale, California, the values of m in Nos. 1, 2 and 3 and α_0/α_c in Nos. 1 and 2 are nearly equal but α_0/α_c in No. 3 is different from these five. If we adopt 54 km as the value of epicentral distance $\varDelta$ instead of 65 km in No. 3, the value of α_0/α_c becomes equal to those of Nos. 1 and 2.

(ii) In the cases of El Centro, California, there is a great difference between the values of α_0/α_c as shown in Nos. 4 and 5. As the reason for this, two cases may be considered; one is that the wave forms are complicated as the observation position is near to the point of origin and the other is that the error of calculation of α_c becomes large as the hypocentral distance is small. In No. 4, if we adopt 50 km as the value of $\varDelta$ instead of 65 km, α_0/α_c becomes nearly equal to m.

(iii) In the case of Los Angeles Subway Terminal and Vernon, California, the values of α_0/α_c as well as m in Nos. 6 and 7 are nearly equal. At any rate, it is a noteworthy result that the amplitude of earthquake motion seems to become maximum at a proper period of each observation station.

4. Conclusions

From the present investigation, we knew that the following empirical formula seems to be applicable to destructive earthquakes. That is

$$A_{m\cdot s}=53T_m^{2.56}\,. \qquad (1)$$

At the same time, the present results tell us that, in the case of destructive earthquakes as well, equipartition of energy is recognized in regard to the waves at bed rock, and there is the considerable modification of wave amplitudes according to the vibration characteristics of the ground.

If we assume (i) magnitude of earthquake, (ii) epicentral distance from engineering judgement according to the results of statistical studies of seismicity for (iii) space as well as (iv) time, we can obtain the spectrum of seismic waves at bed rock. And if, (v) vibration characteristics of the ground are added to them, the seismic factor of the ground for earthquake engineering can be estimated resonably.

At any rate, the results of the present investigations show promise of giving information about the waves to be expected in destructive earthquakes, by means of the general application of the many results of investigations concerning common earthquakes.

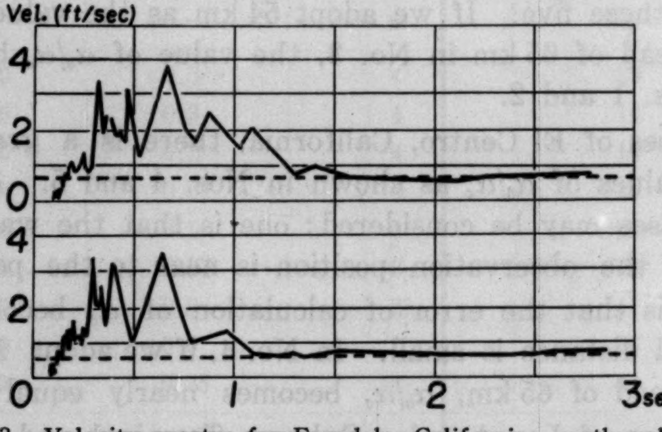

Fig. 3. Velocity spectra for Ferndale, California; earthquake of Oct. 3, 1941. Components: N 45 E (lower), S 45 E (upper).

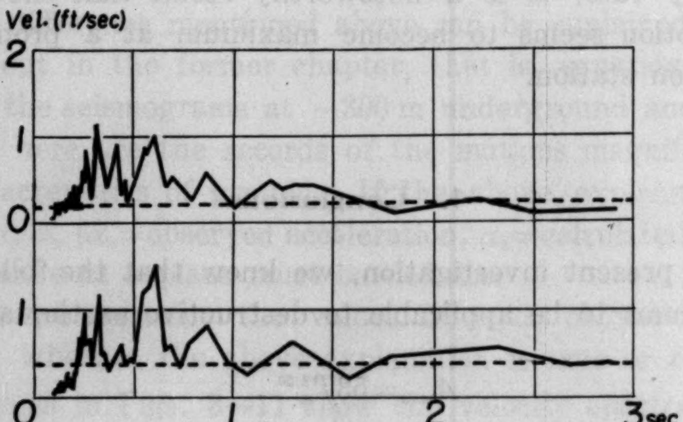

Fig. 4. Velocity spectra for Ferndale, California; earthquake of Feb. 9, 1941. Components: N 45 E (lower), S 45 E (upper).

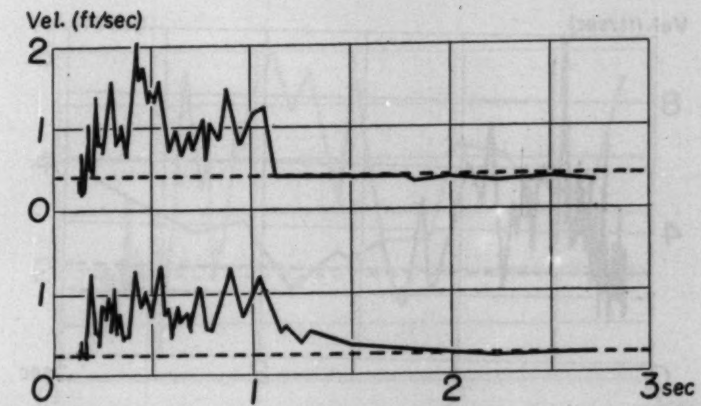

Fig. 5. Velocity spectra for Ferndale, California; earthquake of Sept. 11, 1938. Components: N 45 E (lower), S 45 E (upper).

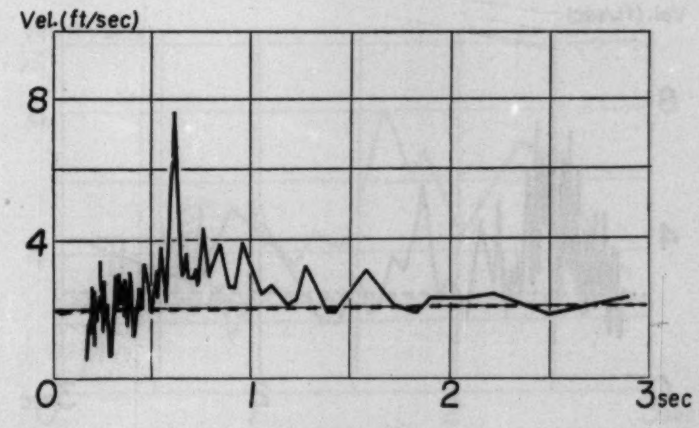

Fig. 6a. Velocity spectrum for El Centro, California; earthquake of Dec. 30, 1934. Component N-S.

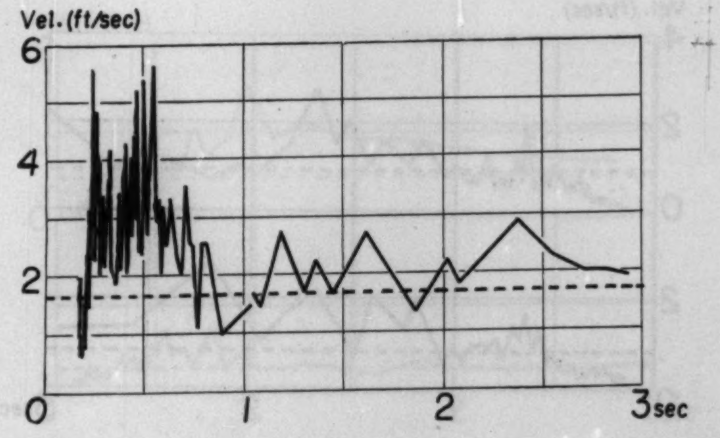

Fig. 6b. Velocity spectrum for El Centro, California; earthquake of Dec. 30, 1934. Component E-W.

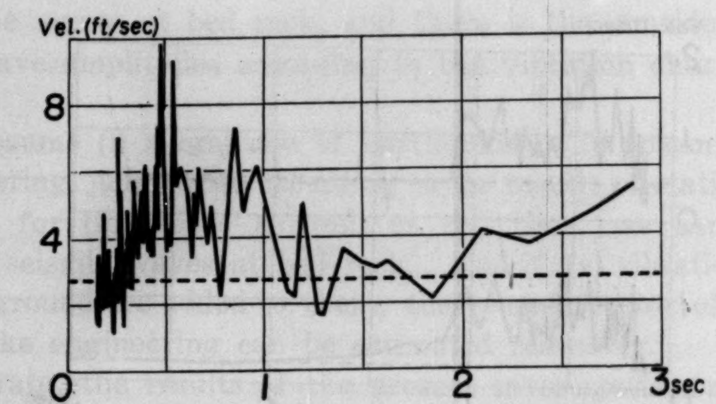

Fig. 7a. Velocity spectrum for El Centro, California; earthquake of May 18, 1940. Component N-S.

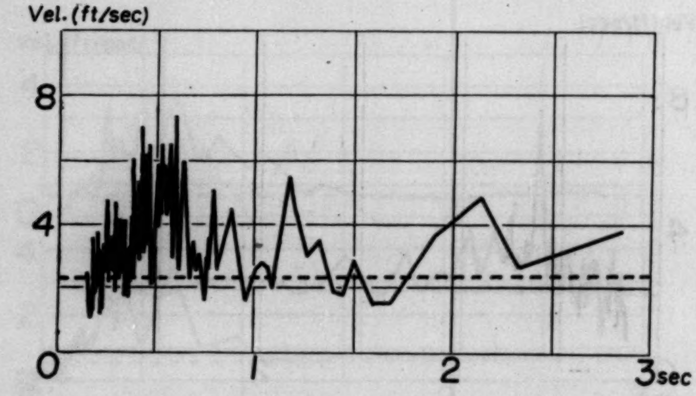

Fig. 7b. Velocity spectrum for El Centro, California; earthquake of May 18, 1940. Component E-W.

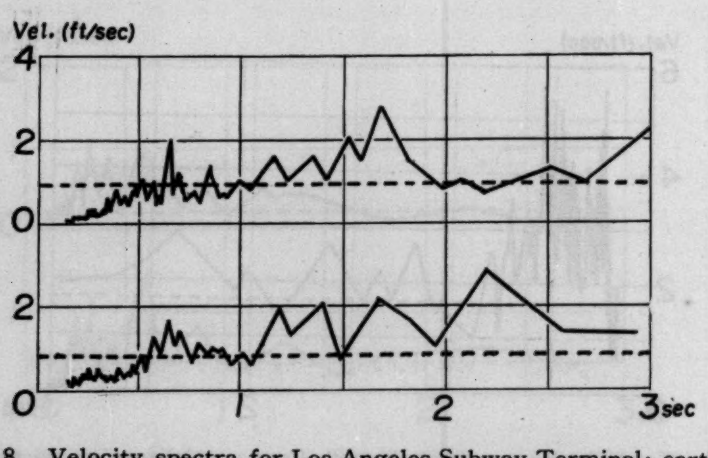

Fig. 8. Velocity spectra for Los Angeles Subway Terminal; earthquake of March 10, 1933. Components: N 39 E (lower), N 51 W (upper).

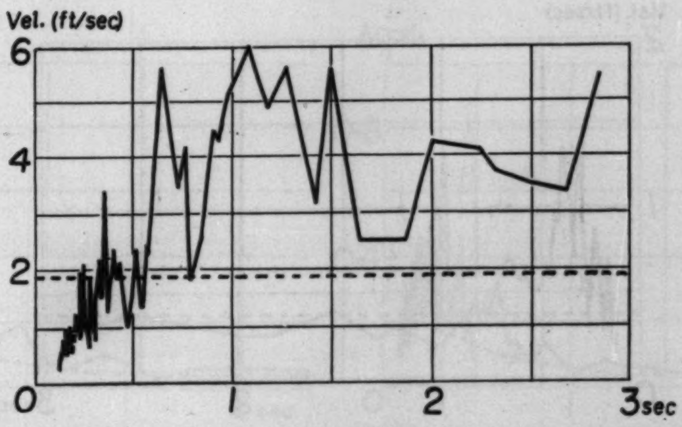

Fig. 9a. Velocity spectrum for Vernon, California; earthquake of March 10, 1933. Component N 08 E.

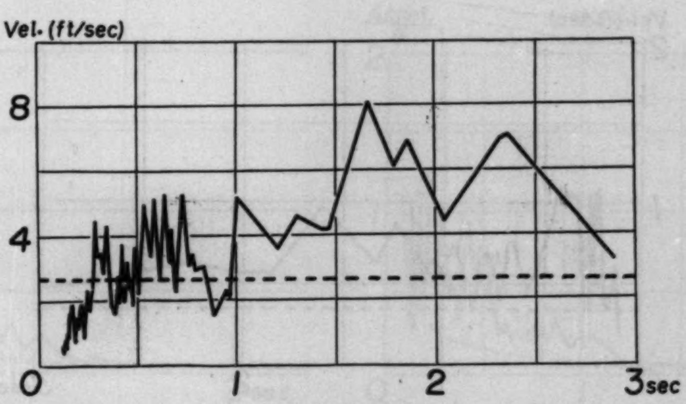

Fig. 9b. Velocity spectrum for Vernon, California; earthquake of March 10, 1933. Component S 82 E.

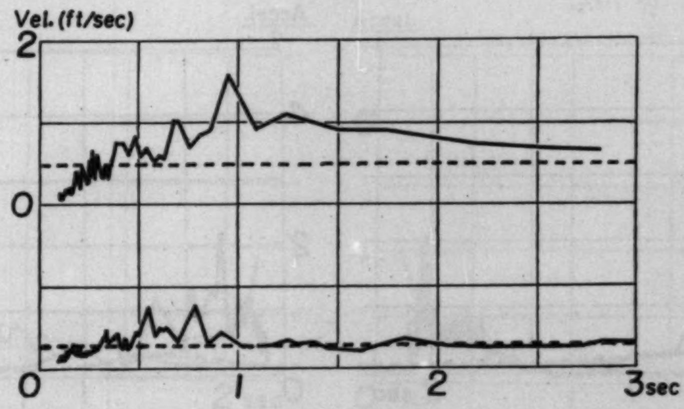

Fig. 10. Velocity spectra for Los Angeles Subway Terminal; earthquake of Oct. 2, 1933. Components: N 39 E (lower), N 51 W (upper).

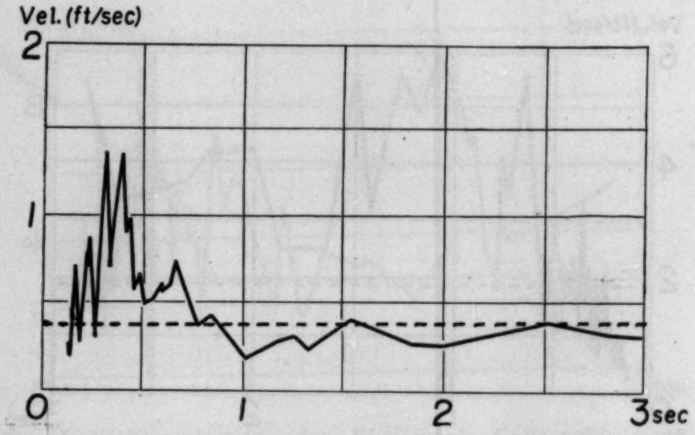

Fig. 11a. Velocity spectrum for Vernon, California; earthquake of Oct. 2, 1933. Component N 08 E.

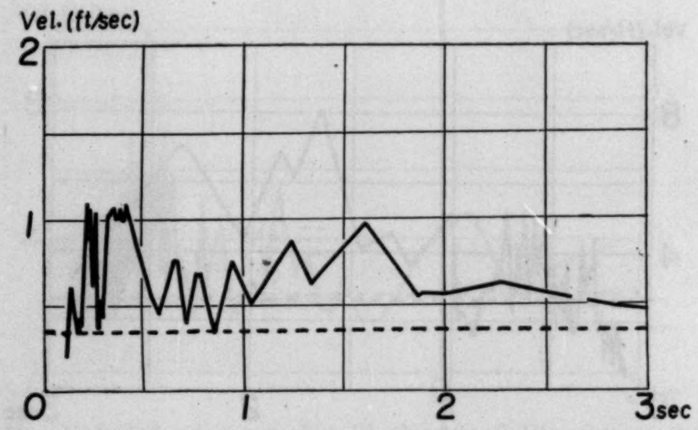

Fig. 11b. Velocity spectrum for Vernon California; earthquake of Oct. 2, 1933. Component S 82 E.

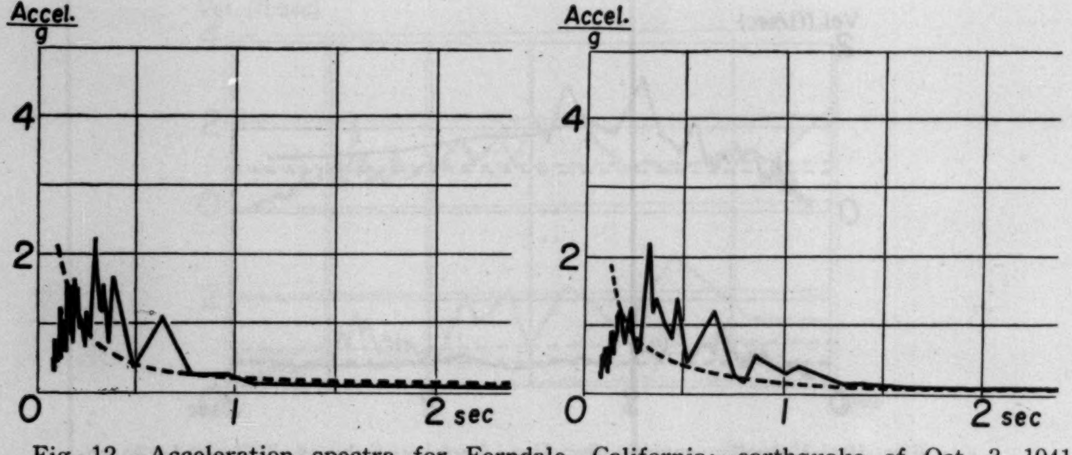

Fig. 12. Acceleration spectra for Ferndale, California; earthquake of Oct. 3, 1941. Components: N 45 E (left), S 45 E (right).

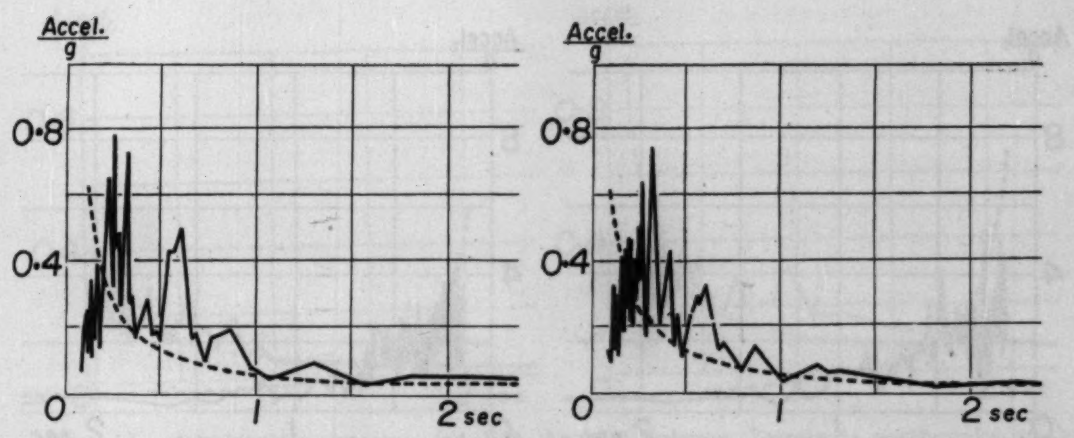

Fig. 13. Acceleration spectra for Ferndale, California; earthquake of Feb. 9, 1941. Components: N 45 E (left), S 45 E (right).

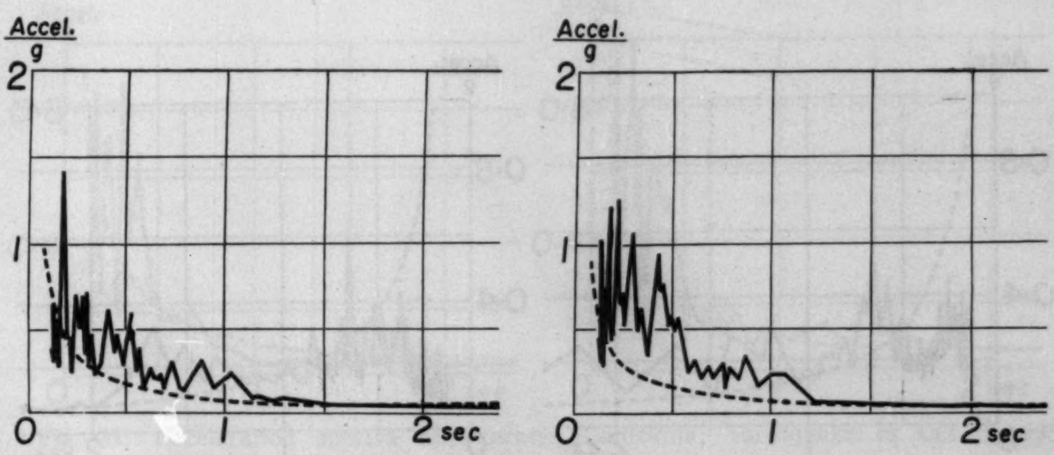

Fig. 14. Acceleration spectra for Ferndale, California; earthquake of Sept. 11, 1938. Components: N 45 E (left), S 45 E (right).

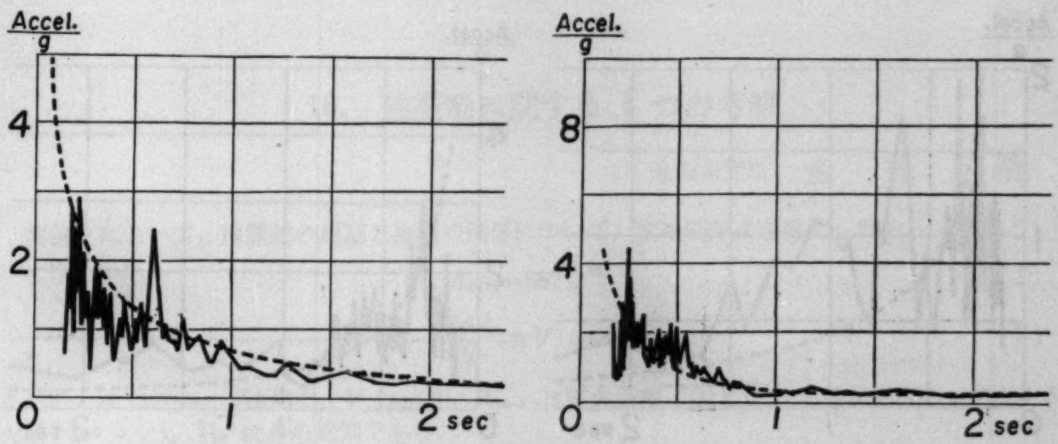

Fig. 15. Acceleration spectra for El Centro, California; earthquake of Dec. 30, 1934. Components: N–S (left), E–W (right).

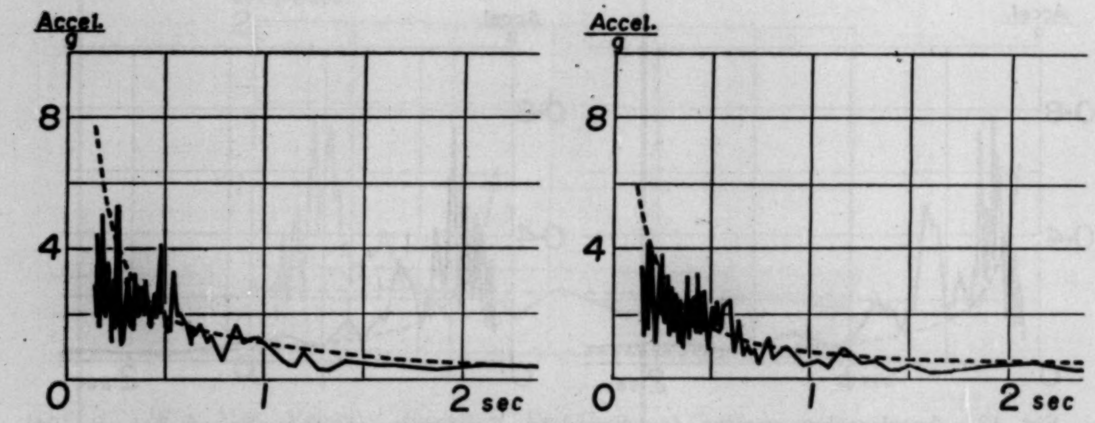

Fig. 16. Acceleration spectra for El Centro, California; earthquake of May 18, 1940. Components: N-S (left), E-W (right).

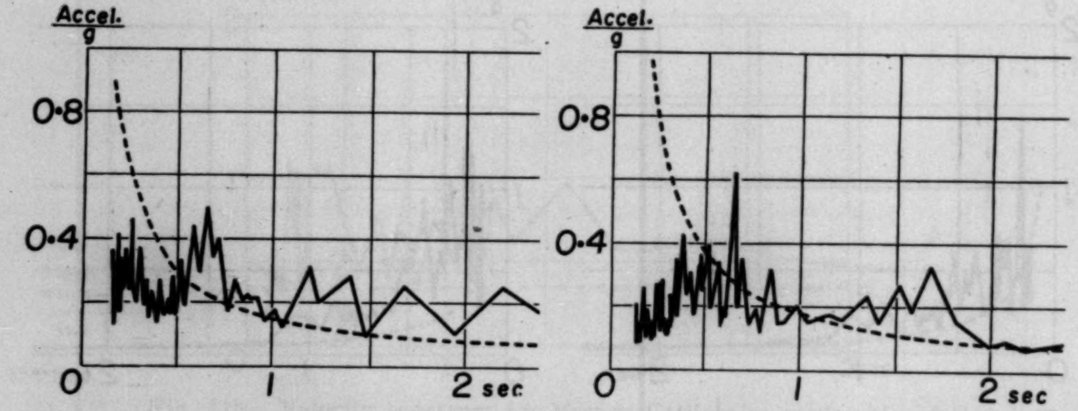

Fig. 17. Acceleration spectra for Los Angeles Subway Terminal; earthquake of March 10, 1933. Components: N 39 E (left), N 51 W (right).

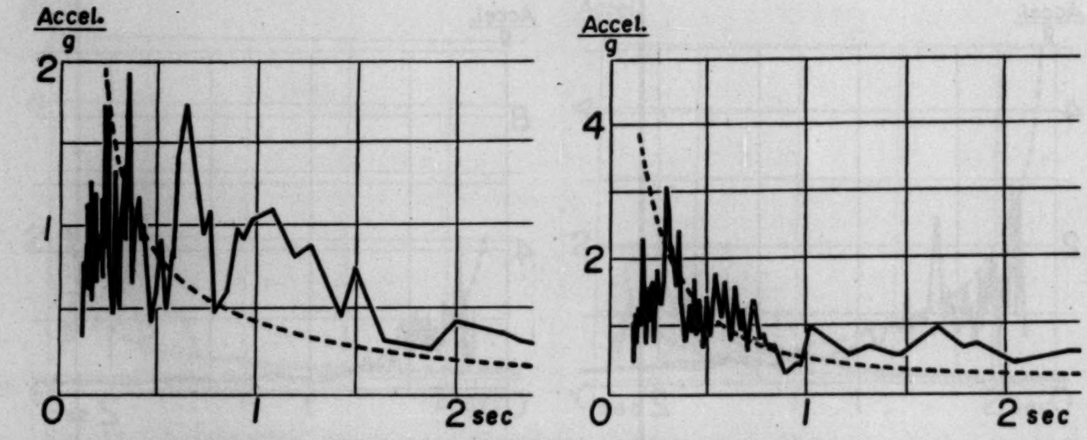

Fig. 18. Acceleration spectra for Vernon, California; earthquake of March 10, 1933 Components: N 08 E (left), S 82 E (right).

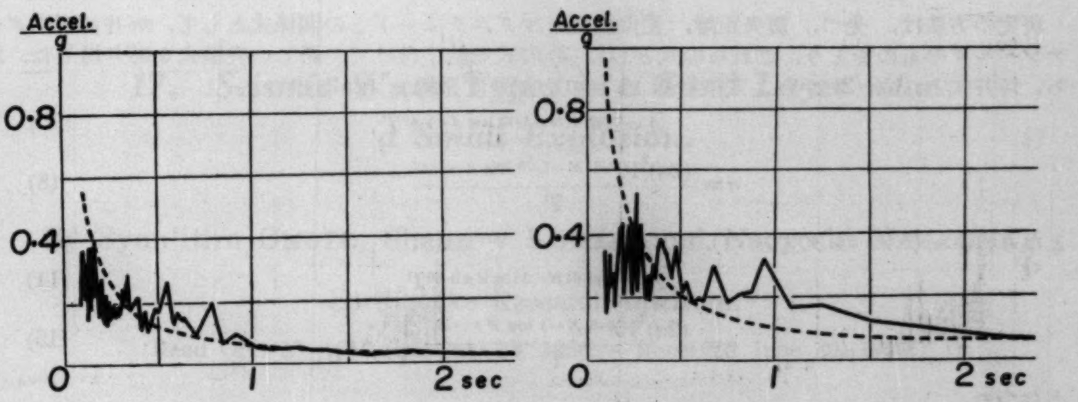

Fig. 19. Acceleration spectra for Los Angeles Subway Terminal; earthquake of Oct. 2, 1933. Components: N 39 E (left), N 51 W (right).

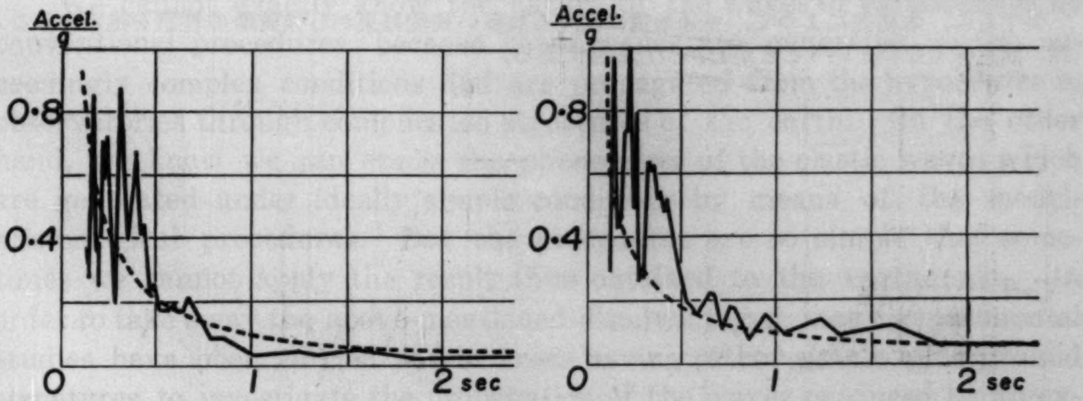

Fig. 20. Acceleration spectra for Vernon, California; earthquake of Oct. 2, 1933. Components: N 08 E (left), S 82 E (right).

---

16. 強震動に関する 1 つの考察

地震研究所　金　井　清

前論文において，地震動の周期と振幅の関係について，次の関係式を得た．即ち，

$$A_{m\cdot s}=53T_m^{2.56}, \qquad (1)$$

$$\frac{2\pi A}{T}(\equiv V)=\text{一定} \qquad (2)$$

ここに，A は振幅，Tは周期，V は速度，$A_{m\cdot s}$ は震央距離 100 km における変位スペクトルの最大値(ミクロン)，T_m はその周期である．

本研究では，普通の大きさの地震で得られた，これらの実験式が，はたして構造物に破壊をもたらすような地震動にもあてはまるかどうかをしらべたものである．

研究の方法は，先づ，震央距離，変位振幅とマグニチュードとの関係式として，坪井並びにグーテンベルグのものをとり，これらの式と(1), (2)の式を結び付けて，新しい実験式を導き出した．即ち，坪井式と(1), (2)から，変位振幅 A (cm)，加速度振幅 α (gal)は，

$$A=10^{0\cdot61M-1\cdot73\log\varDelta-1\cdot47}T\,, \tag{7}$$

$$\alpha=\frac{(2\pi)^2 10^{0\cdot61M-1\cdot73\log\varDelta-1\cdot47}}{T} \tag{8}$$

となり，グーテンベルグ式と(1), (2)からは

$$A=10^{0\cdot61M-3\log\varDelta+0\cdot80}T\,, \tag{14}$$

$$\alpha=\frac{(2\pi)^2 10^{0\cdot61M-3\log\varDelta+0\cdot80}}{T} \tag{15}$$

となつた．

次に，関東地震の東京に於ける地震記象から推定された値及びアメリカ合衆国で得られた強震記録並びにその解析結果と(7), (8)及び(14), (15)を使つた計算結果とを比較した．その結果は，地盤による震動の増幅を考慮に入れると，計算値と実測値が相当によく合うことを示した．

要するに，本研究によつて，普通地震に関する数多い研究結果から強震動の性質を推定することが，無意味でないということがわかつたわけである．

BULLETIN OF THE EARTHQUAKE
RESEARCH INSTITUTE
Vol. 36 (1958), pp. 311-327

17. *Seismic Wave Types in a Sand Layer near a Small Explosion.*

By Syun'itiro OMOTE, Shauzow KOMAKI and Naoyoshi NAKAJIMA,

Earthquake Research Institute.

(Read Oct. 25, 1955 and Oct. 23, 1956.—Received June 30, 1958.)

Introduction

We cannot exactly know the nature of the waves of earthquakes by conventional procedures, because these waves are generated under exceedingly complex conditions and are propagated from the hypocentre to observatories through complicated structures of the earth. On the other hand, we know we can study the phenomena of the elastic waves which are generated under ideally simple conditions by means of the model-seismological procedures. But the procedures are so simple that sometimes we cannot apply the result thus obtained to the earthquake. In order to take away the above-mentioned disadvantages, many experimental studies have been carried out in areas having rather simple underground structures to investigate the propagation of the waves produced by an explosion. We may say that we can expect the simplicity of conditions next to that of model seismology in the case of explosion-seismological experiments, and that a full investigation of the observation results obtained in the course of such experiments is useful for the understanding of earthquake phenomena generated in extremely complex conditions.

Because of these considerations, the Seismic Exploration Group of Japan headed by K. Sassa has been carrying out active research along this line since 1953, and is getting fruitful results. As a part of these activities an experiment was carried out on the sand shore of the Japan Sea in Niigata Prefecture by one of the authors with the cooperation of H. Sima and the Research Team of the Japan Petroleum Exploration Co. Ltd., in 1955. The object of the experiment was to promote the study of the generation and the propagation of seismic waves in sand layers near a small explosion. This experiment was supplemented at the same area in the following year, for the purpose of getting some necessary additional data to improve its results.

Experimental procedures

Location

We made experiments in an area on the skirts of dunes, where there was a fairly thick, uniform layer of coarse sand near the surface as illustrated by the core log in Fig. 1. The slant area of the test site was smooth and of no surface irregularities. The result of the test of grain-size distribution of the coarse sand is tabulated in Table 1 and the cumulative curve of its grain size is steep, as shown in Fig. 1. The area which consists of almost homogeneous and uniform media and has fairly simple underground structures is suitable for seismic experiment by means of a small explosion.

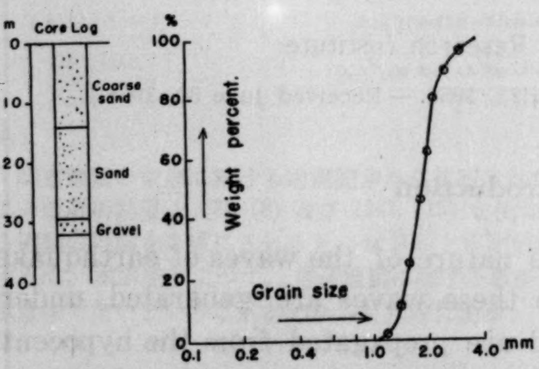

Fig. 1. Sample log and cumulative curve of the coarse sand at the test site.

Table 1. Grain-size distribution of the coarse sand at the test site.

Grain size	Weight percent
> 5 mm	0
5~2.5	5.9
2.5~1.2	93.3
1.2~0.6	0.8
< 0.6	0

In 1955, as will be described later, the experiment was carried out at a site situated about 20 m away from the brink (Traverse A). Judging from the results of the travel-time curves obtained in the observations, it was certain that there was a plane of discontinuity at about 2.8 m below the surface. This seems to be the boundary plane between the sand layer soaked in sea water and the dry sand layer in view of the topography, because there was no geological discontinuity as shown in the core log. Consequently, it means that we conducted the experiment in 1955 on an area having a half space covered with a horizontal single layer. Naturally, the records thus obtained were not so simple as was expected. In 1956, to carry out a seismic experiment on an ideal uniform half space, we set up a traverse (Traverse B) just along the brink which had one layer consisting of saturated sand at the same site. Moreover, the other traverse (Traverse C) was set up on the same line as in 1955.

Equipment

The equipment used in recording the ground motion was similar to that used commonly in seismic prospecting. E. T. L. geophones, having natural frequencies of 27 cps, were used at each traverse. The output of the geophones was connected to an oscillograph without an amplifier. The galvanometers used in the oscillograph were San-ei's G-100 type, having natural frequencies of 100 cps.

Shooting procedure

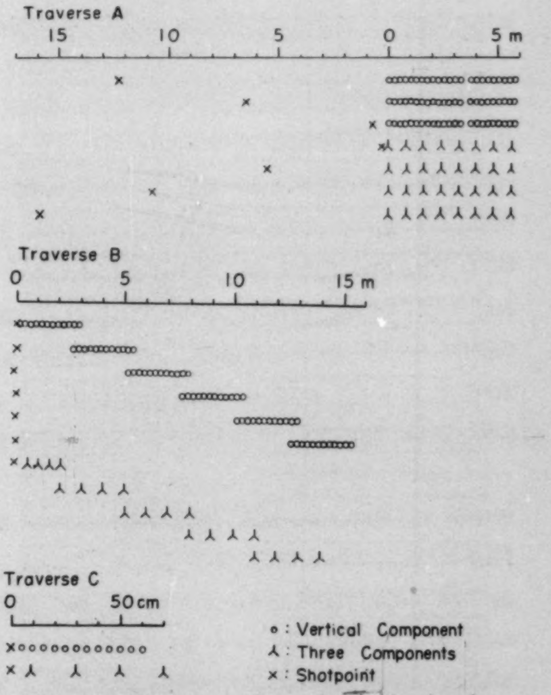

Fig. 2. Location of geophones in the shooting procedure.

In the experiments extending over two years we set up three traverses in all, i.e. A, B and C as shown in Fig. 2. These three traverses were parallel to the straight brink.

Twenty-three vertical geophones were installed along Traverse A at every 25 cm. The epicentral distance spreads from 25 cm to 18 m by removing the shot points. Three-component observations were made at every 75 cm interval.

Along Traverse B, equipment limitations required the use of several spread segments, with common end geophones, to achieve the desired spread coverage. In this case the shot point was fixed. The space of each geophone in the vertical and the three-component observations was 25 cm and 50 cm respectively.

Similar measurement was carried out on a smaller scale along Traverse C. The interval of each geophone in the vertical and the three-component observations was 5 cm and 20 cm respectively.

As vibration sources we used caps and dynamite in 1955 and caps and carlit in 1956. The charge amount was augmented in proportion to the extent of distance.

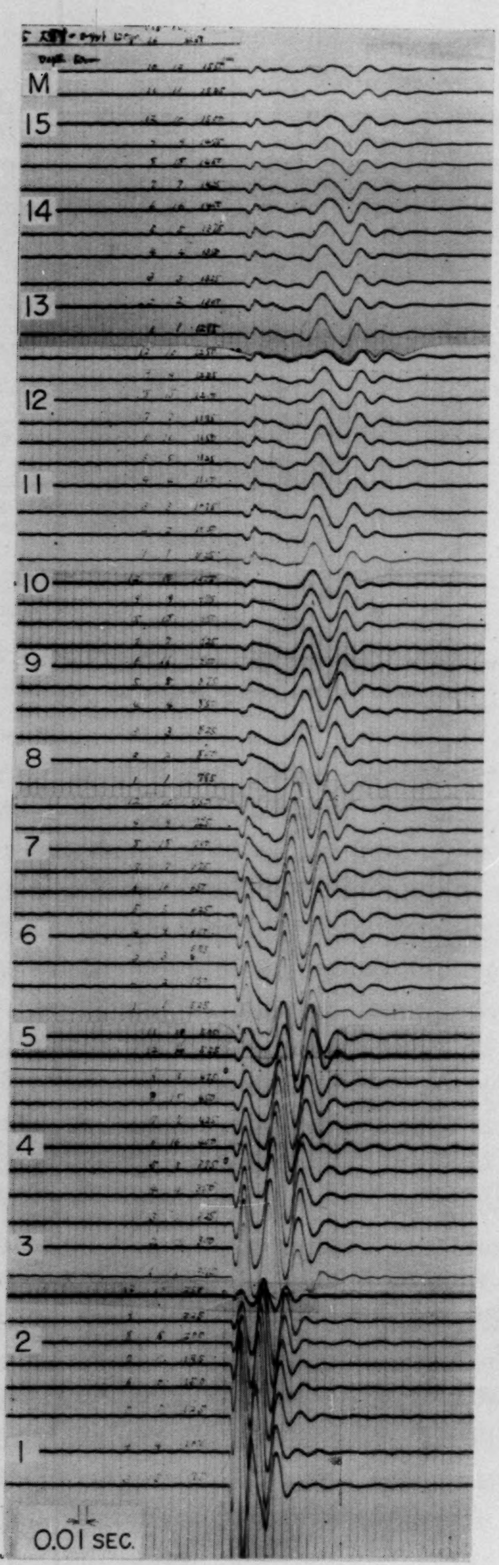

Fig. 3. Typical vertical records obtained along Traverse A.

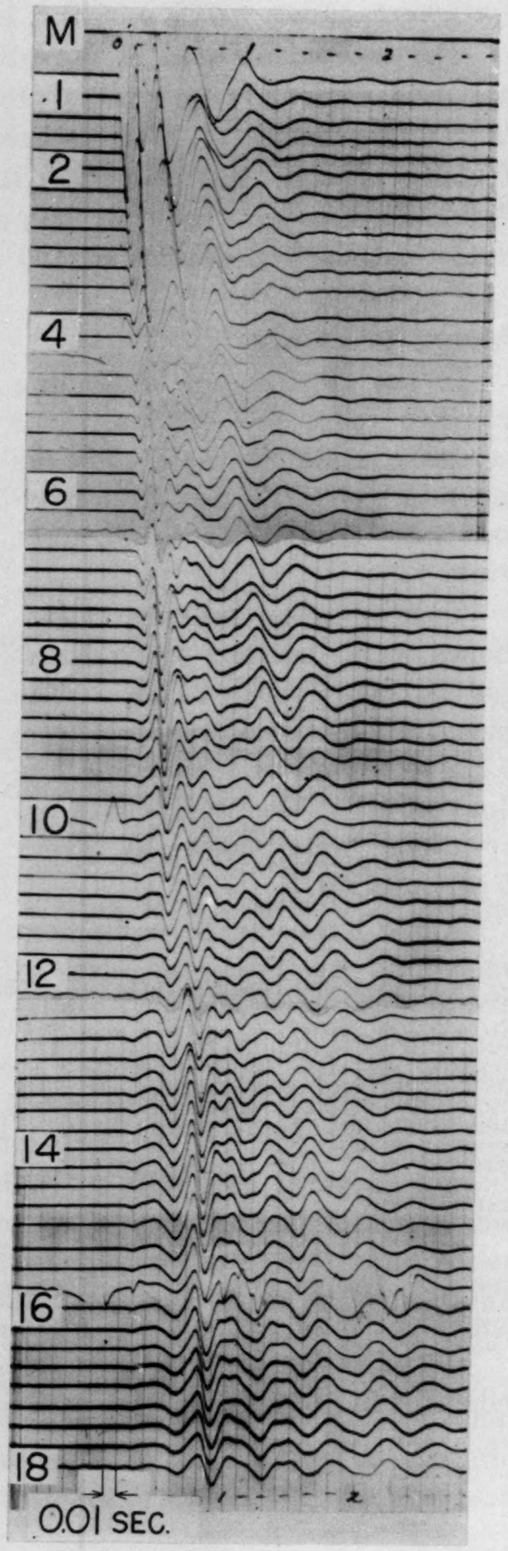

Fig. 4. Typical vertical records obtained along Travese B.

Observed records and travel-time curves

The records of the vertical observations at Traverse A are shown in Fig. 3. The seismograms point out that the experiment has succeeded in getting fairly simple records of small explosions in an area having simple underground structures. The first step in the study of these records was to make travel-time curves. These curves were constructed for all peaks and troughs which had characteristics by which they could be traced. The results on the vertical observations at Traverse A are shown in Fig. 5. This graph will be useful for the classification of wave groups. The slopes of the lines connecting each peak or trough indicate the phase velocities of the respective waves.

In Fig. 5, we have four wave groups having different phase velocities. Roughly speaking, the first wave group shows a similar slope to that of the initial motion at a distance of over 6.5 m. The wave pertaining to this group continues only about half a period. The slope of the second wave group which continues 1∼1.5 periods, is like that of the initial motion at a distance of less than 6.5 m. In another predominant group, i.e. the fourth wave group, the slope is much steeper than those of the two groups, and the duration is 1∼1.5 periods. We find a weak wave group, i.e. the third wave group, between the second and the fourth groups.

Speaking in detail, a train of dots representing the travel-time of peaks or troughs, e.g. II-1U or II-1D, usually do not stand in a straight line, but in the form of the combination of several intermittent lines. That is to say, both the phase velocity and the period of wave gain as the epicentral distance becomes longer. In the second wave group, the phase velocity which shows a value of about 250 m/sec near the shot point amounts to about 350 m/sec and 460 m/sec respectively in the vicinity of 10 m and 15 m from the shot point. Neverthless, the phase velocity of each wave group is given in Table 2 as the mean value of the all phase velocities involved in the group itself. While the period of wave in the second wave group shows values of about 0.013 sec, 0.017 sec and 0.020 sec respectively near the shot point and two other places stated above. The mean values of the period of wave of the four groups are also listed in Table 2 in the same way as those of the phase velocity.

Of these four wave groups, the first one is the bodily P wave propagated through the substratum. The initial arrival and the first peak, i.e. II-1U, of the second wave group represent the bodily P wave

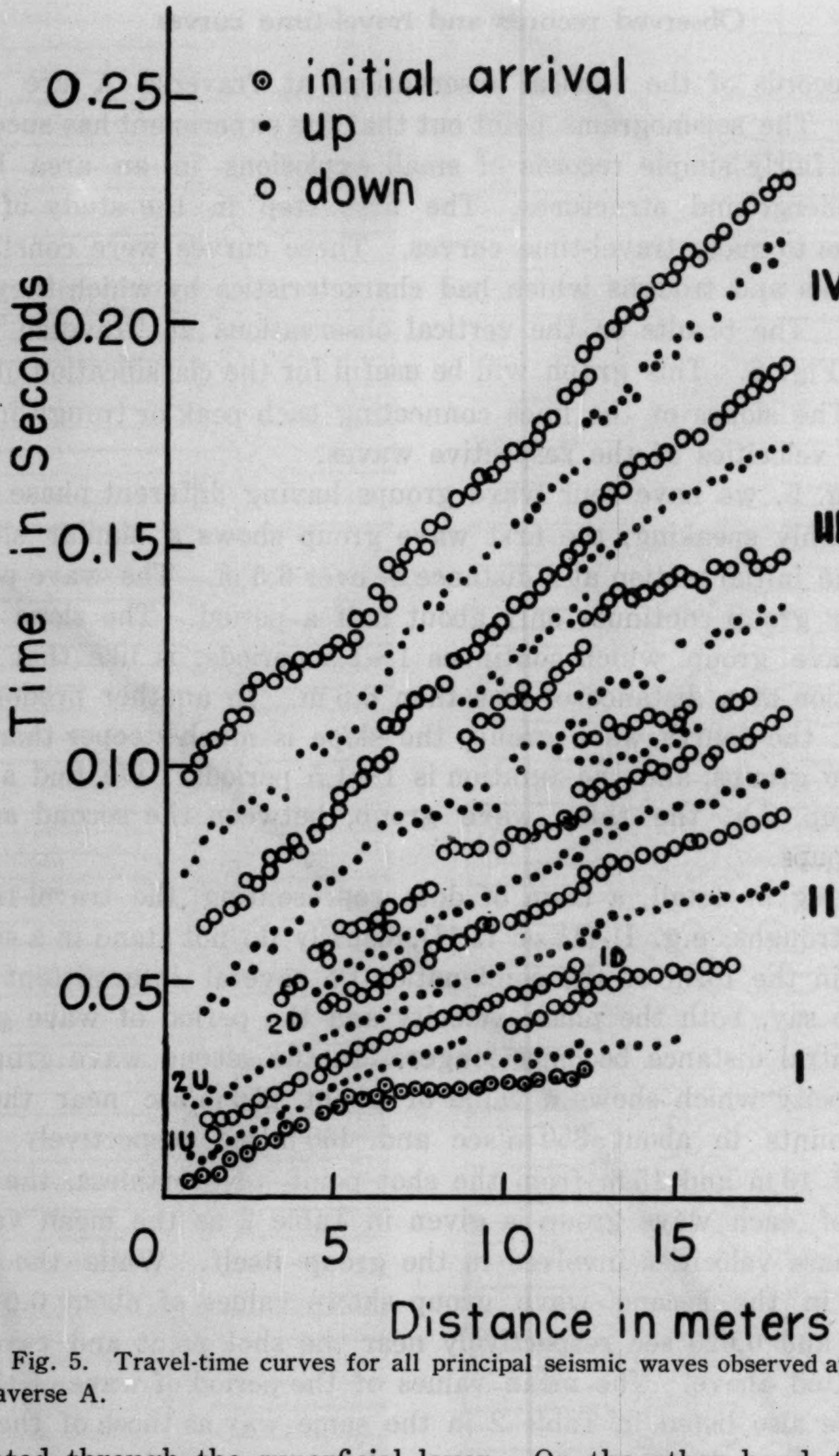

Fig. 5. Travel-time curves for all principal seismic waves observed at Traverse A.

propagated through the superficial layer. On the other hand, the undulation following the initial wave in the same wave group has a dispersive characteristic that the period of wave becomes longer as the phase velocity increases which we have seen in the preceding paragraph.

Table 2. Classification of the wave groups.

Group	Phase velocity	Period
I	1400 m/sec	1.1×10^{-2} sec
II	340	1.6
III	210	2.0
IV	135	3.6

Because of this dispersive characteristic, we considered this part of the waves in the second group as a kind of surface wave. H. Takeuchi and N. Kobayashi[1] had given an opinion that the latter part of the second wave group will be explained as a kind of surface P wave. The third and the fourth wave groups are regarded as surface waves from their dispersive characteristic as in the case of the second wave group.

The travel-time curve from the initial arrival consists of two segments and indicates that the ground structure of the area is not a simple uniform half-space. On the assumption that the ground structure is a half space covered with a horizontal single layer, the depth of the boundary plane is calculated as about 2.8 m. Keeping the topography of the area in mind, it can be concluded that this boundary represents an interface between the dry sand layer and the thick water-soaked sand layer, both of uniform elastic properties, and that the upper layer has a P-phase velocity of 245 m/sec and the lower layer has one of 1400 m/sec which appears to be constant for a spread of distance out to 20 m.

In 1956, in order to conduct the seismic experiment on an ideal uniform half-space, small explosion-seismic observations were made on Traverse B which was set up just along the brink. In this experiment it was reasonablly expected that a superficial overburden of a dry sand layer such as we found in of Traverse A would not be found any longer in Traverse B, because the latter traverse was set up so close to the brink.

The records of the vertical observations on this traverse are illustrated in Fig. 4, arranged in order of epicentral distance. On the basis of these recordes, we made the time-distance plot for all peaks and troughs in the same way as in the case of Traverse A, the result of which is shown in Fig. 6. From this graph it can be seen that the slope of the plot consists of only two groups. The first group has a phase velocity of 1460～1480 m/sec, similar to that of the first group at

---

[1] H. TAKEUCHI and N. KOBAYASHI, *Rep. Seis. Exp. Group of Japan*, **9** (1956), 1, (in Japanese).

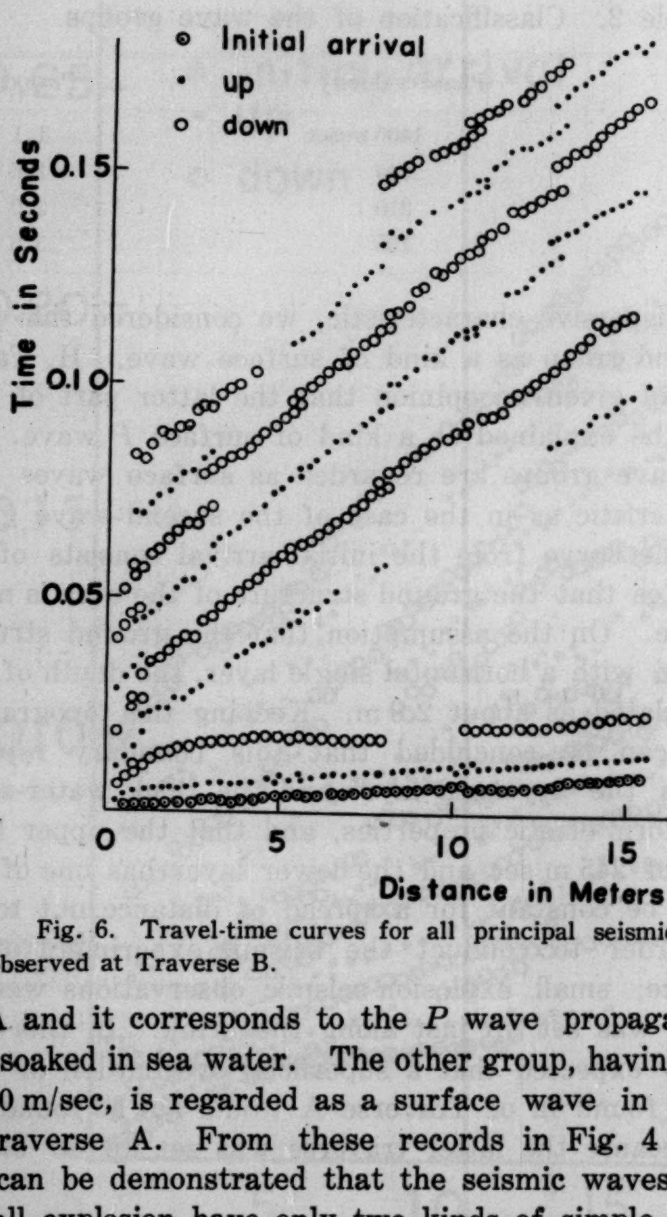

Fig. 6. Travel-time curves for all principal seismic waves observed at Traverse B.

Traverse A and it corresponds to the *P* wave propagated through the sand layer soaked in sea water. The other group, having a phase velocity of 160~180 m/sec, is regarded as a surface wave in reference to the case of Traverse A. From these records in Fig. 4 and the graph in Fig. 6, it can be demonstrated that the seismic waves in a sand layer near a small explosion have only two kinds of simple wave group, provided the observation is made in an area of a really uniform half-space.

Increase and diminution of wave energy

The amplitude of each peak and trough increases or diminishes regularly as the epicentral distance becomes longer, as can be seen in Figs. 3 and 4.

For example, the peak II-1U illustrated in Fig. 5 is predominant near the shot point, but it shows fair decay around 7 m and at last it can hardly be seen in the vicinity of 9 m from the shot point. The trough II-1D which follows II-1U, has a longer life. It shows still considerable predominance around 8 m from the shot point, but it becomes weaker at 10 m and practically disappears around 12 m from the shot point. The trough II-2D can hardly be recognized just near the shot point. It comes in sight for the first time around 4 m and gains energy after that. Though its development reaches the climax at the point of 13～14 m, the trough returns to falling and at last shows a considerable decline in the vicinity of 18 m from the shot point. We find that the same rise and fall as in this case is seen in the other wave groups. The following description is the outline of the increase and diminution of wave energy about the second and the fourth wave groups.

Needless to say, we should pay attention to the existence of the following two unfavorable factors in the case of examining the aspect of the rise and fall of each peak or trough in a given wave group:—i) The error caused by the lack of uniform sensitivity of equipment in each trace. ii) The troubles caused by the fact that the wave generated by an explosion generally has a tendency to attenuate with the extension of the distance from the shot point.

In order to avoid the unfavorable influences caused by these disadvantages, we adopted the following simple methods. The procedure we took to get rid of the first factor was as follows. We concentrated the geophones at a point 30 m from the shot point to test whether each trace keeps uniform sensitivity. In the records thus obtained we read off the values of the amplitudes of the corresponding waves of all traces and then calculated the ratio of the value of each amplitude to the mean value of all the corresponding amplitudes. We regarded the value of the ratio for each trace as each relative sensitivity. Dividing the amplitude of each peak or trough by the corresponding relative sensitivity, we obtained the corrected amplitude.

After this procedure was performed for all amplitudes, the following procedure was taken to get rid of the second factor. We measured the corrected maximum amplitude of each group at respective distances. The relations between the maximum amplitudes thus obtained and the epicentral distance are illustrated in Figs. 7 and 8, which respectively correspond to the second and the fourth groups. Though we can find some disturbance at a great distance in each figure, a regularly logarithmic decrease of the maximum amplitude is seen in each group as

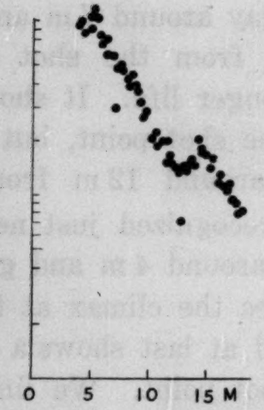

Fig. 7. Corrected maximum amplitude related to the epicentral distance for the second wave group.

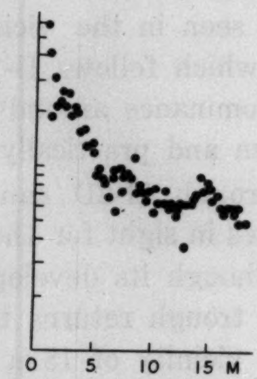

Fig. 8. Corrected maximum amplitude related to the epicentral distance for the fourth wave group.

the distance becomes longer. We calculated the values of the ratio of the corrected amplitude of each peak or trough to the corrected maximum amplitude with regard to each group at respective distances. Now we can know the aspects of the rise and fall of each peak or trough, because we believe we were able to take away the two unfavorable factors through the above procedures.

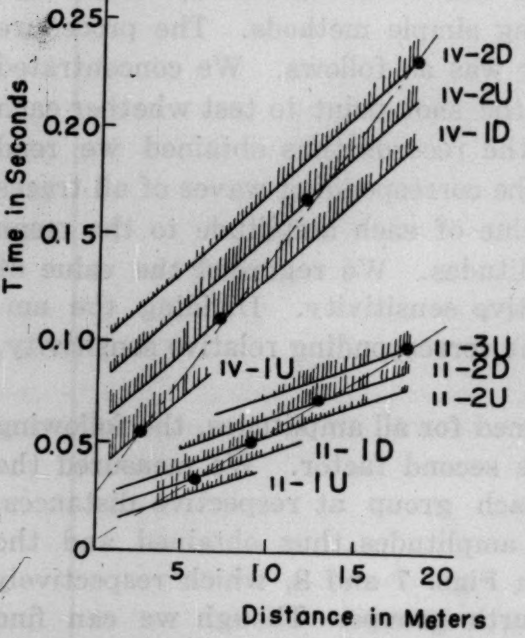

Fig. 9. Rise and fall of each peak ro trough related to the epicentral distance.

Fig. 9 shows the values of the amplitude ratios of the second and the fourth groups, which are drawn on the travel-time curves. The length of the bar is in proportion to the value. We can see clearly the rise and fall of each peak or trough. A wave appears, gains its energy gradually, reaches the climax of energy and after that it loses its energy and in the end disappears. The solid circles in the figure stand for the points where the energy of each peak or trough amounts to maximum. These solid circles of each group seem to stand in a chain line of which the slope shows the minimum group velocity of the wave group, as K. Tazime[2] has pointed out. The values are 190 m/sec and 90 m/sec in the case of the second and the fourth groups respectively. Although the chain line of the second group starts from around the origin, that of the fourth group has a fairly great intercept time. This may be caused by the fact that, in the case of correcting the attenuation of the amplitude of the fourth group derived from the extension of distance, we used the disturbed curve illustrated in Fig. 8 as the standard. Therefore a question arises as to whether each solid circle illustrated in Fig. 9 stands for the maximum energy of each peak or trough of the fourth group or not. As can be seen in Fig. 8, the corrected maximum amplitudes which are used as the denominators of the ratios show greater value as expected in the vicinity of the distance a little farther from the solid circle on the peak IV-2U. So, we may suppose that the apparent energy of a wave at such distance seems to be smaller than it really is. The same question as this may arise in the case of IV-1U and IV-1D and so on. If we put in a strict correction in each case, the apparent slope of the chain line connecting every solid circle in Fig. 9 will pass near the origin. It represents a characteristic of a dispersive surface wave that the chain line whose slope shows the group velocity starts from the origin in the travel-time graph. From this criterion we conclude that the latter part of the second wave group and the fourth wave group are safe to be considered as surface waves.

Energy of wave groups

In order to classify the wave type of the wave groups, we investigated the aspect of the attenuation of energy of each wave group with regard to the epicentral distance.

We calculated the value of the wave energy by means of Howell's method[3], considering that the recorded amplitude represents the particle velocity. Under the assumption that the seismic energy does not spread radially but is confined to the vicinity of the surface plane and that the velocity of transmission is constant for the whole pulse, the energy flowing through a surface element of unit cross section which is perpendicular to a radial line at radius, R, is:

$$E=\frac{\rho c}{2}\sum v^2 \Delta t\,,$$

---

[2] K. TAZIME, *Journ. Physics of the Earth*, **4** (1956), 113.

[3] B. H. HOWELL, Jr. and D. BUDENSTEIN, *Geophysics*, **XX** (1950), 33.

where ρ represents the density of the medium, v the particle velocity, c the velocity of propagation of the energy and Δt the element duration time of the energy. Furthermore, considering the attenuation caused by the viscosity and the solid friction, etc, the formula

$$e^{-\alpha X}=CX^{A}\Sigma v^{2}\Delta t$$

is obtained. Here α stands for the above mentioned rate of attenuation, and A represents the rate of attenuation concerning the distance X, and C is a constant. Between the results of the second and the fourth wave groups on Traverse A, the former proved to be not good. We got $A=1.0\pm0.3$ and $\alpha=0.16\pm0.05/\text{m}$ regarding the fourth group. Therefore, we can guess the energy of the fourth group spreads in a way similar to the surface wave.

As for the energy of the body wave at Traverse B, we calculated the rate of attenuation of the perticle velocity β $(=\alpha/2)$ due to the viscosity, etc, at every spread applying the exponential equation

$$v=v_0X^{-1}e^{-\beta X}$$

to this case under the assumption that the rate of attenuation of the particle velocity as to the distance is 1. In Fig. 10 we plotted the values at every spread thus obtained as corresponding to the middle point of each spread. As can be seen in this figure, β becomes smaller with the extension of the distance from the shot point. Although this may be caused by the fact that we fixed the rate of attenuation regarding the distance as 1, it is possible that there are other causes.

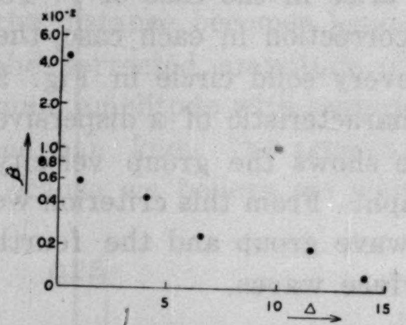

Fig. 10. Relation between the rate of attenuation β and the epicentral distance.

Orbit of ground motion

In order to obtain additional materials for the classification of the wave groups, it is a common procedure to check the orbit of the ground particles due to the seismic waves. In general, the orbit is examined by projecting an actual ground motion on a horizontal or cn a vertical plane containing the seismic source and geophone.

In our measurements, however, we obtained the records of grounb velocity rather than of ground displacement. So the orbits of the particle velocity were drawn except at Traverse B. Fig. 11 shows examples of respective orbits of the second, the third and the fourth wave groups

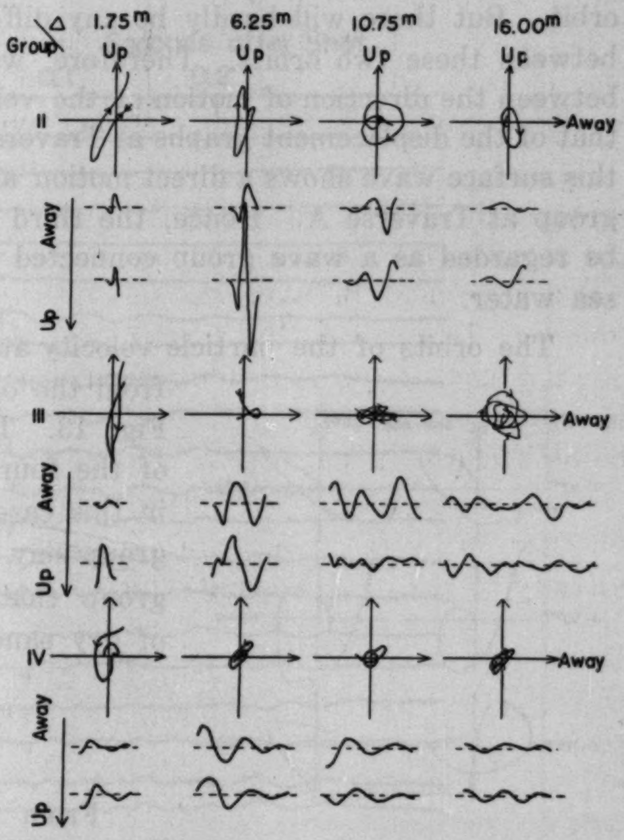

Fig. 11. Ground motion graphs for the second, the third and the fourth wave group at Traverse A.

which were obtained at Traverse A. At the same time, the figure shows the wave forms which were used in the case of drawing the orbits. Judging from the orbits, the second wave group consists of two parts. The first part shows a pull-push motion which is characteristic of a compressional wave. The succeeding part illustrates somewhat vertically polarized motion whose rotational direction is derect. The third group has a direct motion. This group seems to be a kind of typical hydrodynamic wave. H. Sima[4] obtained some reasonable results under the assumption this wave group was an M_{12} wave which was propagated through the surface layer of dry sand underlaid by the water-saturated sand layer. On the other hand, the fourth group shows a retrograde motion. It can be regarded as an ordinary Rayleigh-type wave.

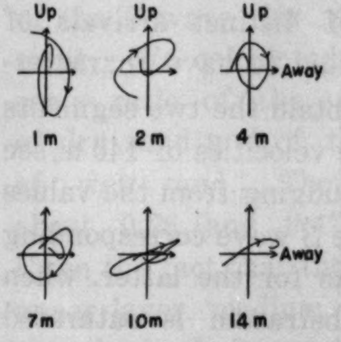

Fig. 12. Ground motion graphs for the surface wave at Traverse B.

We drew the orbits of the actual ground motions on the vertical plane concerning the surface wave at Traverse B. In this case, we obtained the displacement motions by means of integrating the records of the particle velocity according to Sympson's method. On the basis of the result, the particle displacement orbits were shown in Fig. 12. Strictly speaking, the shape of this orbit will be generally different from that of the velocity orbit of the ground motion, because the higher frequency components of ground motion have a greater influence on a velocity orbit than on a displacement orbit. But there will hardly be any difference in a direction of motion between these two orbits. Therefore, we may inquire into the relation between the direction of motion of the velocity orbits at Traverse A and that of the displacement graphs at Traverse B. As can be seen in Fig. 12, this surface wave shows a direct motion and it resembles the third wave group at Traverse A. Hence, the third wave group at Traverse A may be regarded as a wave group connected with the lower layer soaked in sea water.

---

[4] H. SIMA, *Rep. Seis. Exp. Group of Japan,* **11** (1956), 30, (in Japanese).

The orbits of the particle velocity at Traverse C were drawn directly from the observation records, as shown in Fig. 13. The same retrograde orbits as of the fourth group at Traverse A are seen in this case. Therefore, the fourth wave group may be considered as a surface wave group that is related to the upper layer of dry sand.

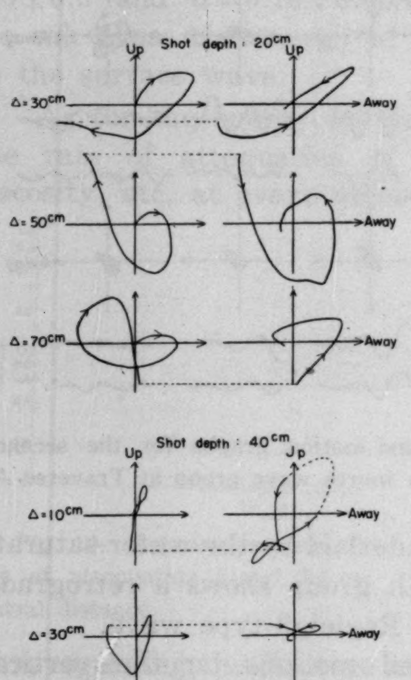

Fig. 13. Ground motion graphs for the surface wave at Traverse C.

S phase

From these vertical observation records, as in any other case of explosion seismic experiments, there can be seen no phase which can be regarded as an *S* phase. On the other hand, as will be seen from the transverse records in Fig. 14, that were obtained at Traverse A and arranged in order of epicentral distance, we can trace a series of distinct arrivals of the events which seem to have characteristics of an *S* wave. Plotting these arrivals, we obtain the two segments of travel-time curves of different phases which give velocities of 140 m/sec and 340 m/sec respectively as shown in Fig. 15. Judging from the values of the velocities, the former seems to represent the *S* wave corresponding to the *P* wave having a velocity of 245 m/sec. As for the latter, when we take into consideration the fact that the substratum is saturated with sea water, it still remains somewhat difficult to call it the *S* wave that corresponds to the *P* wave having a velocity of 1400 m/sec. However, the depth of the interface between the superficial layer and the substratum, calculated from the time-distance graph, gives a value of

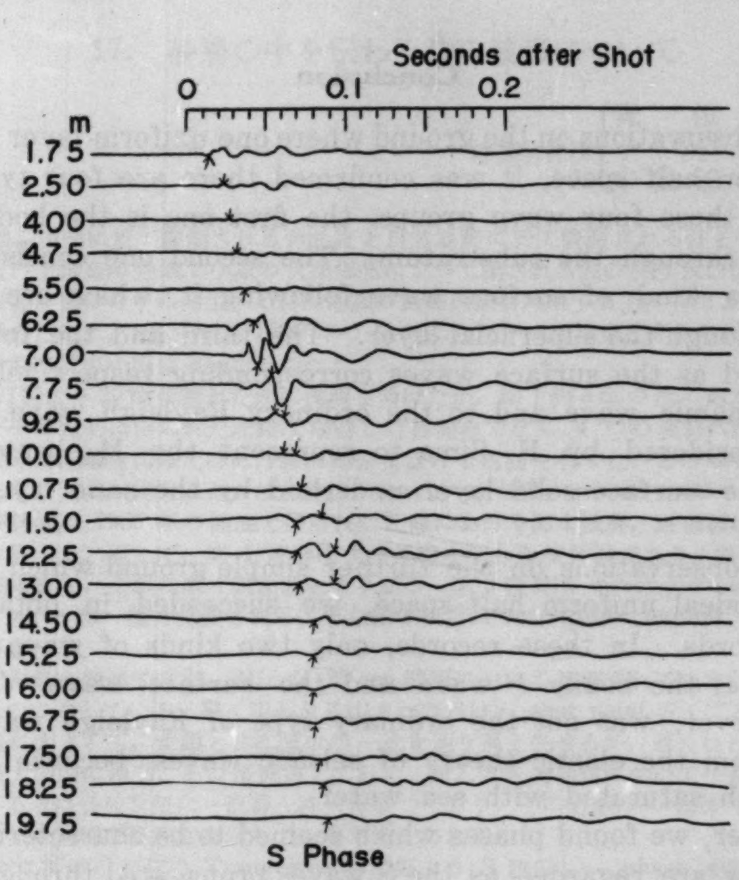

Fig. 14. *S* phases observed on the transverse horizontal geophones along Traverse A.

about 2.6 m, which is in good accord with the value of the depth calculated from *P* wave. This may serve as a positive base for the claim of the *S* wave for the latter segment. We calculated also the Poisson's ratio of the superficial layer of dry sand and of the substratum of wet sand. Their values are about 0.26 and 0.47 respectively. From the fact that the density of the upper layer medium is 1.64 gm/cc, we obtained its rigidity as about 3.2×10^8 dyne/cm^2 and its Lamé's constant as about 3.4×10^8 dyne/cm^2.

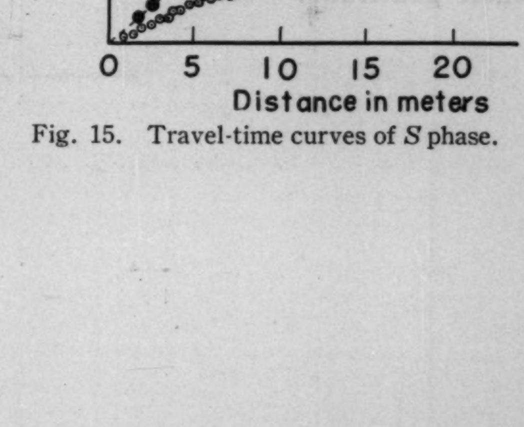

Fig. 15. Travel-time curves of *S* phase.

Conclusion

In the observations on the ground where one uniform layer is underlaid by a uniform half space, it was confirmed there are four types of wave group. Of these four wave groups, the first one is the bodily *P* wave propagated through the substratum. The second one consists of the *P* wave and a kind of surface wave following it, which are propagated together through the superficial layer. The third and the fourth groups are regarded as the surface waves corresponding respectively to a kind of hydrodynamic wave and to the ordinary Rayleigh wave. The third group is considered by H. Sima to represent the M_{12} wave that can exist in the surface solid layer underlaid by the sand layer soaked in sea water.

In the observations on the further simple ground which had a structure of an ideal uniform half space, we succeeded in obtaining much simpler records. In these records, only two kinds of wave group were observed, i.e. the bodily *P* wave and the surface wave. The surface wave, however, was not the ordinary type of Rayleigh wave that was expected from the elastic theory of seismic waves, because the medium was so much saturated with sea water.

Moreover, we found phases which seemed to be characteristic of an *S* wave. They are regarded as the *S* waves propagated through the superficial layer and through the substratum respectively.

Acknowledgements

The authors are very grateful to the Japan Petroleum Exploration Co. Ltd. for their hearty cooperation in these experiments. Their thanks are due to the Seismic Exploration Group of Japan headed by K. Sassa. They further wish to thank Assistant Professor G. Miki of the Institute of Industrial Science in the University of Tokyo, for testing the grain-size distribution of the sand of the field. A part of the expenses necessary for these experiments was defrayed from the funds for scientific research of the Ministry of Education, for which the authors here express their gratitude.

17. 砂層の中を伝わる波の波形について

地震研究所 表　俊一郎
小　牧　昭　三
中島直吉(旧姓小林)

実験室内の模型実験に於て観測される弾性波と自然地震に於て観測される波とを結びつけるものとして，簡単な地下構造の地域で小量の火薬爆発によつて起される波の発生及び伝播の有様を研究することは，複雑な条件の下に発生する自然地震の震動現象を理解する上に有用と思われる．

上の如き目的のために，1955 年と 1956 年の 2 回にわたり一様均質と考えられる砂層より成る，新潟県潟町の砂浜に於て小爆破実験を行つた．

1955 年には汀線より 20 m 程離れた所に測線を設けたが，地下約 3 m の所に海水の浸入による不連続面があり，そのために得られた記録は期待した程簡単でなく 4 つの波群に区分された．1956 年には，より簡単な記録を得るために汀線に測線を設けて観測を行つた．この場合は実体波と表面波とからなる簡単な記録が得られた．位相速度，energy の減衰，ground motion の orbit を調べた結果，この実体波は 1955 年の観測で得られた記録における第 1 波群，表面波は第 3 波群に対応することが大体解つた．而して，第 1 波群は含水砂層を伝わる実体波であり，第 2 波群は乾いた砂層を伝わる実体波と，それに続く表面波とより成る．第 3 波群は direct motion をする表面波で hydrodynamic wave の一種と見做される．また第 4 波群は retrograde motion を示し Raylaigh 型の表面波と解される．

また得られた記録は簡単で而も，PU. を 25 cm 間隔において観測されているために波の消長の有様をしらべるのに適している．早く現われる山または谷は， shot point 近くでその振巾，即ち波の energy は既に大きくて，距離と共に減少の一途を辿り消え失せるが，遅く現われるものは，次第に成長して最大振巾に達し，その後減退して行く．而して走時曲線において一連の山または谷が最大振巾に達する点は各波群毎に一直線上に大体載つており，その直線は origin を通る．これらの直線の傾斜は夫々の波群の群速度を示していると考えられる．

更に，1955 年に於ける観測の Transverse の記録より S 波らしい phase を読み取ることが出来た．走時曲線を描くと 140 m/sec, 340 m/sec を示す二つの分枝が得られ，これは夫々砂層及び含水砂層を伝わる S 波と考えられる．これより両層の境界面の深さを求めると P 波から求められた境界面の深さと殆んど一致する値が得られた．これら P, S 両波の速度から砂層の弾性常数も求めた．

BULLETIN OF THE EARTHQUAKE
RESEARCH INSTITUTE
Vol. 36 (1958), pp. 329-348

18. *Crustal Structure in Northern Kwantô District by Explosion-Seismic Observations.*

Part I. Description of Explosions and Observations.

By The Research Group for Explosion Seismology.

(Read May 28, 1957.—Received June 30, 1958.)

Since the first Nozori explosion of 14th, Nov. 1954, observation areas of our Research Group for Explosion Seismology have been shifted from Tôhoku District to Kwantô District. Since then, we have observed seismic waves due to six explosions in Kwantô District. The first and the second Nozori explosions and the first Hokota explosion were observed to obtain information about the crustal structure of the northern Kwantô District. Temporary observation stations were spread nearly in the direction N 120° E—N 60° W, i.e. on the line joining Nozori and Hokota shot points. A description of the three explosions is given.

1. Description of Explosions.

In order to get blocks of rock necessary for the construction of a rock-fill dam near Lake Nozori, in the northern part of Gunma Prefecture, explosions of dynamite were fired many times. We took advantage of two explosions of comparatively large amounts of dynamite for our study. We call them the first and the second Nozori explosions. Topographic features near these shot points are shown in Fig. 1.

The amount of charge of the first explosion was 3.70 tons and the second one was 1.55 tons. Shot times were generally registered directly on the oscillograph. But in the second Nozori explosion an instrumental disorder prevented direct registration. Fortunately we registered at the same time ground tremors and sound waves of the detonation on a magnetic tape recorder placed near the shot point. Furthermore, the air temperature at the shot time was observed. From these data, we estimated the shot time of the second Nozori explosion as 01 h 05 m 00.291 sec.

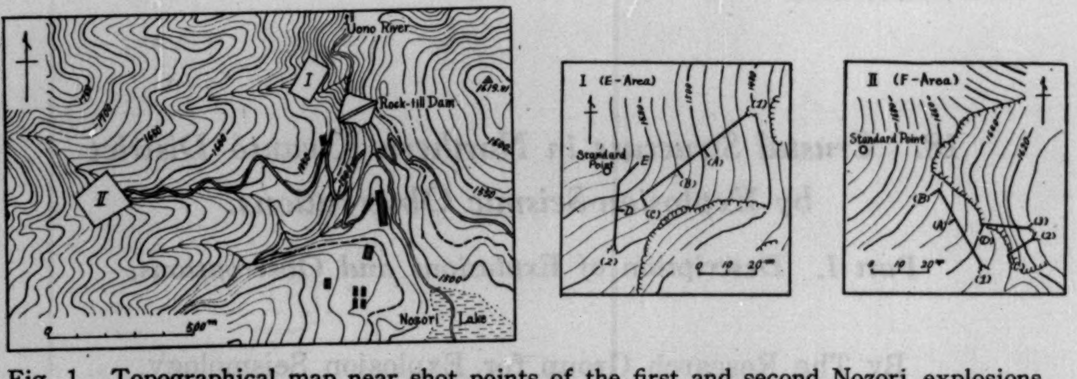

Fig. 1. Topographical map near shot points of the first and second Nozori explosions.
I, II: the first and the second shot points. ⊓: entrance of tunnel.
----: high water level. (A), (B), ···: charge chamber.
——: tunnel.

The first Hokota explosion was planned to obtain more precise knowledge of the crustal structure in the northern Kwantô District. This explosion forms the reverse explosion to the Nozori explosions. A shot position was selected in Taiyô-village, Ibaraki Prefecture. Six holes 70 m deep were located at five apexes and the centre of equilateral pentagon which was inscribed in a circle with 7 m radius. Holes were charged with dynamite from the bottom to 20 m below the ground level and the rest were filled with muddy water. They were blasted simultaneously. Shot time was directly registered on the oscillograph. The amount of charge was one ton in total. The latitude, longitude, height of shot points, amount of charge and shot time of the three explosions are tabulated in Table 1.

Table 1

Name of Explosion	Location of shot point			Amount of Charge	Shot Time
	λ	φ	H		
Nozori I	138°38′35.2″ E	36°42′58.2″ N	1526 m	3.70 ton	1954, Nov. 14, 01 h 05 m 00.865 s
Nozori II	138°37′59.2″	36°42′51.8″	1606	1.55	1955, Aug. 15, 01 h 05 m 00.291 s
Hokota I	140°33′39.6″	36°08′19.8″	41	1.0	1956, Dec. 5, 01 h 05 m 00.200 s

2. Description of Observations.

In total, 33 temporary observation stations were spread nearly in the N 120° E–N 60° W direction along the line joining Nozori and

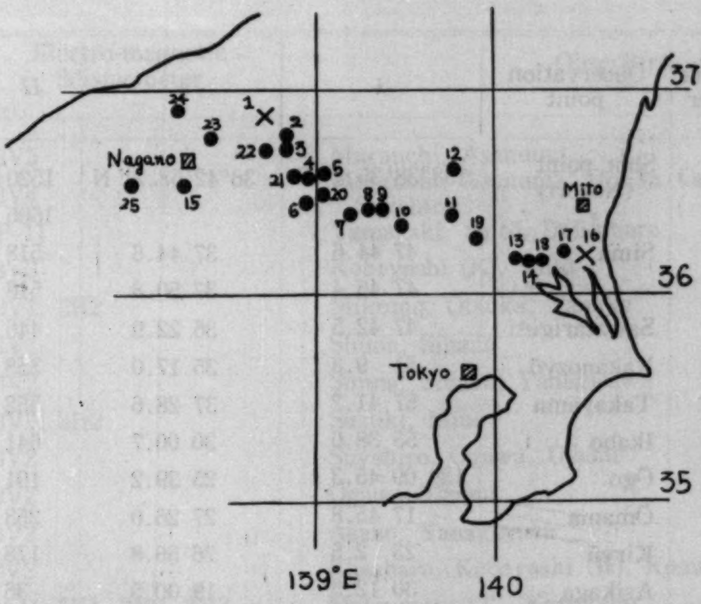

Fig. 2. Shot points and seismic observation stations for the Hokota and Nozori explosions.

×: Shot point ●: Observation point

Hokota shot points. They are shown in Fig. 2. The place names*, latitude, longitude, height, epicentral distance and azimuth of observation stations, type of seismometers and name of observers are tabulated in Table 2. Each station was equipped generally with electromagnetic transducers with amplifiers. But near-by stations made observations without any amplifier. The sensitivity of the transducer was 1–5 volts/kine. The output of the amplifier was connected with a galvanometer of a short proper period. By the combination of a transducer-amplifier-galvanometer, we were able to reach displacement magnification of 10^6–10^7 at 3 c/s. Satisfactory seismograms were obtained at almost all stations. They are shown in Fig. 7.

Measurements of the commencement of the first wave were made by several persons independently and a value was adopted only when satisfactory agreement was found. The running speed of the recording paper was 3 cm/sec or more and minute and second marks were registered on the oscillograph paper directly from the JJY radio time signal. Therefore, the accuracy of determination of the arrival time of first tremors is at least 0.1 sec. even in less favourable cases.

Geographical coordinates of shot and observation points were deter-

---

* In the romanization of place names the Japanese system is adopted instead of the Hepburn system, for example, ti for chi, tu for tsu, etc.

Table

Name of Explosion[1]	Reference Number	Observation point	λ	φ	H	Θ[2]
N 1	1	Shot point (Nozori)	138°38′35.2″E	36°42′58.2″N	1520 m	—
N 2	1′	〃			1606	N83°∼113°E
N 1	2	Sima	47 44.6	37 44.6	518	124°45′E
N 2	2′	〃	47 46.4	37 50.8	516	122 28
N 1	3	Sawatariguti	47 42.5	36 22.9	446	131 53
N 2	4	Nakanozyō	51 9.8	35 17.0	358	125 31
N 1	5	Takayama	57 41.2	37 28.6	552	109 39
N 2	6	Ikaho	55 38.0	30 00.7	641	132 05
N 1	7	Ōgo	139 09 45.3	25 39.2	191	124 34
N 2	8	Ōmama	17 45.8	27 26.0	253	115 41
N 2	9	Kiryū	23 2.5	26 56.8	178	113 39
N 1	10	Asikaga	30 12.5	19 00.5	36	117 55
N 1	11	Totigi	42 36.9	21 38.2	49	112 26
N 2	12	Ōya	49 30.1	35 25.9	152	97 21
N 1	13	Tukuba	140 06 39.9	12 38.6	286	113 05
N 2	13′	〃	〃	〃	〃	112 52
N 2	14	Kakioka	11 28.1	13 45.6	32	111 05
N 1	15	Matusiro	138 12 23.6	32 22.4	383	243 21
H 1	16	Shot point (Hokota)	140 33 39.6	36 08 19.8	41	N 101 00 E 13 00 E
〃	17	Tomoegawa	29 00.1	09 20.8	17	N 74 57 W
〃	18	Tamari	20 14.3	09 34.8	22	83 27
〃	13″	Tukuba	06 39.9	12 38.6	286	78 51
〃	19	Yūki	139 52 40.6	17 32.4	33	74 30
〃	11″	Totigi	43 24.3	22 06.2	44	71 18
〃	10″	Asikaga	30 12.5	19 00.5	36	78 16
〃	7″	Ōgo	09 45.3	25 39.2	191	75 42
〃	20	Sibukawa	138 59 38.5	29 31.7	261	74 26
〃	21	Agatuma	48 55.2	33 51.6	508	73 13
〃	22	Hanasiki	38 37.4	38 44.9	852	71 54
〃	23	Yamanouti	24 17.2	45 16.8	478	70 32
〃	15″	Matusiro	12 23.6	32 22.4	383	78 07
〃	24	Sekiyama	16 47.6	54 55.2	458	67 08
〃	25	Ōmati	137 49 50.6	33 45.4	861	79 08

Survey

---

1) N1....the first Nozori explosion.
N2....the second Nozori explosion.
H1....the first Hokota explosion.

2) Azimuth of observation points measured clockwise from the north.

2

Δ	Electro-magnetic Seismometer	Observers
0.00	3V5	Murauchi, Asanuma
0~0.80	3V4	Murauchi, Asanuma, Honda, Omote, Matuzawa, Suyehiro
16.57	P-11	Yamazaki, Saitō, Daikubara
17.21	3V3	Kobayashi (K), Saitō
18.22	2V1, 2H2	Mikumo, Ōtsuka, Tanaka
24.05	3V1	Shima, Sibano
30.18	3V2	Shima, Sibano, Yanagisawa
35.39	3V3, 3H2	Suzuki, Mine
56.43	3V2	Suyehiro, Ogawa, Usami
65.75	3V2	Ogawa, Usami
73.29	3V2	Asano, Yanagisawa
88.86	3V2	Kasahara, Kobayashi (K), Komaki
103.34	N.D. 3V1, 3V2, 3H2	Matsumoto (T), Karakams
107.37	N.D. 3V1, 3V1	〃 〃
142.99	N.D. 3V1, 3V2	Santō, Shimazu, Tazima
〃	1H1, N.D. 3V1	Asada, Tazime, Akamatu
149.56	N.D. 3V1, 3V1	Hori, Matsumoto (E)
43.53	1H1, 3V1	Utsu, Hisamoto
0~1.24	7V3 (E.T.L.), 7V3	Matuzawa, Tazime, Kaneko, Kawashima, Ōtaki, Hirasawa, Asanuma, Okamura
7.24	3V1, 15V2, 2H2	Okano, Kamo
20.26	2V1, 2H2, Strain meter	Mikumo, Ōtsuka
41.26	1H1, 3V2	Akamatu, Karakama
63.73	3V1, 3V2	Tamaki, Kitamura
79.46	7V12 (E.T.L.)	Noritomi, Ueda, Shibata
97.10	3V2, 2H1	Wada, Muramatsu
129.64	N.D. 3V1, 3V1	Takagi, Nakamura
146.06	N.D. 3V1, 3V1	Utsu, Usami
163.63	N.D. 3V1, 3H1	Suzuki, Mine
180.91	N.D. 3V1, 3V1	Den, Tsunekawa
205.01	N.D. 3V1, 3V3	Asano, Yanagisawa
215.94	N.D. 3V1	Suyehiro
221.72	N.D. 3V1	Sima, Sibano
249.60	N.D. 3V1	Asada, Kobayashi (T), Takeuchi
		Okada

3) For example, 3V5 means that five vertical transducers with natural frequency 3 c/s. were used.
N.D. means transducer with high senstivity (5 volts/kine).

Table 3. Arrival time of tremors at three explosions

Name of Expl.	Ref. No.	Observation points	$\varDelta$	P 0.5 m+	P.U. Number	$P-$shot	$P-\varDelta/6-$shot
N 1	1	Nozori	96.5 m		P.U. 1	00.036 sec	
			506.2		2	0.718	
			770.6		3	0.299	
N 2	1′	〃				0.00	0.00
N 1	2	Sima					
N 2	2′	〃	17.21 km	3.43 sec		03.14	0.27 sec
N 1	3	Sawatariguti	18.22	4.20		03.33	0.29
N 2	4	Nakanozyō	24.05	4.80		04.51	0.50
N 1	5	Takayama	30.18	6.65		05.78	0.75
N 2	6	Ikaho	35.39	6.79	P. U. A	06.50	0.60
N 1	7	Ōgo	56.43	11.17		10.30	0.90
N 2	8	Ōmama	65.75	11.73		11.44	0.48
N 2	9	Kiryū	73.29	12.94		12.65	0.44
N 1	10	Asikaga	88.86	16.18		15.31	0.49
N 1	11	Totigi	103.34	18.58		17.71	0.49
N 2	12	Ōya	107.37	18.81		18.52	0.62
N 1	13	Tukuba	142.99	24.60		23.73	−0.10
N 2	13′	〃	〃				
N 2	14	Kakioka	149.56	25.13		24.84	−0.09
N 1	15	Matusiro	43.53	8.785		07.92	0.665
H 1	16	Hokota	0.0	0.20		0.00	0.00
〃	17	Tomoegawa	7.24	2.51		2.30	1.10
〃	18	Tamari	20.26	4.78		4.57	1.19
〃	13″	Tukuba	41.26	8.08		7.87	0.99
〃	19	Yūki	63.73	12.61		12.40	1.78
〃	11″	Totigi	79.46	14.57		14.36	1.13
〃	10″	Asikaga	97.10	16.97		16.76	0.58
〃	7″	Ōgo	129.64	22.43		22.22	0.62
〃	20	Sibukawa	146.06	25.00		24.80	0.45
〃	21	Agatuma	163.63	27.23		27.00	−0.27
〃	22	Hanasiki	180.91	28.86		28.65	−1.50
〃	23	Yamanouti	205.01	31.8		31.60	−2.57
〃	15″	Matusiro	215.94	34.12		33.91	−2.08
〃	24	Sekiyama	221.72				
〃	25	Ōmati	249.60	38.68		38.47	−3.13

Shot time N1: 1954, Nov. 14th, 01 h 05 m 00.865 sec.
N2: 1955, Aug. 16th, 01 h 05 m 00.291 sec.
H1: 1956, Dec. 5th, 01 h 05 m 00.208 sec.

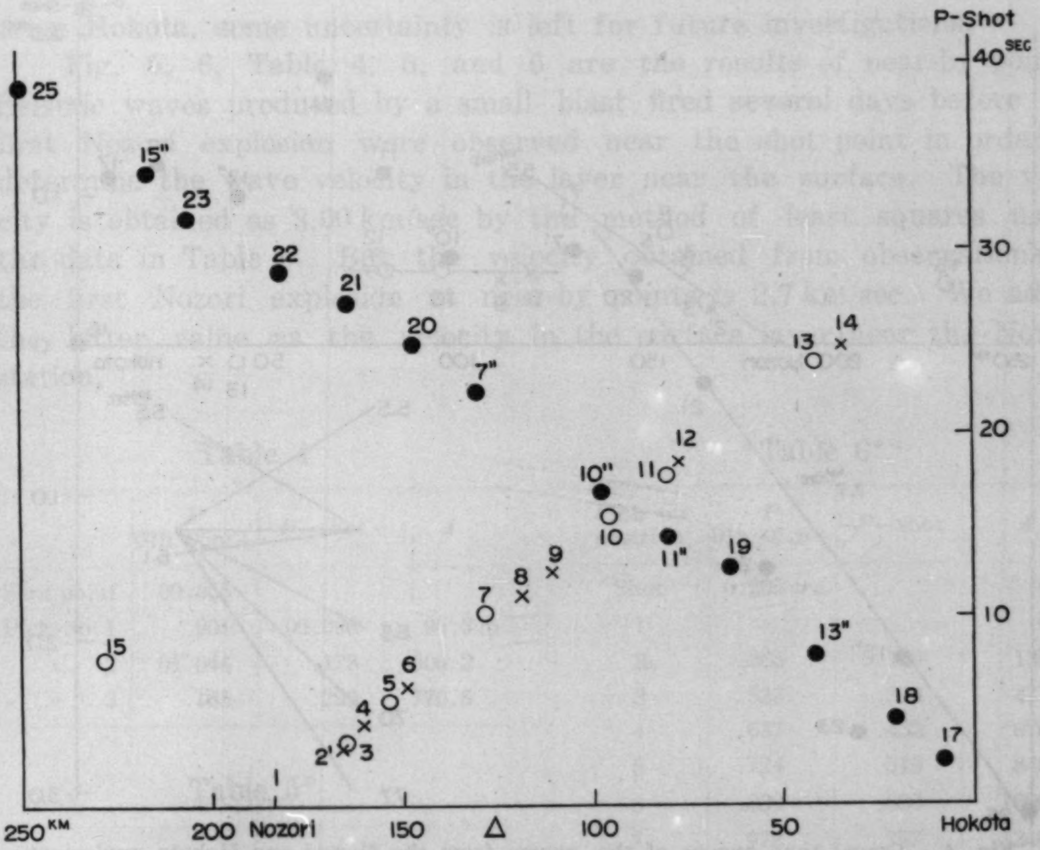

Fig. 3. Travel time graph of seismic waves from the Nozori and Hokota explosions.
○: the first Nozori explosion. ×: The second Nozori explosion.
●: the first Hokota explosion.

mined by the method based upon triangulation, by which we were able to keep errors of latitude and longitude within 0.3″. Therefore errors in epicentral distances were estimated to be less than 10 meters.

Arrival times of P waves and epicentral distances are tabulated in Table 3. They are also shown in Fig. 3, in which all data of three explosions except near-by stations are plotted. In order to visualize deviations from a general trend of travel times, $P-\Delta/6$ was taken as the ordinate, and the same data as in Fig. 3 are plotted in Fig. 4. From a slight inspection of Fig. 4, it is found that a travel time curve with an apparent velocity of 5.5 km/sec, passing through stations near the shot point of Nozori explosions and that with an apparent velocity of 7.7 km/sec., passing through distant stations of the Hokota explosion are plausibly acceptable, but as to the apparent velocity and the extension of a travel time curve which passes through stations between 70–130 km

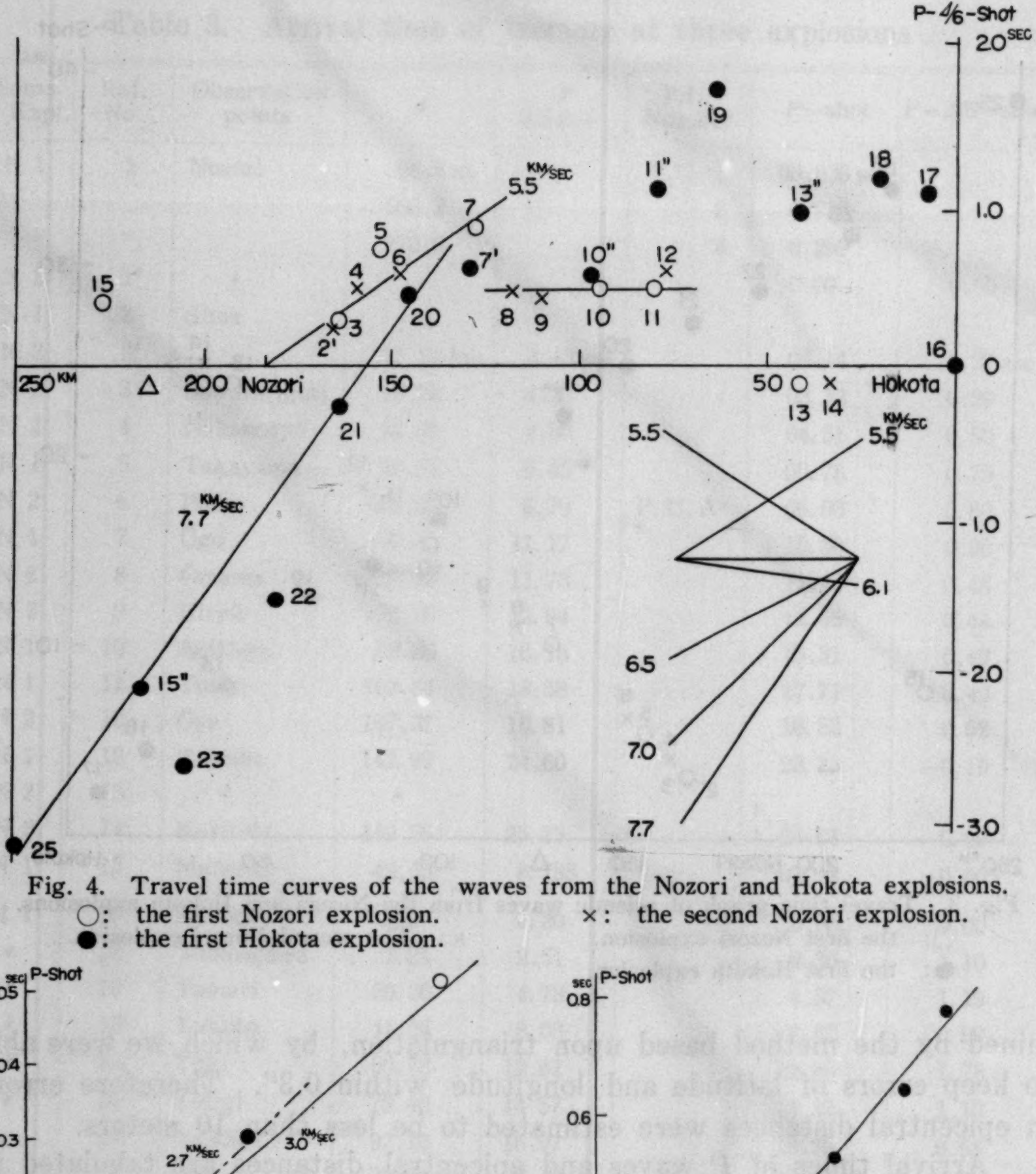

Fig. 4. Travel time curves of the waves from the Nozori and Hokota explosions.
○: the first Nozori explosion. ×: the second Nozori explosion.
●: the first Hokota explosion.

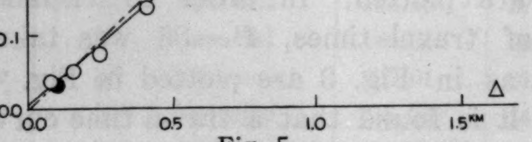

Fig. 5

●-·-·-: Travel times observed at stations near the shot point of the first Nozori explosion.

○——: Travel times from a small explosion fired several days before the day of the first Nozori explosion.

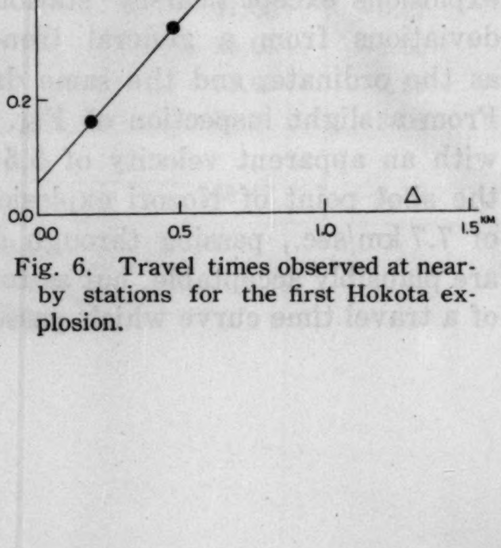

Fig. 6. Travel times observed at nearby stations for the first Hokota explosion.

from Hokota, some uncertainty is left for future investigations.

Fig. 5, 6, Table 4, 5, and 6 are the results of near-by points. Seismic waves produced by a small blast fired several days before the first Nozori explosion were observed near the shot point in order to determine the wave velocity in the layer near the surface. The velocity is obtained as 3.00 km/sec by the method of least squares using the data in Table 5. But the velocity obtained from observations of the first Nozori explosion at near-by points is 2.7 km/sec. We adopt the latter value as the velocity in the surface layer near the Nozori station.

Table 4

	P 01h 05m+	$P-$shot	Δ
Shot point	00.865		
Pick-up 1	.901	00.036	96.5 m
〃 2	01.044	.178	506.2
〃 3	.165	.299	770.6

Table 5*

Pick up position	$P-$shot	Δ
(0)	0.000 sec	0.00 m
1	.039	76.7
2	.056	155.2
3	.077	248.6
4	.138	403.9
5	.202	570.0
6	.512	1454.4

* By the method of least squares, we get
$t=0.000337\Delta(\text{meter})+0.00448$ sec
$V=3.00$ km/sec.

Table 6**

Pick up position	P 01h 05m+	$P-$shot	Δ
Shot	0.205 sec		0 m
1			0
2	.365	0.160	188
3	.523	.318	471
4	.637	.432	676
5	.724	.519	840
6	.839	.634	1090
7	.972	.767	1240

** By the method of least squares, we have

$$t=0.258+\frac{\Delta}{1.79}\,.$$

From the observations at near-by stations of the Hokota explosion, the velocity in the surface layer was found to be 1.79 km/sec by the method of least squares using the data in Table 6. From these results, we consider that a surface layer with the *P*-wave velocity of 1.79 km/sec and one with the *P*-wave velocity of 2.7 km/sec lie respectively near the Hokota and the Nozori shot points.

Crustal structures inferred from data in Part I will be given in the second part of this paper.

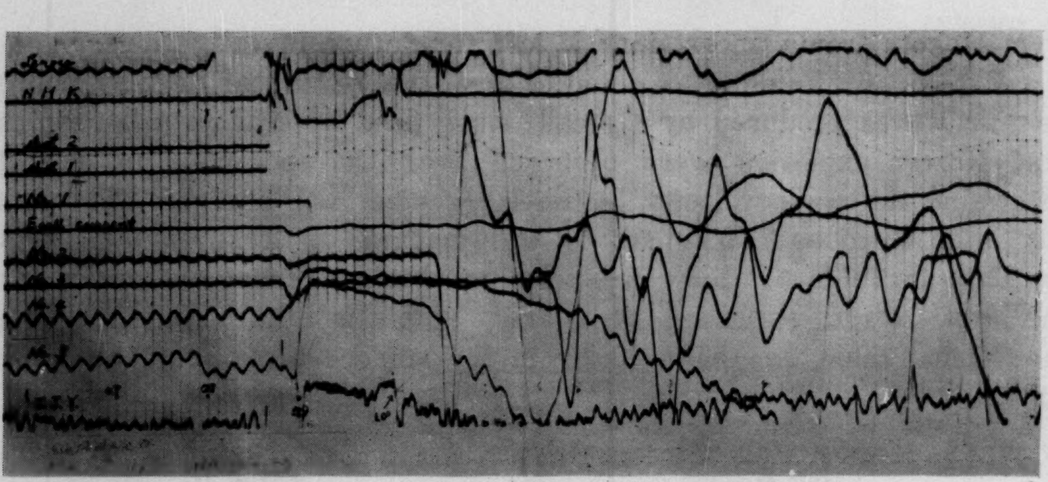

Fig. 7. (1) Seismogram obtained at Nozori in the first Nozori explosion.

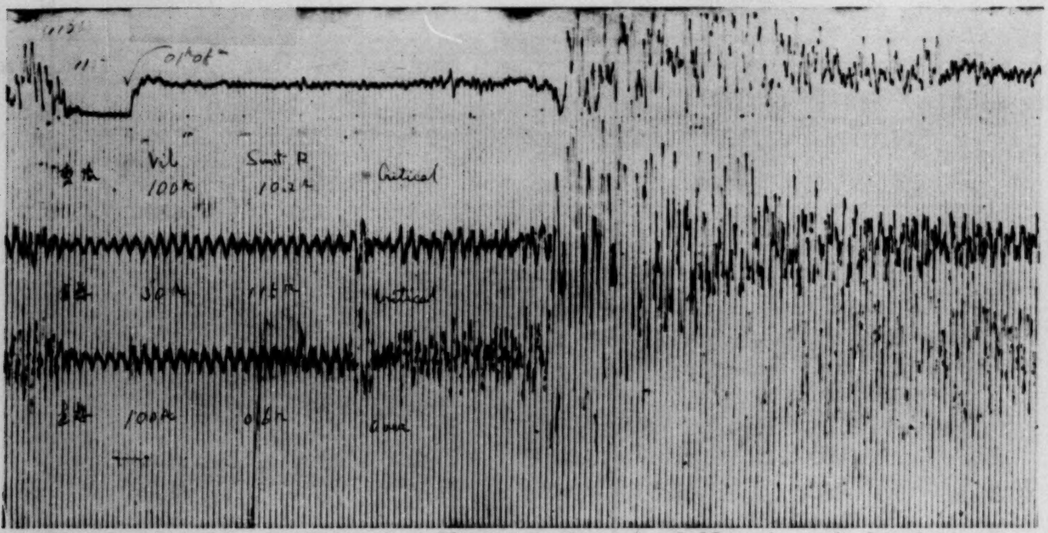

Fig. 7. (2) Record obtained at Nozori in the second Nozori explosion by magnetic tape recorder.

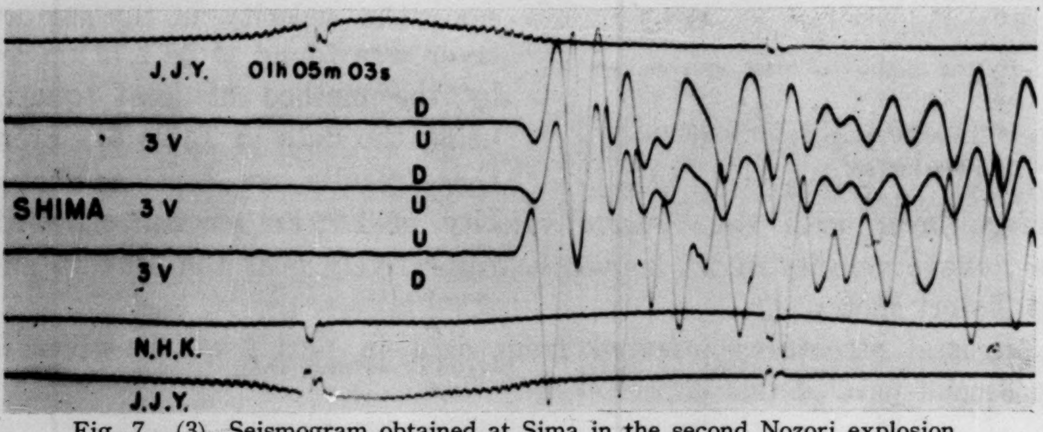

Fig. 7. (3) Seismogram obtained at Sima in the second Nozori explosion.

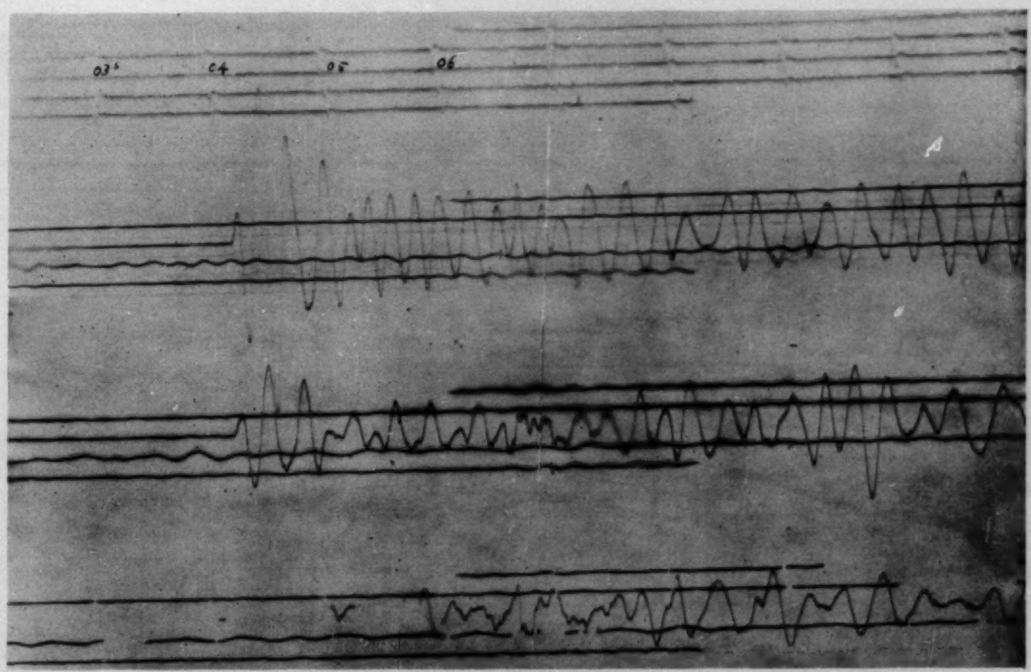

Fig. 7. (4) Seismogram obtained at Sawatariguti in the first Nozori explosion.

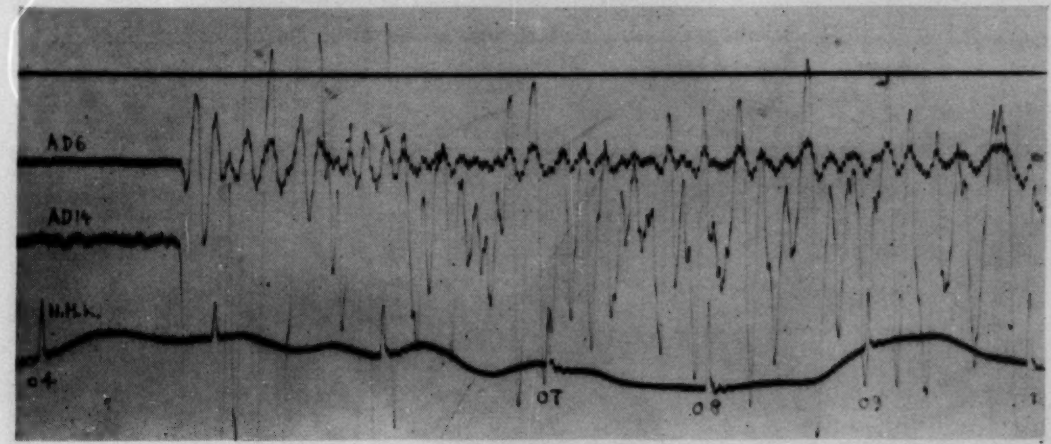

Fig. 7. (5) Seismogram obtained at Nakanozyô in the second Nozori explosion.

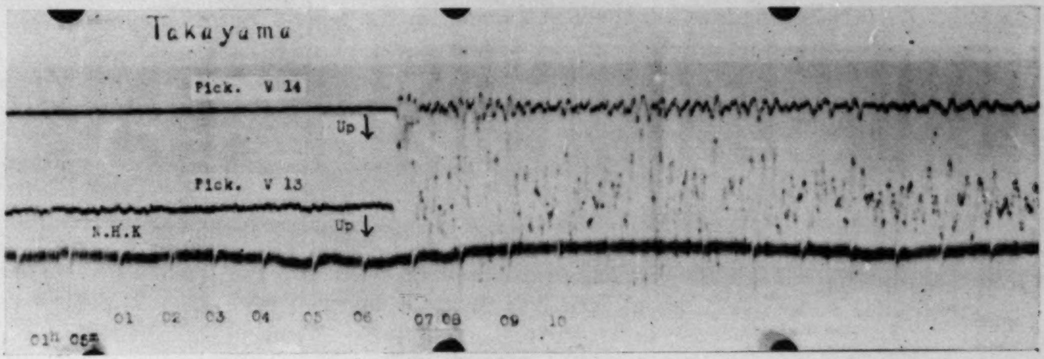

Fig. 7. (6). Seismogam obtained at Takayama in the first Nozori explosion.

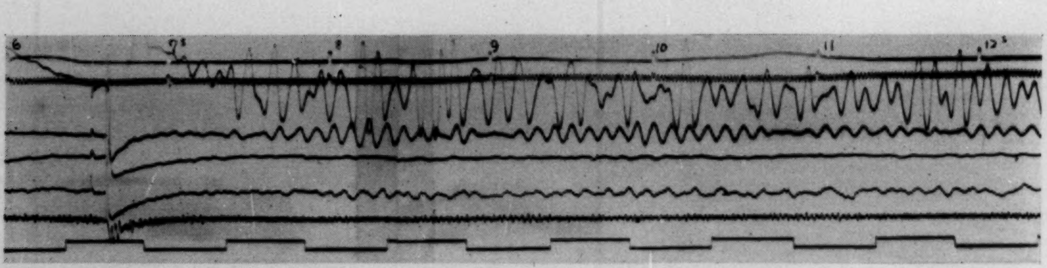

Fig. 7. (7) Seismogram obtained at Ikaho in the second Nozori explosion.

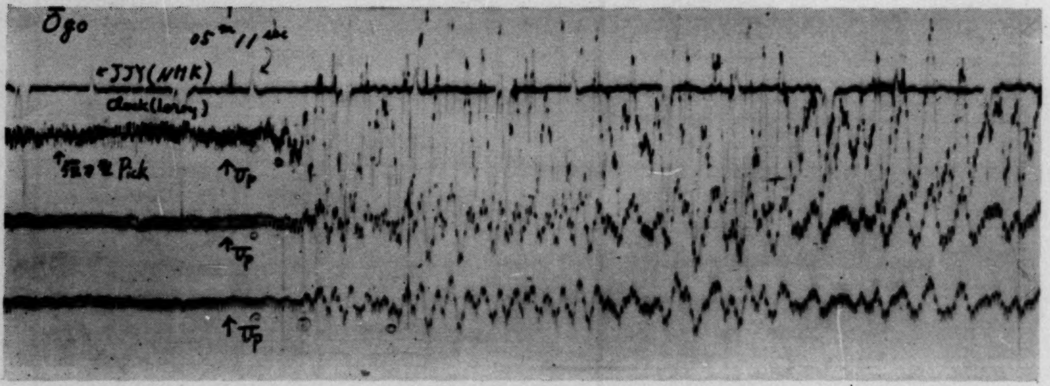

Fig. 7. (8) Seismogram obtained at Ôgo in the first Nozori explosion.

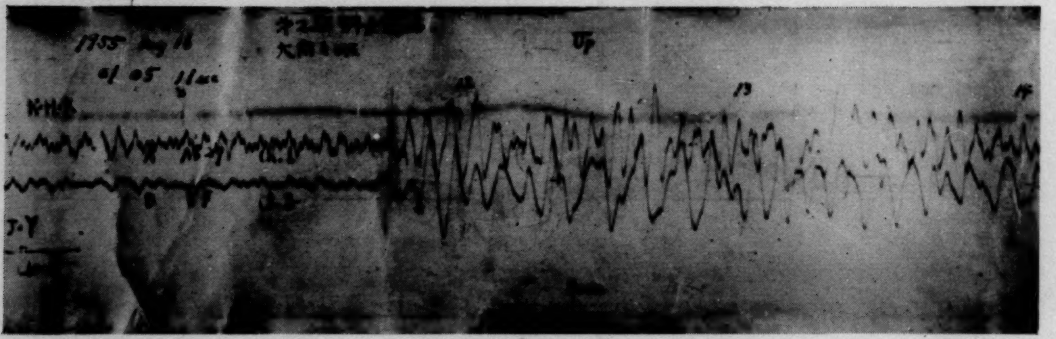

Fig. 7. (9) Seismogram obtained at Ômama in the second Nozori explosion.

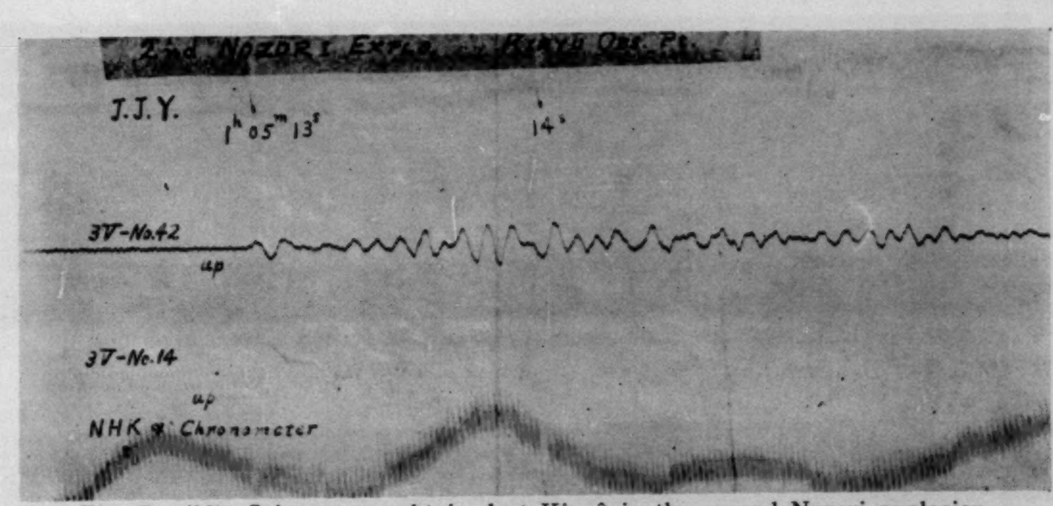

Fig. 7. (10) Seismogram obtained at Kiryû in the second Nozori explosion.

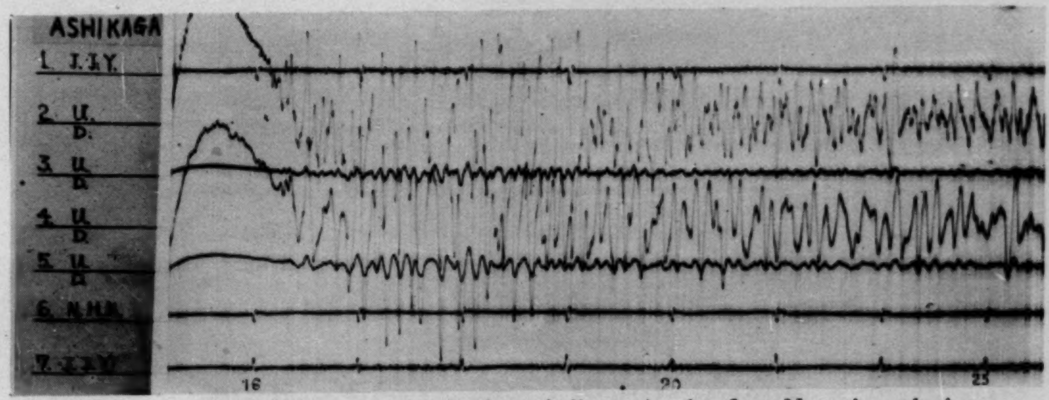

Fig. 7. (11) Seismogram obtained at Asikaga in the first Nozori explosion.

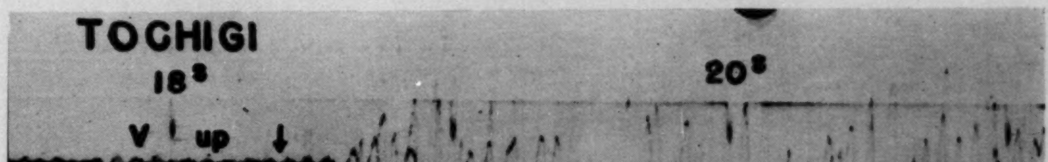

Fig. 7. (12) Seismogram obtained at Totigi in the first Nozori explosion.

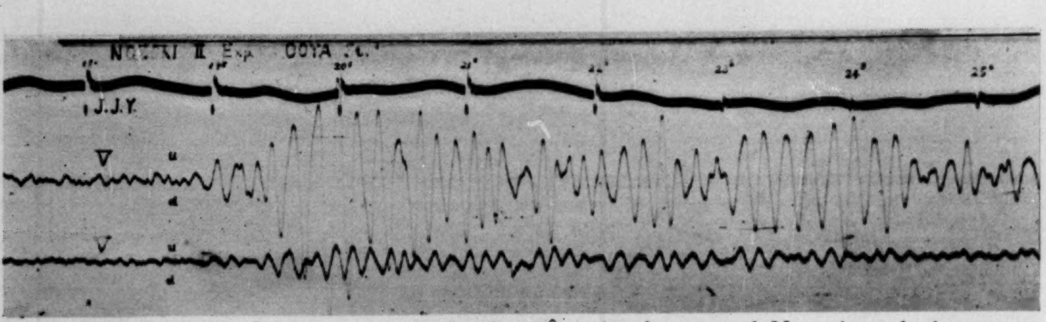

Fig. 7. (13) Seismogram obtained at Ôya in the second Nozori explosion

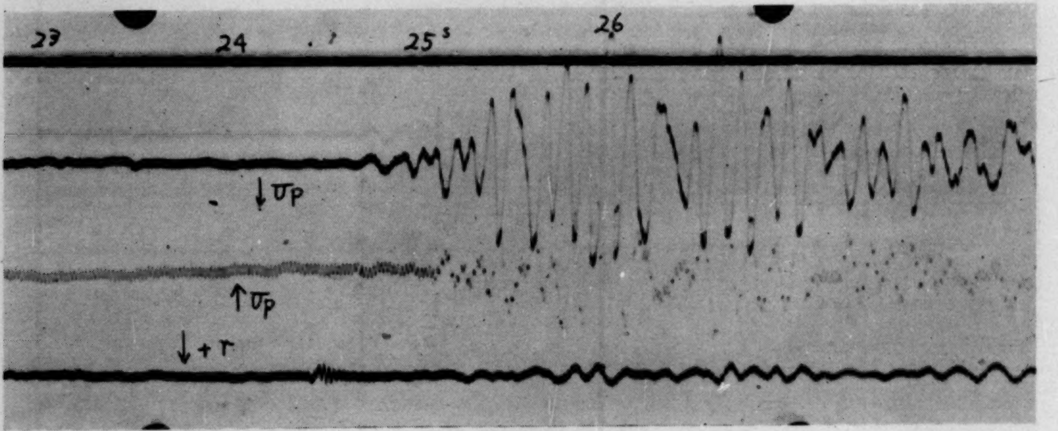

Fig. 7. (14) Seismogram obtained at Tukuba in the first Nozori explosion.

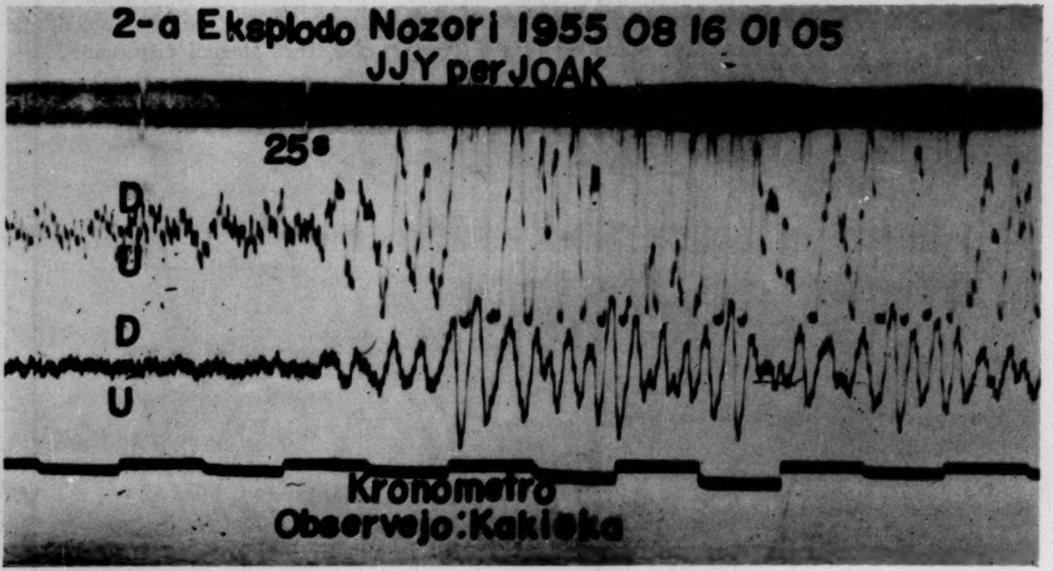

Fig. 7. (15) Seismogram obtained at Kakioka in the second Nozori explosion.

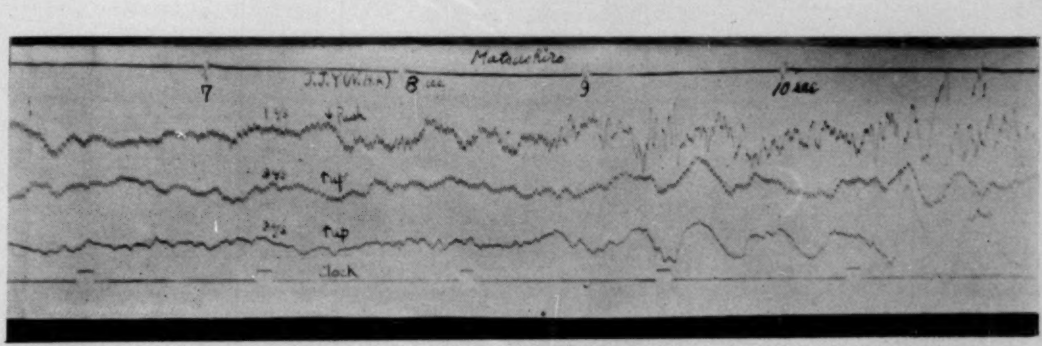

Fig. 7. (16) Seismogram obtained at Matusiro in the first Nozori explosion.

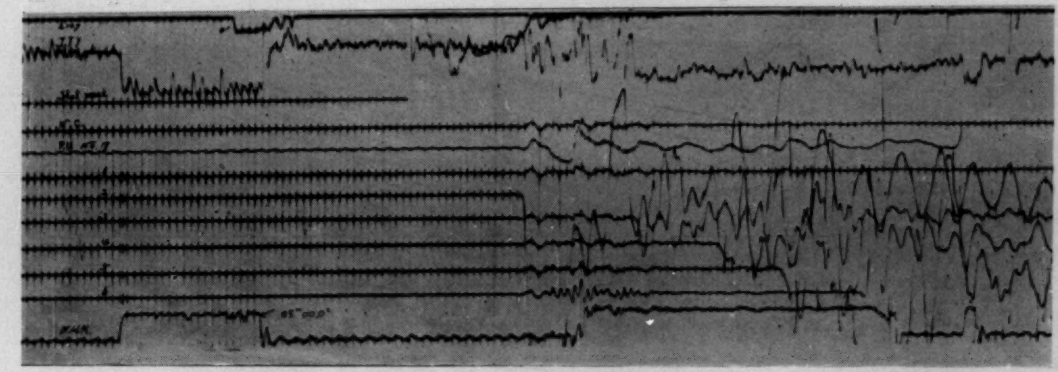

Fig. 7. (17) Seismogram obtained at Hokota in the first Hokota explosion.

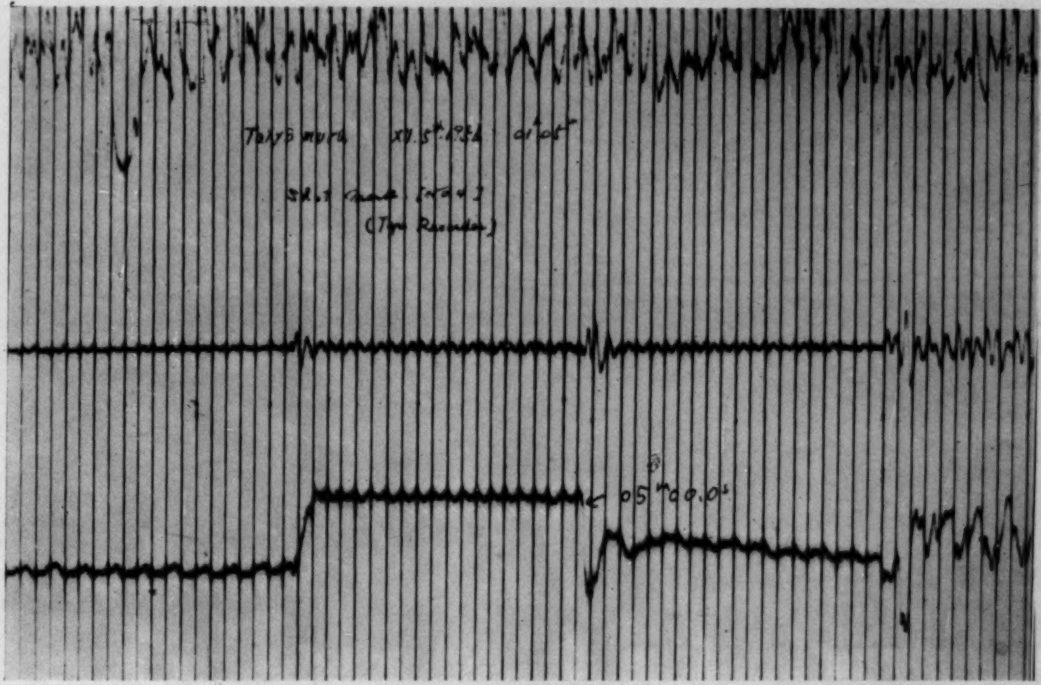

Fig. 7. (18) Record obtained at Hokota in the first Hokota explosion by magnetic tape recorder.

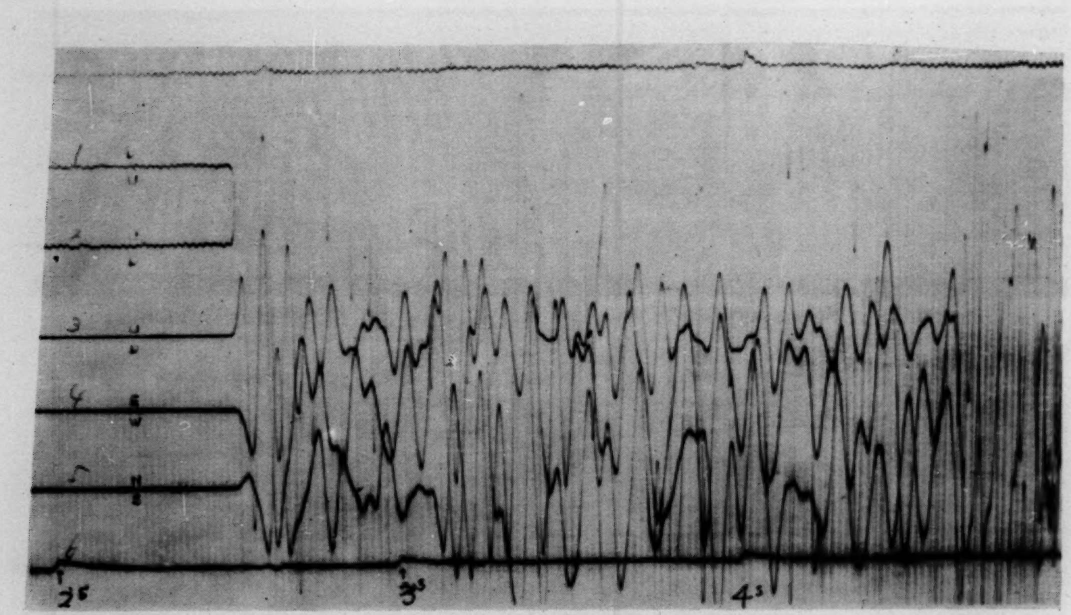

Fig. 7. (19) Seismogram obtained at Tomoegawa in the first Hokota explosion.

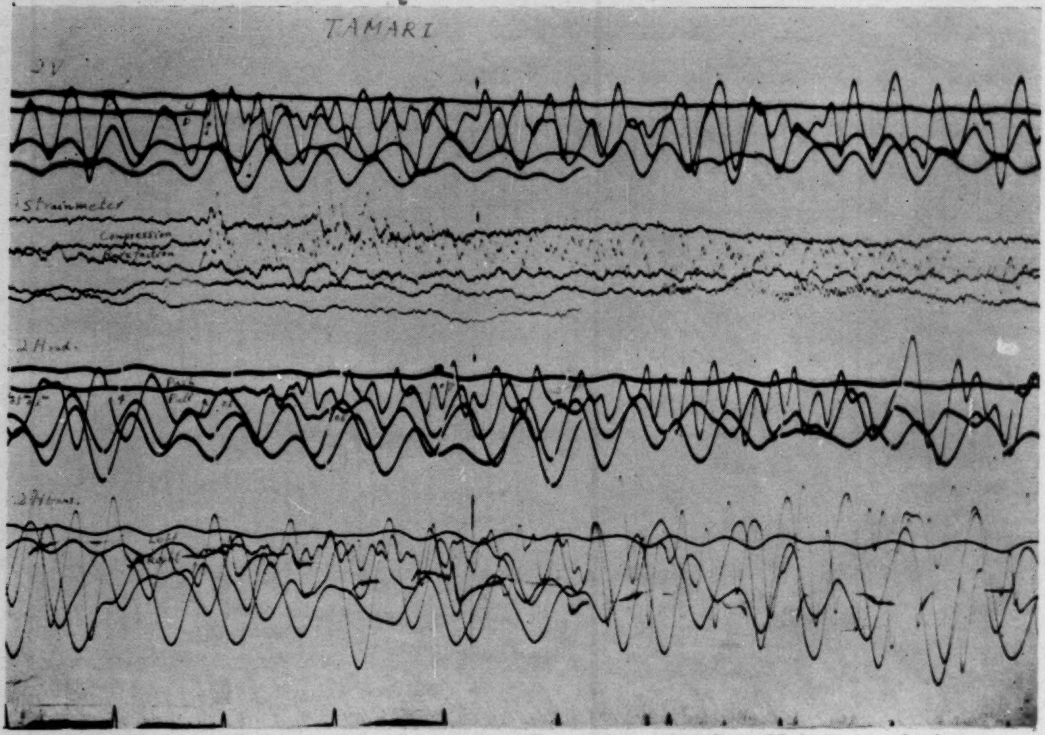

Fig. 7. (20) Seismogram obtained at Tamari in the first Hokota explosion.

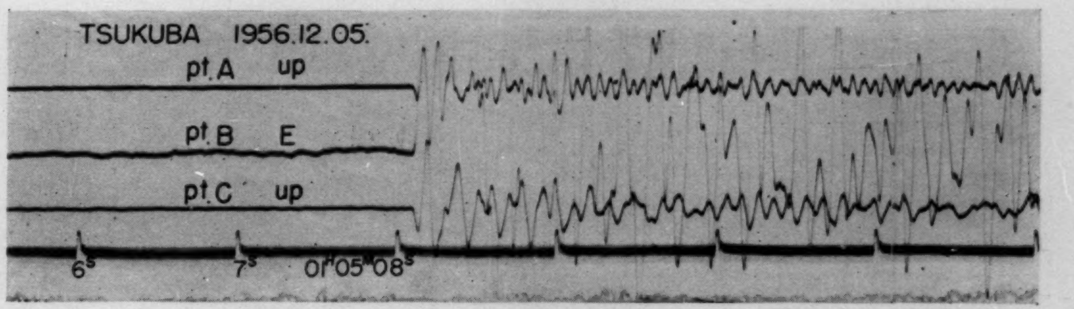

Fig. 7. (21) Seismogram obtained at Tukuba in the first Hokota explosion.

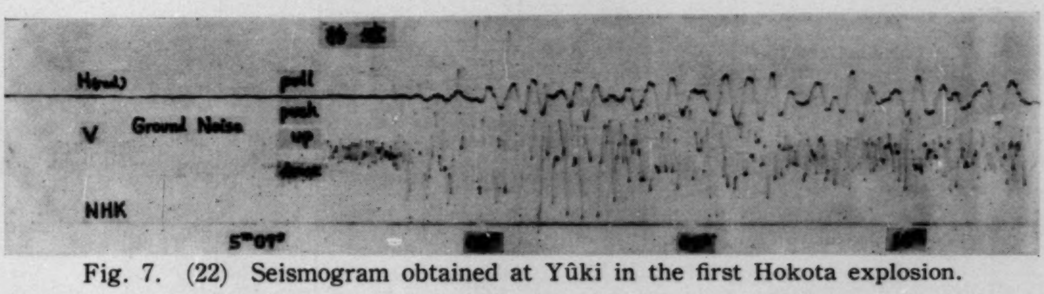

Fig. 7. (22) Seismogram obtained at Yûki in the first Hokota explosion.

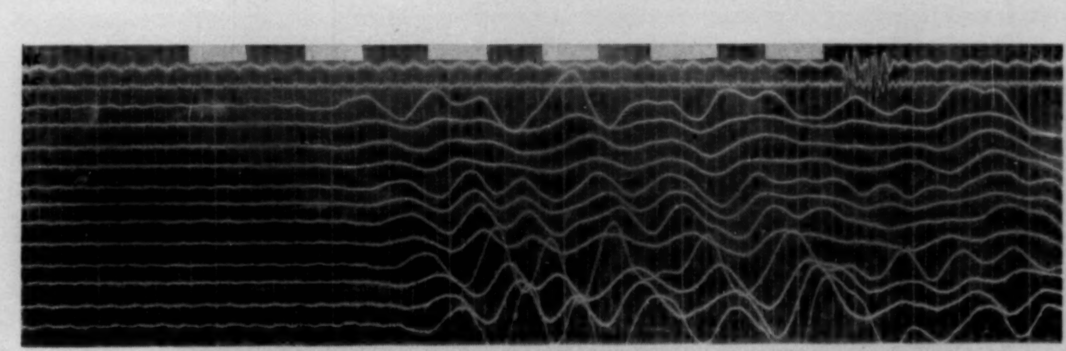

Fig. 7. (23) Seismogram obtained at Totigi in the first Hokota explosion.

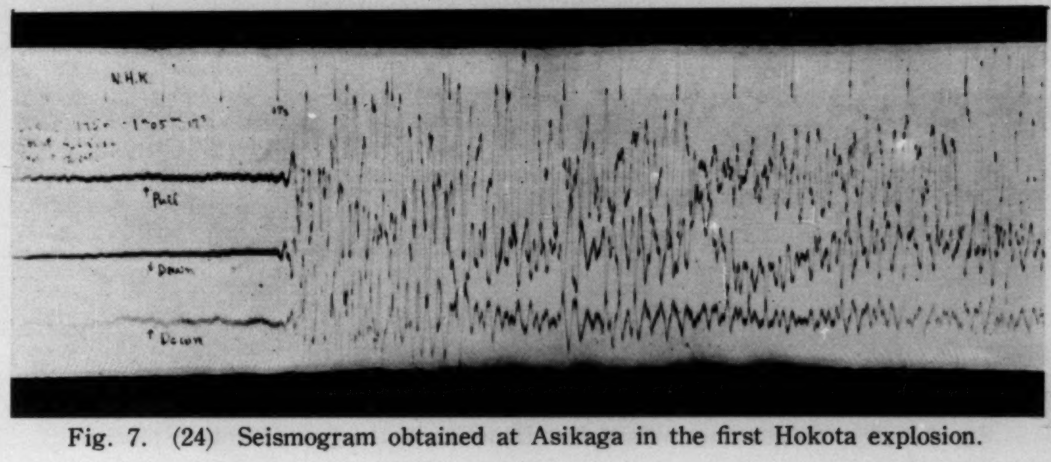

Fig. 7. (24) Seismogram obtained at Asikaga in the first Hokota explosion.

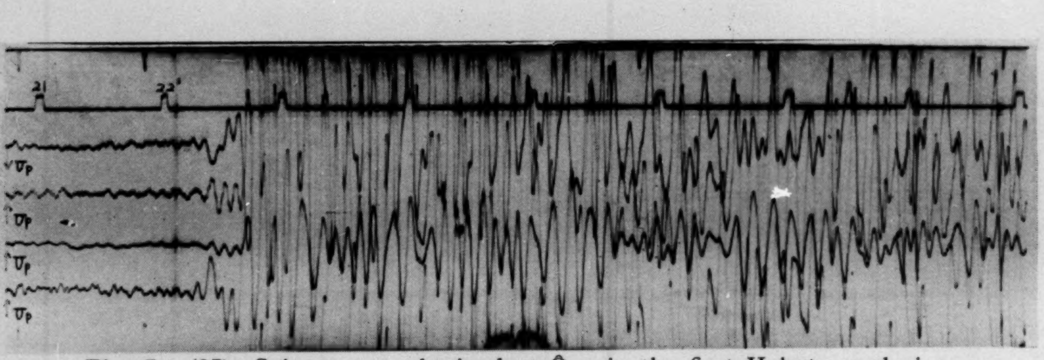

Fig. 7. (25) Seismogram obtained at Ôgo in the first Hokota explosion

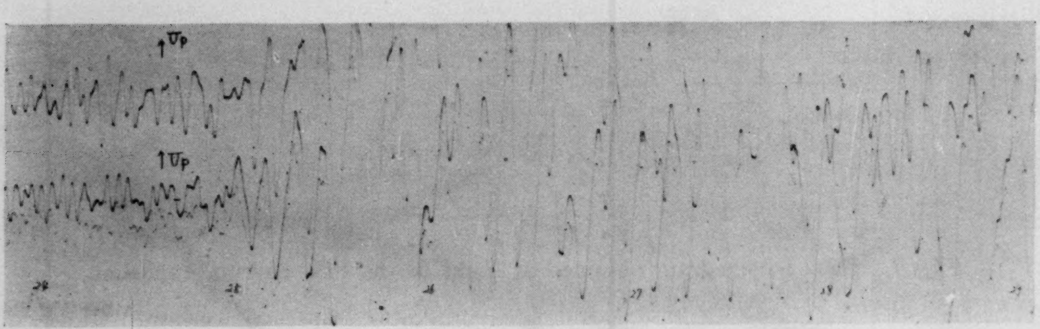

Fig. 7. (26) Seismogram obtained at Sibukawa in the first Hokota explosion.

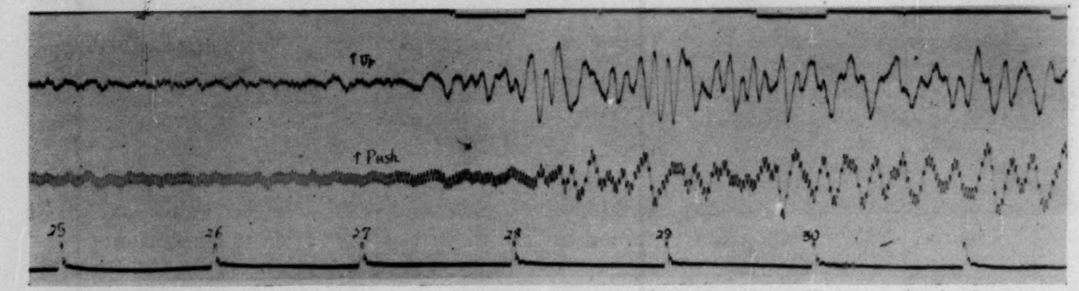

Fig. 7. (27) Seismogram obtained at Agatuma in the first Hokota explosion.

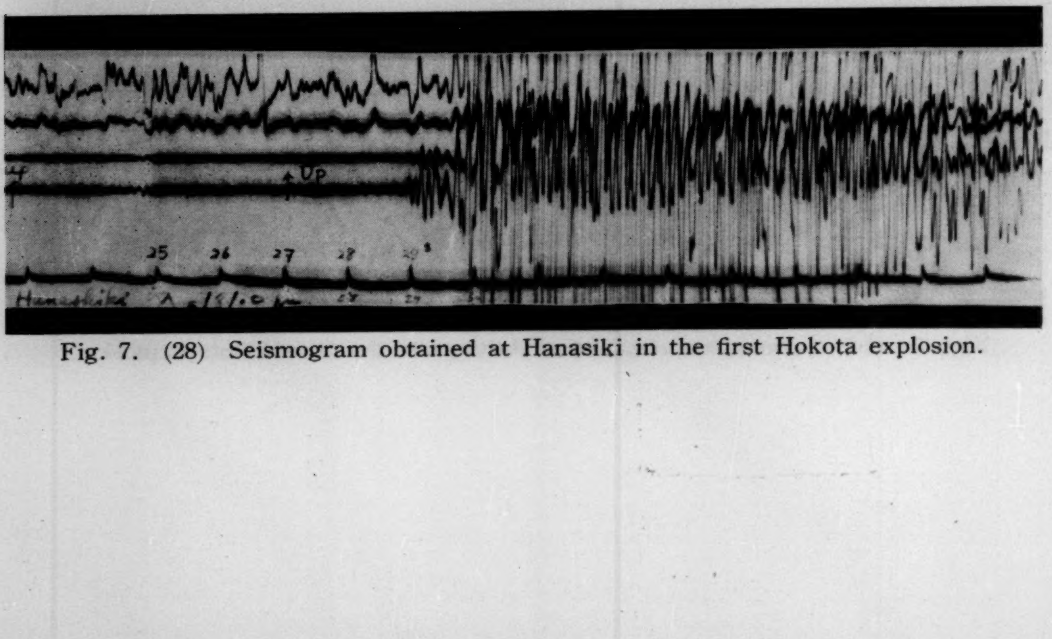

Fig. 7. (28) Seismogram obtained at Hanasiki in the first Hokota explosion.

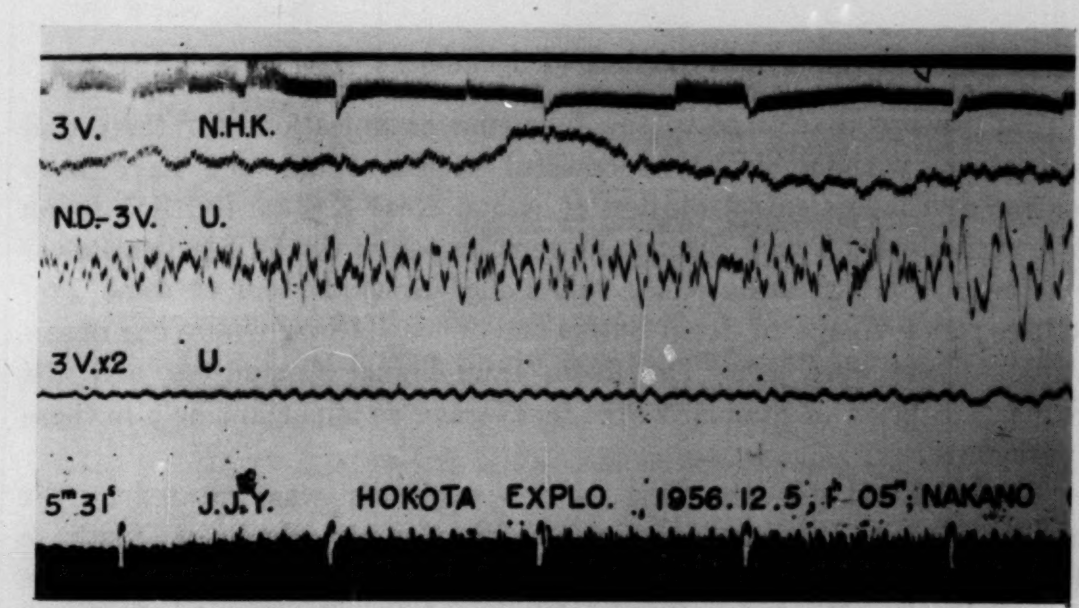

Fig. 7. (29) Seismogram obtained at Yamanouti in the first Hokota explosion.

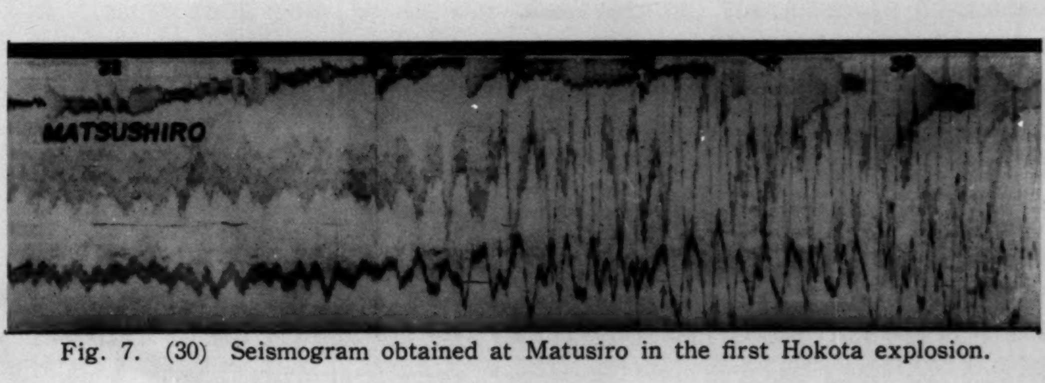

Fig. 7. (30) Seismogram obtained at Matusiro in the first Hokota explosion.

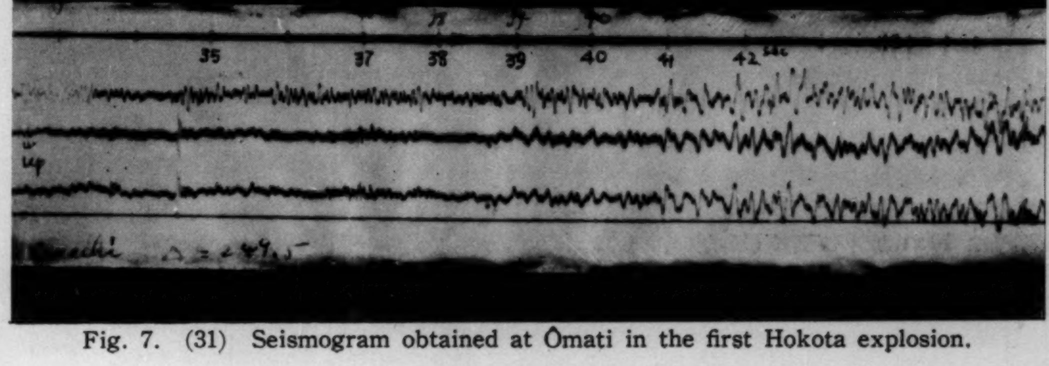

Fig. 7. (31) Seismogram obtained at Ômati in the first Hokota explosion.

3. Acknowledgement.

Our sincere thanks go to the following organizations for their kind cooperation, without which successful results could not have been obtained: Tôkyô Central Station of Nihon Hôsô Kyôkai (NHK): Japan National Railway; Tôkyô Electric Power Company; Chûbu Electric Power Company; Administration offices and Police Headquarters of some prefectures; and village or town offices and police stations where our observation stations were put. The Radio Time Signal Committee and the Broadcast Station of Standard Frequency gave us important help in these experiments.

Financial aid for the first Nozori explosion was granted by the Fund for Special Investigations of the Earthquake Research Institute and those for the second Nozori and for the first Hokota explosions were granted by the Fund for Special Works of the Earthquake Research Institute.

---

18. 大爆破による北関東地方の地殻構造について

其の 1 観 測 報 告

爆破地震動研究グループ

1954 年 11 月 14 日 午前 1 時 05 分に 3.7 トン, 1955 年 8 月 15 日 1 時 05 分に 1.55 トンの火薬による大爆破が群馬県吾妻郡六合村野反池北方で行われた．これは同地に作るダム建設用の石を採る為に行われたが，われわれは，それを利用して，地震動の観測を行つた．合計 18 の観測点は野反と筑波を結ぶ線上に配置された．この観測だけでは地下構造を決めることはできないので 1956 年 12 月 5 日 1 時 05 分に野反・筑波を結ぶ測線の延長上にある茨城県鹿島郡鉾田町の近くの大洋村に爆破点を設けて 1 トンの火薬を爆破させた．測線は爆破点から野反の方向に向つてとり，前 2 回の野反爆破と合せて，正逆両測線による観測を行つた．後者を便宜上鉾田爆破という．観測点は14 である．同爆破点に径 5″ の火薬孔を 70 m の深さに 6 本堀り，これに火薬を50 m の長さに埋めた．

地震計は 3c/s 又は 10c/s の動コイル型換振器が多く，増巾器を通じて短周期のガルバノメーターにつないだ．倍率は 3c/s で最高約 1000 万倍である．

記録のよみとりは，数人の整理委員が行い，一致したものをとつた．その精度は 0.1 sec 以上で，震央距離は 10 m 以下の誤差しかない．

第 1 回野反爆破は地震研究所特殊研究費，第 2 回野反および第 1 回鉾田爆破は地震研究所特別事業費より大部分の費用を出していただきました．心から感謝します．

BULLETIN OF THE EARTHQUAKE
RESEARCH INSTITUTE
Vol. 36 (1958), pp. 349-357

19. *Crustal Structure in Northern Kwantô District by Explosion-Seismic Observations.*

Part II. Models of Crustal Structure.

By Tatsuo USAMI,* Takeshi MIKUMO,** Etsuzô SHIMA,***
Ituo TAMAKI,**** Shûzô ASANO,*** Toshi ASADA***
and Takeo MATUZAWA.***

(Read May 28, 1957.—Received June 30, 1958.)

1. Introduction.

Using the data given in Part I, we can make some plausible models of crustal structure in the vertical section along the line joining Hokota and Nozori shot points. In our observations, the average distance between consecutive stations was about 20 km. Even this density of stations was not large enough for unique determination of the crustal structure. In deriving models for the crustal structure, we first assume a plausible number of layers and the velocity of their *P* waves. The assumptions were based on the travel time data given in Part I, upon due consideration of the crustal structure obtained in Tôhoku District[1]. As a consequence of lack of sufficient data, different models of crustal structures could explain all the travel times in some degree.

In deriving various models, we used the arrival time of the first tremor, and later phases were referred to only when necessary. Arrival times of first tremors for the first Nozori explosion given in Table 2 were read by T. Asada and S. Komaki and those for the second by T. Usami, T. Asada and T. Matumoto.

At the outset we assumed five tentative models as the first approximation and then each model was subjected to small changes in order to make the residue of calculated travel times as small as possible. In each model, $O-C$'s (O stands for the observed travel time of the first wave and C for the calculated one) were calculated graphically, using figures of the vertical section along the line joining Nozori and Hokota shot points, the scale of the figures being 10^{-5} or 5×10^{-6} of the actual.

---

* Japan Meteorological Agency.

** Geophysical Institute, the University of Kyôtô.

*** Earthquake Research Institute, the University of Tôkyô.

**** Ôsaka Institute of Technology.

[1] The Research Group for Explosion Seismology, *Pub. Bureau Central Séism. Int.*, Série A, Trav. Sci., **19** (1956).

2. Model I.

This model was assumed in the following process, using the data of Table 2 in Part I and paying no consideration to the crustal structure of the Tôhoku District[2] obtained by our group.

a) Three layers specified by the velocities 5.5, 6.1 and 7.7 km/sec of the P waves are assumed from top to bottom, each boundary between adjacent layers being taken as horizontal. These layers were called the I, II and III layers respectively. From the travel time in Fig. 4, in Part I the true velocity of the P wave in the II layer cannot be determined precisely, however, it is certain, from the data of Nozori explosions, that the velocity lies between 6.0 and 6.1 km/sec. Thus we take 6.1 km/sec as the first approximation.

b) The thickness of the I layer and that of the II layer were obtained as 6 km and 19 km respectively from the assumed velocity of the P wave and the critical distance determined from travel time curves specified by the I and II layers of Nozori explosions and from those specified by the II and III layers of the Hokota explosion.

From these approximations, we got $O-C=0.37$ sec at station Tukuba for Hokota explosion. Near station Tukuba granitic rocks are found on the ground surface. Therefore, to explain the observed travel time of the Tukuba for the Hokota explosion, we assumed that the II layer comes up to the ground surface near Tukuba and that the weathered layer specified by the velocity 1.79 km/sec of the P wave lies on the I layer near the Hokota shot point with thickness corresponding to $O-C=0.37$ sec. Moreover, the existence of the same weathered layer was assumed between Hokota and station Yûki (19), except near Tukuba, with some thickness so as to make $O-C=0$ sec at these stations for the Hokota explosion. Thickness of the weathered layer thus obtained seems not unreasonable from the geological point of view. In order to make the mean value of $O-C$'s, which is taken for stations near and east of Nozori in the Nozori explosions, zero, a weathered layer specified by the velocity 2.7 km/sec of the P wave was assumed on the I layer with thickness 0.1 km near Nozori shot point.

---

[2] The Research Group for Explosion Seismology, *loc. cit.*, 1).

As stations Matusiro (15) and Ômati (25) do not lie on the line joining Hokota and Nozori shot points, we considered the crustal structure in the section along the line joining Nozori, Matusiro and Ômati separately. In this section, the thickness of the I layer was obtained from the later phases recorded at Matusiro and Ômati for the Hokota explosion, and then the position of the boundary between the II and III layers was determined by using the arrival times of the *P* waves at these two stations observed in the Hokota explosion. With some further trials to make $O-C$'s small as a whole, we obtained a crustal structure which is given in Fig. 8a. In this figure model I is given in thin lines. Model II and model III are superimposed.

Though we examined five models, this model is the simplest and as a whole can explain most satisfactorily the observed travel times of the *P* waves. Therefore we adopt model I as the most plausible one.

3. Models II and III.

These models were examined in order to check how far the observed arrival times of the *P* wave can be explained, if the velocity of the *P* wave in the III layer of the model I be 8.1 km/sec, which is often reported as the velocity of the *P* wave under the Mohorovičić surface. The results are shown in Fig. 8a and Table 7. In the figure, model II is given in thick lines and model III is in chain lines. Structural parts common to model I are not specially mentioned.

Though models II and III were constructed for the same purpose, the results differ remarkably from each other. In deriving model II, the depth of the boundary between the II and III layers was assumed as 25 km everywhere, from which the following contradiction turned out. In order to make $O-C$'s small as a whole, the crustal structure must differ on the north and south sides of the line joining Hokota and Nozori shot points. In model III, the depth of the boundary between the II and III layers was taken as 27 km. This model was rejected, because $O-C$'s at stations Hanasiki, Matusiro and Ômati for the Hokota explosion were too large beyond the observational errors.

These trials indicate that, even with such density of observation stations as this, it is difficult to derive a unique solution of the crustal structure.

4. Model IV.

In deriving this model, the following assumptions were made.

a) Layers specified by the velocity 2.7, 6.0 and 7.5 km/sec of the *P* wave lie from top to bottom in this order, and will be called the I, II and III layers respectively. This model was examined in order to check how far the observed values of travel times can be explained by a model with 7.5 km/sec as the velocity of the *P* wave under the Mohorovičić discontinuity, because the value is often found from the investigations of natural earthquakes.

b) The I layer lies everywhere near the surface.

c) Thickness of the I layer near Nozori is 0.1 km.

Starting from the above assumptions, a crustal structure was obtained by the method of trial and error so as to make $O-C$'s as small as possible. $O-C$'s were calculated from the delay time. The result is shown in Fig. 8b and Table 7. This model can explain the observed value of travel times fairly well except for the following points.

The I layer was obtained from the data of the Hokota explosion as the hatched part of Fig. 8b. But, the same model does not fit well with the data of the Nozori explosions and $O-C$'s for the Nozori explosions remain 0.77, 0.38, 0.34 and 0.40 sec at stations Ôgo, Ômama, Kiryû and Asikaga respectively, these values being far beyond the error of observations. In order to make $O-C$'s small at these stations for the Nozori explosions, we had to add the cross hatched part of Fig. 8b as the I layer. This is a contradiction, because this additional part would have unfavourable effects on $O-C$'s for the Hokota explosion.

5. Model V.

From the following standpoints, this model was tried.

a) At four stations where seismic waves from both the Hokota and Nozori explosions were observed (Totigi, Asikaga, Ôgo, Tukuba), $O-C$'s for both explosions can be compared.

b) Layers specified by the velocity 5.8 and 6.2 km/sec of the *P* wave are assumed, because existence of these layers was plausible in Tôhoku District[3].

c) Layers specified by the velocities 1.8, 2.7, 5.8, 6.2 and 8.0 km/sec of the *P* waves are assumed and they are called the I, II, III, IV and

---

[3] The Research Group for Explosion Seismology, *loc. cit.*, 1).

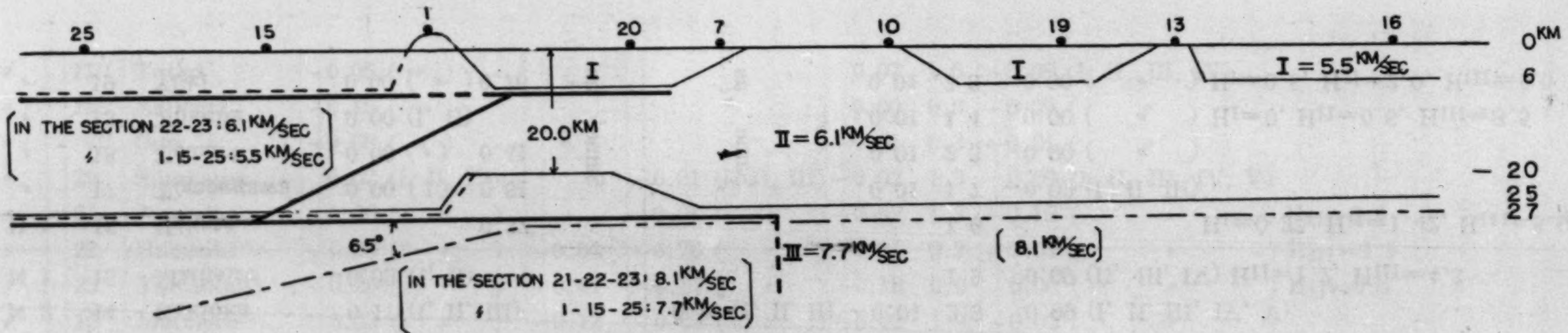
25
15
1
20
7
10
19
13
16
0KM
6
- 20
25
27
I
I
I = 5.5 KM/SEC
IN THE SECTION 22-23 : 6.1 KM/SEC
" 1-15-25 : 5.5 KM/SEC
20.0KM
II = 6.1 KM/SEC
6.5°
IN THE SECTION 21-22-23 : 8.1 KM/SEC
" 1-15-25 : 7.7 KM/SEC
III = 7.7 KM/SEC
8.1 KM/SEC

Fig. 8a.

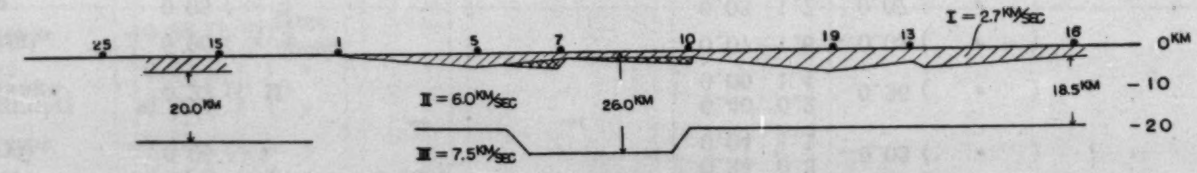
25
15
1
5
7
10
19
13
16
I = 2.7 KM/SEC
0KM
- 10
- 20
20.0KM
II = 6.0 KM/SEC
26.0KM
18.5KM
III = 7.5 KM/SEC

Fig. 8b.

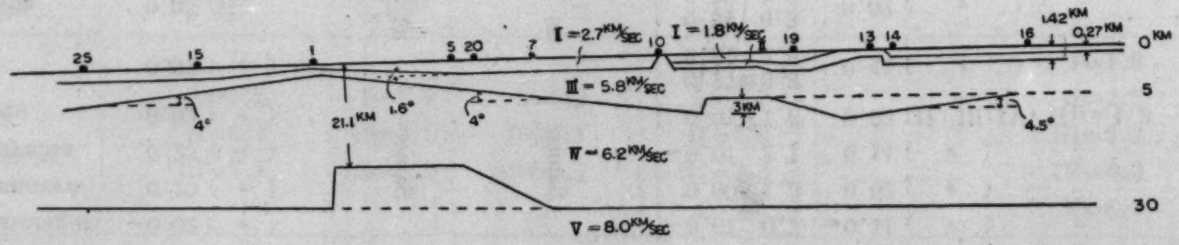
25
15
1
5
20
7
10
19
13
14
16
I = 2.7 KM/SEC
I = 1.8 KM/SEC
1.42KM
0.27KM
0KM
5
30
III = 5.8 KM/SEC
3KM
4°
21.1KM
1.6°
4°
4.5°
IV = 6.2 KM/SEC
V = 8.0 KM/SEC

Fig. 8c

Fig. 8. Crustal structure in the section along the line connecting Nozori and Hokota shot points. Observation lines of Nozori and Hokota explosions were superposed so that the positions of Tukuba station in the cases of the three explosions coincide.

a) model I. ——: boundaries of layers in the section 16-1-23.
- - -: boundaries of layers in the section 1-15(15'')-25.
[ ]—: model II } Only boundaries, which differ from model I, are shown. Others are the same as
-·-·-: model III } model I.
b) model IV. ▨: layer I, obtained from the first and the second Nozori explosions.
c) model V. Upheaval of layer V between stations Nozori and Takayama do not exist in the sections Hokota-Matusiro and Hokota-Ômati.

Table 7. $T_0 - T_c$ (unit in sec).

Name of Exp.	Ref. No.	Observation point	I		II	III	IV		V	
N1, N2	1, 1′	Nozori		sec* 0.1				*** km		$H_{II}=0.15$, $H_{III}=2.8$ ****
N 2	2′	Sima	−0.03 (I, II)		Same as I	Same as I	0.01	0.6	−0.10 (II, III)	
N 1	3	Sawatariguti	−0.02 (〃)				−0.01	0.7	−0.11 (〃)	
N 2	4	Nakanozyō	0.10 (〃)				0.00	1.3	0.02 (〃)	
N 1	5	Takayama	0.23 (〃)				−0.01	2.1	0.14 (〃)	
N 2	6	Ikaho	0.02 (〃)				0.01	1.6	0.03 (II, III IV)	$H_{II}=1.2$
N 1	7	Ōgo	0.07 (〃)				0.77※ 0.01	0.3 2.6	0.41 (〃)	
N 2	8	Ōmama	0.03 (II)				0.38 0.02	0.3 1.2	0.02 (〃)	
N 2	9	Kiryū	0.05 (〃)				0.34 0.04	0.3 1.1	−0.03 (〃)	
N 1	10	Asikaga	0.23 (I, II)				0.40 0.00	0.2 1.4	0.36 (〃)	
N 1	11	Totigi	0.00 (〃)				0.07	1.6	−0.08 (〃)	
N 2	12	Ōya	0.05 (〃)				0.03	1.7	0.07 (〃)	
N 1	13	Tukuba	−0.11 (II, III)			0.01 (II, III)	0.02	1.4	0.97 (II, III, IV, V)	
N 2	14	Kakioka	0.17 (I, II, III)			0.20 (I, II, III)	−0.01	2.9	0.99 (I, II, III, IV, V)	
N 1	15	Matusiro	−0.02 (I, II)					1.9	0.09 (II, III, IV)	$H_{II}=1.2$, $H_{III}=4.3$
H 1	16	Hokota		0.37				1.6		$H_I=0.27$, $H_{II}=1.42$, $H_{III}=5.0$
〃	17	Tomoegawa	0.00 (I)	0.61	Same as	Same as	0.01	1.7	−0.02 (I, II, III)	
〃	18	Tamari	0.00 (〃)	0.41			0.01	2.3	0.00 (〃)	
〃	13″	Tukuba	0.00 (I, II)				0.01	1.4	0.00 (〃)	$H_I=0$, $H_{II}=0.6$, $H_{III} \fallingdotseq 8.5$
〃	19	Yūki	0.00 (〃)	0.76			0.01	3.8	0.00 (〃)	$H_I=0.8$, $H_{II}=2.0$, $H_{III}=6.0$

″	11″	Totigi	−0.05 (″)	—	—	0.07	1.6	−0.09 (I, II, III, IV)	
″	10″	Asikaga	−0.15 (″)			0.00	0.2	−0.09 (″)	
″	7″	Ōgo	−0.09 (″)			−0.01	0.3	−0.21 (″)	
″	20	Sibukawa	0.07 (I, II, III)		−0.01 (I, II, III)	−0.02	1.3	0.09 (I, II, III, IV, V)	
″	21	Agatuma	0.06 (″)		−0.04 (″)	−0.02	1.3	−0.15 (″)	H_{II}=0.8
″	22	Hanasiki	−0.08 (″)	−0.04	−0.78 (″)	0.01	0.2	−0.04 (″)	H_{III}=1.9
″	23	Yamanouti	−0.20 (″)	−0.01	0.17 (″)	−0.18	0.0	0.00 (″)	H_{II}=0.6
″	15″	Matusiro	0.03 (″)	−0.12	0.69 (″)	−0.02	1.9	−0.02 (″)	
″	25	Ōmati	0.05 (″)	0.38	1.02 (″)	−0.03	1.9	0.02 (″)	H_{II}=2.2, H_{III}=7.2
″	15″	Matusiro	−0.83 (I, II) later phase						
″	25	Ōmati	0.27 (″) ″						
″	23	Yamanouti	0.20 (″) ″						
″	21	Agatuma	−0.40 (″) ″						
″	11″	Totigi	0.16 (″) ″	1.08**					
″	10″	Asikaga		0.18**					
Velocity of P wave (unit in km/sec)			I=5.5 II=6.1 III=7.7	I=5.5 II=6.1 III=8.1	I=5.5 II=6.1 III=8.1	I=2.7 II=6.0 III=7.5		I=1.8 II=2.7 III=5.8 IV=6.2 V=8.0	

(I, II, etc.) denote layers through which the first wave that reached the observation point passed.

*···thickness of the weathering layer with V_p=1.79 km/sec.

**···later phase which passed through the layer with V_p=8.1 km/sec.

***···thickness of the layer having P wave velocity of 2.7 km/sec.

****···depth of the lower boundary of a layer shown by I, II···. (unit in km)

※···upper: $O-C$ calculated from the Hokota explosion.
lower: $O-C$ calculated from the Nozori explosion.

V layers respectively. The II layer is assumed everywhere.

From an inspection of travel times, we adopt at the outset travel time curves with apparent velocities of 5.5 and 6.06 km/sec from the Nozori explosions and 5.5, 6.4 and 8.0 km/sec from the Hokoda explosion.

In the process of deriving a model of the crustal structure, shapes of layers specified by the velocities 2.7 and 5.5 km/sec of the P waves were assumed to be symmetric about the Nozori shot point.

From the critical distance determined from the travel time curves specified by the apparent velocities 2.7 and 5.5 km/sec for the Nozori explosions, the thickness of the II layer was obtained as 0.15 km near Nozori. Using the apparent velocity of 6.06 km/sec obtained from the Nozori explosions, the interface between the III and IV layers is considered to be deeper towards the east with a dip of 4°.

From the critical distance 160 km determined by the travel time curves specified by the apparent velocities of 6.4 and 8.0 km/sec of the Hokota explosion, the depth of the interface between the IV and V layers is obtained as 28.8 km.

Starting from these assumptions, small changes were made so as to make $O-C$'s as small as possible, and finally we get the crustal structure shown in Fig. 8c. This model has two disadvantages. The one is that $O-C$'s of Tukuba and Kakioka for the Nozori explosions are 0.97 and 0.99 sec respectively as shown in Table 7, being far beyond the observational errors. The other is that the upheaval of the V layer between stations Nozori and Takayama continues to exist in the Nozori-Hokota section, on the other hand, however, it must not exist in the Hokota-Matusiro and Hokota-Omati section.

6. Concluding remarks.

It is clear that each model obtained above has some advantages as well as some disadvantages. But, as stated before, we adopt model I as the final one, because it is the simplest and can explain the observed values of travel times most satisfactorily.

It is remarkable that the depth of the Mohorovičić discontinuity is obtained in the range of 20–30 km. This value of the depth is remarkably different from the value of 50 km obtained by one of the writers[4] about 30 years ago, which has been used as the standard of the crustal structure in Japan. From this result and that obtained from the investigation of Tôhoku District[5]), it may be said that the depth of the Mohorovičić discontinuity in the north-eastern Honsyû is about 20–30 km. This result was also obtained by one of the writers few years ago from the observed travel time curves of shallow earthquakes[6]).

---

[4] T. MATUZAWA, *Bull. Earthq. Res. Inst.*, **5** (1928), 1; **6** (1929) 177.

The fact that earthquakes near Tukuba occur deeper than 30 km is well-known to Japanese seismologists. Combining this fact and the crustal structure obtained above, it may be said that at least in the northern part of Kwantô District almost all the earthquakes occur below the Mohorovičić discontinuity. Thus, a clear correspondence between the crustal structure and the position of earthquake foci is established in Japan for the first time.

In deriving these models, members of our Research Group for Explosion Seismology joined in our discussions and gave us valuable suggestions for which our sincere thanks are due.

---

19. 大爆破による北関東地方の地殻構造について

其の2 地下構造

宇佐美竜夫* 三雲 健**
嶋 悦三*** 玉城逸夫****
淺野周三*** 淺田 敏***
松沢武雄***

其の1 のよみとり結果を使つて関東北部の東西断面における地下構造を求めた.

結果は Fig. 8a, b, c の通りで，全部でモデルを 5 つ作つた. そのうちモデル I を当グループとして採用することにした. それが最も簡単であり，かつ走時の観測値から計算値を引いた値が全体として小さく，したがつて最もよく走時の観測値を説明できるからである.

モデル II, III はモデル I の Moho 面下の P 波の速さを 8.1 km/sec とした場合，走時の観測値がどの位よく説明できるかを試すために作られた.

モデル IV は Moho 面下の P 波の速度を 7.5 km/sec とし，かつモデル I の 2.7 km/sec 層が地表到る所るあると仮定して試みたものである.

モデル V は，先に東北地方における爆破観測で得られた 5.8 km/sec, および 6.2 km/sec 層を仮定し，これで，どの程度まで走時の観測値が説明できるかを試すために作られた.

Fig. 8 および Table 7 の結果から分るように，Moho 面下の P 波の速度を 7.5～8.1 km/sec の間で変化させても， Moho 面までの深さはやく 25 km になる. これは従来考えられていた 50 km という考えを，大巾に修正するものである.

---

5) The Research Group for Explosion Seismology, *loc. cit.*, 1).

6) I. TAMAKI, *Zisin*, [ii], **7** (1954) 1, 226.

* 気象庁.

** 京都大学理学部地球物理学教室.

*** 東京大学地震研究所.

**** 大阪工業大学.

tigation of Tohoku District[1], it may be said that the depth of the Mohorovičić discontinuity in the north-eastern Honsyû is about 20-30 km. This result was also obtained by one of the writers few years ago from the observed travel time curves of shallow earthquakes.

The fact that earthquakes near Tohoku occur deeper than 30 km is well-known to Japanese seismologists. Combining this fact and the crustal structure obtained above, it may be said that at least in the northern part of Kwantô District almost all the earthquakes occur below the Mohorovičić discontinuity. Thus, a clear correspondence between the crustal structure and the position of earthquake foci is established in Japan for the first time.

In devising these models, members of our Research Group for Explosion Seismology joined in our discussions and gave us valuable suggestions for which our sincere thanks are due.

19. [illegible]

[illegible]

[illegible]

[illegible]

[1] T. Matuzawa, Bull. Earthq. Res. Inst., [illegible]

BULLETIN OF THE EARTHQUAKE
RESEARCH INSTITUTE
Vol. 36 (1958), pp. 359-368

20. *Self-levelling Vibrograph.*

By Kiyoshi KANAI and Teiji TANAKA,

Earthquake Research Institute.

(Read Jan. 24, 1956.—Received June 30, 1958.)

1. Introduction

A transducer of the pendulum type having a natural period of over about 0.2 sec is necessary to keep the supporting bed of the pendulum level. Vibrographs of the usual type can scarcely be operated at such special places as a bored hole, the bottom of a river or the sea, the upper part of tall chimney-like structures, narrow spaces and other complex places.

In order to get round such difficulties in operating vibrographs of comparatively long period, we adopted a system of self-levelling. The principle of the self-levelling type of pendulum adopted here is as follows:

(i) the supporting casing of the vibrograph pendulum consists of a simple pendulum,

(ii) in the stable condition a simple pendulum system can keep the bed of the vibrograph pendulum level,

(iii) before setting a vibrograph, its simple pendulum system is free,

(iv) after the supporting bed of the vibrograph pendulum becomes level, the simple pendulum system is fixed by some mechanism.

The details of the construction of this self-levelling vibrographs are explained in the following sections.

2. Self-levelling type of vibrograph pendulum

Fig. 1 shows the schematic figure of the self-levelling type of vibrograph pendulum designed by us. In Fig. 1, (i) a mass and a spring compose a vibrograph pendulum, (ii) string and inner casing enclosing the vibrograph pendulum form a simple pendulum, (iii) paraffin fixes the simple pendulum system to the outer casing, (iv) a heater makes the simple pendulum system free from the outer casing by melting the paraffin and (v) the outer casing is installed at the measuring place.

Next, the operation process of the self-levelling type of vibrograph will be explained. After the transducer has been installed at the observation place, electric current is sent to the heater in order to melt the paraffin which fixes the inner casing to the outer casing. After about 2~4 minutes, the paraffin melts perfectly and at the same time the inner casing forming a simple pendulum becomes free, and then the supporting bed of transducer pendulum becomes level after the inner casing has repeated damped free vibrations. At that moment when the supporting bed of the transducer pendulum has become level, the buzzer sounds because the electric contacts between the vibrograph pendulum and the inner casing are broken. About 1~2 minutes after the buzzer sounds, the electric current of the heater is cut off. Within about ten minutes after the current of the heater is cut off, the paraffin sets satisfactorily and the inner casing is fixed perfectly to the outer casing. Then all is ready for the observation of vibration. It takes about 15 minutes from the time that the transducer is installed.

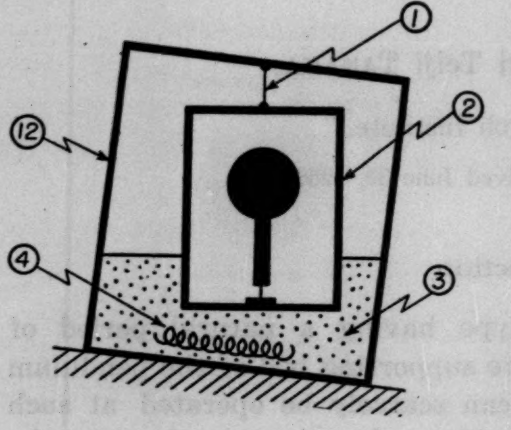

Fig. 1. Schematic figure of the self-levelling system of transducer.
①; hanging string,
②; inner-casing,
③; paraffin,
④; electric heater,
⑫; outer-casing.

3. A self-levelling vibrograph for observation at bored hole-bottom

The plan and the photograph of a self-levelling transducer for observation at 100 mm bored hole-bottom are shown in Figs. 2, 3 and 4. In this design, the natural period of the inverted pendulum is 0.8 sec. In order to make the center of gravity of the inner casing lower, a lead block is set at its bottom, and the natural period of the inner casing becomes about 0.5 sec. As the allowable inclination between the center lines of the inner and outer casings is 15°, the present transducer can be used at the place where the inclination angle is less than 15°. The total weight of transducer is about 4 kg and its sensitivity is 0.58 volt/kine. The overall frequency response curve of the present vibrograph, in which

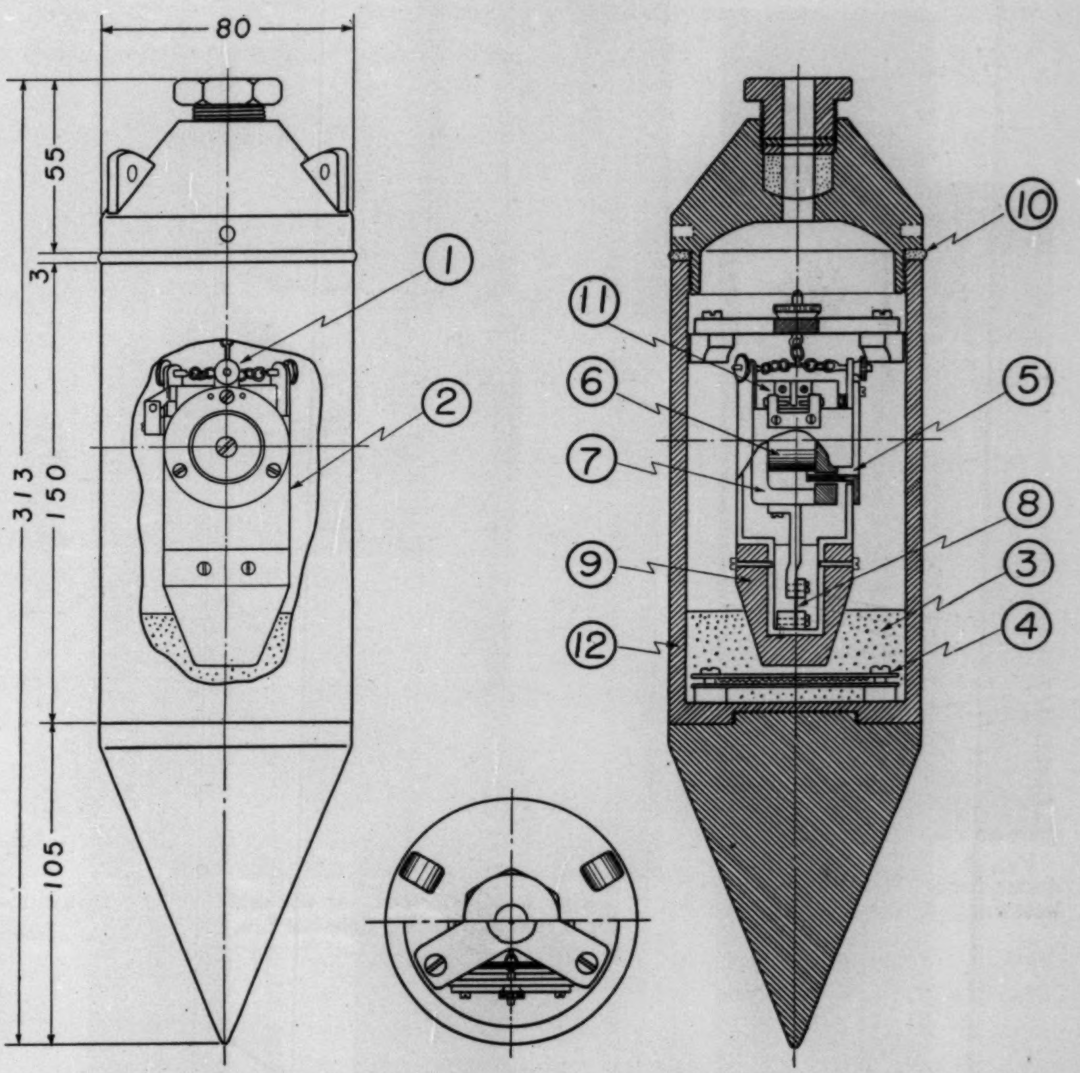

Fig. 2. Plan of the self-levelling transducer for a 100 mm bored hole-bottom. ①; hanging-chain, ②; inner-casing, ③; paraffin, ④; electric heater, ⑤; coil, ⑥; permanent magnet, ⑦; magnetic frame, ⑧; plate spring, ⑨; lead block, ⑩; rubber packing, ⑪; electric contact for buzzer, ⑫; outer-casing.

the transducer is combined with an amplifier and a recoder of the scratching smoked paper type, are shown in Fig. 5.

Simultaneous records of a microtremor at neighbouring places by this vibrograph and a vibrograph of the usual type are shown in Fig. 6. As seen in Fig. 6, the records of the two kinds of vibrograph coincide considerably with each other.

The representative record of an earthquake obtained at a depth of 21 m in a 100 mm bored hole-bottom is shown in Fig. 7. (The results of in-

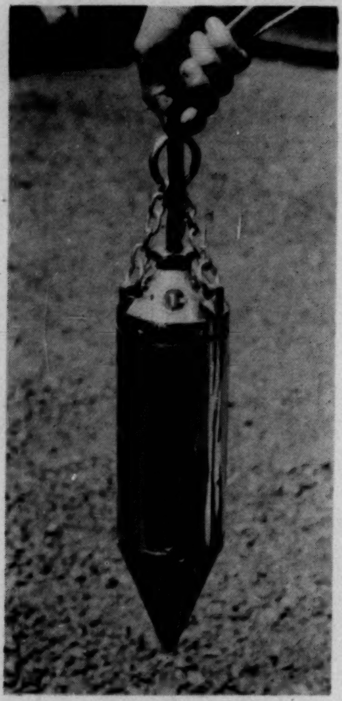

Fig. 3. Self-levelling transducer for a 100 mm bored hole-bottom.

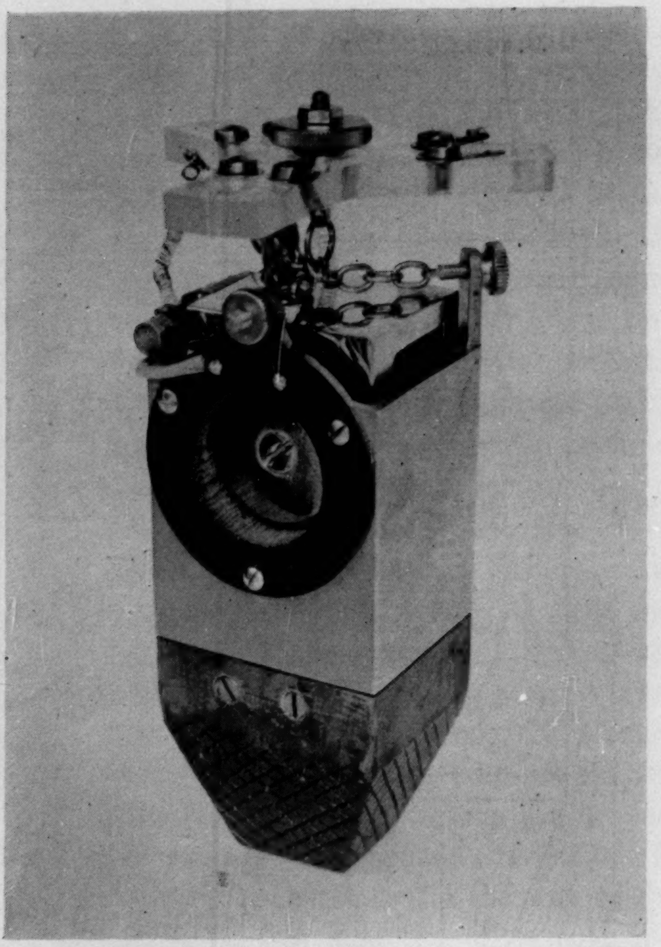

Fig. 4. Inner parts of the self-levelling transducer for a 100 mm bored hole-bottom.

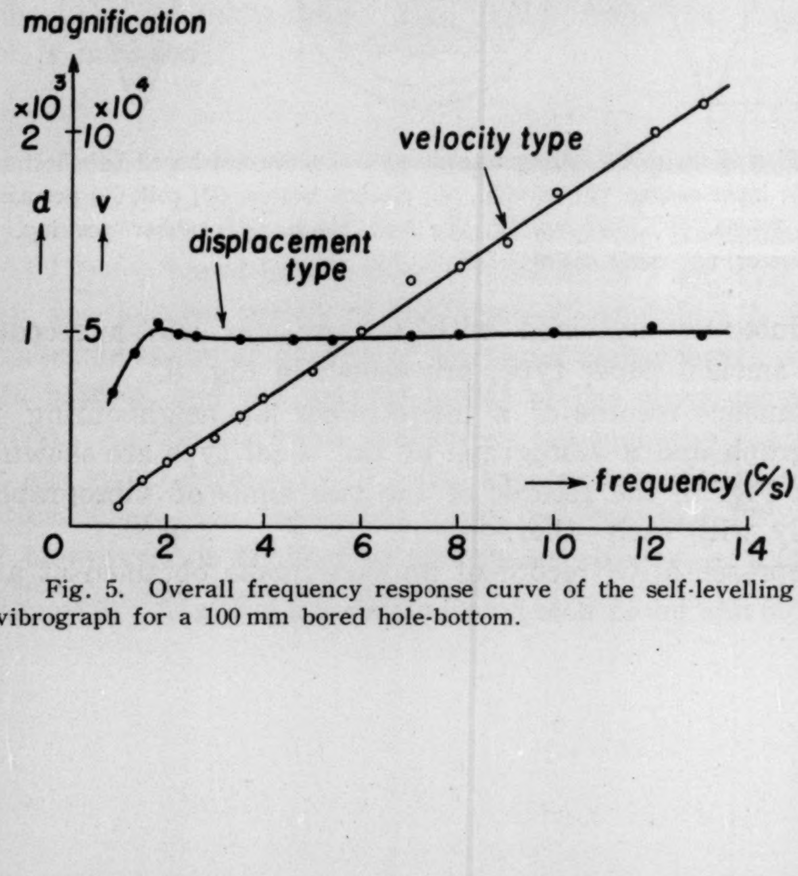

Fig. 5. Overall frequency response curve of the self-levelling vibrograph for a 100 mm bored hole-bottom.

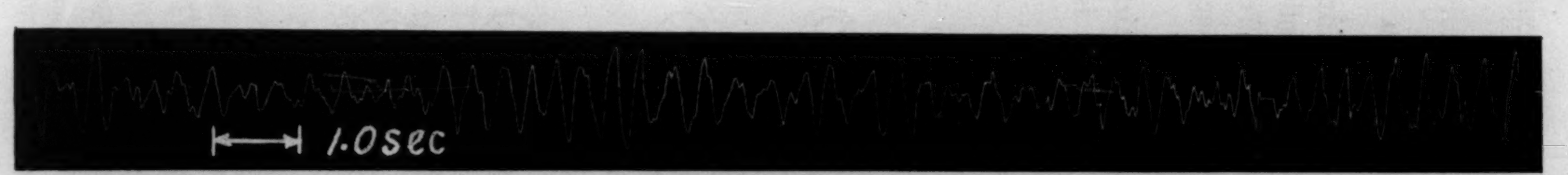

Record of the self-levelling vibrograph for a 100 mm bored hole-bottom.

Record of a vibrograph of the usual type.

Fig. 6. Simultaneous records of a micro-tremor at neighbouring places by two kinds of vibrograph.

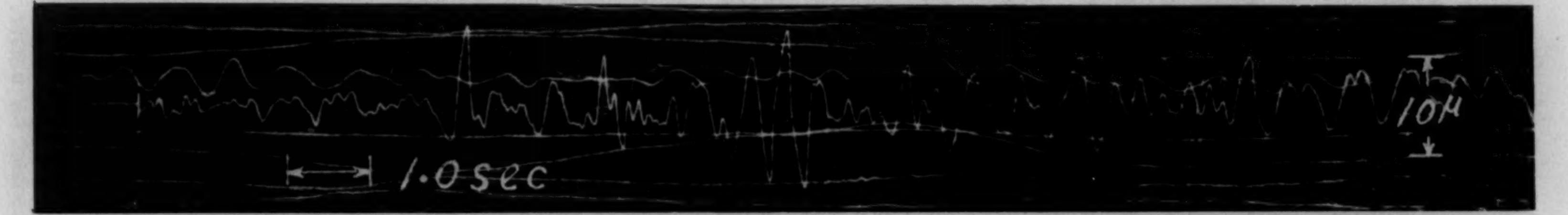

Fig. 7. Representative record of an earthquake obtained at a depth of 21 m in a 100 mm bored hole-bottom.

vestigations concerning these observations will appear in the forthcoming Bulletin.)

4. Self-levelling vibrograph for observation at water-bottom

The plan and the photograph of a self-levelling vibrograph for observations at deep water-bottom are shown in Figs. 8, 9, 10 and 11, respectively. The mechanism of this transducer is somewhat different from that for bored hole use mentioned in the preceding section, because with this the size is scarcely restricted.

The push-pull system of electric circuit consists of two pairs of magnets and coils. The natural period of the inverted pendulum is 1.0

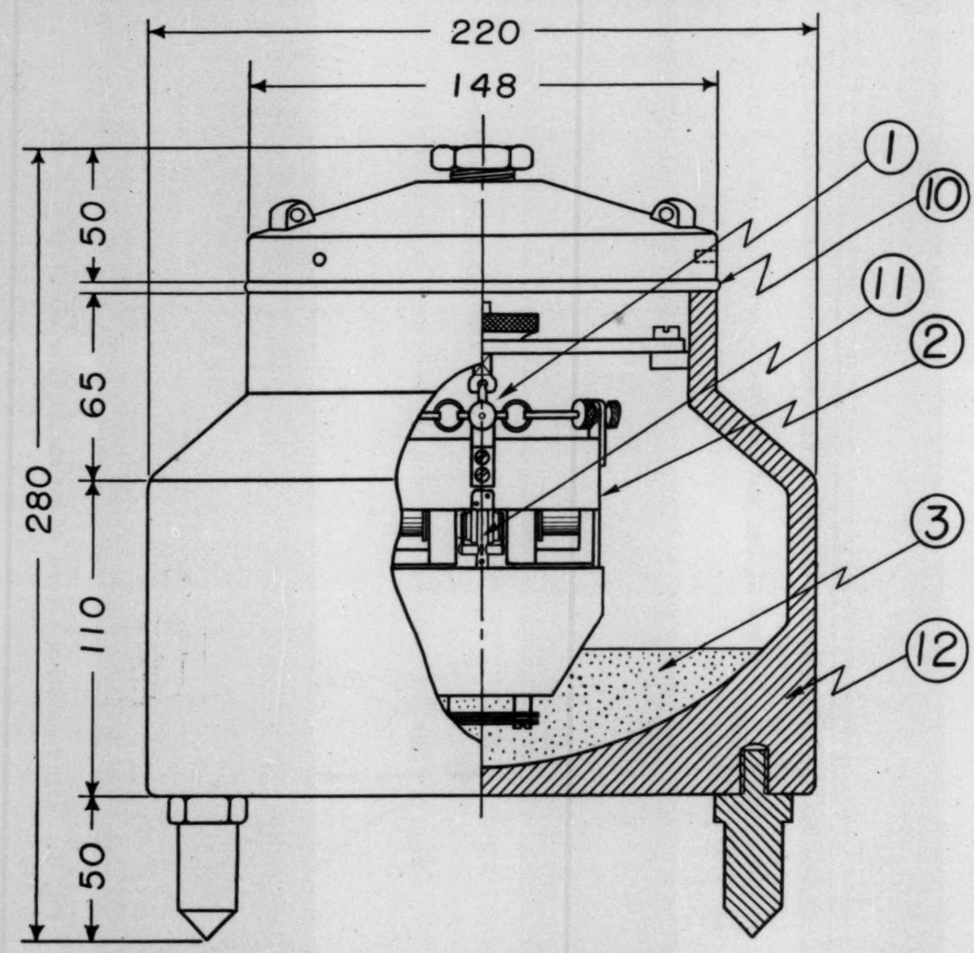

Fig. 8. Plan of the self-levelling transducer for observation at deep water-bottom. ①; hanging-chain, ② inner-casing, ③; paraffin, ⑩; rubber packing, ⑪; electric contact for buzzer, ⑫; outer-casing.

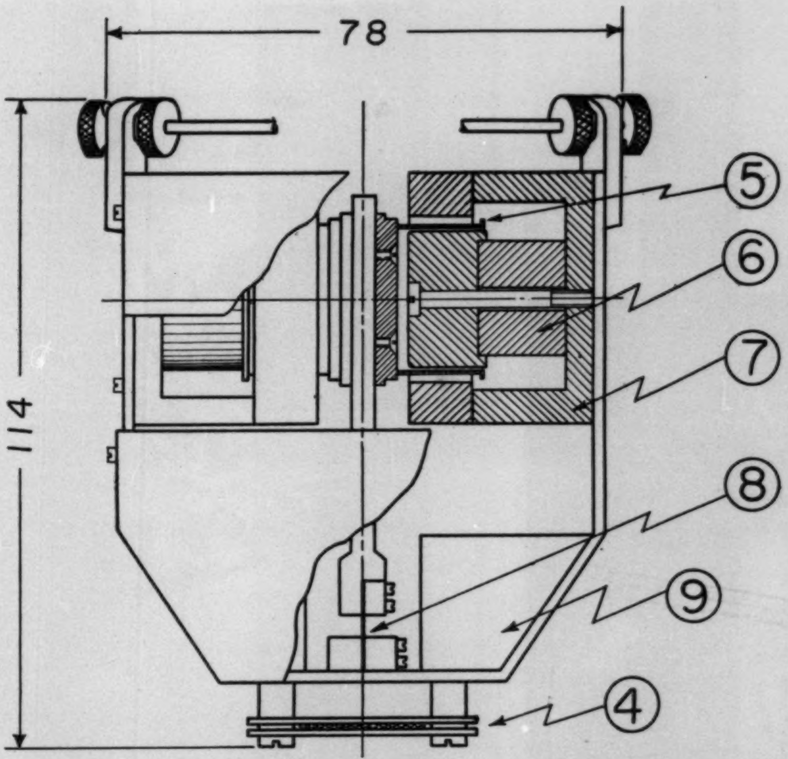

Fig. 9. Plan of the inner parts of the self-levelling transducer for use at deep water-bottom. ④; electric heater, ⑤; coil-bobbin, ⑥; permanent magnet, ⑦; magnetic frame, ⑧; plate spring, ⑨; lead block.

sec. The sensitivity of the transducer is 3.5 volt/kine. The allowable inclination of the place where the transducer will be installed is 45°. The total weight of the transducer is 14.2 kg.

The overall frequency response curve of the vibrograph, in which the transducer is combined with an amplifier and a recorder of the scratching smoked paper type, are shown in Fig. 12.

Simultaneous records of microtremors at neighbouring places by this vibrograph and a vibrograph of the usual type are shown in Fig. 13. As seen in Fig. 13, the vibration-characteristics of two kinds of vibrograph are almost the same.

The representative record of a microtremor at the bottom of the sea of 20 m depth is shown in Fig. 14. (The results of investigations concerning these observations will appear in the forthcoming Bulletin.)

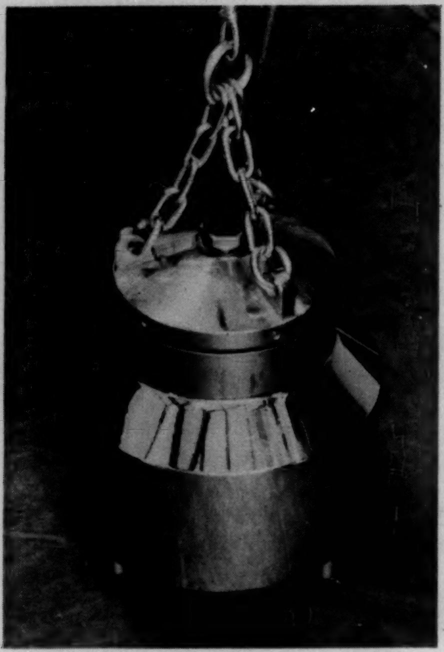

Fig. 10. Self-levelling transducer for deep water-bottom.

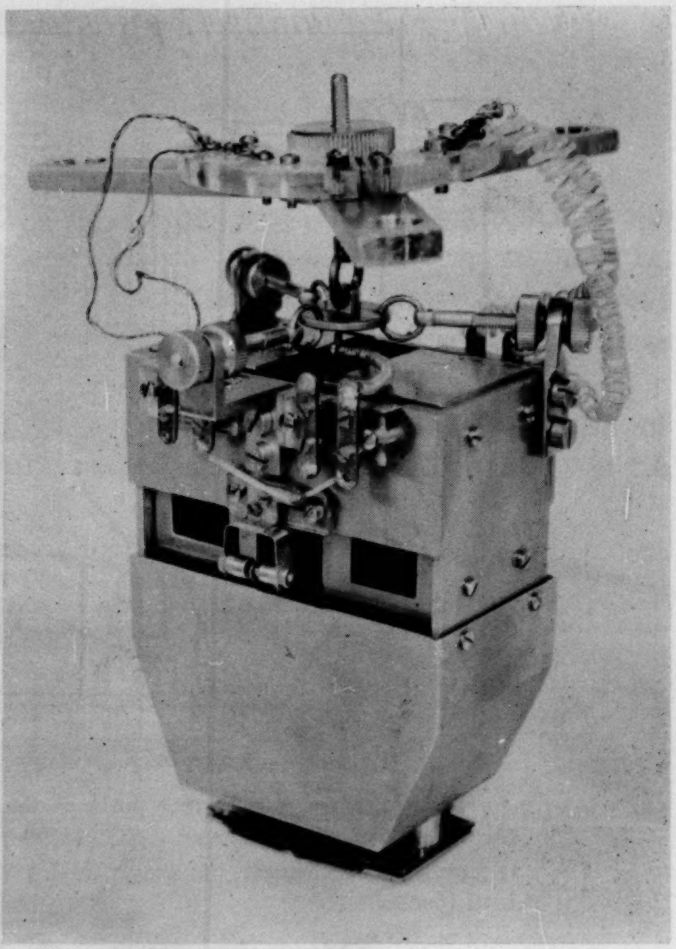

Fig. 11. Inner parts of the self-levelling transducer for deep water-bottom.

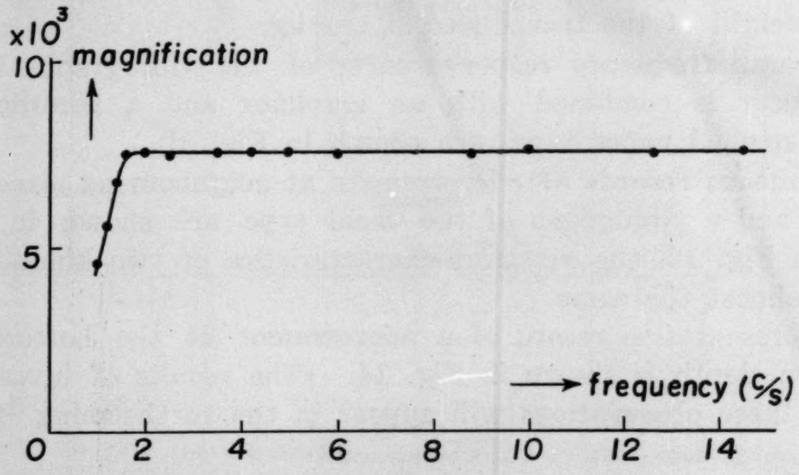

Fig. 12. Overall frequency response curve of the self-levelling vibrograph for deep water-bottom.

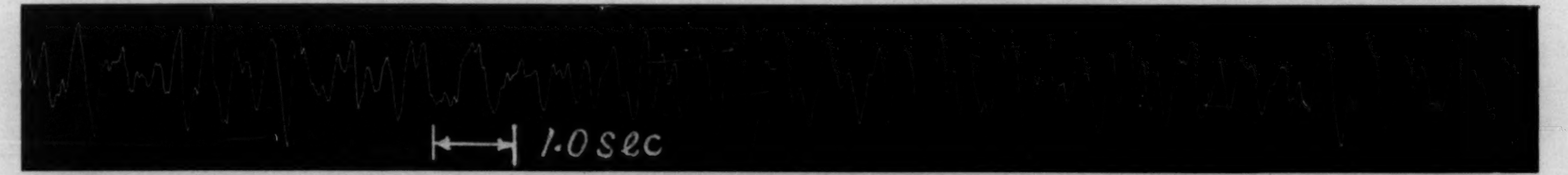

Record of the self-levelling vibrograph for deep water-bottom.

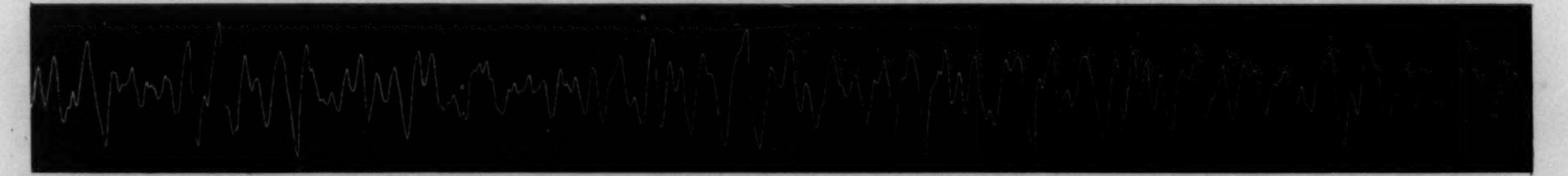

Record of a vibrograph of the usual type.

Fig. 13. Seimultaneous records of a micro-tremor at neighbouring places by two kinds of vibrograph.

Fig. 14. Representative record of micro-tremor at the bottom of the sea of 20 m depth.

20. 自動水準式振動計

地震研究所 {金井 清
田中貞二

0.2 秒位よりも長い周期の振子をもつ換振器は，水準を保たねばならない．従つて，普通の換振器では，試錐孔，河海底，細長い構造物上，狭い場所などでの使用は容易でない．

最近，このような場所で，地震観測，振動測定をしなければならない事情にせまられて，次の原理によつて，自動的に振子の台の水準を出す換振器を試作した．即ち，

(i) 換振器用振子取付け台をもつ枠を，単振子とする．

(ii) 換振器を測定場所に据えてから，単振子を包むパラフィンを電熱器で熔かす．そうすると，枠の振子は減衰自由振動をした後，安定な位置で静止する．

(iii) 枠の振子が安定な位置で静止した状態では，換振器振子取付け台の水準が得られる．

(iv) 取付け台の水準が得られたら，枠を包むパラフィンを熔かしていた電熱器の電流を切る．

(v) このパラフィンが固まると，測定可能になるわけである．

100 mm 試錐孔底用と水底用の 2 種類の換振器を試作した．換振器を据えてから測定できるまでの時間は，10～15 分である．

BULLETIN OF THE EARTHQUAKE
RESEARCH INSTITUTE
Vol. 36 (1958), pp. 369-394

21. *Geological Considerations on Plagioliparite and Associated Extrusives Exposed in the Tendō-Yamagata-Kaminoyama District, Yamagata Prefecture.**

By Takeshi ICHIMURA,
Yamagata University.

(Read June 24, 1958.—Received June 24, 1958.)

Introduction

The frequent occurrence of plagioliparite and associated extrusives is one of the remarkable geological features on the mountainous or hilly land adjacent to the Yamagata Basin. These extrusives are mostly found as dykes and lava flows in the area where Neogene sediments and granitic rocks are well exposed.

They are characterized by succesive extrusions due to repeated igneous activities which took place during or after the sedimentation of green tuff formation and played an important rôle in the formation of metallic or non-metallic mineral deposits. Moreover, the frequency of such extrusives seems to be a key point in making clear the relation between the green tuff formation of the Tendō-Yamagata-Kaminoyama district and that of the adjacent area. There are, therefore, many problem on the geology of these rocks which need to be investigated in detail. The same may be said of their lithological characters and mineral compositions, since they have almost been neglected without any examination.

Since 1956, the writer's field and laboratory work has been done for the purpose of studying them, with the co-operations of his student, Masa Suzuki. The results thus obtained are summarized in this paper.

Distribution

Plagioliparite and associated extrusives are well exposed on the mountainous or hilly land interposed between the Yamagata Basin and Backbone Range as well as between this basin and the Mogami-gawa (Fig. 1). Exclusive of plagioliparite (plagiorhyolite)[1], these various kinds of extrusives are represented by perlite, trachytic andesite, dacite and andesite. Among them, plagioliparite and trachytic andesite are found in high frequency as compared with others. In this case, the occurrence of dacite is restricted to the eastern district, whereas perlite is present in the western area.

---

* Communicated by H. Tsuya.

[1] I. KATŌ, *Sc. Rep. Tōhoku Univ.*, [iii] **5** (1955), 72.

So far as is known at present, the northern distribution of plagioliparite in this district is sporadically traceable up to the area including Suishō-zan, Uzawa-yama, Amayobi-yama, Maizuru-yama near Tendō, the Ōishi-zawa and the ridge between the Iwano-sawa and the Zaimoku-zawa where it is closely associated with green tuff. The frequent occurrence of such a plagioliparite is similarly noticed in the area beyond the Tachiya-gawa. Thus, it can not infrequently be seen at the western side of the Omoshiro Volcanoes which is deeply dissected by such tributaries of the Tachiya-gawa as the Momiji-gawa, Ichino-sawa, Nino-sawa, Bunpeki-zawa, Tashiro-zawa and Magata-zawa. This area is mostly composed of tuffaceous sediments and granitic rocks covered partly by lavas and ejecta of the Omoshiro Volcanoes. Going westwards, however, the geological feature is somewhat different, since plagioliparite and trachytic andesite here are repeatedly exposed in an intricate manner, some of them being underlain or intercalated by Miocene sediments. Such exposures are observable at many places such as those shown by Ōmori-yama, Sanpō'oka, Tamagairi, Shimo-higashiyama, Kirihata, Ōoka-yama and Aono. They extend further south down to the Mamigasaki-gawa, passing through Fukazawa-fudō, Yanbe and Sakazuki-yama. Besides these, plagioliparite and trachytic andesite occasionally cut green tuff and its underlying granodiorite along the uppermost course of the Takase-gawa, but some of them rest upon the green tuff of the ridge behind Namekawa and Niiyama.

At the opposite side of Sakazuki-yama, there are plagioliparite of Chitose-yama and Saruoka-yama as well as dacite of Togami-yama and Iwanami underlain by green tuff beds. It is also noteworthy that small but repeated exposures of plagioliparite are seen in the granitic mass which forms the foundation of the Gando Volcano. Most of these are distributed at Sekizawa, Namekawa, Kami-hōzawa, Shimō-hōzawa, the upper course of the Mamigasaki-gawa, the Happō-zawa, etc., although the occurrence of plagioliparite is partly obscured by overlying lavas and ejecta of the Ryūzan Volcano and Gando Volcano.

It again appears largely in the area of green tuff watered by the Namai-gawa, Shōbu-gawa and Kayadaira-gawa, as is indicated by those

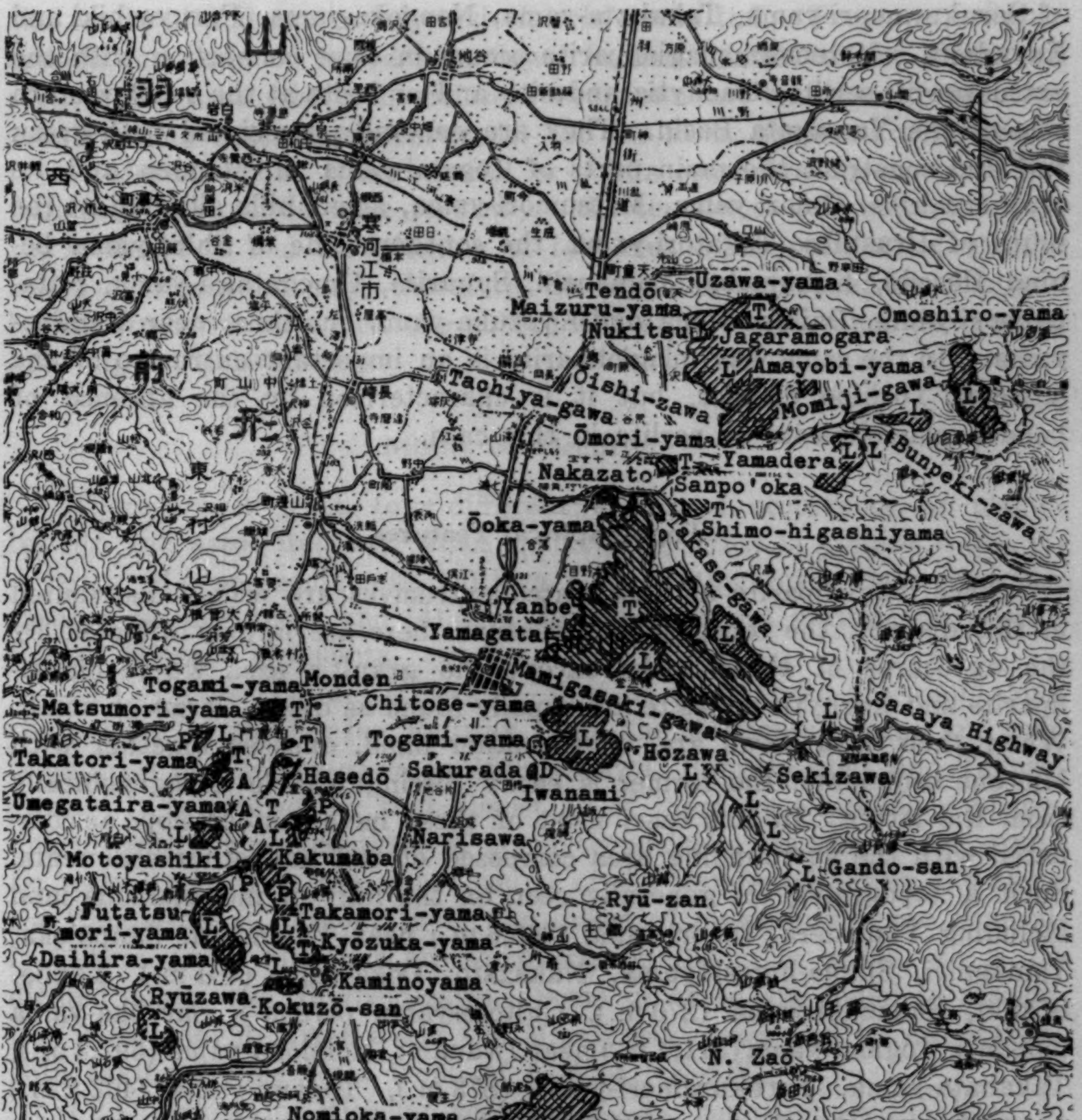
Uzawa-yama
Tendō
Maizuru-yama
Nukitsu
Jagaramogara
Omoshiro-yama
Amayobi-yama
Tachiya-gawa
Oishi-zawa
Momiji-gawa
Ōmori-yama
Yamadera
Bunpeki-zawa
Nakazato
Sanpo oka
Shimo-higashiyama
Ōoka-yama
Takase-gawa
Yanbe
Yamagata
Togami-yama
Monden
Matsumori-yama
Chitose-yama
Mamigasaki-gawa
Sasaya Highway
Togami-yama
Hōzawa
Takatori-yama
Hasedō
Sakurada
Sekizawa
Iwanami
Umegataira-yama
Narisawa
Motoyashiki
Kakumaba
Gando-san
Ryū-zan
Futatsu-mori-yama
Takamori-yama
Kyōzuka-yama
Daihira-yama
Kaminoyama
Ryūzawa
Kokuzō-san
N. Zaō
Nomioka-yama
Ōmizusawa-yama
Shōbu
S. Zaō
Akayama Mine
Kayadaira
Fubira-san
L
1
D
4
P
2
A
5
T
3

Fig. 1. Map showing the distribution of plagioliparite and associated extrusives in the Tendō-Yamagata-Kaminoyama district. 1=Plagioliparite, 2=Perlite, 3=Trachytic andesite, 4=Dacite, 5=Andesite.

of Sarukuramori-yama, Takahata-yama, Nomioka-yama, Furuyashiki and Kayadaira. Moreover, plagioliparite occurs in close connection with the extrusion of perlite, trachytic andesite and andesite at the southwestern side of the Yamagata Basin. They are generally associated with green tuff and construct the main parts of Togami-yama of Monden and its southern hills, Ōmori-yama, Matsumori-yama, small hills situated at the south of Urushibō, Takatori-yama, the southern side of Shiro-yama behind Hasedō, Kakumaba, Yamauchi, Sugarita, Umegataira-yama, Futatsumori-yama, Daihira-yama and Kyōzuka-yama or others near Kaminoyama. In the same way, plagioliparite is an important extrusive of the adjacent Yoshino district, but it is characterized by the absence of banded plagioliparite or perlite in this case.

Topographical Features

Since plagioliparite and associated extrusives are widely distributed in this district, the topographical features here are largely affected by the exposures of these rocks except the granitic area where plagioliparite and trachytic andesite are usually found as dykes, large or small. When their lava flows are, on the other hand, exposed together with Miocene sediments, the former is easily distinguishable topographically from the latter. In this case, most of these have a steep slope as compared with the surrounding area composed of tuff and other sediments. Such a topography is generally seen on the hilly or mountainous land including Yamadera, Ōmori-yama (365.6 m.) near Yamadera, Sanpō'oka, Tamagairi, Shimo-higashiyama, Nakazato, Ōoka-yama (401 m.), Yanbe, Sōzuki, Sakazuki-yama (270 m.), Chitose-yama (472 m.), Saruoka-yama (558 m.), Togami-yama (311.4 m.) near Iwanami, Nomioka-yama (592.4 m.), Takahata-yama, Sarukuramori-yama (873 m.), Togami-yama (402.2 m.) near Moden, Ōmori-yama (606.5 m.) near Urushibō, Umegataira-yama (639.5 m.), Futatsumori-yama (562.4 m.), Daihira-yama (714.4 m.), Kyōzuka-yama and others.

It is also worthy to notice that there are cone-shaped hills or small peaks here and there, being constructed by lava flows composed of plagioliparite, trachytic andesite and dacite. They are represented by Ōmori-yama (plagioliparite and trachytic andesite) near Yamadera, Togami-yama (dacite) near Iwanami, Togami-yama (trachytic andesite) near Monden, etc. which may be mistaken for small volcanoes at a glance (Figs. 2, 5). These conical masses rise up to a height of 311.4 m.–472 m. above the sea-level and are mainly underlain by green tuff. They are probably erosion remnants of folded lava flows, because almost all of them are seen in the area where the Miocene sediments are traversed by syncline axes running north-northeastwards. So far as is observed at present, it is inferable that many cracks or joints concentrating upwards but radiating downwards were formed by the tension or compression due to the syclinal fold and the pitching of fold-axes. The present topography under consideration may, therefore, be supposed to depend on this geological structure by which the subsequent erosion was much favored to build up an isolated cone.

Modes of Occurrence

There are, at least, four different modes of occurrence of plagioliparite and associated extrusives, namely (1) dykes in granitic rocks, (2) dykes in Miocene sediments, (3) lava flows resting upon the eroded surface of granitic rocks and (4) lava flows poured out during the deposition of Miocene sediments.

(1) Dykes in granitic rocks:—Most of these rocks are seen along the cutting of the Senzan Railway Line, the Mamigasaki-gawa and such tributaries of Tachiya-gawa as Momiji-gawa, Bunpeki-zawa and Takase-gawa. It is noteworthy that almost all of them are composed of plagioliparite with some exceptions of trachytic andesite traversing the granitic rocks exposed at the upper course of the Mamigasaki-gawa and along the Hanoki-zawa. Among them, the dykes of plagioliparite are generally 5–20 m. wide, but they are sometimes 60–100 m. in width, as is indicated along the Bunpeki-zawa. Some of these are found in association with propylite dikes along the Mamigasaki-gawa and its tributaries, both taking frequently a trend of N–S or NE–SW.

(2) Dykes in Miocene sediments:—As compared with those in granitic rocks, they appear in low frequency along the Matsutome-zawa, the upper course of the Akakura-zawa, the Sasaya Highway between Namekawa and Niiyama, etc., where plagioliparite was injected into green tuff of the Hōzawa Formation²⁾. The similar mode of occurrence is shown by a trachytic andesite cutting the green tuff on the route between Shōbu and the Fubira Mine.

(3) Lava flows resting upon the eroded surface of grantic rocks:—

---

2) The Hōzawa Formation is composed of green tuff, brecciated tuff and conglomeratic tuff exposed mainly on the ridge behind Hōzawa. Stratigraphically, it corresponds to the lower part of the Kaneyama Formation or the Yoshino Formation.

This type of occurrence is only seen at the upper course of the Takasegawa, the opposite side of Bōbara and on the ridge between Niiyama and Hōzawa. In these cases, the extrusive is represented by plagioliparite and trachytic andesite.

(4) Lava flows poured out during the deposition of Miocene sediments:—There are many lava flows in association with the Sugarita Formation[3], the Yamadera Formation[4] and the upper part of the Yoshino Formation[5]. They were repeatedly erupted during the deposition of the formations composed of green tuff, conglomeratic tuff, brecciated tuff, shale, siltstone and sandstone. Some of them, therefore, interfinger with Miocene sediments and pass laterally into one another. Moreover, it is noticed that the same lava flow overlies occasionally granitic rocks on one hand but green tuff on the other.

So far as has been investigated on Maizuru-yama and its southern hills, plagioliparite is overlain by green tuff and hard shale which grade into the trachytic andesite upwards. The similar feature can be observed on the hills to the south of Nukitsu. In connection with them, a large exposure of plagioliparite flow is known in the area including Uzawa-yama, Jagaramogara and Kami-nukitsu and seems to be traceable southwards down to the Ōishi-zawa where it is found in contact with the brecciated tuff bordered by a fault, indicating that the former is supposed to have been thrown down against the latter.

At the south of the Tachiya-gawa, an extensive area of lava flows represented by plagioliparite and trachytic andesite is distributed in close association with tuffaceous sediments and shale beds. One of them is to be seen along the Magata-zawa or the Tashiro-zawa and overlies tuff beds or granitic rocks. The rock exposed here is plagioliparite with a high frequency of joint structure. In this case, a small isolated hill called Ōmori-yama situated between the Tachiya-gawa and the Senzan Railway Line is constructed of trachytic andesite and plagioliparite intercalated by tuff and shale. The same can be said of the area including Sanpō'oka, Tamagairi and Shimo-higashiyama, where the occurrence of tuff and shale beds is known at the lowest part of the thick lava flow composed of a trachytic andesite. Such a geological feature is confirmed near the hill behind the temple of Sanpō'oka and on the hill-side close to Shimo-higashiyama. The sediments of these places are brecciated tuff and black shale on the hill of Sanpō'oka, but black shale only in the vicinity of Shimo-higashiyama. In the latter case, trachytic andesite interfingers with shale bed in which *Propaemusium tateiwai*, *Sagarites* sp. and small fragments of echinoid are abundantly contained. The lava flow mentioned above were probably displaced downwards by a fault against the alternate beds of shale and tuff near Shimo-higashiyama.

---

[3] The Sugarita Formation corresponds to the Kusanagi Formation of the Shinjō Basin.

[4] The Yamadera Formation is supposed to include the Kusanagi Formation and the uppermost horizon of the Kaneyama Formation. Hence, its lower part may be correlated with the Nishikurosawa Formation of the Akita Prefecture.

[5] The name of the Yoshino Formation was first given by Y. Funayama, and it was also used by Minakawa in his paper [S. MINAKAWA, *Bull. Yamagata Univ.* (*Nat. Sc.*), **4** (1957), 244.], but there may be some difference between them.

The plagioliparite and trachytic andesite with the same mode of occurrence extend further west or south, namely from here to the eastern margin of the Yamagata Basin, the Mamigasaki-gawa and the upper course of the Takase-gawa (Fig. 4). They are sometimes composed only of trachytic andesite. As is shown at several places, such as Nakazato, Kiridome, Fukazawa-fudō, Yanbe, Sōzuki and Namekawa or elsewhere, they are frequently underlain and inserted by tuff and shale beds which are sometimes characterized by the presence of *Propaemusium* and *Sagarites*, being more than 300 m. in the thickest part. It is furthermore confirmed that there are some remnants of tuffaceous or shaly sediments on the hill of trachytic andesite between Nakazato and Ōoka-yama. The plagioliparite and trachytic andesite here are likely to have successively or simultaneously been extruded, and some of these pass laterally or vertically into one another.

In the same way, plagioliparite of Chitose-yama and Saruoka-yama rests upon the green tuff beds, and its lava flow is estimated to be 300 m. or thereabouts in thickness. The same mode of occurrence may be said to be true of the dacite flow extending from Togami-yama to Iwanami and Kami-sakurada. Such an occurrence is equally indicated by the plagioliparite flows of Nomioka-yama, Takahata-yama, Sarukuramori-yama and Kayadaira, where the lava flows overlie the alternate beds of brecciated tuff, conglomeratic tuff, hard shale, sandstone, etc. Of these, the plagioliparite of Nomioka-yama contains occasionally many fragments of black shale. It seems to have a synclinal structure and the maximum thickness of about 300 m. The rock extends further south beyond the Miya-kawa and Kayadaira-gawa, resting on green tuff beds and being highly cliffed here and there. Its exposure is found in a possible connection with several dykes of plagioliparite and trachytic andesite which can be seen along the route between Shōbu and the Fubira Mine.

Very complicated modes of occurrence are revealed by plagioliparite, perlite, trachytic andesite and common andesite exposed repeatedly on the hilly land including Murakizawa, Nishi-yamagata, Motozawa, Yamamoto and Kaminoyama, The most remarkable extrusive of this area is plagioliparite associated frequently with perlite (Fig. 3), trachytic andesite and common andesite. The stratigraphical relationship between them is not exactly determined, but they are likely to be inserted in the Sugarita Formation and the upper horizon of the Yoshino Formation, as is suggested by many examples of Hōhōiwa, Mujinamori, Yamamoto, Matsumori-yama, Futatsumori-yama, Daihira-yama and Kyōzukayama near Kaminoyama. Minakawa[6] believes that plagioliparite begins to appear at the uppermost part of the Yoshino Formation. He also confirmed the occurrence of two plagioliparite flows in the Sugarita Formation distributed at such type localiteis as the tributaries of the Motozawa-gawa situated to the south of Sugarita and on the route between Sugarita and Kaminoyama or Sugarita and Uchiyama. Besides them, a noticeable geological feature here is the frequency of bentonite deposits in green tuff beds which are sometimes associated with the lava flows of banded plagioliparite. These deposits can be examined at Kakumaba and Motoyashiki as well as along the bus road between Yuta and Sugarita, but it is still uncertain whether there are stratigraphical connections between them. Plagioliparite and perlite are mostly found together, showing a gradual transition from one to another. Such a tendency is well investigated along the cutting near Matsumori-yama. The similar occurrence is known on a small hill rising at the south of Urushibō and the bottom of the valley behind Umegataira-yama or others. They extend north-northeastwards, although some complicated structure is revealed in the area including Takatori-yama, Nitazawa, Uchiyama and Umegataira-yama where plagioliparite, perlite and trachytic andesite are found together with andesite. In this case, the ocurrence of several andesite flows is known on the route which passes through Takatori-yama and Sugarita.

The trachytic andesite of Togami-yama and its neighbourhood is, however, isolated from the exposures of banded plagioliparite and perlite mentioned above, but it seems to have a close relationship to the extrusion of trachytic andesite exposed largely on the hills between the Tachiya-gawa and the Mamigasaki-gawa.

---

[6] S. MINAKAWA, *Bull. Yamagata Univ.* (*Nat. Sc.*), **4** (1957), 245.

As can be inferred from the facts already stated, it is very worth noting that the accurrence of lava flows of plagioliparite, perlite, trachytic andesite, dacite and andesite is always confined to the lower half of the Yamadera Formation, the upper or lower horizon of the Sugarita Formation and the upper-most part of the Yoshino Formation. They are, on the other hand, absent at the uppermost horizon of the Yamadera Formation with some fossil brachiopods such as *Terebratalia pacifica*, *Terebratalia tenuis* and *Terebratulina crossei*7).

Lithological Characters

Plagioliparite and its associated extrusives are classified as follow, viz., biotite plagioliparite, hornblende biotite plagioliparite, hornblende plagioliparite, biotite perlite, hornblende perlite, trachytic andesite, two-pyroxene hornblende dacite and two-pyroxene andesite.

(1) Plagioliparite :—Biotite plagioliparite is predominantly exposed as compared with other extrusives, being composed of two varieties with or without a banded structure. The occurrence of non-banded variety is well known along the Kuratsu-gawa, Tachiya-gawa, Takase-gawa, Mamigasaki-gawa and their tributaries. It is also seen in the area which includes Chitose-yama, Saruoka-yama, Nomioka-yama, Takahata-yama, Sarukuramori-yama, Kaneyama, Ōmizusawa-yama, Kakumaba, Takatori-yama near Kubote and others, where columnar or platy joints are seen at many places.

It is compact and hard rock with a porphyritic texture due to the presence of quartz, plagioclase, biotite and hornblende phenocrysts, having a dark grey color in fresh specimens and a grey color when decomposed. Some of it is characterized by the frequency of large phenocrystic quartz. Such a kind of rock is commonly to be observed on the hill behind Kirihata and at the opposite side of Bōbara beyond the Mamigasaki-gawa as well as along the Hanokizawa and near Kaminukitsu. Sometimes, the specimens are rich in small quartz phenocrysts, but they are almost free of them in other cases, as is indicated by the examples which can be observed at the entrance of the Nino-sawa traversed by the Senzan Railway Line or elsewhere. Besides these, there is silicified and partly kaolinized plagioliparite on Chitose-yama, where

---

7) The Similar fossil brachiopods are also contained in the tuffaceous sandstone exposed along the valley between Takatori-yama and Ōmori-yama. This uppermost horizon of the Sugarita Formation is, however, not free of the lava flows composed of plagioliparite and andesite.

the clay deposite are now being used for the porcelain industry of Hirashimizu. Moreover, the occurrence of brecciated plagioliparite is known at the southern foot of Nomioka-yama. It contains many fragments of granodiorite, propylite and black shale.

When non-banded biotite plagioliparite takes a dyke-form, the rock is frequently impregnated by pyrite and is stained by iron oxicides. In another case, it is thinly incrusted with thulite and dendrite, which are occasionally noticed on the cutting of a road opened recently at the southern side of the Tachiya-gawa.

Banded biotite plagioliparite is, on the other hand, a common extrusive at the southwestern part of this district, its occurrence being always restricted to the area of the Sugarita Formation and the upper horizon of the Yoshino Formation. The good exposures are known on Matsumori-yama, Shiro-yama near Hasedō, Umegataira-yama, Daihira-yama, Futatsumori-yama and Kyōzuka-yama as well as at Kakumaba, Uchiyama, Mujinamori and Motoyashiki. Among them, the most remarkable examples are represented by those of Daihira-yama, Futatsumori-yama, Kyōzuka-yama and the ridge along the Motozawa-gawa. In these cases, biotite plagioliparite of Daihira-yama and Futatsumori-yama pass frequently into hornblende-bearing variety.

The rock has a light reddish brown or grey color and reveals distinctly or indistinctly a banded structure in all cases, passing into the ordinary biotite plagioliparite and biotite perlite. When such a plagioliparite shows a remarkable banded structure and is subjected to weathering, it resembles frequently stratified sediments and breaks easily into platy fragments as is the case of Motoyashiki or elsewhere. The columnar joint is almost absent except that of Kyōzuka-yama. Generally, it is a hard rock which is sometimes represented by a porous type whose cavities are occasionally filled up by chalcedony. An example of brecciated biotite plagioliparite is also observable along the bus road near Motoyashiki, and the specimens encrusted with thulite or psilomelane are obtained from the valley behind Umegataira-yama.

Hornblende plagioliparite is found in a small extent as compared with biotite plagioliparite. It is exposed on the ridge extending northeastwards along the Ōishi-zawa near Yamadera, Daihira-yama, Futatsumori-yama and at the entrance of the valley between Suge and Kuromori of Yamamoto. In such cases, the first one has a grey color and contains large quartz phenocrysts and hard shale fragments, whereas the last three are compact and light reddish brown or light grey rocks.

Plagioliparite consists of quartz, orthoclase, plagioclase, biotite, hornblende, augite, magnetite, ilmenite, zircon, apatite, hypersthene, chlorite, pyrite, sericite, limonite, kaolinite, goethite and leucoxene (Fig. 6). The frequency of these minerals reveals a wide range of variation in the different specimens, and the rock is commonly rich in phenocrystic minerals.

Among them, the commonest ingredient is quartz which is found as a phenocryst and a component in the groundmass. Sometimes, its phenocrysts are abundantly present as compared with those of plagioclase, taking a rounded or angular form and being occasionally corroded by the groundmass. The occurrence of well-defined bipyramidal crystal, 4–5 mm. in diameter, is known in the specimen from the Hanoki-zawa and the cutting of truck road between Akayama and Kaneyama-tōge where it is obtained in dyke traversing granodiorite or green tuff. Most of it contain liquid inclusions and minute crystals of magnetite, zircon and chlorite.

Moreover, it is surrounded by a narrow fringe of plagioclase, quartz and sericite as well as of chalcedony and limonite. When such a fringe is composed of plagioclase and quartz, it constructs a spherulitic aggregate or micrographic intergrowth. The phenocrystic quartz ranges mostly from 0.5 mm. to 1.5 mm. in diameter. In the groundmass, this mineral occurs as very small grains with an irregular or rounded form and is intermixed with ill-defined orthoclase and plagioclase crystals.

Plagioclase is also an important ingredient. The phenocrystic plagioclase is very frequently to be seen in the writer's specimens except those obtained from the upper course of the Mamigasaki-gawa and the hill situated at the south of Nukizu-numa. It is oligoclase or andesine with a composition of An_{14-42} and has a rectangular tabular form, 3.48 mm. long and 1.36 mm. across in the largest crystal. Such phenocrysts are usually euhedral or subhedral and almost free of the zonal structure or turbid zone. The crystals are occasionally invaded by the groundmass and are surrounded by a fringe composed of minute quartz and plagioclase grains. They are often subjected to sericitization or kaolinization and to zeolitization in other cases. The plagioclase of the groundmass is oligoclase and is generally represented by ill-defined crystals. In some cases, however, lath-shaped crystals, 0.08 mm.–0.2 mm. long, are also found together.

The occurrence of biotite and hornblende is restricted to a small extent when compared with that of quartz or plagioclase. So far as is known at present, these two minerals are recognized only as phenocrysts in thin sections and are sometimes contained together in the same specimens. In these cases, biotite takes a tabular form, 1.98 mm. in the maximum diameter of its base and 0.57 mm. in the maximum thickness. It is strongly pleochroic from light brown to light yellow (X) to dark yellowish brown (Y or Z), and some of it encloses magnetite crystals. The index of refraction (γ) is 1.674–1.686, but 1.681–1.683 in banded varieties. This mineral is frequently seen in the specimens collected from the northwestern branch of Takatori-yama, Daihira-yama, Futatsumori-yama and the trails between Sumiga-hashi and Tozawa-bashi of the Takase-gawa as well as between Uchiyama and Marumori.

The frequency of hornblende is lower than biotite, and the crystal has a prismatic habit, being characterized by the following pleochroic scheme, viz., X=light yellow, Y=yellowish green or brown, Z=green or dark greenish brown. The absorption is $Z>Y>X$. The indices of refraction are as follows; $N_1=1.665$–1.669, $N_2=1.679$–1.682 on (110). The largest one is 0.97 mm. long and 0.34 mm. across. The extinction angle, $Z \wedge c$, is 17°–18°. When it has a zonal structure, its outer part reveals a smaller extinction angle.

Augite is a rare ingredient with a stout prismatic habit and can be seen in the specimens from the eastern hill-side of the Yamadera Highway and the Ōishi-zawa or elsewhere. It is 0.62 mm. long and 0.25 mm. across in the largest crystal, passing partly into bowlingite. Its extinction angle, $Z \wedge c$, is 40°(±). Besides the example mentioned above, the writer observed some chloritized augite with original crystal forms in the specimens from the Ōishi-zawa.

Magnetite has an octahedral or skeletal form and is scarcely present in almost all specimens. Its crystal is generally very small, and even the largest one does not go beyond 0.05 mm. in diameter.

One of minor ingredients is a pink or colorless zircon which is sometimes overlooked in thin sections. The writer extracted this mineral from crushed specimens by using Thoulet solution (Fig. 13). These two kinds of zircon are contained together, but the colorless variety is mostly absent.

In many specimens, there are several types of crystal characterized by simple or complicated combinations of (100), (111); (110), (111); (110), (111), (311), etc. The commonest form is, however, a combination of (100) and (111) or (110) and (111). They are composed of long or short prismatic crystals, the former being occasionally corroded to a crub-like form with an irregular outline. Such crystals are commonly rich in microlites which have unknown characters. In general, the frequency of zircon crystals seems to be high in the specimens from dykes and lava flows except those of banded plagioliparite. It is, however, noticed that this mineral is almost or entirely absent in some specimens obtained from the western hill of Narasawa, the upper course of the Takase-gawa, the lowermost course of the Happō-zawa and at both the sides of the Motozawa-gawa 500 m. or more east-northeastwards from the bus station of Kakumaba as well as on the ridge between Takatori-yama and Kyōzuka-yama or elsewhere.

Apatite and hypersthene are always negligible minerals. The former is usually colorless, but obtains a brown color when decomposed. The crystal is 0.17 mm. long and 0.03 mm. across in the largest one and occurs in the specimens from the Ōishi-zawa and Chitose-yama. The latter was examined only on the minute crystals extracted from crushed specimens as in the case of zircon. The largest prismatic crystals thus separated are 0.26 mm. or thereabouts in length and are strongly pleochroic from yellow (X) to brownish yellow (Y) or greyish green (Z). This mineral is rarely found in the specimens collected on the hill situated at the south of Nukitsu-numa and the railway cutting between Yamadera and Takase as well as at the junction of the To-zawa and its tributary. Similarly, ilmenite shows very low frequency and is examined only in several specimens. Minute crystals of magnetite are scattered in the groundmass. In this case, it has an octahedral or irregular form which is less than 0.15 mm. in diameter.

Chalcedony or agate(?) fill up generally small cavities in the groundmass and constructs a fringe around plagioclase phenocrysts, affording a characteristic feature to this rock under the microscope. Chlorite is an unimportant alteration product derived from biotite or other ferromagnesian minerals. Some of it is intermixed with quartz and plagioclase in the groundmass. When biotite is chloritized, leucoxene is commonly formed together.

The scaly or flaky sericite is also noteworthy mineral in altered specimens, replacing plagioclase phenocrysts and feldspathic parts of the groundmass. It is 0.2 mm. in the maximum diameter and is extremely abundant, when associated with pyrite which has generally a cubic form and is 0.6 mm. across in the largest crystal.

Moreover, irregular spots or veinlets of limonite are always predominant in the decomposed groundmass, where some of them occur together with chlorite and surround quartz or plagioclase phenocrysts.

Partly, they are supposed to have been derived from pyrite and pass into goethite with a transition stage between them.

The groundmass is constructed by quartz, orthoclase, oligoclase, magnetite, zircon, apatite, hypersthene and several alteration products. It is characterized by a microgranitic texture and reveals frequently a a spherulitic structure. The granular aggregate of quartz, orthoclase and oligoclase is, however, complicated occasionally by the frequent occurrence of small lath-shaped oligoclase crystals. Such a groundmass is entirely free of glassy substance except the case of brecciated varieties from the Ōishi-zawa.

(2) Perlite:—Biotite perlite passes mostly into banded biotite plagioliparite, as is indicated by the exposures on the cutting of truck road opened at the southern foot of Matsumori-yama, Shiro-yama behind Hasedo, two isolated hills about 200 m. southeast of Urushibō, Hōhō-iwa and its vicinity (Fig. 3) as well as on the trail behind Umegataira-yama and others. It has a black color and glassy luster, but obtains a greenish grey or grey or white color in decomposition. The soil derived from this rock exhibits commonly a grey or dark grey color. Among them, those of Matsumori-yama and two small hills near Urushibo as well as of Hōhō-iwa and Sugarita are largely exposed, being partly represented by a porphyritic variety which contains plagioclase and biotite phenocrysts.

At the southern foot of Matsumori-yama, perlite is sometimes rich in irregular cavities with or without the filling substance composed of chalcedony. Besides it, some banded structure is to be seen on the cutting of the hill between Yuta and Urushibō, where it is characterized by the presence of hard brown streaks with quartz phenocrysts and spherulites. There is also a large area where hornblende perlite is well exposed along the valley entering southwestwards from Niōtō-bashi of Kakumaba.

Exclusive of glassy substance, perlite contains quartz, plagioclase, biotite and hornblende in association with magnetite, ilmenite, chalcedony, agate(?), zircon, allanite and hypersthene. They are remarkably increased and decreased in different specimens, and the phenocrystic minerals are restricted to quartz, plagioclase, biotite and hornblende.

Even quartz is changeable in its frequency and is wholly absent in some cases. As is indicated by plagioliparite, the quartz phenocryst is not infrequently affected by the magmatic corrosion and is irregularly invaded by the groundmass. Some of the crystals are remarkably rounded, whereas others are subangular or angular, the largest phenocryst being 2 mm. in diameter. In the chalcedonic part, it is surrounded by a narrow zone of chalcedony and agate(?). Besides these, the sharp hexagonal section is rarely seen. Magnetite, zircon and biotite are included in some of these crystals.

Plagioclase is euhedral or subhedral and occurs in less frequency. It ranges from albite to oligoclase which vary from An_{10} to An_{19} in its composition and reveals a fresh appearance. The crystal is occasionally zoned and includes apatite, magnetite and biotite, being invaded by calcite vein and brown glass.

As a phenocrystic mineral, the platy biotite is less abundant. It lacks in the specimens from the cutting of the truck road between Yuta and Urushibō as well as from that of Shinden. The mineral is pleochroic from yellow (X) to dark brown (Y and Z), and the index of refraction (γ) is 1.683. Its remarkable occurrence is known in the perlite exposed at Hōhō-iwa and near Niōtō-bashi of Kakumaba. In the former case, it is complicatedly branched at the end of crystal which is 1.53 mm. in the maximum length.

Hornblende occurs in the specimens collected from the valley entering southwestwards from Niōtō-bashi. This mineral is occasionally contained strikingly together with biotite. It has a green color and such a pleochroic scheme as light yellow (X), yellowish green (Y) and green (Z). The extinction angle, $Z \wedge c$, is 17°, and the largest crystal is 0.8 mm. long and 0.22 mm. across.

Magnetite has an octahedral or irregular form and is scattered as a single crystal or aggregate. It is 0.2 mm. even in the largest crystal and occurs in a minor amount except the specimen from Shiro-yama near Hasedō. Ilmenite is almost absent, but is noticeably present in the perlite flows cropping out on the cutting near Shinden and traversing the trail situated about 1 km. west of the Hinokizawa-yama.

Allanite is a rare mineral which is found as stout prismatic crystals in the specimens from the southern flank or Futatsumori-yama. In this case, its well-defined crystal is strongly pheochroic from dark brown (X) to dark reddish brown (Y) or light brown (Z).

Pink zircon is a negligible ingredient and takes a stout or long prismatic habit. Chalcedony and agate(?) are associated together in the perlite flow on the cutting of the truck road between Yuta and Urushibō. The perlite here is partly rich in druses filled up with chalcedony and agate(?). The similar feature can be seen in the perlite flow of

Shinden. Moreover, hypersthene has the same frequency as zircon and is so scarce as to be overlooked in thin sections.

The most important feature of this rock is the predominance of the perlitic structure (Figs. 7–8), and it is noteworthy that the perlite exposed on the cutting mentioned above is filled with the swarms of trichites (Fig. 8) or microlites. The latter is also contained in the specimen of Shinden.

(3) Trachytic andesite:—The rock is very commonly exposed in the area between the Tachiya-gawa and Mamigasaki-gawa as well as at Jagaramogara of Nukitsu. In the southwestern district adjacent to the Yamagata Basin, however, it is almost absent except those of Togami-yama, Takatori-yama near Matsumori-yama, Ōmori-yama behind Urushibō and Kyōzuka-yama. The exposures of these localities are somewhat different from place to place in their lithological characters, constructing some columnar joints here and there on the cutting of the Senzan Railway Line between Tateyama and Yamadera as well as along the Mamigasaki-gawa near Sakazuki-yama and on Kyōzuka-yama or elsewhere.

Trachytic andesite reveals a gradual transition to plagioliparite. It is mostly porphyritic in texture, and its appearance resembles common andesite to some extent in fresh specimens. There are also nonporphyritic or slightly porphyritic varieties looking like tuff or shale in alteration, as can be examined on the ridge behind Shimo-higashiyama. The rock mentioned above is black grey in fresh specimens, but gets generally a grey or greyish white color when decomposed. When disseminated pyrite crystals are present, it is stained by brown oxidation products.

The mineral components are plagioclase, orthoclase, quartz, biotite, magnetite, zircon, apatite, hypersthene, chlorite, sericite, goethite, limonite, calcite, and leucoxene (Figs. 9, 10). In this case, the phenocrystic mineral is restricted to a rectangular or lath-shaped plagioclase which is represented by oligoclase or andesine with a composition of An_{16-47}. The amount of the phenocrystic plagioclase varies at different places, and there are some specimens quite devoid of it. The crystal is commonly euhedral or subhedral and lacks frequently the zonal structure, being 3.4 mm. long and 2.38 mm. in the largest one. Generally, it has a fresh appearance, but is occasionally sericitized and chloritized. Moreover, some of this mineral is kaolinized and limonitized. The enclosures are magnetite and apatite.

In the groundmass, plagioclase occurs as irregular of lath-shaped crystals, being intermixed with quartz grains and other minor ingredients. The frequency of these two types of crystal is variable in the writer's specimens. The minute lath-shaped crystals are extremely abundant in the specimens from Yanbe, Sakazuki-yama and Togami-yama near Monden. They are represented by oligoclase showing a fluidal arrangement, and most of them are 0.08 mm.–0.17 mm. in length. The rock rich in such oligoclase crystals is believed to be exposed very widely on the hills extending from the Tachiya-gawa to the Mamigasaki-gawa.

Quartz is found only in the groundmass together with orthoclase and plagioclase, but is entirely absent in the specimens mentioned above. It is hardly distinguishable from feldspar. Orthoclase is quite free of phenocryst. It is sometimes a common ingredient in the groundmass where it is not infrequently sericitized. In the same way, magnetite, ilmenite, biotite, zircon, hornblende, apatite, hypersthene are contained in the groundmass, although they are always low in frequency as compared with other ingredients.

Among them, magnetite is the most noticeable mineral with an octahedral habit or irregular form. In general, its diameter is less than 0.02 mm., and even the largest skeleton crystal is estimated to be 0.85 mm. in longer diameter. The frequent occurrence of ilmenite is known only in the specimens from the eastern or southern foot of small hill (283.1 m.) south to Togami-yama, This mineral is characterized by a hexagonal tabular form and jet-black color. The occurrence of minute biotite flakes is restricted to the rock characterized by the fluidal arrangement of oligoclase laths. They are pleochroic from light yellow (X) to dark yellowish brown (Y, Z) and chlorite is supposed to have derived from them.

Zircon is, on the other hand, a scanty ingredient which has a color and crystal form resembling those of plagioliparite. It is negligible or absent in most specimens. Hypersthene and hornblende are also present scarcely in the writer's specimens. The former is noticed in the specimens from the area including Nakazato, Ōoka-yama and Sanpō'oka, being generally indicated by well-defined prismatic crystals, whereas the latter is to be seen in those collected from Motoyashiki and the northern foot of Ōmori-yama near Urushibō. In these cases, hornblende has a subhedral form and green color. It is pleochroic from light yellow (X) to yellowish green (Y) or green (Z), and its maximum length is 0.74 mm.

Besides them, sericite and calcite are derived from ferro-magnesian minerals and feldspars together with limonite and leucoxene.

The groundmass of this rock consists of above-mentioned ingredients of which oligoclase and quartz are predominant as in the case of plagioliparite. The texture is mostly microgranitic, but obtains some trachytic texture when quartz and orthoclase are gradually replaced by the swarms of lath-shaped oligoclase.

(4) Dacite:—As has already been stated, two-pyroxene hornblende dacite spreads over the area including Togami-yama, Onigoe, Iwanami and Sakurada at the northwestern end of the Ryū-zan Volcano. Some good exposures can be seen on the cutting near the bus station and the adjacent stream bed, exhibiting an indistinct joint structure. The fresh specimen has a black color and compact groundmass in which corroded quartz phenocrysts, 2–4 mm. across are embedded together with phenocrystic plagioclase, hornblende, augite and hypersthene.

The microscopical examination shows that this rock contains quartz, plagioclase, augite, hypersthene, hornblende, magnetite, tridymite, chrorite, limonite and glass (Fig. 11). They are found as phenocrysts and ingredients in the groundmass.

The phenocrystic plagioclase ranges from andesine to labradorite with a composition of An_{47-60}, and the indices of refraction are higher in the specimens from Togami-yama. The crystal is mostly euhedral or subhedral, indicating a rectangular or tabular form and a distinct zonal structure. It has generally a clear appearance, but is sometimes turbid to various extents. In the latter case, such a turbid part is always fringed by a narrow clear zone without any enclosure. Some of it is characterized by the invasion of the groundmass or brown glass and results in the formation of a worm-eaten structure. The largest one is 5.44 mm. long and 3.06 mm. across. Lath-shaped crystals, 0.08 mm.–0.25 mm. in length, are very abundantly present in the groundmass where they are characterized by a fluidal arrangement.

Quartz reveals a low frequency as compared with that of plagioclase and has a round or angular form. It contains liquid inclusions and magnetite crystals, some of it being subjected to the magmatic corrosion. The phenocrystic augite, subhedral or anhedral, occurs in a smaller amount. It is sometimes lower than hypersthene in its frequency and lacks entirely in the dacite exposed on the hill beyond Kamisakurada. Occasionally, the crystal twins on (100), and its extinction angle, $Z \wedge c$, 40°(±). When it is zoned together with hypersthene, the latter is always surrounded by the former. The occurrence of hypersthene is almost restricted to phenocryst. It can be seen in the specimens from the western foot of Togami-yama and its southern hill behind Kami-sakurada, but is unknown in those of Iwanami. This euhedral or subhedral mineral has a long prismatic habit and includes some magnetite crystals. The largest crystal is 1.44 mm. long and 0.25 mm. across.

Green hornblende is a common ingredient with a long prismatic habit. It is strongly pleochroic from light yellow (X) to yellowish green (Y) or green (Z). The absorption is $X<Y<Z$. The largest crystal is 1.19 mm. long and 0.3 mm. across, and the extinction angle, $Z \wedge c$, is 17°. The periphery of crystal is frequently opacitized, and its inner part passes into the confused aggregate of magnetite and augite.

Magnetite is an important ingredient in the groundmass where it is represented by an octahedral or irregular crystal and has a diameter less than 0.08 mm. The crystal with a phenocrystic size is, however, 0.42 mm. in the maximum diameter. Besides these, glass is a remarkable ingredinet in the specimens from Iwanami, whereas tridymite is present only in the dacite of the hill behind Kami-sakurada. Moreover, chlorite and limonite are decomposition products altered from ferromagnesian minerals.

The groundmass is mainly composed of lath-shaped plagioclase, augite, and magnetite together with quartz, hypersthene, tridymite and glass. It has a fluidal structure or microgranitic textutre, being characterized by the presence of gabbroic xenoliths rich in plagioclase, augite, hypersthene and magnetite..

(5) Andesite:—Several exposures of two-pyroxene andesite are found along the trail between the entrance of the Taiko-zawa near Sugarita and Uchiyama as well as between Nitazawa and Takatori-yama. They are characterized by the frequency of joints intersecting at right angle. It is a porphyritic and compact rock with a black or dark grey color in the specimens undecomposed.

The rock is made up of plagioclase, augite, hypersthene, magnetite, apatite and calcite (Fig. 12). Phenocrystic plagioclase has a tabular or rectangular habit and is euhedral or subhedral, being noticed with a fresh appearance and the absence of turbid zones. The indices of refraction suggest that this phenocryst ranges from labradorite to bytownite with a composition of An_{62-78}.

The crystal is sometimes free of the zonal structure, but it is well zoned in other cases. Some of it is invaded by the groundmass, and a worm-eaten structure is thus formed. Its enclosures are magnetite or augite, and the largest crystal is 2.18 mm. long and 1.28 mm. across.

In the groundmass, lath-shaped or rectangular plagioclase is a main ingredient, and it is generally 0.05 mm–0.3 mm. in length.

The phenocrystic augite is always low in its frequency. The subhedral or anhedral crystal of this mineral is 1.24 mm. long and 0.51 mm. across in the largest one. Magnetite is enclosed in such a crystal. Moreover, long or stout prismatic crystal, 0.02 mm–0.08 mm. in length, is, on the other hand, predominant in the groundmass.

Similarly, the long prismatic hypersthene is a scanty phenocryst which is occasionally surrounded by the aggregate of minute augite crystals. Magnetite has an octahedral or ill-defined form, 0.02 mm.–0.05 mm. in its general diameter and 0.35 mm. across in the maximum case. Calcite is a secondary mineral filling up the interstices of other ingredients and is abundantly found in the decomposed part.

The groundmass reveals a pilotaxitic texture, consisting of plagioclase, augite and magnetite as well as hypersthene, and interstitial calcite.

Frequency of Zircon and Its Geological Significance

Zircon reveals a remarkable varirtion of its frequency in plagioliparite and associated extrusives of this district. It is generally found abundantly in plagioliparite as compared with perlite, but seems to be almost or entirely absent in trachytic andesite, dacite and andesite Such a tendency was confirmed by extracting mechanically zircon crystals from the above-mentioned extrusives. For this purpose, 109 specimens of these rocks were crushed, and zircon crystals were carefully separated from each eight grams of crushed specimens by using Thoulet solution. The crystals thus obtained were crystallographically examined and classified into several types of combination. They are separately counted for each specimen to compare their frequency one to another, including ill-defined crystals which are strikingly contained in some specimens.

So far as is known in well-defined crystals, such types of combination as (100), (111); (110), (111) and (110), (111), (311) are more predominant than others. Among them the first two are most abundant in the specimens collected from the dykes of plagioliparite, whereas the last one seems to be present very commonly in the lava flows of the same rock which has no banded structure.

Plagioliparite shows generally a similar but high frequency of zircon crystals in most dykes and lava flows, although there are some exceptional cases which are nearly or wholly free of them. From the facts mentioned above, it is inferred that there is sometimes a difference of crystal habits of this mineral but no remarkable increase or decrease of its frequency between the dykes and lava flows of plagioliparite.

Zircon is also found frequently in perlite. Mostly, it occurs as a combination of (100) and (111) or ill-defined form. The same type of combination and others are also to be seen in trachytic andesite, but they are generally absent as is indicated by dacite and two-pyroxene andesite.

In short, its frequency is likely to depend upon the presence or absence of phenocrystic quartz, augite and hypersthene as well as of glass. If the rock contains quartz or abundant glass and is free of phenocrystic augite and hypersthene, zircon is a common accessory mineral as in the case of plagioliparite and perlite. It is, however, always absent, when phenocrystic augite and hypersthene are found together and these ferromagnesian minerals coexist with phenocrystic quartz and glass. The former is two-pyroxene andesite, and the latter is two-pyroxene hornblende dacite. Similarly, the frequency of zircon is influenced by the absence of the phenocrystic quartz, augite and hypersthene, showing that this mineral is usually lacking in trachytic andesite.

Some Considerations on Volcanic Activities

As has already been stated, the Neogene plagioliparite and associated extrusives are largely found in the Tendō-Yamagata-Kaminoyama district. They are supposed to have been extruded closely one upon the other. In these cases, some of them filled up the fissures of granitic rocks and Neogene sediments, whereas the others poured out as lava flows during the deposition of the Neogene formation.

According to the results of Minakawa's investigation[8], the occurrence of such extrusives seems to be repeated up to the upper horizon of the Hongō Formation at the north of the Sagae-gawa, but it is restricted only to the Sugarita Formation and Yamadera Formation as well as to the upper part of the Yoshino Formation in this district.

So far as is known at present, the first eruption of plagioliparite and associated extrusives is supposed to have taken place during the sedimentation of the lower half of the Yamadera Formation or the upper part of the Yoshino Formation, because there is none of them at the lower horizon of the latter formation. Since that time, the extrusion of these rocks was repeated, and its evidences can be seen even at the upper half of the Sugarita Formation exposed in the southwestern area. Moreover, it happened in co-operation with the violent exprosions which resulted in the deposition of tuffaceous substance to a large extent. The frequency of such volcanic activities are shown by the alternation of lava flows and various kinds of tuff, being characterized by some intricate transitions between them from place to place.

---

[8] S. Minakawa, *op. cit.*, 235–236.

The abundance of tuffaceous or pumiceous substance is the most noticeable feature in the Neogene sediments of this mountainous or hilly land, and it is exceedingly remarkable in the Sugarita Formation, Yamadera Formation and Yoshino Formation which are always associated closely with several kinds of extrusive. Of these, the lower half of the Yoshino Formation is usually accompanied by the dykes or lava flows of andesite, propylite and basalt. It is, therefore, distinguishable from the upper part of the Yoshino Formation, Yamadera Formation and Sugarita Formation associated with acidic or intermediate extrusives.

The influence of volcanic activities is, however, obscure in the Ōisawa Formation and Mizusawa Formation equivalent respectively to the Yoshino Formation and Sugarita Formation. Hence, it seems to have been restricted to the eastern or southwestern area where tuffaceous sediments were extensively accumulated. These types of volcanic activities may partly have a close relationship to those taken place during the deposition of the upper half of the Kaneyama Formation around the Shinjō Basin.

At to the volcanic centers, there is no evidence to confirm them, although pyroclastics and lavas are inferred to have been supplied from many places and some of their origin may be attributed to the submarine eruption. In the area now covered thickly by green tuff or

---

9) The green tuff of the Yoshino Formation is frequently intercalated by hard shale or black shale at its upper horizon corresponding to a part of the Nishi-kurosawa Formation or the Onnagawa Formation. The same may be said of the Yamadera Formation. The formation rich in hard shale or black shale is widely exposed in the area including Maizuruyama, Shimo-higashiyama, Kirihata and Ainohara at the north and Kokuzō-san, Suge, Ryūzawa, etc. at the south. Some of its black shale are characterized by the frequent occurrence of animal or plant fossils. They are *Dentalium* cf. *yokoyamai* MAKIYAMA, *Linthia* sp., *Propaemusium tateiwai* KANEHARA, *Sagarites* sp., *Sardinia* sp., echinoid spines, fish scales, pectoral fins of pisces and plant fossils (gen. and sp. indet.).

other sediments and lava flows, it is very difficult to find out the position of sources from where volcanic products were abundantly supplied. The possible sources may, however, be suggested by the distribution of lava flows which are abnormally thickened and extensively exposed, as is shown by the exposures of Ōoka-yama and its southern extension as well as of Nomioka-yama, Kyōzuka-yama and Daihira-yama or elsewhere.

Besides these, other volcanic centers are supposable to have been located close to the Backbone Range, since many dykes of plagioliparite here traverse granitic masses and Neogene sediments. Some fissures now filled up with dykes may have once been the passages of lava flows.

Importance of Plagioliparite and Associated Extrusives as Sources of Neogene Sediments

Neogene sediments are largely exposed in this district and adjoining areas, where they extend from the Yoshino Formation or Ōisawa Formation up to the Aterazawa Formation intercalated with lignite beds. These formations are composed of various sediments represented mainly by tuff, hard shale, black shale, tuffaceous or pumiceous sandstone, non-tuffaceous sandstone and conglomerate, etc. Among them, tuff and tuffaceous sediments are very predominent, although they pass laterally or vertically into argillaceous rocks. It is also noteworthy that tuff, tuffaceous or pumiceous sandstone, non-tuffaceous sandstone and conglomerate contain generally remarkable amounts of fragments or pebbles consisting of plagioliparite and associated extrusives as well as of minerals derived from them.

As can be inferred from the geological evidences obtained by the writer, the area occupied by the green tuff formations and its base rocks seems to have partly been upheaved one after another during the sedimentation of overlying formations, resulting in a contemporaneous erosion. Several kinds of extrusives including plagioliparite and others may, therefore, be supposed to have been eroded together with green tuff and supplied the material to the younger formations. Besides fragments or pebbles of these rocks, it can be said that a part of such minerals as orthoclase, quartz, plagioclase, green or brown hornblende, biotite, augite, hypersthene, magnetite, pink zircon, etc. were probably supplied from the same sources.

Relationship between the Frequency of Volcanic Activity and the Formation of Metallic Mineral Deposits

The frequent occurrence of metallic mineral deposits is known at the eastern part of this district where granodiorite, plagioliparite, trachytic andesite, dacite, propylite and green tuff are largely exposed. These deposits are represented by quartz veins, networks and impregnations characterized by the predominance of chalcopyrite with or without bornite, covelline, chalcocite, zincblende, galena, pyrite, baryte, gold and silver. Among them, the Chiyonosawa Mine is situated on the northern or northeastern foot of Uzawa-yama (Tendō-machi), whereas the Takase Mine, Ōkubo Mine and Hōzawa Mine (Yamagata-shi) are respectively found near Nakazato and on the northern flank of Minami-omoshiro-yama as well as along several tributaries of the Mamigasaki-gawa. There are also some mines at the southeastern corner of Kaminoyama-shi. They are the Akayama Mine, Fubira Mine, Azuma Mine, Kaneyama Mine, Tōhō Mine, Ōminami Mine and Mikami Mine. The mines mentioned above are now stopped to be worked except the Akayama Mine, Ōminami and Tōhō Mine as well as the Takase Mine reopened recently along the Takase-gawa. The deposits of these mines were formed in granodiorite [Chiyonosawa Mine, Hōzawa Mine (Himesawa deposit), Fubira Mine, Azuma Mine and Ōminami Mine], trachytic andesite (Takase Mine, Akayama Mine, Kukeji Mine and Mikami Mine), propylite (Tōhō Mine and Ōminami Mine), green tuff [Hōzawa Mine (Ōshiozawa, Koshiozawa, Gandozawa and Murakizawa deposits)] and at the contact betweeen granodiorite and green tuff [Hōzawa Mine (Niiyama and Zazanosawa deposits)].

As has already been described, plagioliparite and trachytic andesite are the commonest extrusives on the hilly land or mountainous area including a part of the Backbone Range between Yamagata and Miyagi Prefectures. They are well exposed here and there as dykes or lava flows in the localities where metallic mineral deposits are distributed, and some of them are intensely subjected to the hydrothermal alteration in the mining area. Moreover, plagioliparite is always to be seen even in the vicinity of the deposits which fill up the fissures of propylite or granodiorite in the Tōhō Mine, Fubira Mine, Ōsaka Mine and Ōminami Mine. The same can be said of the veins formed at the contact between green tuff and granodiorite of the Hōzawa Mine.

From such geological features, it is inferable that the volcanic activities connected closely with the repeated extrusions of plagioliparite resulted in the formation of many metallic mineral deposits. The occurrence of plagioliparite and its relationship to the genesis of deposits are, therefore, quite identical with those of the adjacent districts represented by the northern corner of Miyauchi-machi (Kumano Mine, Shuzan Mine, Yoshino Mine, Minamizawa Mine, etc.) and the northern half of Takahata-machi (Futaezaka Mine, Takagami Mine, Kanahara Mine, Monju Mine, etc.).

Summary

(i) Plagioliparite and associated extrusives are widely distributed on the mountainous or hilly land including Tendō-machi, Yamagata-shi and Kaminoyama-shi where granitic rocks and Neogene sediments are extensively exposed.

(ii) Topographically speaking, the area composed of those extrusives has some remarkable features different from others and is characterized by the frequency of small peaks or hills with a conical form.

(iii) They are represented by biotite plagioliparite, hornblende biotite plagioliparite, biotite perlite, hornblende perlite, trachytic andesite, two-pyroxene hornblende dacite and two-pyroxene andesite. Most of them are found as lava flows, although there are various dykes of plagioliparite and trachytic andesite filling up the fissures of granodiorite and green tuff.

(iv) Among them, plagioliparite, perlite and trachytic andesite have a close connection and pass into one another. Moreover, they reveal some similarities between them concerning plagioclase no matter whether it occurs as a phenocryst or ingredient of the groundmass. The plagioclase is always albite, oligoclase and andesine.

(v) To confirm the relationship between zircon and different mother rocks, this mineral was crystallographically and optically examined in connection with its frequency. It has a pink color and several crystal forms represented by the combinations of (100), (111); (110), (111); (100), (111), (311); (100), (110), (311), (331); (100), (110), (311); (100), (101), (311) and (100), (110), (111). Of these, the combinations of (100), (111); (110), (111) and (100), (111), (311) are more commonly present than other types. So far as is known at present, the first two indicate the highest frequency in the specimens of plagioliparite obtained from many dykes, whereas the last one seems to be noticed frequently in the lava flows of the same rock free of a banded structure.

On the whole, zircon is strikingly contained in the specimens of plagioliparite except those from lava flows with a banded structure, but decreases its frequency in perlite and is almost or entirely absent in trachytic andesite. It lacks absolutely in the case of dacite and andesite.

(vi) During the sedimentation of the Sugarita Formation and the upper half of the Yoshino Formation, the volcanic activity took place repeatedly, and these extrusive rocks were successively erupted, being accompanied by violent explosions which resulted in the deposition of such a tuffaceous sediment as green tuff.

(vii) Plagioliparite is an important rock in the area characterized by the abundance of metallic mineral deposits. It is not only distributed here, but in its neighbouring districts, where it is always sericitized intensely and is sometimes subjected to pyritization in the vicinity of deposits. These deposits are, therefore, supposable to owe their formation to repeated eruptions of plagioliparite.

Acknowledgements

The writer's sincere thanks are due to Dr. H. Tsuya and Mr. Watanabe whose kindness greatly facilitated his laboratory work. The expense of this research was partly paid from the fund for Natural Science of the Education Ministry.

---

21. 山形県天童・山形・上ノ山地方の斜長石石英粗面岩及びその関係岩類に関する地質学的考察

山形大学　市村　毅

本地域には斜長石石英粗面岩とこれに伴う真珠岩，粗面岩様安山岩，石英安山岩，安山岩とが広い範囲に亘り露出する．これ等の中，斜長石石英粗面岩，真珠岩，粗面岩様安山岩の間には，しばしば漸移的関係があり，共に曹長石，灰曹長石，又は中性長石を斑晶として含む点に特徴が認められる．一方でかかる各種の火成岩が示す火成活動は，緑色凝灰岩の広大なる堆積を来たさせたものであり，緑色凝灰岩層中に著しく介在するそれ等の熔岩流は，緑色凝灰岩の層位的区分に役立つ様に考えられる．又斜長石石英粗面岩と粗面岩様安山岩とは，山形市とこれに近接する地域とに多い多種多様の金属鉱床と共に見出され，これ等の間に生因上密接なる関係があることを示している．

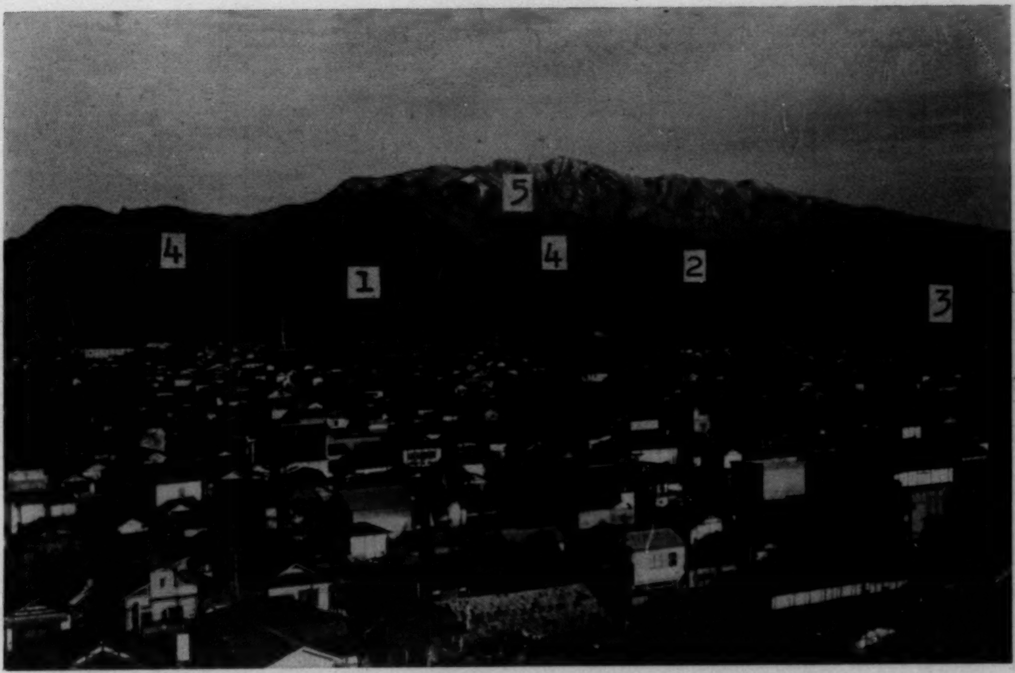

Fig. 2. Chitose-yama, Saruoka-yama, Togami-yama and others viewed from the roof of Marukyū in Yamagata City. 1=Chitose-yama (plagioliparite), 2=Saruoka-yama (plagioliparite), 3=Togami-yama (dacite), 4=Other hills composed of plagioliparite, 5=Ryūzan.

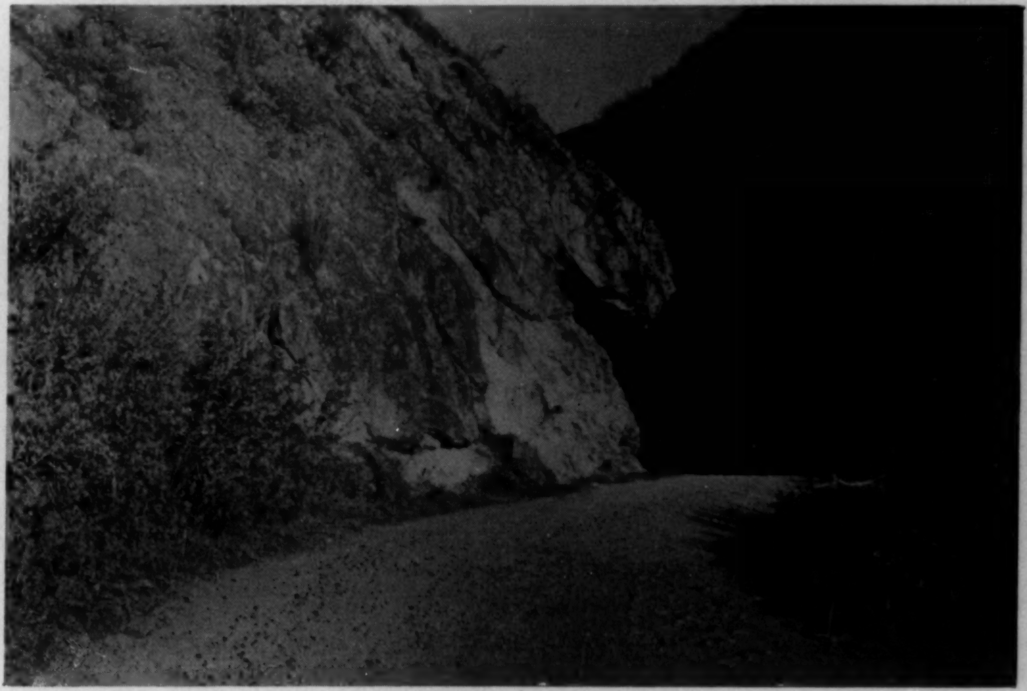

Fig. 3. Perlite exposed along the bus road between Iwanoshita and Sugarita.

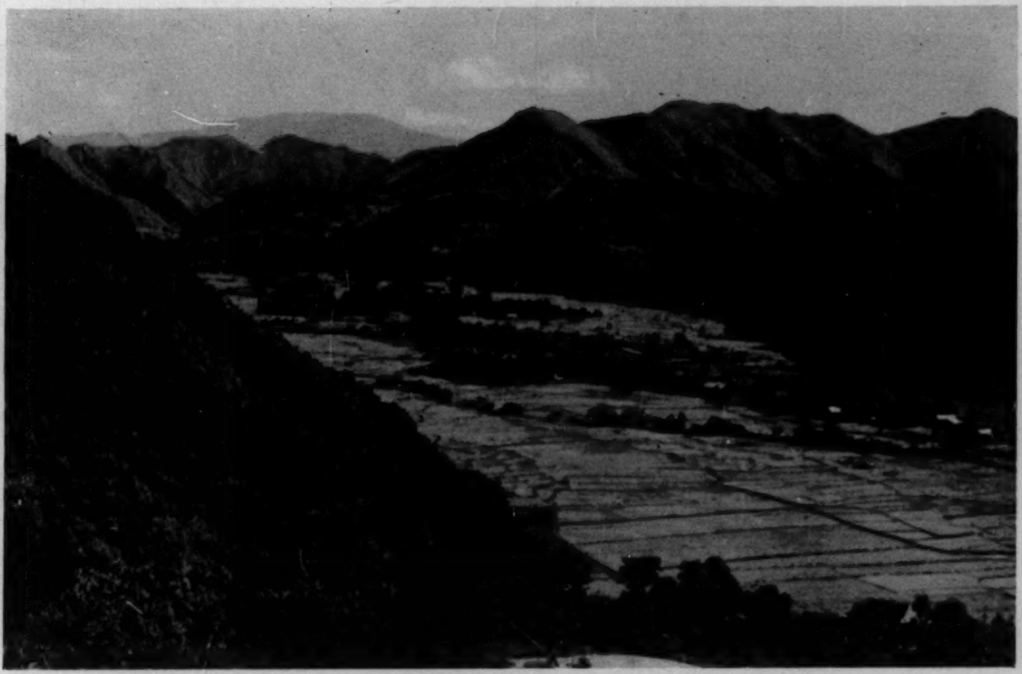

Fig. 4. Mountainous area composed largely of trachytic andesite which are well exposed at the upper course of the Takase-gawa. This picture was taken from Sanpō'oka.

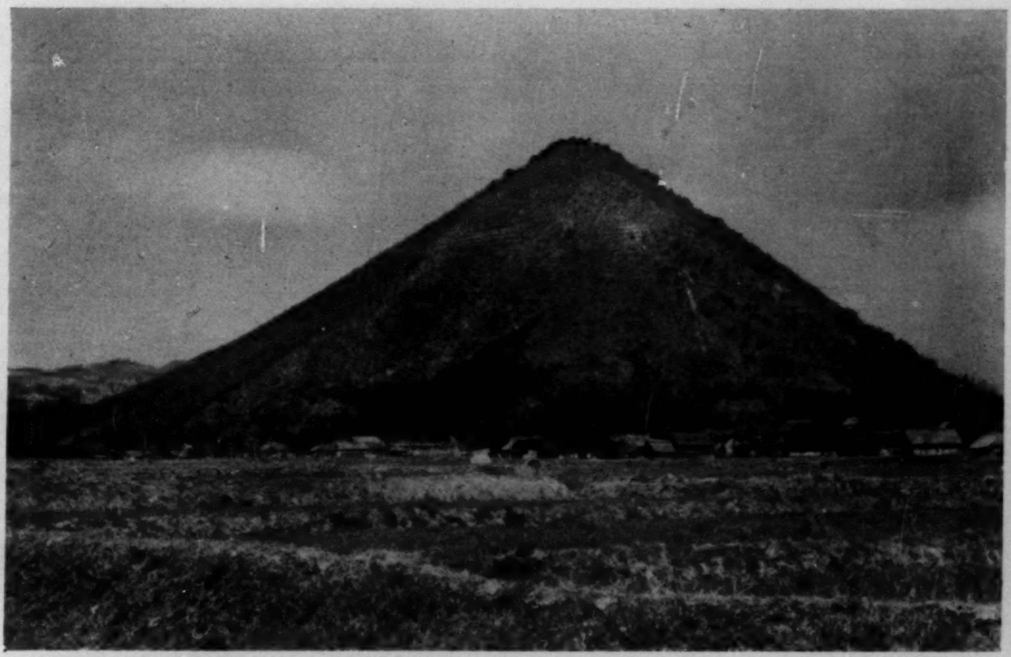

Fig. 5. Togami-yama, a small conical peak near Monden. It is built up of trachytic andesite. Such a topographical feature is very common in the area where plagioliparite, trachytic andesite and dacite are exposed.

R

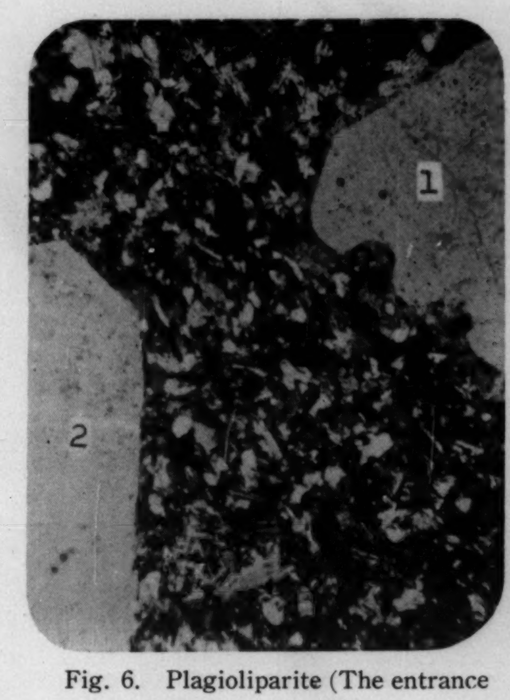

Fig. 6. Plagioliparite (The entrance of the Atera-zawa, a tributary of the Mamigasaki-gawa). 1=Quartz, 2= Plagioclase. ×100.

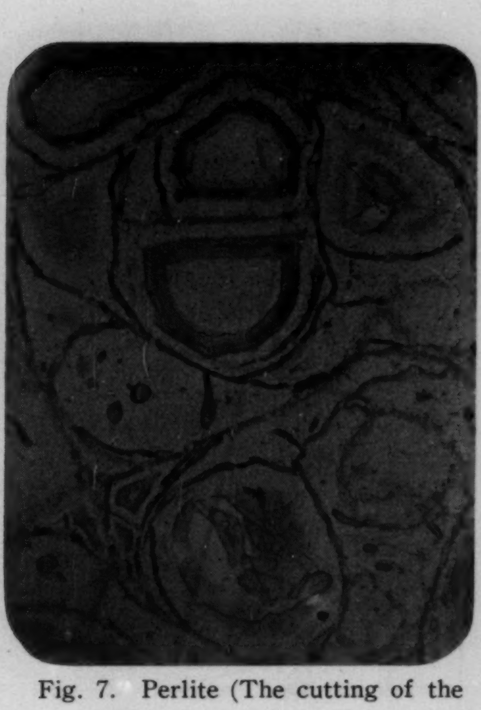

Fig. 7. Perlite (The cutting of the bus road between Iwanoshita and Sugarita). ×100.

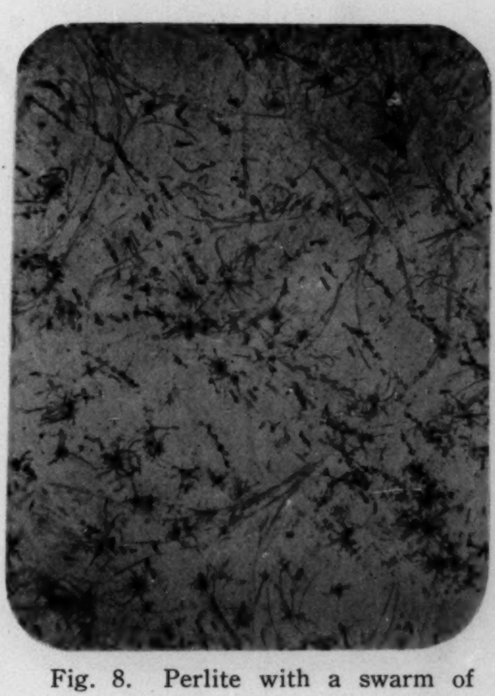

Fig. 8. Perlite with a swarm of trichite (Small hill 700 m. south from Urushibō). ×100.

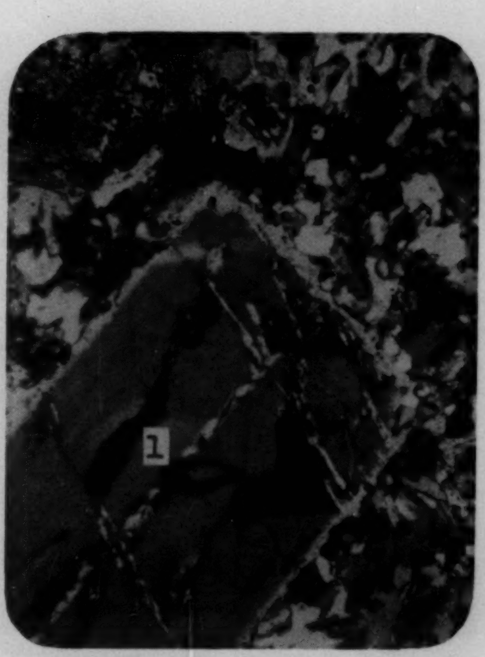

Fig. 9. Trachytic andesite (Fukazawa-fudō). The texture of groundmass resembles that of plagioliparite, but is quite free of quartz phenocrysts. 1=Plagioclase. ×100.

（震研彙報 第三十六号 図版 市村）

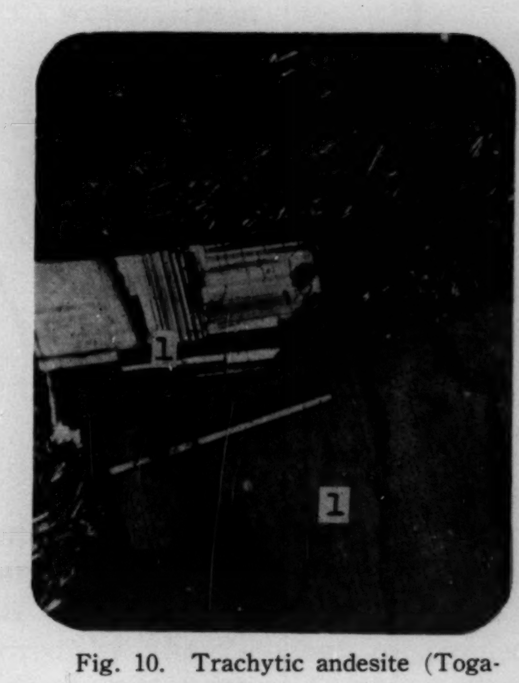

Fig. 10. Trachytic andesite (Togami-yama near Monden). The groundmass shows a trachytic texture. 1=Plagioclase. ×100.

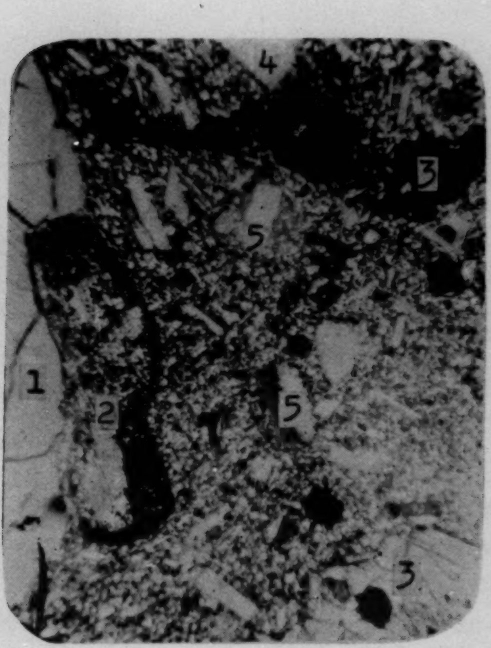

Fig. 11. Two-pyroxene hornblende dacite (Togami-yama near Iwanami). 1=Quartz, 2=Hornblende, 3=Augite, 4=Hypersthene, 5=Plagioclase. ×100.

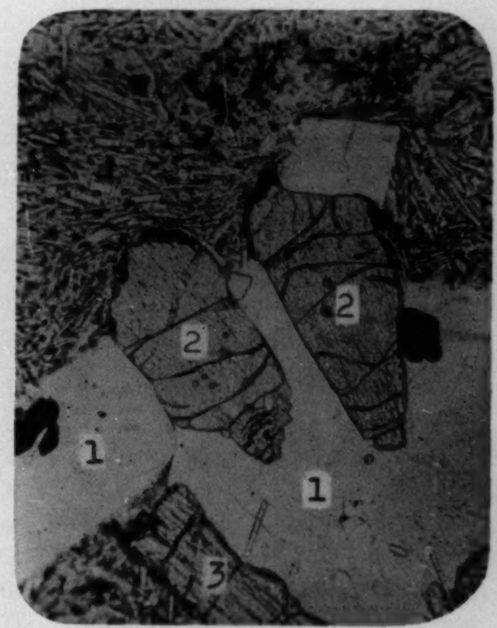

Fig. 12. Two-pyroxene andesite (Uchiyama — Nitazawa). 1 = Plagioclase, 2=Augite, 3=Hypersthene. ×100.

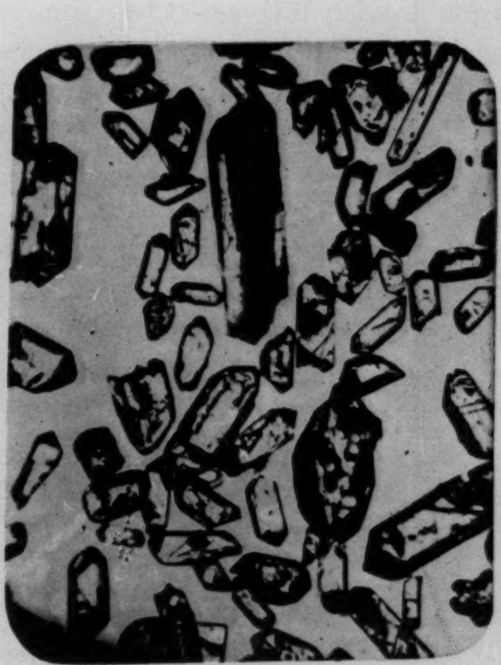

Fig. 13. Pink zircon (Plagioliparite exposed at the entrance of the Aterazawa, a tributary of the Momigasakigawa). ×100.

BULLETIN OF THE EARTHQUAKE
RESEARCH INSTITUTE
Vol. 36 (1958), pp. 395-412

22. *Heavy Minerals in Metamorphosed Sediments from the Tsukuba District, Ibaraki Prefecture.**

By Takeshi ICHIMURA,

Yamagata University.

(Read June 24, 1958.—Received June 24, 1958.)

Introduction

The metamorphosed sediments assigned to the Upper Paleozoic are largely exposed on the hilly land of the Tsukuba district which extends sporadically from the northern corner of Tsukuba-gun to the southern half of Niihari-gun as well as to a part of Ishioka City, being characterized by the frequent occurrence of granitic rocks, abundance of various contact minerals, lit par lit injection of igneous materials, formation of hybrid rocks, etc. These metamorphosed sediments indicate a wide range of alteration from place to place. In this case, some of them were metamorphosed from sandstones, whereas the others were derived from conglomerates, shales and clayslates. They are all subjected to remarkable disturbances here and there. Such geological features have already been studied by H. Yamada,(1) F. Otsuki,(2) K. Jimbo,(3) S. Kōzu,(4) K. Iwasaki,(5) R. Kimura,(6) Y. Ōdaira,(7) H. Satō,(8) K. Sugi,(9) B. Yoshiki(10) and others.

The Tsukuba district is also a well-known area to the writer who was born there, and he was thus in a favorable position to promote his geological and mineralogical works on the metamorphosed sediments of this district. In the latter case, the writer had a special interest in

---

* Communicated by H. Tsuya.

1) H. YAMADA, *Geol. Map, Mito, 1:200,000 and Its Explanatory Text*, (1888).

2) F. ŌTSUKI, *Jour. Geol. Soc. Tokyo*, **8** (1901), 424–428; **9** (1902), 52–57, 115–131.

3) K. JIMBO, *Jour. Geol. Soc. Tokyo*, **12** (1905), 6, 35–42.

4) S. KŌZU, *Jour. Geol. Soc. Tokyo*, **12** (1905), 23–26, 91–94.

5) K. IWASAKI, *Jour. Geol. Soc. Tokyo*, **22** (1915), 372, 388–390.

6) R. KIMURA, *Jour. Geogr.*, **36** (1924), 391.

7) Y. ŌDAIRA, *M. S., Geol. Inst. Univ. Tokyo*, (1925).

8) H. SATŌ, *Geol. Map, Tsukuba, 1:75,000 and Its Explanatory Text*, (1927).

9) K. SUGI, *Jour. Geol. Soc. Tokyo*, **34** (1927); *Jour. Geol. Soc. Tokyo*, **35** (1928), 640–654; *Jap. Jour. Geol. & Geogr.*, **8** (1930), 29–112.

10) B. YOSHIKI, *Jour. Petrog. Min. & Ore Dep.*, **10** (1933), 4, 151–157.

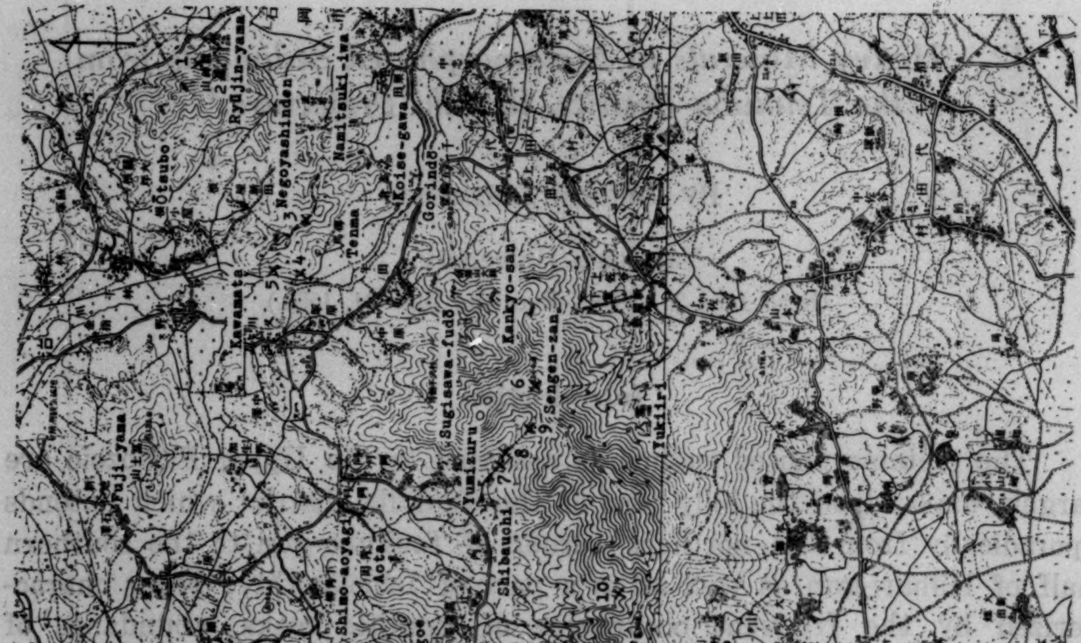
Ryūjin-yama
Ōtsubo
Negoyashinden
Kawamata
Namitsuki-iwa
Tenma
Koise-gawa
Gorindō
Kankyo-san
Sugisawa-fudō
Sengen-san
Yunizuru
Shibauchi
Yukiiri
Fuji-yama
Shimo-aoyagi
Aota
Kami-aoyagi
Onogoe
Asahi-tōge
Ono
Komochi
Sawabe
Tōjōji
Nakayama
Bunchōji
Fudō-tōge
Hōkyō-san
Kowada
Oda
Yamaguchi
Rokusho
Tate
Usui
Kangōri
Hirasawa
Hōjō
Tsukuba-san

Fig. 1. Map showing the location where the specimens of metamorphosed sediments were collected.

heavy mineral components almost free of those in original sediments except zircon crystals. Moreover, his attention was attracted to the presence or absence of some heavy minerals depending upon the distance from the granitic contact. To examine these heavy minerals, he collected abundant specimens from many localities during his field work. They were crushed and analysed mechanically by using heavy solutions. The isolated crystals extracted in this way were crystallographically and optically investigated, their mineralogical characters being furthermore confirmed by microscopical observations of thin sections of each specimen.

The results are summarized in the present paper.

General Features of Mother Rocks

The hilly land of the Tsukuba district (Fig. 1) is geologically a very complicated area, where various kinds of metamorphosed sediments assigned to the Upper Paleozoic are extensively exposed together with granitic rocks (Fig. 2). It extends from Ryūjin-yama to Hōjō westwards, including Negoyashinden, Kankyo-san, Fuji-yama, Sengen-zan, Aoyagi, Onogoe, Busshōji, Asahi-tōge, Tōjōji, Sawabe, Fudō-tōge, Hirasawa, Yamaguchi, Kowada, etc. The metamorphosed sediments here are the alteration products of clayslate, shale, sandstone and conglomerate due to the large intrusion of biotite granite and two-mica granite. In these cases, the grade of metamorphism is very changeable from place to place depending upon the distance from the granitic body and lit par lit injection of the granitic substances.

The Upper Paleozoic sediments of this district are thus affected weakly at the east, but strongly at the west, resulting in the formation of spotted biotite clayslate, hornfels, metamorphosed conglomerate and mica gneiss or schist. Among them, spotted biotite clayslate is widely distributed at the area extending over Ryūjin-yama, Namitsuki-iwa, Negoyashinden and Kankyo-san. This type of clayslate has a black color and is generally characterized by the abundance of biotite spots, 2 mm. in the maximum diameter. Commonly, the rock is composed of quartz, orthoclase, plagioclase, reddish brown biotite, hematite, zircon, apatite, muscovite, tourmaline and graphite. Moreover, some of it contains many andalusite or chiastolite crystals, 3 mm. or more in length, as is indicated by the specimens from the hill behind Tenma. It is frequently intercalated with hornfels derived from arenaceous rocks and has a strike of N40°-70°E and a dip of 50°-70°NW-NNW.

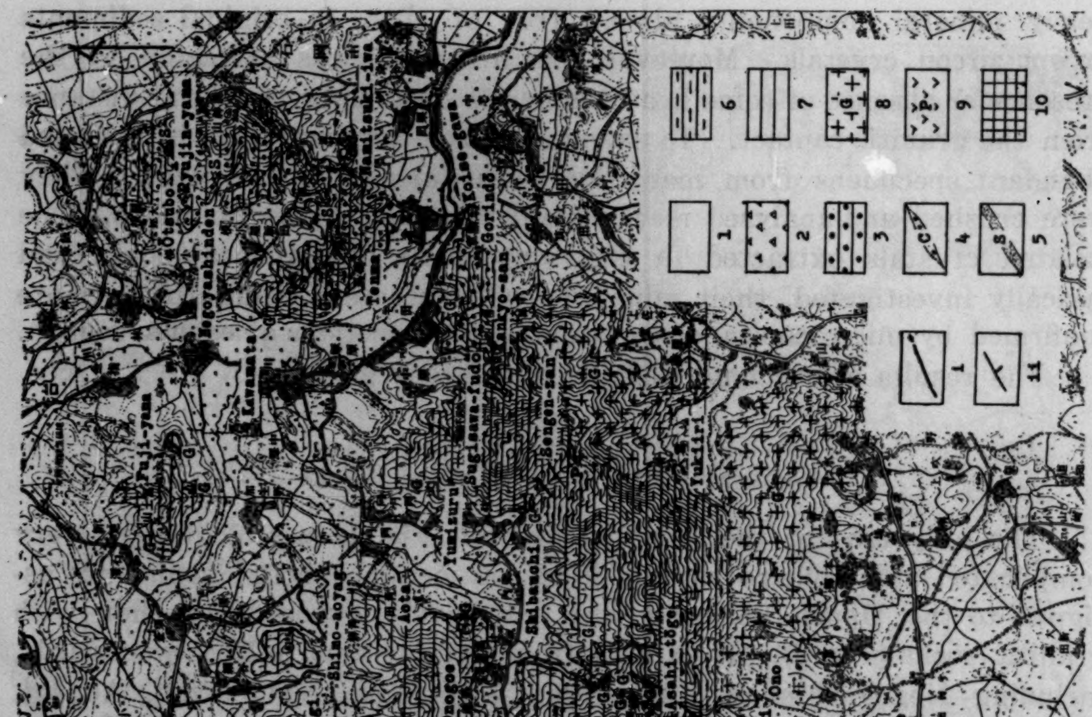
1
2
3
4
5
6
7
8
9
10
i
ii
Hōkyō-san
Shinden
Kowada
Oda
Hōjō
Yamaguchi
Hirasawa
Fudō-tōge
Sawabe

Fig. 2. Geological map showing the distribution of metamorphosed sediments in the Tsukuba district.

1. Recent fluviatile deposits and Pleistocene-Pliocene deposits, 2. Talus deposits, 3. Spotted biotite clayslate, 4. Metamorphosed conglomerate, 5. Hornfels derived from sandstone, 6. Hornfels derived from clayslate or shale, 7. Gneiss or schist, 8. Porphyritic biotite granite and two-mica granite, 9. Pegmatite, aplite and quartz vein, 10. Gabbro, gabbro pegmatite, anorthosite, and amphibolite, i. Fault, ii. Strike and dip.

By going westwards, however, hornfels and injection rock begin to crop out predominantly with the gradual transition and the frequent change of strike and dip. In the case of hornfels, there are several varieties altered respectively from argillaceous, arenaceous and calcareous sediments. They are represented by biotite hornfels, two-mica hornfels, hornblende diopside hornfels, diopside garnet hornblende hornfels, diopside biotite hornfels, andalusite or chiastolite hornfels and cordierite hornfels. The commonest type of these rocks is two-mica hornfels derived from clayslate or shale. Its exposures are traceable from Ryūjin-yama to Sawabe southwestwards, passing through Negoyashinden, Sugisawa-fudō, Sengen-zan and Tōjōji and intercalating other kinds of hornfels changed from arenaceous sediments as well as from rudaceous rocks. The occurrence of andalusite or chiastolite-bearing biotite or two-mica hornfels is known near Sengen-tōge and also on the ridge extending from here southwestwards, whereas cordierite hornfels is found at Sugisawa-fudō. Minerallogically speaking, biotite hornfels or two-mica hornfels consists of quartz, orthoclase, magnetite, apatite, zircon, tourmaline and graphite together with reddish brown biotite and muscovite. Such mineral components are quite similar even when phenoblastic andalusite, chiastolite and cordierite are present. The distribution of hornblende-bearing diopside hornfels and diopside garnet hornblende hornfels is restricted to a small extent as compared with other metamorphosed sediments. So far as is known at present, the former is to be seen on the hill just behind Kangōri, and the latter is found at the Hirasawa quarry. Besides these, quartzose diopside plagioclase hornfels is noticed by Sugi[11] on the hill near Sugisawa-fudō, Kami-aoyagi and Nakayama.

Hornblende-bearing diopside hornfels is highly quartzose, and the main part of this rock is composed of quartz, plagioclase, orthoclase and diopside with a subordinate amount of green hornblende, magnetite and zircon. Diopside garnet hornblende hornfels is a hard and compact rock with a light green or dark green color, being constructed by a granoblastic aggregate of quartz, orthoclase, plagioclase, titanite, magnetite, apatite zoisite, allanite and zircon as well as green hornblende, diopside and garnet. It is a xenolith in porphyritic biotite granite and grades into biotite-bearing variety at its marginal part.

Metamorphosed conglomerate is exposed in connection with spotted biotite clayslate, two-mica hornfels and injection mica gneiss. The most

---

11) K. SUGI, *op. cit.*, (1930), 75, 89–92.

remarkable one can be observed on the southern flank of a ridge rising up close to the truck road between Sawabe and Oda. Its exposure extends from north to south within the area of two-mica gneiss or schist.

The western half of this area is almost built up of injection mica gneiss characterized by a lit par lit injection of porphyritic biotite granite and other igneous materials. Frequently, it has a banded structure due to the repetition of mica-rich parts and quartzose laminae or lenses. In general, they are represented by intricate aggregates of quartz, orthoclase, plagioclase, biotite, muscovite, hematite, zircon, apatite, tourmaline and graphite, containing occasionally sillimanite, cordierite, garnet and andalusite or chiastolite. When biotite and muscovite are found together, the former is always more predominant than the latter, and some spotted structure is not infrequently formed by shimmer aggregates of these two minerals. In the specimens collected from near the exposures of granitic rocks, biotite flakes are sometimes associated closely with confused swarms of sillimanite needles. The occurrence of such sillimanite crystals seems to be restricted to the area which was subjected to the intense contact metamorphism, and it is well known at Hirasawa, Kowada and on Jō-yama as well as along the truck road of Fudō-tōge and in its vicinity where porphyritic biotite granite is repeatedly and complicatedly exposed.

Of these, the metamorphosed sediments of the Hirasawa quarry (Fig. 3) are biotite gneiss, biotite hornfels and diopside garnet hornblende hornfels. In this case, biotite gneiss is the most predominant rock, having thin layers of biotite or two-mica hornfels derived from sandstone. They are traversed and intercalated by porphyritic biotite granite, aplite, pegmatite and other igneous materials (Fig. 4). Such metamorphosed sediments are smoothly or intricately bordered against granitic rocks, and a sudden or gradual transition can be seen between them, being subjected to the complicated injection of igneous materials near the granitic contact (Figs. 5–6). Most of biotite gneiss here have a distinct banded structure and are remarkably folded close to the contact where biotite flakes are exceedingly increased and some aplitic or granitic veins are found together.

As to the chemical characters of metamorphosed sediments mentioned above, there are only few available data.[12] Some of them are shown in the following table (Table 1).

---

[12] K. SUGI, *op. cit.*, (1930), 103.

Table 1.

	(1)	(2)	(3)
SiO_2	63.63	65.54	60.20
Al_2O_3	16.09	16.27	16.98
Fe_2O_3	0.55	1.10	5.89
FeO	5.00	3.54	3.80
MgO	2.28	2.15	2.98
CaO	1.24	2.00	1.57
Na_2O	2.09	2.99	0.83
K_2O	4.52	3.00	3.42
H_2O_+	1.02	1.42	4.14 (ig. loss.)
H_2O_-	0.17	0.40	
TiO_2	0.74	0.50	not det.
P_2O_5	0.08	0.56	not det.
MnO	0.10	0.07	not det.
C	2.00	not det	not det.
Total	99.53	99.54	99.81

(1) Sillimanite biotite gneiss from the Hirasawa quarry. Anal., S. Tanaka.
(2) Injection biotite gneiss from Fudō-tōge. Anal., T. Katō.
(3) Spotted biotite clayslate from Ryūjin-yama. Anal., Y. Ōdaira.

Mineralogical and Optical Characters of Heavy Minerals

The mineralogical and optical characters of heavy minerals can be well investigated by isolating them from their mother rocks. For this purpose, the writer crushed various types of metamorphosed sediments collected from many localities of the Tsukuba district (Fig. 1) and used Thoulet solution to extract them. In this operation, he could concentrate such heavy minerals as allanite, andalusite (chiastolite), apatite, biotite, garnet, hematite, magnetite, monazite, muscovite, sillimanite, titanite, tourmaline, zircon and zoisite. They are sometimes in high frequency, but are scarcely present, or absent in other cases.

Among them, biotite is the most remarkable heavy ingredient in all of metamorphosed sediments which include biotite gneiss (schist), two-mica gneiss (schist), biotite hornfels, two-mica hornfels and spotted biotite clayslate. The mineral is commonly scattered through the rock, but crowds together occassionally to form rounded spots here and there. It is strongly pleochroic from light brownish yellow (X) to reddish brown (Y, Z), having an index of refraction (γ) between 1.639 and 1.649. The crystal contains apatite, graphite and zircon.

Muscovite is less important than biotite. Both the minerals are frequently associated together, particularly at Hirasawa, Yamaguchi, Kowada and Oda as well as on Asahi-tōge and Fudō-tōge. It is often characterized by the presence of a worm-eaten structure and the abundance of enclosures represented mostly by graphite crystals.

The occurrence of andalusite (chiastolite) and sillimanite is restricted to a small extent. Andalusite takes a long prismatic habit, and its crystal is imperfectly terminated. Sometimes, the interior of this mineral is rich in the carbonaceous matter and passes into chiastolite. It alters to minute sericite scales when decomposed. The indices of refraction are as follows:

$$\alpha=1.613-1.627\ ,\qquad \gamma=1.637-1.642$$

Sillimanite consists of transparent and colorless needles, 0.5 mm. in the maximum length. The crystal shows the highest frequency in biotite gneiss of the Hirasawa quarry (Fig. 9) and constructs confused aggregates which are distinguishable even with naked eyes. The indices of refraction are $\alpha=1.651$, $\beta=1.653$ and $\gamma=1.673$.

Diopside and hornblende (Fig. 7) are characteristic ingredients in hornfeles metamorphosed from sandstones rich in lime and magnesia. Both the minerals are found together, and some of them are associated with garnet, taking a subhedral or anhedral form in most specimens. In the case of hornblende, it has usually a poikilitic texture and is often intergrown with diopside in an intricate manner. The largest crystal is 1.52 mm. long and 0.72 mm. across. The mineral is distinctly pleochroic from light yellow or light brown (X) to greenish brown or brownish green (Y) and green or bluish green (Z). Moreover, its extinction angle, $c\wedge Z$, is 15°. When the crystal encloses zircon, the pleochroic halo is seen along the contact between them.

The amount of hornblende is more abundant than diopside in the specimens from the Hirasawa quarry, but is *vice versa* in those from Mukō-yama.

Diopside has a diameter of 0.3 mm. or thereabouts even in the largest crystal and contains zoisite crystals. Its extinction angle, $c\wedge Z$, is 40°.

The most remarkable accessory heavy mineral is tourmaline which is present in most specimens of biotite gneiss (schist), two-mica gneiss (schist), biotite hornfels, two-mica hornfels, spotted biotite clayslate, etc. It occurs as a stout or long prismatic crystal (Figs. 10–11), the former taking frequently a well-defined form as compared with the latter. They are composed of *m*$(10\bar{1}0)$, *a*$(11\bar{2}0)$ and *o*$(02\bar{2}1)$ as well as of *r*$(10\bar{1}1)$. So far as has been examined by the writer, the commonest form is represented by a combination of $(10\bar{1}0)$, $(11\bar{2}0)$ and $(10\bar{1}1)$. When the elongated crystal is truncated at the end, $(10\bar{1}1)$ is always absent as is indicated in the specimens of two-mica gneiss or schist from the area including Hōkyō-zan and Kowada. The size of such crystals shows a wide range. The largest one is 0.93 mm. long and 0.42 mm. across in the crystal with a stout prismatic habit, whereas it is 0.81 mm. long and 0.15 mm. across in the long prismatic variety. In this case, the refractive indices are as follows:

$$N_E=1.622-1.628\ ,\quad N_O=1.648-1.655\ .\quad N_O-N_E=0.026-0.027\ .$$

The mineral strongly pleochroic from light brownish yellow or light brown (N_E) to dark yellowish brown or dark brown (N_O). Some of it is faintly zoned and reveals a darker color at its inner part. The crystal has occasionally a clear appearance without any inclusion, but it is commonly rich in graphite and gas (?) inclusions. In the elongated crystal, they are exceedingly abundant and a dark core is formed by the high frequency of graphite inclusions.

The occurrence of zircon (Fig. 12) is not so remarkable as tourmaline, although this ingredient is contained in most of metamorphosed sediments. Its frequency seems to depend on the lithological characters of original sediments and has a tendency to be high in hornfelses derived from arenaceous sediments, but it lacks occasionally in gneisses and hornfelses altered from argillaceous rocks.

The mineral is found as colorless, purple and pink crystals with a short or long prismatic habit and well-rounded form (Fig. 12). In the writer's specimens, the frequency of the colorless zircon is much higher than that of the purple or pink variety, and sharp prismatic crystals are rarely found. It constructs the combinations of (100), (111); (110), (111) and (110), (100), (111), (311). Among them, the common type is composed of (100) and (111) or (110) and (111). In these cases, the colorless zircon is quite free of such a long and sharp prismatic form as found frequently in porphyritic biotite granite of the Hirasawa quarry and two-mica granite of Kankyo-san or elsewhere.

The purple zircon is contained in the specimens obtained from Ryūjin-yama, Negoya and Fudō-tōge, where the mother rock is two-mica hornfels changed from sandstone. It usually takes an ill-defined form and is sometimes worn to a spherical grain. In the specimens from Ryūjin-yama, the crystal has a bright purple color and is slightly pleochroic. The pink variety occurs only in two-mica hornfels exposed at the western side of Fudō-tōge. The original rock of hornfels here is also sandstone.

The length or diameter of various zircon crystals mentioned above ranges from 0.03 mm. to 0.22 mm., and their minute grains enclosed in biotite flakes afford a pleochroic halo along the contact between them.

Apatite is not so widely distributed as tourmaline and zircon in metamorphosed sediments. This mineral is almost or entirely absent in spotted biotite clayslate and associated hornfels of Ryūjin-yama and the adjacent area, but has a tendency to be increased in biotite gneiss (schist), two-mica gneiss (schist) and biotite or two-mica hornfels of Hirasawa, Kowada and others, where granitic rocks are exposed here and there. It is, therefore, always noticeable in the specimens obtained from the granitic contact of the Hirasawa quarry and also in their xenoliths captured by porphyritic biotite granite of the same place. Even in these cases, its frequency is not very high when compared with porphyritic biotite granite, particularly biotite-rich part of the contact which has already been described in the writer's previous paper.[13)]

Apatite has a stout prismatic habit or rounded form, the good crystal being a combination of prism, pyramid and base. It is mostly colorless and clear without any enclosure, but has rarely a dark grey core supposed to be a decomposed part. Such a crystal is occasionally associated with biotite flakes and sillimanite needles. The largest one is 0.14 mm. long and 0.09 mm. across.

The frequent occurrence of pink garnet is known in some specimens of biotite hornfels or two-mica hornfels collected from Mukō-yama, Hirasawa and the ridge between Busshōji and Rokusho, where they are believed to have been derived from various kinds of sandstone. Commonly, the mineral has a rounded form with the exception of beautiful rhombic dodecahedron formed in two-mica hornfels of Busshōji-Rokusho. At the Hirasawa quarry, garnet is complicatedly intermixed with green hornblende and diopside in the mother rock enclosed by porphyritic biotite granite. The round crystal mentioned above is 0.06 mm–1.12 mm. across and has an uneven surface, being characterized by the frequency of a mesh structure in thin sections (Fig. 8).

Monazite is a very rare ingredient in metamorphosed sediments of

---

13) T. ICHIMURA, *Bull. Earthq. Res. Inst.*, **33** (1955), 392.

this district, although it shows a high frequency in porphyritic biotite granite near its contact of the Hirasawa quarry. The writer separated out this mineral from biotite hornfels and two-mica hornfels which alternate with two-mica gneiss or schist at the western side of Fudōtōge and are undoubtedly alteration products of arenaceous rocks. The crystal occurs as minute round grains, 0.07 mm.–0.17 mm. in diameter and is slightly pleochroic from light greenish yellow to light yellow or almost colorless. Moreover, it has a dark border due to the effect of refractive indices and is easily distinguishable from zircon or titanite.

The restricted occurrence of heavy minerals is also indicated by titanite and allanite which are present together only in the xenolith of diopside garnet hornblende hornfels found at the Hirasawa quarry. The former has an irregular or rounded form and is frequently associated with green hornblende or diopside, including occasionally ill-defined magnetite crystals. The latter is, on the other hand, very scarcely contained in the rock mentioned above. It is strongly pleochroic from light brown (X) to reddish brown (Y) or light yellow (X). The crystal is 1.07 mm. long and 0.3 mm. across.

In addition, there are some metallic minerals such as hematite, magnetite and pyrite, but they are negligible or absent in most specimens.

The heavy minerals in many specimens are summarized in Table 2.

Geological Considerations on the Occurrence of Heavy Minerals

As has already explained, metamorphosed sediments of the Tsukuba district contain various kinds of heavy minerals which change their frequency from place to place. In many specimens collected by the writer, biotite is the most predominant mineral. Even in the sediments affected slightly by contact metamorphism, this ingredient is always present with a high frequency. Its amount seems to depend on the grade of metamorphism and the lithological character of original sediments. It increases its frequency in metamorphosed sediments derived from clayslate and is especially abundant at or near the granitic contact.

The same may be said of muscovite which has a tendency to gradually increase in frequency in the area, where granitic rocks are sporadically exposed and some of them are still concealed under the present surface.

Sillimanite and andalusite (chiastolite) are, on the other hand,

Table 2. Heavy minerals in metamorphosed sediments

	1*	2*	3	4	5	6	7	8	9	10	11	12*	13*	14	15	16*	17*	18*	19*	20*	21	22	23
Allanite	—	—	—	—	—	—	—	—	—	—	—	—	—	—	—	—	—	—	—	—	—	—	—
Andalusite (chiastolite)	—	—	×	—	—	—	—	—	×	—	—	—	—	—	—	—	—	—	—	—	—	—	—
Apatite	—	—	—	—	—	—	×	—	—	—	×	—	×	—	×	—	—	—	×	×	—	×	—
Biotite	⊠	⊗	⊗	⊗	⊗	⊗	⊗	⊗	⊗	⊗	⊗	⊗	⊗	⊗	⊗	⊗	⊗	⊗	⊗	⊗	×	⊗	⊗
Diopside	—	—	—	—	—	—	—	—	—	—	—	—	—	—	—	—	—	—	—	—	—	—	—
Garnet	—	—	—	—	—	—	—	—	—	—	—	—	—	—	—	—	—	—	—	—	—	—	—
Hematite	×	×	—	×	×	×	—	×	—	—	—	—	—	—	—	—	—	—	—	×	—	—	—
Hornblende	—	—	—	—	—	—	—	—	—	—	—	—	—	—	—	—	—	—	—	—	—	—	—
Magnetite	—	—	—	—	—	—	—	—	—	—	—	—	—	—	—	—	—	—	—	—	—	—	—
Monazite	—	—	—	—	—	—	—	—	—	—	—	—	—	—	—	—	—	—	—	—	—	—	—
Muscovite	⊠	×	⊗	⊗	⊗	⊠	⊗	⊗	⊗	⊗	⊗	⊗	⊗	⊗	⊗	—	⊗	⊗	×	⊠	⊗	⊗	⊗
Pyrite	—	—	—	—	—	—	—	—	—	—	—	—	—	—	—	—	—	—	—	×	—	—	—
Sillimanite	—	—	—	—	—	—	⊗	—	—	—	—	—	—	—	—	—	—	—	—	—	—	—	×
Titanite	—	—	—	—	—	—	—	—	—	—	—	—	—	—	—	—	—	—	—	—	—	—	—
Tourmaline	⊠	×	⊠	⊠	⊠	×	⊠	⊠	×	×	×	×	⊠	×	×	×	—	—	×	×	×	×	×
Colorless zircon	⊠	×	×	×	⊠	×	×	×	×	×	×	⊠	×	×	×	⊠	×	×	×	×	×	×	×
Pink zircon	—	—	—	—	—	—	—	—	—	—	—	—	—	—	—	—	—	—	—	—	—	—	—
Purple zircon	—	—	—	—	—	—	—	—	—	—	—	—	—	—	—	—	—	—	—	—	—	—	—
Zoisite	—	—	—	—	—	—	—	—	—	—	—	—	—	—	—	—	—	—	—	—	—	—	—

	24	25	26*	27*	28*	29	30	31	32	33*	34*	35	36*	37	38	39	40	41	42	43	44	45	46
Allanite	—	—	—	—	—	—	—	—	—	—	×	—	—	—	—	—	—	—	—	—	—	—	—
Andalusite (chiastolite)	—	—	—	—	—	—	—	—	—	—	—	—	—	—	—	—	—	—	—	—	—	—	—
Apatite	—	—	—	—	—	×	—	×	⊠	×	×	×	×	×	×	—	⊠	⊠	×	×	—	×	—
Biotite	⊗	⊗	⊗	⊠	⊠	⊗	⊗	⊗	⊗	⊗	×	⊗	—	⊗	⊗	⊗	⊗	⊗	⊗	⊗	⊗	⊗	⊗
Diopside	—	—	—	—	—	—	—	—	—	—	⊗	—	⊗	—	—	—	—	—	—	—	—	—	—
Garnet	—	—	⊠	—	—	—	—	—	—	—	⊗	—	—	⊠	—	—	—	—	—	—	—	—	—
Hematite	—	—	—	×	×	×	—	×	×	×	×	—	—	—	—	—	—	—	—	—	—	×	—
Hornblende	—	—	—	—	—	—	—	—	—	—	⊗	—	×	—	—	—	—	—	—	—	—	—	—
Magnetite	—	—	—	—	—	—	—	—	—	—	×	—	×	—	—	—	—	—	—	—	—	—	—
Monazite	—	—	—	×	×	—	—	—	×	—	—	—	—	—	—	—	—	—	—	—	—	—	—
Muscovite	⊗	⊗	×	×	×	⊗	⊗	×	×	—	—	×	—	—	×	⊠	⊗	⊠	⊗	⊗	⊠	⊗	⊠
Pyrite	—	—	—	—	×	—	—	×	—	—	—	—	—	×	—	—	—	—	—	—	—	—	—
Sillimanite	—	—	×	—	—	—	×	⊗	⊗	—	—	⊗	—	—	⊠	×	×	—	×	×	×	—	—
Titanite	—	—	—	—	—	—	—	—	—	—	⊠	—	×	—	—	—	—	—	—	—	—	—	—
Tourmaline	⊠	×	⊠	×	—	×	×	×	⊗	—	—	×	—	×	⊠	×	—	⊠	×	⊠	⊠	⊠	—
Colorless zircon	×	×	×	⊠	⊠	⊠	×	×	×	×	×	×	×	×	×	×	×	×	×	×	×	×	×
Pink zircon	—	—	—	—	×	—	—	—	—	—	—	—	—	—	—	—	—	—	—	—	—	—	×
Purple zircon	—	—	—	×	×	—	—	—	×	—	—	—	—	—	—	—	—	—	—	—	—	—	—
Zoisite	—	—	—	—	—	—	—	—	—	—	×	—	×	—	—	—	—	—	—	—	—	—	—

⊗ Extremely abundant. ⊠ Fairly abundant. * Hornfels derived from sandstone.

Table 3. Localities of metamorphosed sediments in the preceeding table

	Village or town	District or city
(1) Ryūjin-yama (Two-mica hornfels)		Ishioka-shi .
(2) 〃 (〃 〃)	〃	〃 .
(3) Negoyashinden-Tenma (Andalusite spotted biotite clayslate)	Yasato-machi	Niihari-gun .
(4) Negoya-Tenma (Two-mica hornfels)	〃	〃 .
(5) 〃 (Two-mica gneiss)	〃	〃 .
(6) The summit of Sengen-zan (Two-mica hornfels)	Chiyoda-mura	〃 .
(7) Yumizuru (Two-mica hornfels)	Yasato-machi	〃 .
(8) 〃 (〃)	〃	〃 .
(9) 〃 (〃)	〃	〃 .
(10) Shibauchi (〃)	〃	〃 .
(11) Komachi (〃)	Niihari-mura	〃 .
(12) Tōjōji (〃)	〃	〃 .
(13) 〃 (〃)	〃	〃 .
(13) 〃 (〃)	〃	〃 .
(14) 〃 (〃)	〃	〃 .
(15) Tōjōji-Sawabe (〃)	〃	〃 .
(16) Sawabe (〃)	〃	〃 .
(17) 〃 (〃)	〃	〃 .
(18) 〃 (〃)	〃	〃 .
(19) 〃 (〃)	〃	〃 .
(20) 〃 (〃)	〃	〃 .
(21) Oda 〃	Tsukuba-machi	Tsukuba-gun.
(22) Nakayama-Busshōji (Two-mica gneiss)	Yasato-machi	Niihari-gun .
(23) Busshōji (〃)	〃	〃 .
(24) 〃 (〃)	〃	〃 .
(25) Fudō-tōge (Two-mica schist)	Tsukuba-machi	Tsukuba-gun.
(26) Rokusho-Busshōji (Garnet two-mica hornfels)	〃	〃 .
(27) Yamaguchi (Two-mica hornfels)	〃	〃 .
(28) 〃 (〃)	〃	〃 .
(29) Hirasawa-yama (Two-mica schist)	〃	〃 .
(30) 〃 (Two-mica gneiss)	〃	〃 .
(31) 〃 (Sillimanite two-mica gneiss)	〃	〃 .
(32) Hirasawa (〃)	〃	〃 .
(33) 〃 (Biotite hornfels, xenolith)	〃	〃 .
(34) 〃 (Diospide garnet hornblende hornfels)	〃	〃 .
(35) Mukō-yama (Sillimanite two-mica gneiss)	〃	〃 .
(36) 〃 (Hornblende-bearing diopside hornfels)	〃	〃 .
(37) 〃 (Biotite hornfels)	〃	〃 .
(38) Jō-yama (Sillimanite two-mica gneiss)	〃	〃 .
(39) Yamaguchi (Two-mica gneiss)	〃	〃 .
(40) Kowada (Two-mica gneiss)	〃	〃 .
(41) 〃 (〃)	〃	〃 .
(42) 〃 (〃)	〃	〃 .
(43) 〃 (〃)	〃	〃 .
(44) 〃 (〃)	〃	〃 .
(45) Hōkyō-zan (Two-mica schist)	〃	〃 .
(46) Hōkyō-zan—Fudō-tōge (Two-mica gneiss)	〃	〃 .

restricted in distribution, both the minerals not being found together in the Tsukuba district. Generally speaking, the former occurs frequently in the area where metamorphosed sediments are closely associated with granitic rocks. In short, sillimanite is a stable mineral and is more abundant in biotite gneiss exposed close to the granitic contact, but it has some tendency to decrease its frequency with the increase of muscovite. Such a feature can be seen at the Hirasawa quarry and its adjacent area.

Andalusite is seen in metamorphosed sediments derived only from shale or clayslate which was less affected by the granitic intrusion. It is, therefore, contained in biotite hornfels or spotted biotite clayslate formed at the distance from the main granitic body.

Green hornblende and diopside are, however, noticed only in hornfels which were originally siliceous sediments rich in lime and magnesia. Geologically, they are not important minerals, since such kinds of mother rocks are scarcely distributed in this district.

One of the common heavy accessory minerals is tourmaline. Generally, it has a high frequency in gneisses and hornfelses derived from clayslate or shale, but is occasionally lacking even in these kinds of rock.

The similar tendency is also seen in hornfelses metamorphosed from sandstones and spotted biotite clayslate subjected to the least metamorphism, although the occurrence of this mineral is restricted to a smaller extent. These facts suggest that such a volatile component as boron was not uniformly circulated in the metamorphosed area, and the distribution of tourmaline crystals seems, therefore, independent of the distance from the granitic body, the lithological character of original sediments as well as of grade of metamorphism, spreading over all parts of the contact aureole. Its formation is supposed to have largely been facilitated by the sedimentary structure disturbed by the granitic intrusion.

Zircon is less frequently present than tourmaline, when both the minerals are found together in metamorphosed sediments. Commonly, it takes a rounded form and has some appearance of an ingredient in the original sediments, being almost free of such well-defined crystals as those of the Tsukuba type granite and Inada type granite.[14] These granites are characterized by coexistence of colorless and pink varieties in which the former occurs as the beautiful crystal with a sharp outline. Among them, the pink zircon is generally contained in two different types of granite of the Tsukuba district, whereas the occurrence of the colorless one seems to be more remarkable in the Tsukuba type granite, particularly near its contact. It is, therefore, necessary to confirm whether zircon crystals of the granites were partly supplied from the Upper Paleozoic sediments exposed here or not.

---

[14] S. OKADA, N. SHIMODA & H. SHIBATA, *Stud. Geol. & Min. Inst. T.K.D.*, (1954), 217-307.

So far as is known at present, the colorless zircon of metamorphosed sediments is, however, nearly wanting in well-defined crystals and reveals a quite different feature from that of granites. Accordingly, the ill-defined crystals of the colorless zircon derived from abovementioned sediments and enclosed in granites are impossible to get a sharp outline without the subsequent addition of zirconium. The sharp crystals of colorless zircon in granites, however, always have a clear appearance and lack a zonal structure. This evidence seems to suggest that there is no genetical connection between colorless zircon crystals of metamorphosed sediments and those of granites.

The same may be said of the pink zircon which has mostly a well-defined form in granites. In this case, it is supposed that the original zircon will lose its color by the thermal effect of the granitic magma.

The occurrence of apatite seems to depend on the distance from the granitic contact and the grade of metamorphism. Hence, it has a tendency to increase its frequency when approaching the granitic body. Such features are somewhat different from those of tourmaline which is found even at the periphery of the contact aureole and indicate an irregular distribution without any connection to the lithological characters of the original sediments. These facts may suggest that fluorine or chlorine acted only on the sediments adjacent to the granitic body. The frequency is, therefore, high at the contact, but decreases strikingly within a short distance from it.

Monazite is rarely contained in two-mica hornfels exposed at the western side of Fudō-tōge, where porphyritic biotite granite was intruded together with pegmatite. This mineral is, however, always absent in other metamorphosed sediments including those of the Hirasawa quarry. From these facts, it can be inferred that the formation of monazite was restricted to a small extent in the sediments subjected to metamorphism and took place largely within the granitic body in which it is a common accessory ingredient and increases its amount at the periphery.

Allanite, garnet, hematite, magnetite, pyrite, titanite and zoisite are also unimportant heavy accessory minerals, and their occurrence has no geological significance, since they are found in a negligible amount.

Among various heavy minerals mentioned above, zircon is specially noticed as an original ingredient of the Upper Paleozoic sediments. It was least affected by metamorphism and seems to have been preserved even when other minerals wholly disappeared by recrystallization. In the investigation of these heavy minerals, it is very desirable to examine those of the Upper Paleozoic sediments exposed on the Toriashi mountain land[15] which is situated farther north. The formation here is chiefly composed of sandstone and shale with occasional intercalations of limestone lenses and chert layers. It is, therefore, expected to contain many kinds of heavy minerals as in the case of the similar formation distributed largely in the Chichibu district.[16]

Summary

i) Various kinds of metamorphosed sediments assigned to the Upper Paleozoic are extensively exposed in the Tsukuba district which includes a part of Ishioka City, Niihari-gun and Tsukuba-gun. They are mostly the alteration products of argillaceous or arenaceous sediments due to the large intrusion of the Tsukuba type granite (porphyritic biotite granite and two-mica granite), being represented by biotite or two-mica gneiss (schist), several types of hornfels, metamorphosed conglomerate and spotted biotite clayslate.

ii) These metamorphosed sediments were crushed, and heavy minerals were extracted from them by using Thoulet solution. The heavy minerals thus obtained were examined under the microscope together with those in thin sections of the mother rocks. Besides biotite and muscovite, there are allanite, andalusite (chiastolite), apatite, diopside, garnet, hematite, hornblende, magnetite, monazite, sillimanite, titanite, tourmaline, zircon and zoisite.

iii) Among them, the commonest ingredient is biotite which is contained in almost all metamorphosed sediments. It seems to increase its amount in biotite or two-mica gneiss (schist) and biotite or two-mica hornfels derived from argillaceous sediments and is abundantly present at or near the granitic contact. The same tendency is also shown by muscovite which is more predominant when approaching the granitic body.

---

15) K. KAWADA, *Sc. Rept. T. B. D.*, (C), **2** (1953), 217-307.

16) T. ICHIMURA & H. MATSUBAYASHI, *Bull. Earthq. Res. Inst.*, **31** (1953), 159-164.

iv) Sillimanite and andalusite (chiastolite) are restricted in distribution, the former being found in biotite or two-mica gneiss (schist) close to the granitic mass, whereas the latter being contained in two-mica hornfels or spotted biotite clayslate less affected by the granitic intrusion. Hornblende and diopside occur only in hornfelses altered probably from sandstones rich in lime and magnesia.

v) Of accessory heavy minerals, most remarkable is tourmaline which has a wide distribution even in spotted biotite clayslate. Its formation seems to be independent of original sediments as well as of the grade of metamorphism, but reveals a close relationship to the sedimentary structure and disturbance due to the granitic intrusion.

vi) Zircon is the next important heavy accessory mineral. It is supposed to have been an ingredient of the original Upper Paleozoic sediments, since there is no evidence to suggest its formation due to the addition of zirconium from the granitic magma. In this case, the crystal seems to have been preserved without any striking alteration during metamorphism. Moreover, it may be said that Paleozoic sediments subjected to contamination were not the source of colorless zircon crystals coexisting with the pink variety in the Tsukuba type granite and Inada type granite.

vii) Apatite seems to increase its frequency in the neighbourhood of the granitic body. It is, therefore, abundant in biotite or two-mica gneiss (schist) near the granitic contact, but is almost absent in spotted biotite clayslate.

Allanite, hematite, magnetite, monazite, titanite and zoisite are negligible heavy accessory ingredients.

---

22. 茨城県筑波地方産変質堆積岩の重鉱物

山形大学 市村毅

石岡市から新治郡及び筑波郡に跨る丘陵地域には上部古生層と見做される変質堆積岩が広く露出している．この岩石の原岩は頻繁に黒雲母花崗岩や複雲母花崗岩，或はこれ等に伴うペグマタイト，アプライトなどの貫入を受け，元来の岩石の内容，花崗岩からの距離，地層の構造その他の差により，様々なる変質岩を生ずるに至つた．黒雲母片麻岩又は片岩，複雲母片麻岩又は片岩．黒雲母ホルンフエルス，複雲母ホルンフエルス，点紋黒雲母粘板岩などはこれ等の代表的なるものであり，頁岩や粘板岩から変化した片麻岩，片岩，ホルンフエルスの中には紅柱石（空晶石），菫青石，珪線石を多く含む場合が知られている．若し堆積岩が石灰や苦土に富む場合には，透輝石，ザクロ石，緑色角閃石がしばし認められる．

黒雲母，白雲母，紅柱石，珪線石，ザクロ石，透輝石，角閃石の他に，重鉱物としては，電気石ジルコン，褐簾石，黝簾石，燐灰石，クサビ石，モナヅ石，赤鉄鉱，磁鉄鉱，黄鉄鉱などが存在する．それ等の中で最も多いのが黒雲母と白雲母とであり，大方の変質堆積岩に含まれる．又黒雲母や白雲母に次いで頻度が高いのは電気石，ジルコン，燐灰石であるが，珪線石とか紅柱石，透輝石，角閃石の如きは，時に多いことがあつても，その範囲が限られている．その他の重鉱物には重要視すべきものがない．

副成分重鉱物としては，電気石が最も著しく存在する．然もその分布は貫入火成岩からの距離とか岩質とかに関係なく，その原岩が原料の滲透に都合のよい構造を有する処に特に集中している様に思われるばかりでなく，場所によつては，これが結晶形に著しい変化が見られる．又ジルコンは大概円味を有し，その上無色透明なるものが大部分を占め，紫色種や淡紅色種は至つて少い．これ等は何れも原岩が変質する以前からその鉱物成分として存在したものであり，花崗岩漿からジルコニウムが特に供給されたために生じたものでない．又堆積岩を変質せしめたこの地方の花崗岩中に淡紅色ジルコンと共存する無色透明の美晶は，堆積岩からの捕獲晶が脱色し，ジルコニウムの供給により生長したと見做される証拠もなく，むしろ花崗岩の中で，結晶形や色を全然異にするジルコンの結晶が，岩漿的に且つ同時に生じたことを考える方が合理的である．ジルコンは一般に砂岩から生じた変質岩に多い様見受けられる．燐灰石は花崗岩との接触部にやや著しく集り，これを遠ざかると急劇に頻度の減少を見せている．

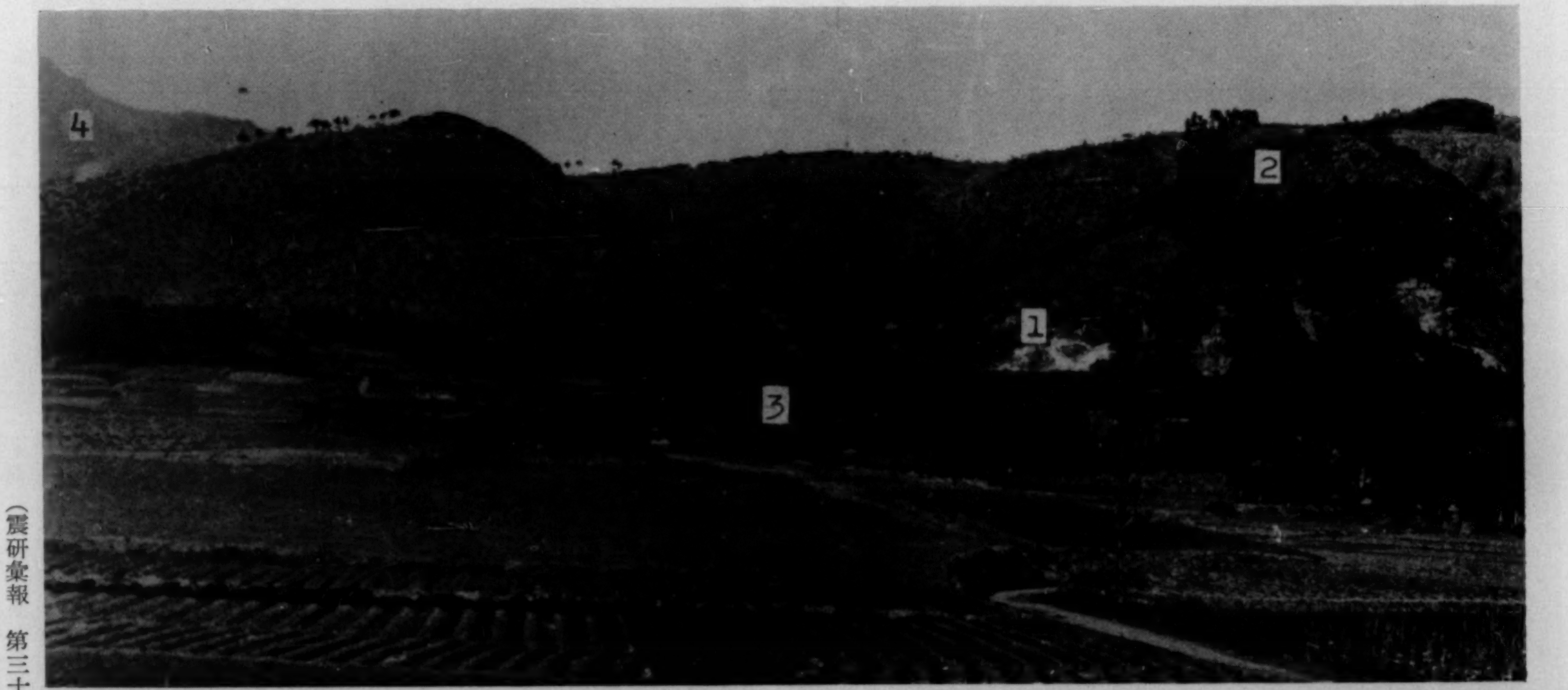

Fig. 3. The Hirasawa quarry viewed from near Hōjō. Various kinds of metamorphosed sediments and granitic rocks are well exposed at this quarry and on the hill in its background.

1=Hirasawa quarry, 2=Hirasawa-yama, 3=Hirasawa-mura, 4=Tsukuba-san.

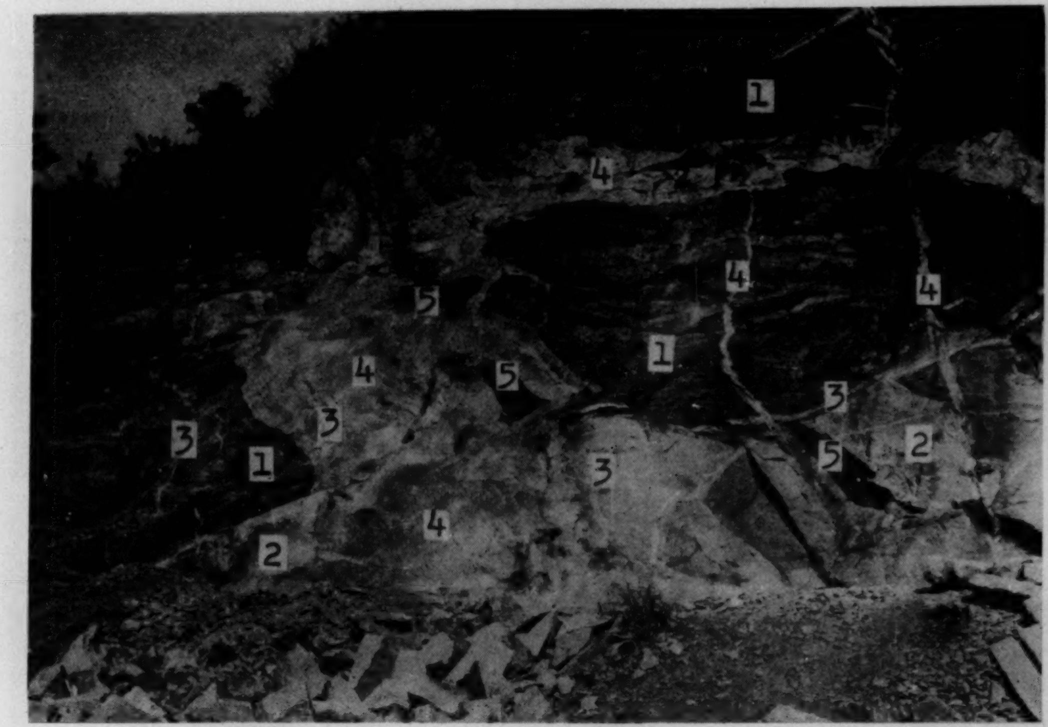

Fig. 4. Metamorphosed sediments and granitic rocks exposed at the Hirasawa quarry. Metamorphosed sediments here are intricately traversed by porphyritic biotite granite, pegmatite and aplite. In this case, the intrusion of biotite granite was succesively followed by those of pegmatite and aplite. 1=metamorphosed sediments, 2=Porphyritic biotite granite, 3=Pegmatite, 4=Aplite, 5=Xenolith.

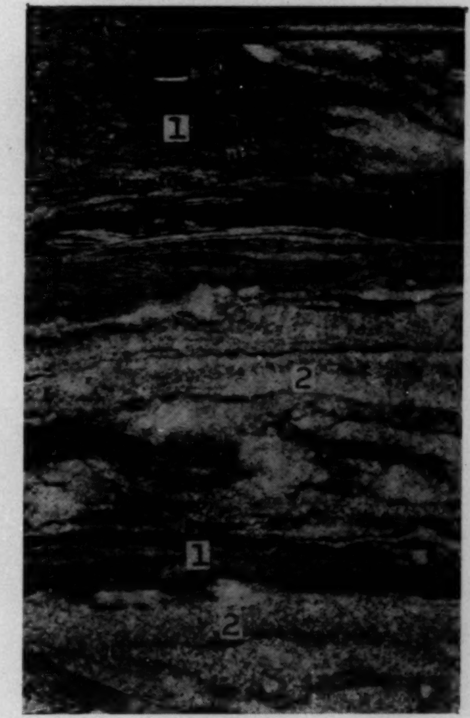

Fig. 5. Lit par lit injection of biotite granite. 1=Biotite gneiss, 2=Biotite porphyritic granite.
(Hirasawa quarry)

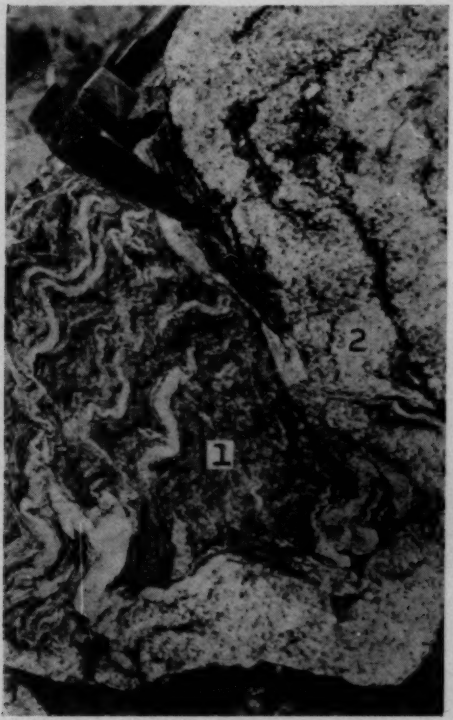

Fig. 6. Biotite gneiss contorted by the granitic intrusion. 1=Biotite gneiss, 2=Porphyritic biotite granite.
(Hirasawa quarry)

（震研彙報 第三十六号 図版 市村）

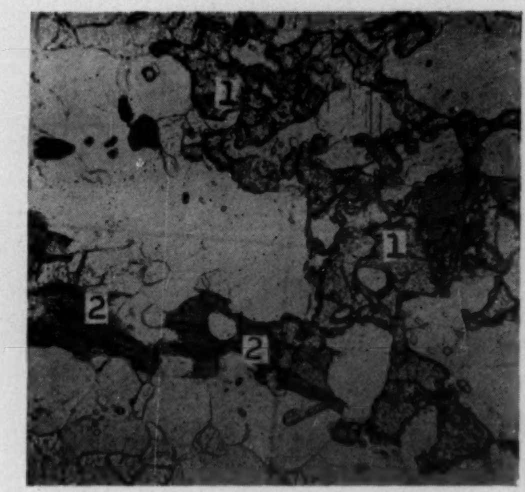

Fig. 7. Diopside and hornblende. 1= Diopside, 2=Green hornblende. (Diopside garnet hornblende hornfels, Hirasawa quarry). ×100.

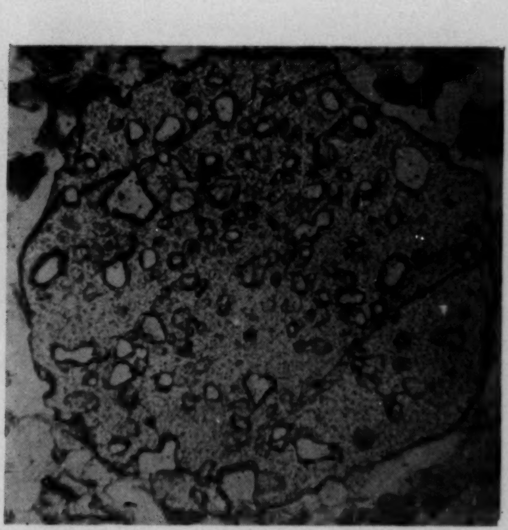

Fig. 8. Garnet crystals with a mesh structure. (Garnet two-mica hornfels, Rokusho-Busshōji). ×100.

Fig. 9. Sillimanite needles. (Sil. two mica hornfels, Mukō-yama). ×100.

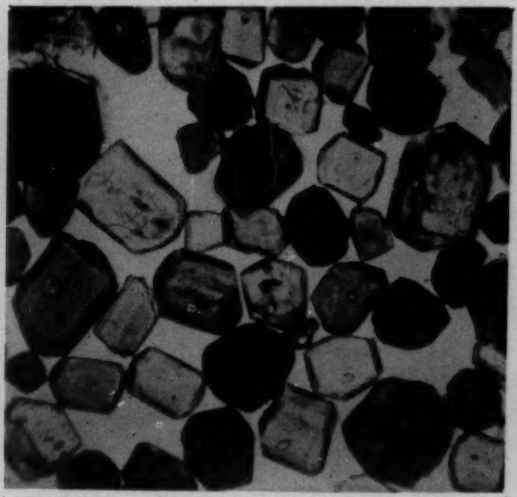

Fig. 10. Short prismatic crystals of tourmaline (Sil. two-mica gneiss, Hirasawa quarry). ×100.

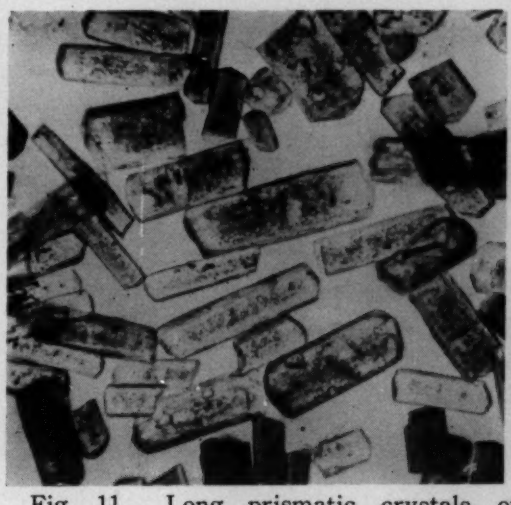

Fig. 11. Long prismatic crystals of tourmaline (Two-mica hornfels, Yumizuru). ×100.

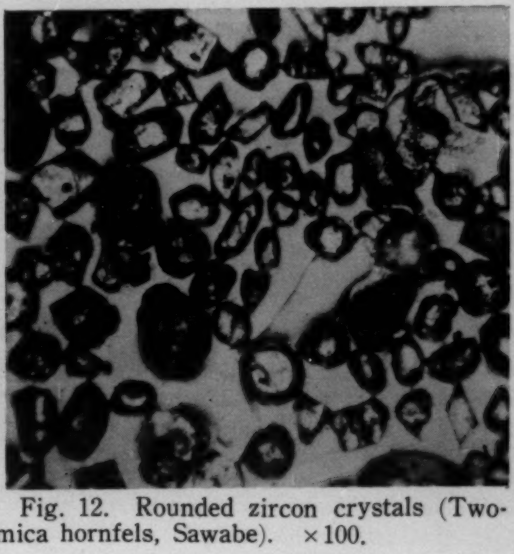

Fig. 12. Rounded zircon crystals (Two-mica hornfels, Sawabe). ×100.

(震研彙報　第三十六号　図版　市村)

地震研究所彙報
第36号(1958)413—431頁

23. 小諸附近に分布する浅間火山軽石の粒度組成

地震研究所 津屋弘達
村井勇
細谷与七

(昭和33年4月22日発表—昭和33年6月30日受理)

I まえがき

火山噴出物のうちで，砕屑性の噴出物の研究は，従来とかくなおざりにされがちであつた．ところが，最近に至り，噴火型式の1つである *nuée ardente* の現象が，火山学上極めて重要なものとして注目されるようになり，*nuée ardente* の堆積物の研究がしだいに行われるようになつた．これらの研究の先駆をなしたのは，FENNER, Clarence N. の Valley of Ten Thousand Smokes の凝灰岩の研究である1)．

又，MOORE, Bernard N. は，Crater Lake 地域の軽石の研究を行い，"Older Pumice" と呼んだ軽石層を *nuée ardente* の産物であると結論した．この MOORE の研究においては，軽石の粒度組成が論ぜられ，"Older Pumice" が *nuée ardente* 堆積物の粒度組成の特徴を示すものとされた2)．日本でも，最近，*nuée ardente* 或いは pyroclastic flow の堆積物であると認められるものが各地で報告されており，詳細な研究がしだいに行われるようになつた．それらの研究の中で，種子田定勝の南九州の"しらす"の研究は，粒度組成の特徴が，"Older Pumice" と共通であるとして，"しらす"を *nuée ardente* 或いは pumice flow の堆積物であると結論し，注目される3)．このように火山砕屑堆積物の研究は，*nuée ardente* 堆積物からはじめられ，多くの成果があげられている．筆者等は浅間火山において火山砕屑堆積物の研究を行い，いくつかの成果を得ることができた．とくに小諸附近に分布する軽石質堆積物の粒度組成について興味ある結果を得たので，ここに報告する．

II 軽石層の分布と構造

浅間火山の南側中腹より山麓部一帯にわたつて，軽石質の火山砕屑堆積物の層が非常に

---

1) Clarence N. FENNER, "The Origin and Mode of Emplacement of the Great Tuff Deposit of the Valley of Ten Thousand Smokes", *National Geog. Soc. Contr. Tech. Papers, Katmai Ser.*, No. 1 (1923)

2) Bernard N. MOORE, "Deposits of Possible Nuée Ardente Origin in the Crater Lake Region, Oregon", *Jour. Geol.*, **42** (1934), 358～375.

3) Sadakatu TANEDA, "Geological and Petrological Studies on the Shirasu in South Kyushu, Japan, Part I. Preliminary Note", *Memoirs of the Faculty of Sci., Kyushu Univ. Series D. Geol.*, **4** (1954), 167～177.

広い範囲にわたつて分布している(第１図参照)．特に小諸市東部では広い分布を示し，これを開析する小谷(“田切り”と呼ばれている)の谷壁に，その断面を見ることができる．

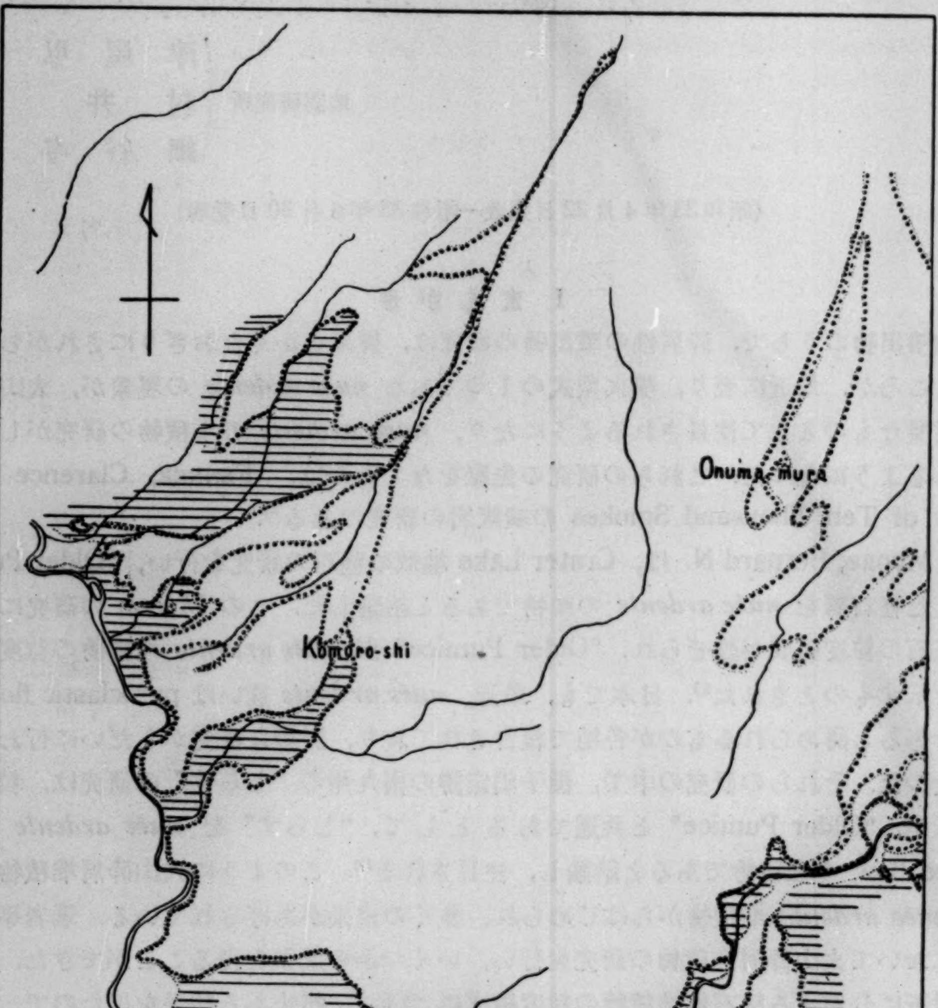
Onuma-mura
Komoro-shi
Asama-machi
Regend
pumiceous deposits
scoriaceous deposits
basement
0
2 Km

第１図　小諸附近における軽石の分布を示す地質概略図

分布の西端は小諸駅南の懐古園の西側まで達し，南端は南佐久郡中込町北部にまで延びている．東方の北佐久郡小沼村では，岩滓質の火山砕屑堆積物（八木貞助はこれを追分火山弾流と呼んでおり[4]，又荒牧重雄は ***nuée ardente***堆積物と考えて追分熱雲と呼んでいる[5]）によつておおわれている．蛇堀川の谷に沿つて，同様の岩滓質堆積物が軽石層の上をおおつている．八木はこれを蛇堀岩屑流と呼んでいる．南方の軽井沢町伍賀附近，及び東方の中軽井沢附近にも同様の軽石質の火山砕屑堆積物が分布しており，これもおそらく小諸附近に分布するものと一連のものと思われる．この軽石質火山砕屑堆積物は，基盤の第三紀或いは更新世の地層や熔岩流，火山砕屑堆積物（千曲層，信州熔岩，岩尾層等）の上に不整合的にのつている．層厚はだいたい20～25mで，分布範囲全体にわたつてあまりいちぢるしく変化しない．ただし，基盤の表面はかなりの起伏を示すために，その谷の部分を埋めている場合には40m，あるいはそれ以上の厚さに達している．又基盤の丘稜状の突出部の上にはのつていない．分布の限界は判然としており，“田切り”もその限界の部分で消えている．

軽石層の内部には層理のような構造はほとんど見られず，全体を通じて概して均質である．ただし，部分的に粒径の大きな軽石の集積したポケット状の部分や，砂丘の構造のような偽層状の構造が認められる．層の中央部附近（表面より約10m附近）に水磨された巨大な礫が並んでいるのを認められる場合があり，だいたいにおいてこの部分を境にして上下2層に分れるようである．しかし場所によつては層内がさらに複雑に幾層にも分れている場合も見られる．分布範囲の南部では最上部の層が細粒の火山灰質の薄層になつている．最南端の中込町北部では，この細粒の層が全層厚の半分以上を占めている．層内は概して均質であるが，軽石の含み方が部分的に又地域的に異ることも多い．たとえば，小諸市の市街部より四ツ谷にかけての部分では特に大粒径の軽石が多量に含まれている．このような層内の細い分層の場所ごとの変化や，その相互関係については，綿密な調査を行つて明らかにしなければならず，その詳細な検討は別の機会に譲ることにする．

この軽石層の中にはしばしば自然木炭が含まれている．これは堆積当時かなりの高温であつたことを物語つている．層の表面には一般に30cmほどの土壌層が形成されている．この土壌層の下1～1.5mほどの部分は，酸化されて赤褐色ないし黄褐色に変色している．蛇堀川及び追分原の岩滓質火山砕屑堆積物はこの土壌層の上にのつており，これらの堆積物が軽石層の堆積にくらべてはるかに新期の噴火によるものであることを示している．軽石層の表面はまだいちぢるしい侵蝕を受けていないが小諸市より東南の地域では小さな開析谷“田切り”の発達が顕著である．

浅間火山の北麓，吾妻川の南岸にそつても，小諸附近と同じように基盤の上に同様の軽石層が分布している．その分布範囲は，東は北軽井沢北方，西は田代湖南方姥が原にまで

---

4)　八木貞助「浅間火山」長野県北佐久教育会 (1930).

5)　S. ARAMAKI, “The 1783 activity of Asama Volcano”, *Part I, J. J. G. G.*, **27** (1956), 189～229.

達している．この軽石層も小諸附近の軽石層と一連のものである可能性が大きい．

これらの軽石層は，その分布の状態などから判断して，普通の降下軽石とは異る様相を示している．八木貞助はこれに対して“灰流 ash flow”と呼び，1930 年の Stromboli の

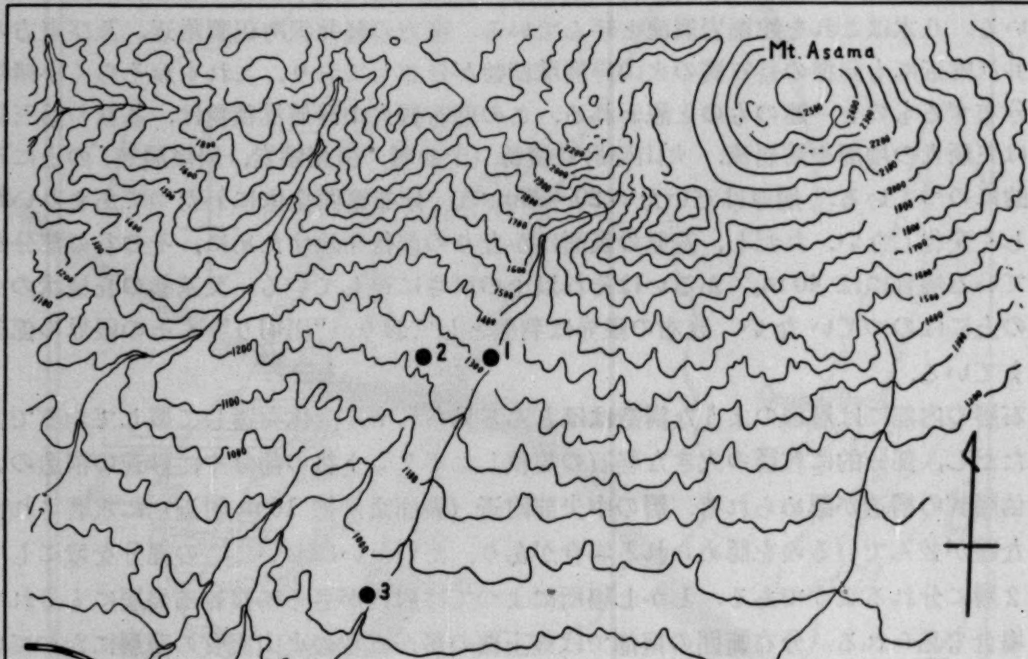
Mt. Asama
Komoro
1
2
3
4
5
6
7
8
9
10
0
2
4 Km

第 2 図　　試料の採集地点を示す図

噴火に相当するような第二次熱流によるものであろうと述べている．又，荒牧重雄は仏岩火山体より噴出した軽石流であるとしている．

この軽石質火山砕屑物は，１つの試料を検査したところでは，複輝石安山岩質のもので，glass の屈折率は低く（1.498_5），斑晶に当る斜長石の粒はいずれも累帯構造が著しい．

III　機械分析のための試料の採取

試料の採取にあたつては，できるかぎり条件のよいところをえらんで行つた．即ち，新しい道路の切り割りや“田切り”の谷壁などのような層全体を見渡すことのできる大きな露頭面をえらび，その中で特別の構造が認められない均質な部分から試料を採取した．かつ採取した試料の中でも，特に新鮮なものを用いて機械分析を行つた．試料は 2〜4kg 程度採集し，この中で約 50 g を保存用試料として予め分け，残りの全量を分析にあてた．露頭面で粒径の特に大きな軽石塊を多く含むと認められる場合には，その粒径について現場で実測を行い，機械分析の補助的資料とした．

試料を採取した場所は第２図に示す通りである．又，各試料の層内の位置は第 I 表の備考欄に記載してある．

IV　機械分析の方法

保存用試料を予め分け，残りの全量を分析にあてたが，このうち 50〜80 g を取りだして全粒度についての分析を行い，残り全部は８メッシュ（網目の径約 2mm）以上を水洗いしたのち篩分けを行つた．全粒度の分析は２段階に分けて行つた．即ち傾瀉法により直径 1/32 mm 以下の粒子とそれ以上の粒子とに分け，粗粒部分は乾燥したのち篩分けを行い，細粒部分は口径 10cm，高さ 15cm のガラス円筒瓶に入れてピペット法により分析した．この方法の詳細については，ここでは省略する[5]．以上の８メッシュ以上の粒度についての分析の結果と全粒度の分析の結果をまとめて機械分析の結果とした．これは，少量の試料について行う全粒度の分析においては粗粒部分の分析結果に大きな誤差が入りやすいのを避けるためである．

V　機械分析の結果

機械分析の結果は第１表に示す．これをヒストグラム及び累積和曲線で示せば第３図及び第５図のようになる．つぎに累積和曲線上で５%，16%，25%，50%，75%，84%，95%にあたる粒径を ϕ スケールで読みとり，夫々 ϕ_5，ϕ_{16}，ϕ_{25}，$\phi_{50}=Md_\phi$，ϕ_{75}，ϕ_{84}，ϕ_{95} とする．ただし $\phi=-\log_2\xi$（ξ は粒径を mm で表わしたもの）である．さらに，これらの値を用いて粒度分布のパラメター Q'，Q''，M_ϕ，σ_ϕ，α_ϕ，$\alpha_{2\phi}$，β_ϕ を計算する．ただし

---

5)　村井勇「江戸川河口附近の三角州上の干潟堆積物」地震研究所彙報 **34** (1956)，97．

第1表　機械分析の結果

1, 2～12, 13 は試料の番号. 1～10 は軽石, 11, 12 は蛇堀岩屑流, 13 は天明噴火の降下軽石である. 欄内の数字は各区間の占める重量%を示す. 各試料の採集地点は第1図に示してある.

ϕ	1	2	3	4	5	6	7	8	9	10	11	12	13
～-6				4.0								6.6	
-6～-5				3.4	6.3	0.7	4.9					4.9	
-5～-4				2.7	4.0	3.7	6.4	1.2	2.6			4.7	
-4～-3	4.2	8.1	3.1	2.6	8.4	3.7	6.7	1.9	6.9			4.1	14.3
-3～-2	4.9	5.7	5.4	2.2	7.6	4.0	6.2	2.5	12.3		0.7	3.2	23.8
-2～-1	7.1	6.5	8.5	3.4	7.3	6.2	7.4	3.6	9.8	0.1	1.2	4.3	17.9
-1～ 0	11.0	13.0	15.4	14.7	10.4	11.5	11.5	12.5	11.2	0.2	2.4	10.3	15.4
0～ 1	21.6	21.8	23.8	23.0	17.2	25.9	18.8	21.5	17.5	4.4	10.2	18.9	12.6
1～ 2	16.7	19.0	15.6	15.8	13.7	17.1	11.8	15.2	11.7	13.2	17.8	16.5	1.6
2～ 3	11.2	14.1	10.5	11.0	9.2	9.9	8.3	10.9	7.9	19.5	23.4	12.2	0.3
3～ 4	8.4	6.1	5.7	5.8	4.7	5.5	4.6	8.0	5.1	19.2	21.2	7.5	1.3
4～ 5	4.9	2.2	3.1	2.5	2.6	3.0	2.4	6.2	4.2	12.0	12.6	3.2	1.6
5～ 6	4.0	0.7	1.7	1.9	1.8	3.6	3.1	6.5	5.6	9.2	9.0	0.5	4.9
6～ 7	1.2	1.1	2.9	2.4	2.7	1.9	3.2	3.9	2.8	7.4	0.9	1.9	3.4
7～ 8	1.8	0.8	2.0	2.5	2.1	1.7	2.7	3.0	1.0	5.6	0.3	0.6	1.5
8～ 9	1.4	0.2	1.1	0.6	1.2	0.9	1.0	1.7	1.4	3.3	0.3	0.2	1.3
9～	1.6	0.7	1.2	1.5	0.8	0.9	1.0	1.4		5.9		0.4	0.1

$$Q' = (\phi_{75}-\phi_{25})/2$$

$$Q'' = (\phi_{75}+\phi_{25}-2\phi_{50})/Q'$$

$$M_\phi = (\phi_{16}+\phi_{84})/2$$

$$\sigma_\phi = (\phi_{84}-\phi_{16})/2$$

$$\alpha_\phi = (M_\phi-\phi_{50})/\sigma_\phi$$

$$\alpha_{2\phi} = \frac{\frac{1}{2}(\phi_5+\phi_{95})-\phi_{50}}{\sigma_\phi}$$

$$\beta_\phi = \frac{\frac{1}{2}(\phi_{95}-\phi_5)-\sigma_\phi}{\sigma_\phi}$$

M_ϕ; σ_ϕ; α_ϕ; $\alpha_{2\phi}$; β_ϕ は, 夫々 INMAM, D.L. (1952) による平均値, 偏差, 歪度, 尖度の近似値である[6]. 又 Md_ϕ, Q', Q'' は普通に用いられる中央値, 及び偏差, 歪度の近似値である. 実際に積率を計算してこれらの近似値と比較した結果では, 偏差は σ_ϕ に, 又歪度は $\alpha_{2\phi}$ にほぼ一致する場合が多いようである. 以上のような粒度分布のパラメターの値を第2表に示す.

軽石の試料 10 個についての分析の結果は, 細粒の "試料 10 番" を除いた他のものについては, 以下に列記するような特徴が認められる.

1) Md_ϕ の値は 0.3～1.5 (1～3 mm に相当) で, 火山灰 (4～1/4mm) の粒度に相

---

[6] D. L. INMAN, "Measures of describing the Size Distribution of Sediments", *Jour. Sed. Petrol.*, **22** (1952), 125～145.

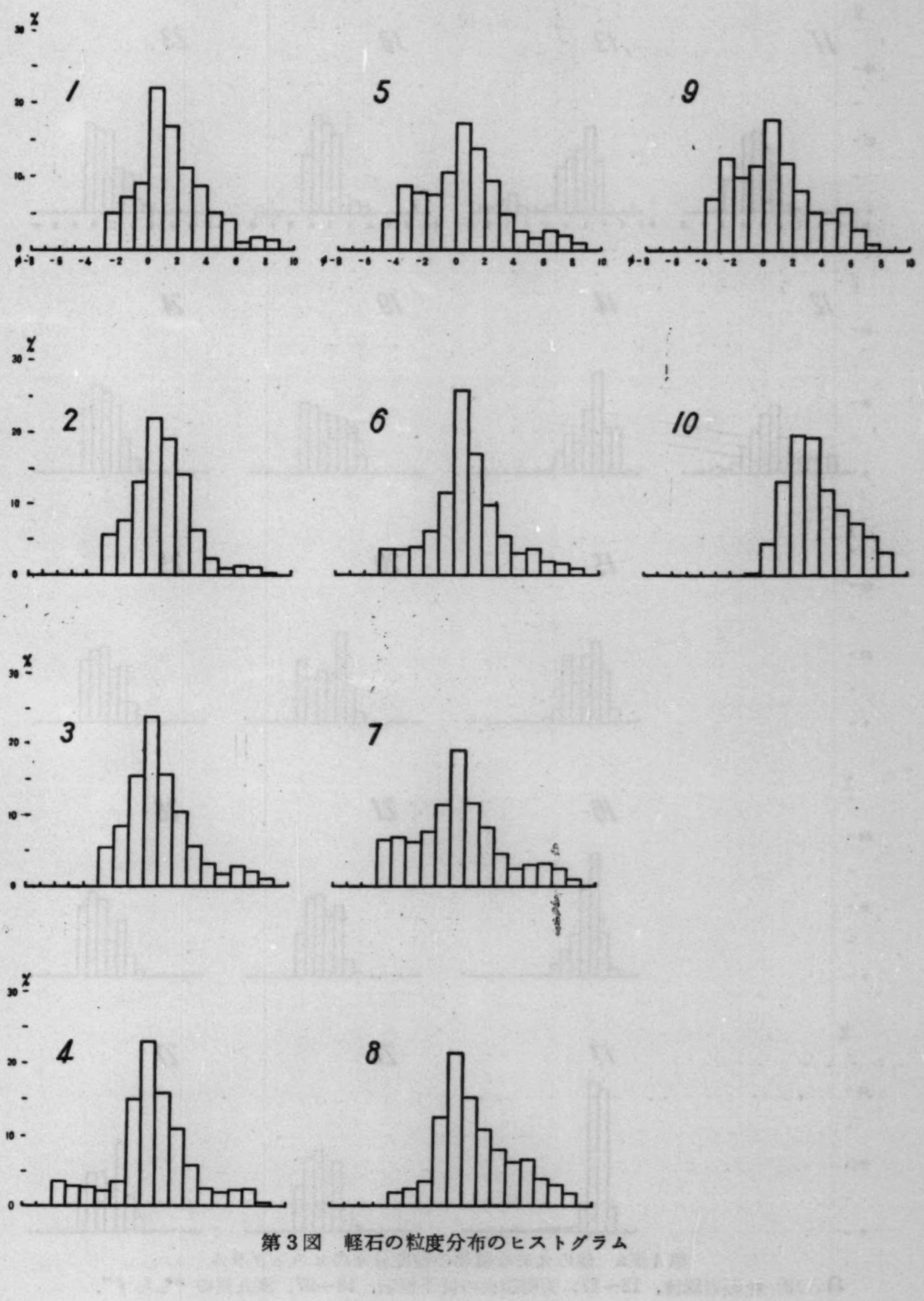

第3図　軽石の粒度分布のヒストグラム

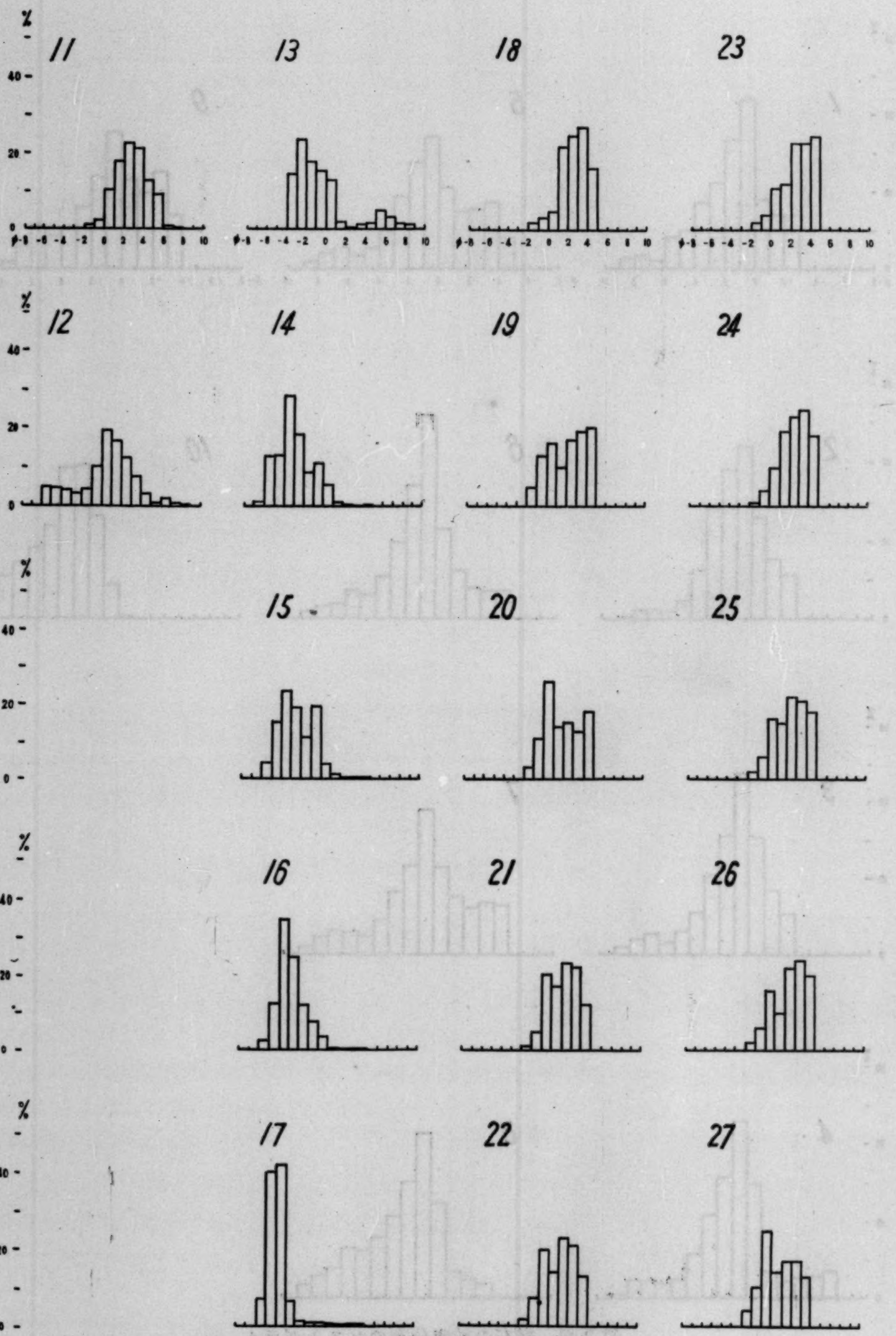

第4図a 他の火砕堆積物の粒度分布のヒストグラム
11，12；蛇堀岩屑流，13～17；天明噴火の降下軽石，18～27；南九州の“しらす”.

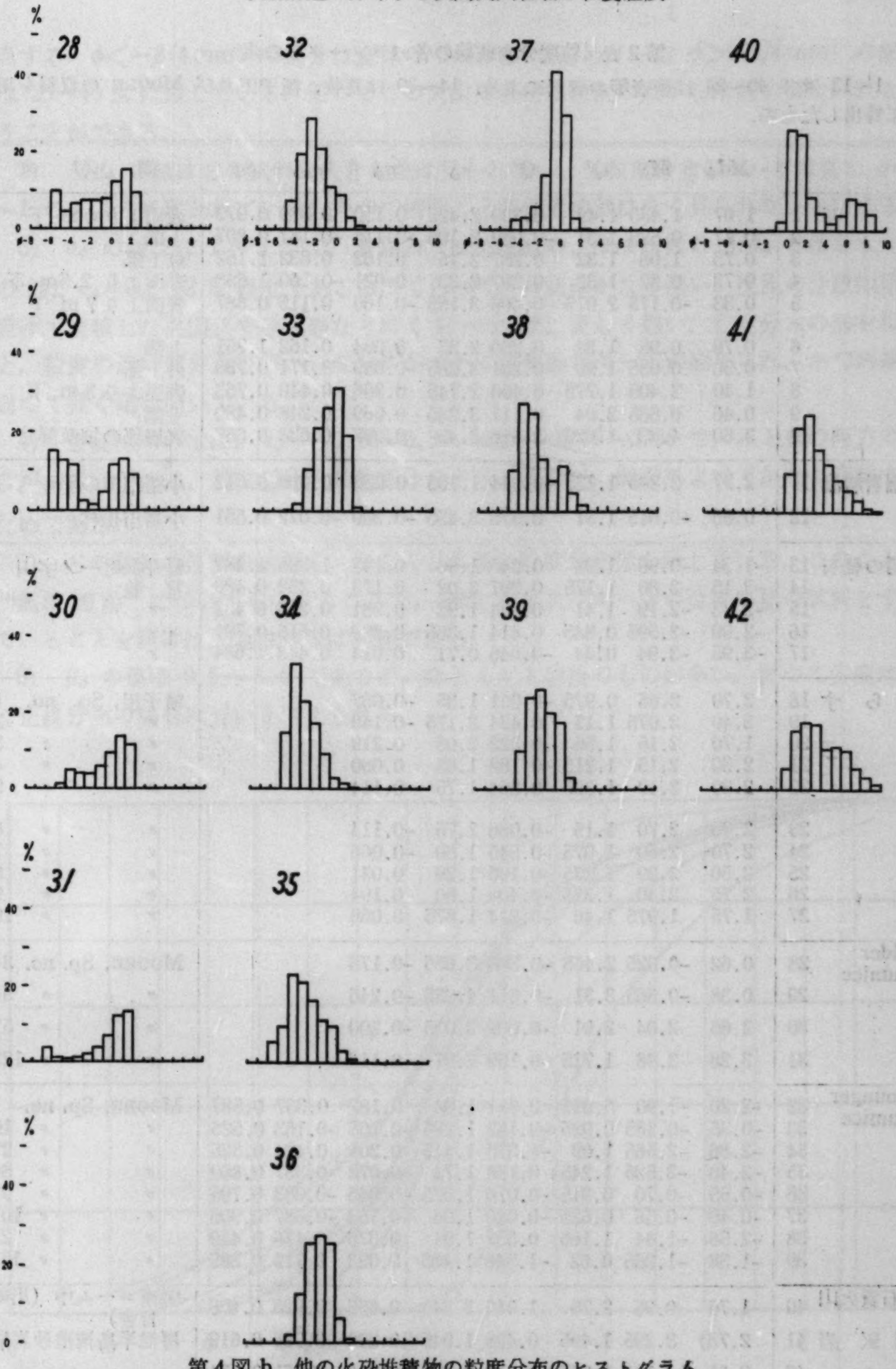

第4図 b　他の火砕堆積物の粒度分布のヒストグラム
28～31; Crater Lake 地域の "Older Pumice"
32～39; 〃 "Younger Pumice",
40; 関東ローム中の軽石質火山灰，41，42; 第三系の凝灰岩.

第2表 粒度分布曲線の各パラメーターの値

1～13 及び 40～24 は筆者等の資料による. 14～39 は荒牧, 種子田及び MOORE の資料を用いて算出したもの.

		Md_ϕ	M_ϕ	Q'	Q''	σ_ϕ	α_ϕ	$\alpha_{2\phi}$	β_ϕ	備考
軽石	1	1.07	1.435	1.49	0.389	2.425	0.150	0.389	0.973	表面より4m 下
	2	0.77	0.525	1.31	−0.030	2.105	−0.116	−0.187	0.807	上部
	3	0.73	1.08	1.32	0.287	2.15	0.162	0.632	1.162	最上部
	4	0.73	0.82	1.32	0.287	2.33	0.021	−0.100	1.658	表面より 2.5m 下
	5	0.33	−0.175	2.075	−0.409	3.155	−0.160	0.115	0.887	表面より7m 下
	6	0.79	0.98	1.28	0.250	2.25	0.084	0.162	1.251	上部
	7	0.36	0.035	1.99	−0.231	3.285	−0.089	0.171	0.788	最上部
	8	1.40	2.405	1.775	0.400	2.745	0.366	0.440	0.763	表面より3m 下
	9	0.46	0.685	2.04	0.117	3.245	0.069	0.248	0.480	上部
	10	3.60	4.33	1.625	0.516	2.45	0.297	0.638	0.687	表層部の細粒部分
蛇堀岩屑流	11	2.77	2.805	1.125	−0.044	1.705	0.020	0.029	0.612	小諸市芦の平
	12	0.66	−0.615	1.81	0.375	3.455	−0.369	−0.072	0.551	小諸市松林
天明の軽石	13	−1.34	−0.96	1.38	0.246	1.96	0.193	1.395	1.487	軽井沢町一ノ字山
	14	−3.15	−2.80	1.175	0.297	2.02	0.173	0.252	0.480	荒牧
	15	−2.73	−2.19	1.41	0.524	1.92	0.281	0.276	0.432	〃
	16	−2.99	−2.595	0.845	0.414	1.365	0.289	0.516	0.791	〃
	17	−3.95	−3.94	0.44	−0.045	0.71	0.014	0.443	1.684	〃
しらす	18	2.70	2.65	0.975	−0.051	1.35	−0.037			種子田, Sp. no. 1
	19	2.40	2.075	1.15	0.434	2.175	−0.149			〃 〃 2
	20	1.70	2.15	1.55	0.322	2.05	0.219			〃 〃 3
	21	2.30	2.15	1.215	−0.189	1.65	0.060			〃 〃 4
	22	2.30	2.10	1.325	−0.264	1.75	−0.114			〃 〃 5
	23	2.90	2.70	1.15	−0.086	1.75	−0.114			〃 〃 6
	24	2.70	2.60	1.075	−0.046	1.50	−0.066			〃 〃 7
	25	2.50	2.29	1.275	−0.196	1.29	0.031			〃 〃 8
	26	2.75	2.40	1.375	−0.400	1.80	−0.194			〃 〃 9
	27	1.75	1.975	1.40	−0.214	1.875	0.066			〃 〃 10
Older Pumice	28	0.62	−0.025	2.455	−0.386	3.655	−0.176			MOORE, Sp. no. 34
	29	0.38	−0.665	3.31	−0.311	4.235	−0.246			〃 〃 54a
	30	2.65	2.04	2.01	−0.009	3.035	−0.200			〃 〃 53a
	31	3.28	2.98	1.715	−0.169	2.57	−0.116			〃 〃 123
Younger Pumice	32	−2.20	−1.90	0.995	0.311	1.60	0.187	0.337	0.587	MOORE, Sp. no. 1
	33	−0.35	−0.485	0.925	−0.162	1.285	−0.105	−0.163	0.525	〃 〃 10
	34	−2.86	−2.565	1.09	−1.376	1.415	0.201	0.424	0.526	〃 〃 27
	35	−2.40	−2.525	1.245	0.168	1.72	−0.072	0.337	0.860	〃 〃 86
	36	−0.65	−0.70	0.915	−0.076	1.075	−0.046	−0.093	0.795	〃 〃 97
	37	−0.40	−0.56	0.625	−0.080	1.04	−0.153	−0.687	0.908	〃 〃 107
	38	−2.56	−1.84	1.165	0.557	1.91	0.376	0.476	0.439	〃 〃 21
	39	−1.38	−1.265	0.62	−1.548	1.465	0.023	0.112	0.389	〃 〃 153
軽石質火山灰	40	1.76	0.95	2.70	1.348	3.34	0.655	0.923	0.408	関東ローム中（川崎市日吉）
凝灰岩	41	2.73	3.295	1.495	0.428	1.945	0.290	0.585	0.619	房総半島清澄砂岩層中
〃	42	3.61	4.135	1.775	0.411	2.425	0.216	0.461	0.554	〃

当する．$\phi<-2$(4mm) の部分は全体の 5～30% を占め，一方 $\phi>2$(1/4mm) の部分は 25～40% に達している．従つてこの火山砕屑物は粒度の点からは軽石質火山灰ということができる．

2)　Md_ϕ の値はどの試料も大きな差は見られない．又粒度分布のモードは常に $\phi=0$～1 のところに現われている．従つて場所ごとの粒度の差は全く見られないといえる．

3)　σ_ϕ の値は 2.1～2.3 で，普通の水成堆積物の，ほぼ同様の Md_ϕ の値をもつものでは $\sigma_\phi=0.5$～2.5 程度であるのにくらべて，分級はかなり悪い．又風の分級作用を受けて堆積した火山灰や砂丘砂などにくらべれば，著しく悪い．粒度分布の形を見ると，粒度の粗い部分及び細かい部分にかすかに副次的なモードが認められ，かつ両端に向つて長く尾を引いている，

4)　歪度については，$\alpha_\phi=-0.16$～0.37，$\alpha_{2\phi}=-0.19$～0.64 で，正と負の両方の場合がある．これは，粗粒部分と細粒部分の占める割合が，試料によつてかなり変動するためである．

5)　どの試料の分析の結果も，ほとんど共通の粒度分布型を示している．このことは“試料10番”についてもいえることで，Md_ϕ の値及びモードの位置が他の試料とずれていることを除けば，他の特徴は共通である．

6)　β_ϕ の値は 0.5～1.6 であるが，ほとんど1前後のものが多い．従つて尖度はほぼ正規分布の場合に近いと考えられる．

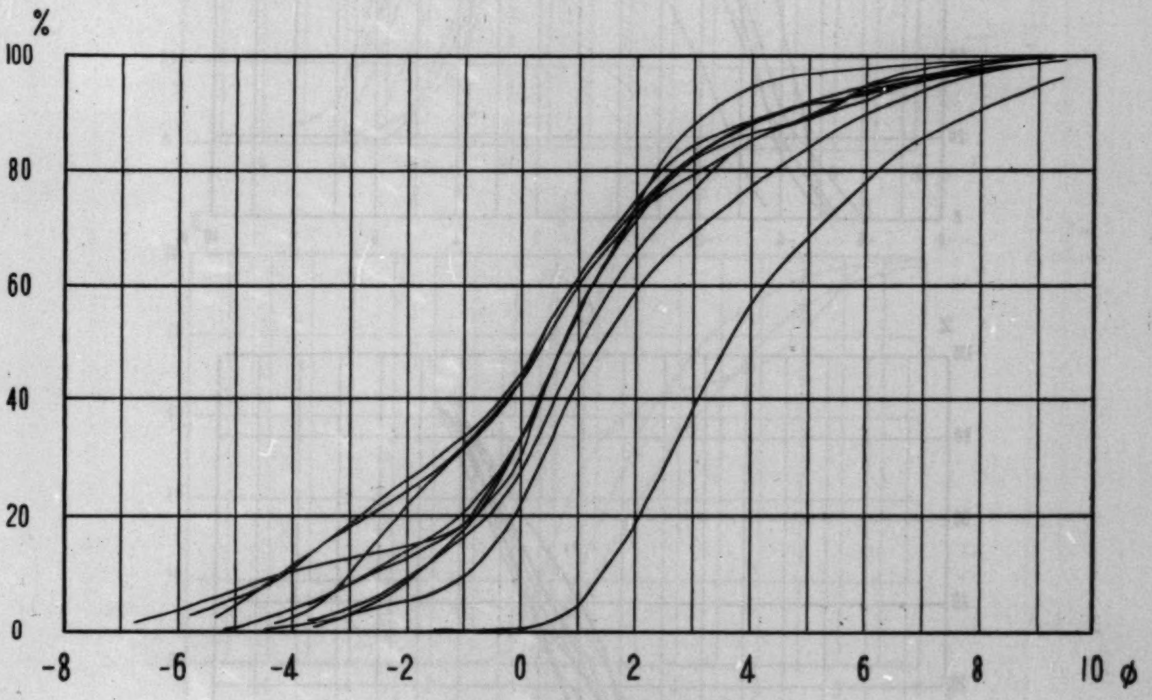

第5図　軽石の粒度分布の累積和曲線

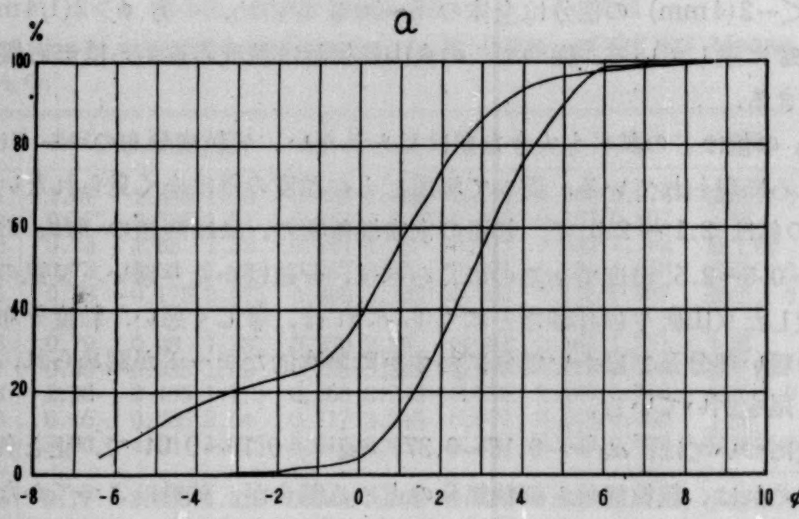
a
%
100
80
60
40
20
0
-8
-6
-4
-2
0
2
4
6
8
10
φ

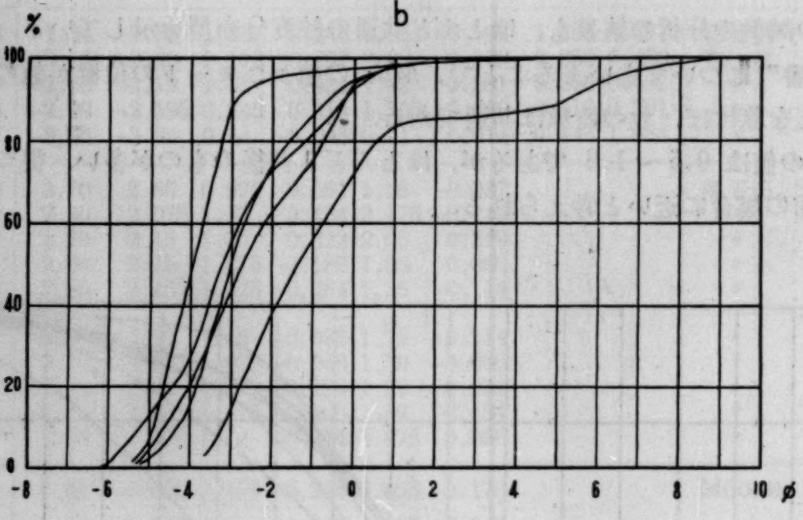
b
%
100
80
60
40
20
0
-8
-6
-4
-2
0
2
4
6
8
10
φ

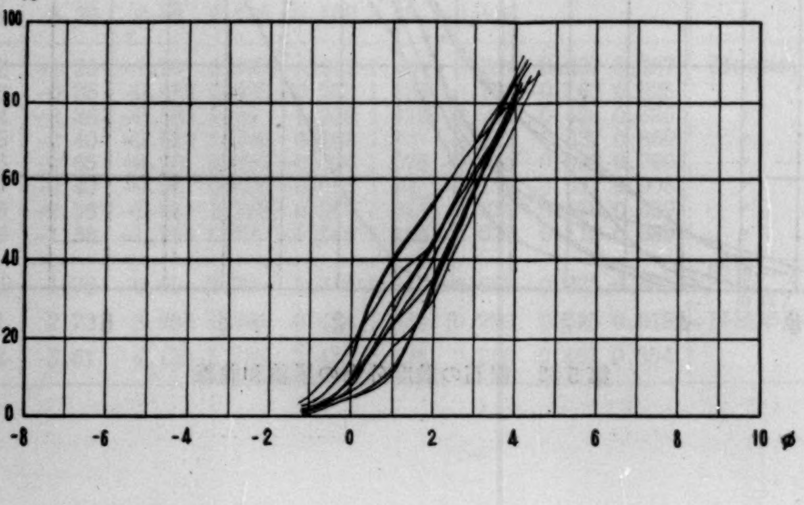
C
%
100
80
60
40
20
0
-8
-6
-4
-2
0
2
4
6
8
10
φ

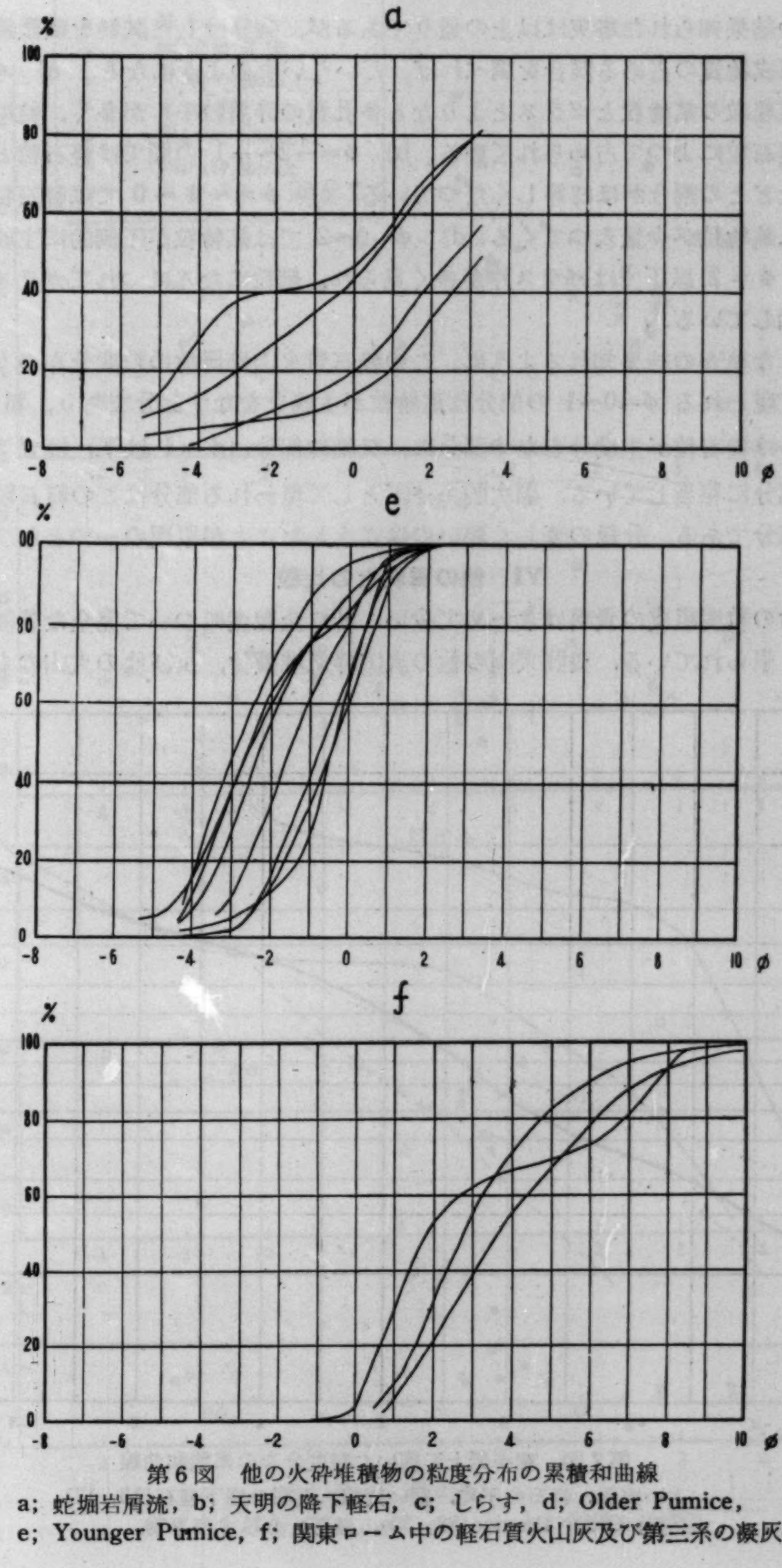

第６図　他の火砕堆積物の粒度分布の累積和曲線
a; 蛇堀岩屑流，b; 天明の降下軽石，c; しらす，d; Older Pumice,
e; Younger Pumice, f; 関東ローム中の軽石質火山灰及び第三系の凝灰岩.

機械分析の結果知られた事実は以上の通りであるが，篩分けした試料を顕微鏡下で検査して，その構成物質の占める割合を調べれば，だいたい次のようになる．a） $\phi=-2$ 以上は軽石粒（粗粒の鉱物粒とガラスとよりなる多孔質の砕屑粒子）が多く，特に $\phi=3$ 以上は殆んど軽石粒によつて占められている．b） $\phi=-2\sim-1$ の間では軽石粒と熔岩片及び捕獲岩片などとの割合がほぼ等しくなつている．c） $\phi=-1\sim0$ では軽石粒は少くなり，かわりに鉱物粒が少量入つてくる．d） $\phi=0\sim2$ では鉱物粒が圧倒的に主成分を占めている．e） $\phi=2$ 以下ではガラス片が多く見られ，細粒になるにつれてガラス片の占める割合は増加している．

以上のような検査の結果知れるように，この軽石質火山砕屑物の粒度分布のうち，常にモードとして現われる $\phi=0\sim1$ の部分は鉱物粒が主成分をなす部分であり，粗粒部分（$\phi=-2$ 以上）は軽石粒が主成分をなす部分に，又細粒部分（$\phi=4$ 以下）はガラス片が主成分をなす部分に相当している．副次的モードとして現われる部分はこの軽石粒の部分とガラス片の部分である．分級の著しく悪いのはこうしたことが原因の一つとなつている．

VI 他の資料との比較

火山砕屑物の粒度組成の資料はきわめて少い．特に全粒度について完全な機械分析を行つた例はごく限られている．浅間火山の他の火山砕屑堆積物，及び他の火山のものについ

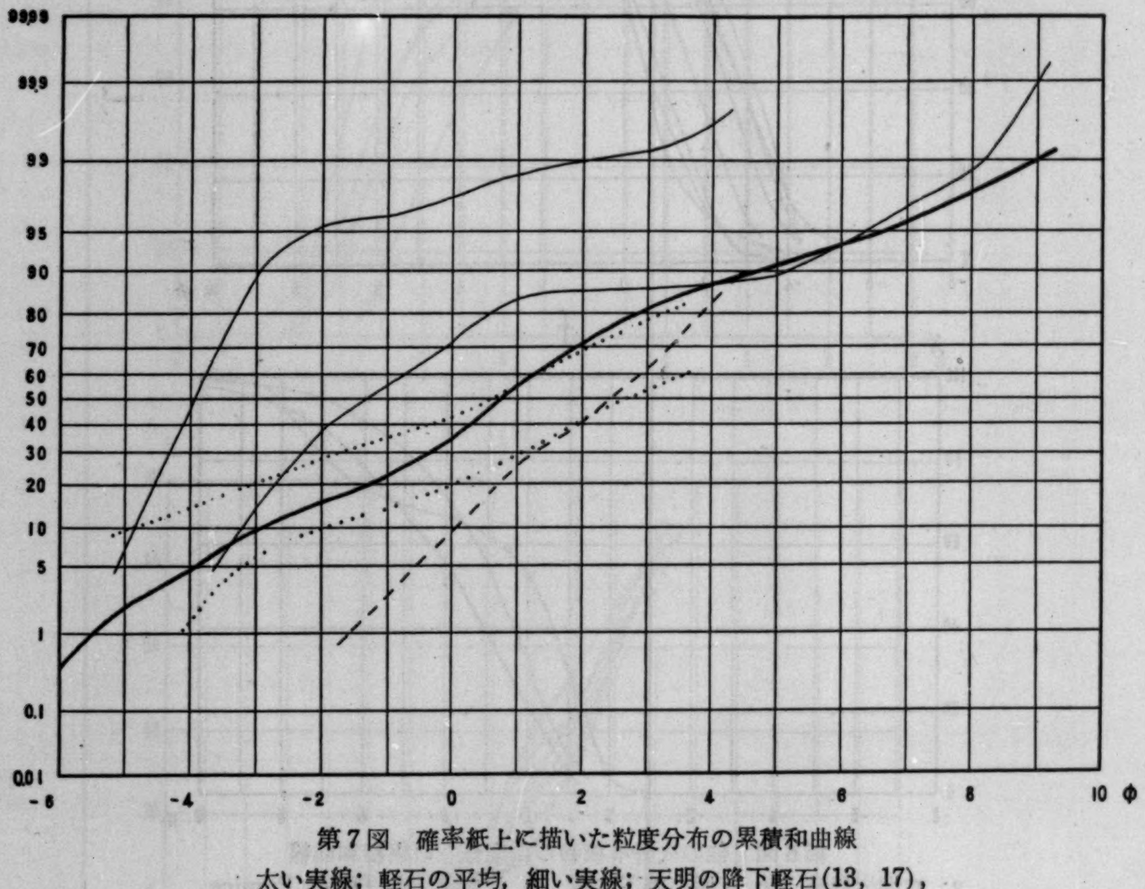

第7図 確率紙上に描いた粒度分布の累積和曲線

太い実線；軽石の平均，細い実線；天明の降下軽石(13，17)，点線；Older Pumice(28，30)，破線；しらすの平均．

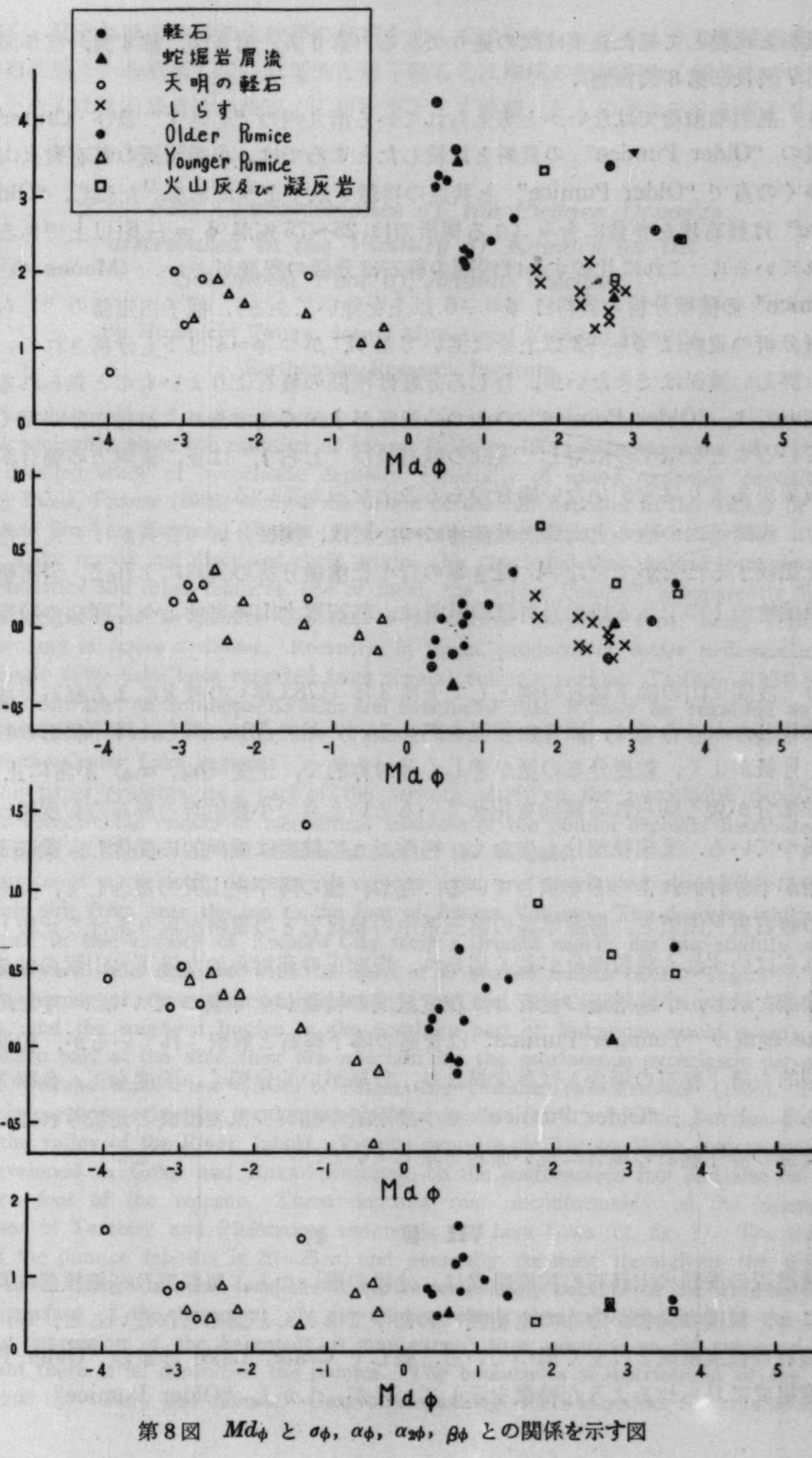

第8図 Md_ϕ と $\sigma\phi$, $\alpha\phi$, $\alpha_2\phi$, $\beta\phi$ との関係を示す図

ての資料と比較して見た結果は次の通りである（第Ⅱ表，第3図，第4図，第5図，第6図，第7図及び第8図参照）．

1）　熱雲堆積物ではないかと考えられている南九州の“しらす”及び Crater Lake 地域の“Older Pumice”の資料と比較したところでは，小諸附近の軽石質火山砕屑物は多くの点で“Older Pumice”と共通の特徴を示すようである．ただし，“Older Pumice”は軽石塊を多量に含み（ある個所では 25〜75％が $\phi=-6$ 以上であると報告されている），これに比較すれば浅間の軽石は分級の程度がよい．（MOORE の“Older Pumice”の機械分析の資料は $\phi=-6$ 以上を除いてある）．種子田定勝の“しらす”の機械分析の資料は $\phi=-2$ 以上をはぶいてあり，かつ $\phi=4$ 以下も分析されていないので，詳しい検討はできないが，むしろ分級は浅間の軽石よりよいものと見られる．歪度については，“Older Pumice”の4つの資料がすべて負であり，粗粒部分が長く尾を引いていることを示すのに対して浅間の軽石及び“しらす”は正，負両方の場合があり，粗粒部があまり尾を引かない場合のあることを示している．

2）　浅間火山の他の火山砕屑堆積物については，機械分析の資料がほとんどないので十分比較することができない．筆者等の行つた機械分析の資料によれば，岩屑質火山砕屑堆積物の1つである蛇堀岩屑流の試料は，軽石質火山砕屑物と全く同様の粒度分布を示した．

3）　浅間火山の降下軽石の例として天明3年（1783年）の噴火による軽石を取りあげて比較したところでは，顕著な相異を認めることができた．即ち，降下軽石の粒度組成は，分級がよく，粒度分布の型が著しく非対称的で，歪度（α_ϕ，$\alpha_{2\phi}$）が常に正であり，粗粒部分が鋭く切られる傾向を見せているという点で小諸附近の軽石の粒度組成とは全く異つている．又細粒部分も少なく，場所ごとに粒度は規則的に変化し，風による分級作用が十分行われたことを示している．なお，他の降下火山灰の例として，関東ローム中の軽石質火山灰と，房総半島の第三系中の凝灰岩との資料を取りあげて比較したが，これらはいずれも粗粒部分が鋭く切られ，歪度正の非対称的な降下火山灰の特徴的な粒度分布を示し，小諸附近の軽石とは粒度組成の特徴が全く異つていた．なお，Crater Lake 地域の“Younger Pumice”は普通の降下軽石と解釈されているが，粒度分布は典型的な降下軽石の場合とは多少異なり，分級がいく分悪く，歪度も正，負両方の場合がある．しかし，“Older Pumice”や小諸附近の軽石の粒度組成と比較すれば，はるかに普通の降下軽石の場合に近い様相を示している．

VII　要　　約

小諸附近の浅間火山軽石の粒度組成は，分級の悪いこと，粗粒部及び細粒部に長く尾を引くこと，粒度の変化が分布の全範囲にわたつてほとんど認められないこと，等の点で，降下軽石の粒度組成とは全く異つている．概して Crater Lake 地域の“Older Pumice”の粒度組成に見られるような特徴を示しているが，しかし“Older Pumice”ほど分級は

悪くなく，又それほど多量の大粒径の軽石を含んではいない．このような粒度組成の特徴と，分布状態とから判断して，典型的な降下軽石とは堆積の機構が全く異るものと見られる．おそらくは火山砕屑流の状態で山腹を流下して堆積したものであろうと考えられる．

23. *Size Characteristics of the Pumice Deposits distributed in the Vicinity of Komoro on the Southwest Foot of Asama Volcano.*

By Hiromichi TSUYA, Isamu MURAI and Yoshichi HOSOYA,
Earthquake Research Institute.

The phenomena of *nuées ardentes* or burning clouds have attracted much attension by volcanologists since the eruption of Mount Pelée in 1902, inducing some of them to do a detailed study of pyroclastic deposits, especially of *nuées ardentes* deposits. Among those, Fenner (1923) studied the origin of the tuff deposits in the Valley of Ten Thousand Smokes, Katmai. MOORE (1934) described the recent pumice deposits of the Crater Lake region and discussed their origin. He concluded that, judged from the size characteristics and other features, one of them, the "Older Pumice", is apparently different in origin from the pumice deposits of the normal projected type, being regarded as a product of *nuées ardentes*. Recently, in Japan, products of *nuées ardentes* or of pyroclastic flows have been reported from several volcanic regions. TANEDA (1954) studied the "Shirasu" in Southern Kyushu and concluded that it may be regarded as the *nuées ardentes* products showing size characteristics similar to those of the "Older Pumice" of the Crater Lake region.

This paper presents, as a part of the writers' study on the pyroclastic deposit of Asama Volcano, the results of mechanical analyses of the pumice deposits distributed in the vicinity of Komoro on the southwest foot of the volcano.

Pumiceous pyroclastic deposits of various ages are distributed extensively on the mountain side from near the top to the foot of Asama Volcano. The deposits which are developed in the vicinity of Komoro City form a ground nearly flat but slightly slope southwestward, and are cut with the walls of *U*-shaped gullies called "Tagiri". The western border of their distribution area is on the west side of Komoro Railway Station, and the southern border in the northern part of Nakagomi-machi (town). In the eastern part of the area they are overlain by the scoriaceous pyroclastic deposits, YAGI's "Oiwake Bomb Flow" (1930) or ARAMAKI's "Oiwake *Nuée Ardente*" (1956). They are also partly overlain by another scoriaceous deposit (YAGI's "Jabori detritus Flow") along the valley of the River Jabori. Pumice deposits similar to those just mentioned are developed in Goka and Naka-karuizawa, on the southeastern foot and also on the northern foot of the volcano. These deposits rest unconformably on the basement composed of Tertiary and Pleistocene sediments and lava flows (cf. fig. 1). The thickness of the pumice deposits is 20～25 m, and generally constant throughout the distribution area, though in some localities it varies remarkably because of the irregularities of the surface of the basement. In the places where they are deposited in the preexisting depression of the basement, it may exceed 40 m, whereas on the ridges of the basement there is no deposit of the pumice. The boundaries of distribution of the deposits are very sharp and definite. Generally speaking, there is neither remarkable stratification nor structure of special meaning, in the deposits, although large blocks of pumice some times occur in pockets and cross beddings are often seen. In some localities rounded boulders occur in a layer at the middle horizon dividing the deposits into two parts. Moreover, fine stratifications are locally developed. Natural charcoals are often found in the deposits, showing that these pyroclastics were very hot when they were deposited.

With the object of carrying out mechanical analyses, samples of 2~4 kg weight of the deposits wers collected from the homogeneous part in the large outcrop such as new roadcuts or walls of gullies. Localities of sampling are shown in fig. 2. If very large blocks of pumice were embedded in the outcrop, their diameters were measured on the spot. Each sample was divided into three parts: one, about 50 gr weight, was put aside for preservation; another, 50~80 gr weight, was prepared for thorough mechanical analysis; and the rest was used for analysis of grains coarser than 8 mesh (about 2 mm in diameter). Mechanical analyses were carried out by means of the sieving, decantation and pipette methods. In thorough analyses the specimens were sized by the decantation method and divided into two parts: one coarser and the other finer than 1/32 mm in grain diameter. The coarser part was dried up and was sized by means of sieving with woven wire screens. The finer part was analysed by the pipette method. The weight of each fraction separated by the sieving and pipette method was calculated as the percentage in the total weight of the specimen. Analyses have been made on ten specimens of the pumice deposits, and the results are shown in table 1 and fig. 3 and fig. 5.

The diameters of particles in millimeters ξ are replaced here by ϕ as expressed $\phi = -\log_2 \xi$ for convenience. Approximate value of every sort of parameter of the size distribution, that is mean M_ϕ, median $M_{d\phi}$, deviation or sorting Q and σ_ϕ, skewness Q', α_ϕ and $\alpha_{2\phi}$, and kurtosis β_ϕ, in ϕ scale are obtained from the following relations.

$$M_\phi = (\phi_{16} + \phi_{84})/2, \quad M_{d\phi} = \phi_{50},$$

$$Q' = (\phi_{75} - \phi_{25})/2, \quad \sigma_\phi = (\phi_{84} - \phi_{16})/2,$$

$$Q'' = (\phi_{75} + \phi_{25} - 2\phi_{50})/Q',$$

$$\alpha_\phi = (M_\phi - \phi_{50})/\sigma_\phi, \quad \alpha_{2\phi} = \{(\phi_5 + \phi_{95})/2 - \phi_{50}\}/\sigma_\phi,$$

$$\beta_\phi = \{(\phi_{95} - \phi_5)/2 - \sigma_\phi\}/\sigma_\phi$$

Here, $\phi_5, \phi_{16}, \cdots, \phi_{95}$ are the ϕ values of the percentiles, or the size associated with the percentage values on the cumulative curves. The values of these parameters are listed in table 2.

The results of the mechanical analyses of nine specimens of the pumice deposits, except sp. no. 10, are summarized as follows: 1) The median diameters of the pumice deposits are exclusively within a range of 0.3 to 1.5 in ϕ scale, and these deposits may be called pumiceous ash. 2) The variation of coarseness with distance from the source could not be found, for the values of median diameters are almost constant and the mode of the size distribution always lies in the fraction of 0~1 in ϕ scale. 3) The sorting is rather bad, as the values of σ_ϕ are 2.1 to 2.3. Tailingout of both the coarser and finer fractions are found in every case, and the secondary maxima may be sometimes found in these tailingout parts. 4) The degree of skewness varies widely, as the values of α_ϕ are -0.16 to 0.37, and the values of $\alpha_{2\phi}$ are -0.19 to 0.64. 5) The size distribution of every specimen shows quite similar feature. This is also true for sp. no. 10, the median diameter of which is far smaller than those of the other specimens. (Sp. no. 10 was collected from the uppermost fine layer.) 6) The values of β_ϕ, the parameter of kurtosis, is 0.5 to 1.6.

It may be recognized that the pumice deposits consist of several different constituents, when observed under the microscope. The material above $\phi = -2$ consists dominantly of pumice. Pumice itself is composed mainly of finely vesicular or fibrous glass, and phenocrysts of plagioclase, augite and hypersthene are present. The finer particles are of grains of minerals and of glass. The material from $\phi = 0$ to 2 consists largely of mineral grains, and below $\phi = 2$ the particles are mainly angular fragments of glass.

In general, the pumice deposits concerned show size characteristics similar to those of the "Older Pumice" (cf. table 2, 28~31, fig. 4b, fig. 5d), in that both show fairly bad sorting, tailingout of both the coarser and finer fractions, lack of the variation of coarseness and the other features. The "Shirasu" also may have similar characteristics, but the sorting is rather good (cf. table 2, 18~27, fig. 4a, fig. 5c).

The size characteristics of the pumice deposits are quite different from those of the normal pumice fall. For example, the size characteristics of pumice fall of the 1783 activity of Asama show good sorting, lack of tailingout of the coarser fractions, regular variation of coarseness with distance from the crater and other features (cf. table 2, 13~17, fig. 4a, fig. 5b). These features may be the typical characteristics of the normal projected pyroclastic deposits. The "Younger Pumice" of the Crater Lake region also shows the similar size characteristics (cf. table 2, 32~39, fig. 4b, fig. 5e). Other examples of ash and tuff also show the similar features (cf. table 2, 40~42, fig. 4b, fig. 5f).

There are few data of mechanical analyses of other pyroclastic deposits of Asama. The writers have tried the analyses of two specimens of the "Jabori Detritus Flow", the results being similar to those of the pumice deposits (cf. table 2, 11, 12, fig. 4a, fig. 5a).

The pumice deposits which are distributed in the vicinity of Komoro may be entirely different in origin from that of the normal pumice fall, as may be judged from their size characteristics, distribution and other features, and are regarded as the products of pyroclastic flows.

fractions of [illegible] in table 3, 5 and 6.

It may be recognized that the pumice deposits consist of several different constituents, which are [illegible] under the microscope. The material above $\phi = 0$ consists dominantly of pumice. Pumice itself is composed mainly of [illegible] or fibrous glass, and phenocrysts of plagioclase, augite and hypersthene are present. The finer particles are of grains of minerals and of glass. The material from $\phi = 0$ to 2 consists largely of [illegible] and below 2 all the particles are mainly angular fragments of crystals.

In general, the pumice deposits concerned show size characteristics similar to those of the "Older Pumice" (cf. table 2, M-12, fig. 4b, fig. 5b), in that both show fairly bad sorting, [illegible] of both the coarser and finer fractions, lack of the variation of coarseness with other features. The "Older Pumice" also may have similar characteristics, but the sorting is rather good (cf. table 4, fig. 4 and fig. 5).

The size characteristics of the pumice deposits are quite different from those of the several pumice falls. For example, the characteristics of pumice fall of the 1783 activity of Asama-yama are good sorting, lack of tailing out of the coarser fractions, regular variation of coarseness with distance from the crater and other features (cf. table 3, [illegible], fig. 4 and fig. 5b). These features may be the typical characteristics of the normal pyroclastic fall deposits. The "Younger Pumice" of the [illegible] region also shows the similar size characteristics (cf. table 3, [illegible], fig. 4b, fig. 5b). Other examples of [illegible] and [illegible] also show the similar features (cf. table 2, [illegible], fig. 4b and 5b).

There are few data of mechanical analyses of other pyroclastic deposits of Asama. The writers have tried the analyses of two specimens of the [illegible], the results being similar to those of the pumice deposits (cf. table 2, [illegible] 11, fig. 4a, fig. 5a).

The pumice deposits which are distributed in the vicinity of Tomioka may be entirely different in origin from that of the normal pumice fall, as may be judged from their size characteristics, distribution and other features, and are regarded as the products of pyroclastic flows.

地震研究所彙報
第36号(1958)433-446頁

24. プロトン磁力計の試作研究

文部省科学試験研究費研究班
（代表者 力武常次）

(昭和33年5月27日発表—昭和33年6月14日受理)

1. 緒言

Packard と Varian[1] が水中のプロトンの核磁気モーメントを利用し，地球磁場中に於ける自由歳差運動周波数を測定して，地球磁場全磁力の絶対測定を行う方法を提唱して以来，各国に於てこの方法による地球磁場測定の実用化が試みられている．例えば Waters と Phillips[2] は約500 *cc* の水のはいつたびんに励磁コイルをまいて，約100ガウスの人工磁場を地球磁場とほぼ直角に加え，この磁場を急に切断することにより，水中のプロトンに自由歳差運動を起させる方法を採用した．この歳差運動は同じびんに巻かれた受信コイルによつてピック・アップされ，狭帯域増巾器を経て周波数計数器により計数される．計数は100 *kc/s* の水晶発振器を基準としている．この方法により，10^{-5} の精度で周波数を計数することができるから，英国の地球磁場全磁力に相当する約2000 *c/s* の計数にあたつては $\pm 0.02\,c/s$ の精度を保つことになり，全磁力が $\pm 0.5\gamma$ の精度で測定できることになつた．英国 Abinger 地磁気観測所に於て，地磁気変化計と比較観測を行つたところでは良好な一致を得ている．

Cahill および Allen[3] はこの方式の磁力計を気球にのせて，高空の地球磁場測定を行つた．蒸溜水約300 *cc* を用い，切換リレーにより同一コイルを励磁および検出に共用，タイマーを用いて1分毎に約5秒間励磁するようにした．信号はトロイダル変圧器を経て増巾され，91 *Mc/s* FM 発信器により地上に送られる． このような方式により高さ 10^4 *ft* に達する高空の全磁力が $\pm 2\gamma$ の精度で測定されている．

本邦に於ても，このような方式の磁力計は物理学者および地球物理学者の注目するところとなり，建設省地理調査所[4,5]，気象庁地磁気観測所，東京教育大学[6,7] 等に於て各種の実験が行われるようになつた．これら各機関の関係者を統合して相互に情報を交換するとともに，プロトン磁力計を製品化することを目的として「プロトン磁力計の試作研究」に関する研究組織がつくられ，昭和32年度文部省科学試験研究費をうけて研究活動を開

---

1) M. PACKARD and R. VARIAN, *Phys. Rev.*, **93** (1954), 941.
2) G. S. WATERS and G. PHILLIPS, *Geophys. Prosp.*, **4** (1956), 1.
3) L. J. CAHILL, JR. and J. A. VAN ALLEN, *Journ. Geophys. Res.*, **61** (1956), 547.
4) 坪川家恒・田島稔・瀬戸孝夫 測地学会誌 **4** (1957), 24.
5) 坪川家恒 科学 **28** (1958), 73.
6) 小島昌治・大井喜久夫・小川静子・鳥塚一男 科学 **27** (1957), 255.
7) 小島昌治・小川静子・鳥塚一男・大井喜久夫 計測 **7** (1957), 456.

始した.

1957 年 4 月，第一次南極地域観測隊が帰国したが，南極大陸プリンスハラルド海岸の地球磁場が異常に弱いことを報告し，その異常地域の範囲を明らかにするためには，海上磁気測量を行うことが必要であるとし，そのためにはプロトン磁力計検出部を観測船で曳航する方式が望ましく，至急南極地域観測用プロトン磁力計を製作してほしいという要請が本研究組織に対し申込まれた．かくして，本組織としては南極地域観測用磁力計を優先的に試作することとなり，1957 年 10 月に出港した観測船「宗谷」にはその試作器械が積込まれた．時間的制約のために，器械の調整その他に不備の点があつたが，船上での調整修理の結果，東支那海，印度洋，南極海域等の磁気測量が実施され，地球磁気学上貴重な資料を得ることができた.

一方，固定観測所用プロトン磁力計 1 台を試作するという本来の目的に対しては，本邦中部にて使用するため，標準周波数として 2000 および 1900 *c/s* を有する装置を作製し，信号周波数との唸周波数をペン書きオッシログラフ記録上で数える方式とした．この磁力計は 1958 年 3 月一応完成し，神奈川県油壷に於て地磁気変化計と比較して良好な結果を得たので，1958 年 4 月 19 日の金環食に際しては，八丈島に於ける観測に実用された．これらの試験の結果，この形式の磁力計は固定観測所用プロトン磁力計としては一応満足できる性能を有することがわかつた.

本研究組織はさらに，南極地域観測用プロトン磁力計に類似した性能を有する海底地質探査用磁力計の製作に協力するほか，各種記録方式の研究，周波数直読方式の研究，ロケット塔載の可能性の検討等を行つた．また本研究組織に参加している各機関に於ては，それぞれの目的に応じて研究を進めていることはもちろんであるが，その結果は別の機会に発表されるであろうから，ここには重複をさけて，主として科学試験研究費補助金により製作した固定観測所用プロトン磁力計について報告することにする.

2. 研究組織

「プロトン磁力計の試作研究」に関する研究班の組織は次のようなものである.

分担事項	所属	氏名	分担事項	所属	氏名
記録方式の研究	東京教育大学 お茶の水女子大学 東京学芸大学	小島昌治 小川静子 鳥塚一男	比較測定	東京大学理学部 東京大学地震研究所	秋本俊一 上田誠也
標準周波計および増幅器の製作	日本電子光学研究所 同	関　利正 草鹿履一郎	比較測定および南極観測	東京大学理学部 東京大学地震研究所	永田　武 力武常次*
比較測定	建設省地理調査所 同 同	坪川家恒 瀬戸孝夫 田島　稔	比較測定およびロケット観測	東京大学理学部	福島　直
			海上観測	工業技術院地質調査所 同	佐藤光之助 長谷川　博

*) 代表者

3. 測定原理

プロトンの自由歳差運動を利用する地球磁場の測定原理については，上述の文献に詳細に報告されているから，ここではきわめて簡単に述べる．

プロトンは磁気モーメント μ をもつているから，偏極磁場 H_p を与えることにより，単位体積あたりの有効なプロトンの数を n とすれば，全体として

$$M_0 = n\mu \tag{1}$$

という磁気モーメントを発生することができる． H_p は地球磁場とそれに直角な人工磁場とよりなるが，前者は後者にくらべてはるかに小さいから， H_p は励磁コイルの発生する磁場と考えてよい．プロトンのスピンが 1/2 で熱平衡にあるときボルツマン分布に従うことを考えれば， n は

$$n = \frac{\mu N}{kT} H_p \tag{2}$$

で与えられる． N は単位体積中のプロトンの数， k はボルツマン常数， T は絶対温度である．

偏極磁場を充分長い時間与えた後， $t = 0$ で磁場を急に取りのぞいたとすれば，緩和時間を T_1 として

$$M = M_0 \, exp\,(-t/T_1) \tag{3}$$

であらわされるように帯磁が減少する． T_1 は水中のプロトンに対して約3秒である[2)].
磁場の急変にともなつて，プロトンは地球磁場のまわりに自由歳差運動を起し，その周波数 f は

$$2\pi f = \gamma F \tag{4}$$

となる．ここに F は地球磁場の全磁力， γ は gyromagnetic ratio というプロトンに固有の常数で，プロトンのスピン角運動量を $\hbar I$ としたときに

$$\mu = \gamma \hbar I \tag{5}$$

という関係がある．

結局，全体の磁気モーメントベクトルも周波数 f で歳差運動を起すことになる．励磁コイルを受信コイルに使えば，その軸方向の磁束密度成分は

$$4\pi M \cos 2\pi f t$$

という時間的変化をすることになるから，コイル中に誘起される電圧 V は，（3）を考慮して，

$$V = V_0 e^{-t/T_1} \cos 2\pi f t \tag{6}$$

となる．したがつて f を測定し，（4）式により F を求めることができることになる．
γ の値は水では

$$\gamma = (2.67528 \pm 0.00006) \times 10^4 \, sec^{-1} \, gauss^{-1} \tag{7}$$

と与えられている．したがつて f を c/s で測れば

$$F = 23.4861 f \, \gamma \tag{8}$$

という計算式が得られる．

地球磁場の不均一があると，各プロトンの周波数がわずかにちがつてくるから歳差運動の位相に不一致をきたし，信号の減衰時間は（6）で与えられるものより小さくなる．

4．装置の説明

1）構成

第1図は固定観測所用プロトン磁力計のブロック・ダイヤグラムを示したものである．

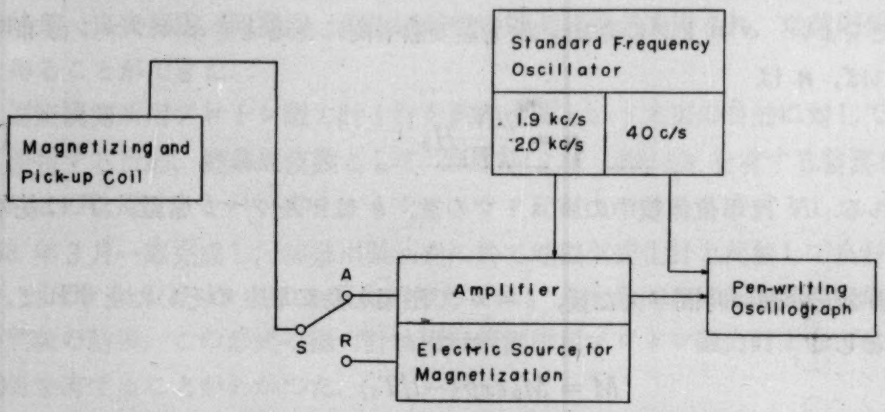
Standard Frequency Oscillator
1.9 kc/s
2.0 kc/s
40 c/s
Magnetizing and Pick-up Coil
A
S
R
Amplifier
Electric Source for Magnetization
Pen-writing Oscillograph

Fig. 1. Block diagram of the proton magnetometer.

2）偏極および検出コイル

内径67*mm*，内長70*mm*の円筒型硬質塩化ビニール製容器に蒸溜水約200*cc*をいれ，その外側に径1*mm*エナメル銅線を540回巻いてある．

3）励磁電源

励磁電源は交直両用とし，増幅器と同一シャーシーに納められている．直流用のときには，24V蓄電池をパネルの所定端子に接続する。

励磁電源からの電流（約5アンペア）で，励磁コイルを励磁するが，その際はスイッチSをR側とし，数秒後スイッチをA側に切り換えることにより，励磁コイルは検出コイルと兼用される．緩和時間を考慮して，プロトンを飽和値にまで配向するためには，数秒の励磁時間が必要である．

4）増幅器

検出コイルに誘起した信号電圧は約25*m*のシールド線にて結合変圧器に導かれ，前置増幅器，2*kc/s*狭帯域増幅器により増巾される．50*c/s*リジェクター2組を用いハム除去を行つている．この増幅器の電圧利得は約140*db*である．第2図に励磁電源および増幅器の結線図を示す．

増幅器の出力は，第2図に見られるように，平衡型混合回路に導かれ，標準周波電圧（標準周波発振器より端子J_6を経て混合回路に加えられる）との唸周波数が出力として取出される．この出力は記録計に導かれる．

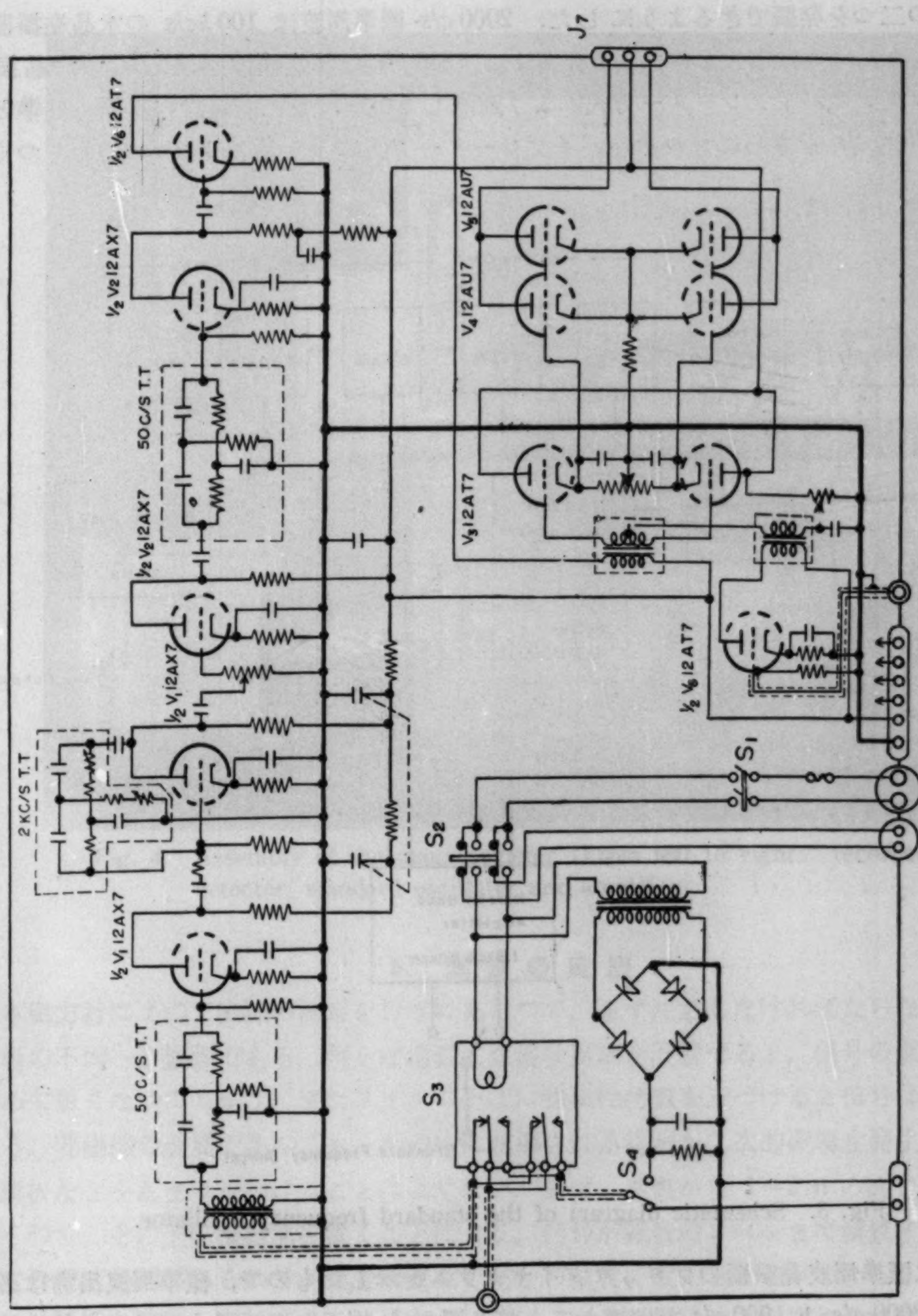
J7
½ V6 12AT7
½ V2 12AX7
50C/S T.T
½ V2 12AX7
½ V1 12AX7
2KC/S T.T
½ V1 12AX7
50C/S T.T
J1
V5 12AU7
V4 12AU7
V3 12AT7
J6
½ V6 12AT7
J5
S1
J4
J3
S2
S3
S4
J2

Fig. 2. Electric circuits of the electric source for magnetization and the amplifier.

5) 標準周波発振器

標準周波発振器としては，本邦中部に於て使用することを目的として，2000 および 1900 *c/s* の二つを発振できるようにした．2000 *c/s* 標準周波は 100 *kc/s* の水晶発振器から，ブロッキング発振方式２段により逓降し，1900 *c/s* 標準周波は 3.8 *kc/s* の水晶振発器から，マルティバイブレーター方式により逓降している．また記録計の時間の標準とするため，2000 *c/s* をさらにマルティバイブレーター方式により逓降して 40 *c/s* をつくつてある．

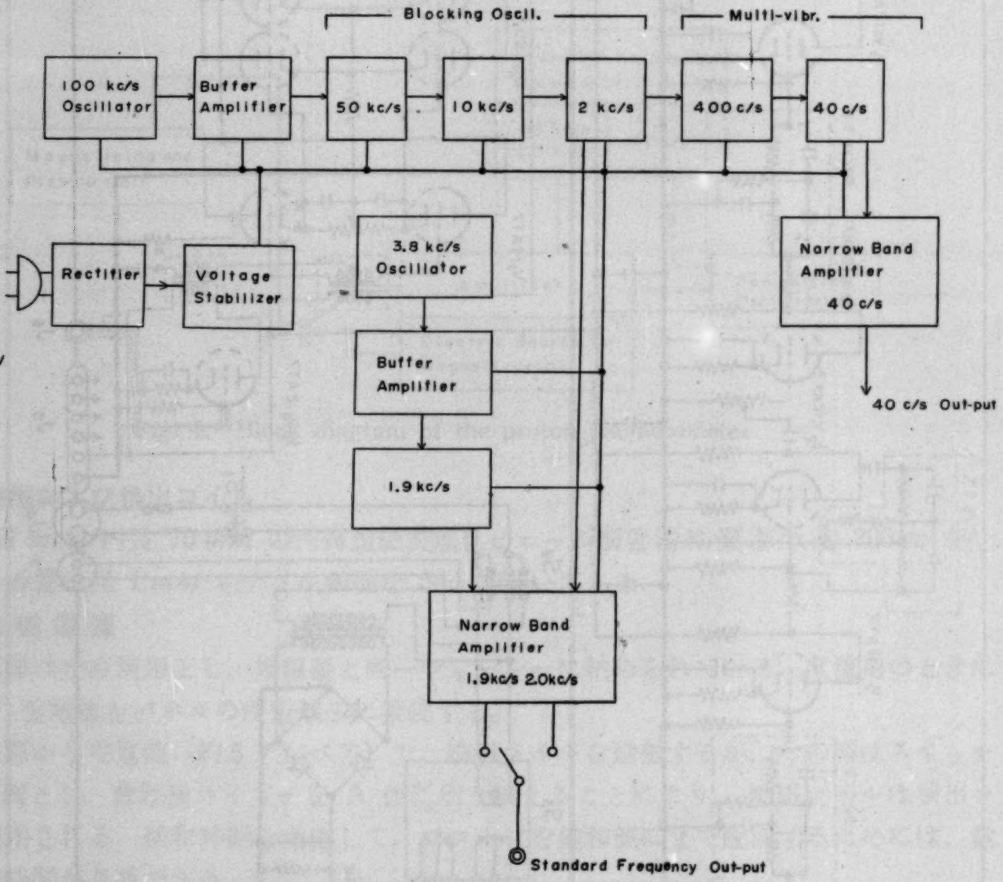
Blocking Oscil.
Multi-vibr.
100 kc/s Oscillator
Buffer Amplifier
50 kc/s
10 kc/s
2 kc/s
400 c/s
40 c/s
Narrow Band Amplifier 40 c/s
40 c/s Out-put
Rectifier
Voltage Stabilizer
A.C. 100 V
3.8 kc/s Oscillator
Buffer Amplifier
1.9 kc/s
Narrow Band Amplifier 1.9kc/s 2.0kc/s
Standard Frequency Out-put

Fig. 3. Schematic diagram of the standard frequency oscillator.

第３図は標準周波発振器のブロックダイヤグラムを示したもので，標準周波出力は必要に応じて 2000 *c/s* と 1900 *c/s* を切換えて，第２図の J_6 端子を経て混合回路に供給する．標準周波数発振器の結線図は省略する．

6) 記録計

記録計としては２成分ペン・オッシログラフを使用し，感度は 0.5 *mm/mA* で 60 *c/s* ぐらいまではほぼ平坦な特性を有する．記録紙の送りは通常 12.5 *cm/sec* である．

第4図は記録計，偏極および検出コイル，増幅器および励磁電源，標準周波発振器をとりまとめて，その外観を示したものである．

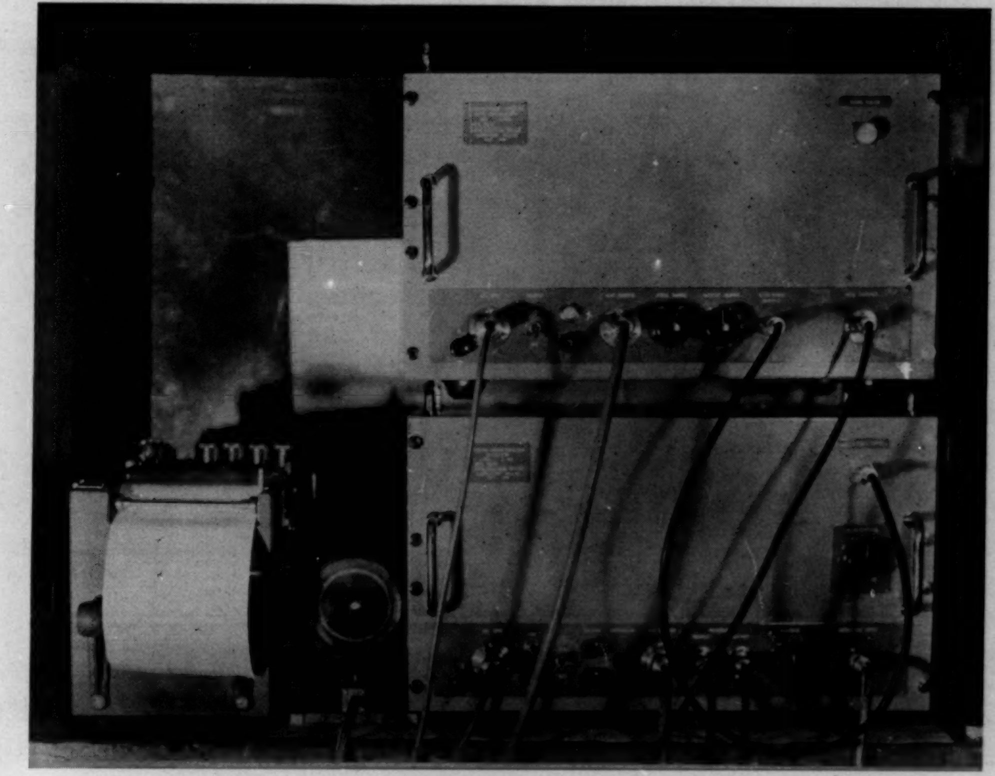

Fig. 4. Assembly of the magnetometer (From left to right: recorder, detector, standard oscillator and amplifier).

5. 測定の実際

本磁力計によつて実際の測定を行うにあたつて，まず注意しなければならないことは，磁場の不均一の影響である．例えば地表に直接検出部を設置すると，信号の継続時間がきわめて短くなつてしまう．またコイルのそばに強磁性物質を近づけると信号は全く出なくなる．非磁性の金属であつても，その中に誘導される電流が二次的磁場を発生するから，金属板などをあまり近づけることはよくない．通常，地表から 1～2 *m* の高さに木の台をつくつて，その上に検出部を置くことにより，信号が雑音のレベルまで減衰するのに3秒程度の継続時間があるので，信号周波数を充分の精度で数えることができる．もし，すべて直流電源を使用して雑音のレベルをさげれば，さらに継続時間を増加さすことも可能であろう．

測定のための操作はつぎのようなものである．増幅器および発振器のスイッチをいれて作動状態とした後，押しボタンスイッチ S_1 を押す．押しつづけている間は励磁電流が励磁コイルに送られる．つぎに記録計のモーターのスイッチをいれる．しかし，S_1 を押し

ている間は，モーターは回転しないようになつているので，記録紙は送られない．約10秒後，記録計の検流計スイッチを2成分ともいれると同時に押しボタンを離す．そうすると記録紙が送られ，信号および40 *c/s* 標準周波が記録されるから，数秒後に検流計スイッチおよびモータースイッチを切る．これで1回の操作が終了するわけであるが，適当な工夫をすれば1箇のスイッチによる単一操作も可能である．

測定記録としては，第5図および第7図のような記録が得られる．これらの記録上で，40 *c/s* 標準周波により1秒あるいは2秒を定め，その間にはいる信号の波数を求める．あるいは適当な信号波数をえらび，その間に標準周波数がいくつあるかを数える．このようにして記録紙の信号周波数が10〜20 *c/s* の場合には0.05 *c/s* の精度で読みとることは容易であるから，(8) 式により1 γ の精度が容易に保たれることになる．記録紙上の周波数がさらに少くなつてゼロ・ビートの状態に近くなつたり，あるいは50 *c/s* 以上にもなると，周波数の読取りがやや困難になるので，このような場合にはさらに50 *c/s* おきの標準周波との唸をとることが望ましい．

本装置に於ては，2000 *c/s* および1900 *c/s* の2つの標準周波があるので，例えば1900 *c/s* 標準周波を使用して唸周波数10 *c/s* を得た場合に，プロトンの歳差運動周波数が1910 *c/s* であるか1890 *c/s* であるかを直ちに判別できる．

6. 神奈川県油壺に於ける比較観測

1958年4月3—4日にわたつて，神奈川県油壷の臨海実験所構内に於て本磁力計の試験を行い，地磁気変化計と比較した．油壷に於ては，1952年以降地磁気3成分の連続観測を実施しており[8]，今回の比較観測では，磁力計検出部は観測壕より約400 *m* の距離に設置され，約21時間にわたつてほぼ30分から1時間間隔で測定を行つた．第5図は2000 *c/s* を標準周波とした場合の記録の1例である．

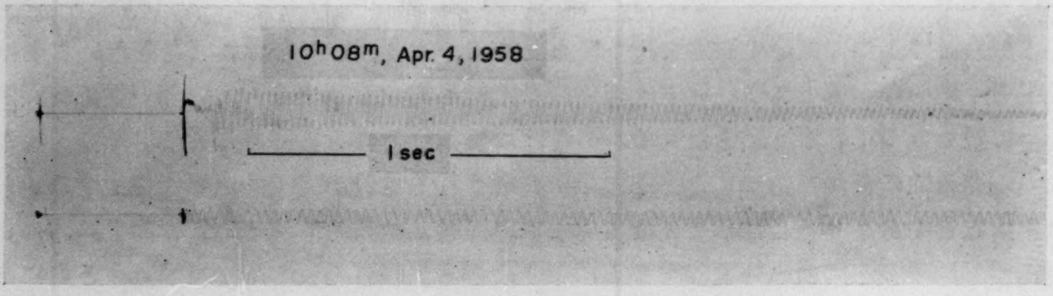

Fig. 5. One example of the records at Aburatsubo.

測定結果は第1表の通りであつた．

---

8) T. RIKITAKE, I. YOKOYAMA and Y. HISHIYAMA, *Bull. Earthq. Res. Inst.*, **33** (1952), 207.

Table 1. Results of the observation at Aburatsubo

Time (JST)	Standard freq.	Signal freq.	Total force	Time (JST)	Standard freq.	Signal freq.	Total force
Apr. 3, 1958	*kc/s*	*c/s*	γ		*kc/s*	*c/s*	γ
17*h* 30*m*	2.0	1948.00	45750.9	4*h* 08*m*	2.0	1948.56	45764.1
17 31	2.0	1947.44	45737.8	5 08	2.0	1948.58	45764.5
18 05	2.0	1947.68	45743.4	6 06	2.0	1948.64	45766.0
18 10	1.9	1947.54	45740.1	7 06	2.0	1948.89	45771.8
18 18	2.0	1947.44	45738.8	8 04	2.0	1948.36	45759.4
19 36	2.0	1947.88	45748.1	8 46	2.0	1947.38	45736.4
19 38	1.9	1947.84	45747.2	9 42	2.0	1946.31	45711.2
20 05	2.0	1947.96	45750.0	10 08	2.0	1946.20	45708.6
20 07	1.9	1947.88	45748.1	10 32	2.0	1945.92	45702.1
21 11	2.0	1947.96	45750.0	10 43	2.0	1945.75	45698.1
22 05	2.0	1948.40	45760.3	11 06	2.0	1946.15	45707.5
23 04	2.0	1948.16	45754.7	11 29	2.0	1946.30	45711.0
23 05	2.0	1948.16	45754.7	12 03	2.0	1946.52	45716.2
Apr. 4, 1958				12 24	2.0	1946.93	45725.8
0 03	2.0	1948.80	45769.7	12 25	1.9	1946.84	45723.7
1 03	2.0	1948.92	45772.5	13 08	1.9	1948.18	45755.2
2 05	2.0	1948.76	45768.8	13 38	2.0	1948.50	45762.7
3 05	2.0	1948.60	45765.0	13 39	1.9	1948.35	45759.1
3 17	2.0	1948.75	45768.5	13 50	2.0	1948.05	45752.1

測定結果を図に示すと，第6図の黒点のようになり，較差 70γ に達する地球磁場全磁力の日変化が顕著にあらわれている.

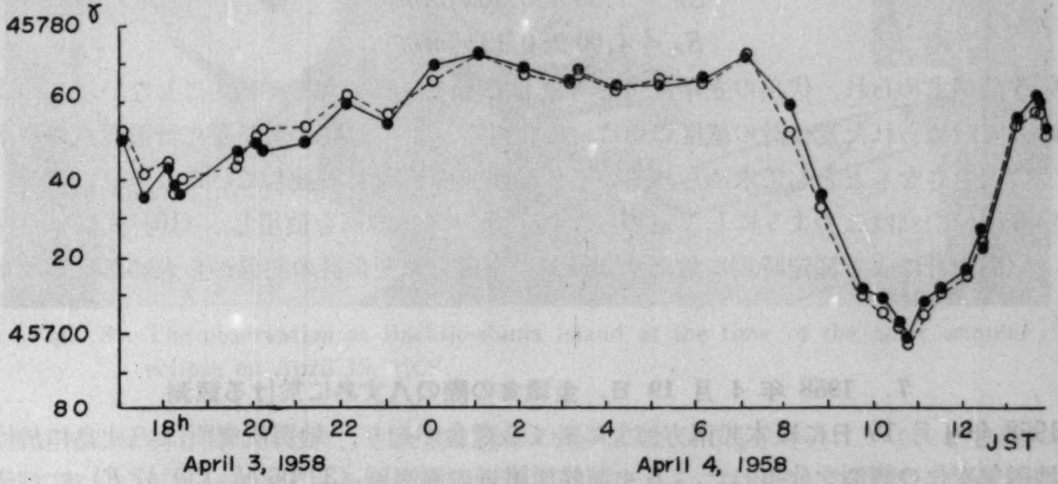

Fig. 6. Comparison of the results observed by the proton magnetometer (black circle) with those observed by a magnetograph of ordinary type (hollow circle). From Apr. 3 to 4, 1958 at Aburatsubo.

変化計の基線の絶対値の正確な値は不明であるから，基線より測つた水平分力および鉛直分力の変化をそれぞれ ΔH, ΔZ とすれば

$$F=\sqrt{(H_0+\Delta H)^2+(Z_0+\Delta Z)^2}$$

という関係がある．H_0 および Z_0 は水平分力および鉛直分力の基線値で，F は全磁力とし，その基線値を F_0 とする．$\Delta H \ll H_0$, $\Delta Z \ll Z_0$ であるから

$$F=F_0+\frac{H_0}{F_0}\Delta H+\frac{Z_0}{F_0}\Delta Z$$

という関係が得られる．これはまた基線値に対応する伏角を I_0 として

$$F=F_0+\cos I_0\cdot\Delta H+\sin I_0\cdot\Delta Z \qquad (9)$$

と書くこともできる．

変化計の平均感度をも検定する意味で，変化計記録を基線値から mm 単位で読取つて，水平分力および鉛直分力の変化をそれぞれ Δh, Δz とあらわせば

$$F=F_0+S_H\cos I_0\cdot\Delta h+S_Z\sin I_0\cdot\Delta z \qquad (10)$$

という関係があることになる．F はプロトン磁力計により測定されているから，F_0, $S_H\cos I_0$, $S_Z\sin I_0$ をパラメターとして，その値を最小自乗法により決定することができる．

計算の結果は

$$F_0=45750.4\pm0.5\,\gamma$$
$$S_H\cos I_0=0.849\pm0.070\,\gamma/mm$$
$$S_Z\sin I_0=2.993\pm0.095\,\gamma/mm$$

ということになり，S_H および S_Z がわかつているとして，伏角 I_0 が求められることになるが，S_H および S_Z の値は充分な精度では知られていないから，むしろ I_0 を与えて S_H, S_Z を求めることにする．1952 年の絶対測定の平均値[8)] は $I_0=48°22'$ であるから

$$S_H=1.28\pm0.10\,\gamma/mm$$
$$S_Z=4.00\pm0.13\,\gamma/mm$$

という値が求められ，伏角の永年変化を考慮してもこの値はほとんど変化しない．このようにして定められた変化計の感度の値は，変化計のコイル常数および変化計設置点の水平分力の大きさをもととして求められている値に誤差の範囲で一致している．

第6図の白点はこのようにして定められたパラメターの値を使用し，(10) 式によりプロトン磁力計による測定時刻に対応する時刻の全磁力を変化計の記録から求めたものである．

7. 1958 年 4 月 19 日，金環食の際の八丈島に於ける観測

1958 年4月 19 日には本邦南方海上に於て金環食が起り，地震研究所は八丈島に於ける地磁気変化の観測を分担した．八丈測候所附近の観測壕 (33°06′N, 139°47′E) に地磁気変化計を設置して，連続観測を実施するとともに，数 10 m 離れた地点にプロトン磁力計検出部を設置し，食甚をはさんで6時間にわたり，10 分間隔で測定を行つた．八丈島

は玄武岩質の火山であるので，地球磁場の局地的勾配が大きく，このために信号継続時間は約 2 秒ぐらいになつている．第 7 図は記録の 1 例で，測定実施中の状況は第 8 図に示してある．

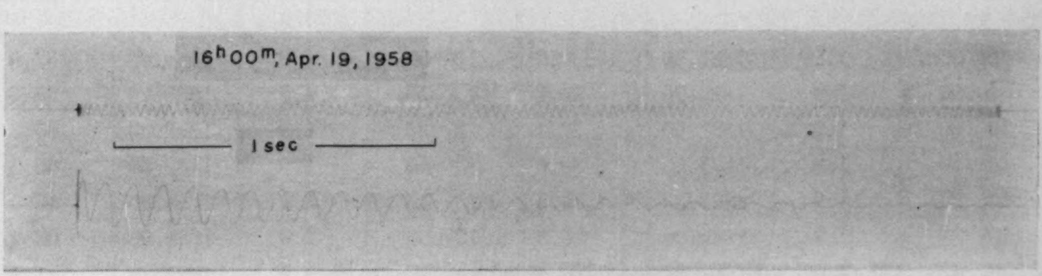

Fig. 7. One example of the records at Hachijo-shima Island.

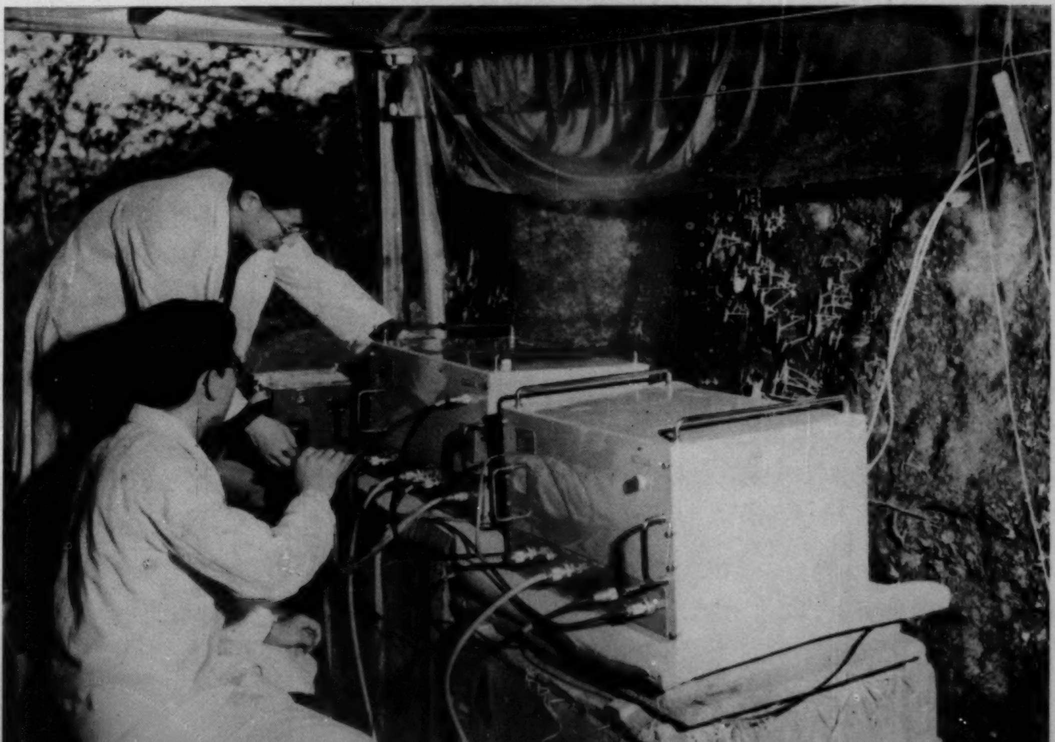

Fig. 8. The observation at Hachijo-shima Island at the time of the solar annular eclipse on April 19, 1958

測定結果は第 2 表に示され，また第 9 図中の黒丸によつても示されている．第 9 図には日食のはじめとおわりおよび金環食時間が書きこんである．本報告に於ては，日食と地磁気変化の関係を論じることは目的でないから，これは別の機会にゆずり，このような変化を測定したことを報告するにとどめる．

Table 2. Results of observation at Hachijo-shima Island

Time (JST)	Standard freq.	Signal freq.	Total force	Time (JST)	Standard freq.	Signal freq.	Total force
Apr. 19, 1958	kc	c/s	γ		kc	c/s	γ
9h 00m	1.9	1887.50	44330.0	*13h 00m*	1.9	1888.65	44357.0
9 35	1.9	1887.70	34.7	13 10	1.9	1888.70	58.2
10 00	1.9	1887.60	32.4	13 20	1.9	1888.80	60.5
10 10	1.9	1887.50	30.0	13 30	1.9	1888.80	60.5
10 20	1.9	1887.30	25.3	13 40	1.9	1888.80	60.5
10 30	1.9	1887.30	25.3	13 50	1.9	1888.90	62.9
10 40	1.9	1887.30	25.3	14 00	1.9	1889.25	71.1
10 50	1.9	1887.50	30.0	14 10	1.9	1889.35	73.5
11 00	1.9	1887.50	30.0	14 20	1.9	1889.42	75.1
11 10	1.9	1887.70	34.7	14 30	1.9	1889.40	74.6
11 20	1.9	1887.75	35.9	14 40	1.9	1889.40	74.6
11 30	1.9	1887.90	39.4	14 50	1.9	1889.27	71.6
11 40	1.9	1888.25	47.6	15 00	1.9	1889.15	68.8
11 50	1.9	1888.30	48.8	15 10	1.9	1889.00	65.2
12 00	1.9	1888.40	51.2	15 20	1.9	1888.86	62.0
12 10	1.9	1888.45	52.3	15 30	1.9	1889.00	65.2
12 20	1.9	1888.45	52.3	15 40	1.9	1889.10	67.6
12 30	1.9	1888.80	60.5	15 50	1.9	1889.10	67.6
12 40	1.9	1888.76	59.6	16 00	1.9	1889.00	65.2
12 50	1.9	1888.70	58.2	16 22	1.9	1889.00	65.2

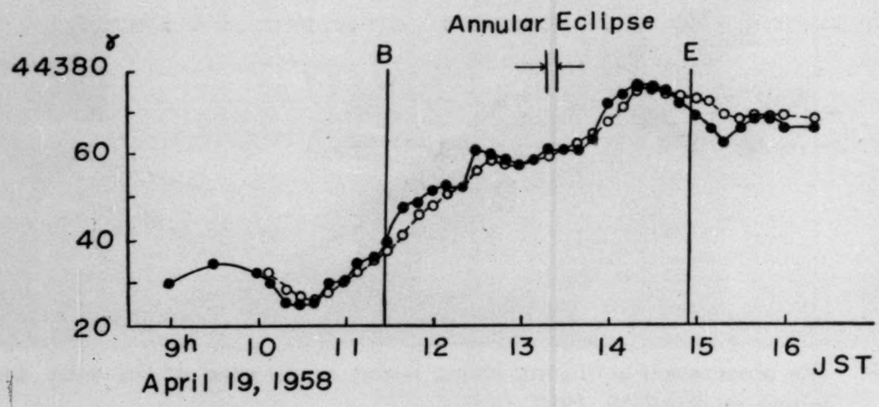

Fig. 9. Comparison of the results observed by the proton magnetometer (black circle) with those observed by a magnetograph of ordinary type (hollow circle). During the eclipse period on April 19, 1958 at Hachijo-shima Island.

変化計の対応する記録から，前節に準じて（10）式により計算すると

$$F_0 = 44383.8 \pm 0.3\,\gamma$$
$$S_H = 0.86 \pm 0.06\,\gamma/mm$$
$$S_Z = 1.51 \pm 0.08\,\gamma/mm$$

という結果が得られ，この値を用いて，変化計より得られた対応する時刻の全磁力の値を白丸で第9図に示してある．上述の計算には地理調査所型二等磁気儀による絶対測定の結果にもとづいて $I_0 = 43°52'$ としてある．

第9図を見ると，プロトン磁力計測定値と変化計記録よりの計算値との間に若干の不一致があるが，その原因についてははつきりしたことはわからない．

8. 性能に対する意見および将来の計画

油壷および八丈島に於ける試験の結果から判定して，本装置は固定観測点用としてはほぼ充分の性能を有し，注意して測定を実施することにより 1γ の精度で，地球磁場全磁力の絶対測定を行うことができる．測定は原子核固有の常数をもととしているから，温度その他の環境の変化に無関係に測定し得ることは，従来標準電池を基準として行つてきた絶対測定に比して，大きな利点である．従つて，各地磁気観測所にプロトン磁力計を設置して，絶対値の基準とすることはきわめて望ましいことである．

南極地域観測用および海上磁気測量用プロトン磁力計の成果からもわかるように，本方式の磁力計は動揺に対してきわめて鈍感である．この特徴を利用して，航空機用およびロケット用のプロント磁力計を早急に実用化することが望ましい．

今回試作したプロトン磁力計の欠点としては雑音がやや大きいことがあげられる．この点は改良を要する．また標準周波として 2000 および 1900 *c/s* を設けたが，実用上からはさらに 1950 *c/s* があることが望ましく，さもないと信号周波数が 1950 *c/s* に近いときに，周波数計数の精度が悪くなるおそれがある．また器械全体を小型軽量化することもさらに可能と考えられる．

将来の計画としては次のような点が重視される．

1) 本研究組織の東京教育大学グループによつて研究されたように，周波数直読方式を実用化し，できればカードにパンチすることを考える．

2) 米国に於て実用化されていると伝えられるように，トランジスターを利用して，きわめて軽量小型のプロトン磁力計をつくり，磁気探鉱に役立てる．

3) ロケットに搭載可能な超小型プロトン磁力計およびテレメータータリングの研究を促進する．

終りに本研究に対し財政的援助を賜つた文部省当局に感謝の意を表する．

24. *A Proton Magnetometer*.

By Research Group for Proton Magnetometer.

A nuclear precession magnetometer is constructed by the Research Group for Proton Magnetometer. The group, represented by T. RIKITAKE of the Earthquake Research Institute, has been active since April, 1957. Although the group was first formed in the hope of constructing a practicable magnetometer of nuclear precession type for station-use, the members of the group have cooperated in constructing the magnetometer which was used by the Japanese Antarctic Research Expedition on the Antarctic, Indian and Chinese Oceans. A magnetometer for magnetic prospecting on the sea was also designed and constructed with the cooperation of the group. Some of the members of the group have studied various methods of recording related to magnetometers of the principle, direct counting method of signal frequency, possibility of rocket-mounting and so on.

In this report, however, only the magnetometer specially designed for a magnetic station is described. The instrument was made with the financial help of the Research Grant from the Ministry of Education.

The principle of the magnetometer is more or less the same as those appearing in many references. Protons in 200*cc* water contained in a bottle are magnetized by the magnetic field produced by the magnetizing coil wound around the bottle. When the electric currents in the coil are abruptly switched off, precession of protons around the earth's magnetic force is excited. By using the magnetizing coil as the pick-up one as well, the induced electromotive force is introduced to the narrow-band amplifier. Since the frequency of the precession is slightly less than 2000*c/s* in the central part of Japan, beat frequency can be easily recorded by mixing the signal with the standard 1.9 or 2.0 *kc/s* frequencies. The standard frequencies are supplied from the standard oscillator containing quartz oscillators. A two-component pen-writing oscillograph is used for recording. With the aid of the 40*c/s* standard frequency which is also supplied from the standard oscillator and is recorded on the same paper, the beat frequency is readily counted with an accuracy of 0.05*c/s*.

Comparisons of the present instrument with magnetic variometers have been made at Aburatsubo and Hachijo-shima Island. It is likely that the magnetometer can be used at ordinary magnetic stations with satisfactory accuracy.

The research group is now going to continue its activity in relation to construction of a portable magnetometer on the same principle. A direct reading or punched-card instrument will also be attempted in the future.

昭和33年10月27日印刷
昭和33年10月31日発行

東京都文京区本富士町一番地
東京大学構内
編纂兼発行者　東京大学地震研究所

東京都新宿区山吹町一八四番地
印刷者　笠井康頼

東京都新宿区山吹町一八四番地
印刷所　株式会社 国際文献印刷社

売捌所
東京都中央区日本橋通二丁目六番地
丸善株式会社

Sold by Maruzen Co., Ltd., Nihonbashi-dôri, Chûô-ku, Tôkyô.
Price of this copy: 624 Yen. (Postage exclusive.)

BULLETIN OF
THE EARTHQUAKE RESEARCH INSTITUTE
UNIVERSITY OF TOKYO

Vol. 36, Part 3. September, 1958.

Contents.

Papers and Reports.

Page
14. S. UYEDA, T. YUKUTAKE and I. TANAOKA, Studies of the Thermal State of the Earth. The First Paper: Preliminary Report of Terrestrial Heat Flow in Japan. (in English) 251
15. K. KANAI and S. YOSHIZAWA, The Amplitude and the Period of Earthquake Motions. II. (in English) 275
16. K. KANAI, A Study of Strong Earthquake Motions. (in English) 295
17. S. OMOTE, S. KOMAKI and N. NAKAJIMA, Seismic Wave Types in a Sand Layer near a Small Explosion. (in English) 311
18. The Research Group for Explosion Seismology, Crustal Structure in Northern Kwantô District by Explosion-Seismic Observations. Part I. Description of Explosions and Observations. (in English) 329
19. T. USAMI, T. MIKUMO, E. SHIMA, I. TAMAKI, S. ASANO, T. ASADA and T. MATUZAWA, Crustal Structure in Northern Kwantô District by Explosion-Seismic Observations. Part II. Models of Crustal Structure. (in English) 349
20. K. KANAI and T. TANAKA, Self-levelling Vibrograph. (in English) 359
21. T. ICHIMURA, Geological Considerations on Plagioliparite and Associated Extrusives Exposed in the Tendō-Yamagata-Kaminoyama District, Yamagata Prefecture. (in English) 369
22. T. ICHIMURA, Heavy Minerals in Metamorphosed Sediments from the Tsukuba District, Ibaraki Prefecture. (in English) 395
23. H. TSUYA, I. MURAI and Y. HOSOYA, Size Characteristics of the Pumice Deposits distributed in the Vicinity of Komoro on the Southwest Foot of Asama Volcano. (in Japanese) 413
24. Research Group for Proton Magnetometer, A Proton Magnetometer. (in Japanese) . 433

(For the papers written in Japanese or in occidental languages, the abstracts are given in occidental languages or in Japanese respectively.)

BULLETIN OF THE EARTHQUAKE RESEARCH INSTITUTE,
UNIVERSITY OF TOKYO. Vol. 36, Part 4. December, 1958.

東京大學
地震研究所彙報

第36號　第4册

昭和33年12月

目　次

論文及報告

頁
25. Phototransistor を使つた Starter の試作（英文）……………… 河角　広・嶋　悦三・柴野睦郎・柳沢馬住 447
26. 地震断層の性状について（英文）……………………………… 笠原慶一 455
27. 地震観測用スターター（邦文）………………………………… 田中貞二 465

所　報

索　引

(The titles in occidental languages are given on the back cover.)

地震研究所彙報は，年４回定期に（ただし，第１号より第６号までは不定期に，第７号は３冊として刊行された），彙報別冊は不定期に刊行される．

この彙報に載せられた論文及び報告についての責任は，すべてその著者のみにある．

この彙報についての照会通信は，すべて東京大学地震研究所長にあてられたい．

The Bulletin is published quarterly. (Vols. 1-6 were published at irregular intervals and Vol. 7 consisted of three parts.)
Supplementary Volume is published at irregular interval.

The authors of the papers alone are responsible for the statements and opinions contained in their respective papers.

All communications relating to this Bulletin should be addressed to the Director of the Earthquake Research Institute, University of Tokyo, Japan.

Earthquake Research Institute, University of Tokyo
Address:
No. 1, Motofuji-cho, Bunkyo-ku,
Tokyo Metropolis, Japan.
Telephone: 92-3161-Extension 6506
Cable address: ZISINKEN, TOKYO.

東京大学地震研究所
所在地
東京都文京区本富士町一番地
電話　小石川 92―3161（代）構内 6506
電略　ブンケウ　トウダイ　ヂシン

**Bulletin of the Earthquake
Research Institute**
Vol. 36 (1958), pp. 447-453

25. *A Seismographic Starter Using a Phototransistor.*

By Hirosi KAWASUMI, Etsuzo SHIMA, Muturo SIBANO
and Masumi YANAGISAWA,

Earthquake Research Institute.

(Read Sept. 16, 1958.—Received Sept. 30, 1958.)

1. Starters of recording apparata for seismic observations have frequently been used since early times for the purpose of saving the care and expense of continuous observations. Recently demands for seismograms rendering detailed analyses of earthquake motions have been made by both theoretical and practical workers. To cope with this demand, fine recording or high speed drivings of recording papers and films have been introduced in earthquake observations. But for engineering purposes, it has been realized that motions of twenty cycles or more per second must be made legible. This raised a new problem, since continuous observation on photographic paper driven with such a high velocity involves technical difficulties in addition to the high expense. If we are to use a revolving drum type record receiver, it is very difficult to obtain a light spot bright enough to leave its trace, in high frequency oscillations, on the photographic paper without fogging the background in the course of the long exposure. These circumstances compel us to use a recording apparatus equipped with a starter. The light source may then be made bright enough, and the recording paper may be driven fast enough to make the record of high frequency oscillations easily legible.

Although we cannot but lose initial portions of seismograms if we use a starter, the amplitudes of P-phases are usually small in comparison with those of S-phases, and the loss is of no vital consequence from the engineering point of view. With these facts in mind, a number of starters have been made and used practically. All of them have their respective merits, but some are of too low sensitivities as they only are set free by a strong earthquake or by an earthquake strong enough to be felt by unaided human senses, while others are made very sensitive by means of electronic amplifiers, and are safely used only by trained operators. These disadvantages make it difficult to use them in an area of low seismicity or in rural districts where trained operators are not easily accessible. Additional difficulty may also be found in areas where no commercial AC power supply is available.

But recently phototransistors with sensitivities as high as 10,000 times of the photocells have been made and used in various fields. If we use one in our starter, the use of a delicate electronic amplifier and the need of a trained operator may be dispensed with. With this in mind, we have made a starter for a seismograph using a phototransistor. In it, the transistor is illuminated continuously by the light from a lamp after being reflected by the mirror of a galvanometer, which is connected to a pickup. The sustained collector current of the transistor keeps, by the first relay, breaking the circuits to operate the record receiver. By the onset of an earthquake motion with an amplitude larger than a prescribed limit, the light on the phototransistor is deflected to nullify the collector current, and the record receiver may begin its function.

This starter may also be used where no AC power supply is available, and it has a tolerable sensitivity without using an electronic amplifier. The reason for not using the usual mechanical starter is the difficulty of obtaining a sufficient sensitivity by such means. But our new device is not without drawbacks, because the use of a phototransistor makes it necessary, as we have mentioned, to constantly illuminate the transistor. This will necessitate special consideration for minimizing the required power supply to the light source. We have endeavoured to do so, and have been able to make two storage batteries maintain the necessary power for half a month without recharging, which we will explain further later. Other points provided for in the construction of our starter are as follows:

a) It is stably responsibe to high frequency oscillations up to at least 30 cycles per second, with a prescribed threshold amplitude of the element of the ground motions.

b) It dispenses with a dummy pickup, and uses in its stead the same pickup used for the observation also for the starter.

c) It avoids the trouble encountered in emergencies such as breaking of the filament of the lamp or permanent deflections of the light of the lamp which is illuminating the phototransistor in too strong an earthquake.

2. The final model is described schematically in Fig. 1. It's function will be explained briefly as follows. First the galvanometer for the starter is connected through the relay R2 to the pickup, and the

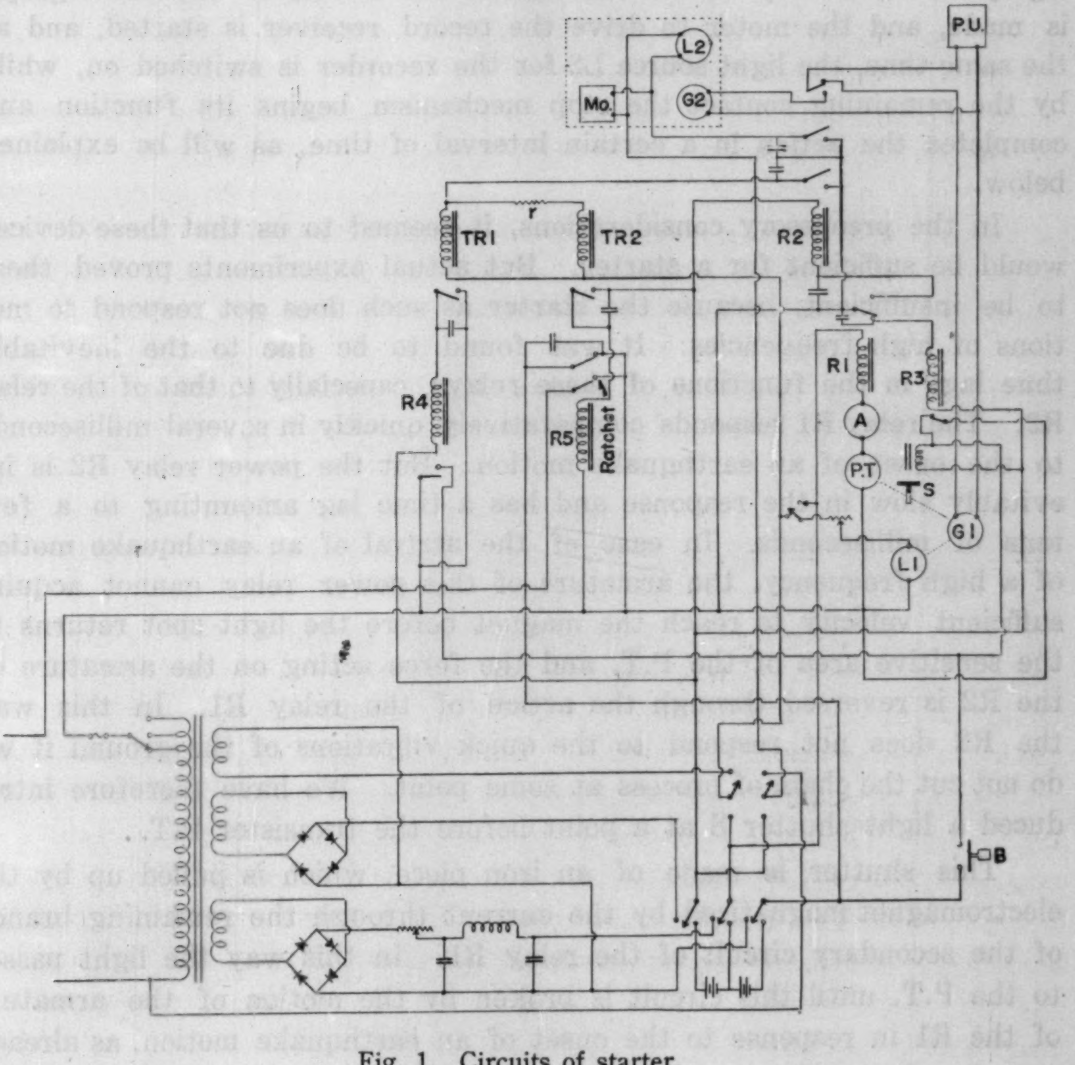

Fig. 1. Circuits of starter.

light from a lamp L1 is reflected by the mirror of the galvanometer G1, and illuminates the phototransistor P.T.. The collector current from the P.T. flows through the relay R1, by which action all functioning of the record receiver is kept in suspense. By the onset of an earthquake motion, the galvanometer mirror is rotated, and the light spot on the P.T. is deflected away from its sensitive area. The collector current will then be nullified, and the contact point of the relay R1 will go back and make the secondary circuit. The current will now flow through the coil of R2, and the magnet will pull the armature with three contacts. By the first contact the pickup P.U. (which has been connected to the galvanometer G1) is switched back to the galvanometer G2 in the oscillograph unit, and by the second contact the circuit to the oscillograph is made, and the motor to drive the record receiver is started, and at the same time, the light source L2 for the recorder is switched on, while by the remaining contact the stop mechanism begins its function and completes the action in a certain interval of time, as will be explained below.

In the precursory considerations, it seemed to us that these devices would be sufficient for a starter. But actual experiments proved them to be insufficient, because the starter as such does not respond to motions of high frequencies. It was found to be due to the inevitable time lags in the functions of these relays, especially to that of the relay R2. The relay R1 responds comparatively quickly in several milliseconds to the onset of an earthquake motion. But the power relay R2 is inevitably slow in the response and has a time lag amounting to a few tens of milliseconds. In case of the arrival of an earthquake motion of a high frequency, the armature of this power relay cannot acquire sufficient velocity to reach the magnet before the light spot returns to the sensitive area of the P.T. and the force acting on the armature of the R2 is reversed through the action of the relay R1. In this way the R2 does not respond to the quick vibrations of the ground if we do not cut the chain of process at some point. We have therefore introduced a light shutter S at a point before the transistor P.T..

This shutter is made of an iron piece, which is pulled up by the electromagnet magnetized by the current through the remaining branch of the secondary circuit of the relay R1. In this way the light passes to the P.T. until this circuit is broken by the motion of the armature of the R1 in response to the onset of an earthquake motion, as already stated. In such an event, the shutter is released and begins to fall. If the earthquake motion is of high frequency, the armature of the R1 returns to its original position quickly, and pulls up the falling iron piece of this shutter. But if the attraction of the electromagnet is adjusted to be not much stronger than the force due to gravity, the falling motion of the shutter which has started a moment ago can be made almost infallible. To test these circumstances, we experimentally connected an oscillator to the galvanometer G1 in our starter and the output voltage of the oscillator was very slowly increased until the amplitude of the light spot at the P.T. slightly exceeded the threshold value. In this way we could find that our starter functions very stably even by the oscillations of as high as 50 cycles per second. Part of provision a) mentioned above is thus fulfilled.

The rest of provision a) and provision b) is accomplished by the action of the second contact of R2, because we use in the starter a similar galvanometer to that used in the oscillograph unit, while the one pick-up used in the starter is switched over to the galvanometer G2 in the oscillograph without a changing. According, therefore, as the seismometer in use is designed to record the displacement, or the velocity or the acceleration of the ground motion, the same element of the ground motion actuates the starter when its amplitude exceeds the prescribed threshold value of the element.

Now the function of the stopping mechanism will be explained. By the third contact of R2, the electric current begins to flow through the thermal relays TR1 and TR2. This current heats the bimetal strips each of which is provided with an electric contact. These bimetal strips will thus slowly be bent, and the contact point attached to the strip in the TR1 will touch another contact point in a certain prescribed time, say one minute, while the contact on the strip of the TR2 will touch the other in 65 seconds in our model. By these contacts, circuits are made to pull the armatures of the relays R4 and R5. Then by the relay R4 the electric current flows through the electromagnet to pull up the shutter, and the light of the lamp L1 is now able to illuminate the P.T.. The relay R1 and consequently all the other parts of our starter thus return to the original state, provided the light spot remains on the sensitive area of the P.T.. In case when the filament of the L1 would have been broken or the mirror of the G1 would have been shifted by too strong an impulse and others, the relay R1 begins its function and the record receiver starts over again. But as the thermal relays have already been heated and have no time to cool, the TR2, which has a longer time lag than the TR1 and has not yet made contact, now makes contact in an appreciably short interval of time, and the R5 will then be actuated to cut the main current flowing through the secondary circuits of this relay. And by this break of the negative side of all the circuits, all the function of the record receiver will be stopped. As a ratchet is provided to cramp the armature of the R5 the stopping action is securely maintained. It cuts the chain of infinite succession of the function of this starter, which might occur if it were not for the TR2, R5 and the ratchet. Thus provision c) is fulfilled.

In the event of such an emergency when the ratchet has caught the armature of the relay R5, we first examine the cause and eliminate it by changing the bulb L1 or readjusting the light spot coming from the mirror of galvanometer G1 etc.. And second we push the button B to raise the shutter S and then release the ratchet. If we can thus assure the collector current flowing through ammeter A we release the button B. Thus the state of perfect preparation is regained.

The resistance r is inserted in the primary circuit of the TR2 in order to prolong the time lag by several seconds as compared with that of the TR1, because it is necessary to resume the initial state of perfect preparation for the recording in case when all the recording system is in good condition. This state is easily verified by the needle of the ammeter A, which indicates the collector current of the phototransistor.

The capacities in Fig. 1 are used as usual to reduce the sparks in the gaps of the contacts in the relays and to suppress undesirable vibrations of the armatures which considerably retard the final touches of the contacts of the relays concerned.

3. The main drawback of our starter, as we have mentioned, is the constant power loss due to keeping the lamp L1 lit and keeping the shutter pulling up, so we endeavoured to minimize the necessary current. We selected a suitable bulb for the lamp L1 and introduced an appropriate optical lens system for that purpose. Fortunately the phototransistor has its maximum sensitivity for the infrared rays so that the filament voltage of the lamp can be lowered appreciably. We can safely drop the voltage as low as 2.5 volts from the normal 6 volts without dropping the collector current below the working level of 2 milliamperes of the relay R1. The necessary power supply is about 0.7 ampere in our lamp at that voltage, while the electromagnet operating the shutter S requires about 0.1 ampere, so that total current constantly needed is about 6 watts at maximum.

The necessary current to operate the oscillograph is 5 amperes at 12 volts. But as the working time is only 1 minute, this loss of power is almost negligible in comparison with the above mentioned constant consumption of 6 watts. If we use two batteries of 6 volts with a capacity of 200 ampere hours each, and exchange their line up at the end of one week, we can safely use the batteries another week more without recharging. Perhaps it will be wise to change one of the batteries every week alternately with a recharged battery.

In view of general usage of these recorder sets also at places where AC power supply is available, we have shown in Fig. 1 a line up of a model to be operated by AC as well as by DC sources. It is pro-

vided with a rectifier circuit and turn over switches from the DC storage batteries.

---

25. Phototransistor を使つた Starter の試作

地震研究所
河角広
嶋悦三
柴野睦郎
柳沢馬住

Phototransitor を使用した Relay 回路による Starter を試作したが充分使用に耐えることがわかつた.

設計にあたつて特に注意したのは次の点である.

a) 交流 100 V, 50～60 サイクル或は直流 12 V 何れでも使用出来る.

b) 30 c/s 以下の周波数できめられた振巾（加速度，速度，変位，何れでもよい）の地震動に対してはすべて安定に作動する.

c) Dummy の換振器は使用しない.

d) Lamp が切れるというような事故に対しては最小限に被害を喰いとめる様にする.

欠点は Lamp をつけ通して置かねばならない事で常時 6 W の電力を消耗する. このため直流を使用する場合には Battery の消耗に注意しなければならない. 例えば 6 V 200 A.H. の Battery 2 ケを使用し，Lamp に電力を供給する方の Battery を一週間で他方と交換すると，充分充電してあれば 2 週間は連続観測することが出来る.

which with a rectifier circuit and turn over switches from the DC storage batteries.

86. Photoelectric ... Starter ...

[illegible]

BULLETIN OF THE EARTHQUAKE
RESEARCH INSTITUTE
Vol. 36 (1958), pp. 455-464

26. *Physical Conditions of Earthquake Faults as Deduced from Geodetic Data.*

By Keichi KASAHARA,

Earthquake Research Institute.

(Read July 15, 1958—Received September 30, 1958.)

Summary

Horizontal displacement of triagulation points around an earthquake fault provides valuable information about physical conditions of faulting. The writer applies his theory of a strike-slip fault to some actual cases for the purpose of finding their probable conditions, such as the depth, the magnitude of stress change in the fault plane, and the strain energy associated with the crustal deformations. The analysis is effected for the San Andreas fault, the Gômura fault, the Tanna fault, the Imperial Valley fault, and the Fairview Peak fault, geodetic data of which have been reported in detail by several geophysicists.

It is proved that these faults are as deep as 6～15 km approximately, the San Andreas fault being the shallowest whereas the Gômura fault and the Fairview Peak fault are the deepest. This tendency seems to be in good harmony with distribution of their focal depths which were determined seismometrically. The stress change and the total strain energy are also estimated as shown in Table 1, where the rigidity is assumed as 5×10^{11} c.g.s.. The agreement of the strain energy with that of seismic waves can be seen in the respective cases, which confirms the view that sudden occurrence of such a faulting is the immediate cause of the earthquake.

Another notable bit of information is also obtained from the triangulation data. Theory predicts antisymmetric distribution of v_0 (horizontal displacement of triangulation stations) on both sides of a fault. In the actual distribution of v_0, however, this characteristic is more or less disturbed by overlapping of another type of deformation. Quantitative discussion of this effect leads us to a conclusion that it can be attributed to strain accumulation in the earth's crust which developed gradually before the earthquake.

1. Introduction

The significance of faulting as the immediate cause of a great earthquake was first pointed out by H. F. Reid when he proposed the elastic rebound theory⁽¹⁾. This idea has attracted the notice of many seismologists, especially of those in the United States and Canada, who worked out laborious investigations of earthquake-generating mechanism on the basis of this hypothesis. Although Reid's model seemed to provide a reasonable explanation for the fundamental characteristics of a strike-slip fault, more detailed examination was necessary for its widespread acceptance.

The present writer conducted, in his previous papers, a study of the nature of earthquake origins, wherein he proposed an improvement of the model⁽²⁾. It is proved theoretically that this model provides more reasonable explanation for the crustal deformation which appears around the fault. Applying the theory to the actual geodetic data, we are able to estimate the probable conditions of the fault, such as the depth, the stress change in the fault plane, and the total strain energy.

The similar model has also been investigated by L. Knopoff, recently⁽³⁾. With the aid of theory of electrostatic field he showed an exact solution for the problem, with which the writer's results agreed practically. P. Byerly and DeNoyer have presented another theory of crustal deformation for the purpose of estimating the depth and the energy of some earthquake faults⁽⁴⁾. Their model assumes constant amplitude of deformation with depth, which is different from the one taken by Knopoff and the writer.

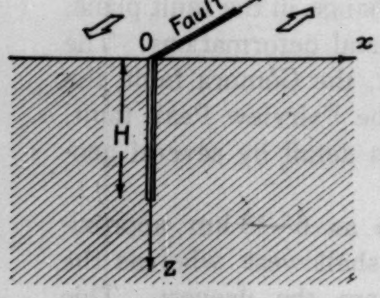

Fig. 1. Fault origin model fo earthquakes.

On the basis of these theories we are, now, able to discuss physical conditions of an earthquake fault, provided it is of strike-slip type and the deformation around it is known in detail by precise geodetic means. Accumulation of this sort of knowledge would be very useful for further investigations of the mechanism of great earthquakes, so the writer intends to study more examples, to which the fault model is applicable.

---

1) H. F. REID, *Bull. Dept. Geol. Sci., Univ. California*, **6** (1911), 413–444.

2) K. KASAHARA, *Bull. Earthq. Res. Inst.*, **35** (1957), 473–532; *ibid.*, **36** (1958), 21–53. *Journ. Phys. Earth*, **6** (1958), 15–22.

3) L. KNOPOFF, *Geophys. Journ. R.A.S.*, **1** (1958), 44–52.

4) P. BYERLY and J. DENOYER, *Contributions in Geophysics in Honor of Beno Gutenberg* (1958), 17–35.

2. Method of analysis

The method of the following analysis is based on the fault model which has been presented previously[5]. It is assumed that the earth's crust (homogeneous and perfectly elastic) is subject to a uniform shear stress, which increases with time and causes a fracture plane when it exceeds the strength of the medium. We also assume that the fracture is represented by a vertical plane of infinite length and of finite depth, in which the initial shear stress is liberated (Fig. 1). With the aid of the theory of elasticity, we calculate mathematically the deformation which is to be observed after the fracture. Fig. 2 illustrates the distribution of v_0 (displacement of a point at the earth's surface) diminishing with distance from the fault, in which the depth of the fault (H) is taken as a parameter.

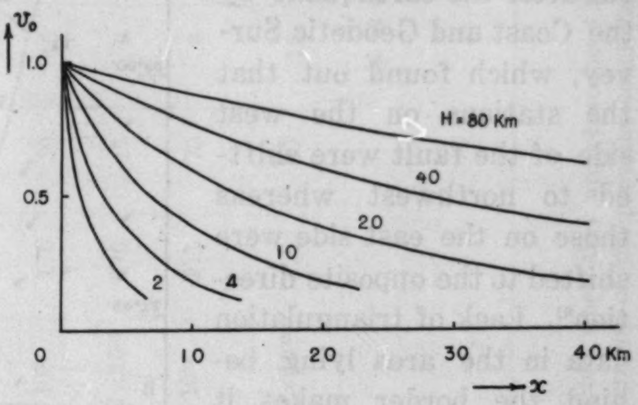

Fig. 2. Diminution curves of v_0 with distance from the fault (x).

These curves indicate that the earth's deformation predominates only in the limited regions lying on both sides of the fault and that the greater the value of H is, the wider the region of deformation becomes. Such a tendency being in good harmony with some of the observational data, we are able to find out the most probable value of H from their comparison. The theory also provides a way to compute the stress change in the fracture plane, $(Y_x)_0$, and the total amount of strain energy, E_f, as the functions of H, L, μ, v_{00}, where these symbols denote, respectively, the depth, the half-length of the actual fault, the rigidity of the crust, and the value of v_0 at the fault trace.

3. Data used in the analysis

The following analysis is carried out for the cases of the California earthquake (1906), the Tango earthquake (1927), the North-Izu earthquake (1930), the Imperial Valley earthquake (1940), and the Fairview

---

[5] *loc. cit.*, 2).

Peak earthquake (1954), all of which are accompanied by strike-slip faults. Descriptions of the first three cases have already been given in the previous papers, so that the following description is given only of the last two, which are newly added to our discussion.

The Imperial Valley fault (1940)

A great earthquake took place on May 18, 1940 in the Imperial Valley, California. This earthquake was accompanied by a long fault which was traceable across the epicentral area. Resurvey of the triangulation network over the area was carried out after the earthquake by the Coast and Geodetic Survey, which found out that the stations on the west side of the fault were shifted to northwest whereas those on the east side were shifted to the opposite direction[6]. Lack of triangulation data in the area lying behind the border makes it impossible to get complete knowledge about the deformation. However, geological survey proves that the fracture extended to several tens of kilometres south of the border. Taking this fact into account, we assume that movements of the triangulation stations along the border line represent the most predominant part of the deformation. On this assumption, we plot the amplitudes of displacement

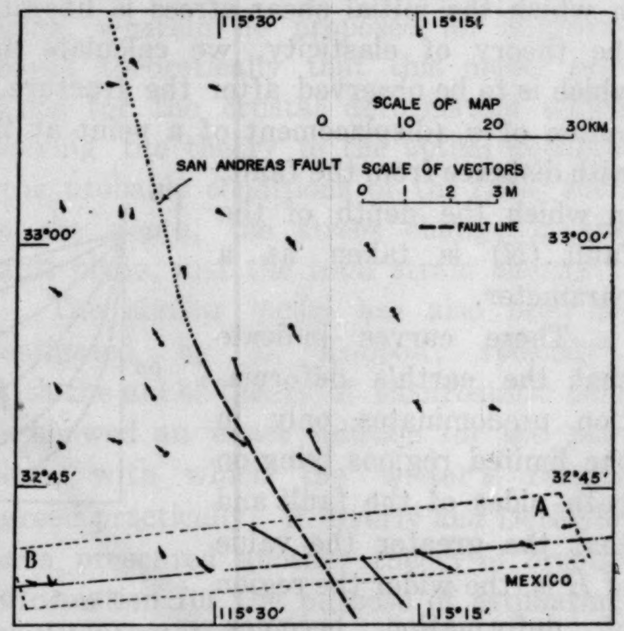

Fig. 3. Movements of triangulation stations around the Imperial Valley fault (after C. A. Whitten).

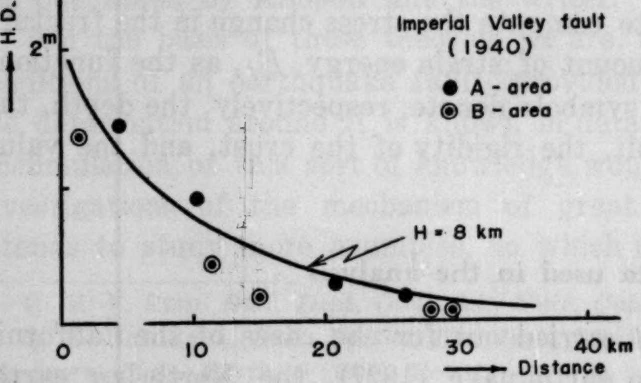

Fig. 4. Diminution curve of v_0 in the Imperial Valley area.

---

[6] C. A. WHITTEN, *Journ. Coast and Geodetic Survey*, **2** (1949), 84–88.

Table 1. Physical Conditions of Earthquake Faults*)

Name	Main Shock					Fault						Remarks
	Date	Epicentre	Depth	M	E_s	v_{00}	$2L$	H	$2L/H$	$(Y_x)_0$	E_f	
					ergs	m	km	km		c.g.s.	ergs	
San Andreas	1906 IV 18	38°N 123°W	Shallow	$8^1/_4$	2×10^{24}	2.5	440	6	73	2.8×10^{8}	3×10^{24}	$H=3.2$ km (KNOPOFF) $H=10$ km (BYERLY & DENOYER)
Gômura	1927 III 7	35.6°N 135.2°E	10 km	7.5	10^{23}	1.5	30	15	2	5×10^{7}	4×10^{22}	
Tanna	1930 XI 26	35.1°N 139.0°E	0~5	7.0	2×10^{22}	2.0	15	8	2	1.2×10^{8}	3×10^{22}	
Imperial Valley	1940 V 18	32.7°N 115.5°W	Shallow	6.7	10^{22}	2.1	70	8	10	1.3×10^{8}	1.5×10^{23}	$H=12$ km (BYERLY & DENOYER)
Fairview Peak	1954 XII 16	35.2°N 118.1°W	15	7.4	6×10^{22}	1.5	60	15	4	5×10^{7}	7×10^{22}	$H=23$ km (BYERLY & DENOYER)

(μ is assumed as 5×10^{11} c.g.s.)

---

*) Numerical values of some items are corrected when they are reproduced from the previous papers. However, such correction is not so remarkable as to cause great alteration of the previous conclusions.

vectors for the eleven stations mentioned in Fig. 4, where data from both sides of the fault are plotted in the same coordinates. Applying the theoretical curves to them, we know that the most probable values of H and v_{00} are as follows.

$$H=8\text{ km}, \text{ and } v_{00}=200\text{ cm}.$$

This estimation enables us, then, to compute $(Y_x)_0$ and E_f for the present case, the results of which are shown in Table 1.

The Fairview Peak fault (1954)

Two great earthquakes took place on December 16, 1954 in the Dixie Valley-Fairview Peak area of Nevada. They were accompanied by two major faults which appeared on the side of Fairview Peak and in Dixie Valley, respectively. Since the former one was the most conspicuous, the following discussion deals only with it.

Numbers of minor fractures appearing along the Fairview Peak fault made it difficult to determine the direction of the principal fault plane by geological survey. However, a seismometrical study conducted by C. Romney has concluded that one of the nodal planes lies in the direction of N11°W dipping 62° to east[7]. This value being in good harmony with the direction of earth movements near the fault, we assume here that it represents the strike of the actual fault plane (see the chain line in Fig. 5). Triangulations prepared before and after the earthquake

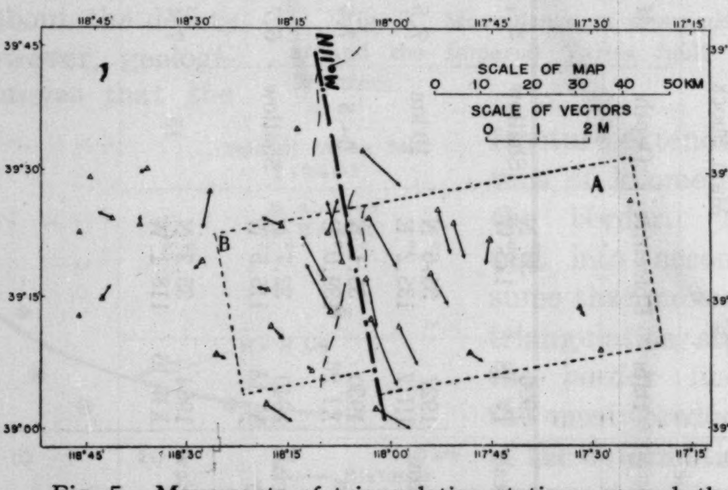

Fig. 5. Movements of triangulation stations around the Fairview Peak fault (after C. A. Whitten).

---

[7] C. ROMNEY, *Bull. Seis. Soc. Amer.*, **47** (1957), 301-320.

by the Coast and Geodetic Survey have clarified the features of the deformation associated with the fault[8]. Geodetic observations as well as the seismometrical solution for this fault indicated that the movement in the vertical direction was half of the horizontal one. So that it is not a strike-slip fault in the strict sense, however a tentative application of the theory of a strike-slip fault might be allowed in the present step of approximation.

The amplitudes of displacement vectors for the triangulation stations in A and B areas (see Fig. 5) are plotted against the distance, from which we find out that the diminution of v_o can be explained by taking $H=15$ km and $v_{00}=150$ cm (Fig. 6). $(Y_x)_0$ and E_f are computed, then, as shown in Table 1.

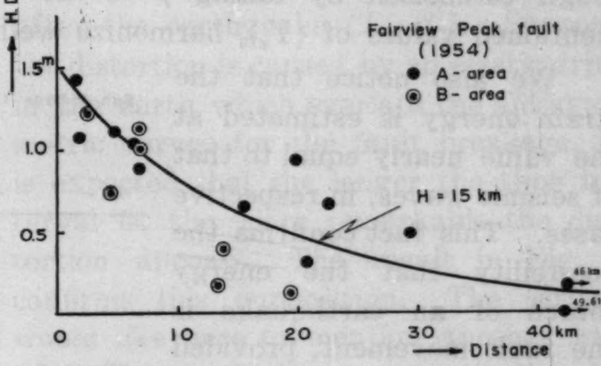

Fig. 6. Diminution curve of v_0 in the Fairview Peak area.

4. Faulting and elastic drift in the earth's crust.

The results of the foregoing analysis are compiled in Table 1, in which the conditions of the main shocks are also given for the sake of comparison. We notice, first, the relation between the depth of the seismic focus and of the fault plane. The present writer found out, previously, that the focus of the Tango earthquake was located at the lower part of the Gômura fault. Such a relation is likely to hold good in all of the present cases. This fact is of essential meaning for the elastic rebound theory of earthquakes, which premises the spatial coincidence of the earthquake origin with the fault plane.

From the table we know that the aspect ratio of the faults $(2L/H)$ differs much from each other, in which we notice, however, that the ratios for the faults in California are estimated at larger values than those for the others. D. Tocher, who investigated ground breakages in California and Nevada, expressed a view that the volume of elastic strain was no thicker for the largest shocks than it is for the smallest shock that produced a fault[9]. The writer would not like here to check this only with the above-mentioned data, but he considers that it is

---

8) C. A. WHITTEN, *Trans. Amer. Geophys. Union,* **37** (1956), 393–398.

9) D. TOCHER, *Bull. Seis. Soc. Amer.,* **48** (1958), 147–153.

worth examining how H or $2L/H$ depends on the local conditions, by taking more examples.

$(Y_x)_0$ distributes in a range between 5×10^7 and 3×10^8 c.g.s.. From the viewpoint of our model, this quantity should be understood as the strength of the medium. C. Tsuboi has concluded, from another standpoint, that the ultimate strain of the earth's crust is about 10^{-4}.[10] After rough estimation by taking $\mu=5\times10^{11}$ c.g.s., we see that the above-mentioned values of $(Y_x)_0$ harmonize well with Tsuboi's conclusion.

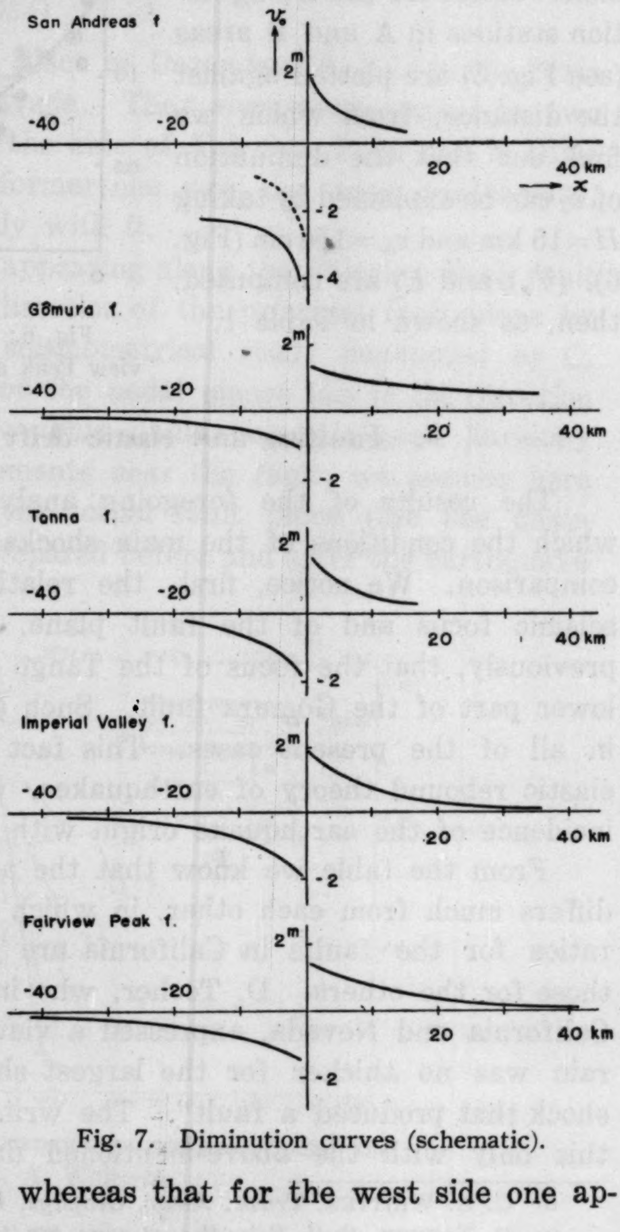

Fig. 7. Diminution curves (schematic).

We also notice that the strain energy is estimated at the value nearly equal to that of seismic waves, in respective cases. This fact confirms the possibility that the energy source of an earthquake is the fault movement, provided it occurs in a very short time. Both sorts of energy being computed after rough approximation, more detailed investigation would be necessary for decisive conclusion. However, as long as we regard the estimation as order-of-magnitude one, the above-mentioned view can be accepted.

The theory predicts that the diminution curves on both sides of a fault are antisymmetric with one another. This prediction is likely to hold good in such a case as the Imperial Valley fault; however, in the case of the San Andreas fault, for instance, we see some distortion of the curves. The curve for the east side area approaches zero with distance, whereas that for the west side one approaches a certain finite value of v_0, 200 cm say. This type of distortion can be seen, more or less, in the other cases as shown in Fig. 7, which might be attributed to the strain accumulation in the crust developed before the earthquake. In order to ascertain this supposition, we plot, in Fig. 8, the magnitude of distortion ($\Delta v_0/v_{00}$) against the time interval between the surveys conducted before and after the earthquake (T_2-T_1). Suppose the distortion is caused by an elastic drift in the earth which overlaps the antisymmetric curves for the fault breakage, it is expected that the longer the time interval is, the more remarkable the distortion appears. The result in Fig. 8 confirms this supposition. The writer would like here to mention another important fact which proves more directly the elastic drift in the California district. Geodetic triangulation prepared by C. A. Whitten has clearly indicated the drift of triangulation stations developing at a constant rate[11]. Taking this fact as well as the result of Fig. 8 into consideration, we might accept the reality of strain accumulation in the other districts, too.

---

[10] C. Tsuboi, *Journ. Phys. Earth*, **4** (1956), 63–66.

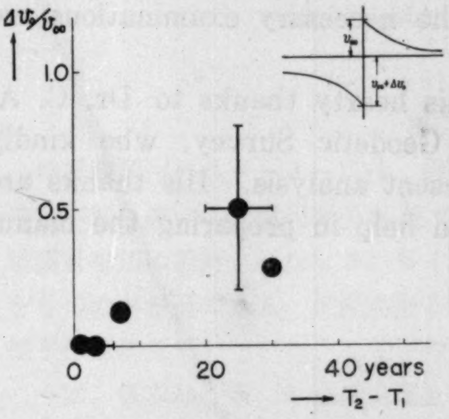

Fig. 8. Distortion of diminution curves versus time interval between the surveys.

5. Conclusions and acknowledgement.

The writer applied his theory of a strike-slip fault to five representative cases and estimated their physical conditions of faulting as shown in Table 1. The conclusions which are obtained from the present analysis are as follows.

1. The depths, to which the fault planes appeared from the earth's surface, are estimated at the values between 6 km and 15 km. They are nearly equal to the focal depths of the respective shocks.

2. The stress changes amounting to $5\times10^7\sim3\times10^8$ c.g.s. took place in the fracture planes. These values agree well with the strength of the crust, that has been concluded from another point of view.

3. The energy of crustal deformation and that of seismic waves are of the same order, in the respective cases.

4. The diminution curves of deformation indicate some distortion

---

[11] C. A. WHITTEN, *loc. cit.*, 8).

due to the elastic drift in the earth's crust. The longer the time interval between the surveys before and after the earthquake is, the more remarkable the distortion becomes.

These results are likely to confirm the view that the faultings were the immediate causes of the respective earthquakes; however, a definite conclusion will be postponed until all the necessary examinations are carried out.

The writer wishes to acknowledge his hearty thanks to Dr. C. A. Whitten of the United States Coast and Geodetic Survey, who kindly offered the triangulation data for the present analysis. His thanks are also due to Miss R. Iwaya for her kind help in preparing the manuscript.

---

26. 地震断層の性状について

地震研究所　笠　原　慶　一

さきに提出した断層模型の立場から，代表的な横辷り断層と思われる San Andreas 断層，郷村断層，丹那断層 (以上の 3 例については一部報告済み), Imperial Valley 断層，Fairview Peak 断層についてその性状を考察した．おもな結論は次の通りである．

1.　これらの断層面はそれぞれ 6 km から 15 km の深さに達していたものと推定されるが，験震学的に求められている震源の深さもまた，ほぼこれに匹敵する．

2.　断層面上の shear 歪力の変化は 5×10^7 c.g.s. から 3×10^8 c.g.s. の間に求められる．これは地殻の力学的強さに関する従来の常識から見ても妥当な数値と思われる．

3.　地殻変動の歪エネルギーと地震波動のエネルギーとは，それぞれの場合において同じ order であることが判つた．

4.　断層両側における水平変動の分布は逆対称であることが予想されるが，取扱つた実例のうちには分布曲線にある種の歪みが認められるものもある。この歪みの程度は，最初の測量から地震に至るまでの期間が長かつた場合ほど顕著であつて，地震前に地殻歪みが進行していた事実を裏書きするものと思われる．

以上の結果はいずれも断層地震説を主張する上に都合のよい事実であるが，単にこれだけの資料から決定的な議論はできない．更に地震学的その他の立場から検討を加える必要がある。

地震研究所彙報
第36号 (1958) 465-470頁

27. 地震観測用スターター

地震研究所 田中貞二

(昭和30年12月20日発表—昭和33年9月31日受理)

1. まえがき

地震観測用のスターターには，従来から，種々の形式の考案があるが，それらの機構上の根本的な違いは起動用振子を使う1),2),3),4)か，使わない5),6),7)かである．後者は電磁型地震計専用に設計されたものが多く，一般の機械式地震計に使うものは，別に起動用振子をもつのが普通である．起動用振子には，水平動のものと，上下動のものとがあり，又，振子接点に使われる材料にも色々の種類がある．

今回，煤書地震計の記録紙速度を速め，地震動波形の解析精度をよくする目的で，新しい型のスターターを試作した．設計にあたつては，既に使われている種々のスターターの利点をとり入れ，次のような方針をとつた．

1) 種々の地震計に使用できるように，起動用振子を使い，その固有周期は地震計の周期に応じて容易に変えられるようにする．

2) 記録紙がなくなるまで，何回でも自動的に繰り返し作動する．

3) 構造をできるだけ簡単にし，故障がおこる度合を少くする．

4) 成るべく高感度のものとする．

2. スターターの構造

スターターは起動用振子と限時リレー回路とからなる．第1図にその写真を示す．

(1) 起動用振子

起動用振子は，第2図に示すように，重錘と板バネからなる無制振の水平振子で，重錘の動きをエデン・バネ8)で拡大する方法をとつた．又，この振子は縦に使うと逆立振子となる．

---

1) U. S. A. COAST and GEODETIC SURVEY, *Earthquake Investigations in California 1934–1935*, (1936), 9–10.
2) 友田 好文 地震 **5** (1952), 28.
3) 高橋竜太郎 地震 **6** (1953), 1.
4) 矢橋徳太郎 地震 **10** (1957), 162.
5) 浅田 敏・田 望 地震 **5** (1952), 29.
6) 岡本舜三・清宮勝行 生産研究 **7** (1955), 116.
7) H. KAWASUMI, E. SHIMA, M. SIBANO and M. YANAGISAWA, *Bull. Earthq. Res. Inst.*, **36** (1958), 447.
8) G. NISHIMURA, M. SUZUKI and E. FURUKAWA, *Bull. Earthq. Res. Inst.*, **32** (1954), 87.

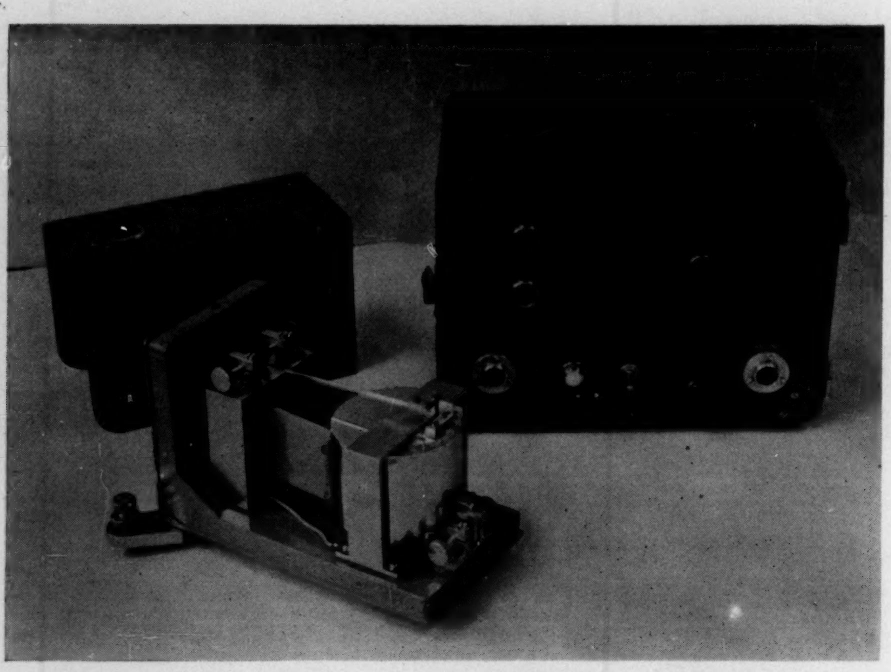

Fig. 1. Newlybuilt starter pendulum (left) and its relay-box (right).

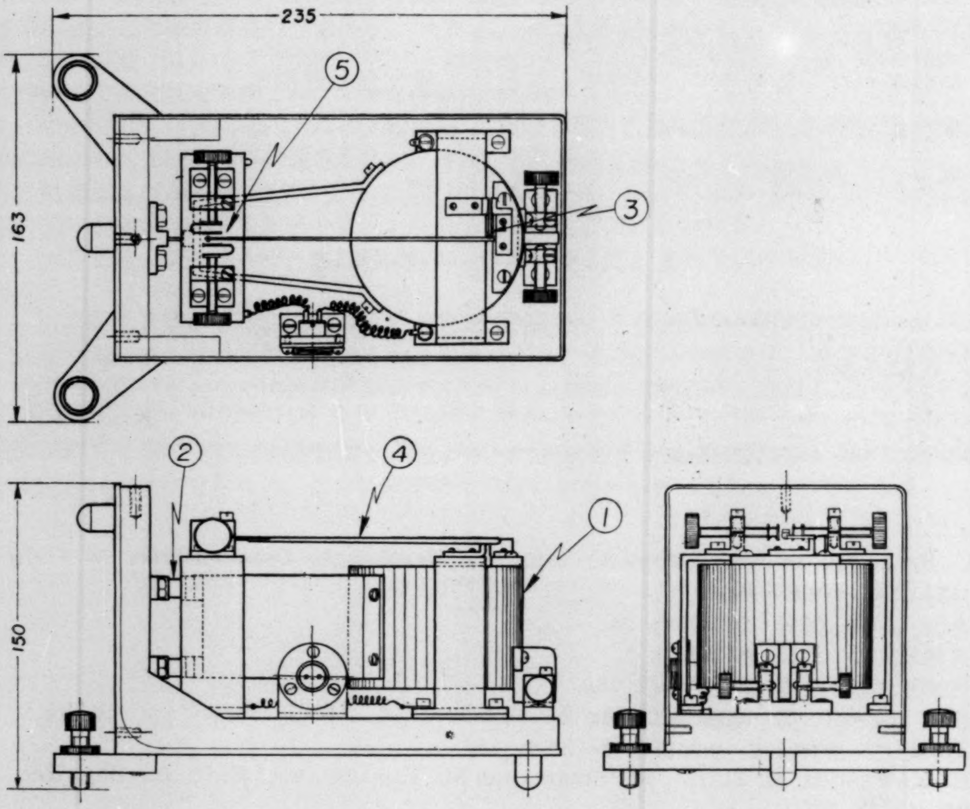

Fig. 2. Construction diagram of the newlybuilt starter. ①; mass of pendulum, ②; plate spring, ③; Eden's twin strip, ④; aluminium lever, ⑤; electric contact-point.

この振子の質量は 2.6 kg，幾何倍率は 125 倍である．板厚の違うエデン・バネを付けかえると，幾何倍率を変化することなく，振子の固有周期を第1表のように変えることができる．

経験によれば，起動用振子を使うスターターの故障の原因は，振子の電気接点の酸化，又は汚染による接触抵抗の増大に起因することが多いので，特に接点材料の選択に留意した．この起動用振子に使用した材料は，可動接点はオスミウム，白金，ロヂウムの合金，固定接点は銀，パラヂウムの合金である．このスターターにおいては，動作時の接点電流が極めて少ないこととあいまつて，振子接点の劣化は殆んど完全に防止することができた．

第1表　起動用振子の固有周期

エデン・バネの厚さ (mm)	固有周期 (sec)
0.07	0.58
0.08	0.42
0.10	0.31
0.13	0.25
0.23	0.14

第3図は，起動用振子（固有周期 0.14 sec）の振動台による検定結果で，感度は約 3 gal/mm，減衰常数 (h) は約 0.03 であつた．

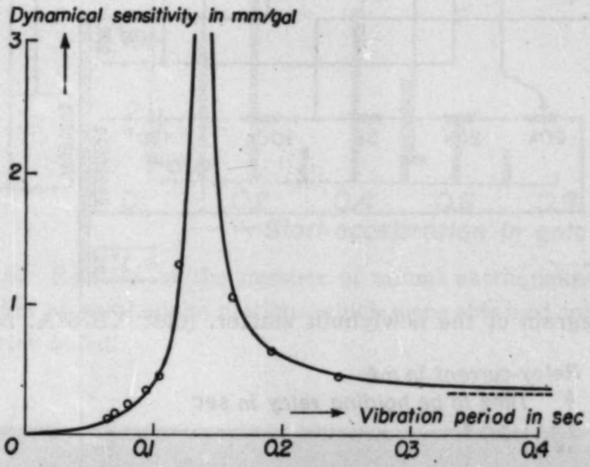

Fig. 3. Dynamical sensitivity of the newlybuilt starter. Circles represent the results of observations which were carried out by means of vibration table of simple harmonic motion, and the full line indicates mathematical results.

(2) 限時リレー回路

限時リレー回路は第4図に示すように4極放電管と多接点継電器を使い，なるべく簡略に構成した．放電管の格子は常に負に保たれ，継電器が開放されている状態では，蓄電器は常に充電されている．今，地動により起動用振子の電気接点が閉じると，放電管の格子電位は負から正に変り，放電管は放電する．従つて継電器が作動し，地震計記録装置は駆動される．それと同時に，蓄電器は高抵抗を通じて放電管格子へ切換えられ，その蓄積電荷が格子回路の高抵抗を通じて放電し，格子電位が放電維持電圧以下に低下するまで放電

管は放電を持続する． 或る時間の後， 放電が停止すると， 継電器は開放され， 初めの待機姿勢に戻る．限時リレー回路はこのような動作を繰り返し行うものである．放電管の放電継続時間，即ち，地震計記録装置の動作時間は放電管格子の負電位を変化することによつて，1～3 分の間で任意に調整することができる．この回路では起動用振子の接点電流は数 μA 程度であるから， 火花放電による接点の損傷は起り難いし，例え， その接触抵抗が数 MΩ まで増大しても，リレー回路は確実に動作する．又，地震動による振子接点の断続はリレー回路の動作に影響しない． この回路の消費電力は常時約 7W である． 第 5 図は電源電圧の変化に対する継電器保持時間及び継電器電流の変化を示すもので，電源電圧に対する安定度はきわめて良好である．

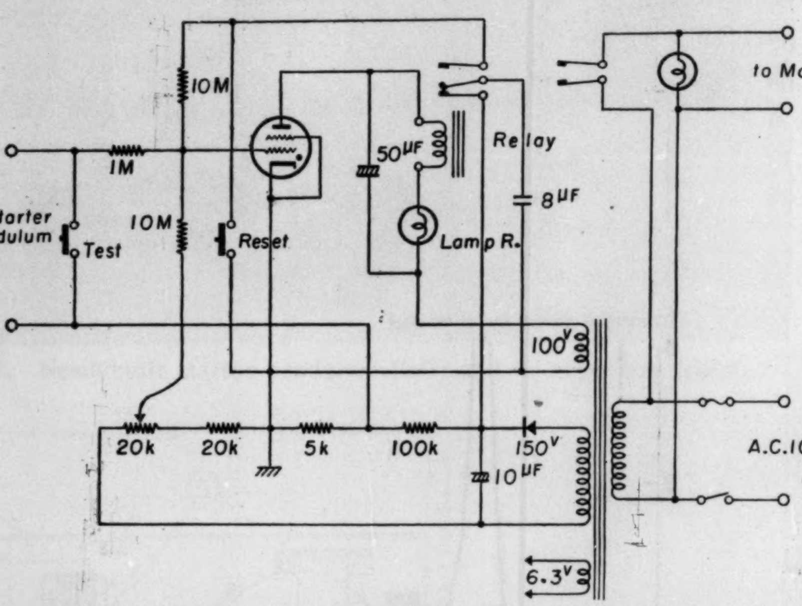
XB785A
10M
1M
to Starter Pendulum
Test
10M
Reset
50μF
Relay
8μF
Lamp R.
to Motor
100V
A.C.100V
20k
20k
5k
100k
150V
10μF
6.3V

Fig. 4. Circuit diagram of the newlybuilt starter. (old: XB785A. new: XB785B, 2D21.)

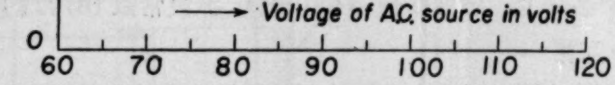

Fig. 5. Characteristic curves of relay-circuit of the newlybuilt starter. White and black circles represent the relation of time of holding relay and relay-current to the value of valtage of A. C. source.

3. 観測結果

固有周期0.14 secの起動用振子(接点間隙1 mm)をもつスターターの試験のための地震観測を，固有周期1 sec，幾何倍率200倍の水平動地震計で行い，約3ケ月の間に22ケの地震記録をとつた．

地震記録の描き始めの振巾と，その直後の平均周期とから，スターター始動時の加速度振巾を推定すると，第6図のような頻度分布が得られた．従つて，22ケの地震の大部分は0.5 gal以下の加速度で始動したことになり，起動用振子の振動特性から期待される値にくらべてかなり小さい．これは起動用振子の減衰が小さいので，自由振動が誘発されるためと考えられる．

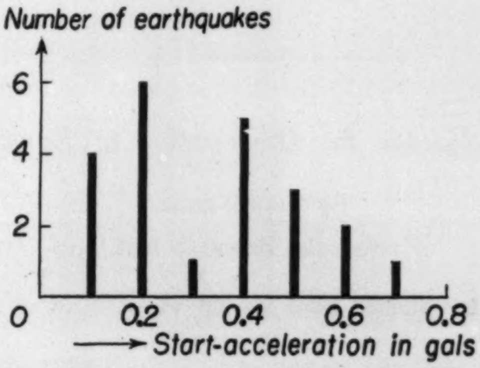

Fig. 6. Relation of the number of actual earthquakes to the values of acceleration of earthquake motions which were obtained soon after the newly-built starter acted.

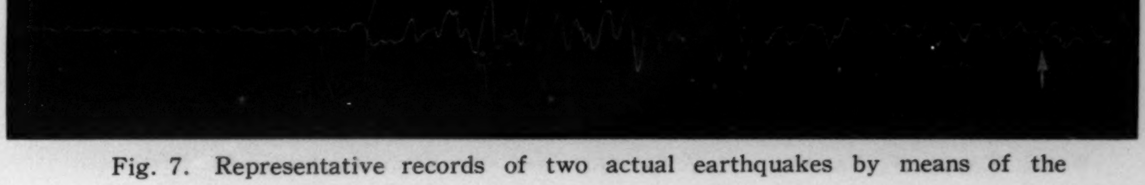

Fig. 7. Representative records of two actual earthquakes by means of the newlybuilt starter. (Original ×0.7.)

第7図に茨城県日立鉱山での地震観測[9]で得られた記録の一例を示す．この場合には，起動用振子の固有周期を 0.42 sec とし，周期 1 sec，倍率 200 倍の水平動地震計 4 台と組合せて使用したが，有効な記録振巾をもつ 42 ケの地震のうち 38 ケまでは初期微動の部分から記録することができた．

4. むすび

比較的高感度をもち，長期の安定性があり，自動的に繰り返し動作するスターターを設計，試作して各種の試験を行つた．

このスターターは，その後数台製作され，地震観測に実用されている[10),11)]．日立鉱山の坑内においては委託観測により約2ケ年連続使用したが故障は起らなかつた．

終りに，この仕事について終始御指導を頂いた金井清先生に厚く御礼を申し述べる．

27. *A Starter for Observation of Earthquakes.*

By Teiji TANAKA,
Earthquake Research Institute.

The strong points of the starter built for the observation of earthquakes presented in this paper are as follows:

(1) its sensitivity is high and, at the same time, stability is good, though the mechanism is considerably simple,

(2) recording time is changeable,

(3) automatic operations of starting and stopping recording are repeatable many times.

Next, the figure captions are written in the subsequence. Fig. 1 Newlybuilt starter pendulum (left) and its relay-box (right). Fig. 2 Construction diagram of the newlybuilt starter. 1; mass of pendulum, 2; plate spring. 3; Eden's twin strip, 4; aluminium lever, 5; electric contact-point. Fig. 3 Dynamical sensitivity of the newlybuilt starter. Circles represent the results of observations which were carried out by means of vibration table of simple harmonic motion, and the full line indicates mathematical results. Fig. 4 Circuit diagram of the newly-built starter. Fig. 5 Characteristic curves of relay-circuit of the newlybuilt starter. White and black circles represent the relation of time of holding relay and relay-current to the value of voltage of A. C. source. Fig. 6 Relation of the numbers of actual earthquakes to the values of acceleration of earthquake motions which were obtained soon after the newlybuilt starter acted. Fig. 7 Representative records of two actual earthquakes by means of the newly-built starter.

---

[9] K. KANAI, T. TANAKA and T. SUZUKI, *Bull. Earthq. Res. Inst.*, **36** (1958), 201.

[10] 鈴木正治 地震研究所彙報 **36** (1958), 235.

[11] 金井 清・田中貞二・鈴木富三郎・長田甲斐男・吉沢静代 地震研究所談話会（昭和 33 年 7 月).

所報

◎談話会記事

第356回談話会（昭和33年6月24日）

1.	能代・大館間の重力再測 特に二ツ井地震による重力場の変化	実川顕 田島広一
2.	分散性媒質に於ける地震波の初動に就いて	吉山良一
3.	地盤の震動特性に関する半実験式（補遺）	金井清
4.	地震動の大きさと周期との関係（再補遺）	金井清
5.	房総半島清澄砂岩層中の一凝灰岩の機械的組成	村井勇
6.	三原山におけるガス組成の変化と火山活動（続報）	野口喜三雄 島誠 綿抜邦彦 （野口研究員紹介） 神谷宏 （野口研究員紹介）
7.	茨城県筑波地方に於ける変質堆積岩中の重鉱物	市村毅 （津屋所員紹介）
8.	山形県天童，山形，上の山地方の斜長石石英粗面岩及びその関係岩類に関する地質学的考察	市村毅 （津屋所員紹介）
9.	浅間火山の活動と同火山に発生する地震の研究（続報） 特に噴火予知に関連して	水上武 茂木清夫 内堀貞雄 平賀士郎 宮崎務 伊東喜久子

第357回談話会（昭和29年7月15日）

1.	超短波遠隔記録地震計（第2報）	宮村摂三 辻浦賢
2.	大地震に伴う地殻変動の研究（第4報） （地震断層の深さについて）	笠原慶一
3.	富士火山の重力測量	横山泉 田島広一
4.	屈斜路湖及び阿寒湖面上の重力測量	横山泉 田島広一 村瀬勉 （力武所員紹介） 音田功 （力武所員紹介）
5.	日立，東海，水戸における地震動比較観測	金井清 田中貞二郎 鈴木富三郎 長田甲斐男 吉沢静代
6.	島根県大社町の地盤調査 （南海地震異常震害地）	金井清 田中貞二郎 鈴木富三郎

第358回談話会（昭和33年9月16日）

1.	大理石の変形及び破壊（第1報） （特に強度と加重速度）	茂木清夫
2.	Phototransistor を使つた Starter について	河角広 嶋悦三 柴野睦郎 柳沢馬住
3.	東京三崎間の水準点の変動 特に油壷験潮場内固定点の変動量について	山口生知
4.	超短波多重遠隔記録地震計による小六点観測	宮村摂三 辻浦賢
5.	近地地震波動のスペクトル的研究（第2報） （筑波山における六点観測）	安芸敬一 辻浦賢

第359回談話会（昭和33年10月29日）

1.	有層弾性体の伝播波について （特に接触部の水平変位差が及ぼす影響）	夏目正太郎 （金井技官紹介）
2.	G 波の研究	佐藤泰夫
3.	日本に於ける地磁気変化の異常（続報）	力武常次 上田誠也 行武毅 中川英子 棚岡巌
4.	三鷹市新川における土地脈動の三点観測	岸上冬彦
追加	最大振巾と震央距離との関係	吉山良一

第360回談話会（昭和33年11月25日）

1.	本邦火山岩の微量成分について	桂敬 （南所員紹介）
2.	地磁気永年変化と地球中間層の導電性	行武毅 （力武所員紹介）
3.	火薬爆発による地震動の発生（その 2）	笠原慶一
4.	多点観測による脈動の研究（その 1）	三東哲夫
5.	垂直方向に任意の物質分布をもつ半無限弾性体内を伝わる表面波の方程式の数値解法	佐藤泰夫
6.	地震波のスペクトル構造について（第1報） ―そのマグニチュード決定におよぼす影響―	松本利松
7.	地盤の震動増幅度を求める一方法	金井清 吉沢静代

Index to Vol. 36.

Page

AKI, K.; TSUJIURA, M.; HORI, M. and GOTÔ, K., (5) Spectral Study of Near Earthquake Waves (1). (in English) 71

ASADA, T.; USAMI, T.; MIKUMO, T.; SHIMA, E.; TAMAKI, I.; ASANO, S. and MATUZAWA, T., (19) Crustal Structure in Northern Kwantô District by Explosion-Seismic Observations. Part II. Models of Crustal Structure. (in English) 349

ASANO, S.; USAMI, T.; MIKUMO, T.; SHIMA, E.; TAMAKI, I.; ASADA, T. and MATUZAWA, T., (19) Crustal Structure in Northern Kwantô District by Explosion-Seismic Observations. Part II. Models of Crustal Structure. (in English) 349

GOTÔ, K.; AKI, K.; TSUJIURA, M. and HORI, M., (5) Spectral Study of Near Earthquake Waves (1). (in English) 71

HAGIWARA, T., (8) A Note on the Theory of the Electromagnetic Seismograph. (in English) 139

HORI, M.; AKI, K.; TSUJIURA, M. and GOTÔ, K., (5) Spectral Study of Near Earthquake Waves (1). (in English) 71

HOSOYA, Y.; TSUYA, H. and MURAI, I., (23) Size Characteristics of the Pumice Deposits distributed in the Vicinity of Komoro on the Southwest Foot of Asama Volcano. (in Japanese) 413

ICHIMURA, T., (21) Geological Considerations on Plagioliparite and Associated Extrusives Exposed in the Tendō-Yamagata-Kaminoyama District, Yamagata Prefecture. (in English) 369

ICHIMURA, T., (22) Heavy Minerals in Metamorphosed Sediments from the Tsukuba District, Ibaraki Prefecture. (in English) ... 395

KANAI, K., (16) A Study of Strong Earthquake Motions. (in English) 295

KANAI, K. and TANAKA, T., (20) Self-levelling Vibrograph. (in English) 359

KANAI, K. and YOSHIZAWA, S., (15) The Amplitude and the Period of Earthquake Motions. II. (in English) 275

KANAI, K.; KISHINOUYE, F.; NASU, N. and KAWASUMI, H., (9) Vibration of a Reinforced Concrete Building moved with Vibration Generators. (in English) 165

KANAI, K.; TANAKA, T. and SUZUKI, T., (10) Rocking and Elastic Vibrations of Actual Building. I. (Experiments by Vibration Generator). (in English) 183

KANAI, K.; TANAKA, T. and SUZUKI, T., (11) Rocking and Elastic

Vibrations of Actual Building. II. (Observation of Earthquake Motion). (in English) 201

KASAHARA, K., (2) The Nature of Seismic Origins as Inferred from Seismological and Geodetic Observations (2). (in English) 21

KASAHARA, K., (26) Physical Conditions of Earthquake Faults as Deduced from Geodetic Data. (in English) 455

KAWASUMI, H.; KANAI, K.; KISHINOUYE, F. and NASU, N., (9) Vibration of a Reinforced Concrete Building moved with Vibration Generators. (in English) 165

KAWASUMI, H.; SHIMA, E.; SIBANO, M. and YANAGISAWA, M., (25) A Seismographic Starter Using a Phototransistor. (in English) 447

KISHINOUYE, F., (12) A Study of the Shōnai Earthquake of 1894. (in Japanese) 227

KISHINOUYE, F.; KANAI, K.; NASU, N. and KAWASUMI, H., (9) Vibration of a Reinforced Concrete Building moved with Vibration Generators. (in English) 165

KOMAKI, S.; OMOTE, S. and NAKAJIMA, N., (17) Seismic Wave Types in a Sand Layer near a Small Explosion. (in English) 311

MATUMOTO, T., (3) Calibration of an Electromagnetic Seismograph by Means of the Frequency Analysis. (in English) 55

MATUZAWA, T.; USAMI, T.; MIKUMO, T.; SHIMA, E.; TAMAKI, I.; ASANO, S. and ASADA, T., (19) Crustal Structure in Northern Kwantô District by Explosion-Seismic Observations. Part II. Models of Crustal Structure. (in English) 349

MIKUMO, T.; USAMI, T.; SHIMA, E.; TAMAKI, I.; ASANO, S.; ASADA, T. and MATUZAWA, T., (19) Crustal Structure in Northern Kwantô District by Explosion-Seismic Observations. Part II. Models of Crustal Structure. (in English) 349

MINAMI, E. and SHIMA, M., (7) On the Geochemical Study of Carbon 14. (II). Agedating of Volcanic Product and the Rate of Peat Sedimentation. (in English) 135

MOGI, K., (6) Relations between the Eruptions of Various Volcanoes and the Deformations of the Ground Surfaces around them. (in English) 99

MURAI, I.; TSUYA, H. and HOSOYA, Y., (23) Size Characteristics of the Pumice Deposits distributed in the Vicinity of Komoro on the Southwest Foot of Asama Volcano. (in Japanese) 413

NAKAGAWA, E.; RIKITAKE, T.; YOKOYAMA, I.; UYEDA, S. and

YUKUTAKE, T., (1) The Anomalous Behaviour of Geomagnetic Variations of Short Period in Japan and Its Relation to the Subterranean Structure. The 7th report. (in English) 1

NAKAJIMA, N.; OMOTE, S. and KOMAKI, S., (17) Seismic Wave Types in a Sand Layer near a Small Explosion. (in English) 311

NASU, N.; KANAI, K.; KISHINOUYE, F. and KAWASUMI, H., (9) Vibration of a Reinforced Concrete Building moved with Vibration Generators. (in English) 165

OKADA, A., (4) Shiroishi Earthquake of Sept. 30th, 1956, and Precise Levelling Resurvey of its Epicentral Area, Miyagi Prefecture. (in Japanese) 65

OMOTE, S.; KOMAKI, S. and NAKAJIMA, N., (17) Seismic Wave Types in a Sand Layer near a Small Explosion. (in English) 311

Research Group for Proton Magnetometer, (24) A Proton Magnetometer. (in Japanese) 433

RIKITAKE, T.; YOKOYAMA, I.; UYEDA, S.; YUKUTAKE, T. and NAKAGAWA, E., (1) The Anomalous Behaviour of Geomagnetic Variations of Short Period in Japan and Its Relation to the Subterranean Structure. The 7th report. (in English) 1

SHIMA, E.; KAWASUMI, H.; SIBANO, M. and YANAGISAWA, M., (25) A Seismographic Starter Using a Phototransistor. (in English).. 447

SHIMA, E.; MIKUMO, T.; USAMI, T.; TAMAKI, I.; ASANO, S.; ASADA, T. and MATUZAWA, T., (19) Crustal Structure in Northern Kwantô District by Explosion-Seismic Observations. Part II. Models of Crustal Structure. (in English) 349

SHIMA, M. and MINAMI, E., (7) On the Geochemical Study of Carbon 14. (II). Agedating of Volcanic Product and the Rate of Peat Sedimentation. (in English) 135

SIBANO, M.; KAWASUMI, H.; SHIMA, E. and YANAGISAWA, M., (25) A Seismographic Starter Using a Phototransistor. (in English).. 447

SUZUKI, M., (13) Aseismic Properties of a Wooden House. Part 2. (Observation of Earthquakes) (in Japanese) 235

SUZUKI, T.; KANAI, K. and TANAKA, T., (10) Rocking and Elastic Vibrations of Actual Building. I. (Experiments by Vibration Generator). (in English) 183

SUZUKI, T.; KANAI, K. and TANAKA, T., (11) Rocking and Elastic Vibrations of Actual Building. II. (Observation of Earthquake Motion). (in English) 201

TAMAKI, I.; USAMI, T.; MIKUMO, T.; SHIMA, E.; ASANO, S.; ASADA,

T. and Matuzawa, T., (19) Crustal Structure in Northern Kwantô District by Explosion-Seismic Observations. Part II. Models of Crustal Structure. (in English) ... 349

Tanaka, T., (27) A Starter for Observation of Earthquakes. (in Japanese) ... 465

Tanaka, T. and Kanai, K., (20) Self-levelling Vibrograph. (in English) ... 359

Tanaka, T.; Kanai, K. and Suzuki, T., (10) Rocking and Elastic Vibrations of Actual Building. I. (Experiments by Vibration Generator). (in English) ... 183

Tanaka, T.; Kanai, K. and Suzuki, T., (11) Rocking and Elastic Vibrations of Actual Building. II. (Observation of Earthquake Motion). (in English) ... 201

Tanaoka, I.; Uyeda, S. and Yukutake, T., (14) Studies of the Thermal State of the Earth. The First Paper: Preliminary Report of Terrestrial Heat Flow in Japan. (in English) ... 251

The Research Group for Explosion Seismology, (18) Crustal Structure in Northern Kwantô District by Explosion-Seismic Observations. Part I. Description of Explosions and Observations. (in English). 329

Tsujiura, M.; Aki, K.; Hori, M. and Gotô, K., (5) Spectral Study of Near Earthquake Waves (1). (in English) ... 71

Tsuya, H.; Murai, I. and Hosoya, Y., (23) Size Characteristics of the Pumice Deposits distributed in the Vicinity of Komoro on the Southwest Foot of Asama Volcano. (in Japanese) ... 413

Usami, T.; Mikumo, T.; Shima, E.; Tamaki, I.; Asano, S.; Asada, T. and Matuzawa, T., (19) Crustal Structure in Northern Kwantô District by Explosion-Seismic Observations. Part II. Models of Crustal Structure. (in English) ... 349

Uyeda, S.; Rikitake, T.; Yokoyama, I.; Yukutake, T. and Nakagawa, E., (1) The Anomalous Behaviour of Geomagnetic Variations of Short Period in Japan and Its Relation to the Subterranean Structure. The 7th report. (in English) ... 1

Uyeda, S.; Yukutake, T. and Tanaoka, I., (14) Studies of the Thermal State of the Earth. The First Paper: Preliminary Report of Terrestrial Heat Flow in Japan. (in English) ... 251

Yanagisawa, M.; Kawasumi, H.; Shima, E. and Sibano, M., (25) A Seismographic Starter Using a Phototransistor. (in English).. 447

Yokoyama, I.; Rikitake, T.; Uyeda, S.; Yukutake, T. and Nakagawa, E., (1) The Anomalous Behaviour of Geomagnetic

Variations of Short Period in Japan and Its Relation to the Subterranean Structure. The 7th report. (in English)............ 1
YOSHIZAWA, S. and KANAI, K., (15) The Amplitude and the Period of Earthquake Motions. II. (in English) 275
YUKUTAKE, T.; RIKITAKE, T.; YOKOYAMA, I.; UYEDA, S. and NAKAGAWA, E., (1) The Anomalous Behabiour of Geomagnetic Variations of Short Period in Japan and Its Relation to the Subterranean Structure. The 7th report. (in English) 1
YUKUTAKE, T.; UYEDA, S. and TANAOKA, I., (14) Studies of the Thermal State of the Earth. The First Paper: Preliminary Report of Terrestrial Heat Flow in Japan. (in English) 251

Variations of Short Period in Japan and its Relation to the Subterranean Structure. The 7th report. (in English) 1
YOSHIZAWA, S. and KASAHARA, K., (15) The Amplitude and the Period of Earthquake Motions in the Epicentral Area. (in English) .... [illegible]
YUKUTAKE, T., RIKITAKE, T., YOKOYAMA, I., UYEDA, S. and NAKAGAWA, E., (1) The Anomalous Behaviour of Geomagnetic Variations of Short Period in Japan and its Relation to the Subterranean Structure. The 7th report. (in English) 1
YUKUTAKE, T., UYEDA, S. and TAKAOKA, T., (14) Studies of the Thermal State of the Earth. The First Paper: Preliminary Report of Terrestrial Heat Flow in Japan. (in English) 251

索引 第36号

頁

安芸敬一·辻浦　賢·堀　実·後藤健一 (5) 近地地震波動のスペクトル的研究 (1) (英文) 71

浅田　敏·宇佐美竜夫·三雲　健·嶋　悦三·玉城逸夫·浅野周三·松沢武雄 (19) 大爆破による北関東地方の地殼構造について　其の 2　地下構造 (英文)........ 349

浅野周三·宇佐美竜夫·三雲　健·嶋　悦三·玉城逸夫·浅田　敏·松沢武雄 (19) 大爆破による北関東地方の地殼構造について　其の 2　地下構造 (英文) 349

後藤健一·安芸敬一·辻浦　賢·堀　実 (5) 近地地震波動のスペクトル的研究 (1) (英文) 71

萩原尊礼 (8) 電磁地震計の倍率その他について (英文) 139

堀　実·安芸敬一·辻浦　賢·後藤健一 (5) 近地地震波動のスペクトル的研究 (1) (英文) 71

細谷与七·津屋弘逵·村井　勇 (23) 小諸附近に分布する浅間火山軽石の粒度組成 (邦文) 413

市村　毅 (21) 山形県天童·山形·上ノ山地方の斜長石石英粗面岩及びその関係岩類に関する地質学的考察 (英文)........ 369

市村　毅 (22) 茨城県筑波地方産変質堆積岩の重鉱物 (英文) 395

金井　清 (16) 強震動に関する 1 つの考察 (英文) 295

金井　清·田中貞二 (20) 自動水準式振動計 (英文) 359

金井　清·吉沢静代 (15) 地震動の振幅と周期の関係 (英文) 275

金井　清·岸上冬彦·那須信治·河角　広 (9) 鉄筋コンクリート造建物の振動実験 (英文) 165

金井　清·田中貞二·鈴木富三郎 (10) 建物の動揺，弾性振動 第 1 報 (起振機による振動実験) (英文) 183

金井　清·田中貞二·鈴木富三郎 (11) 建物の動揺，弾性振動 第 2 報 (地震観測) (英文) 201

笠原慶一 (2) 震源の性状に関する地震学的及び測地学的研究 (二) (英文) 21

笠原慶一 (26) 地震断層の性状について (英文) 455

河角　広·金井　清·岸上冬彦·那須信治 (9) 鉄筋コンクリート造建物の振動実験 (英文) 165

河角　広·嶋　悦三·柴野睦郎·柳沢馬住 (25) Phototransistor を使つた Starter の試作 (英文) 447

岸上冬彦 (12) 1894 年の庄内地震の研究 (邦文) 227

岸上冬彦·金井　清·那須信治·河角　広 (9) 鉄筋コンクリート造建物の振動実験 (英文) 165

小牧昭三・表　俊一郎・中島直吉（旧姓小林） (17) 砂層の中を伝わる波の波形について (英文)……………… 311

松本利松 (3) 電磁地震計の特性を周波数分析によつて求める方法 (英文) …… 55

松沢武雄・宇佐美竜夫・三雲　健・嶋　悦三・玉城逸夫・浅野周三・浅田　敏 (19) 大爆破による北関東地方の地殼構造について 其の 2 地下構造 (英文)……… 349

三雲　健・宇佐美竜夫・嶋　悦三・玉城逸夫・浅野周三・浅田　敏・松沢武雄 (19) 大爆破による北関東地方の地殼構造について 其の 2 地下構造 (英文)……… 349

南　英一・島　誠 (7) ^{14}C による地球化学的研究 (II) 火山噴出物の年代および泥炭の沈積速度について (英文)……………… 135

茂木清夫 (6) 火山の噴火とその周辺の地殼変動との関係 (英文) ……… 99

村井　勇・津屋弘逵・細谷与七 (23) 小諸附近に分布する浅間火山軽石の粒度組成 (邦文) ……………… 413

中川英子・力武常次・横山　泉・上田誠也・行武　毅 (1) 日本に於ける地磁気短周期変化の異常と地下構造 (第 7 報) (英文) ……………… 1

中島直吉（旧姓小林）・表俊一郎・小牧昭三 (17) 砂層の中を伝わる波の波形について (英文) ……………… 311

那須信治・金井　清・岸上冬彦・河角　広 (9) 鉄筋コンクリート造建物の振動実験 (英文) ……………… 165

岡田　惇 (4) 宮城県白石市附近の地震 (1956 年 9 月 30 日) と水準測量の結果 (邦文) ……………… 65

表　俊一郎・小牧昭三・中島直吉（旧姓小林） (17) 砂層の中を伝わる波の波形について (英文)……………… 311

文部省科学試験研究費研究班 (代表者 力武常次) (24) プロトン磁力計の試作研究 (邦文)……………… 433

力武常次・横山　泉・上田誠也・行武　毅・中川英子 (1) 日本に於ける地磁気短周期変化の異常と地下構造 (第 7 報) (英文) ……………… 1

嶋　悦三・河角　広・柴野睦郎・柳沢馬住 (25) Phototransistor を使つた Starter の試作 (英文)……………… 447

嶋　悦三・宇佐美竜夫・三雲　健・玉城逸夫・浅野周三・浅田　敏・松沢武雄 (19) 大爆破による北関東地方の地殼構造について 其の 2 地下構造 (英文)……… 349

島　誠・南　英一 (7) ^{14}C による地球化学的研究 (II) 火山噴出物の年代および泥炭の沈積速度について (英文)……………… 135

柴野睦郎・河角　広・嶋　悦三・柳沢馬住 (25) Phototransistor を使つた Starter の試作 (英文)……………… 447

鈴木正治 (13) 木造家屋の耐震性 (第 2 報) (自然地震の観測) (邦文) ……… 235

鈴木富三郎・金井　清・田中貞二 (10) 建物の動揺, 弾性振動 第 1 報 (起振機に

よる振動実験）（英文）........................ 183

鈴木富三郎・金井　清・田中貞二　(11)　建物の動揺，弾性振動　第 2 報（地震観測）（英文）........................ 201

玉城逸夫・宇佐美竜夫・三雲　健・嶋　悦三・浅野周三・浅田　敏・松沢武雄　(19)　大爆破による北関東地方の地殻構造について　其の 2 地下構造（英文）........ 349

田中貞二　(27)　地震観測用スターター（邦文）........................ 465

田中貞二・金井　清　(20)　自動水準式振動計（英文）........................ 359

田中貞二・金井　清・鈴木富三郎　(10)　建物の動揺，弾性振動　第 1 報（起振機による振動実験）（英文）........................ 183

田中貞二・金井　清・鈴木富三郎　(11)　建物の動揺，弾性振動　第 2 報（地震観測）（英文）........................ 201

棚岡　巌・上田誠也・行武　毅　(14)　地球熱学（第 1 報）日本に於ける地殻内熱流量についての序報（英文）........................ 251

爆破地震動研究グループ　(18)　大爆破による北関東地方の地殻構造について　其の 1 観測報告（英文）........................ 329

辻浦　賢・安芸敬一・堀　実・後藤健一　(5)　近地地震波動のスペクトル的研究 (1)（英文）........................ 71

津屋弘逵・村井　勇・細谷与七　(23)　小諸附近に分布する浅間火山軽石の粒度組成（邦文）........................ 413

宇佐美竜夫・三雲　健・嶋　悦三・玉城逸夫・浅野周三・浅田　敏・松沢武雄　(19)　大爆破による北関東地方の地殻構造について　其の 2 地下構造（英文）........ 349

上田誠也・力武常次・横山　泉・行武　毅・中川英子　(1)　日本に於ける地磁気短周期変化の異常と地下構造（第 7 報）（英文）........................ 1

上田誠也・行武　毅・棚岡　巌　(14)　地球熱学（第 1 報）日本に於ける地殻内熱流量についての序報（英文）........................ 251

柳沢馬住・河角　広・嶋　悦三・柴野睦郎　(25)　Phototransistor を使つた Starter の試作（英文）........................ 447

横山　泉・力武常次・上田誠也・行武　毅・中川英子　(1)　日本に於ける地磁気短周期変化の異常と地下構造（第 7 報）（英文）........................ 1

吉沢静代・金井　清　(15)　地震動の振幅と周期の関係（英文）........................ 275

行武　毅・力武常次・横山　泉・上田誠也・中川英子　(1)　日本に於ける地磁気短周期変化の異常と地下構造（第 7 報）（英文）........................ 1

行武　毅・上田誠也・棚岡　巌　(14)　地球熱学（第 1 報）日本に於ける地殻内熱流量についての序報（英文）........................ 251

BULLETIN
OF THE
EARTHQUAKE RESEARCH INSTITUTE
UNIVERSITY OF TOKYO

VOL. 36

1958

東京大学

地震研究所彙報

第 36 號

昭和 33 年

CONTENTS.

Vol. 36.

Part 1. March, 1958.

Papers and Reports.

Page

1. T. RIKITAKE, I. YOKOYAMA, S. UYEDA, T. YUKUTAKE and E. NAKAGAWA, The Anomalous Behaviour of Geomagnetic Variations of Short Period in Japan and Its Relation to the Subterranean Structure. The 7th report. (in English) 1
2. K. KASAHARA, The Nature of Seismic Origins as Inferred from Seismological and Geodetic Observations (2). (in English) ... 21
3. T. MATUMOTO, Calibration of an Electromagnetic Seismograph by Means of the Frequency Analysis. (in English) 55
4. A. OKADA, Shiroishi Earthquake of Sept. 30th, 1956, and Precise Levelling Resurvey of its Epicentral Area, Miyagi Prefecture. (in Japanese) 65

Part 2. June, 1958.

5. K. AKI, M. TSUJIURA, M. HORI and K. GOTÔ, Spectral Study of Near Earthquake Waves (1). (in English)............... 71
6. K. MOGI, Relations between the Eruptions of Various Volcanoes and the Deformations of the Ground Surfaces around them. (in English) 99
7. M. SHIMA and E. MINAMI, On the Geochemical Study of Carbon 14. (II). Agedating of Volcanic Product and the Rate of Peat Sedimentation. (in English) 135
8. T. HAGIWARA, A Note on the Theory of the Electromagnetic Seismograph. (in English).. 139
9. K. KANAI, F. KISHINOUYE, N. NASU and H. KAWASUMI, Vibration of a Reinforced Concrete Building moved with Vibration Generators. (in English)................................ 165
10. K. KANAI, T. TANAKA and T. SUZUKI, Rocking and Elastic Vibrations of Actual Building. I. (Experiments by Vibration Generator). (in English) 183
11. K. KANAI, T. TANAKA and T. SUZUKI, Rocking and Elastic

Vibrations of Actual Building. II. (Observation of Earthquake Motion). (in English) 201
12. F. KISHINOUYE, A Study of the Shōnai Earthquake of 1894. (in Japanese) 227
13. M. SUZUKI, Aseismic Properties of a Wooden House. Part 2. (Observation of Earthquakes) (in Japanese) 235

Part 3. September, 1958.

14. S. UYEDA, T. YUKUTAKE and I. TANAOKA, Studies of the Thermal State of the Earth. The First Paper: Preliminary Report of Terrestrial Heat Flow in Japan. (in English) 251
15. K. KANAI and S. YOSHIZAWA, The Amplitude and the Period of Earthquake Motions. II. (in English) 275
16. K. KANAI, A Study of Strong Earthquake Motions. (in English) .. 295
17. S. OMOTE, S. KOMAKI and N. NAKAJIMA, Seismic Wave Types in a Sand Layer near a Small Explosion. (in English) 311
18. The Research Group for Explosion Seismology, Crustal Structure in Northern Kwantô District by Explosion-Seismic Observations. Part I. Description of Explosions and Observations. (in English) 329
19. T. USAMI, T. MIKUMO, E. SHIMA, I. TAMAKI, S. ASANO, T. ASADA and T. MATUZAWA, Crustal Structure in Northern Kwantô District by Explosion-Seismic Observations. Part II. Models of Crustal Structure. (in English) 349
20. K. KANAI and T. TANAKA, Self-levelling Vibrograph. (in English) 359
21. T. ICHIMURA, Geological Considerations on Plagioliparite and Associated Extrusives Exposed in the Tendō-Yamagata-Kaminoyama District, Yamagata Prefecture. (in English) 369
22. T. ICHIMURA, Heavy Minerals in Metamorphosed Sediments from the Tsukuba District, Ibaraki Prefecture. (in English) 395
23. H. TSUYA, I. MURAI and Y. HOSOYA, Size Characteristics of the Pumice Deposits distributed in the Vicinity of Komoro on the Southwest Foot of Asama Volcano. (in Japanese) 413
24. Research Group for Proton Magnetometer, A Proton Magnetometer. (in Japanese) 433

Part 4. December, 1958.

25. H. KAWASUMI, E. SHIMA, M. SIBANO and M. YANAGISAWA, A Seismographic Starter Using a Phototransistor. (in English) . 447

26. K. **KASAHARA**, Physical Conditions of Earthquake Faults as Deduced from Geodetic Data. (in English) 455
27. T. **TANAKA**, A Starter for Observation of Earthquakes. (in Japanese) 465

(in Japanese) 227
13. M. Suzuki, Aseismic Properties of a Wooden House. Part 2. (Observation of Earthquakes) (in Japanese) 235

Part 3. September, 1958.

14. S. Uyeda, T. Yukutake and I. Tanaoka, Studies of the Thermal State of the Earth. The First Paper: Preliminary Report of Terrestrial Heat Flow in Japan. (in English) 251
15. K. Kanai and S. Yoshizawa, The Amplitude and the Period of Earthquake Motions. II. (in English) 275
16. K. Kanai, A Study of Strong Earthquake Motions. (in English) 295
17. S. Omote, S. [illegible] and [illegible], Seismic Wave Types in a Sand Layer near a Small Explosion. (in English) 311
18. The Research Group for Explosion Seismology, Crustal Structure in Northern Kwantō District by Explosion-Seismic Observations. Part I. Description of Explosions and Observations. (in English) 329
19. T. Usami, T. Mikumo, E. Shima, I. Tamaki, S. Asano, T. Asada and T. Matuzawa, Crustal Structure in Northern Kwantō District by Explosion-Seismic Observations. Part II. Models of Crustal Structure. (in English) 349
20. K. Kanai and T. Tanaka, Self-levelling Vibrograph. (in English) 359
21. [illegible], Geological Considerations on Plagioliparite and Associated Extrusives Exposed in the Tendō-Yamagata-Kaminoyama District, Yamagata Prefecture. (in English) 369
22. [illegible], Heavy Minerals in Metamorphosed Sediments from the Tsukuba District, Ibaraki Prefecture. (in English) 395
23. H. Tsuya, I. Murai and [illegible], Size Characteristics of the Pumice Deposits distributed in the Vicinity of Komoro on the Southwest Foot of Asama Volcano. (in Japanese) 413
24. Research Group for Proton Magnetometer, A Proton Magnetometer. (in Japanese) 433

Part 4. December, 1958.

25. [illegible], E. Shima, [illegible] and M. [illegible], A [illegible] Using a Phototransistor. (in English) 447

目　次

第 36 号

第 1 冊　昭和 33 年 3 月

論文及報告　　頁

1. 日本に於ける地磁気短周期変化の異常と地下構造（第 7 報）（英文）…… 力武常次 横山泉 上田誠也 行武毅 中川英子 1
2. 震源の性状に関する地震学的及び測地学的研究（二）（英文）…… 笠原慶一 21
3. 電磁地震計の特性を周波数分析によつて求める方法（英文）…… 松本利松 55
4. 宮城県白石市附近の地震（1956 年 9 月 30 日）と水準測量の結果（邦文）…… 岡田惇 65

第 2 冊　昭和 33 年 6 月

5. 近地地震波動のスペクトル的研究（1）（英文）…… 安芸敬一 辻浦賢 堀実 後藤健一 71
6. 火山の噴火とその周辺の地殻変動との関係（英文）…… 茂木清夫 99
7. ^{14}C による地球化学的研究（II）火山噴出物の年代および泥炭の沈積速度について（英文）…… 島誠 南英一 135
8. 電磁地震計の倍率その他について（英文）…… 萩原尊礼 139
9. 鉄筋コンクリート造建物の振動実験（英文）…… 金井清 岸上冬彦 那須信治 河角広 165
10. 建物の動揺，弾性振動 第 1 報（起振機による振動実験）（英文）…… 金井清 田中貞二 鈴木富三郎 183
11. 建物の動揺，弾性振動 第 2 報（地震観測）（英文）…… 金井清 田中貞二 鈴木富三郎 201
12. 1894 年の庄内地震の研究（邦文）…… 岸上冬彦 227
13. 木造家屋の耐震性（第 2 報）（自然地震の観測）（邦文）…… 鈴木正治 235

第 3 冊　昭和 33 年 9 月

14. 地球熱学（第 1 報）日本に於ける地殻内熱流量についての序報（英文）…… 上田誠也 行武毅 棚岡巌 251

15.	地震動の振幅と周期の関係 (英文)…………………	金井　清 吉沢静代	275
16.	強震動に関する 1 つの考察 (英文)…………………	金井　清	295
17.	砂層の中を伝わる波の波形について (英文)…………………	表　俊一郎 小牧昭三 中島直吉 (旧姓 小林)	311
18.	大爆破による北関東地方の地殻構造について 其の 1 観測報告 (英文)…………………	爆破地震動研究グループ	329
19.	大爆破による北関東地方の地殻構造について 其の 2 地下構造(英文)…………………	宇佐美竜夫 三雲　健 嶋　悦三 玉城逸夫 浅野周三 浅田　敏 松沢武雄	349
20.	自動水準式振動計 (英文)…………………	金井　清 田中貞二	359
21.	山形県天童・山形・上ノ山地方の斜長石石英粗面岩及びその関係岩類に関する地質学的考察 (英文)…………………	市村　毅	369
22.	茨城県筑波地方産変質堆積岩の重鉱物 (英文)…………………	市村　毅	395
23.	小諸附近に分布する浅間火山軽石の粒度組成 (邦文)…………………	津屋弘逵 村井　勇 細谷与七	413
24.	プロトン磁力計の試作研究 (邦文)…………………	文部省科学試験研究費研究班 (代表者 力武常次)	433

第 4 冊　昭和 33 年 12 月

25.	Phototransistor を使つた Starter の試作 (英文)…………………	河角　広 嶋　悦三 柴野睦郎 柳沢馬住	447
26.	地震断層の性状について (英文)…………………	笠原慶一	455
27.	地震観測用スターター (邦文)…………………	田中貞二	465

昭和33年12月20日印刷
昭和33年12月25日発行

東京都文京区本富士町一番地
東京大学構内
編纂兼発行者　東京大学地震研究所

東京都新宿区山吹町一八四番地
印刷者　笠井康頼

東京都新宿区山吹町一八四番地
印刷所　株式会社国際文献印刷社

売捌所
東京都中央区日本橋通二丁目六番地
丸善株式会社

Sold by Maruzen Co., Ltd., Nihonbashi-dôri, Chûô-ku, Tôkyô.
Price of this copy: 120 Yen. (Postage exclusive.)

BULLETIN OF

THE EARTHQUAKE RESEARCH INSTITUTE

UNIVERSITY OF TOKYO

Vol. 36, Part 4. December, 1958.

Contents.

Papers and Reports.

Page

25. H. KAWASUMI, E. SHIMA, M. SIBANO and M. YANAGISAWA, A Seismographic Starter Using a Phototransistor. (in English) 447
26. K. KASAHARA, Physical Conditions of Earthquake Faults as Deduced from Geodetic Data. (in English) 455
27. T. TANAKA, A Starter for Observation of Earthquakes. (in Japanese).......... 465

Institute Notes.

Index.

(For the papers written in Japanese or in occidental languages, the abstracts are given in occidental languages or in Japanese respectively.)